ISSN 2542-1565

Vol. 15 2022 No. 04

GEOGRAPHY ENVIRONMENT SUSTAINABILITY

Special issue «LARGE RIVERS HYDROLOGY AND HYDROGEOCHEMESTRY»

«The journal GEOGRAPHY, ENVIRONMENT, SUSTAINABILITY was founded in 2008 by Russian Geographical Society, the Lomonosov Moscow State University Geography Department, and the Russian Academy of Sciences Institute of Geography. Since that time the journal publishes **4 issues per year**, containing original research papers and reviews. The journal issues are open source and distributed through subscriptions, library exchanges of leading universities, and via the website through the world»

FOUNDERS OF THE JOURNAL: Russian Geographical Society, Faculty of Geography, Lomonosov Moscow State University and Institute of Geography of the Russian Academy of Sciences

The journal is published with financial support of the Russian Geographical Society.

The journal is registered in Federal service on supervision of observance of the legislation in sphere of mass communications and protection of a cultural heritage. The certificate of registration: ПИ № ФС77-67752, 2016, December 21.

PUBLISHER
Russian Geographical Society
Moscow, 109012 Russia
Novaya ploshchad, 10, korp. 2
Phone 8-800-700-18-45
E-mail: press@rgo.ru
www.rgo.ru/en

EDITORIAL OFFICE
Lomonosov Moscow State University
Moscow 119991 Russia
Leninskie Gory, 1,
Faculty of Geography, 1806a
Phone 7-495-9391552
Fax 7-495-9391552
E-mail: ges-journal@geogr.msu.ru
www.ges.rgo.ru

DESIGN
Layout designer: Tereshkin Anton
Moscow, 115088,
26 Simonovsky Val str., bldg. One
Phone: +7 (903) 108-04-44
E-mail: smile.tai@gmail.com

DOI prefix: 10.24057

Format A4 (210x297mm)

"GEOGRAPHY, ENVIRONMENT, SUSTAINABILITY" is the only original English-language journal in the field of geography and environmental sciences published in Russia. It is supposed to be an outlet from the Russian-speaking countries to Europe and an inlet from Europe to the Russian-speaking countries regarding environmental and Earth sciences, geography and sustainability. The main sections of the journal are the theory of geography and ecology, the theory of sustainable development, use of natural resources, natural resources assessment, global and regional changes of environment and climate, social-economical geography, ecological regional planning, sustainable regional development, applied aspects of geography and ecology, geoinformatics and ecological cartography, ecological problems of oil and gas sector, nature conservations, health and environment, and education for sustainable development.

OPEN ACCESS POLICY. "GEOGRAPHY, ENVIRONMENT, SUSTAINABILITY" is an open access journal. All articles are made freely available to readers immediately upon publication. Our open access policy is in accordance with the Budapest Open Access Initiative (BOAI) definition - it means that articles have free availability on the public internet, permitting any users to read, download, copy, distribute, print, search, or link to the full texts of these articles, crawl them for indexing, pass them as data to software, or use them for any other lawful purpose, without financial, legal, or technical barriers other than those inseparable from gaining access to the internet itself.

Date of publication: December 31st, 2022.

EDITORIAL BOARD

EDITORIAL OFFICE

CONTENTS

Nayanne S. Benfica, Andrea da Silva Gomes, Carlos E. I. Drumond, Fabrício B. Zanchi
THE RELATION BETWEEN NET PRIMARY PRODUCTIVITY AND HUMAN ACTIVITIES FOR THREE BIOMES IN BAHIA STATE, BRAZIL 6

Maxim V. Bocharnikov
CLIMATE-RELATED GRADIENTS ON VEGETATION DIVERSITY OF THE ALTAI-SAYAN OROBIOME (SOUTHERN SIBERIA) 17

Aysha Hanif, Safdar A. Shirazi, Muhammad Jabbar, Anum Liaqat, Sahar Zia, Mariney M. Yusoff
EVALUATING THE VISITORS' PERCEPTION AND AVAILABLE ECOSYSTEM SERVICES IN URBAN PARKS OF LAHORE (PAKISTAN) 32

Anton A. Iurmanov, Igor Yu. Popov, Mikhail S. Romanov
SEAGRASSES AT THE ISLANDS ITURUP AND URUP OF KURIL ARCHIPELAGO 39

Ronnel C. Nolos, Akhmad Zamroni, Kathleen Faith P. Evina
DRIVERS OF DEFORESTATION AND FOREST DEGRADATION IN PALAWAN, PHILIPPINES: AN ANALYSIS USING SOCIAL-ECOLOGICAL SYSTEMS (SES) AND INSTITUTIONAL ANALYSIS AND DEVELOPMENT (IAD) APPROACHES 44

Afrinia L. Permatasari, Ika A. Suherningtyas, Putu P. K. Wiguna
DEVELOPMENT AND EVALUATION OF THE WEBGIS APPLICATION TO SUPPORT VOLCANIC HAZARD MITIGATION IN THE SOUTHERN FLANK OF MERAPI VOLCANO, SLEMAN REGENCY, YOGYAKARTA PROVINCE, INDONESIA 57

Citra F. Utami, Kosuke Mizuno, Hayati S. Hasibuan, Tri E. B. Soesilo
DISCOVERING SPATIAL DEVELOPMENT CONTROL FOR INDONESIA: A SYSTEMATIC LITERATURE REVIEW 64

Raed Al Tal, Rawan Theodory, Subhi M. Bazlamit
ASSESSING THE INTERSECTED RELATIONSHIP BETWEEN LAND USE AND TRANSPORTATION PLANNING 80

Roman A. Babkin, Svetlana V. Badina, Alexander N. Bereznyatsky
ASSESSMENT OF TEMPORAL VARIABILITY IN THE LEVEL OF POPULATION VULNERABILITY TO NATURAL AND MAN-MADE HAZARDS (THE CASE OF MOSCOW DISTRICTS) 90

Dwi Ariyani, Perdinan, Mohammad Y. J. Purwanto, Euis Sunarti, Atie T. Juniati, Mochammad Ibrahim
CONTRIBUTED INDICATORS TO FLUVIAL FLOOD ALONG RIVER BASIN IN URBAN AREA OF INDONESIA 102

Anna A. Cherkasova, Anton A. Iurmanov, Alexey A. Maslakov, Matija Petkovich, Marina N. Petrushina, Aida Tabelinova, Azamat Tolipov, Georgy Yakubov, Yulia Yushina
PRIELBRUSYE NATIONAL PARK ENVIRONMENTAL CHANGES DUE TO INCREASING TOURISM ACTIVITY 115

Nayot Kulpanich, Morakot Worachairungreung, Katawut Waiyasusri, Pornperm Sae-Ngow, Pornsmith Chaysmithikul, Kunyaphat Thanakunwutthirot
RELATIONSHIP BETWEEN URBANIZATION AND ROAD NETWORKS IN THE LOWER NORTHEASTERN REGION OF THAILAND USING NIGHTTIME LIGHT SATELLITE IMAGERY 124

Mikhail A. Lokoshchenko, Eugeniya A. Ehukova
SURFACE URBAN HEAT ISLAND IN MOSCOW DURING LOCKDOWN OF COVID-19 PANDEMIC IN 2020 134

SPECIAL ISSUE
«LARGE RIVERS HYDROLOGY AND HYDROGEOCHEMESTRY»

Anatoly Tsyplenkov, Sergey Chalov, Markus Eder, Helmut Habersack
LARGE RIVERS HYDROLOGY AND SEDIMENT TRANSPORT 145

HYDROLOGY, HYDRAULICS AND HYDROCLIMATIC IMPACT

Olga N. Nasonova, Yeugeny M. Gusev, Evgeny E. Kovalev
CLIMATE CHANGE IMPACT ON WATER BALANCE COMPONENTS IN ARCTIC RIVER BASINS 148

Alexander N. Vasilenko, Dmitry V. Magritsky, Natalia L. Frolova, Artem I. Shevchenko
LONG-TERM HEAT FLUX FORMATION OF THE LARGE RUSSIAN ARCTIC RIVERS
UNDER THE INFLUENCE OF CLIMATE-INDUCED AND DAM-INDUCED EFFECTS 158

Djan'na K. Houteta, Kossi Atchonouglo, Julien G. Adounkpe, Badabate Diwediga, Yao Lombo, Kossi E. Kpemoua, Komi Agboka
CHANGES IN LAND USE/ COVER AND WATER BALANCE COMPONENTS DURING
1964-2010 PERIOD IN THE MONO RIVER BASIN, TOGO-BENIN 171

Natalia Yaitskaya, Igor Sheverdyaev
DIGITAL ELEVATION MODEL DEVELOPMENT OF THE VOLGA AND DON RIVER'S DELTA
AND APPLICATION IN HYDROLOGICAL MODELING 181

Valeriy P. Bondarev
SOCIAL CONSEQUENCES OF FLOODS: CASE STUDY OF FIVE EMERGENCIES
IN DIFFERENT GLOBAL DRAINAGE BASINS 188

SEDIMENT TRANSPORT AND RIVER MORPHOLOGY

Lisa Schmalfuß, Christoph Hauer, Liubov V. Yanygina, Martin Schletterer
LANDSCAPE READING FOR ALPINE RIVERS: A CASE STUDY FROM THE RIVER BIYA 196

Olga A. Petrovskaya, Andrey A. Maltsev
TESTING BED LOAD TRANSPORT FORMULAS: A CASE STUDY OF THE LOWER AMUR
MULTI-BEAM ECHO-SOUNDERS (MBES) DATA 214

Ellina D. Zaharova, Vladimir R. Belyaev
CONTRIBUTION OF THE DIFFERENT SOURCES TO THE FORMATION OF ALLUVIAL SEDIMENTS
IN THE SELENGA RIVER DELTA (EASTERN SIBERIA, RUSSIA) 222

Nausheen Mazhar, Kanwal Javid, Muhammad A. N. Khan, Amna Afzal, Kiran Hamayon, Adeel Ahmad
INDEX-BASED SPATIOTEMPORAL ASSESSMENT OF WATER QUALITY
IN TARBELA RESERVOIR, PAKISTAN (1990-2020) 232

RESEARCH PAPER

THE RELATION BETWEEN NET PRIMARY PRODUCTIVITY AND HUMAN ACTIVITIES FOR THREE BIOMES IN BAHIA STATE, BRAZIL

Nayanne Silva Benfica[1*], Andrea da Silva Gomes[2], Carlos Eduardo Iwai Drumond[2], Fabrício Berton Zanchi[3]
[1]Development and Environment, State University of Santa Cruz, 45662-900, Ilhéus (Bahia), Brazil
[2]Economics Department, State University of Santa Cruz, 45662-900, Ilhéus (Bahia), Brazil
[3]Environmental Science Center, Federal University of Southern Bahia, 45810-000, Porto Seguro (Bahia), Brazil
***Corresponding author:** nayannebenfica@gmail.com
Received: February 24th, 2022 / Accepted: November 11th, 2022 / Published: December 31st, 2022
https://DOI-10.24057/2071-9388-2022-021

ABSTRACT. Brazilian biomes are hotspots of global biodiversity, important biomass producers and, consequently, help maintain the world's carbon balance. Net primary production (NPP) is a variable used to determine carbon uptake by land cover. As environmental factors and human activities vary, net primary production increases or decreases. This study aimed to evaluate NPP in three Brazilian biomes – Atlantic Forest, Cerrado, and Caatinga – in the state of Bahia for the last 17 years, and to understand its relationship with human activities by analyzing burned areas, as well as interrelated environmental factors, such as climate variability and soil heat flux, using remote sensing. Using the MOD17 dataset, we find evidence that the Atlantic Forest biome is the one that absorbs more carbon in comparison to the Caatinga and Cerrado biomes, with a mean annual net primary production in each one of these three biomes equal to 1,227.89 g C m^{-2}, 913.81 g C m^{-2}, and 803.56 g C m^{-2}, respectively. The years of El Niño influenced all biomes, and the results showed a strong relationship between climate and NPP in the studied biomes, especially in Caatinga, which is the most sensitive to climatic variations. Besides these results, we find evidence that, in all these biomes, the NPP dynamics have been affected by the increase in land use for agricultural and livestock activities, mainly because of deforestation and burning.

KEYWORDS: Atlantic Forest, Cerrado, Caatinga, MODIS, Carbon, Land use change

CITATION: Benfica N.S., da Silva Gomes A., Drumond C.E.I. , Zanchi F.B. (2022). The Relation Between Net Primary Productivity And Human Activities For Three Biomes In Bahia State, Brazil. Geography, Environment, Sustainability, 4(15), 6-16
https://DOI-10.24057/2071-9388-2022-021

ACKNOWLEDGEMENTS: The authors are grateful to the Doctoral Program in Development and Environment at the State University of Santa Cruz (UESC) and the Doctoral scholarship for the first author supported by, the Research Support Foundation of the State of Bahia (FAPESB).

Conflict of interests: The authors reported no potential conflict of interest.

INTRODUCTION

Vegetation in Brazilian biomes is considered one of the richest in the world (Forzza et al. 2012). The Cerrado and Atlantic Forest biomes are global biodiversity hotspots (Myers et al. 2000). Of the 20,000 plant species in the Atlantic Forest, an estimated 8,000 are endemic (Myers et al. 2000) and the flora and fauna of the biome may include 1%-8% of total world species (Silva and Casteleti 2003). The Cerrado biome is the largest and richest savanna in the neotropical region (Klink and Machado 2005; Mendonça et al. 2008). It covers around 2 million km^2 and it is home to a vascular flora of 12,300 species, of which 4,400 are endemic (Mittermeier et al. 2011). The Caatinga biome covers 70% of northeastern Brazil (Silva et al. 2017) and connects to the Cerrado, with which it shares many forest species (Teixeira et al. 2017). The biodiversity of Brazilian biomes comprises important biomass producers, and is, consequently, responsible for the world's carbon turnover (De Miranda et al. 2014; Althoff et al. 2016; Barni et al. 2016; Morais et al. 2017).

Net primary production (NPP) is an important variable for understanding carbon flow in different ecosystems (Chen et al. 2019; Novenko et al 2019; Zhang et al. 2019) and is defined as the difference between photosynthesis and autotrophic respiration of natural vegetation (Wang et al. 2018). NPP increases or decreases as variables such as precipitation and temperature (Liu et al. 2016; Delgado et al. 2018), solar radiation, diffuse light fraction and vapor pressure deficit (Wu et al. 2016), soil characteristics and water availability cause stress due to excess or scarcity to vegetation (Dyukarev et al. 2019; Chen and Yu 2019). Root depth and soil hydraulic redistribution can also determine NPP in drought periods (Oliveira et al. 2005). Moreover, climate change and human activity resulting in changes in land use and cover are intrinsically linked to variations in carbon uptake (Neumann et al. 2016; Chen et al. 2019).

In Brazil, human activity has caused many of the changes in land use and cover, mainly due to burning and deforestation (Barni et al. 2016; De Santana et al. 2020). Based on the annual deforestation report of the non-governmental organization MapBiomas, in 2019, an estimated 408,6 thousand ha were

deforested in the Cerrado, 10,6 thousand ha in the Atlantic Forest and 12,1 thousand ha in the Caatinga. These data corroborate Brazil's position as the world's seventh-largest greenhouse gas emitter, with an average of 1,939 billion tons of Greenhouse Gases emitted per year (SEEG 2018). Another impact of burning and deforestation is that the increased levels of atmospheric aerosols from biomass burning, in addition to pollution, cause a reduction in diffuse radiation and, consequently, NPP (Oliveira et al. 2007; Rap et al. 2015). Also, regarding changes on land cover, the replacement of natural vegetation for areas of human occupation such as pastures, can alter water balance and, possibly, the water content in the atmosphere and rainfall patterns (Dias et al. 2002; Staal et al. 2018). Therefore, understanding the relationship between human activity and NPP is essential to mitigate present and future impacts in Brazilian biomes.

Changes in precipitation and climate anomalies play an important role in the regional and global carbon cycle (Wu et al. 2016; Fu et al. 2018). Some studies have shown a decline in global NPP due to deforestation and droughts in recent decades (Medlyn et al. 2011; Althoff et al. 2016), and due to El Niño anomalies (Gushchina et al 2019; Wigneron et al. 2020). On the other hand, in some specific cases, depending on the sort of land handling, an increase in NPP can be verified, despite the increase in the use of the soil for agriculture and the temperature rise (Li et al. 2017; Chen et al. 2019). Therefore, the effect of environmental factors on the dynamics of NPP can vary from region to region (Ji et al. 2020), which stresses the need to evaluate these factors. Few studies have been conducted in Brazilian biomes regarding the effects of climate events and human action on NPP.

Images of the Moderate Resolution Imaging Spectroradiometer (MODIS) have been used in numerous studies on NPP (including for model input) due to its accuracy and spatial and temporal representativeness (Liu et al. 2016; Neumann et al. 2016; Morais et al. 2017). MODIS can provide results to better understand the spatial dynamics of NPP and increase or decrease trends based on environmental and human factors in Brazilian biomes. Moreover, MODIS provides information on potential carbon areas and helps create environmental and socio-economic policies. Thus, this study aims (1) to evaluate the spatial and temporal dynamics of NPP in the Atlantic Forest, Caatinga and Cerrado biomes as a whole and for each land use and cover in the state of Bahia, Brazil, in the last 17 years, (2) understand the relationship between NPP and human activity through the analysis of burned areas in the biomes, and (3) verify the influence of environmental factors in net primary productivity of each biome (whole) through the study of climate variability and soil heat flux.

MATERIALS AND METHODS

Study area

The studied biomes are the Atlantic Forest, Caatinga, and Cerrado located in the state of Bahia, northeastern Brazil. The biomes cover an area of approximately 56 million hectares with 417 municipalities (Figure 1). Around 14 million people live in the areas of these biomes (IBGE 2021) and the territory is considerably occupied by productive activities.

The Atlantic Forest biome is characterized by dense, open, and mixed ombrophilous forests, and semi-decidual and decidual seasonal forests. In its latitudinal extent, it has tropical and subtropical regions, while in its longitudinal extent, it comprises different forest compositions due to the decreasing precipitation gradient from the coast to the interior (Ribeiro et al. 2009). Its climate, according to the new classification of Alvares et al. (2013), the climate is tropical without dry season (Af) on the coast, which covers 47% of the Atlantic Forest. Inland, climate is tropical monsoon (Am) and tropical with dry winter (Aw) in 10% and 24% of this biome, respectively. Moreover, the climate in the borders of the Caatinga biome has been recorded as humid subtropical (Cwa) in 3,7 % of its area, subtropical with hot summer (Cfa) (3%) and tropical dry summer (As) (10%), dry semi-arid (BSh) (0,71%), temperate with mild summer (Cfb) (1,11%), and dry winter and temperate summer (Cwb) (0,48%), respectively.

The Cerrado biome is composed of savannas with

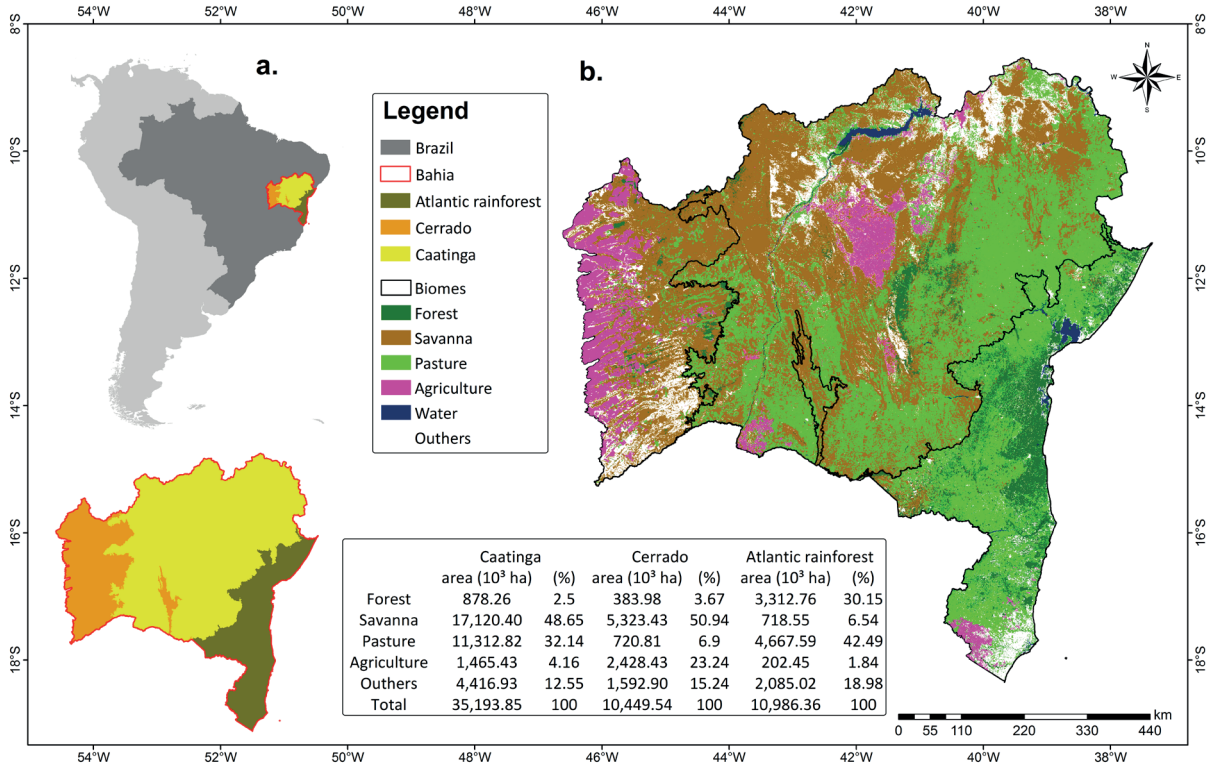

	Caatinga		Cerrado		Atlantic rainforest	
	area (10^3 ha)	(%)	area (10^3 ha)	(%)	area (10^3 ha)	(%)
Forest	878.26	2.5	383.98	3.67	3,312.76	30.15
Savanna	17,120.40	48.65	5,323.43	50.94	718.55	6.54
Pasture	11,312.82	32.14	720.81	6.9	4,667.59	42.49
Agriculture	1,465.43	4.16	2,428.43	23.24	202.45	1.84
Outhers	4,416.93	12.55	1,592.90	15.24	2,085.02	18.98
Total	35,193.85	100	10,449.54	100	10,986.36	100

Fig. 1. Location map (a) biomes of the state of Bahia and (b) land use and cover of the biomes in the state of Bahia, Brazil in 2019

defined arboreal and shrub-herbaceous strata. The climate for the state of Bahia in 94% of the biome is tropical with dry winter (Aw), with heavy rainfall in summer. Only a small portion of its area, located to the east of the biome, is classified as As in 4,62% of its area, and Cwb in 1,38% of its area, respectively (Alvares et al. 2013).

The Caatinga biome has savannas with a predominance of semi-continuous canopy species, which are classified as woodland steppe savannas and woodland savannas. In the northern area of the Caatinga, the climate is semi-arid (BSh) in 53% of the biome. In the central region, the climate is Aw and As in 18% and 25% of the Caatinga, respectively. Small portions of the Caatinga have Cwb and Cfb climates, in 2,24% of its area, and 1,76% of its area, respectively (Alvares et al. 2013).

Net primary production

To achieve the Net Primary Production (NPP) between the years 2003 and 2019, were used MOD17A3 images from collection 6, which are provided in HDF format with an annual NPP layer and a pixel resolution of 500 meters. Net primary production is obtained from the difference between Gross Primary Production (GPP) and vegetation respiration. Initially, according to Eq. (1), to collect the GPP the algorithm is based on the concept of the efficiency of use of solar radiation by vegetation (ε). The gross primary production derives from absorbed photosynthetically active radiation (APAR). Where APAR is estimated by multiplying the fraction of photosynthetically active radiation absorbed by vegetation cover (FPAR) (from MOD15 images) and incident photosynthetically active radiation (PAR), assumed to be 45% of total incident solar radiation (Monteith 1972; Running and Zhao 2019), according to Eq. (2):

Due to the variability of vegetation cover and

$$GPP = \varepsilon \times APAR \quad (1)$$

$$APAR = PAR \times FPAR \quad (2)$$

environmental factors in large areas, it is difficult to find the efficiency of light use (ε). However, the model is based on a maximum efficiency value (ε_{max}), including the environmental contributions, where it assumes the minimum air temperature ($Tmin_{scalar}$) and the water status of the vegetation, found through the deficit of water vapor pressure (VPD_{scalar}) (Field et al. 1995; Running and Zhao 2019), as per Eq. (3):

However, to arrives at annual NPP, the maintenance

$$\varepsilon = \varepsilon_{\max} \times T\min_{scalar} \times VDP_{scalar} \quad (3)$$

(R_m) and growth respiration (R_g) are subtracted from GPP as the Eq. (4):

The MODIS tiles that cover the Atlantic Forest, Cerrado,

$$NPP = GPP - Rm - Rg \quad (4)$$

and Caatinga biomes of the state of Bahia, Brazil, are 13H and 09V, 13H and 10V, 14H and 9V, and 14H and 10V and they are available for free on the NASA website (https://search.earthdata.nasa.gov/). In the MODIS Reprojection Tool (MRT) software, the tiles were unified, with conversion from HDF to GeoTIFF and sinusoidal projection to WGS84. In ArcGis 10.4.1, the areas of each biome were cut off and the NPP layer was multiplied by the conversion factor of 0.1 to obtain the biophysical values (g C m^{-2}) (Running and Zhao 2019).

To estimate the carbon uptake of each annual land use and cover, the most relevant classes were selected in all studied biomes, forest, savanna, pasture and agriculture for MapBiomas year 2019 (https://mapbiomas.org/) (Figure 1). The images provided by MapBiomas have a resolution of 30 meters. For use in the overlap, the image was resampled to 500 meters using the nearest neighbor method.

Burned area

The MCD64A1 images of the burned area in the 500-meter spatial resolution MODIS sensor, collection 6, resulted from the algorithm that uses active fire observations and a burn-sensitive vegetation index, which identifies the date the burn occurred on each pixel (Giglio et al. 2016). MCD64A1 images are available with the layers: burn date; uncertain burn date; pixel quality control; and first day, and last reliable detection day of the year (last day) of burned areas (Giglio et al. 2016). The burn date layer made available for each month was used to obtain the values for each year between 2003 and 2019 in hectares for each biome. Given the accuracy of the burn date layer (Libonati et al. 2015; Fornacca et al. 2017), it was the only layer used in this study.

Climate data

To obtain the annual precipitation of each biome, the secondary GPM_3IMERGM 06B version of the Integrated Multi-satellite Retrievals (IMERG) algorithm of the Global Precipitation Measurement (GPM) program was used, available in GeoTIFF format at Giovanni-NASA (https://giovanni.gsfc.nasa.gov/). The IMERG algorithm is based on the analysis of cloud surface temperature, humidity, and pressure and provides precipitation estimates from images with resolution of approximately 10x10 km for the entire planet (Huffman et al. 2019).

MOD11A2 land surface temperature (LST) images of the MODIS sensor have been frequently used due to their accuracy and proximity with air temperature variations (Zhu et al. 2013; Aguilar-Lome et al. 2019). These images are available with the mean temperature of 8 days for each pixel and with spatial resolution of 1 km. For this study, land surface temperature (LST_day) and the pixel quality control indicator (QC_Day) were used.

The LST_day layer was multiplied using ArcGis 10.4.1 software by the scale factor of 0.02 and subtracted from 273.15 to obtain the temperature in Celsius (Eq. (5)) (Wan 2013). Then, for the entire study period, the LST_day band was multiplied by the quality layer with QC = 0, since quality control values equal to zero indicate greater accuracy of the data (Sun et al. 2017).

$$LSTDay = (P \times F) - 273.15 \quad (5)$$

where,

LST Day is the daytime surface temperature (°C), P is the original pixel value, F is the conversion factor (0.02).

Based on the eight-day mean values of the land surface temperature MOD11A2 images, annual means were obtained for the Atlantic Forest, Cerrado, and Caatinga biomes.

The water availability index (WAI) is estimated from the ratio of actual evapotranspiration to potential evapotranspiration (Reichstein et al. 2007; Chen and Yu 2019). The actual evapotranspiration and potential evapotranspiration bands of the MOD16A3 images were used to determine the index. The MOD16A3 images are available annually and have a resolution of 500 meters.

Soil

Soil heat flux and influence on NPP were analyzed using «GLDAS_NOAH025_» version 2.1 soil heat flux images of the Global Land Data Assimilation System (GLDAS-2.1) and spatial resolution of 0.25° x 0.25° (Rodell et al. 2004; Beaudoing and Rodell 2019). The images are available in GeoTIFF format at Giovanni-NASA (https://giovanni.gsfc.nasa.gov/)

Statistical analysis

For all the analyses we performed here, we use the mean of the interest variable for the geographical sub-areas of our investigation. To determine NPP for each land use and cover (forest, savanna, agriculture, and pasture) of the Atlantic Forest, Cerrado, and Caatinga biomes, one-way ANOVA and the Tukey test were performed, according to normal waste distribution and variance homogeneity requirements. One-way ANOVA and t-test methods have been commonly used for this type of analysis (Liu et al. 2016; Yang et al. 2017; Chen and Yu 2019). A decreasing/increasing trend analysis was also performed for the 2003–2019 time series in all the annual variables of this study, namely, NPP, precipitation, burned areas, land surface temperature, evapotranspiration, water availability index, and soil heat flux, based on the Mann-Kendall nonparametric test. A positive or negative Z value in the Mann-Kendell test indicates an increasing or decreasing trend, respectively (Mann 1945; Kendall 1975). All statistical analyses were performed using R 3.6.1 software, at a significance level of $\alpha < 0.05$. To verify the relationship of the variables with NPP, a series of regressions were also estimated.

RESULTS

Spatial and temporal analysis of net primary production

According to the results of the MOD17A3 images, the Atlantic Forest has the highest average NPP for the studied period in comparison to the other biomes. The Atlantic Forest, Cerrado, and Caatinga have a mean annual NPP of 1,227.89 g C m^{-2}, 913.81 g C m^{-2}, and 803.56 g C m^{-2}, respectively (Figure 2).

For the studied series (2003–2019), a sharp decrease in NPP was observed in 2015 and 2016 in the Atlantic Forest biome. For the Cerrado biome, lower NPP was recorded in 2003, 2007, 2012, and 2016, while, for the Caatinga biome, the most critical years for NPP were 2012, 2015, and 2017 (Figure 2).

The Atlantic Forest biome absorbed the most carbon, especially on the coast (Figure 3), which is known for having extensive forest remnants (Figure 1). In the west of the biome, high mean annual NPP values, between 1,500 and 1,750 g C m^{-2}, were also observed. In the west and the extreme south of the state, however, where agriculture is predominant (Figure 1), low mean annual NPP values were observed (Figure 3). In the Caatinga biome, to the north, values less than 250 g C m^{-2} were observed; nevertheless, in the center of the biome, some sites had a mean annual NPP of up to 2,500 g C m^{-2}. Chapada Diamantina, located in the center of the Caatinga biome, comprises a mixture of native vegetation, between savanna and forest, as observed in Figure 1. Throughout the Cerrado, mean annual NPP ranged from 750 to 1,250 g C m^{-2}.

Net primary production and land use and cover

Higher and lower NPP variations were observed for the forest areas of the Atlantic Forest, 1,434.55 g C m^{-2}, followed by the savanna areas of the Atlantic forest biome, 1,228.99 g C m^{-2}, and the forest areas of the Caatinga biome, 1,226.24 g C m^{-2}, and they do not differ statistically ($\alpha = 0.05$) (Figure 4).

Considering the division of these biomes in terms of land use for human activities, mean annual NPP in pastures observed in the Atlantic Forest (1,092.91 g C m^{-2}) and NPP in agriculture in the same biome (971.99 g C m^{-2}) are statistically equal to the NPP observed in the forest areas of the Cerrado biome (1,059.09 g C m^{-2}).

Moreover, mean annual NPP observed in the agricultural areas of the Atlantic Forest (971.99 g C m^{-2}), savanna of the Atlantic Forest (965.18 g C m^{-2}), grassland of the Cerrado (916.56 g C m^{-2}), and savanna of the Caatinga (858.11 g C m^{-2}) did not differ statistically. Agriculture of the Caatinga biome has a lower mean NPP (628.77 g C m^{-2}) and differs statistically from the other studied categories.

The NPP observed for each land use and cover in the different biomes varied throughout the study period (Figure 5). In the Atlantic Forest biome, in the years 2015 and 2016, reductions of 6% to 22% of NPP were observed in all land covers and uses with respect to the historical average value of the time series. In the agriculture area of this biome, a 21% reduction in NPP was observed in 2013, in comparison with the mean of all studied years.

For the Cerrado biome, annual NPP in all land use and cover was lower in 2003, 2007, 2012, and 2016, with reductions ranging between 10% and 22% with respect

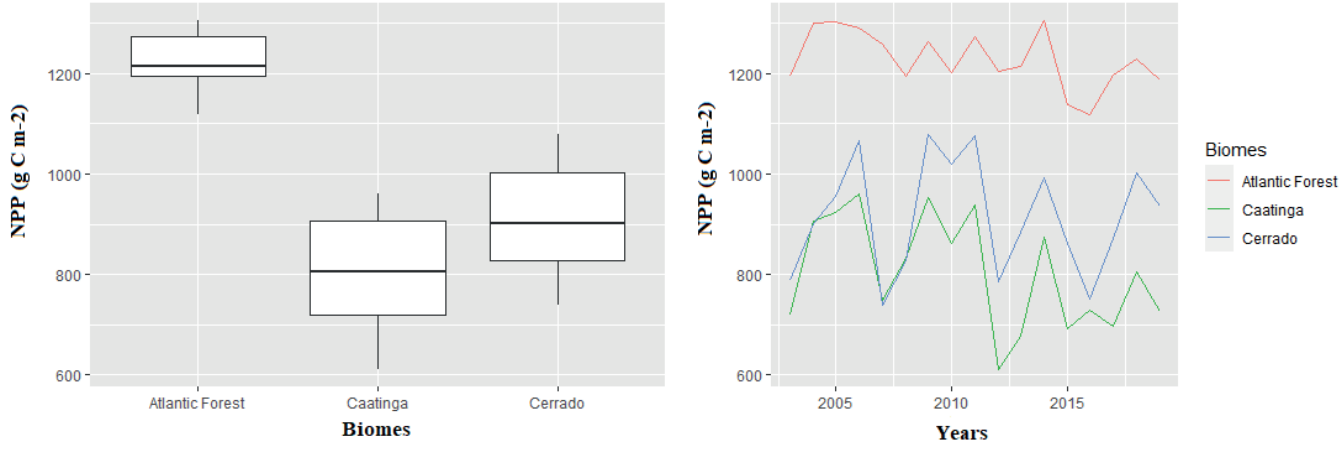

Fig. 2. Annual average and temporal variation of NPP in the Atlantic Forest, Cerrado, and Caatinga biomes of state Bahia, Brazil between 2003-2019

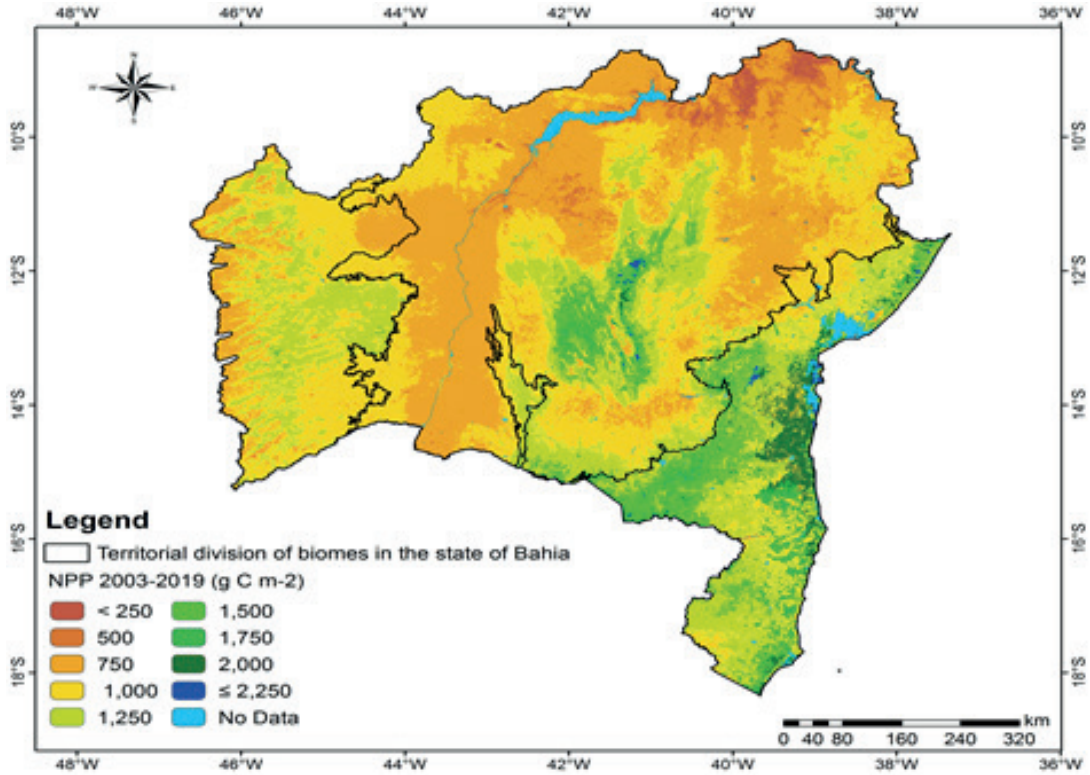

Fig. 3. Spatial mean NPP in the Atlantic Forest, Cerrado, and Caatinga biomes of state Bahia, Brazil between 2003-2019

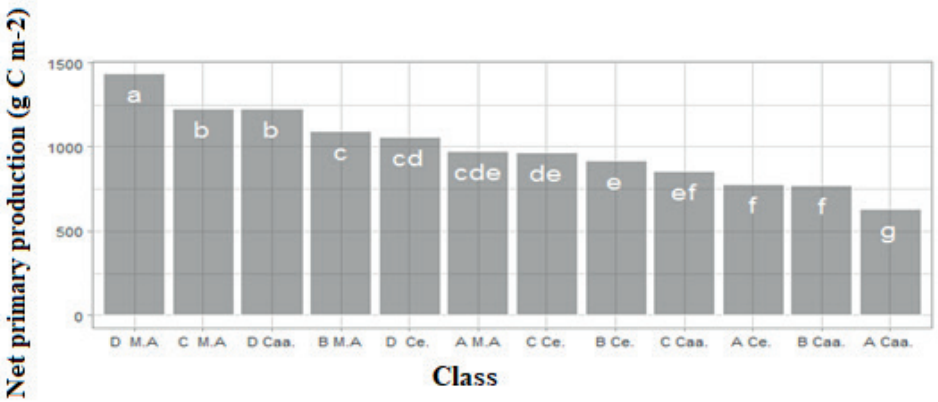

Fig. 4. One-way ANOVA and the Tukey test applied to NPP of class A, Agriculture; B, pasture; C, savanna; and D, forest; in M.A, Atlantic Forest; Ce, Cerrado; and Caa, Caatinga biomes of Brazil

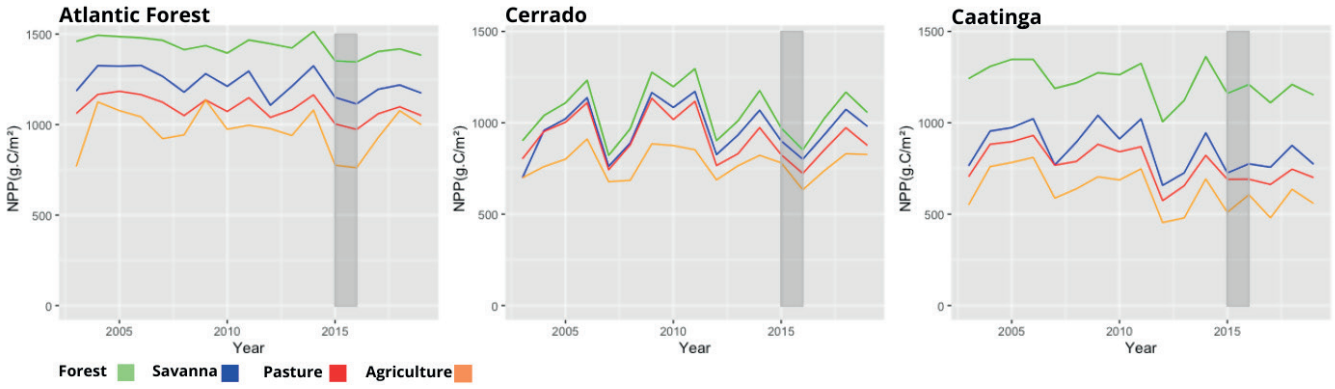

Fig. 5. Temporal variation between 2003 and 2019 of net primary production for each land use and cover (forest, savanna, agriculture, and pasture) in the Atlantic Forest, Cerrado, and Caatinga biomes, with gray markings for periods of high intensity El Niño events in Brazil available at http://enos.cptec.inpe.br/ (INPE, 2020)

to the annual mean, except for the savanna, in which a 27% reduction in NPP was observed in 2003, compared to the mean. In the Caatinga biome, 2012 was more critical, with reductions between 18% and 28% in NPP and annual values of 454.24 g C m^{-2} for agriculture, 573.92 g C m^{-2} for pasture, 657.78 g C m^{-2} for savanna, and 1,005.58 g C m^{-2} for forest.

The high intensity El Niño event in Brazil in the 2015–2016 period (INPE 2020) is related to the decrease in NPP in all biomes, especially the Atlantic Forest. Other low-intensity occurrences of El Niño were observed in Brazil in the periods 2002–2003, 2006–2007, and 2009–2010 (INPE 2020).

Decreasing/increasing trend

The Mann-Kendall statistical test results for the 2003 to 2019 time series showed statistically significant decreasing trend in carbon flux for the categories NPP forest Atlantic Forest, NPP Atlantic Forest pasture and NPP Caatinga pasture (Table 1). For environmental factors, an increasing trend was observed for Caatinga LST, Cerrado LST and Cerrado HF. Moreover, a decreasing trend was observed for Caatinga Precipitation. No statistically significant results were observed for overall NPP and burned areas of the Atlantic Forest, Caatinga, and Cerrado.

Effects of environmental and human factors on NPP

Regarding to the variables that controls the Net Primary Production, in the Caatinga biome there was a greater and positive relationship between NPP and precipitation than in the Atlantic Forest and Cerrado biomes (Figure 6). For the evapotranspiration variable, a strong positive relationship was found in the Cerrado (R^2 =0.97, p-value = 4.56e-13) and Caatinga (R^2 =0.94, p-value = 4.84e-11) biome. The water availability index shown to be the most important variable for net primary production in all biomes, with a positive and extremely significant relationship. The surface temperature was more significant for the Caatinga biome and negatively related to NPP. While, the heat flux variable, negatively impacts the NPP of the Atlantic Forest and Cerrado biomes. However, there are no statistically significant relationship between burned areas and net primary production in all biomes evaluated.

DISCUSSION

Spatial and temporal dynamics of net primary production

The spatial and temporal analyses of NPP in the 17 studied years showed that the Atlantic Forest biome has higher carbon stock and lower variation than the Cerrado and Caatinga biomes. Similar results were found in other studies (Bazame et al. 2019; Gomes et al. 2019). The forest of the Atlantic Forest biome in the state of Bahia, Brazil, is exceptionally superior to savannas and cultivated areas in terms of carbon uptake, with annual NPP of 1,434.55 g C m^{-2}, which is higher than the global average NPP of 1,032 g C m^{-2} in tropical forests and 577 g C m^{-2} in temperate forests (Li et al. 2017). This result demonstrates the importance of conserving the natural vegetation of the Atlantic Forest biome for regional and global carbon flux.

Significant NPP differences between natural vegetation areas and human occupation areas were found. The forest NPP of the Atlantic Forest biome is approximately 50% higher than the agricultural NPP of the Caatinga biome, this is the biggest difference found between land use and cover, and it is similar to results found in China when comparing areas of natural and unnatural vegetation (Yang et al. 2017). In contrast, the natural vegetation of the savannas of the

Table 1. Mann-Kendall test Z-statistics for the variables of interest (Time-series period 2003–2009)

Area	NPP	LST	Prec.	WAI	Eta	HF	BA
Atlantic Forest (whole)	-1.60 (0.11)	1.11 (0.27)	-1.36 (0.17)	-1.36 (0.17)	-0.37 (0.72)	1.24 (0.22)	-0.62 (0.54)
Atlantic Forest class Forest	-2.59 (0.0094*)						
Atlantic Forest class Savanna	-1.69 (0.091)						
Atlantic Forest class Pasture	-2.02 (0.043*)						
Atlantic Forest class Agriculture	-0.62 (0.54)						
Cerrado (whole)	0.042 (0.97)	2.18 (0.029*)	-1.94 (0.052)	0.00 (1)	0.12 (0.90)	2.14 (0.032*)	-1.11 (0.26)
Cerrado class Forest	0.20 (0.83)						
Cerrado class Savanna	0.45 (0.65)						
Cerrado class Pasture	-0.53 (0.59)						
Cerrado class Agriculture	0.041 (0.96)						
Caatinga class (whole)	-1.36 (0.17)	2.59 (0.094*)	-2.26 (0.023*)	-1.60 (0.1)	-1.68 (0.091)	1.41 (0.15)	-1.27 (0.20)
Caatinga class Forest	-1.77 (0.076)						
Caatinga class Savanna	-1.19 (0.23)						
Caatinga class Pasture	-2.02 (0.043*)						
Caatinga class Agriculture	-1.60 (0.10)						

NPP, net primary production; LST, land surface temperature; Prec, precipitation; WAI, water availability index; ETa, actual evapotranspiration; HF, soil heat flux; and BA, burned area;. P-value in parentheses, where (*) stands for the 5% significance level.

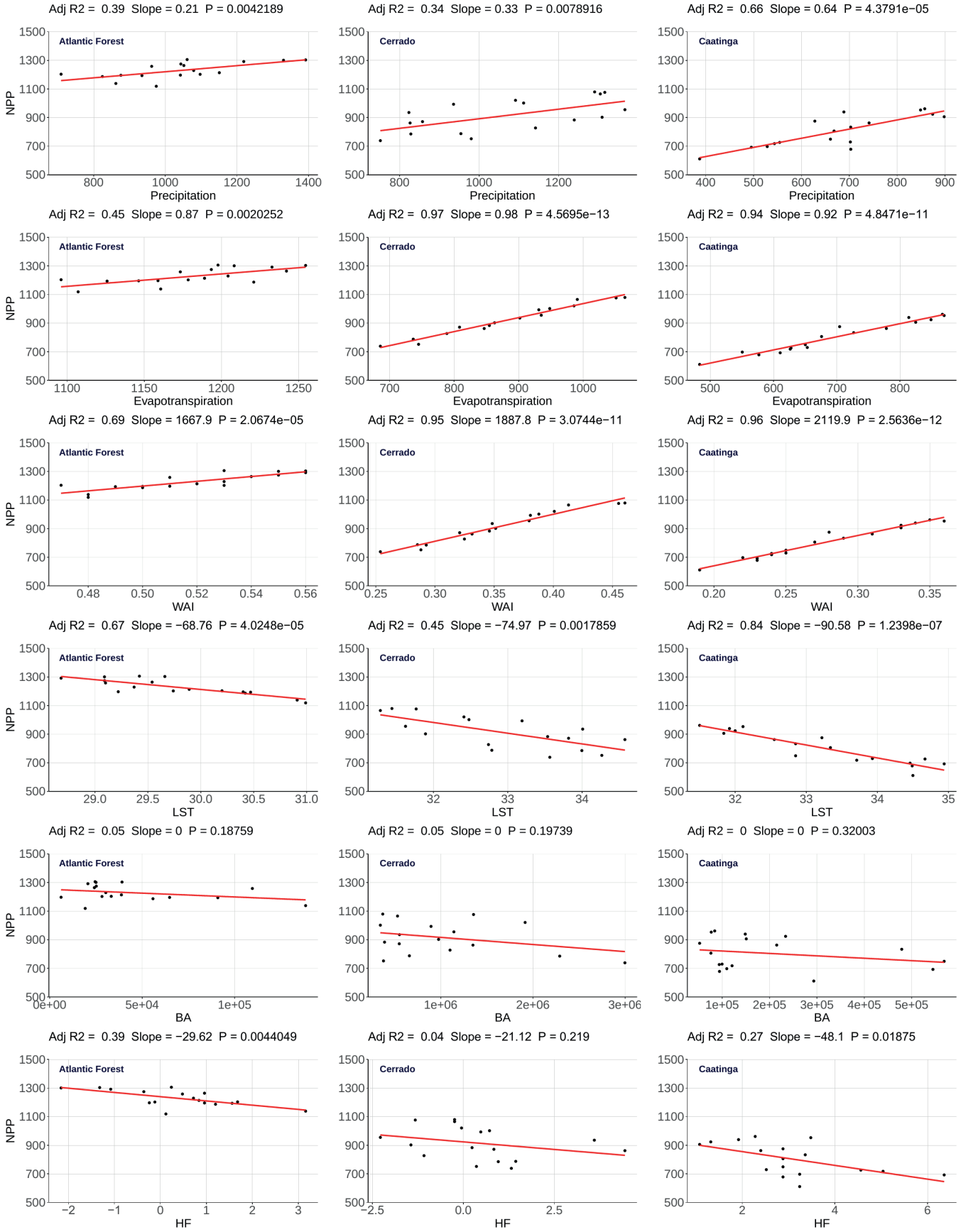

Fig. 6. Linear regression between NPP and controllers in biomes Atlantic Forest, Cerrado and Caatinga. NPP, net primary production (g C m^{-2}); Precipitation (mm); Actual evapotranspiration (mm); WAI, water availability index (mm mm^{-1}); LST, land surface temperature; BA, burned area (ha) and HF, soil heat flux (W m^{-2})

Cerrado and Caatinga biomes resemble areas with human occupations of agriculture and pasture. Similar results are reported by Morais et al. (2017), who observed similar NPP values in the savannas of the Caatinga to those found in irrigated areas. According to Chen et al. (2019), control of favorable conditions such as irrigation and nutrient supply in the soil has increased the leaf area and the «greening» of plantations, which are fundamental components for carbon flux.

The NPP temporal variation analysis indicated that high-intensity El Niño events in the 2015–2016 period and low-intensity El Niño events in 2003 and 2007 impacted the NPP of the studied biomes. A cross-continent analysis showed that the severe drought in 2015–2016 mainly affected the carbon stock of America's humid forests, which, by the end of 2017, forests showed slight signs of recovery (Wigneron et al. 2020). Also regarding temporal variation, a decreasing trend of NPP for the forest of the Atlantic Forest biome was observed and can be linked to deforestation and burning. Based on the non-governmental organization Mapbiomas, between 2003 and 2019 there was an increase of approximately 215,000 hectares of agricultural areas in the Atlantic Forest biome, for the Cerrado and Caatinga biome the expansion of agricultural and pasture areas was 1.5 million and 1 million hectares, respectively. A global analysis revealed that 5% of Earth is in a «browning» process, mainly caused by human activity; in Brazil, the loss of leaf area of natural vegetation, which is an essential attribute of this process, has been reported, with consequences for carbon flux (Chen et al. 2019). For the pastures of the Caatinga and Atlantic Forest biomes, decreasing trends of NPP were also found, triggered by the large-scale degradation of pastures in the state of Bahia and Brazil. Based on the Digital Atlas of Brazilian Pastures, in 2019, 51% of the pasture areas in the state of Bahia were classified as «severe degradation» Brazil has approximately 41 million hectares of degraded pasture, which directly affects the health of vegetation and soil and disturbs carbon absorption. An analysis in the Cerrado biome compared the carbon stock between improved brachiaria grassland, degraded brachiaria grassland and savanna areas and showed that improved grassland areas store more carbon in more than half of the value found for degraded grassland, while for the savanna, the carbon stock values were close to those of improved brachiaria grassland (Rosendo and Rosa, 2012). These results highlight the importance of conservation and the need for proper management of cultivated areas for carbon flux.

Relation of NPP with environmental and human factors

The results reveal different responses of NPP to environmental changes in each studied biome. The correlations between precipitation and NPP in the Atlantic Forest and Cerrado biomes found in this study are lower than the same correlations for the Caatinga biome. An intuitive explanation for this stems from the fact that Caatinga has systematically lower annual mean precipitation than the other biomes studied. Therefore, small variations in terms of precipitation have a greater impact on NPP (Figure 6). In 2012, the Caatinga suffered the most severe drought in the last 50 years, which led to 57% lower precipitation in some localities of the biome than the historical mean of 606.4 mm (Gutiérrez et al. 2014). Also in 2012, NPP in the savannas of the state of Pernambuco suffered a reduction of 42% (NPP = 400 g C m^{-2}) (Morais et al. 2017), while in the state of Bahia, our results showed a reduction of 23% (NPP = 657.78 g C m^{-2}) in this atypical year.

Land surface temperature had a negative relationship with NPP for all biomes, with greater negative correlation in the Caatinga biome. As indicated in the literature, extreme temperature variations cause forest mortality (Pau et al. 2018) and, associated with water restriction, may be a limiting factor in carbon uptake (Wu et al. 2016). Doughty and Goulden (2008) indicate that forests decrease photosynthesis and carbon uptake when leaf temperatures are near or exceed 35°C. High temperatures are related to increased vapor-pressure deficit, which in turn induces stomatal closure and, thus, reduces carbon absorption and evapotranspiration (Lloyd and Farquhar 2008). This relationship between carbon absorption and evapotranspiration was also observed in the present study, in which a positive linear relationship with NPP was observed in all biomes. In addition to evapotranspiration, the water availability index showed a positive and strong correlation with NPP, perhaps the most important variable studied here, especially in the Caatinga and Cerrado biomes, where the water availability index is often half the value observed in the Atlantic Forest biome and increases strongly control NPP. The importance of water availability was also observed in Europe and Asia (Reichstein et al. 2007; Chen and Yu 2019). In addition to these results, an increasing trend for LST was identified in the Cerrado and Caatinga biomes and a decreasing trend for precipitation in the Caatinga biome, climatic conditions that, if confirmed over time, may threaten NPP in these biomes. According to Yang et al. (2017), low soil moisture and high temperatures of some arid and semi-arid regions hinder vegetation growth, which directly reduces NPP.

Regarding soil heat flux, which is an important component in studies on thermal properties of soils and soil-plant-atmosphere interactions (Singh et al. 2020), no strong correlations were found with NPP. However, lower heat flux values were observed in the Atlantic Forest biome, suggesting cover conditions with lower soil heating capacity.

Although no significant results were found between burned areas and NPP for the Atlantic Forest, Cerrado, and Caatinga in this study, loss of carbon stock by burning vegetation and deforestation, induced mainly by agricultural expansion (De Santana et al. 2020), and the consequent increase in atmospheric carbon has been reported in the biomes of Brazil (Silva Júnior et al. 2020). In that regard, we believe our time-series statistics, regarding the association of NPP and the burned areas, should be analysed with caution. One step ahead in our research agenda consists in exploring this issue by accessing longer time series to make it possible to address this issue with different methods. Based on future projections, a decrease in CO_2 emissions in the Brazilian biomes is not expected, and these emissions will exceed 5.7 Gt of CO_2 by 2030, which compromises Brazil's emission reduction targets set by the Paris Agreement (Silva Júnior et al. 2020).

CONCLUSION

The analyses conducted in this study provided valuable insight into the dynamics of NPP in the Brazilian biomes Caatinga, Cerrado, and Atlantic Forest of the state of Bahia. Of all the studied land covers and uses, the forests of the Atlantic Forest biome are the most important for regional and global carbon flux; however, a decreasing trend was identified by the Mann-Kendall test for NPP in this type of cover, which may be associated with deforestation. Moreover, the NPP of the savanna areas of

the Caatinga and Cerrado biomes resembles that of the areas of human occupation for pastures and agriculture.

The results showed a strong relationship between climate and NPP in the studied biomes, especially in the Caatinga biome, which was more sensitive to variations of the studied climate variables. In the time series, reductions in NPP were observed resulting from El Niño (2015–2016) and atypical climate years, such as the 2012 drought in the Caatinga biome. Finally, the results can shed light on the dynamics of NPP in response to possible future climate change, enable management of potential carbon areas, and support future environmental and socioeconomic policies.

REFERENCES

Aguilar-Lome J., Espinoza-Villar R., Espinoza J.C., Rojas-Acuña J., Willems B.L. & Leyva-Molina W.M. (2019). Elevation-dependent warming of land surface temperatures in the Andes assessed using MODIS LST time series (2000–2017). International Journal of Applied Earth Observation and Geoinformation 77, 119-128, DOI: 10.1016/j.jag.2018.12.013.

Althoff T.D., Menezes R.S.C., de Carvalho A.L., de Siqueira Pinto A., Santiago G. A.C.F., Ometto J.P.H.B., Randow V.C. & Sampaio E.V.S.B. (2016). Climate change impacts on the sustainability of the firewood harvest and vegetation and soil carbon stocks in a tropical dry forest in Santa Teresinha Municipality, Northeast Brazil. Forest Ecology and Management 360, 367-375, DOI: 10.1016/j.foreco.2015.10.001.

Alvares C.A., Stape J.L., Sentelhas P.C., de Moraes G., Leonardo J. & Sparovek G. (2013). K¨oppen's climate classification map for Brazil. Meteorologische Zeitschrift 22, 711-728, DOI: 10.1127/0941-2948/2013/0507.

Atlas Digital das Pastagens Brasileiras (2019). https://pastagem.org/atlas/map. [Accessed 01 January 2021].

Barni P.E., Manzi A.O., Condé T.M., Barbosa R.I. & Fearnside P.M. (2016). Spatial distribution of forest biomass in Brazil's state of Roraima, northern Amazonia. Forest Ecology and Management 377, 170-181, DOI: 10.1016/j.foreco.2016.07.010.

Bazame H.C., Althoff D., Filgueiras R., Calijuri M.L. & de Oliveira J.C. (2019). Modeling the Net Primary Productivity: A Study Case in the Brazilian Territory. Journal of the Indian Society of Remote Sensing 47, 1727-1735, DOI: 10.1007/s12524-019-01024-3.

Beaudoing H. & Rodell M. (2020). GLDAS Noah Land Surface Model L4 monthly 0.25 x 0.25 degree V2.1, Greenbelt, Maryland, USA, Goddard Earth Sciences Data and Information Services Center (GES DISC), DOI: 10.5067/SXAVCZFAQLNO. [Accessed 12 August 2020].

Chen C., Park T., Wang X., Piao S., Xu B., Chaturvedi R.K., Fuchs R., Brovkin V., Ciais P., Fensholt R., Tømmervik H., Bala G., Zhu Z., Nemani R.R., Ranga B. & Myneni R.B. (2019). China and India lead in greening of the world through land-use management. Nature sustainability 2, 122-129, DOI: 10.1038/s41893-019-0220-7.

Chen Z. & Yu G. (2019). Spatial variations and controls of carbon use efficiency in China's terrestrial ecosystems. Scientific Reports, 9, 1-10, DOI: 10.1038/s41598-019-56115-5.

da Silva Junior C.A., Teodoro P.E., Delgado R.C., Teodoro L.P.R., Lima M., Pantaleão A., Baio F.H.R., de Azevedo G.B., Azevedo G.T.O.S., Capristo-Silva G.F., Arvor D. & Facco C.U. (2020). Persistent fire foci in all biomes undermine the Paris Agreement in Brazil. Scientific Reports 10, 1-14, DOI: 10.1038/s41598-020-72571-w.

de Miranda S. do C., Bustamante M., Palace M., Hagen S., Keller M. & Ferreira L.G. (2014). Regional Variations in Biomass Distribution in Brazilian Savanna Woodland. Biotropica 46, 125-138, DOI: 10.1111/btp.12095.

de Santana R.O., Delgado R.C.& Schiavettic A. (2020). The past, present and future of vegetation in the Central Atlantic Forest Corridor, Brazil. Remote Sensing Applications: Society and Environment, 20, 1-14, DOI: 10.1016/j.rsase.2020.100357.

Delgado R.C., Pereira M.G., Teodoro P.E., dos Santos G.L., de Carvalho D.C., Magistrali I.C. & Vilanova R.S. (2018). Seasonality of gross primary production in the Atlantic Forest of Brazil. Global Ecology and Conservation 14, 1-12, DOI: 10.1016/j.gecco.2018.e00392.

Dias M.S., Rutledge S., Kabat P., Dias P.S., Nobre C., Fisch G., Dolman A.J., Zipser E., Garstang M., Manzi A.O., Fuentes J.D., Rocha H.R., Marengo J., Plana-Fattori A., Sá L.D.A., Alvalá R.C.S., Andreae M.O., Artaxo P., Gielow R. & Gatti L. (2002). Cloud and rain processes in a biosphere-atmosphere interaction context in the Amazon region. Journal of Geophysical Research: Atmospheres 107, 1-20, DOI: 10.1029/2001JD000335.

Doughty C.E. & Goulden M.L. (2008). Are tropical forests near a high temperature threshold? Journal of Geophysical Research: Biogeosciences 113, 1-12, DOI: 10.1029/2007JG000632.

Dyukarev E.A., Godovnikov E.A., Karpov D.V., Kurakov S.A., Lapshina E.D., Filippov I.V., Filippova N.V., Zarov E.A. (2019). Net Ecosystem Exchange, Gross Primary Production And Ecosystem Respiration In Ridge-Hollow Complex At Mukhrino Bog. GEOGRAPHY, ENVIRONMENT, SUSTAINABILITY, 12(2), 227-244, DOI: 10.24057/2071-9388-2018-77.

Field C.B., Randerson J.T. & Malmstreom C.M. (1995). Global net primary production: combining ecology and remote sensing. Remote Sens. Environ, 51(1), 74-88, DOI: 10.1016/0034-4257(94)00066-V.

Fornacca D., Ren G. & Xiao W. (2017). Performance of three MODIS fire products (MCD45A1, MCD64A1, MCD14ML), and ESA Fire_CCI in a mountainous area of Northwest Yunnan, China, characterized by frequent small fires. Remote Sensing 9, 1131, DOI: 10.3390/rs9111131.

Forzza R.C., Baumgratz J.F.A., Bicudo C.E.M., Canhos D.A., Carvalho Jr A.A., Coelho M.A.N., Costa A.F., Costa D.P., Hopkins M.G., Leitman P.M., Lohmann L.G, Lughadha E.N., Maia L.C., Martinelli G., Menezes M., Morim P.M., Peixoto A.L., Pirani J.R., Prado J., Queiroz L.P., Souza S., Souza V.C., Stehmann J.R., Sylvestre L.S., Walter B.M. T. & Zappi D.C. (2012). New Brazilian floristic list highlights conservation challenges. BioScience 62, 39-45, DOI: 10.1525/bio.2012.62.1.8.

Fu Z., Gerken T., Bromley G., Araújo A., Bonal D., Burban B., Darren Ficklin D., Fuentes J.D., Goulden M., Hirano T., Kosugi Y., Liddell M., Nicolini G., Niu S., Roupsard O., Stefani P., Mi C., Tofte Z., Xiao Z., Valentini R., Wolf S. & Stoy P.C. (2018). The surface-atmosphere exchange of carbon dioxide in tropical rainforests: Sensitivity to environmental drivers and flux measurement methodology. Agricultural and Forest Meteorology 263, 292-307, DOI: 10.1016/j.agrformet.2018.09.001.

Giglio L., Boschetti L., Roy D., Hoffmann A.A., Humber M., Hall J.V. (2016). Collection 6 MODIS Burned Area Product User's Guide Version 1.0. NASA EOSDIS Land Processes DAAC: Sioux Falls, SD, USA. https://lpdaac.usgs.gov/. [Accessed 02 February 2020].

Gomes L.C., Faria R.M., de Souza E., Veloso G.V., Schaefer C.E.G.R. & Filho E.I.F. (2019). Modelling and mapping soil organic carbon stocks in Brazil. Geoderma 340, 337-350, DOI: 10.1016/j.geoderma.2019.01.007.

Gutiérrez A.P.A., Engle N.L., De Nys E., Molejón C. & Martins E.S. (2014). Drought preparedness in Brazil. Weather and Climate Extremes 3, 95-106, DOI: 10.1016/j.wace.2013.12.001.

Gushchina D., Heimsch F., Osipov A., June T., Rauf A., Kreilein H., Panferov O., Olchev A., Knohl A. (2019). Effects Of The 2015–2016 El Niño Event On Energy And CO2 Fluxes Of A Tropical Rainforest In Central Sulawesi, Indonesia. GEOGRAPHY, ENVIRONMENT, SUSTAINABILITY, 12(2), 183-196, DOI: 10.24057/2071-9388-2018-88.

Huffman G.J., Stocker E.F., Bolvin D.T., Nelkin E.J., Jackson T. (2019). GPM IMERG Final Precipitation L3 1 month 0.1 degree x 0.1 degree V06, Greenbelt, MD, Goddard Earth Sciences Data and Information Services Center (GES DISC). 10.5067/GPM/IMERG/3B-MONTH/06. [Accessed 04 April 2020].

Instituto Brasileiro de Geografia e Estatística – IBGE, 2021. População estimada. https://cidades.ibge.gov.br/brasil/ba/panorama. [Accessed 04 March 2021].

Instituto Brasileiro de Geografia e Estatística – IBGE, 2021. População estimada. https://cidades.ibge.gov.br/brasil/ba/panorama. [Accessed 04 March 2021].

Instituto Nacional de Pesquisas Espaciais – INPE, 2021. http://enos.cptec.inpe.br/ [Accessed 01 January 2021].

Ji Y., Zhou G., Luo T., Dan Y., Zhou L.& Lv X. (2020). Variation of net primary productivity and its drivers in China's forests during 2000–2018. Forest Ecosystems 7, 1-11, DOI: 10.1186/s40663-020-00229-0.

Kendall K. (1975). Thin-film peeling-the elastic term. J. Phys. Appl. Phys. 8, 1449.

Klink C.A. & Machado R.B. (2005). Conservation of the Brazilian cerrado. Conservation biology 19, 707-713, DOI: 10.1111/j.1523-1739.2005.00702.x

Li P., Peng C., Wang M., Li W., Zhao P., Wang K., Yang Y. & Zhu Q. (2017). Quantification of the response of global terrestrial net primary production to multifactor global change. Ecological Indicators 76, 245-255, DOI: 10.1016/j.ecolind.2017.01.021.

Libonati R., DaCamara C.C., Setzer A.W., Morelli F. & Melchiori A.E. (2015). An algorithm for burned area detection in the Brazilian Cerrado using 4 µm MODIS imagery. Remote Sensing 7, 15782-15803, DOI: 10.3390/rs71115782.

Liu L.B., Yang H.M., Xu Y., Guo Y.M. & Ni J. (2016). Forest Biomass and Net Primary Productivity in Southwestern China: A Meta-Analysis Focusing on Environmental Driving Factors. Forests 7, 1-16, DOI: 10.3390/f7080173.

Lloyd J. & Farquhar G.D. (2008). Effects of rising temperatures and [CO2] on the physiology of tropical forest trees. Philosophical Transactions of the Royal Society B: Biological Sciences 363, 1811-1817, DOI: 10.1098/rstb.2007.0032.

Mann H.B. (1945). Nonparametric tests against trend. Econometrica 245-259.

Mapbiomas – Coleçãoo 5 da Série Anual de Mapas de Cobertura e Uso de Solo do Brasil. https://mapbiomas.org/. [Accessed 12 March 2020].

Mapbiomas – Relatório Anual do Desmatamento do Brasil – 2019. http://alerta.mapbiomas.org/relatorios. [Accessed 04 November 2020].

Medlyn B.E., Duursma R.A. & Zeppel M.J.B. (2011). Forest productivity under climate change: a checklist for evaluating model studies. Wiley Interdisciplinary Reviews: Climate Change 2(3), 332-355, DOI: 10.1002/wcc.108.

Mendonça R.C., Felfili J.M., Walter B.M.T., Silva Júnior M.C., Rezende A.V., Filgueiras T.S, Nogueira P.E & Fagg C.W. (2008). Flora vascular do bioma Cerrado: Check list com 12.356 espécies. In: Sano S.M, Almeida S.P, Ribeiro J.F (eds) Cerrado: ecologia e flora. Embrapa Cerrados, Planaltina, 421-1181. https://www.bdpa.cnptia.embrapa.br/. [Accessed 05 January 2021].

Mittermeier R.A., Turner W.R., Larsen F.W., Brooks T.M. & Gascon C. (2011). Global biodiversity conservation: the critical role of hotspots. In: Zachos, F., Habel, J. (eds) Biodiversity Hotspots. Springer, Berlin, 3-22, DOI: 10.1007/978-3-642-20992-5_1.

Morais Y.C.B., de Araújo M.S.B., de Moura M.S.B., Galvíncio J. D. & de Queiroga R.M. (2017). Análise do Sequestro de Carbono em áreas de Caatinga do Semiárido Pernambucano. Revista Brasileira de Meteorologia 32, 585-599, DOI: 10.1590/0102-7786324007.

Monteith J.L. (1972). Solar radiation and productivity in tropical ecosystems. J. Appl. Ecol. 9(3), 747-766.

Myers N., Mittermeier R.A., Mittermeier C.G., Fonseca G.A.B. & Kent J. (2000). Biodiversity hotspots for conservation priorities. Nature 403, 853-858. https://www.nature.com/articles/35002501.

Neumann M., Moreno A., Thurnher C., Mues V., Härkönen S., Mura M., Bouriaud O., Lang M., Cardellini G., Thivolle-Cazat A., Bronisz K., Merganic J., Alberdi I., Astrup R., Mohren F., Zhao M. & Hasenauer H. (2016). Creating a Regional MODIS Satellite-Driven Net Primary Production Dataset for European Forests. Remote Sensing 8, 1-18, DOI: 10.3390/rs8070554.

Novenko E.Yu., Tarasov P.E., Olchev A.V. Special Issue «Climate-Vegetation Interaction: Natural Processes Versus Human Impact». (2019). GEOGRAPHY, ENVIRONMENT, SUSTAINABILITY, 12(2), 128-131.

Oliveira P.H.F., Artaxo P., Pires C., De Lucca S., ProcóPio A., Holben B., SCHAFER J., CARDOSO L.F., WOFSY S.C. & ROCHA H.R. (2007). The effects of biomass burning aerosols and clouds on the CO2 flux in Amazonia. Tellus B: Chemical and Physical Meteorology 59(3), 338-349, DOI: 10.1111/j.1600-0889.2007.00270.x.

Oliveira R.S., Dawson T.E., Burgess S.S.O. & Nepstad D.C. (2005). Hydraulic redistribution in three Amazonian trees. Oecologia 145, 354-363, DOI: 10.1007/s00442-005-0108-2.

Pau S., Detto M., Kim Y. & Still C.J. (2018). Tropical forest temperature thresholds for gross primary productivity. Ecosphere 9(7), 1-12, DOI: 10.1002/ecs2.2311.

Rap A., Spracklen D.V., Mercado L., Reddington C.L., Haywood J.M., Ellis R.J., Phillips P., Artaxo D., Bonal N. & Restrepo Coupe N.B. (2015). Fires increase Amazon forest productivity through increases in diffuse radiation. Geophysical Research Letters 42(11), 4654-4662, DOI: 10.1002/2015GL063719.

Reichstein M., Papale D., Valentini R., Aubinet M., Bernhofer C., Knohl A., Laurila T., Lindroth A., Moors E., Pilegaard K. & Seufert G. (2007). Determinants of terrestrial ecosystem carbon balance inferred from European eddy covariance flux sites. Geophysical Research Letters 34, 01402, DOI: 10.1029/2006GL027880.

Ribeiro M.C., Metzger J.P., Martensen A.C., Ponzoni F.J. & Hirota M.M. (2009). The Brazilian Atlantic Forest: How much is left, and how is the remaining forest distributed? Implications for conservation. Biological Conservation 142(6), 1141–1153, DOI: 10.1016/j.biocon.2009.02.021.

Rodell M., Houser P.R. U., Jambor J., Gottschalck K., Mitchell C. Meng K. & Arsenault B. (2004). The Global Land Data Assimilation System. Bulletin of the American Meteorological Society 85, 381-394, DOI: 10.1175/BAMS-85-3-381.

Rosendo J.D.S. & Rosa R. (2012). Comparação do estoque de C estimado em pastagens e vegetação nativa de Cerrado. Sociedade & Natureza 24(2), 359-376, DOI: 10.1590/S1982-45132012000200014.

Running S.W. & Zhao M. (2019). User's Guide Daily GPP and Annual NPP (MOD17A2H/A3H) and Year-end GapFilled (MOD17A2HGF/A3HGF) Products NASA Earth Observing System MODIS Land Algorithm (For Collection 6). https://lpdaac.usgs.gov/. [Accessed 03 March 2020].

SEEG – Sistema de Estimativas de Emissões e Remoções de Gases de Efeito Estufa. Observatório do clima. Sistema de estimativas de emissões de gases de efeito estufa 2018. https://seeg.eco.br/. [Accessed 10 October 2020].

Silva J.M.C., Barbosa L.C.F., Leal I.R. & Tabarelli M. (2017). The caatinga: understanding the challenges. In: Silva, J.M.C., Leal, I.R., Tabarelli, M. (eds) Caatinga. Springer, Cham, DOI: 10.1007/978-3-319-68339-3_1.

Silva J.M.C. & Casteleti C.H.M. (2003). Status of the biodiversity of the Atlantic Forest of Brazil. In: Galindo-Leal C., Câmara I.G. (Eds.), The Atlantic Forest of South America: Biodiversity Status, Threats, and Outlook. CABS and Island Press, Washington, 43-59.

Singh R.P., Paramanik S., Bhattacharya, B.K. & Behera, M.D. (2020). Modelling of evapotranspiration using land surface energy balance and thermal infrared remote sensing. Tropical Ecology 61, 42-50, DOI: 10.1007/s42965-020-00076-8.

Staal A., Tuinenburg O.A., Bosmans J.H.C., Holmgren M., van Nes E.H., Scheffer M., Zemp, D. C. & Dekker, S. C. (2018). Forest-rainfall cascades buffer against drought across the Amazon. Nature Climate Change 8(6), 539-543, DOI: 10.1038/s41558-018-0177-y.

Sun L., Chen Z., Gao F., Anderson M., Song L., Wang L., Hu B. & Yang Y. (2017). Reconstructing daily clear-sky land surface temperature for cloudy regions from MODIS data. Computers & Geosciences 105, 10-20, DOI: 10.1016/j.cageo.2017.04.007.

Teixeira A.M.C., Pinto J.R.R., Amaral A.G. & Munhoz C.B.R. (2017). Angiosperm species of «Cerrado» sensu stricto in Terra Ronca State Park, Brazil: floristics, phytogeography and conservation. Brazilian Journal of Botany 40, 225-234, DOI: 10.1007/s40415-016-0341-4.

Wan Z. (2013). Collection-6 MODIS Land Surface Temperature Products Users' Guide. https://lpdaac.usgs.gov/. [Accessed 10 May 2020].

Wang X.F., Wang H.B., Li X. & Ran Y. (2018). Photosynthesis (NPP, NEP, Respiration). In: Li X., Vereecken H. (eds) Observation and Measurement. Ecohydrology. Springer, Berlin, Heidelberg, DOI: 10.1007/978-3-662-47871

Wigneron J.-P., Fan L., Ciais P., Bastos A., Brandt M., Chave J., Saatchi S., Baccini A. & Fensholt R. (2020). Tropical forests did not recover from the strong 2015–2016 El Niño event. Science Advances 6(6), 1-10, DOI: 10.1126 / sciadv.aay4603.

Wu J., Guan K., Hayek M., Restrepo-Coupe N., Wiedemann K.T., Xu X., Wehr R., Christoffersen B.O., Miao G., da Silva R., de Araujo A.C., Oliviera R.C., Camargo P.B., Monson R.K., Huete A.R. & Saleska S.R. (2016). Partitioning controls on Amazon forest photosynthesis between environmental and biotic factors at hourly to interannual timescales. Global Change Biology 23, 1240-1257, DOI: 10.1111/gcb.13509.

Yang J., Zhang X.C., Luo H.Z. & Yu X.J. (2017). Nonlinear Variations of Net Primary Productivity and Its Relationship with Climate and Vegetation Phenology, China. Forests 8(10), 1-21, DOI: 10.3390/f8100361.

Zhang Q., Wang C. & Zhou Z. (2019). Does the net primary production converge across six temperate forest types under the same climate? Forest Ecology and Management, 448, 535-542, DOI: 10.1016/j.foreco.2019.06.035.

Zhu W., Lű A. & Jia S. (2013). Estimation of daily maximum and minimum air temperature using MODIS land surface temperature products. Remote Sensing of Environment 130, 62-73, DOI: 10.1016/j.rse.2012.10.034.

RESEARCH PAPER

CLIMATE-RELATED GRADIENTS ON VEGETATION DIVERSITY OF THE ALTAI-SAYAN OROBIOME (SOUTHERN SIBERIA)

Maxim V. Bocharnikov
Lomonosov Moscow State University, Leninskie gory, 1, Moscow, 119991, Russia
*Corresponding author: maxim-msu-bg@mail.ru
Received: April 5th, 2022 / Accepted: November 11th, 2022 / Published: December 31st, 2022
https://DOI-10.24057/2071-9388-2022-043

ABSTRACT. An analysis of the spatial organization of vegetation cover has been carried out for the Altai-Sayan orobiome in connection with climatic conditions in the Southern Siberian mountains based on original relevés of plant communities at the 4 altitudinal spectra. Basic bioclimatic parameters on the altitudinal spectra of vegetation have been determined according to latitudinal and longitudinal differentiation of climate. Correlation and discriminate analyses allowed to identify the regional features of altitudinal gradients in species diversity of the spectra as well as the role of parameters in the structure of typological diversity of vegetation for belts of high-mountain tundra, alpine and subalpine meadows and sparse forests, dark coniferous mountain taiga forests, chern-taiga forests, small leave – light coniferous subtaiga forests, forest-steppe. A compiled bioclimatic scheme characterizes the spatial organization of orobiome's vegetation by basic bioclimatic parameters on the regional level (continentality index, average temperature of January). This scheme shows regional features of the diversity of vegetation in Southern Siberia, in adjacent plain and mountain regions according to climatic conditions. Identified patterns determine unity of the Altai-Sayan orobiome as well as regional differentiation that reflected on the development of types of vegetation zonality. They can be used to analysis of vegetation forming in different mountain systems.

KEYWORDS: ecosystem, biodiversity, bioclimate, altitudinal zonality, mountain territories, ordination

CITATION: Bocharnikov M. V. (2022). Climate-Related Gradients On Vegetation Diversity Of The Altai-Sayan Orobiome (Southern Siberia). Geography, Environment, Sustainability, 4(15), 17-31
https://DOI-10.24057/2071-9388-2022-043

ACKNOWLEDGEMENTS: The investigation has been completed based on the theme of Lomonosov Moscow State University's fundamental research «Spatial and temporary organization of ecosystems in conditions of environmental changes» and the MWG Herbarium Center for Collective Use (created with the support of the Moscow University Development Program). I am thankful to colleagues of Lomonosov Moscow State University (Faculty of geography, department of biogeography) and Sukachev Institute of Forest SB RAS (laboratory of phytocoenology and forest resource science) for their support and assistance.

Conflict of interests: The authors reported no potential conflict of interest.

INTRODUCTION

Ecological gradients in the structure of biodiversity is one of the fundamental problems of biogeography. The spatial differentiation of ecosystems and their components is influenced by external factors, and climate is one of the main factors. Climatic justification of vegetation diversity is a traditional direction of botanical and geographical investigations at different spatial levels with thermic and moisture parameters (Francis and Currie 2003; Rivas-Martinez et al. 2004; Whittaker et al. 2001). The variety of functional parameters of plant species (Yang et al. 2019), key phytocoenotic characteristics (Dolezal and Srutek 2002), and also biodiversity indices have connections with climatic gradients at different levels of biota spatial structure (Shao and Halpin 1995; Qian et al. 2007). The spatial organization of large zonal and altitudinal-belt subdivisions of vegetation is determined on a global scale (Holdridge 1967; Tuhkanen 1984). The structure of typological diversity (types of vegetation, vegetation formations) can be explained by climate on a regional scale (Grebenshchikov 1974; Nakamura et al. 2007; Bocharnikov 2019).

There are more opportunities for strong analysis in connection with new environmental data. They are represented by spatial models of ecological and geographical conditions. Such climatic models allow using a wide spectrum of key bioclimatic parameters and indices to reveal vegetation-climate patterns. The examples of these models are global model Bioclim created by interpolation of data of meteorological stations, altitude, and MODIS data (Fick and Hijmans 2017), and global model CHELSA created by orographic predictors among others (wind fields, valley exposition) (Karger at al. 2017). They can be used in medium- and small-scale investigations all over the world according to global coverage of the models (spatial resolution is about 1 km and below). The relevance of the work is increasing in connection with vegetation reactions on climate change in the past (Otto-Bliesner et al. 2006), and potential forecast scenarios in the future (De Dios et al. 2007; Navarro-Racines et al. 2020).

The concept of biome diversity describes biomes as basic ecosystem complexes on a regional spatial level. The development of ecosystems in the contemporary period connects to climatic conditions on certain amplitudes of key bioclimatic parameters. They determine compositions, spatial structure, and functions of ecosystems. Altitudinal-belts spectra of vegetation as a strong ecosystem complex in mountains have the name «orobiome» (Walter and Breckle 1991; Ogureeva and Bocharnikov 2017). The differences in relations of species and vegetation communities to environmental factors in the various parts of spatial distribution and a variation of coenotic role of plant communities in vegetation cover (Alberto et al. 2013; Svenning et al. 2014; Bocharnikov et al. 2018) determine regional level as a basis for biogeographical researches. They find integral reflection in the diversity of altitudinal-belt spectra with the specific composition of belts for each spectrum (Ogureeva 1991). Regional differentiation on spectra with different levels of biodiversity can be identified by climatic conditions (del Rio and Penas 2006). This characterizes the advantage of the biome concept in research of vegetation-climate relations.

The main purpose of the investigation is the evaluation of climate as a factor of the spatial organization of vegetation for the Altai-Sayan orobiome. The determination of the key bioclimatic parameters connected to the vegetation and regional patterns of its distribution is the basic task of research. Types of vegetation, classes, and groups of formations are used as basic typological units that are the background for altitudinal belts. At a higher level, altitudinal belts and spectra are considered to determine of types of altitudinal zonality within the Altai-Sayan group of zonality that characterizes the orobiome (Ogureeva and Bocharnikov 2017). Types of altitudinal zonality are described as basic units of the comparative regional analysis. Chosen key areas for climatic interpretation of the spatial structure of vegetation diversity in the South Siberian mountains correspond to these types.

MATERIAL AND METHODS

Reviling of the diversity of vegetation in connection with climatic conditions is based on the analysis of original geobotanical and model climatic data. Relevés of vegetation communities, completed from 2008 to 2015 in different regions of Southern Siberia on key areas, cover full altitudinal spectra on ranges (Fig. 1). They characterize the diversity of the Altai-Sayan orobiome and its 4 geographical variants with specific types of altitudinal zonality. All relevés have been completed according to traditional methods of phytocoenosis analysis (Sukachov and Zonn 1964). Species composition of vascular plants, ground mosses and lichens with an evaluation of projective cover, mean altitude, and phenophases for each species have been described on key plots by 100 м^2 (non-forest communities) и 400 м^2 (forest communities). Tree, shrub, and herb layers' density (by percent) have been described. Geographical coordinates, as well as altitude, have been measured by GPS.

Choosing of key areas has been determined by tasks of investigations connected with spatial patterns in the structure of vegetation in different ranges by climatic conditions and altitudinal gradients of temperature and moisture parameters. It is reflected in the development of different types of altitudinal zonality which relate to the Altai-Sayan group of boreal class with a prevalence of mountain taiga belt (Ogureeva 1991). Cyclonic provinces, shown on the scheme of forest regionalization (Polikarpov et al. 1986), are characterized by a low level of continentality. Dark coniferous forests (*Abies sibirica, Pinus sibirica*) and small-leaved (*Populus tremula, Betula pendula*) – dark coniferous («chern-taiga») forests develop in these regions (Nazimova et al. 2014). In regions with a higher level of continentality larch (*Larix sibirica*) forests are typical. High-mountain vegetation of boreal class relates to alpine type (Tolmachev 1948).

Relevés of vegetation communities have been completed on different levels of catena and slopes according to tasks of revealing spatial patterns of diversity with the main role

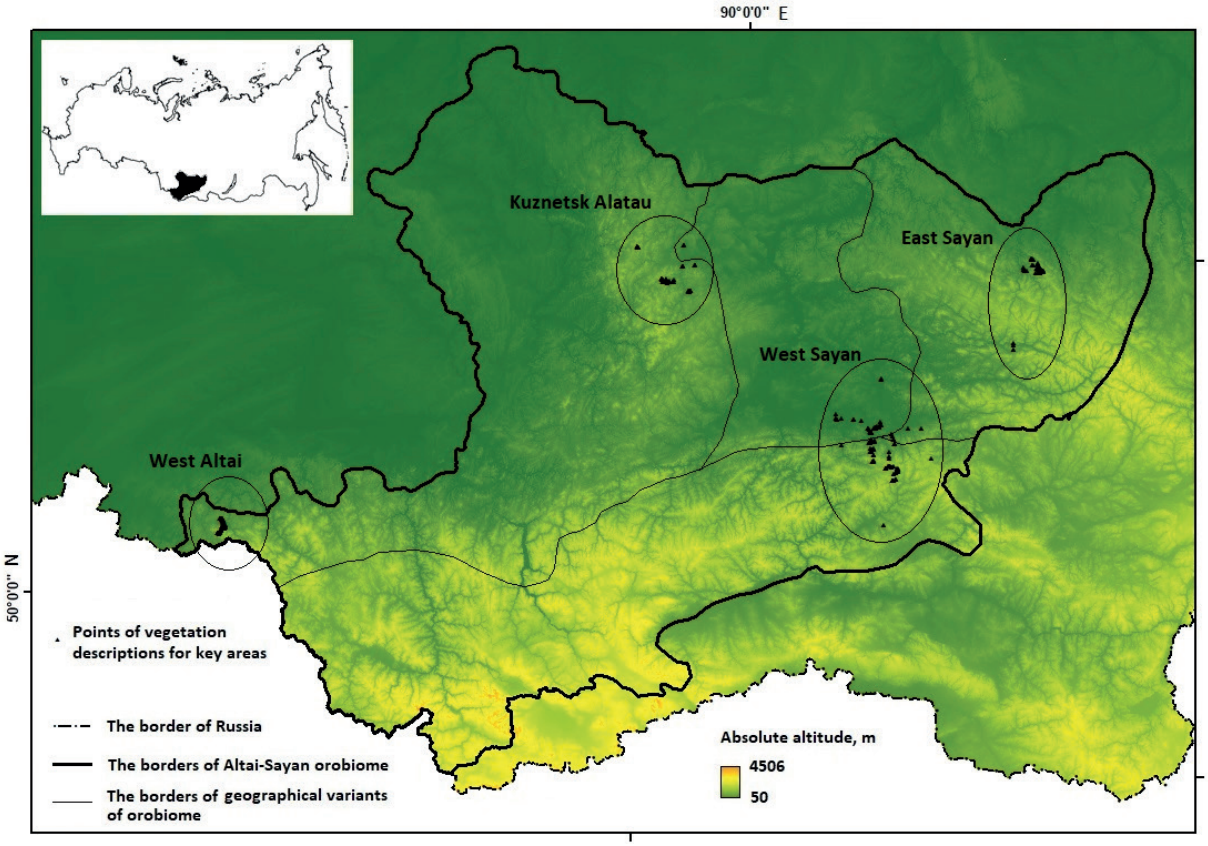

Fig. 1. Points of relevés on key areas

of climate. It is known a significant influence of ecological conditions through slope gradients which are reflected on vegetation (Ogureeva 1997; Namzalov 2020). Generally, they are associated with the middle parts of drained slopes of the ranges (transit positions of catena). The analysis has been performed by 396 relevés on 4 general profiles (Table 1). Relevés are included in groups (general profiles) presented by altitudinal-belt spectra of 4 types of altitudinal zonatily (basic types for orobiome).

Climatic data have been derived from the global model CHELSA (Karger et al. 2017). It contains data on 19 bioclimatic parameters with 30´´ spatial resolution averaged on period 1979-2013. There are temperature and moisture parameters and their ratio (average values for the year, each quarter of the year, July and January). Basic parameters have been used to calculate bioclimatic indices which apply to the analysis of vegetation and climate (del Rio and Penas 2006; Rivas-Martinez et al. 2011; Bocharnikov 2019). The values of bioclimatic variables for each vegetation community have been determined by extraction of these in points of relevés based on the climatic model. Altitude has been used as an integral parameter that characterizes gradients of climatic conditions in the mountains. 25 bioclimatic parameters including 8 bioclimatic indices have been used (Table 2).

Nonmetric multidimensional scaling (NMS-ordination) (Clarke 1993) allowed to identify the character of vegetation communities' variation in the system of ecological and geographical factors. This method is one of the most used for

Table 1. Relevés in the Southern Siberian mountains

Region	Geographical location	Number of relevés	Years of investigations	Types of altitudinal zonality of vegetation	Geographical variant of Altai-Sayan orobiome
West Sayan	Kulumys, Kedranskiy, Oiskiy, Ergaki ridges	147	2008, 2009, 2010	Alpine-subalpine-mountain taiga-chern-taiga	Central Altai
West Altai	Tigirek ridges	143	2015	Alpine-subalpine-mountain taiga-chern-taiga-shrub-forest-steppe-steppe	North Altai
East Sayan	Sayan ridges	52	2012	Alpine-subalpine-mountain taiga	Sayan
Kuznetsk Alatau	Profile the Black Lake – Ivanovskie lakes	54	2008	Alpine-subalpine-mountain taiga-forest-steppe-steppe	North Altai, Minusinsk depression

Table 2. Bioclimatic parameters for ordination analysis of vegetation

Parameters	Symbol
Average annual temperature	Bio1
Average temperature of summer	Bio10
Average temperature of winter	Bio11
Average annual precipitation	Bio12
Average precipitation of summer	Bio18
Average precipitation of winter	Bio19
Average temperature of January	T_January
Average temperature of April	T_april
Average temperature of July	T_July
Average temperature of October	T_october
Average maximum temperature of January	T_max_January
Average maximum temperature of July	T_max_July
Average minimum temperature of January	T_min_January
Average minimum temperature of July	T_min_July
Average precipitation of January	P_January
Average precipitation of July	P_July
Continentality index	Ic
Thermicity index	It
Aridity index	Ia
Ombrothermic index of summer	Ios_summer

Ombrothermic index of July	Ios_July
Oceanity index	OCE
Pluviothermic quotient	Q_pluv
Evapotranspiration estimate	Pet
Altitude above sea level	Alt_gps

the ordination of species and communities (Aynekulu et al. 2012; Rahman et al. 2020). Interpretation of spatial structure of vegetation cover has been carried out in connection with bioclimatic parameters. Euclidian metric has been used as a measure of similarity. The evaluation of conjugacy of vegetation and climate has been carried out based on a correlation between values of communities on ordination scheme and bioclimatic parameters. We used 3 axes to interpretation of ordination. Linkage and reliability of each axis and each parameter have been determined by Spearmen's nonparametric coefficient of linear correlation (p-value < 0.001).

The analysis of climate patterns in vegetation has been carried out on the different levels of its spatial organization. ***Complete altitudinal spectra of types of altitudinal zonality*** describe a high level. The vegetation cover of key areas is formed as a part of altitudinal spectra of the Altai-Sayan group of boreal class (Ogureeva 1991; Ogureeva et al. 1999). It belongs to West Altai, West-East Sayan, and Salair-Kuznetsk types of altitudinal zonality. The dominant position of dark and light coniferous forests in the mountain taiga belt, the alpine type of high-mountain vegetation with alpine and subalpine belts character this group. Regional specificity finds expression in the typological diversity of different vegetation belts. West Altai and West-East Sayan types are developed in the very wet climate of the rain-barrier ranges (Polikarpov et al. 1986). They are characterized by the basic participation of dark coniferous forests and unique relict chern-taiga forests in the warmest and humid conditions of low mountains with a high level of botanical diversity (Nazimova 1975; Nazimova et al. 2005, 2014; Stepanov 2012). The basis of chern-taiga forests is consisted by small-leave – dark coniferous communities. The lower part of altitudinal spectra is occupied by the forest-steppe belt with a high level of shrub communities in West Altai (Ogureeva 1980). High mountains are characterized by a high level of typological diversity and relatively low amplitudes of ecological conditions suitable for the development of alpine and subalpine meadows and high-mountains tundra. Salair-Kuznetsk type of altitudinal zonality is connected with the east macroslope of the Kuznetsky Alatay with lower humidity. The dominance of larch forests in the forest-steppe belt, Siberian fir, and Siberian pine forests in the mountain taiga and subalpine belts describe the diversity of this type.

The next level of the spatial organization of vegetation relates to ***altitudinal belts.*** Types of altitudinal zonality for key areas are described by forest-steppe, sub-taiga, mountain taiga (with chern-taiga forests), subalpine and alpine-tundra belts. The altitudinal amplitude, development of sub-belts, different phytocoenotic optimum of basic communities characterize each type. The most important regional patterns are connected with vegetation of the low part of altitudinal spectra. Chern-taiga forests dominate in warm and wet conditions in the low parts of West Altai and West Sayan. Forest-steppe belt with exposure combinations of larch forests and grass steppes is developed in the low parts of Kuznetsk Alatau and West Altai.

The third level of the spatial organization of vegetation is determined by the ***typological composition of vegetation.*** It can be evaluated through basic formations and types of vegetation according to geographical-genetic classification (Sochava 1980). Vegetation communities are presented by three phratries of formations: Altai-Sayan alpine, Ural-South Siberian boreal, and Transvolga-Kazakhstan steppe. Following V.B. Sochava, a «phratry» are described as a complex of plant formations with genetic and geographic unity of formations. Altai-Sayan phratry is presented by alpine and subalpine meadows, sparse forests. Dark coniferous (*Abies sibirica, Pinus sibirica*) and light coniferous (*Larix sibirica*) forests of Ural-South Siberian form the mountain taiga belt. Larch and pine (*Pinus sylvestris*) forests and grass steppes (*Stipa pennata, Helictotrichon altaicum, Koeleria cristata*) of Transvolga-Kazakhstan phratry form the forest-steppe belt. The basic typological units of vegetation are associated with the general structure of diversity of altitudinal belts for key areas (Table 3). Each type of altitudinal zonality has common features and also regional specifics in diversity (Table 4).

Table 3. Typological diversity of vegetation communities of Altai-Sayan orobiome

<table>
<tr><td rowspan="3"></td><td rowspan="3">Altitudinal belts</td><td colspan="4">Typological diversity of vegetation</td></tr>
<tr><td colspan="4">Geographic-genetic complexes</td></tr>
<tr><td colspan="2">Altai-Sayan</td><td>Ural-South Siberia</td><td>Transvolga-Kazakhstan</td></tr>
<tr><td>I</td><td>Alpine-tundra</td><td>1. Alpine meadows</td><td>2. High-mountain tundra</td><td rowspan="2"></td><td rowspan="5"></td></tr>
<tr><td>II</td><td>Subalpine</td><td>1. Subalpine meadows</td><td>2. Subalpine sparse forests</td></tr>
<tr><td>III</td><td>Mountain taiga</td><td colspan="2" rowspan="4"></td><td>III.1. Siberian pine-fir forests</td></tr>
<tr><td>IIIa</td><td>Chern-taiga</td><td>IIIa.1. Birch and aspen-Siberian pine-fir forests</td></tr>
<tr><td>IV</td><td>Subtaiga</td><td>IV.1. Birch-pine forests</td><td>IV.2. Birch-larch forests</td></tr>
<tr><td>V</td><td>Forest-steppe</td><td colspan="2">1. Birch-larch forests</td><td>2. Herb-grass steppes, shrubs, steppe meadows</td></tr>
</table>

The role of climate as a factor of vegetation diversity has been determined at different levels of its organization (for complete altitudinal spectra of vegetation, altitudinal belts, and typological units of vegetation). The significance of differentiation of altitudinal belts and typological units by bioclimatic parameters has been determined based on discriminant analysis (F-statistic and p-value have been used).

The relations between vegetation and climate are presented on the integral bioclimatic scheme of the Altai-Sayan orobiome. The experience of creating such schemes determines the opportunity of explanation of the spatial organization of vegetation cover at the regional level (Nakamura et al. 2007; Bocharnikov 2019). Key bioclimatic parameters on the integral axes of ordination have been used to create a scheme. The scheme is presented by a matrix with cells containing typological units of vegetation of different types of altitudinal zonality for the Altai-Sayan orobiome. Additional interpretation of vegetation-climate connections has been reflected in the picture.

The analysis of species diversity distribution correlated with key bioclimatic parameters has become one of the ways of revealing vegetation-climate relations. Two indicators have been used: species richness per area (alpha-diversity) and gradient differentiation between altitudinal belts (Whittaker beta-diversity index). Beta-diversity has been determined to groups of communities into 100-m stages on the spectrum (before 1700 m a.s.l.). Gradients of diversity have been analyzed by each key area and by complete data. Altitude above sea level has been used as an integral factor of the spatial structure of species diversity in the mountains (Odland 2009; Mokarram and Sathyamoorthy 2015). The relation patterns between diversity and ecological factors have been given based on correlation analysis.

The spatial analysis of data has been completed using Saga 2.1.4, ArcGIS Pro Advanced 10.8.1, and Statistica 12.5.192.5.

RESULTS

The conjugation of vegetation and climate along altitudinal gradients in different types of altitudinal zonality

The altitude above sea level as an integral parameter characterizes the differentiation of vegetation diversity on the spectrum for each type of altitudinal zonality (Table 5). The strongest connection is marked for the West Sayan type (correlation coefficient 0.65). Axes 1 and 3 of ordination schemes have the main contribution in connection with climate. This is confirmed by maximum significant values of correlation with bioclimatic parameters (Table 5). There are 2 main gradients determined by bioclimatic parameters. The first includes temperature parameters with the highest values of correlation. The second is connected with altitude and humidity. Moisture parameters in every type of altitudinal zonality have more close connections. Ombrothermic indices based on the ratio of temperature and moisture parameters in the warmest quarter of the year have the maximum values among these.

Comparison of ordination schemes in different types of altitudinal zonality determines a differentiation in connections between the vegetation and bioclimatic parameters. Maximum values of correlation coefficients are identified on general profiles on key areas in West Sayan and West Altai. They have maximum diversity of altitudinal subdivisions with the development of chern-taiga sub-belt. Fewer strong connections are determined to East Sayan. It is characterized by a simpler structure of altitudinal zonality including a sub-taiga belt of pine forests, a mountain taiga

Table 4. Typological diversity of vegetation of altitudinal zonality types for Altai-Sayan orobiome

Typological subdivisions of altitudinal belts	Types of altitudinal zonality			
	West Sayan	East Sayan	West Altai	Salair-Kuznetsk
I.1. Alpine meadows	1		2	
I.2. High-mountain tundra	3	4	5	6
II.1. Subalpine meadows	7	8	9	10
II.2. Subalpine sparse forests	11	12	13	14
III.1. Siberian pine-fir forests	15	16	17	18
IIIa.1. Birch and aspen-Siberian pine-fir forests	19		20	
IV.1. Birch-pine forests	21	22		23
IV.2. Birch-larch forests		24		
V.1. Birch-larch forests and steppes			25	26
V.2. Herb-grass steppes, shrubs, steppe meadows			27	28

Vegetation of altitudinal belts: 1-2 – alpine meadows (*Schulzia crinita, Viola altaica, Carex aterrima, Festuca sphagnicola, Bupleurum triradiatum*); 3-6 – high-mountain tundra (*Betula rotundifolia, Rhododendron aureum, Dryas oxyodonta, Sibbaldia procumbens, Omalotheca norvegica, Empetrum nigrum, Cladina rangiferina*); 7-10 – subalpine meadows (*Veratrum lobelianum, Heracleum dissectum, Geranium albiflorum, Euphorbia lutescens, Delphinium elatum*); 11-14 – subalpine sparse forests (*Pinus sibirica, Abies sibirica*); 15-18 – Siberian pine-fir forests (*Abies sibirica, Pinus sibirica*); 19-20 – birch and aspen-Siberian pine-fir forests (*Abies sibirica, Pinus sibirica, Betula pendula, Populus tremula*); 21-23 – birch-pine forests (*Pinus sylvestris, Betula pendula*); 24 – birch-larch forests (*Larix sibirica, Betula pendula*); 25-26 – birch-larch forests and steppes (*Larix sibirica, Betula pendula; Stipa capillata, Carex pediformis, Cleistogenes squarrosa, Bupleurum scorzonerifolium*); 27-28 – herb-grass steppes, shrubs, steppe meadows (*Stipa capillata, Poa attenuata, Carex pediformis, Artemisia santolinifolia, Phleum phleoides, Pulsatilla flavescens*).

Table 5. Correlation between species diversity of the altitudinal spectra and bioclimatic parameters (Spearman's rank correlation coefficient; reliable values at p <0.001 are bold font)

Bioclimatic parameters	Correlation coefficients for types of altitudinal zonality									
	Altai-Sayan group of types of zonality		West-Sayan		East-Sayan		West-Altai		Salair-Kuznetsk	
	Axis 1	Axis 3	Axis 1	Axis 3	Axis 1	Axis 3	Axis 1	Axis 3	Axis 1	Axis 3
Alt_gps	-0.054	**-0.420**	**0.648**	-0.083	**0.304**	**-0.520**	**-0.522**	**-0.238**	**0.485**	**-0.247**
Bio1	**0.232**	**0.262**	**-0.661**	0.083	**-0.232**	**0.371**	**0.532**	**0.244**	**-0.462**	**0.248**
Bio10	0.106	**0.411**	**-0.659**	0.079	**-0.237**	**0.382**	**0.530**	**0.241**	**-0.465**	**0.238**
Bio11	**0.390**	-0.032	**-0.681**	0.085	-0.199	**0.324**	**0.536**	**0.244**	**-0.456**	**0.248**
Bio12	0.121	0.034	**0.272**	0.076	**0.232**	**-0.283**	**-0.639**	**-0.224**	**0.479**	**-0.276**
Bio18	**-0.241**	0.123	0.200	**0.278**	**0.233**	**-0.372**	**-0.479**	**-0.267**	**0.367**	**-0.383**
Bio19	**0.255**	0.080	**0.350**	-0.186	0.153	-0.052	**-0.631**	-0.197	**0.504**	**-0.265**
T_January	**0.393**	-0.045	**-0.679**	0.086	-0.120	**0.329**	**0.541**	**0.242**	**-0.459**	**0.248**
T_april	**0.209**	**0.268**	**-0.657**	0.082	**-0.233**	**0.379**	**0.529**	**0.243**	**-0.463**	**0.261**
T_July	0.090	**0.423**	**-0.654**	0.079	**-0.236**	**0.379**	**0.531**	**0.243**	**-0.463**	**0.237**
T_october	**0.253**	**0.241**	**-0.661**	0.080	**-0.228**	**0.364**	**0.527**	**0.244**	**-0.461**	**0.240**
T_max_January	**0.399**	-0.060	**-0.682**	0.086	-0.189	**0.312**	**0.534**	**0.243**	**-0.461**	**0.265**
T_max_July	0.155	**0.355**	**-0.657**	0.078	**-0.236**	**0.375**	**0.526**	**0.243**	**-0.467**	**0.239**
T_min_January	**0.386**	-0.025	**-0.680**	0.086	**-0.213**	**0.343**	**0.542**	**0.246**	**-0.445**	**0.241**
T_min_July	0.028	**0.484**	**-0.653**	0.079	**-0.243**	**0.383**	**0.528**	**0.243**	**-0.464**	**0.242**
P_January	**0.276**	0.077	**0.346**	-0.194	0.146	-0.047	**-0.629**	-0.195	**0.506**	**-0.269**
P_July	**-0.264**	0.143	**0.218**	**0.278**	**0.226**	**-0.381**	**-0.441**	**-0.270**	**0.349**	**-0.408**
Ic	**-0.360**	**0.519**	-0.050	-0.026	**-0.321**	**0.490**	**0.499**	**0.245**	**-0.469**	0.208
It	**0.358**	0.051	**-0.675**	0.085	**-0.213**	**0.344**	**0.536**	**0.244**	**-0.457**	**0.252**
Ia	-0.061	-0.053	**0.476**	-0.082	0.132	**-0.315**	**-0.590**	**-0.240**	**0.427**	**-0.304**
Ios_summer	**-0.229**	-0.104	**0.468**	0.080	0.168	**-0.368**	**-0.520**	**-0.256**	**0.395**	**-0.350**
Ios_July	**-0.249**	-0.084	**0.467**	0.090	0.167	**-0.371**	**-0.507**	**-0.260**	**0.388**	**-0.363**
OCE	**0.224**	**-0.230**	**0.383**	-0.120	**0.223**	**-0.518**	**-0.435**	-0.121	**0.359**	**-0.513**
Q_pluv	**0.202**	-0.100	**0.294**	0.067	**0.234**	**-0.303**	**-0.635**	-0.231	**0.476**	**-0.276**
Pet	0.155	0.050	0.208	0.113	**0.265**	**-0.268**	**-0.643**	-0.221	**0.483**	**-0.270**

Bioclimatic parameters – see table 2. Axes 1, 3 – according to NMS-ordination data.

belt of dark coniferous forests, and high-altitudinal belts with less diversity of alpine and subalpine meadows and mountain tundra.

The conjugation of vegetation and climate along altitudinal gradients in a general altitudinal gradient of types of altitudinal zonality

The strongest connection has been detected with a temperature of January and winter months, and also thermicity index (correlation coefficient with axis 1 is about 0.4) (Table 5). They limit the position of the upper level of distribution of key vegetation communities according to the integral altitudinal gradient. Moisture parameters, and also bioclimatic indices have fewer clear connections but with statistical confidence ($p < 0.001$). The ordination scheme on a general set of communities is similar to schemes for each type of altitudinal zonality. Differentiation of humidity (annual precipitation of year, July and January) reflects the spatial structure of types of altitudinal zonality with forest-steppe belt (West Altai, Kuznetsk Alatau). The development of hemiboreal forests (the subtaiga and chern-taiga belts) is determined by a high level of temperature and moisture supply. The development of the forest-steppe belt is connected with a relatively low level of humidity (annual precipitation – 600-800 mm, ombrothermic index of summer – 130-160).

The conjugation of the key typological divisions of vegetation and climate in the different types of altitudinal zonality

The main formation complexes of vegetation determine each type of altitudinal zonality (Table 3). The correlation of climatic parameters with vegetation on the ordination scheme characterizes the close connection of spatial structure of climate and vegetation. The bioclimatic parameters with maximum correlation connections with vegetation communities have been determined for the axes of NMS-ordination. They are mean annual temperature and continentality index (Rivas-Martinez et al. 2004). The reliability of differences in altitudinal belts of vegetation in each type of altitudinal zonality and between types has been determined by choosing bioclimatic parameters using the Kruskal-Wallis test.

The confidence intervals for each altitudinal belt in different types of altitudinal zonality on the ordination scheme characterize differences between vegetation communities (Fig. 2). They are significantly different on the ordination scheme by the first and the third axes (Wilks' Lambda = 0.06286, F = 40.623, $p < 0.000$). Based on the proximity of areas of altitudinal belts determined by the confidence intervals different types of altitudinal zonality have a high level of phytocoenotic similarity. The alpine and subalpine belts are the closest in different regions. The similarity of these communities can be determined by development in a cold climate with typical conditions for high mountains (Kolomyts 1966). The regional differentiation of the lower-lying belts is clearer. For example, the area of the mountain taiga belt of the East Sayan is located within the area formed by the subalpine sparse forests of the West Sayan without intersecting with its mountain taiga belt. This characterizes the warmer conditions for the mountain taiga of the West Sayan, which is distinguished by a high level of floristic and coenotic diversity with the development of large-herb, large-fern (*Dryopteris expansa, Athyrium distentifolium*) forest types. A similar position in the scheme is occupied by the area of the chern-taiga of the West Altai, which partially overlaps with the area of subalpine sparse forests of this region. The most differences between key areas are noted in the lower parts of the altitudinal-belt spectra. A separate position in the diagram is occupied by birch-pine subtaiga forests of the West Sayan. They belong to the most moisture variant of the subtaiga of the mountains of Southern Siberia with dominance of bracken and large-herb types of forest communities with the participation of nemoral elements (Drobushevskaya and Nazimova 2007). Subtaiga forests in other regions form intersecting areas under conditions of increasing continentality of the climate. Areas of forest-steppe complexes in all types of altitudinal zonality in the scheme are superimposed on each other in the conditions of high heat supply.

The horizontal axis of NMS-ordination, in general, characterizes the change of communities of different altitudinal subdivisions according to the change in the temperature supply of the cold season. By these parameters, the altitudinal change of the complexes of basic forest-steppe, subtaiga, mountain-taiga, and high-mountain communities is expressed. The values on the vertical axis are closely related to the climate continentality index, heat supply indicators for the summer period and July, as well as altitude above sea level.

The conjugation of species diversity of vegetation communities with climate

The altitudinal gradient is expressed in the change in the relative species diversity of communities in all types of altitudinal zonality. This parameter decreases with an increase of altitude. It is described by a linear model for every mountain profile (Fig. 3–6). The range of values of parameters is large at each altitudinal level for every profile. The degree of conjugation of changes in the species diversity of communities with climatic conditions along altitudinal gradient is varied in different types of zonality. The closest relationship is observed on the profile on the northern macroslope of West Sayan (R^2 = 0.52). It is characterized by the participation of subtaiga and chern-taiga forests with the high level of diversity (Ermakov 2003). The high abundance of communities of the forest-steppe belt on the profile in the Kuznetsk Alatau and its sharp decrease in the mountain-taiga belt and high-mountain belts

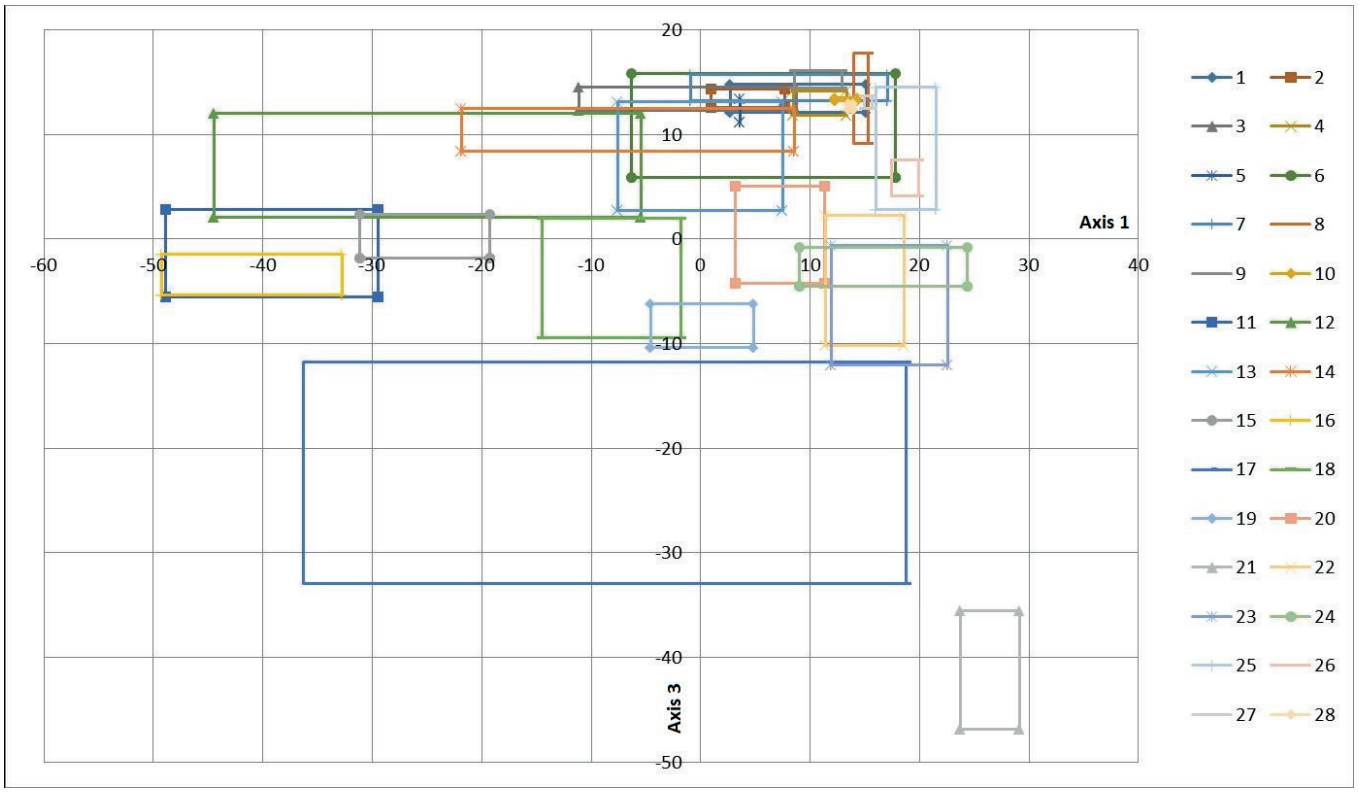

Fig. 2. Confidence intervals of typological subdivisions of vegetation on the first and third axes of the NMS-ordination

Typological subdivisions of vegetation of altitudinal belts – see table 4.

determine a rather high degree of correlation of this parameter with the altitude ($R^2 = 0.37$). A more even distribution of species diversity is expressed in conditions of high floristic richness for every altitudinal belt (West Altai) and in a lower level of diversity (East Sayan).

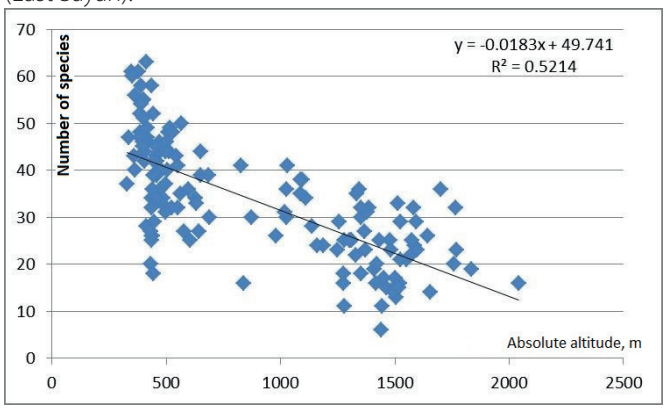

Fig. 3. Changing of relative species richness of communities on altitudinal profile in West Sayan type of zonality

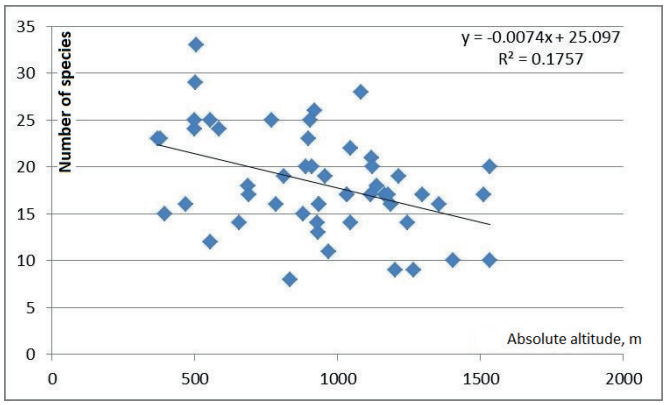

Fig. 4. Changing of relative species richness of communities on altitudinal profile in East Sayan type of zonality

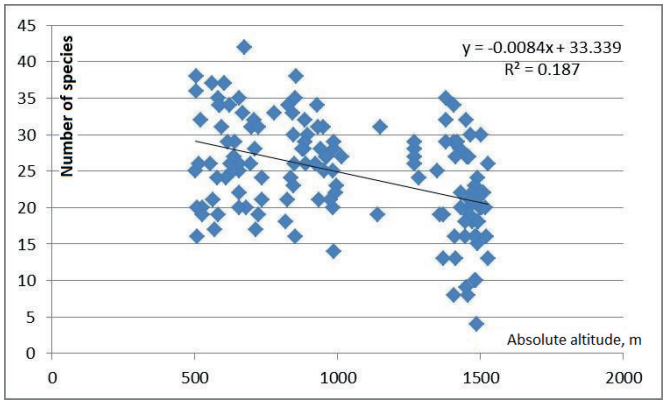

Fig. 5. Changing of relative species richness of communities on altitudinal profile in West Altai type of zonality

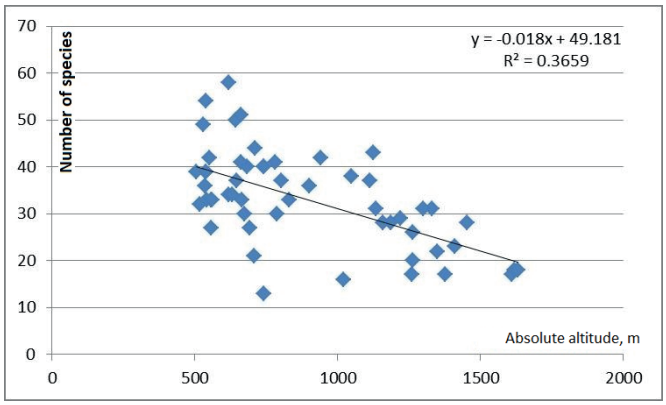

Fig. 6. Changing of relative species richness of communities on altitudinal profile in Salair-Kuznetsk type of zonality

There is a tendency to a decreasing the relative species richness (species abundance) of vegetation communities with an increase of altitude for the mountains of Southern Siberia in general (Fig. 7). The communities with the largest floristic diversity connect with the lower part of the altitudinal spectrum in conditions of increased temperature supply.

Differential diversity, calculated using the Whittaker index for elevation segments on the generalized profile for key areas in the aggregate, has a non-linear character of variation along the elevation gradient (Fig. 8). There are several peaks of diversity. The maximum values are connected with an altitude of 500-600 m (the optimum development of chern-taiga forests in West Sayan and West Altai, the forest-steppe belt of the Kuznetsk Alatau and subtaiga forests of East Sayan). The high level of floristic diversity corresponds to an increased level of differential diversity under the large temperature supply conditions in the low part of altitudinal-belt spectra of mountain ranges. A decrease in the diversity index is observed in the mountain-taiga belt. It is increased again near the upper limit of the distribution of forests at the contact with subalpine sparse forests (900-1000 m). The third extremum is connected with an altitude of 1500-1600 m (the optimum development of the subalpine meadows on contact with the alpine-tundra belt). An increased level of phytocoenotic diversity of the subalpine belt is typical for different mountain systems (Molozhnikov 1986; Sedel'nikov 1988). Based on the identified trends in the change of diversity, it is determined its increasing at the contact of altitudinal-belt divisions, characterized by the mixing of communities at different altitudinal levels.

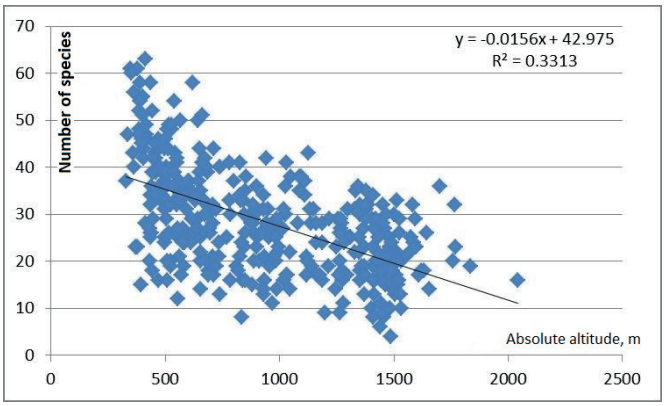

Fig. 7. Changing of relative species richness of communities on complex altitudinal profile in Altai-Sayan group of zonality types

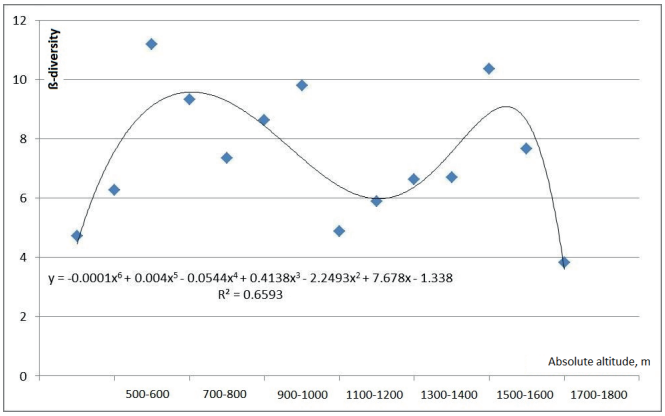

Fig. 8. Changing β-diversity of communities (Whittaker index) on complex altitudinal profile in Altai-Sayan group of zonality types

Moisture characteristics (average precipitation of July and summer) have significant correlations among the bioclimatic parameters (Table 6). The diversity is increased with moisture decreasing in the lower part of the altitudinal spectrum. A deviation from the linear dependence is observed in the subalpine belt, where the level of diversity increases with increasing moisture. January temperatures also have high positive relationships with the level of diversity. It confirms the general pattern according to which an increase in temperature supply contributes to an increase in the diversity of biota at different spatial levels (Currie and Paquin 1987; Shao and Halpin 1995; Morozova 2011).

The revealed gradients of temperature and moisture supply are summarized on the bioclimatic matrix of the vegetation of the Altai-Sayan orobiome (Table 7). The compiled scheme makes it possible to determine the patterns of vegetation diversity at the regional spatial level. The horizontal and vertical rows of the matrix are characterized by differences in conditions along the integral vectors of bioclimatic parameters through temperature and moisture indicators. Data on the key climatic conditions, which are basic in the differentiation of typological subdivisions of vegetation, are given for the most closely related bioclimatic variables. The continentality index and the average temperature of January are taken as a basis. In addition, the indicators of the average annual temperature, the average temperature of July, the average precipitation of July, and the thermicity index are given.

Vegetation diversity of the Altai-Sayan orobiome is formed under climatic conditions, which determine the development of altitudinal-belt units within the climatic sectors (Fig. 9). The average temperature of January and the continentality index characterize the spatial structure of vegetation through basic complexes of altitudinal belts of different types of zonality.

Table 6. Correlations between β-diversity (Whittaker index) with bioclimatic parameters (Spearman's rank correlation coefficient; reliable values at p <0.001 are bold font)

Bioclimatic parameters	Correlation coefficient
Bio1	**0.328**
Bio10	0.206
Bio11	**0.533**
Bio12	**-0.437**
Bio18	**-0.597**
Bio19	**-0.394**
T_January	**0.540**
T_april	**0.314**
T_July	0.195
T_october	**0.349**
T_max_January	**0.558**
T_max_July	**0.258**
T_min_January	**0.525**
T_min_July	0.132
P_January	**-0.388**
P_July	**-0.608**
Ic	**-0.565**
It	**0.477**
Ia	**-0.431**
los_summer	**-0.459**
los_July	**-0.463**
OCE	0.161
Q_pluv	**-0.367**
Pet	**-0.439**

Bioclimatic parameters – see table 2.

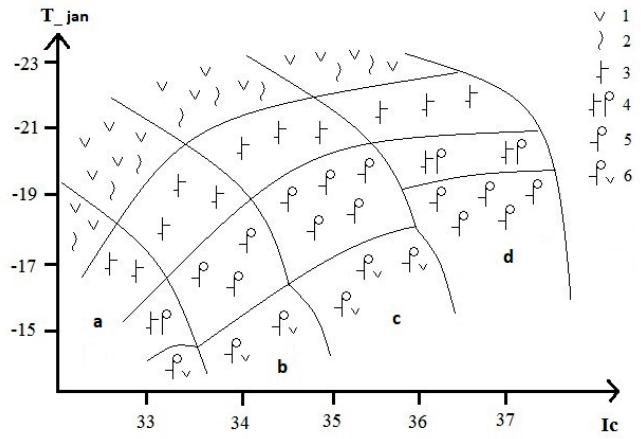

Fig. 9. Bioclimatic scheme of altitudinal belts of vegetation for Altai-Sayan orobiome

Vegetation: 1 – high-mountain tundra; 2 – alpine and subalpine meadows and sparse forests; 3 – dark coniferous mountain taiga forests; 4 – chern-taiga forests; 5 – small leave – light coniferous subtaiga forests; 6 – forest-steppe.
Types of altitudinal zonality: a – West-Altai; b – Salair-Kuznetsk; c – East-Sayan; d – West-Sayan.
Axes: Ic – continentality index, T_jan – the average temperature of January.

DISCUSSION

According to the classification of continentality types of climate (Rivas-Martinez et al. 2004), the vegetation cover of considering types of altitudinal zonality are developed in the continental sector (Ic = 31-37). It connects with boreal macrobioclimate and a low level of temperature supply (Table 7). There are significant differences between altitudinal divisions in the level of continentality (the parameter of Ic varies from 31 to 37, the parameter of It varies from 33 to 47) and in the temperature supply (the average temperature of January varies from –14 °C to –24 °C, the average temperature of July varies from +12 °C to +20 °C). Bioclimatic parameters allow determining the patterns, which characterize the changing of belts within types of altitudinal zonality and between spectra in the

The area of the increased temperature supply is occupied by the vegetation of the low part of altitudinal spectra (forest-steppe, sub-taiga, and chern-taiga belts). They are developed by an average temperature of about 0 °C. Regional features are expressed in the level of continentality and moisture supply. The sub-taiga forests are the most moisture ecosystems (the average precipitation of July is above 120-130 mm). Low mountains of the West Sayan are characterized by maximum amplitudes of temperature that reflect on maximum values of continentality index and minimum values of thermicity index. The vegetation cover of this region belongs to the humid geographical variant of sub-taiga birch-pine forests

Table 7. The vegetation of the Altai-Sayan orobiome in the system of bioclimatic parameters

Bioclimatic parameters		Ic	31±0.04	31.4±0.07	32±0.0	32.5±0.22	33±0.0	33.4±0.3	34±0.2	34.6±0.2	37.2±0.2
		P_July	102.5±2.3	102.5±0.9	95±0.0	112.5±10.2	147.3±1.2	90.3±12.4	114.7±13	90±18.6	141±18.7
		It	-39.2±0.2	-37.7±1.1	-32.9±0.0	-36.2±1.6	-47.4±0.3	-37.7±2.5	-40.1±1.9	-35.4±3.9	-45.6±2.3
T_January	T_July	T_year									
-23.8±0.8	13.3±1.1	-3.9±0.9									3 7 11
-23.1±0.3	13.9±0.5	-3.3±0.4									1
-22.1±1.5	15.2±1.6	-2.1±1.5									15
-21.4±0.1	11.9±0.1	-4.5±0.1					4				
-20.3±0.3	12.9±0.4	-3.2±0.4				6 10			8 12		
-19.7±0.3	13.2±0.3	-3.1±0.3				14					
-19±0.6	15±0.8	-1.8±0.7							16		
-18.3±2.1	15.2±1.1	-1.3±1	2 5 9	13				18		22 24	19
-17.5±0.5	19.7±0.4	2.2±0.4									21
-17.3±0.7	16.7±1	-0.1±0.9							23		
-16.6±0.2	17.6±0.1	0.7±0.1			17					26 28	
-15.3±0.6	17.2±0.8	1.5±0.7				25 27					
-14.6±0.7	17.9±0.9	2.2±0.8				20					

Vegetation typological subdivisions of altitudinal belts – see table 4.
Bioclimatic parameters (mean ± standard deviation) – see table 2.

of South Siberia (Drobushevskaya and Nazimova 2007). Shrub (*Caragana arborescens, Spiraea chamaedrifolia*), bracken (*Pteridium pinetorum* ssp. *sibiricum*), herb (*Lathyrus humilis, L. frolovii, Vicia sepium, Cruciata glabra* ssp. *krylovii*) and grass (*Calamagrostis arundinacea, Brachypodium pinnatum*) forests are the basis of these vegetation diversity. These communities have a high species abundance (about 40 species of vascular plants on a key area of 400 m^2). Forest-steppe vegetation complexes are formed in the low part of the altitudinal spectra of West Altai and Kuznetsk Alatau. Forest-steppe belt is an example of the complicated spatial organization of vegetation cover with a combination of forest, steppe, meadow, and shrub communities on the slopes of different temperature and moisture supply (Chytry et al. 2007; Ogureeva 1980). The conditions of moisture favor the development of meadow steppes (*Stipa pennata, Helictotrichon altaicum*), shrub communities (*Caragana arborescens, Spiraea trilobata, Rosa acicularis*) in the West Altai type of zonality (Ogureeva 1980). They develop in combination with larch and birch-pine herb-grass forests. The least humid geographical variant of the forest-steppe, associated with the eastern macroslope of the Kuznetsk Alatau, is distinguished by the predominance of herb-sod-bunch-grass steppes, (*Stipa pennata, Helictotrichon altaicum, Iris ruthenica, Filipendula stepposa, Schizonepeta multifida*) and larch forests. The sub-taiga forests of the East Sayan are developed in conditions of the lowest temperature supply (the average annual temperature is negative; the average temperature of July does not exceed +15…+16 °C). Sedge (*Carex macroura*) – grass (*Calamagrostis arundinacea*) and herb-grass birch-pine forests are charactered. They are distinguished by a relatively low typological diversity and lower floristic diversity in comparison with their analogs in other types of the Altai-Sayan group (Nazimova et al. 1987).

The mountain taiga belt is formed under conditions of a decreasing heat supply with a high level of moisture. Differences in the types of altitudinal zonality are well expressed. In West Altai, mountain taiga forests are formed at the highest temperatures (the average temperature of July is +16...+17 °C). In West Sayan, mountain taiga is developed in conditions of high humidity. Differentiation of the belt into two sub-belts characterize West Altai and West Sayan types of altitudinal zonality. The diversity is based on large-herb birch-aspen-Siberian pine-fir large-herb (*Cacalia hastata, Verathrum lobelianum, Senecio nemorensis*) and large-fern (*Athyrium filix-femina, Dryopteris filix-mas, Matteucia struthyopteris*) communities. The chern-taiga complexes, which are characterized by the development of nemoral relict species of the Neogene age and a high level of biota diversity (Ermakov 2003; Kuminova 1960; Nazimova 1967), are determined by modern climatic conditions, primarily high moisture with increased temperature supply (the average precipitation of July exceeds 110 mm, and the average temperature of July exceeds +15 °C). The increased moisture of the winter period also contributes to the preservation of relict complexes. At the same time, the chern-taiga of West Sayan is formed under conditions of slightly higher moisture and lower temperature supply compared to West Altai (Table 7).

The purely mountain-taiga belt in the humid climate of the middle mountains of the Altai-Sayan group of types of altitudinal zonality is represented by dark-coniferous Siberian pine-fir fern (*Dryopteris expansa*), large-herb, herb-green moss forests. The lowest level of moisture supply is observed in larch (*Larix sibirica*) forests on altitudinal profiles in West Altai and Kuznetsk Alatau (average precipitation of July is less than 100 mm). Here these communities are distributed at a narrow altitude amplitude (about 500 m). In East Sayan, the increased moisture of the mountain taiga belt does not contribute to an increase in its species diversity due to the low heat supply (the average temperature of January is –19 °C).

The high altitudinal belts of all key areas are characterized by a significant amplitude of the values of climate conditions. At the same time, within the types of altitudinal zonality for high mountain communities, there are no significant differences between the key bioclimatic indicators. It can be explained by a decrease in contrasts in the climatic conditions of high mountain regions reflected in the vegetation cover (Sedel'nikov 1988). In all types of altitudinal zonality, the subalpine belt is represented by polydominant large-herb (*Verathrum lobelianum, Cirsium helenioides, Bupleurum aureum* ssp. *longifolium*) subalpine meadows and Siberian pine and fir sparse forests. Alpine (*Schulzia crinita, Bistorta major, Myosotis krylovii*) meadows and high mountain tundra (*Rhododendron aureum, Festuca sphagnicola, Empetrum nigrum*) are characterized by a high similarity of typological diversity. In different types of altitudinal zonality, they are developed with low-temperature supply (the average temperature of January is below –13 °C) and, in general, an increased level of moisture with some regional differences (the average precipitation of July is more than 100 mm). The differences between the subalpine and alpine-tundra belts are mainly regulated by thermic conditions. The high heterogeneity of the ecotopic conditions of the highlands contributes to an increase in vegetation diversity, which is reflected in the richness of plant communities of high-mountain belts of different types of altitudinal zonality in the mountains of Southern Siberia and their close relationship with ecological factors (Molozhnikov 1986; Sedel'nikov 1988). Regional differences between high-mountain belts in relation to the complex of bioclimatic parameters are expressed to a greater extent between the types of altitudinal zonality in comparison with the differences between belts within each of the types.

The spatial structure of vegetation of the Altai-Sayan orobiome is characterized by the altitudinal gradient of climatic conditions. Temperature parameters are most closely related to gradients (especially, temperatures of the cold season) (Fig. 9). The climatic areas of the basic vegetation types of the altitudinal belts, determined by a set of key parameters (average temperature of January, continentality index), do not intersect, which provides a climatic identification for the distinguished types of altitudinal zonality.

Differences in the temperature supply and climate continentality, which characterize the zonal structure of the vegetation cover in large territories, for example, in Northern Eurasia (Nazimova et al. 2004), find similar patterns of influence for the altitudinal spectra. At the same time, the contrast of the vegetation cover increases significantly. The continentality of the climate in the mountains of Southern Siberia marks the altitudinal-belt spectra of vegetation, which are formed under a certain ecological and geographical specificity of mountain ranges. By the prevailing Atlantic transport of air masses, the spatial structure is dependent on the relative position of the ranges, their latitudinal position, and orientation. The entire altitudinal spectrum of the West Sayan type of altitudinal zonality is developed within the same sector of continentality with the maximum values for the group of zonality types, which do not have significant differences between the belts (Table 7). Temperature parameters play a key role in regulating the change of altitudinal belts. The

remaining types of altitudinal zonality are differentiated according to the degree of continentality, reflecting changes in moisture along the altitudinal gradient. The largest amplitude of the parameter has been noted for the West Altai and Salair-Kuznetsk types with forest-steppe belts in the lower part of the spectra. The climatic areas of the corresponding belts in different spectra are partially intersected but do not completely correspond to each other. It is expressed in different aspects of the diversity of vegetation (the level of absolute and relative floristic richness, the ratio of basic and associated types of communities, etc.).

Traditionally the analysis of vegetation cover in relation to climate altitudinal gradient is based on the warm season parameters mainly (Nakamura et al. 2007). The average temperature of January has been used to characterize the thermic conditions. The role of the cold season parameters is not given sufficient attention, while they determine the functioning of ecosystems in different belts during a long frosty period. Extreme temperatures and their annual amplitudes are limiting in the distribution of individual plant species and communities (Bocharnikov 2021). Under the conditions of the development of the Altai-Sayan group of types of altitudinal zonality, the lowest temperatures occur in January. The greatest variation in vegetation diversity is associated with their change.

The conditions for the development of belts of different types of altitudinal zonality are not identical and can differ quite significantly due to a change in the continental climate. The basis of each spectrum is the mountain-taiga belt of dark-coniferous forests. Regional differences in the mountain-taiga belt are clearly expressed in the formation of the chern-taiga sub-belt in the West Altai and the West Sayan types. Despite the increased values of the continentality index, the development of the chern-taiga in West Sayan is determined by a high level of moisture, including a large amount of precipitation of summer. It contributes to forming relict nemoral complexes, which are possible even under low negative average annual temperatures.

The species diversity patterns in the orobiome find some particularities in comparison with mountain gradients of biodiversity. The maximum diversity relates to the lowest part of the spectra (about 400-600 m). The position of maximum in the world is changed in the wide range with gravitation to middle mountains (about 1500 m at 50-60° of North latitude) (Sang 2009; Guo et al. 2013). The orobiome has a similar species diversity pattern in different types of altitudinal zonality that characterizes its unity. Each type has a specific spread of diversity values with a general trend. The differentiation of beta-diversity confirms a complicated character of mountain diversity (Zhu et al. 2009; Bueno et al. 2021). It can not describe by linear models on the basis of certain bioclimatic parameters. The explanation of diversity trend is in changing of vegetation belts as the basic ecosystems in mountains.

The unity of the groups of types of altitudinal zonality connects with a certain amplitude of bioclimatic parameters (Ogureeva 1991). Changes between types concern the altitudinal limits of belts, the development of individual sub-belts, the variations in the level of absolute and relative species richness of communities founded in each type of altitudinal zonality. At the regional level of the evaluation of the spatial structure of vegetation in connection with climatic conditions, it corresponds to the first level of bioclimatic organization, characterizing the group of types of zonality (Table 8). At the second level, the diversity of climatic conditions determines the development of certain types of zonality, differing in the level of temperature and moisture supply and the degree of continentality. The third level of bioclimatic organization characterizes the conditions of the formation of individual altitudinal vegetation belts, contributing to their development in the composition of the spectra. The amplitude of the values of bioclimatic parameters that determine the unity of its typological subdivisions decreases with a decrease in the hierarchical level of the bioclimatic organization of the vegetation cover. At the same time, different parameters respond to this to a different extent. The level of moisture and continentality of the climate vary rather weakly within individual types of zonality, while temperature supply marks the change of individual belts. It is especially expressed in the lower part of the altitudinal spectra.

Belts in different types of altitudinal zonality have differences in their climatic conditions, depending on the development in the certain type for the particular profile. These differences are reflected not only in the occupied altitudes on the profiles but also in the most important features of vegetation diversity. The predominance of formations and the indicators of the diversity of their communities determine the differences in the spectra by preserving basic formational complexes of vegetation for all the spectra. In the warmest conditions, vegetation belts of West Altai are formed. High-mountain vegetation receives limited development, and relict chern-taiga forests develop in the lower part of the spectrum (the West Altai sector of their distribution) (Ogureeva 1980). The optimal ratio of temperature and moisture contributes to

Table 8. Bioclimatic organization of the spatial structure of vegetation cover for the Altai-Sayan orobiome

A level of bioclimatic organization	Typological levels of altitudinal zonality				
I	Group of types of altitudinal zonality	Altai-Sayan			
II	Zonality types	West Sayan	East Sayan	West Altai	Salair-Kuznetsk
III	Altitudinal belts	I.1 I.2 II.1 II.2 III.1 IIIa.1 IV.1	I.2 II.1 II.2 III.1 IV.1 IV.2	I.1 I.2 II.1 II.2 III.1 IIIa.1 V.1 V.2	I.2 II.1 II.2 III.1 IV.1 V.1 V.2

Vegetation typological subdivisions of altitudinal belts – see table 3.

the development of a forest-steppe belt with a complex composition and structure. Shrub communities participate in the composition of the belt, characterizing the region's connections with the continental regions of Kazakhstan and Central Asia (Karamysheva and Rachkovskaya 1973). West Sayan sector of chern-taiga forests is associated with conditions of a higher amplitude of annual temperatures. However, due to the high level of moisture, including during the vegetation season, they get the opportunity for the development of typologically rich hemiboreal complexes (Nazimova et al. 1987; Ermakov 2003; Bocharnikov 2015). From the climatic point of view, the botanical and geographical specificity of the Altai-Sayan group of types of altitudinal zonality can be determined only by a set of parameters characterizing the temperature, moisture, and their ratio. Under similar conditions of temperature supply, specific altitudinal subdivisions of different spectra are developed (Fig. 9). Moreover, they are strictly separated in the space of climatic conditions.

The obtained results of the work are valuable not only as fundamental knowledge but for practical use. Understanding of regional differences in climatic prerequisites for the formation of vegetation creates the basis for identifying ecosystem problems and planning the rational use of plant resources (Zheng, Zhu 2017). In addition, the constructed bioclimatic system will serve as a basis for identifying trends in the structure of vegetation in connection with climate changes, to which the biota responds (Ramachandran et al. 2020).

CONCLUSION

The conducted bioclimatic interpretation of the vegetation characterizes the general trends in its spatial organization in the Altai-Sayan orobiome, determined by the differentiation of temperature and moisture supply. The unity of altitudinal spectra for the entire group of types of altitudinal zonality is reflected in a similar composition of belts with individual features of belts and sub-belts of vegetation (for example, chern-taiga forests). These features characterize the regional specificity of types of altitudinal zonality.

The vegetation diversity is associated with the climate at different spatial levels marked by bioclimatic parameters. The proposed system of levels of bioclimatic organization of the vegetation cover on the example of types of altitudinal zonality characterizes the differences in the role of specific parameters that determine the differentiation of different belts and different types of zonality within Altai-Sayan group. These differences are associated with a change of the conjugation between parameters and typological subdivisions of vegetation, different amplitudes of the values of parameters that limit the distribution of individual belts and total altitudinal spectra. The conditions of temperature supply are key in the change of altitudinal belts of vegetation of individual spectra. The parameters of moisture and climate continentality have a dominant in determination of the differences in the complete spectra of different types of zonality. At the same time, within the group of types of altitudinal zonality, the unity of gradients of climatic conditions is preserved.

The thermic gradient prevails over the moisture gradient in terms of the degree of influence on the vegetation diversity within specific altitudinal spectra in the mountains of Southern Siberia. The temperatures of the vegetation season, winter period, as well as the ratio of average temperature extremes, have the most important limiting value. The moisture and continentality gradients characterize a change in altitudinal spectra. Each spectrum has a specific trend of changes in bioclimatic parameters by altitude, which determines differences in the types of vegetation zonality according to the diversity of belts from climatic positions. An increase in the typological diversity of vegetation within the altitudinal-belt spectra is associated with a large variation in the values of bioclimatic parameters differentiated by altitudinal profiles. An increase in the diversity of climatopes, as a reflection of the diversity of temperature and moisture supply conditions, contributes to the functioning of unique relict ecosystems, in particular, chern-taiga forests with an excessive level of moisture.

The increased floristic richness of vegetation complexes in the lower part of the altitudinal-belt spectra of the Altai-Sayan group of altitudinal zonality (forest-steppe, subtaiga, chern-taiga complexes) determines a clear trend in the decrease of relative species diversity of communities with the increase of altitude. It is marked by thermic parameters. A more even distribution of relative species diversity on altitudinal profile connects with a high level of diversity of high-mountain vegetation, and also with a more homogeneous altitudinal-belt structure with a few typological subdivisions. Differentiation diversity is associated with the moisture of the warm period and the temperature supply of the cold period. It has a non-linear trend by the altitudinal gradient. The maximum values of diversity are expressed in the lower part of the altitudinal spectrum and the contact of subalpine and alpine-tundra belts. The spatial structure of high-mountain vegetation forms in relative homogenous climatic conditions with a smooth gradient of climatic parameters according to the low continentality of climate. It depends on ecotopic conditions mostly. The regional differentiation by climatic conditions of development of vegetation is in different types of altitudinal zonality of the Altai-Sayan group.

REFERENCES

Alberto F.J., Aitken S.N., Alia R., Gonzalez-Martinez S.C., Hänninen H., Kremer A., Lefevre F., Lenormand T., Yeaman S., Whetten R. and Savolainen O. (2013). Potential for evolutionary responses to climate change-evidence from tree populations. Glob. Change Biol., 19, 1645-1661, DOI: 10.1111/gcb.12181.

Aynekulu E., Aerts R., Moonen P.E., Denich M., Gebrehiwot K., Vågen T., Mekuria W. and Boehmer H. J. (2012). Altitudinal variation and conservation priorities of vegetation along the Great Rift Valley escarpment, northern Ethiopia. Biodivers. Conserv, 21, 2691-2707, DOI: 10.1007/s10531-012-0328-9.

Bocharnikov M.V. (2015). Eco-ptytocoenotic structure of the forest cover on the northern macroslope of Western Sayan. Lesovedenie, 1, 10-19 (in Russian with English abstract).

Bocharnikov M.V., Ogureeva G.N. and Jargalsaikhan L. (2018). Regional features of the altitudinal gradients in Northern Transbaikalia vegetation cover. Geography, Environment, sustainability, 11(4), 67-84, DOI: 10.24057/2071-9388-2018-11-4-67-84.

Bocharnikov M.V. (2019). Role of climate in the spatial structure of vegetation of the Kodar-Kalar orobiome. Contemp. Probl. Ecol., 12, 193-203, DOI: 10.1134/S1995425519030028.

Bocharnikov M.V. (2021). Species distribution in cenofloras of the cryophytic steppes and cushion plants with the participation of Stellaria pulvinata Grub. in the Mongolian Altai. Arid Ecosystems, 11, 1, 52-61, DOI: 10.1134/S2079096121010042.

Bueno M.L., Rezende V.L., De Paula L.F. A., Meira-Neto J.A.A., Pinto J.R.R., Neri A.V.and Pontara V. (2021). Understanding how environmental heterogeneity and elevation drives the distribution of woody communities across vegetation types within the campo rupestre in South America. Journal of Mountain Science, 18, 1192-1207, DOI: 10.1007/s11629-020-6125-0.

Chytry M., Danihelka J., Kubešová S., Lustyk P., Ermakov N., Hájek M., HajkovanP., Kočí M., Otypková Z., Roleček J., Řezníčková M., Šmarda P., Valachovič M., Popov D. and Pišút I. (2007). Diversity of forest vegetation across a strong gradient of climatic continentality: Western Sayan Mountains, southern Siberia. Plant Ecology, 196, 61-83, DOI: 10.1007/s11258-007-9335-4.

Clarke K.R. (1993). Non-parametric multivariate analyses of changes in community structure. Austral. J. Ecol., 18, 117-143, DOI: 10.1111/J.1442-9993.1993.TB00438.X.

Currie D.J. and Paquin V. (1987). Large-scale biogeographical patterns of species richness in trees. Nature, 329, 32-327, DOI: 10.1038/329326A0.

De Dios V.R., Fischer C. and Colinas C. (2007). Climate change effects on Mediterranean forests and preventive measures. New Forests, 33, 29-40, DOI: 10.1007/s11056-006-9011-x.

Del Rio S. and Penas A. (2006). Potential distribution of semi-deciduous forests in Castile and Leon (Spain) in relation to climatic variations // Plant Ecology, 185, 269-282, DOI: 10.1007/s11258-006-9103-x.

Dolezal J. and Srutek M. (2002). Altitudinal changes in composition and structure of mountain-temperate vegetation: a case study from the Western Carpathians. Plant Ecology, 158, 2, 201-221, DOI: 10.1023/A:1015564303206.

Drobushevskaya O.V. and Nazimova D.I. (2006). Climatic variants of the light-coniferous low-mountain subtaiga in Southern Siberia. Geography and Natural Resources, 2, 21-27 (in Russian with English abstract).

Ermakov N.B. (2003). Diversity of boreal vegetation in North Asia. Hemiboreal forests. Classification and ordination. Novosibirsk, 232. (in Russian).

Fick S.E. and Hijmans R.J. (2017). WorldClim 2: new 1-km spatial resolution climate surfaces for global land areas // International Journal of Climatology, 37, 4302-4315, DOI: 10.1002/JOC.5086.

Francis A.P. and Currie D.J. (2003). A globally consistent richness-climate relationship for angiosperms. American Naturalist, 161, 523-536, DOI: 10.1086/368223.

Grebenshchikov O.S. (1974). An essay of climatic characteristics for the main plant formations of the Caucasus. Botanical journal, 59, 2, 161-173 (in Russian).

Holdridge L.R. (1967). Life zone ecology. San Jose: Tropical Science Center, 206.

Karger D.N., Conrad O., Böhner J., Kawohl T., Kreft H., Soria-Auza R. W., Zimmermann N. E., Linder H. P. and Kessler M. (2017). Climatologies at high resolution for the earth's land surface areas. Scientific Data, 4, 170122, DOI: 10.5061/dryad.kd1d4.

Kolomyts E.G. (1966). Snow cover of mountain taiga landscapes of Northern Transbaikalia. Moscow-Leningrad, 184. (in Russian).

Kuminova A.V. (1960). The vegetation cover of the Altai. Novosibirsk, 450. (in Russian).

Mokarram M. and Sathyamoorthy D. (2015). Modeling the relationship between elevation, aspect and spatial distribution of vegetation in the Darab Mountain, Iran using remote sensing data. Model. Earth Syst. Environ., 1, 30, DOI: 10.1007/s40808-015-0038-x.

Morozova O.V. (2011). Spatial trends in the taxonomic richness of the vascular plant flora. Biosfera 3(2), 190-207 (in Russian with English abstract).

Nakamura Y., Krestov P. V. and Omelko A. M. (2007). Bioclimate and vegetation complexes in Northeast Asia: first approximation to an integrated study. Phytocoenologia, 37, 3-4, 443-470, DOI: 10.1127/0340-269X/2007/0037-0443.

Namzalov B.B. (2020). Extrazonal Steppe Phenomena in the Mountains of Southern Siberia: Features of Spatial Organization and Centers of the Latest Speciation and Cenogenesis. Contemp. Probl. Ecol., 13, 495-504, DOI: 10.1134/S199542552005008X.

Navarro-Racines C., Tarapues J., Thornton P., Jarvis A. and, Ramirez-Villegas J. (2020). High-resolution and bias-corrected CMIP5 projections for climate change impact assessments. Scientific Data, 7, 7, DOI: 10.1038/s41597-019-0343-8.

Nazimova D.I. (1967). Relics of nemoral flora in the forests of the Western Sayan. Lesovedeniye, 3, 76-88 (in Russian).

Nazimova D.I. (1975). Mountain dark coniferous forests of the Western Sayan: an experience of ecological-phytocenotic classification. Leningrad, 119. (in Russian).

Nazimova D.I., Danilina D.M. and Stepanov N.V. (2014). Biodiversity of rain-barrier forest ecosystems of the Sayan mountains // Botanica Pacifica. A journal of plant science and conservation, 3(1), 39-47, DOI: 10.17581/bp.2014.03104.

Nazimova D.I., Ermakov N.B., Andreeva N.M. and Stepanov N.V. (2004). Conceptual model of structural biodiversity of zonal forests in North Eurasian forests. Contemp. Probl. Ecol., 5, 745-755 (in Russian with English abstract).

Nazimova D.I., Korotkov I.A. and Cherednikova Y.S. (1987). The main altitudinal-belt divisions of the forest cover in the mountains of Southern Siberia and their diagnostic features. Lectures in Commemoration of V.N. Sukachev. Moscow, 30-64 (in Russian).

Nazimova D.I., Ponomarev E.I., Stepanov N.V. and Fedotova E.V. (2005). Chern dark coniferous forests in southern Krasnoyarsk krai and problems of their general mapping. Lesovedeniye, 1, 12-18 (in Russian with English abstract).

Odland A. (2009). Interpretation of altitudinal gradients in South Central Norway based on vascular plants as environmental indicators. Ecological Indicators, 9(3), 409-421, DOI: 10.1016/j.ecolind.2008.05.012.

Ogureeva G.N. (1980). Botanical geography of Altai. Moscow, 192. (in Russian).

Ogureeva G.N. (1991). Botanical and geographical zoning of the USSR. Moscow, 78. (in Russian).

Ogureeva G.N. (1997). Structure and dynamics of high mountain ecosystems of Mongolian Altai. Arid ecosystems, 3, 6-7, 119-133 (in Russian with English summary).

Ogureeva G.N. and Bocharnikov M.V. (2017). Orobiomes as the basic units of the regional evaluation of the mountain region biodiversity. Ecosystems: Ecology and Dynamics, 1, 2, 52-81 (in Russian with English abstract).

Ogureeva G.N., Miklyaeva I.M., Safronova I.N. and Yurkovskaya T.K. (1999). Zones and types of altitudinal zonation of vegetation of Russia and adjacent territories. Scale 1: 8 000 000. Moscow.

Otto-Bliesner B.L., Brady E.C., Clauzet G., Tomas R., Levis S. and Kothavala Z. (2006). Last glacial maximum and Holocene climate in CCSM3. Journal of Climate, 19, 11, 2526-2544, DOI: 10.1175/JCLI3748.1.

Polikarpov N.P., Chebakova N.M. and Nazimova D.I. (1986). Climate and mountain forests of Southern Siberia. Novosibirsk, 225. (in Russian).

Qian H., Fridley J.D. and Palmer M.W. (2007). The latitudinal gradient of species-area relationship for vascular plants of North America // American Naturalist, 170, 5, 690-701.

Guo Q., Kelt D., Sun Z., Liu H., Hu L., Ren H. and Wen J. (2013). Global variation in elevational diversity patterns // Scientific Reports, 8, 1-7, DOI: 10.1038/srep03007.

Rahman I.U., Khan N., Ali K. and Ahmad S. (2020). Vegetation-environment relationship in Pinus wallichiana forests of the Swat Hindukush range of Pakistan. J. For. Res., 31, 185-195, DOI: 10.1007/s11676-018-0864-6.

Ramachandran R.M., Roy P.S., Chakravarthi V., Joshi P.K., Sanjay J. (2020). Land use and climate change impacts on distribution of plant species of conservation value in Eastern Ghats, India: a simulation study. Environmental Monitoring and Assessment, 192, 86, DOI: 10.1007/s10661-019-8044-5

Rivas-Martinez S., Penas A. and Diaz T.E. (2004). Bioclimatic map of Europe, thermoclimatic belts. Cartographic Service. University of Leon, Spain.

Rivas-Martinez S., Rivas Saenz S. and Penas A. (2011). World-wide bioclimatic classification system. Global Geobotany, 1(1), 1-634.

Sang W. (2009). Plant diversity patterns and their relationships with soil and climatic factors along an altitudinal gradient in the middle Tianshan Mountain area, Xinjiang, China. Ecological Research, 24, 303-314, DOI: 10.1007/s11284-008-0507-z.

Sedel'nikov V.P. (1988). High mountain vegetation of the Altai-Sayan mountainous region. Novosibirsk, 222. (in Russian).

Shao G. and Halpin P.N. (1995). Climatic controls of Eastern North American coastal tree and shrub distributions. Journal of Biogeography, 22, 6, 1083-1089, DOI: 10.2307/2845837.

Sochava V.B. (1980). Geographical aspects of the Siberian taiga. Novosibirsk, 256. (in Russian).

Stepanov N.V. (2012). Endemism of boreal rainforest region of the Sayan mountains. Abstracts of the symposium The East Asian Flora and its role in the formation of the world's vegetation. Vladivostok, 85.

Sukachov V.N. and Zonn S.V. (1961). Methodical instructions for the study of forest types. Moscow, 144. (in Russian).

Svenning C., Gravel D., Holt R. D., Schurr F. M., Thuiller W., Münkemüller T., Schiffers K.H., Dullinger S., Edwards T.C., Hickler J.T., Higgins S.I., Nabel J.E.M.S., Pagel J. and Normand S. (2014). The influence of interspecific interactions on species range expansion rates. Ecography, 37, 1198-1209, DOI: 10.1111/j.1600-0587.2013.00574.x.

Tolmachev A.I. (1948). The main ways of vegetation formation in high-mountain landscapes of the northern hemisphere. Botanical journal, 33, 2, 161-180 (in Russian).

Tuhkanen S. (1984). A circumboreal system of climatic-phytogeographical regions. Acta Botanica Fennica 127, 1-50.

Walter H. and Breckle S.-W. (1991). Okologishe Grundlagen in global sicht. Stuttgart: G. Fischer, 586, DOI: 10.1007/BF02902905.

Whittaker R.J., Willis K.J. and Field R. (2001). Scale and species richness: towards a general hierarchical theory of species diversity. Journal of Biogeography, 28, 453-470, DOI: 10.1046/J.1365-2699.2001.00563.X.

Yang Y., Wang H., Harrison S.P., Prentice I.C., Wright I.J., Peng C. and Lin G. (2019). Quantifying leaf-trait covariation and its controls across climates and biomes. New Phytologist, 221, 1, 155-168, DOI: 10.1111/nph.15422.

Zheng X., Zhu J. (2017). A new climatic classification of afforestation in Three-North regions of China with multi-source remote sensing data. Theoretical and Applied Climatology. 127, 465-480, DOI: 10.1007/s00704-015-1646-0

Zhu Y., Jiang Y., Liu Q., Kang M., Spehn E.M. and Korner C. (2009). Elevational trends of biodiversity and plant traits do not converge – a test in the Helan Range, NW China. Plant Ecology, 205, 273-283, DOI: 10.1007/s11258-009-9616-1.

RESEARCH PAPER

EVALUATING THE VISITORS' PERCEPTION AND AVAILABLE ECOSYSTEM SERVICES IN URBAN PARKS OF LAHORE (PAKISTAN)

Aysha Hanif[1], Safdar A. Shirazi[2], Muhammad Jabbar[3*], Anum Liaqat[2], Sahar Zia[1], Mariney M. Yusoff[3]

[1]Lahore College for Women University, Lahore, Pakistan

[2]University of the Punjab, Lahore, Pakistan

[3]University of Malaya, Malaysia

***Corresponding author:** jabbar.lhr@gmail.com

Received: December 3rd, 2022 / Accepted: November 11th, 2022 / Published: December 31st, 2022

https://DOI-10.24057/2071-9388-2021-133

ABSTRACT. Ecosystem services provided by urban parks play a significant role in visitors' well-being. The provision of these services depends upon the well-designed green spaces built to fulfil the needs of people. As these services are linked with visitors' well-being, particular emphasis to indicate them is needed. However, minimal documentation is found regarding these valuable services, particularly in the context of Lahore. So, in this study, an effort was made to highlight visitors' preferences for the available ecosystem services provided by urban parks in Lahore, Pakistan. These ecosystem services are beneficial in enhancing the well-being of people. Fifteen parks in Lahore were selected in this study to highlight the visitors' preferences in visiting the parks. A questionnaire-based survey was conducted in these parks to collect information. The questionnaire was compiled to record socio-demographical profiles, usage patterns, choices, and visitors' opinions about the services provided by the parks. A total of 300 responses were recorded to depict the survey findings. The result highlights that 60-80% of visitors like to come to the parks having maximum services regardless of how distant is from their residence. It also reveals that large-sized parks with maximum facilities attract more visitors than small and medium-sized parks. As in these parks, people only from neighbouring areas visit due to their accessibility. The findings will be helpful for the managers and planners of the urban park to improve the ecosystem services for the well-being of people. It will also indicate the choices of people based on that information, the status of parks can be improved, and new parks can be developed to meet the visitors' needs.

KEYWORDS: Ecosystem Services; preferences; urban parks; Visitors' Well-being; Principal Component Analysis

CITATION: Hanif A., Shirazi S.A., Jabbar M., Liaqat A., Zia S., Yusoff M.M. (2022). Evaluating The Visitors' Perception And Available Ecosystem Services In Urban Parks Of Lahore (Pakistan). Geography, Environment, Sustainability, 4(15), 32-38
https://DOI-10.24057/2071-9388-2021-133

ACKNOWLEDGEMENTS: We are thankful to the respondents who spare time to respond to the questionnaire. We highly appreciate the role of editors and reviewers who provide their intensive input to make this piece of research into a research article.

Conflict of interests: The authors reported no potential conflict of interest.

INTRODUCTION

As urbanization is increasing worldwide, enhancing the quality of life for citizens in a sustainable way is becoming challenging. However, it also creates opportunities by focusing on the areas for improvement. More people are living in urban areas as compared to rural areas globally. 55% of the world's population resided in cities in 2018, which is expected to be 68% in 2050 (McCormack et al. 2010). In this scenario, ecosystem services are considered a practical approach in achieving sustainable development goals. They also support the environmental policies in designing urban plans for cities. Various methods can be applied to assess city ecosystem services (Gatersleben et al. 2014). Primarily they are based on one of these three approaches; spatially precise biophysical measurements, models, or web-based modelling platforms and qualitative approaches based on experts' evaluation (Battisti et al. 2019). The literature revealed that the benefits rendered by urban green spaces are mostly related to environmental, social, and economic values as urban green space contributes significantly to social aspects by promoting physical activities, space for relaxing, reducing stress, and enhancing social interaction (Ambiental et al. 2010). They also play their role economically by increasing the property value due to proximity and generating revenues from tourist attractions. Similarly, environmental benefits are also rendered by urban green spaces like regulation and conservation services. Thus, their presence in cities is considered a significant sustainability indicator (Delgadillo Polanco, 2012).

Ecosystem services assist humanity in various ways and are referred to as ecosystem benefits. Natural drivers can be evaluated but not controlled; anthropogenic drivers, on the other hand, may be evaluated and controlled. The most obvious reason for this is to represent the effects of human actions on

ecological services (Dalton 2011; Lü et al. 2012; Sinchembe & Ellery 2010; Wang et al. 2009). Purification of air, temperature and noise regulation, carbon absorption, flood reduction, recreational opportunities, and provision of social connections can be provided by urban parks as ecosystem services (Hanif et al. 2020b). Ecosystem services can be supplied for natural, semi-natural, or controlled ecosystems to satisfy societal development demands. However, due to the rapid rise of the economy and society, the current gap between ecosystems' capability to offer services and human requirements increases. Furthermore, humans affect ecosystem services by changing the land habitat, ecosystem structure, and biogeochemical cycle. These human activities positively and negatively affect ecosystem services (Jardine et al. 2007; Liu et al. 2013; Rechkemmer & Von Falkenhayn 2009).

Various factors influence the use of green spaces/parks in cities. These factors encompass the quality and quantity of space, attributes of potential users (age, gender, race, socio-economic profile), psychological factors (capability, identified hindrance) influencing personal preferences, accessibility, provision of facilities according to needs of users, parks maintenance and safety (Giles-Corti et al. 2005). Green areas create a better human environment by controlling the city's climate, cooling temperature and filtering air (Jabbar & Yusoff, 2022a). It has been recognized that green space is a vital source of a sustainable urban environment (Jabbar et al. 2021).

As the quality of green spaces is essential for optimizing benefits, the characteristics of parks are also considered keystone aspects. Pieces of evidence show that the characteristics of every park vary according to its community to get maximum advantages (Jabbar & Mohd Yusoff 2022b). Thus to enhance the well-being of people, a comprehensive study of the urban parks is inevitable (Ayala-Azcárraga et al. 2019). Variables like type and area covered by vegetation in adjacent areas, accessibility to green spaces, people's participation in outdoor activities, nearness of water bodies and any association with the natural environment can be utilized to gauge people's exposure to their natural surroundings within cities. Research also shows that various landscape variables in various scenarios impact physical, social, and mental health and well-being, enhancing the mood of people and kids (Dushkova & Ignatieva 2020). Although the provision of ecosystem services and the well-being of people in cities are associated, written documents to reflect their importance are rare in Lahore. Similarly, people benefit from these facilities by visiting the parks; however, they are unaware of ecosystem services. In this context, this study aims to highlight the visitors' preferences to visit the parks by examining the available ecosystem services. It will be helpful for the park's administration and planners to improve the ecosystem services for the well-being of people according to their choices.

MATERIAL AND METHODS

Study area

Lahore, a metropolitan city, has an almost 11 million population, according to the census of 2017. The urban population worldwide ranked 56th in 1975, 38th in 2007, and will be at 24th in 2025. Due to the high growth rate and fast urbanization, the city has physically and socially transformed. The metropolitan has just 3% green area, which is very low compared to the global standard, 25-30% minimum value (Imran & Mehmood 2020). They were classified into three categories based on their size, i.e., small <1 hectare, medium 1.1 – 4.5 ha, and large >4.6 ha, according to Ballester-Olmos and Morata's classification. Thus, available green spaces become insufficient for many people, and parks' constraints can be easily observed. It is also worth mentioning that per capita green space is shallow in Lahore except for Gulberg town, compared to the world's minimum value of 9 m^2 per inhabitant (Alam et al. 2014). Consequently, the parks in the study area are insufficient and unequally distributed, directly influencing the quality of life. In this study, fifteen parks in Lahore (Bagh e Jinnah, Botanical Garden Jallo, Family Park Samanabad, Fatima Jinnah Ladies Park, FCC Park, Greater Iqbal Park, Gulabi Park, Gulshan e Iqbal Park, Jam e Shirin Park, Jillani Park, Nadra begum Park, Nasir Bagh, National Bank Park, Rahmania Park and Tomb Nur Jahan Park) were chosen for the study as shown in figure 1.

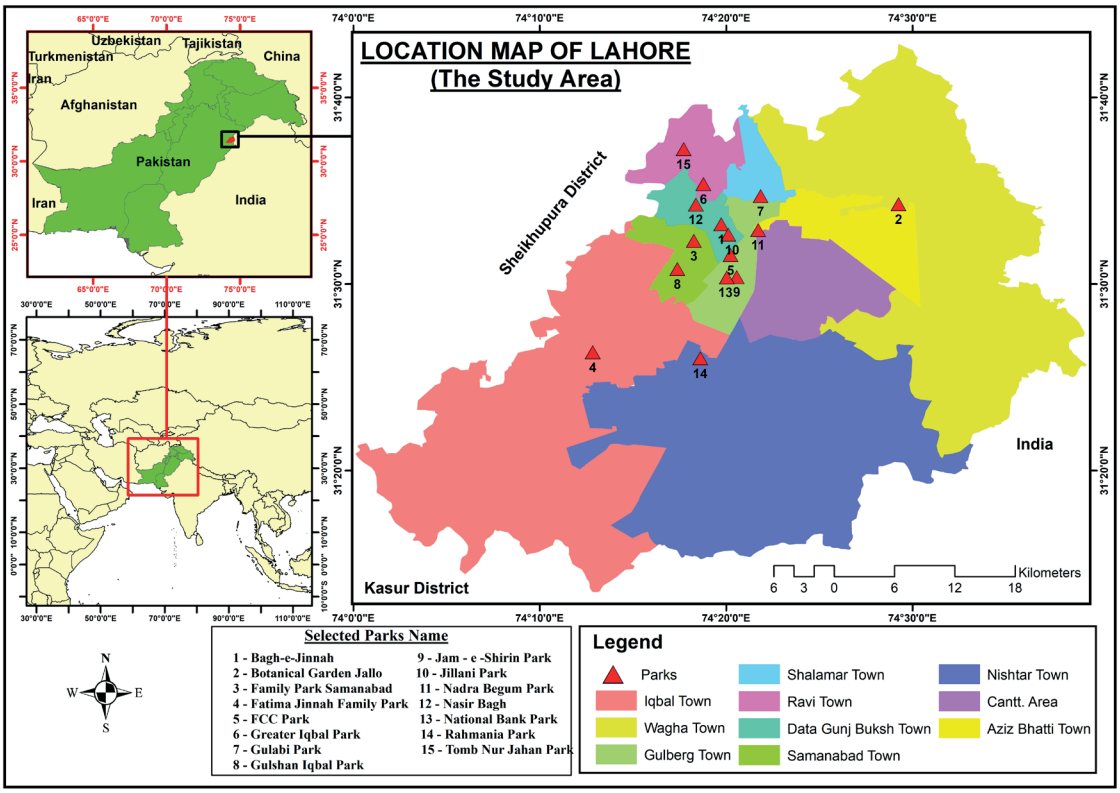

Fig. 1. Location of the Study Area and Selected parks

Data Collection

The study was based on primary data; therefore, a questionnaire-based survey was conducted in the selected parks (shown in figure 1) to observe and record the information. The questionnaire was divided into socio-demographic information, usage pattern, visitors' preferences, and perceptions. A total of 300 questionnaires were get filled out by visitors.

Statistical analysis

The study performed Principal Component Analysis (PCA) according to the nature of the data. The usage of PCA was to highlight the association between spatial, socio-economic, and ecological components and the park's area (Ayala-Azcárraga et al. 2019). In contrast, the suitability of the data was checked by performing the KMO and Bartlett's test of sphericity. Previously, European researchers performed it to check the homogeneity of variance (Kothencz & Blaschke 2017). In addition, the agglomerative Hierarchical Clusters and Preference Map was drafted in XLstat version 2014.05.03. A Chi-square test was also conducted to show the association between different variables identified in parks. For example, the Chi-square test with Cramer's V showed the association of socio-demographic attributes and visitors' choices to the parks (Mak & Jim 2019).

The variables computed by SPSS for conducting PCA were denoted under eight factors shown in table 1.

The perceived variables by the visitors, as shown in table 1, were utilized in Principal Component Analysis. The Correlation Matrix examined the association between these variables. KMO and Bartlett's test depicts a .000 significance level smaller than the alpha value .05, as shown in table 2. Kaiser-Meyer-Olkin also indicates the significant means of variables with a sampling adequacy value of .726. In this way, a total of eight factors were generated through PCA. The Rotated component matrix of these eight factors is shown in Annexure A.

RESULTS AND DISCUSSION

The results showed that visitors rated small size parks with the lowest score due to few facilities. It is also evident that very few visitors came to these parks. Usually, the people residing near these parks come there more often. In comparison, parks of medium and large size have spacious areas and generate many ecosystem services. Thus, more people came to visit these parks. The number of visitors to various parks is depicted

Table 1. Variables that integrate the eight factors evaluated for urban parks

Sr. No.	Factors	Variables
1	Visitors' opinions on the present condition of the park	• Vegetation in park • Size of park • Diversity in Parks • Attractiveness • Accessibility • Crowd in park • Pleasant to spend time in parks
2	Usage pattern of Parks	• Means of transportation. • Distance of park from residency • Frequency of visit • The most satisfying facility in a park
3	Socio-environmental perspective	• Accompanied with • Importance to live near a park
4	Social status of visitors	• People's familiarity with the benefits of park • Education level • Employment status
5	Health satisfaction with parks	• Satisfaction level of health by visiting a park. • Gender
6	Preference dependency and age group	• Preference for any green area near the residence • Age Groups
7	The socio-economic pattern of visitors	• Time to stay. • Income group
8	Services attraction	• Wish to find any activity to do in a park. • Preferred activity to do in a park. • Quality of park for which it is famous. • Purpose of visit

Table 2. KMO and Bartlett's test of sphericity

KMO and Bartlett's Test		
Kaiser-Meyer-Olkin Measure of Sampling Adequacy.		.726
Bartlett's Test of Sphericity	Approx. Chi-Square	1468.768
	Df	300
	Sig.	.000

in figure 2. The maximum number of people coming to Greater Iqbal Park is due to its vast area, ideal location, and various ecosystem services. Similarly, many visitors visited Jillani park due to its scenic beauty and good quality of services.

People usually do not compromise on the facilities. So, they travel a long distance to seek their desired services in parks. Therefore, it can be assumed that the visitors' preference is available parks' services rather than the size. It can also be understood from figure 3 that without considering the park's size, 225 respondents (75%) had to travel for more than 1000 meters distance to access the park.

It also shows that 9.3% of people visit the parks between 500-1000 meters. At the same time, 15.7% can access parks by covering 500 meters distance. It can be assessed that these are mostly community parks or located very near people's residences.

PCA was performed based on the park's attributes and availability of facilities. On the x-axis and y-axis, the value range of Pearson's Correlation matrix is shown from -1 to +1, as shown in figure 4. PCA was also used to highlight respondents' preferences for the existing infrastructure of urban green spaces in Oslo, Norway (Soy Massoni, Barton, Rusch, & Gundersen 2018). According to the result, principal component analysis reveals 60.35% of the total variance. Previously, a similar result (60.74%) was shown between environmental and infrastructural attributes in the study of urban parks in Mexico City (Ayala-Azcárraga et al. 2019). Fig 4 indicates the variation in visitors' opinion on these attributes with a change in parks. It is worth mentioning that only positively associated variables are shown through PCA. Variables of parks analyzed for PCA are mentioned in Annexure A. Most visitors choose to visit those parks, where different appetence is fulfilled such as near the homes, a speciality of the park for which they are famous, the most satisfying services.

On the other hand, few visitors do not choose to visit the parks due to little greenery, populace place, and minor diversities. The parks with medium and large areas provide many facilities, e.g., more greenery, silent area, rich diversities, more panoramic views, spacious places, and leisure time. Thus, large and medium parks provide much more facilities and have a good framework than small parks.

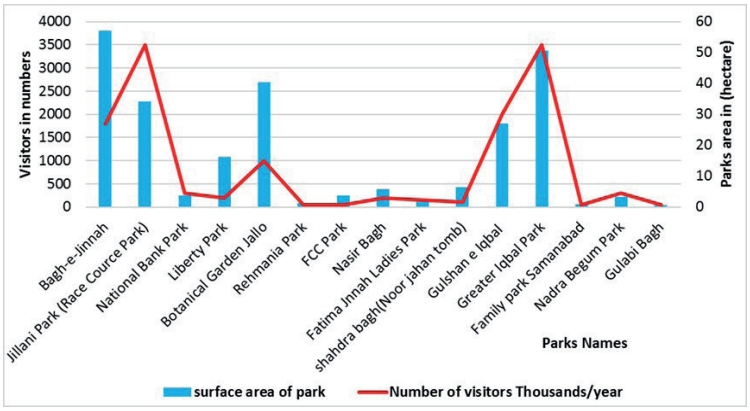

Fig. 2. Park area and number of visitors

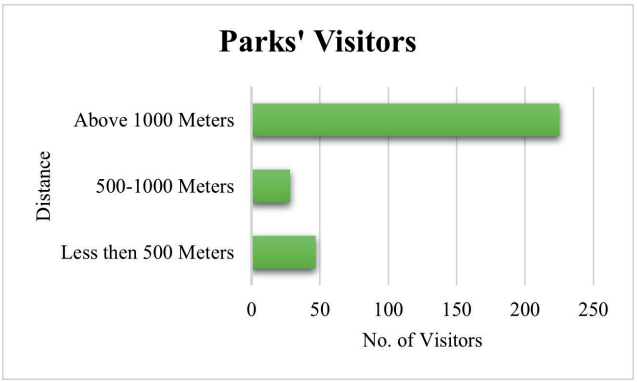

Fig. 3. Number of respondents and range of distance to access parks

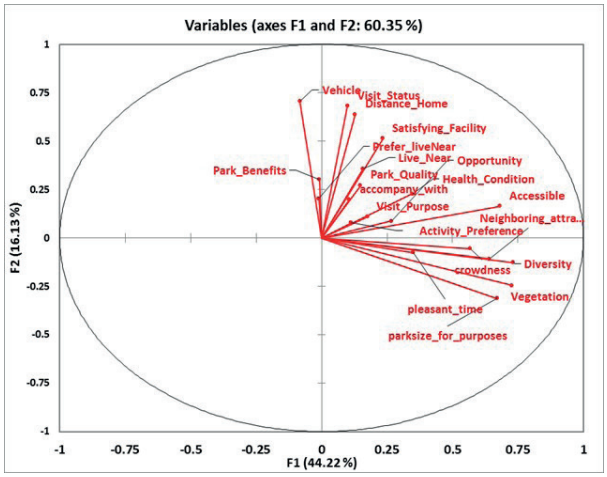

Fig. 4. Patterns of association between variables and size of parks

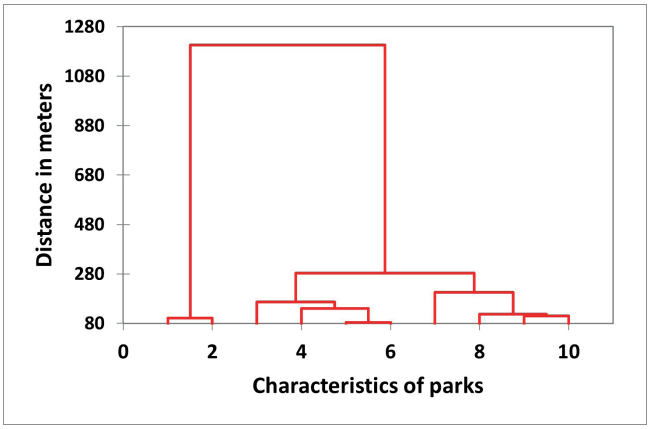

Fig. 5. The dendrogram based on Dissimilarity

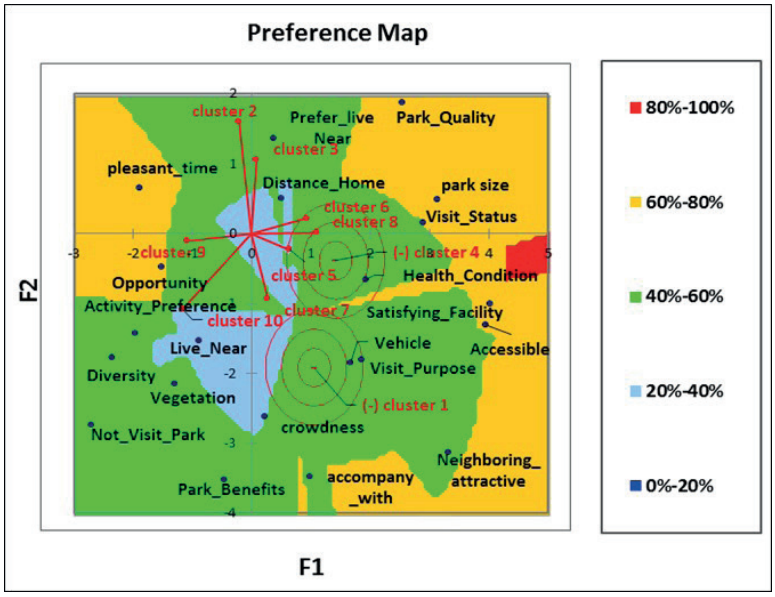

Fig. 6. Preference map

Ten (10) parcels based on dissimilarities found in the attributes of parks according to people's preferences for visiting the parks are shown in figure 5. Dendrogram usually shows natural grouping among a set of variables. The two adjacent parcels fuse at every phase of analysis until all the attributes form a set of clusters called dendrogram (Vieira et al. 2018). The dendrogram highlights ten parcels generated by utilizing the factor loading value of PCA.

In figure 6, the preferences of people who visit the parks are presented based on their liking scores. It is observed that 20-40% of visitors preferably visit the parks near or at a minimum distance from their homes. So, most of the time, people residing adjacent to parks choose to visit small and medium-sized parks. While, 40-60% of visitors come to medium-sized parks, where various services like high diversity, more greenery, satisfactory health level, and accessibility of preferred services can be found. Despite that, 60-80% of visitors like to come to large parks due to the wide range of facilities both in quantity and quality, as they have passion and want to enjoy nature by investing time in large-sized parks. So, they covered a long distance to come to large parks to utilize the services generated by parks. Therefore, it shows that visitors are attracted to the services regardless of the distance to reach the parks.

CONCLUSION AND SUGGESTIONS

Urban parks provide various ecosystem services, which are beneficial for the citizens. Identification of these services is essential for the better management of green spaces in cities. Due to their contribution to improving well-being, visitors' preferences are also inevitable for improving existing and developing new parks. In this context, 15 parks in Lahore, a megapolitan city in Pakistan, were studied to record the visitors' preferences for visiting the parks. The study found that visitors have different preferences in visiting the parks. They mostly preferred those parks with maximum ecosystem services regardless of the distance of parks. Therefore, it is concluded that the availability of ecosystem services is a primary preference for visitors visiting Lahore parks.

Moreover, the city residents ignored distance to avail more ecosystem services as people enjoy services even though they must travel long distances like more than 1000 meters. This study also determines that the attributes of urban parks in generating services for the well-being of people cannot be ignored. Therefore, it is suggested that the attributes of parks like the diversity of vegetation, recreational activities, and easy access to parks should be considered for future planning. These specified attributes should be identified and conveyed to the management for developing urban parks in this context. It is expected that the study may be helpful in the improvement of existing facilities and the establishment of parks in the future to gain maximum benefits for the visitors' well-being.

REFERENCES

Alam R., Shirazi S.A., Zia S., & Minallah M. (2014). SPATIAL DISTRIBUTION OF URBAN GREEN SPACES IN LAHORE, PAKISTAN: A CASE STUDY OF GULBERG TOWN. Pakistan journal of science, 66, 277-281.

Ambiental P., & del Distrito Federal O. T. (2010). Presente y Futuro de las Áreas Verdes y del Arbolado de la Ciudad de México. México, DF, México.

Ayala-Azcárraga C., Diaz D., & Zambrano L. (2019). Characteristics of urban parks and their relation to user well-being. Landscape and Urban Planning, 189, 27-35.

Battisti L., Pomatto E., & Larcher F. (2019). Assessment and Mapping Green Areas Ecosystem Services and Socio-Demographic Characteristics in Turin Neighborhoods (Italy). Forests, 11, 25, DOI:10.3390/f11010025

Dalton S.E. (2011). Application of the human ecosystem model in warfare ecology. In Warfare Ecology (pp. 245-257): Springer.

Delgadillo Polanco V.M. (2012). El derecho a la ciudad en la Ciudad de México.¿ Una retórica progresista para una gestión urbana neoliberal? Andamios, 9(18), 117-139.

Dushkova D., & Ignatieva M. (2020). New trends in urban environmental health research: from geography of diseases to therapeutic landscapes and healing gardens. GEOGRAPHY, ENVIRONMENT, SUSTAINABILITY, 13, 159-171, DOI:10.24057/2071-9388-2019-99

Gatersleben B., & Andrews M. (2013). When walking in nature is not restorative—The role of prospect and refuge. Health & place, 20, 91-101.

Giles-Corti B., Johnson M., Knuiman M., Collins C., Douglas K., Ng K., . . . Donovan R. (2005). Increasing walking:: How important is distance to, attractiveness, and size of public open space? American journal of preventive medicine, 28, 169-176.

Hanif A., Shirazi S.A., & Majid A. (2020a). ASSESSING QUALITY OF LIFE THROUGH PEOPLE'S PERCEPTION: A CASE STUDY OF LAHORE-PAKISTAN. J. Agric. Res, 58(4), 289-295.

Hanif A., Shirazi S.A., & Majid A. (2020b). Role of community for improvement of ecosystem services in urban parks. Pakistan Journal of Agricultural Sciences, 57(6).

Imran M., & Mehmood A. (2020). Analysis and mapping of present and future drivers of local urban climate using remote sensing: a case of Lahore, Pakistan. Arabian Journal of Geosciences, 13, DOI:10.1007/s12517-020-5214-2

Jabbar M., Yusoff M.M. & Shafie A. (2021). Assessing the role of urban green spaces for human well-being: a systematic review. GeoJournal, DOI:10.1007/s10708-021-10474-7

Jabbar M., Yusoff M.M. (2022a). Assessing The Spatiotemporal Urban Green Cover Changes and Their Impact on Land Surface Temperature and Urban Heat Island in Lahore (Pakistan). GEOGRAPHY, ENVIRONMENT, SUSTAINABILITY, 15(1):130-140, DOI:10.24057/2071-9388-2021-005

Jabbar M., & Yusoff M.M. (2022b). Assessing and Modelling the role of urban green spaces for human well-being in Lahore (Pakistan), Geocarto International, DOI: 10.1080/10106049.2022.2087757

Jardine A., Speldewinde P., Carver S., & Weinstein P. (2007). Dryland salinity and ecosystem distress syndrome: human health implications. EcoHealth, 4(1), 10-17.

Kothencz G., & Blaschke T. (2017). Urban parks: Visitors' perceptions versus spatial indicators. Land Use Policy, 64, 233-244, DOI:10.1016/j.landusepol.2017.02.012

Liu Y., Fan Y., & Huang K. (2013). Service ecosystem evolution and controlling: A research framework for the effects of dynamic services. Paper presented at the 2013 International Conference on Service Sciences (ICSS).

Lü Y., Fu B., Feng X., Zeng Y., Liu Y., Chang R., . . . Wu, B. (2012). A policy-driven large scale ecological restoration: quantifying ecosystem services changes in the Loess Plateau of China. PloS one, 7(2), e31782.

Mak B.K.L., & Jim C.Y. (2019). Linking park users' socio-demographic characteristics and visit-related preferences to improve urban parks. Cities, 92, 97-111, DOI: 10.1016/j.cities.2019.03.008

McCormack G.R., Rock M., Toohey A. M., & Hignell D. (2010). Characteristics of urban parks associated with park use and physical activity: A review of qualitative research. Health & place, 16(4), 712-726.

Pazhouhanfar M., & Kamal M. (2014). Effect of predictors of visual preference as characteristics of urban natural landscapes in increasing perceived restorative potential. Urban Forestry & Urban Greening, 13(1), 145-151.

Rechkemmer A., & Von Falkenhayn L. (2009). The human dimensions of global environmental change: Ecosystem services, resilience, and governance. Paper presented at the EPJ Web of Conferences.

Rey Gozalo G., Morillas J., González D., & Moraga P. (2017). Relationships among satisfaction, noise perception, and use of urban green spaces. Science of The Total Environment, 624, 438-450, DOI:10.1016/j.scitotenv.2017.12.148

Sinchembe M., & Ellery W. (2010). Human impacts on hydrological health and the provision of ecosystem services: a case study of the eMthonjeni–Fairview Spring Wetland, Grahamstown, South Africa. African Journal of Aquatic Science, 35(3), 227-239.

Vieira J., Matos P., Mexia T., Silva P., Lopes N., Freitas C., . . . Pinho P. (2018). Green spaces are not all the same for the provision of air purification and climate regulation services: The case of urban parks. Environmental research, 160, 306-313.

Wang Z., Liu Z., Song K., Zhang B., Zhang S., Liu D., . . . Yang F. (2009). Land use changes in Northeast China driven by human activities and climatic variation. Chinese Geographical Science, 19 (3), 225-230.

Annexure A

Rotated Component Matrix

	Component							
	1	2	3	4	5	6	7	8
Present condition of vegetation in park	.770							
Presence of diversity	.764							
Present condition of park's size	.721							
crowd in park	.676							
Accessibility	.670							
Attractiveness	.646							
Means of transportation		.772						
Distance of park from residency		.763						
Frequency of visit		.741						
Most satisfying facility in park		.510						
Time to stay			.798					
Income group			.728					
Accompanied with			.698					
Employment status			.697					
Importance to live near park			-.513					
Satisfaction level of health by visiting park				.696				
Gender				-.660				
Feel pleasant to spend time in park								
Preference of any green area near residence					.692			
Age Groups					-.516			
Quality of park for which it is famous						.754		
Purpose of visit						.818		
Preferred activity to do in park						.601		
people's familiarity about benefits of park							.688	
Education level							.592	

RESEARCH PAPER

SEAGRASSES AT THE ISLANDS ITURUP AND URUP OF KURIL ARCHIPELAGO

Anton A. Iurmanov[1*], Igor Yu. Popov[2], Mikhail S. Romanov[1]
[1]Main Botanical Garden named after N. V. Tsitsin RAS, Botanicheskaya st., 4, Moscow, 127276, Russia
[2]Saint-Petersburg State University, Universitetskaya Embankment, 7/9, Saint-Petersburg, 199034, Russia
***Corresponding author:** yurmanov–anton.ya.ru@yandex.ru
Received: October 2nd, 2022 / Accepted: November 11th, 2022 / Published: December 31st, 2022
https://DOI-10.24057/2071-9388-2022-017

ABSTRACT. The islands Iturup and Urup of Kuril Archipelago have been understudied in respect of seagrasses. The research aimed to fill this gap. In 2019 during the expedition of the Russian Geographical Society a part of the coastline has been surveyed by walking, the beached remains of seagrasses and the seagrasses growing on the littoral have been registered. The length of the routes was 95 km. The possible sources of negative anthropogenic impact have been examined. Herbarium collections of several institutions (LE, LECB, MHA, MW, MWG, SAK, Kamchatka Branch of Pacific Geographical Institute of the RAS, the Herbarium of Kronotsky Nature Reserve) have been explored. Three species of seagrasses occur at Iturup and Urup: *Zostera marina* L., *Zostera asiatica* Miki, and *Phyllospadix iwatensis* Makino. The last two species are of particular interest as they are threatened and distributed over a relatively small area. Unlike the habitats of the main part of their range located at the coasts of Japan and Korea, the habitats of the studied islands do not suffer from anthropogenic pressure. The discovered northern refuge is significant for the seagrasses conservation. Current global warming and increasing anthropogenic pressure on the southern habitat would increase its significance. It is especially important for *Phyllospadix iwatensis* as it turned out to be rather numerous at the studied islands. The other two species occur in small numbers there.

KEYWORDS: seagrasses, *Zosteraceae, Zostera marina, Zostera asiatica, Phyllospadix iwatensis*, Kuril Islands

CITATION: Iurmanov A. A., Popov I. Yu., Romanov M. S. (2022). Seagrasses At The Islands Iturup And Urup Of Kuril Archipelago. Geography, Environment, Sustainability, 4(15), 39-43
https://DOI-10.24057/2071-9388-2022-017

ACKNOWLEDGEMENTS: The authors are grateful to the Russian Geographical Society for the organization of the expedition to Iturup and Urup islands. A. Iurmanov and M. Romanov acknowledge the support of the Russian Foundation for basic research, the project No 19–34–90164, and the project of Main Botanical Garden No 18–118021490111–5. The work was carried out by M. Romanov in accordance with institutional research project No 122042700002-6.

Conflict of interests: The authors reported no potential conflict of interest.

INTRODUCTION

Seagrasses are a group of underwater monocotyledonous plants (Monocotylendoneae - Alismatales) widely distributed over coastal waters of all continents except Antarctica (Hogarth 2015). Their congregations form «underwater meadows» providing an environment for numerous animals and algae; these meadows are especially valuable habitats (Nagelkerken and Velde 2004). Seagrasses are sensitive to anthropogenic influences. Economic activity in the coastal zone increases eutrophication, siltation, and turbidity in shallow waters causing the decline of the underwater meadows (Duarte 2002; Short et al. 2011; Unsworth et al. 2014). The intentional extermination of seagrasses by humans also occurs as they are used as raw materials for the manufacture of various products. Many species of seagrasses are declining (Orth 2006; Waycott and Williams 2006). This happens especially dramatically in the case of species having a small range. Such species are known for the coastal waters of Japan, Korea, and neighboring territories of Russia and China. *Phyllospadix iwatensis* Makino and *Zostera asiatica* Miki belong to this category. The first one was assigned to the «vulnerable» category of the IUCN red list, the second one – to «near-threatened» but approaching «vulnerable»; in Japan, it is considered «vulnerable» (Short and Waycott 2010ab). The northern parts of the range of these species, i.e. coastal waters of Russia are insufficiently studied. Most of the performed studies took place on the southern coasts of the mainland (Kalita and Skriptsova 2014; Levenets and Lebedev 2015; Mitina et al. 2016; Kulepanov and Drobyazin 2018). The relatively northern waters including the Kuril Islands remain especially understudied. The specimens from the Kuril Islands were mentioned in Russian sources, but without details; most of the studies in this field were carried out in the 1960s (Kusakin et al. 1974; Ivanova and Tsurpalo 2017). Moreover, some data on the seagrasses of southern Kuril Islands were obtained in 1990-2000 in process of studies of algae (Evseeva 2007). According to these sources, *Phyllospadix iwatensis* occurs at Iturup Island; and its occurrence at Urup is likely as it was noted at Simushir Island located northwards from Urup. Moreover, *Zostera marina* L. was reported for Iturup. This species is not considered threatened globally and has a big range (Short et al. 2010). However, it still draws attention. In the past, it was especially abundant forming underwater meadows,

but now these meadows are shrinking rapidly. It concerns not only general challenges to biodiversity conservation but commercial fisheries as well, as fishes use them as substrates for spawning (Klimova et al. 2015).

The information of the seagrasses at Kuril Islands required updating. We have done this work for the Urup and Iturup islands, which are the largest islands of the Kuril archipelago. Our hypothesis was that threatened seagrasses are in a good state at these islands in contrast to the main part of the range, because, unlike the latter, the islands are poorly developed in terms of economic activity and settlement. Here we present the results of its testing.

MATERIAL AND METHODS

Iturup and Urup islands are ribbon-shaped with uneven edges stretching out from southwest to the northeast (Fig. 1). Iturup is 200 km long, its width is from 7 to 27 km; Urup is 117 km long and up to 20 km wide. Iturup is populated and developed compared to the other Kuril Islands, but the developed plots occupy a small part of its territory. Only 6500 people live there, while most of the population is concentrated in the middle of the island. The southern half of the island is considered a protected area; visits are usually not allowed there. Urup is almost undeveloped and unpopulated (Atlas of the Kuril Islands 2009). There are two lighthouses located at its southern and northern extremes, where a few people reside. Recently, mining for gold has started on the southern end of the island, and a small shift camp was built. Both islands are distant from the mainland; the possibilities for their survey are limited by short expeditions.

In 2019, an expedition for a comprehensive study of the islands Iturup and Urup was organized by the Russian Geographical Society. It took place from July 17 to September 25. We took this opportunity to study seagrasses. On both islands we surveyed sections of the coastlines by traveling on foot; doing so, we recorded congregations of seagrasses in the water, visible from the shore, as well as the beached remains. In such a way most of the obtained data concern *Phyllospadix iwatensis* as it inhabits the shallow waters up to the depths of 4.5 m. The other seagrasses usually occur deep, therefore we could only register their beached remains. We described the specifics of surveyed habitats, including possible sources of negative impacts. The length of the routes was 55 km on Iturup and 40 km on Urup (Fig. 1). The herbarium specimens have been collected and stored in Tsitsin Main Moscow Botanical Garden of Academy of Sciences (MHA); they have been used in the studies on phylogeny and morphology (Iurmanov et al., 2020, 2021). The species identification was carried out using the Keys to Plants of the Soviet Far East (Voroshilov 1982).

In addition to the survey we looked for the information on seagrasses at Urup and Iturup islands in the herbarium collections of several institutions: Komarov Botanical Institute (LE), Saint Petersburg State University (LECB), Tsitsin Main Moscow Botanical Garden of Academy of Sciences (MHA), Moscow State University Faculty of Biology (MW), and Faculty of Geography (MWG), Institute of Marine Geology and Geophysics Far Eastern Branch Russian Academy of Sciences (SAK), Kamchatka Branch of Pacific Geographical Institute of the Russian Academy of Sciences (PGI FEB RAS, Petropavlovsk-Kamchatsky, the acronym of the herbarium is missing), the Herbarium of Kronotsky Nature Reserve (KR, Elizovo, the acronym of the herbarium is missing).

RESULTS

We have found *Phyllospadix iwatensis* on both islands. On Iturup Island the growing individuals and beached remains occurred at south-eastern and western coasts. It was registered at the coastline growing on various substrates – boulders, sand plots between stones, or dense tufa (Fig. 1). In some places it formed small underwater meadows, solitary individuals also occurred. The seagrasses growing on tufa had especially big rhizomes; it was up to 7 mm thick; these rhizomes formed dense tussocks. The grasses on sand have not formed such tussocks; they were much thinner;

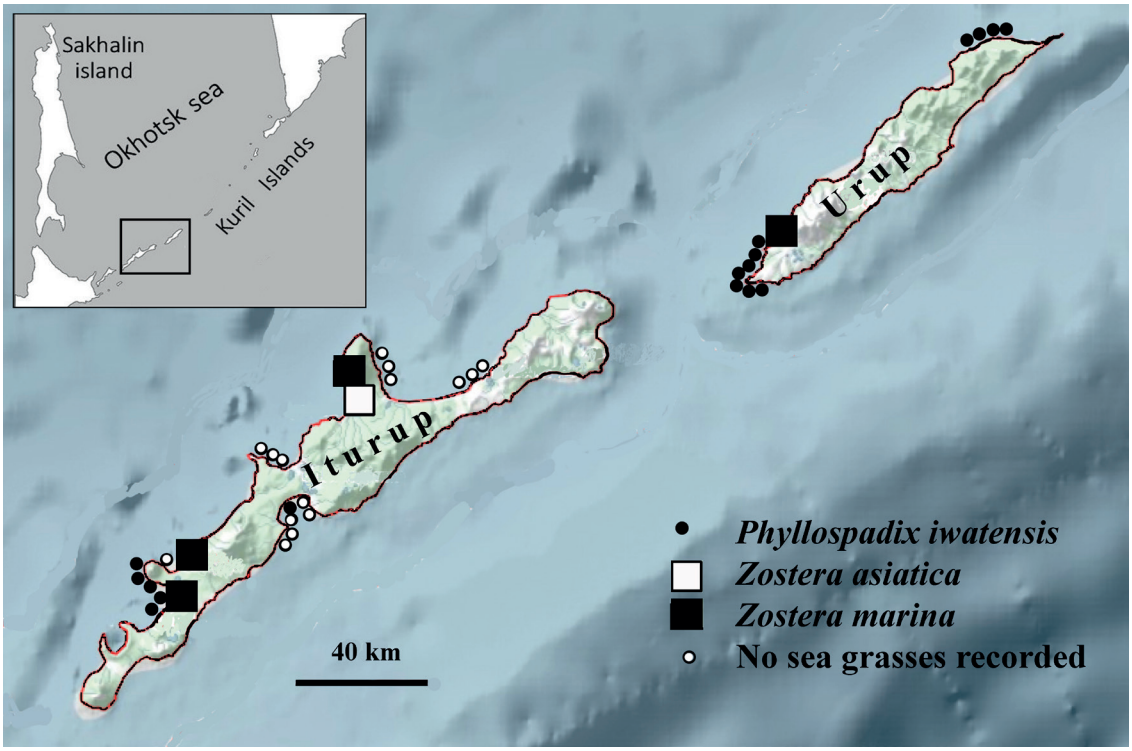

Fig. 1. Study area and the results of the survey: ● – records of *Phyllospadix iwatensis* , ■ – records of *Zostera marina*, – record of *Zostera asiatica*, ❍ – no sea grasses found

(decipher the symbols on the map: square, empty circle, full circle)

their rhizome was about 1.5 mm. thick. The coast section, in which it was not found, represented beaches with sand or peddles. As for the Urup island, *Phyllospadix iwatensis* was found over the entire surveyed area. Especially big aggregations were observed in the northern section. In addition to *Phyllospadix iwatensis* we registered species of *Zostera*. The beached remains of *Zostera marina* were found in both islands. One specimen of *Zostera asiatica* was found at the Kurilsk City on Iturup; it is the most populated place. All beached remains were not numerous compared to algae. The latter were abundant; they often composed long stripes several meters wide at the coastline. Most of the bottom of the littoral was also covered by algae. The seagrasses usually occupied small depressions between stones covered by algae (Fig. 2).

No strong negative anthropogenic impacts on seagrasses have been identified. All surveyed areas of the coastline and littoral have been in their natural state. Development in the coastal zone affects an insignificant part of the water area – except for a few small berths, we have not seen any constructions. There was no aquaculture in the coastal area. Any other sources of intensive eutrophication were not found. The main economic activity on Iturup is associated with fishing, which is carried out by trap-nets affecting a little the seagrass habitats. The deposit exploration on Urup, at least at the time of the study, was distant from the coastal zone.

The studied herbarium collections do not have specimens from Iturup and Urup. There are some data only for the territory nearby. In the islands located southwards from Iturup the same species were registered, as well as the other species *Zostera japonica*. Northern Kuril Islands represent a gap in collections. Further north, in Kamchatka and Commander Islands, only *Zostera marina* occurs.

DISCUSSION

The obtained data indicate the fact that seagrasses are rather common around the islands Urup and Iturup. However, their biomass is not very big and they hardly form big areas of underwater meadows. Had they been abundant, their beached remains would be much more numerous. In the case of big numbers of seagrasses, their remains in wrack zone formed barrages up to 1.5 m. high after storms; their commercial use was possible (Morozova-Vodianitskaya 1939). The amount of such organic materials can be so large that it affects to development of marine shores (Vacchi et al., 2017). In the case of Kurils, the storms can be very strong, but even small «stacks» of seagrasses were not found. Probably, the lack of suitable substrates and relatively small areas of shallow waters restrict their number. Despite this, the revealed habitats are significant at least for *Phyllospadix iwatensis*. A small number of registration sites are known for this species in the main part of the range, and they are located near the coasts exposed to strong anthropogenic pressure. In our case, the habitats occupy a large area and nothing threatens them so far. The economic activity develops slowly and has little effect on seagrasses. The direct extermination of seagrasses is also not expected in a near future over studied area. Seagrasses were harvested in the 1930-1960s in the Russian Far East as stuff for upholstered furniture and a packaging material (Kulepanov 2005), as well as for the manufacture of paper and fertilizers (Kardakova 1953). But currently seagrasses are not in use for this. The use of seagrasses is considered in the context of possibilities for extraction of therapeutic and prophylactic substances (Aminina 2005), but large-scale harvesting still does not take place. Although it should be noted that seagrasses are not considered protected in Russia, they are still discussed by scientists in the context of the search for potential raw materials, but not an object requiring conservation measures (Dulenin 2012; Mitina et al. 2016).

Since the seagrasses were not properly investigated in the past in the area under consideration, we do not know for sure whether the *Phyllospadix iwatensis* or *Zostera asiatica* lived there «initially», or they have recently increased in numbers and expanded the range due to climatic changes. Anyway, the surveyed islands turned out to be a «reserve» for vulnerable species of seagrasses, at least for *Phyllospadix iwatensis*. The lack of suitable substrates is believed to be the reason for the limited distribution

Fig. 2. Typical aggregation of *Phyllospadix iwatensis*, the northern coast of Urup Island. 2.09.2019. (Photo by Igor Popov)

of this species (Iurmanov, 2022a). Unlike most seagrasses it inhabits the specific congregations of stony substrates. Suitable habitats have a small area for natural reason, therefore with an increase of anthropogenic impact the risk of catastrophic decline is high. In the Chinese part of the range, this has already happened because of extensive kelp aquaculture (Short and Waycott 2010a). In our case, the habitats occupy a large area. Probably, the same is true for the northern Kuril Islands. Taking into account the current global warming this extension can be relatively large. The boundaries of the ranges of several species are currently shifting northwards (Loarie et al. 2009). It is possible that this also concerns the seagrasses at the Kuril Islands. When discussing the impact of climate warming on seagrasses, the negative impacts drew main attention: overgrowth of algae, increase of eutrophication, increase of frequency of storms that either directly destroy grasses, or increase turbidity, etc. (Short and Neckles 1999; Björk et al. 2008). However, the impact of climate warming may be rather positive for some species as it contributes the extension of their habitats.

As for the observed *Zostera* species, they remain understudied during our survey, because only beached remains were registered. They could have been brought from anywhere. However, it is more likely that they sailed from a nearby point than from afar (Iurmanov et al., 2022b). This is especially true for *Zostera asiatica* as it is not abundant. Probably, the Kuril Islands is a «reserve» for this species as well.

CONCLUSIONS

A refuge for the vulnerable seagrasses species was formed at the southern Kuril Islands. There are no negative anthropogenic influences on the habitats of seagrasses. The role of this refuge will increase in the foreseeable future because the main part of their range is located southwards, while in the south the anthropogenic pressure is strong, the habitats of seagrasses are undergoing negative changes. At the same time, northern habitats are becoming more favorable for seagrasses due to global warming. The coastal waters of surveyed islands Urup and Iturup are especially important for the species *Phyllospadix iwatensis*. It turned out to be rather numerous, but it is rapidly declining in the main part of the range located in the waters at Japan, Korea, and the neighboring part of China.

REFERENCES

Aminina N. (2005). Main trends of the studies on algae and sea grasses of Far East. Isvestiya TINRO, 141, 348-354 (In Russian with English summary).

Atlas of Kuril Islands (2009). Moscow, Vladivostok: Russian Academy of Siences. (In Russian).

Björk M., Short F., Mcleod E. and Beer S. (2008). Managing Seagrasses for Resilience to Climate Change. Gland, Switzerland: IUCN.

Duarte C. (2002). The future of seagrass meadows. Environmental Conservation, 29, 192-206.

Dulenin A. (2012). Resources and distribution of commercial macrophytes in the western Tartar Strait (Khabarovsk Territory). Izvestia TINRO, 170, 17-29 (In Russian with English summary).

Evseeva N. (2007). Macrophytobenthos of the coastal zone of southern Kuril Islands. In: Biology, state and environment of hydrobionts in Skhalin-Kuril region and its coastal waters. Proceedings of Sakhalin institute for fisheries. SakhNIRO, 9, 125-145 (In Russian).

Hogarth P. (2015). The Biology of Mangroves and Seagrasses. 3rdEd. Oxford etc.: Oxford University Press.

Iurmanov A., Romanov M. and Bobrov A. (2020). Phylogenetic phytogeography of the family Zosteraceae. Problems of Botany of South Siberia and Mongolia, 19(2), 98-101. (In Russian with English summary).

Iurmanov A., Romanov M. and Bobrov A. (2021). Fruit morphology and histology of Zostera asiatica Miki and Phyllospadix iwatensis Makino (Zosteraceae) in connection with comparative carpology of higher Alismatales. Botany Letters. 168(4), 570-576.

Iurmanov A.A. (2022a). Phylogenetic phytogeography of selected groups of seagrasses (Monocotylendoneae – Alismatales) based on analysing of genes 5.8S rRNA and RuBisCo large subunit. Geography, environment, sustainability. 15(1), 61-69.

Iurmanov A.A., Romanov M.S., Gerb M.A., Volodina A.A., Baikova I.B., Popov I.Y., Markovets M.Y. (2022b). Seagrass Zostera In the Russian Section Of the Baltic Sea. Geography, Environment, Sustainability, 2(15), 111-115.

Ivanova M. and Tsurpalo A. (2017). The Phyllospadix iwatensis community in the intertidal zone of the Far Eastern seas of Russia. Izvestia TINRO, 188, 173-180 (In Russian with English summary).

Kalita T. and Skriptsova A. (2014). Current status of subtidal macrophyte communities in Ussuriysky and amursky bays, Sea of Japan. Russian Journal of Marine Biology, 40, 6. 427-434 (In Russian with English summary).

Kardakova E. and Kizevetter I. (1953). Sea grasses of Far East. Vladivostok: Primorskoye knizhnoye izdatelstvo (In Russian).

Klimova A., Klyukina R., Bonk A. and Klochkova N. (2015). The role of sea weeds in formation of spawning substrate of Pacific herring. Vestnik Kamchat GTU, 31, 60-66 (In Russian with English summary).

Kulepanov V. (2005). Researches of macrophytobenthos at the coast of Primorye. Izvestiya TINRO, 141, 355-364 (In Russian with English summary).

Kulepanov V. and Drobyazin E. (2018). Species composition and quantitative distribution of seaweeds in the sublittoral zone and on the continental slope in the northwestern Japan Sea. Izvestiya TINRO, 195, 151-160 (In Russian with English summary).

Kusakin O., Kudriashov O., Tarakanov T. and Shornikov E. (1974). Belt-forming floristic-faunistic groups of littoral of Kuril Islands. In: Plant and animal world of littoral of Kuril Islands. Novosibirsk: Nauka. 5-75 (In Russian).

Levenets I. and Lebedev E. (2015) Diversity of the intertidal macrophytes of Far eastern marine biosphere reserve FEB RAS (Peter the Great bay, sea of Japan). Proceedings of Dalrybvtuz, 36, 37-48 (In Russian with English summary).

Loarie S., Duffy P., Hamilton H., Asner G., Field C. and Ackerly D. (2009). The velocity of climate change. Nature, 462, 1052-1055.

Mitina N., Malashenkov B. and Gordeev A. (2016) An Assessment of Natural Resource and Economic Potential of the Coastal Waters of the Middle Primorye. Gosudarstvennoye upravleniye, Elektronnny Vestnik, 58, 147-163 (In Russian with English summary).

Morozova-Vodianitskaya N. (1939). Zostera as an Object of Gathering in the Black Sea. Priroda, 8, 49-52. (In Russian).

Nagelkerken I., Velde G. van der (2004). Relative importance of interlinked mangroves and seagrass beds as feeding habitats for juvenile reef fish on a Caribbean island. Marine Ecology Progress Series, 274, 153-159.

Orth R. (2006). A Global Crisis for Seagrass Ecosystems. BioScience, 56, 987-996.

Short F. and Neckles H. (1999). The effects of global climate change on seagrasses. Aquatic Botany, 63, 169-196.

Short F. and Waycott M. (2010a). Phyllospadix iwatensis. The IUCN Red List of Threatened Species. e.T173344A6995596. [online] Avalible at: http://dx.doi.org/10.2305/IUCN.UK.2010-3.RLTS.T173344A6995596.en [Accessed 05 January 2021].

Short F. and Waycott M. (2010b). Zostera asiatica. The IUCN Red List of Threatened Species. e.T173339A6994461. [online] Avalible at: http://dx.doi.org/10.2305/IUCN.UK.2010-3.RLTS.T173339A6994461.en [Accessed 05 January 2021].

Short F., Carruthers T., Waycott M., Kendrick G., Fourqurean J., Callabine, A., Kenworthy, W. and Dennison W. (2010). Zostera marina. The IUCN Red List of Threatened Species. e.T153538A4516675. [online] Avalible at: http://dx.doi.org/10.2305/IUCN.UK.2010-3.RLTS.T153538A4516675.en [Accessed 05 January 2021].

Short F., Polidoro B., Livingstone S., Carpenter K., Bandeira S., Bujang J., Calumpong H., Carruthers T., Coles R., Dennison W., Erftemeijer P., Fortes M., Freeman A., Jagtap T., Kamal A., Kendrick G., Kenworthy W., La Nafie Y., Nasution I., Orth R., Prathep A., Sanciangco J., van Tussenbroek B., Vergara S., Waycott M. and Zieman J. (2011). Extinction risk assessment of the world's seagrass species. Biological Conservation, 144, 1961-1971.

Unsworth R., Keulen van M. and Coles R. (2014). Seagrass meadows in a globally changing environment. Marine Pollution Bulletin, 83, 383-386.

Vacchi M., De Falco G., Simeone S., Montefalcone M., Morri C., Ferrari M., and Bianchi C. N. (2017). Biogeomorphology of the Mediterranean Posidonia oceanica seagrass meadows. Earth Surface Processes and Landforms. 42(1), 42-54.

Voroshilov V. (1982). Keys to Plants of the Soviet Far East. Moscow: Nauka (In Russian).

Waycott M. and Williams S. (2006). A global crisis for seagrass ecosystems. Bioscience, 56, 987-996.

RESEARCH PAPER

DRIVERS OF DEFORESTATION AND FOREST DEGRADATION IN PALAWAN, PHILIPPINES: AN ANALYSIS USING SOCIAL-ECOLOGICAL SYSTEMS (SES) AND INSTITUTIONAL ANALYSIS AND DEVELOPMENT (IAD) APPROACHES

Ronnel C. Nolos[1,2*], Akhmad Zamroni[1,3], Kathleen Faith P. Evina[1,4]
[1]School of Environmental Science and Management, University of the Philippines, Los Baños, Laguna, 4031, Philippines
[2]Department of Environmental Sciences, College of Natural and Allied Health Sciences, Marinduque State College, Boac, 4900, Philippines
[3]Department of Geological Engineering, Institut Teknologi Nasional Yogyakarta, Indonesia
[4]Forestry and Environmental Science Department, College of Agriculture, Forestry, and Environmental Sciences, Western Philippines University, Palawan, Philippines 5302
***Corresponding author:** ronnelnolos@gmail.com
Received: May 26th, 2022 / Accepted: November 11th, 2022 / Published: December 31st, 2022
https://DOI-10.24057/2071-9388-2022-081

ABSTRACT. Palawan Island is home to one of Southeast Asia's largest, oldest, and most diversified rainforests hence it was called the «Last Frontier.» However, the island province's forest is contending with increased conversion of forest lands to plantation and household-level agriculture, intensive mineral mining, illegal logging, and other pressures on its ecosystems. Understanding these factors in relation to the prevalence of deforestation and forest degradation in Palawan is imperative. This paper analyzed these drivers of deforestation and forest degradation in Palawan using the social-ecological systems (SES) and institutional analysis development (IAD) frameworks. A literature review was conducted using a variety of web-based databases and sources and additional data were collected from official websites and reports. The identified major drivers of deforestation and forest degradation in the province include increasing population, migration from lowland to upland areas, illegal logging, mining, wide-scale *kaingin* and oil palm plantation, wildlife poaching, and weak policy implementation and enforcement. These identified drivers can be the target of the government of Palawan for their forest management plans. Additional findings and recommendations of this paper will also aid in the forest management planning in Palawan and other areas where similar settings exist.

KEYWORDS: deforestation, Palawan, social-ecological systems, institutional analysis and development, resource conflict

CITATION: Nolos R. C., Zamroni A., Evina K.F.P. (2022). Drivers Of Deforestation And Forest Degradation In Palawan, Philippines: An Analysis Using Social-Ecological Systems (SES) And Institutional Analysis And Development (IAD) Approaches. Geography, Environment, Sustainability, 4(15), 44-56
https://DOI-10.24057/2071-9388-2022-081

ACKNOWLEDGEMENTS: The authors thank Dr. Jessica Villanueva-Peyraube and Prof. Eduardo Roquiño who gave insights into this paper. They also want to extend their gratitude to Haris Nur Eka Prasetya who created some maps in the paper. They also thank Deutscher Akademischer Austauschdienst (DAAD) and Southeast Asian Regional Center for Graduate Study and Research in Agriculture (SEARCA) for giving scholarship funding for one of the authors (Akhmad Zamroni).

Conflict of interests: The authors reported no potential conflict of interest.

INTRODUCTION

Forests provide some of the world's most important ecosystem services. These include carbon sequestration (Richards and Stokes 2004), hydrologic cycle and nutrient cycling (Waring and Schlesinger 1985), watershed protection (Kramer et al. 1997), habitat for animals and biodiversity (Reeves and Daniels 2020), and livelihood for humans (Chechina et al. 2018) among others. However, just like any other ecosystems, forests are faced with a myriad of threats such as natural and anthropogenic forest fires (Johnson and Miyanishi 2001; Dugarjav et al. 2010; López and Saavedra 2021), climate change (Nikitin et al. 2019; Seidl et al. 2017), pollution (Smith 2012), and deforestation and forest degradation which are considered to be the biggest threats to the forests worldwide (Gichuki 2019). The act or process of converting forest land to non-forest land is known as deforestation, while forest degradation is

a decrease in forest production capacity as measured by forest quality, carbon stock, and vegetation type (Van Khuc et al. 2018). Both threats have far-reaching and long-term detrimental environmental repercussions. Degradation of habitat and loss of biodiversity, impairment of water quality, air pollution, increased emission of greenhouse gases, and diminution of ecosystem goods and services are just a few of these repercussions (Austin et al. 2019; Birhan et al. 2021; Engdaw, 2020; Ghazoul 2015).

The world's total forest area is 4.06 billion hectares (ha), or 31% of the total land area. Since 1990, deforestation has caused the loss of an estimated 420 million hectares of forest around the world (FAO 2020). Between 2015 and 2020, deforestation is expected to increase by 10 million hectares each year, with agricultural development remaining the primary cause of deforestation and forest degradation (Jayathilake et al. 2021). In 2010, 593 million people lived in Southeast Asia, comprising 11 nations (Brunei, Cambodia, East Timor, Indonesia, Laos, Malaysia, Myanmar, Philippines, Singapore, Thailand, and Vietnam). Primary land use and land cover changes, as well as significant deforestation, have taken place in the area due to the increasing need for food, fiber, water, and shelter. Following the Amazon and the Congo Basin as the largest tropical rainforest regions in the world, Southeast Asia saw more dramatic annual deforestation than any other continent in the 1990s. From 2000 to 2010, this area was also a focal point for changes in the forest cover. For instance, Indonesia and Myanmar were listed among the top ten countries with the most significant annual net loss of forests (Dong et al. 2014). Southeast Asian nations had a crucial causal relationship between environmental-demographic factors and a lack of forest cover. The residual forest area was adversely associated with population density. According to numerous studies, the low remaining forest area results from high population pressure. Several factors also contribute to forest degradation, including irresponsible selective logging (both legal and illegal), shifting cultivation, small-holder forest encroachment, fuel wood collection, wood extraction for charcoal production, overgrazing, fires, and even modifications to natural water regimes (Koike et al. 2013). Southeast Asia's leading cause of forest loss has been the expansion of agriculture in the lowlands. In Southeast Asia, conflicts over the ownership and control of natural resources and ecological advantages have a long history. These conflicts range from land occupations and resistance to forest eviction to opposition to mega-dams and mining operations. Land politics has been heavily influenced by land control, alienation, and dispossession since colonial domination (Pichler and Brad 2016).

The Philippines, like many other tropical countries, had a long history of forest loss, with the peak of deforestation occurring between 1977 and 1988, owing to 25-year logging concessions (Araza et al. 2021). The surviving rainforest in the country has been drastically decreased, from almost 70% in the 1900s to less than 10% now (Perez et al. 2020). Palawan Island is home to one of Southeast Asia's largest, oldest, and most diversified rainforests (Supsup et al. 2020). In addition to providing a home for wildlife and a source of income for its citizens, its forests prevent soil erosion, preserve watersheds, and mitigate the impacts of climate change. Despite possessing substantial protected areas and a large share of the country's surviving forests, Palawan is contending with increased conversion of forest lands to plantation and household-level agriculture, intensive mineral mining, illegal logging, and other pressures on its ecosystems. Palawan's natural forest cover decreased from 55 to 48% between 1992 and 2010, with an annual forest loss of 5,500 hectares (Supsup et al. 2020). Other socioeconomic difficulties in Palawan include a lack of renewable energy sources, poor solid waste management in city centers, low conservation activity, and a high poverty rate (Fuentes n.d.). Hence, understanding these factors in relation to the prevalence of forest degradation and deforestation in Palawan is imperative. Analyzing connections between biological and socioeconomic components of forest ecosystems, as well as their ramifications for ecosystem integrity, need a multidisciplinary framework that may give a shared lexicon for understanding emergent interaction patterns (Houballah 2019) as well as the possible causes of its degradation. This can be done by using various frameworks such as the social-ecological systems (SES) and institutional analysis and development (IAD). Such frameworks were used in various settings such as in small-scale fisheries (Basurto et al. 2013), mining (Nilsson et al. 2021), water resource management (Gain et al. 2021), resource governance (Clement 2010) and urban ecosystems (Mincey 2013). However, there were very few studies which analyzed the drivers of deforestation and forest degradation in Palawan with the mentioned frameworks, hence, this study was conducted. Institutional gaps were further identified and policy recommendations were provided.

MATERIALS AND METHODS

Study Area

Palawan is a 1 768-island province in the Philippines located at 9.8349° N and 118.7384° E (Figure 1). The main island is a narrow strip of land that stretches for 625 kilometers and is 40 kilometers broad at its widest point. It is located to the southwest of Luzon. The Sulu Sea is to the southeast and the South China Sea is to the northwest. It is separated from Borneo by the Balabac Strait, with Mindoro Island looming beyond the northeastern Mindoro Strait (NSO 2000). It is a long, narrow island that is the country's largest province and is known to have primary forests with high endemicity of flora and fauna (Araza et al. 2021). On mainland Palawan, there are two major climatic regions: the south-eastern side, which has little rainy season (maximum annual precipitation ≤ 2 000 mm), and the north-western side, which has a more noticeable rainy season (maximum annual precipitation 3 000 mm); both have mean annual temperatures of 27.3–28.0 °C (Supsup et al. 2020).

Literature Review and Data Collection

A literature review was conducted using a variety of web-based databases and sources. Some of the most major web-based databases used in this study include Google Scholar, Science Direct, and Scopus. The search focused on deforestation and forest degradation in the Philippines' Palawan province. A thorough grasp of this case study necessitates a review of some past research (Zamroni et al. 2020). Reading abstracts to comprehend the main idea of the previous study was conducted to deepen understanding of the article (Suprapto et al. 2017).

Annual statistics on forest cover and forest cover decline in Palawan were provided by Global Forest Watch (GFW), an open-source web program that uses real-time data to monitor global forests, Philippines from 2001 to 2020. Other secondary data were collected from the websites of

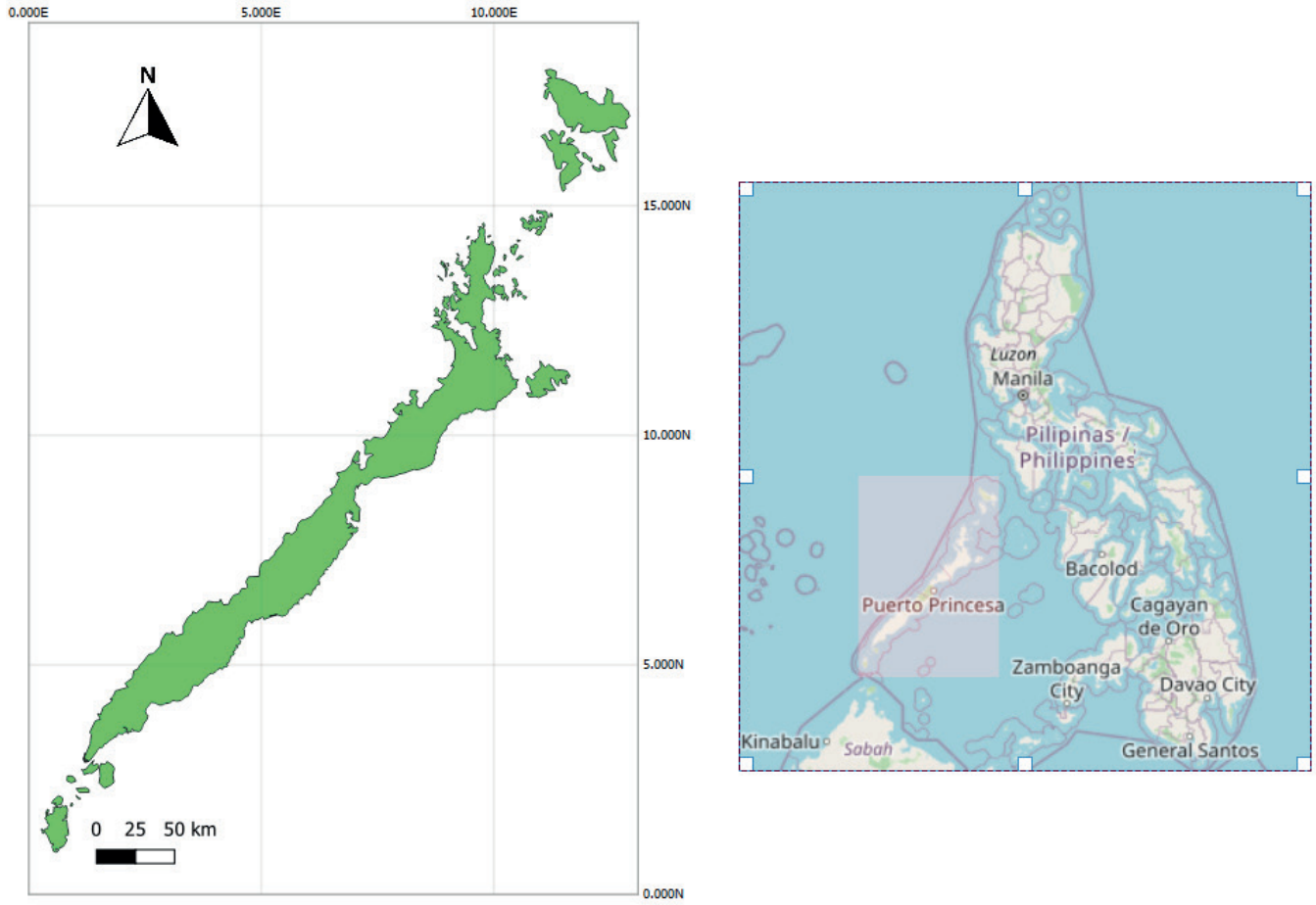

Fig. 1. Map of the study area

DENR-Forest Management Bureau and Philippine Statistics Authority. National and local reports were also utilized in this study.

Social-Ecological Systems (SES) Framework

The SES framework was used to analyze and understand the plethora of variables, its interaction, and outcomes to the forest ecosystem of Palawan, especially the drivers of forest degradation and deforestation (Partelow 2018). It is an important diagnostic tool which can be used to organize variables of interest and level of tier into connected groups. It identifies the characteristics and interactions of resource units, resource system, actors, and governance system, in a specific economic, social, and political setting. Because it is multi-tiered, the SES framework is hierarchical. Each of the variables in the first tier unpacks to expose a number of variables in the second tier, which can then unpack into a third tier, and so on (Basurto et al. 2013; Ostrom 2009). It is utilized a lot in the field of sustainability research.

Institutional Analysis and Development (IAD) Framework

The IAD framework is a multi-tiered conceptual map. Identification of an action arena, subsequent patterns of interactions and repercussions, and evaluation of these outcomes are all part of the framework (Ostrom 2010). Through a nested collection of operational, collective-choice rules, and constitutional, the IAD framework connects the decisions of actors at several governance levels (Clement 2010). It is a powerful analytical tool, particularly when looking at how local institutional structures affect natural-resource governance. This framework could be useful for a variety of tasks in decentralized forest governance research, including 1) establishing favorable conditions for good natural-resource governance, and 2) organizing efforts to track and learn about the impact of previous and current policy initiatives on sustainability (Andersson 2006).

RESULTS AND DISCUSSION

In the Lens of Socio-Ecological Systems Framework

The SES framework used in the Palawan forest case study is shown in Figure 2. The solid boxes represent first-tier categories, such as resource units, resource systems, actors, and governance systems, which are the highest-level variables. At the lower tiers, they have several variables. All of the actions in an action situation take place as interactions and then transform into outcomes. Dashed arrows show feedback from action circumstances to each of the top-tier categories. Any component of the SES can be affected by exogenous effects from linked natural systems or social-economic-political situations.

Social, economic, and political settings

Under this first-tier category, three (3) second-tiers were considered which include the demographic trends (S1), economic development (S2), and political stability (S3). For the demographic trends, there was an increase in the population of both the Palawan province and its capital, the Puerto Princesa City (PSA 2021). In 2000, the population in Palawan province (including Puerto Princesa City) was 755 412. In 2010, the population was 994 340 and in 2015, it was 1 104 585 (Figure 3). In the study of Carandang et al. (2013), it was found that the rapid growing population has a direct impact on the loss of forest cover in the Philippines. They selected sites in various provinces of the country which included Palawan.

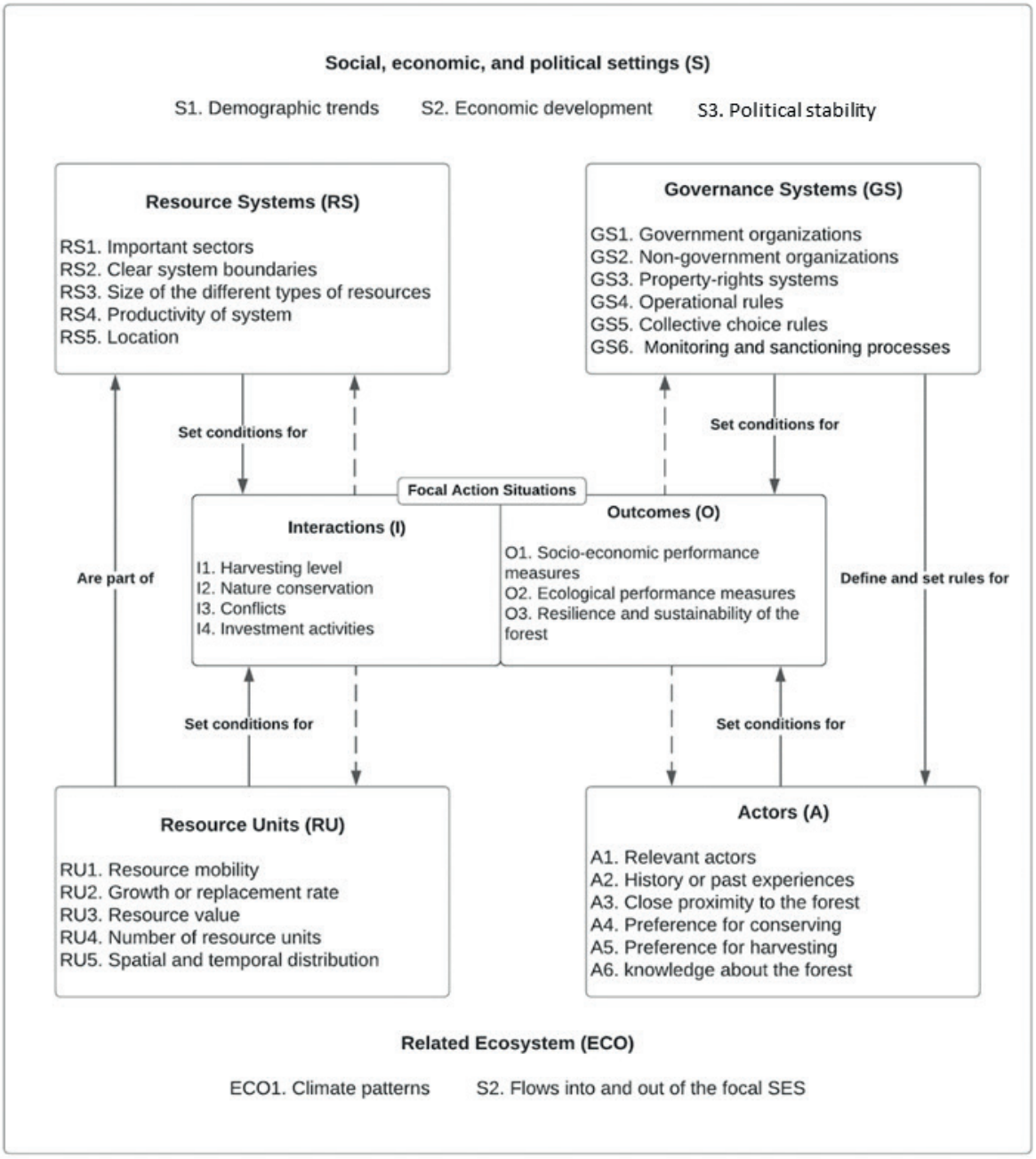

Fig. 2. The modified SES framework for the Palawan case study (Ostrom 2009)

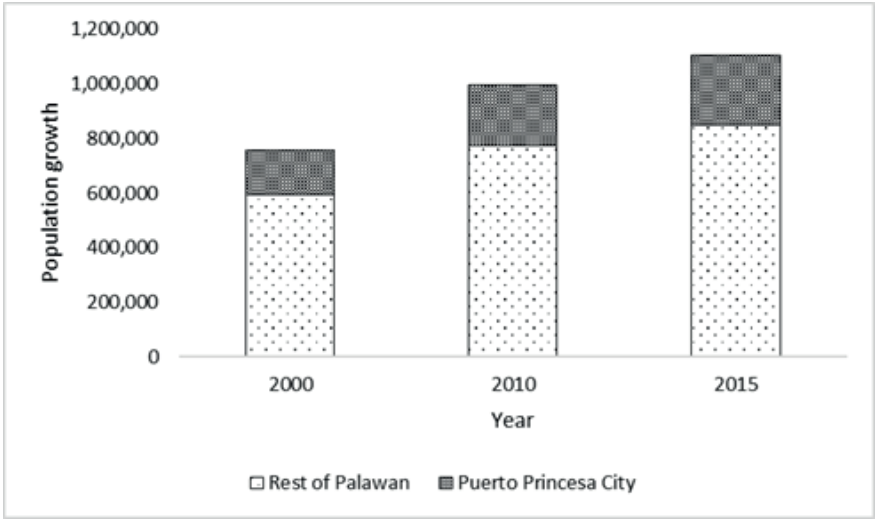

Fig. 3. Population growth in the Palawan province and Puerto Princesa City (2000-2015)

The immediate causes of the disappearance of the forests at a shocking rate are also brought by the settlement of lowlanders and commercial logging. The impacts of immigration and development are also found to increase the impacts not only on the forest but to other resources as well such as fishery, corals, and mangroves among others (Eder 1990).

For economic development, the Palawan province's employment sector is dominated by industry sectors. Figure 4 shows the labor productivity per sector in Palawan from 2009-2017. For agriculture, forestry, and fishing, there was an increasing trend from 68 365 (2009) to 119 321 (2017). The same goes for services where an increasing trend was shown from 116 839 (2009) to 191 751 (2017). However, a decreasing trend was observed for the industry sector where the labor productivity of 488 268 (2009) decreased to 374 266 (2017) (PSA, 2021).

There was also an increasing annual per capita income in the province of Palawan from 1994-2000 (PSA, 2018). The annual income per capita in the province was Php10 582 in 1994, Php18 673 in 1997, and Php26 279 in 2000. Additionally, the National Economic and Development Authority (NEDA) reported that the average annual family income in the province of Palawan in 2009 was Php132 640 (NEDA 2022). Although this figure was in average annual family income, it is still larger than the annual per capita income reported in the years 1994, 1997, and 2000.

For political stability, there were conflicts identified not only in the study area but in the entire country, as well. Many politicians and well-connected persons saw the forests as an asset from which they could derive benefits, which explains why many politicians were also loggers at the same time. During the 1950s-1970s, these perspectives supplied the push to rationalize and campaign for enormous mechanization of logging, which severely degraded natural forests (Guiang et al. 2001). Land-use conflicts between conservation and mining activities were also possible due to the lack of a clear delineation of protected area boundaries and uncertainty about the idea of intact forests (Carandang et al. 2013). As a result, disagreements are common when it comes to forest management, particularly when it comes to ownership and allocating resource rights.

Resource system

The environmental circumstances in which the resources are situated or produced are described in this first-tier category. Five (5) second-tier variables were considered which include important sectors (RS1), clear system boundaries (RS2), size of the different types of resources (RS3), productivity of the system (RS4), and location (RS5). The forest is considered to be the important sector here. The forest in Palawan is divided into five (5) major classifications as shown in Figure 5. National parks account for 51% of the total forest area in Palawan. This was followed by certified alienable and disposable land (30%), established timberland (12%), established forest reserves (5%), and civil reservation (2%) (DENR-FMB 2020).

Boundaries of regions such as forest can emerge over time or be imposed abruptly; they can be enforced by an external authority or a local faction in control, or they can be approved by vote or agreement. Custom, ritual, consensus, and/or compulsion can all be used to keep boundaries in place. By design or by accident, they may be more or less permeable (McDermott 2000). Also, unclear forest boundaries still exist in Palawan.

Moreover, based on the 19-year forest cover data of GFW in Palawan from 2001-2020, there was an increasing trend of forest cover loss in the province (Figure 6). A major forest cover loss was reported in 2016 which was more than 20 000 ha. This can be attributed to anthropogenic activities, especially illegal logging. Some of the illegal logging hotspots in Palawan are the municipalities of Brooke's Point and Taytay. On the other hand, the forest cover is slowly regained due to the reforestation projects of the government like the National Greening Program (NGP).

Resource units

The natural resource units created by the resource system are described by this variable. Five (5) second-tier variables were considered which include resource mobility (RU1), growth or replacement rate (RU2), resource value (RU3), number of resource units (RU4), and spatial and temporal distribution (RU5). The extent of Palawan's forests in 2010 (692 288 hectares) can be conservatively evaluated at Php 161 billion, based on multiple research, and includes regulating services (Php 111 billion), supporting services

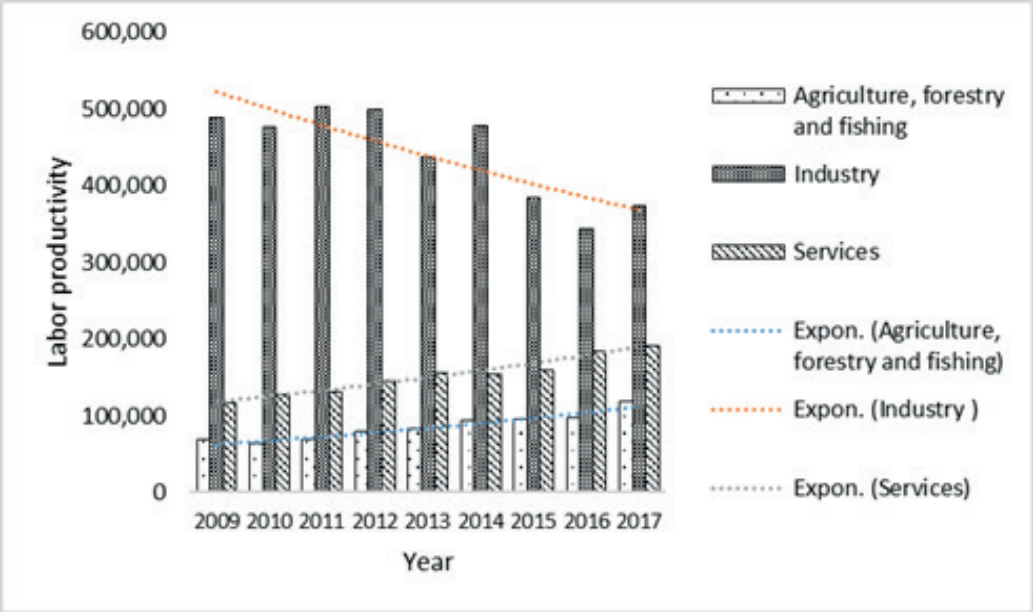

Fig. 4. Labor productivity per sector in Palawan from 2009-2017

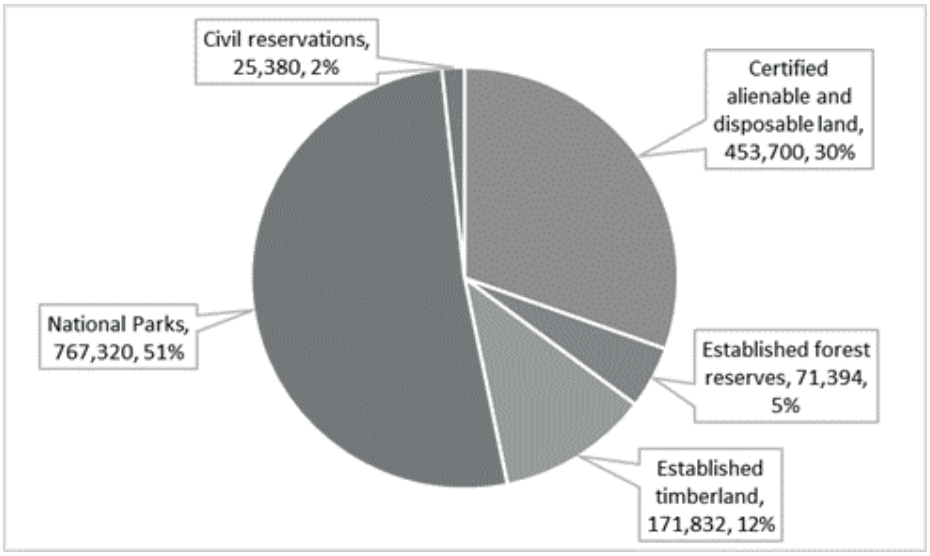

Fig. 5. Structure of forest lands in Palawan (ha)

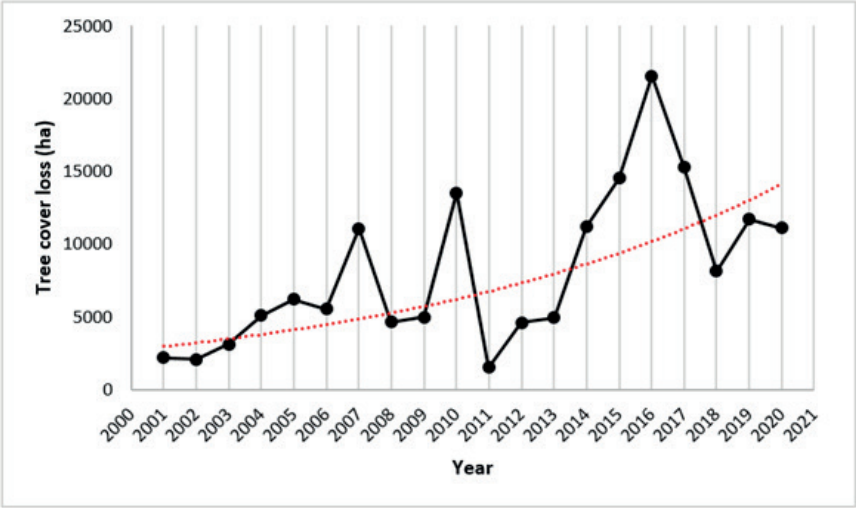

Fig. 6. Forest cover loss (ha) in Palawan, Philippines from 2001-2020

(Php 29 billion), and provisioning services (Php 21 billion) provided by forest ecosystems (Palawan LGU n.d.). One of the forest resources includes logs. The log production in Palawan in 2018, 2019, and 2020 was 9 601, 9 821, and 6 372.25 m^3, respectively.

Despite the fact that 48% of urban households and 71% of rural households in mainland Palawan got their fuelwood from their own farms, 25% of urban and 28% of rural residents still got it from public forest areas (Carandang et al. 2013). Moreover, extraction of non-timber forest products (NTFPs) continues to degrade forests in various parts of the Philippines, including Palawan. Many rural households in the Philippines benefit from NTFP gathering and harvesting since it provides them with additional monetary income. These can be utilized for either survival or commercial purposes. Some of the NTFPs derived from the forests of Palawan include wild honey, almaciga resin (*Agathis philippinensis*), stick broom from batbat leaf midribs (*Caryota sp.*), local bamboo poles, rattan, and buri (*Corypha elata*) among others (Matias et al. 2018).

Actors

Actors are simply the people affecting or affected by the resource. Six (6) second-tier variables were considered which include relevant actors (A1), history or past experiences (A2), close proximity to the forest (A3), preference for conserving (A4), preference for harvesting (A5), and knowledge about the forest (A6). Relevant actors include the community or people, private organizations, government organizations, and non-government organizations (NGOs). Despite its abundant natural resources, the province of Palawan has a high poverty rate. According to the 2014 Community-Based Monitoring System (CBMS) census, 61% of total households in Palawan's 20 (out of 23) municipalities earn less than the poverty line (Palawan LGU n.d.). The impacts of immigration and development are also found to increase the impacts on forest ecosystems. Special groups must also be considered under this sector which includes persons with disabilities, elderlies, and minority groups such as Tagbanua, Palaw'an, Tau't bato and the Bataks. Community and traditions values related to natural resource use include agricultural practices (i.e. monoculture and slash-and-burn activities) which are all contributing to Palawan's forest loss (Supsup et al. 2020).

Governance systems

Government, either local or national, is indispensable in the management and conservation of natural resources. Six (6) second-tier variables were considered which include government organizations (GS1), non-government organizations (GS2), property-rights systems (GS3), operational rules (GS4), collective choice rules (GS5), monitoring and sanctioning processes (GS6). Some of the line agencies when it comes to the management of natural resources like forest in Palawan are the Department of

Environment and Natural Resources (DENR), Department of Agriculture (DA), National Economic Development Authority (NEDA), Department of Interior and Local Government (DILG), and Department of Agrarian Reform (DAR). The roles of local government units (LGUs) in the management of forest resources cannot be neglected. They are on the ground, hence, they are knowledgeable of the things which are happening in their respective territories. However, it was also found out that some government officials are accomplices of illegal loggers and/or they are the ones owning illegal logging companies. NGOs, on the other hand, have spearheaded political projects aimed at mediating local–state relations in order to minimize, correct, and/or improve the effects of development and conservation. NGOs and their partners can use political action to help alter bad policies (Austin and Eder 2007).

Interactions

In Palawan, it is crucial to understand the relationships between the resource system and units, the governing system, and the actors. Four (4) second-tier variables under the subsystem interactions were considered. These are harvesting level (I1), nature conservation (I2), conflicts (I3), and investment activities (I4). Logs, fuelwood, and non-timber forest products are commonly harvested in the province either for subsistence or commercial uses. One of the well-known conservation efforts in the province is the World Network of Biosphere Reserves under the Man and Biosphere (MAB) Program of UNESCO (R. Fuentes n.d.) which encourages solutions that balance biodiversity protection with long-term use. However, resource conflicts exist in the province such as resource extraction, onshore mineral extraction using open pit technologies, land use change and conversion, expansion of exotic species plantations, and illegal wildlife trade (R. Fuentes n.d.) among others.

Outcomes

This subsystem represents the outcomes of the variables' interactions. Three (3) second-tier variables were considered namely socio-economic performance (O1), ecological performance measures (O2), and resiliency and sustainability of the forest (O3). It's noteworthy that the actors and the governance system are the major variables which greatly affect the conditions of the resource system and resource units. Good interactions among these variables will lead to the resource's efficiency and sustainability. On the other hand, the management measures that the actors do to the forest resources will be reciprocated by good environmental quality, resiliency, and abundant resources. This will, in turn, entail win-win conditions for all the variables involved. However, these ideal interactions are still persisted with negative ones which hamper the good outcomes that can arise from these.

Using the Institutional Analysis Development (IAD) framework

The IAD framework used in the Palawan forest case study is shown in Figure 7. These include the exogenous variables, action arena, interactions, outcomes, and the management plans. The exogenous variables include the biophysical/material conditions, attributes of the community, and the rules/governance. Action arena, on the other hand, consists of the interacting action situations and the participants. The exogenous variables affect the action arena resulting in particular interactions. These will result in outcomes which will require management plans and will have feedback loops to the exogenous variables and the action arena.

Exogenous variables
Biophysical/Material conditions

Palawan is a long, narrow island that is the country's largest province. Primary forests with high endemism of flora and fauna are known to exist in Palawan, although they are being threatened by a rise in active mining operations, slash-and-burn farming, oil palm expansion, and timber poaching (Araza et al. 2021). Due to its great biodiversity, it is recognized as the Philippines' «Last Frontier» (Matias et al. 2018). It has the country's largest terrestrial forest cover, accounting for 46% of the land area of Palawan Province. Palawan is also noted for having a

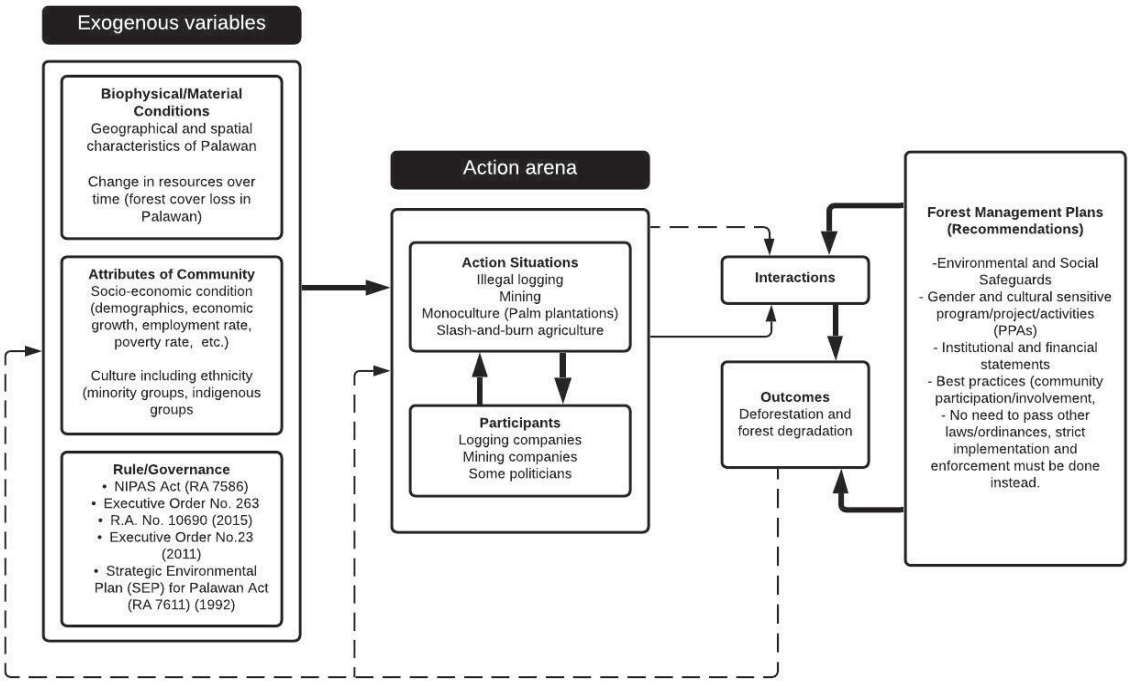

Fig. 7. The IAD framework for Palawan forest resources

large number of endemic plants and animals (Fuentes et al. 2015). However, an increasing trend of forest cover loss in Palawan was reported by the GFW from 2001-2020 as shown in Figure 6. Deforestation hotspots in Palawan are primarily located in the southern portion of the province which includes the Mt. Matalingahan and Malamplaya Protected Landscape (Araza et al. 2021). During the Marcos administration, deforestation became even worse. Timber Licensing Agreements (TLAs) and other timber license holders controlled over 10 million ha of land in the country, indicating that the logging sector was on the rise (Pamintuan 2011). Based on Landsat imagery from 1979, the government's Strategic Environmental Plan for Mainland Palawan estimated that 68% of the island was still forested. However, the forest is rapidly disappearing, at a rate of 19,000 hectares each year.

Attributes of the community

It describes the primary actors' historical background, values, culture, beliefs, religion, skills, knowledge, poverty level, health problems, and other socioeconomic aspects. This component was elaborated in the SES framework which shows the socio-demographic and economic conditions of the province (Figure 2). Increased demand for food, as a result of demographic variables such as population growth, may need the clearance of more land for agricultural expansion or subsistence farming (Carandang et al. 2013). Likewise, to make ends meet, many people who couldn't find jobs in the area turned to illegal logging, wood poaching, and *kaingin* production. On the other hand, local communities that rely on forest services become stewards of these resources, protecting them against illegal actions such as indigenous people. Environmental stewardship is becoming increasingly important to rural community leaders, who see it as a key component of their towns' long-term existence (Johnson 1993).

Indigenous people like Tagbanwa and Palawano are occupying the forest lands in Palawan. However, they are affected by the deforestation and forest degradation that are happening in the province. They mainly rely on the services provided by the forests, hence, these greatly affect their way of life. They have their cultural practices such as slash-and-burn methods of agriculture but for subsistence purposes only and these have very minimal impact on the forest ecosystem. What contribute largely to the land cover change and deforestation in Palawan are the logging activities for timber production, mining, and oil palm production. Malaysian and Filipino investors are reportedly cooperating to establish oil palm plantations in Palawan by renting smallholder farmers' and indigenous peoples' lands. Many smallholder agricultural farms, including indigenous fallow areas within forestlands, have already been turned to oil palm plantations, which require enormous tracts of land. The majority of oil palm farms are in the municipality of Espanola, but they are spreading to other towns in Palawan, including Brooke's Point, Quezon, and Bataraza (Carandang et al. 2013). In addition to local dynamics, macro-scale factors such as poverty, international prices of agricultural commodities and forest products, high rural population growth, and government land tenure policy all have a role in reducing forest cover.

Rules and Governance

The forests in the Philippines just like in Palawan are protected and conserved under various laws and provisions. These include the Executive Order (EO) 192 (1987), Local Government Code of 1991, National Integrated Protected Areas System (NIPAS) Act (RA 7586) of 1992, EO 263 (1995), and Indigenous People's Rights Act (RA 8371) of 1997 (Guiang et al. 2001).

Despite these many rules and laws on forest management, deforestation and forest degradation, not only in Palawan, but in the entire country still persist. According to Domingo and Manejar (2019), forest protection, as a policy, lacked adequate provisions for enforcement and institutionalization. Conflicting policy also opened forestlands to various extractive industries such as mining, exportation, timber and lumber businesses, contracting, and land conversions. In addition, Pulhin (2002) revealed that there (3) are three major concerns in forest policy formulation. These include the difficulty of achieving consensus among many policy actors, the urgent need for legislation that incorporates community-based forest management (CBFM's) methodology and aims, and the necessity to place a greater emphasis on monitoring and evaluating existing policies. Gradel et al. (2019) also argue that effective forest administration with local participation is significant to better support sustainable forestry.

Action arena

The action arena is made up of action situations and participants. The action situation is a social space in which actors interact, solve common problems, and trade services and goods; participants are those who participate in the situation (Nigussie et al. 2018).

Action situations

The action situations that were found to be imperative on the prevalence of forest degradation and deforestation in Palawan were the illegal logging, mining, monoculture, slash-and-burn type of agriculture, and immigration patterns. Land grabbing and illegal logging have increased in the frontier province, owing to the expansion of plantations and mining (Dressler 2021). The main issue is the difficulty of government forest guards to stop illegal logging activities in woods that are generally located in remote locations which they can barely protect due to lack of equipment and personnel support (Carandang et al. 2013). Just like a Palawan municipal official who attempted to curb illegal logging but was assassinated allegedly by the bodyguards of one of the province's most powerful politicians (Broad and Cavanagh 2020).

Mining is also prevalent in the province. In Southern Palawan province, specifically in Narra, Bataraza, and Quezon, about four (4) mining enterprises operate. While mining benefits mining towns and the country economically, it also has many social and environmental consequences (Agarin et al. 2021; Asih et al. 2022; Carandang et al. 2013; Nolos et al. 2022; Senoro et al. 2022; Zamroni et al. 2022). For example, the Rio Tuba Mine represents one of the Philippines' largest nickel ore reserves. In that area, chromium in the nickel laterite has polluted the surrounding surface water (Delina et al. 2020). To increase low-grade ore and laterite operations around the Mount Bulangao range in southern Palawan, the Rio Tuba Nickel Mining Corporation, a Filipino-Japanese partnership founded in 1973, has pushed to enclose ancestral territories and clear more forests. Up to 2176 hectares of ancestral lands of the Palawan have been claimed by Citi-Nickel Mining Corporation in Sofronio Española, located further north. Due to widespread evictions, toxic tailing

pond overflows into highland rivers, and lowland paddy irrigation schemes, NGOs and allies in Palawan have tried to prevent these practices (Dressler 2021). Figure 8 shows Google Earth images of the conditions before Rio Tuba Mine was developed in 1985 and after Rio Tuba Mine was developed in 2021. It can be seen also in the figure that the forest changes to mining land.

Participants

The IAD framework divides contextual elements into three (3) categories, which can be used to describe each actor's conduct in certain action situations: 1) physical factors, 2) community characteristics, and 3) institutional structures in the local area (Andersson 2006). The participants considered under the IAD framework were the logging and mining companies, government agencies, NGOs, and the community. Pagdanan Timber Products is the main logging enterprise in Palawan, and its politically powerful owner has Timber License Agreements covering a staggering 168 000 hectares. On the other hand, some of the major mining companies in the province are the Rio Tuba Nickel Mining Corporation in Puerto Princesa, Citinickel Mines and Development Corporation in Sofronio Española, and the Berong Nickel Corporation in Quezon, Palawan. The DENR-Mines and Geosciences Bureau has reported that the province of Palawan has the second largest nickel mine output in the Philippines in 2014 (PCSDC 2015). Figure 9 shows the nickel ore production in metric tons (MT) of the three (3) nickel mines in the province of Palawan in 2014. It is shown in the figure that the Rio Tuba Nickel Mining Corporation has the highest nickel mine output averaging to 4 800 000 MT. The Citinickel Mines and Development Corporation has a nickel mine output of approximately 2 200 000 MT while the Berong Nickel Corporation has 813 300 MT. Despite these mineral outputs which are important in the economy, mining causes deforestation and soil erosion of the area (Zambales 2021).

The role of government is also crucial in the management of forest resources. On the other hand, there were cases where many politicians and «well-connected» persons saw the forests as an asset from which they could derive benefits, which explains why many politicians were also loggers at the same time.

Interactions and Outcomes

By identifying the exogenous variables and the action arena, as well as their interactions, it's much clearer now why forest degradation and deforestation are prevalent in the province of Palawan. There were a myriad of drivers why these resource conflicts happen. The province has an increasing population which demands additional resources, land for housing or agriculture, and rapid migration to upland areas. These were then aggravated by major threats which include illegal logging, mining, oil palm plantation, wildlife poaching, and a wide-scale *kaingin* system. The slow rejuvenation of the forest makes it difficult to compensate for these lost resources, hence, degradation happens. Figure A1 shows a comparison of some parts of Palawan in year 2000 and 2020. It was evident from the images that parts of the province experienced deforestation and land cover changes, in general.

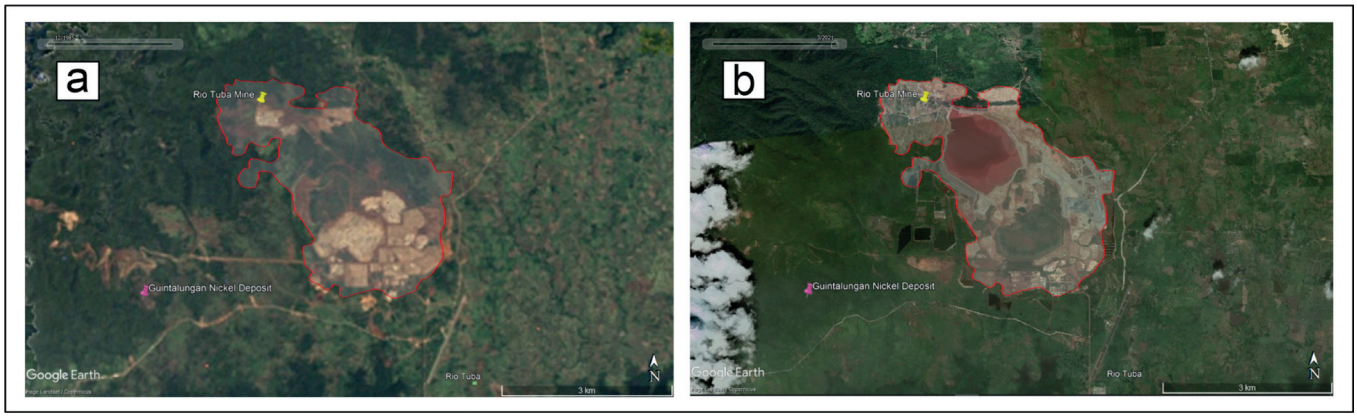

Fig. 8. Google Earth images, a) Before Rio Tuba Mine developed (1985), b) After Rio Tuba Mine developed (2021)

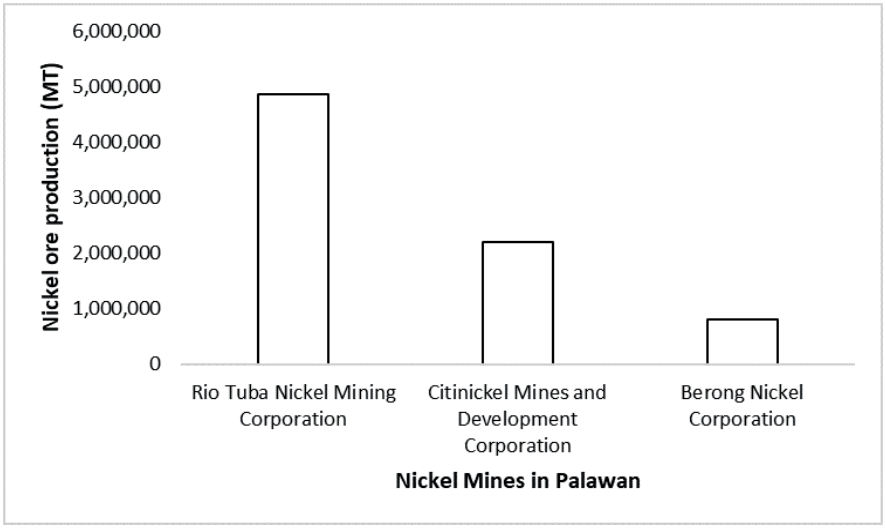

Fig. 9. Nickel ore production (MT) in the province of Palawan in 2014

Forest Management Plans

Inclusive and holistic approaches to the management and conservation of the forests in Palawan are to be considered. The institutional analysis revealed important aspects in the forest resources management in the province. Some of the recommended forest management plans are environmental and social safeguards, strict adherence to land use plan, culturally-sensitive programs, clear institutional and financial statements, community-involvement such as CBFM, reforestation such as the NGP, and the need for proper enforcement and implementation of existing forest laws instead of passing additional ones.

CONCLUSIONS

This paper analyzed and assessed the drivers of deforestation and forest degradation in the province of Palawan using the social-ecological systems (SES) and institutional analysis development (IAD) frameworks. Palawan Island is home to one of Southeast Asia's largest, oldest, and most diversified rainforests hence it was called the «Last Frontier». However, the island province's forest is contending with increased conversion of forest lands to plantation and household-level agriculture, intensive mineral mining, illegal logging, and other pressures on its ecosystems. Palawan's natural forest cover decreased from 55 to 48% between 1992 and 2010, with an annual forest loss of 5 500 ha. Further, the province still experienced forest cover loss in recent times as it was reported that approximately 23 400 ha of forest was lost from 2002 to 2021. The SES evaluated the variables like resource systems and units, governance systems, and actors considering the economic, social, and political settings of the study area. It revealed that aside from timber and logs, non-timber forest products (NTFPs) were also harvested in Palawan. These were initially harvested by indigenous peoples (IPs) for subsistence use but lowland communities partook on this which contributed to forest degradation. The increasing population and rapid migration from lowland areas to upland areas also contributed to this issue. On the other hand, the IAD identified major drivers of forest degradation and deforestation in the province which include illegal logging, mining, wide-scale *kaingin* and oil palm plantation, and wildlife poaching. Most of the illegal logging activities are in remote locations which the government forest guards can barely protect due to lack of equipment and personnel support. There were also cases where many politicians, who should be the frontline in forest management, saw the forests as an asset from which they could derive benefits, which explains why many of them were also loggers at the same time. There were already many laws on the Palawan forest resources conservation and management but the issue of deforestation still remains. The IAD also identified policy recommendations for forest management in Palawan which include strict adherence to land use plan, culturally-sensitive programs, clear institutional and financial statements, community-involvement such as CBFM, reforestation such as the NGP, and the need for proper implementation and enforcement of existing forest laws instead of passing additional ones. The findings and recommendations of this paper will aid in the policy-making of forest management plans in Palawan and other areas where similar settings exist.

REFERENCES

Agarin C.J.M., Mascareñas D.R., Nolos R., Chan E., and Senoro D. B. (2021). Transition Metals in Freshwater Crustaceans, Tilapia, and Inland Water: Hazardous to the Population of the Small Island Province. Toxics, 9(4), 71.

Andersson K. (2006). Understanding decentralized forest governance: an application of the institutional analysis and development framework. Sustainability: Science, Practice and Policy, 2(1), 25-35.

Araza A.B., Castillo G.B., Buduan E.D., Hein L., Herold M., Reiche J., and Razal R.A. (2021). Intra-annual identification of local deforestation hotspots in the Philippines using earth observation products. Forests, 12(8), 1008.

Asih A.S., Zamroni A., Alwi W., Sagala S.T., and Putra A.S. (2022). Assessment of Heavy Metal Concentrations in Seawater in the Coastal Areas around Daerah Istimewa Yogyakarta Province, Indonesia. The Iraqi Geological Journal, 14-22.

Austin K.G., Schwantes A., Gu Y., and Kasibhatla P. S. (2019). What causes deforestation in Indonesia? Environmental Research Letters, 14(2), 024007.

Austin R.L., and Eder J.F. (2007). Environmentalism, development, and participation on Palawan Island, Philippines. Society and Natural Resources, 20(4), 363-371, DOI: 10.1080/08941920601161379.

Basurto X., Gelcich S., and Ostrom E. (2013). The social–ecological system framework as a knowledge classificatory system for benthic small-scale fisheries. Global Environmental Change, 23(6), 1366-1380.

Beth J., Jontila S., Anthony R., Balisco T., Matillano J.A., and Jontila J.B.S. (2014). AACL BIOFLUX the Sea cucumbers (Holothuroidea) of Palawan, Philippines 1, 2. 7(3). http://www.bioflux.com.ro/aacl.

Birhan E., Assefa E., and Petrova M.A. (2021). Challenges of Forest Governance in Addressing Redd+: Status, Effects And Prospects. The Case of Bale Eco-Region, Oromia Regional State, Ethiopia. Geography, Environment, Sustainability, 14(1), 185-195.

Blomquist W., and deLeon P. (2011). The design and promise of the institutional analysis and development framework.

Broad R., and Cavanagh J. (2020). 3. The Last Rainforests. In Plundering Paradise (pp. 39-55). University of California Press.

Carandang A.P., Bugayong L.A., Dolom P.C., Garcia L.N., Villanueva M.M.B., and Espiritu N.O. (2013). Analysis of key drivers of deforestation and forest degradation in the Philippines. https://ovcre.uplb.edu.ph/research/our-projects/article/13430-analysis-of-key-drivers-of-deforestation-and-forest-degradation-in-the-philippines.

Chechina M., Neveux Y., Parkins J. R., and Hamann, A. (2018). Balancing conservation and livelihoods: A study of forest-dependent communities in the Philippines. Conservation and Society, 16(4), 420-430.

Clement F. (2010). Analysing decentralised natural resource governance: proposition for a «politicised» institutional analysis and development framework. Policy Sciences, 43(2), 129-156.

DENR. (2021). Forestry Related DENR Policies. https://forestry.denr.gov.ph/index.php/issuances/laws-and-policies

DENR-FMB. (2020). Philippine Forestry Statistics - 2020. https://drive.google.com/file/d/1FsTVnJeC4FRDKcU6FQREMBKc08opGtjj/view.

Department of Environment and Natural Resources (DENR). (2021). Philippine Forestry Statistics. <https://forestry.denr.gov.ph/index.php/statistics/philippines-forestry-statistics>. Accessed on 12/3/2021.

Dressler W., McDermott M., Smith W., and Pulhin J. (2012). REDD policy impacts on indigenous property rights regimes on Palawan Island, The Philippines. Human Ecology, 40(5), 679-691.

Dressler W. (2014). Green governmentality and swidden decline on Palawan Island. Transactions of the Institute of British Geographers, 39(2), 250-264.

Dressler W. (2021). Defending lands and forests: NGO histories, everyday struggles, and extraordinary violence in the Philippines. Critical Asian Studies, 1-32.

Domingo S. and Manejar A.J. (2019). Forest protection in the Philippines: Policy evolution and sector outcomes. Philippine Institute for Development Studies.

Dugarjav C., Gunin P., Bazha S., and Saandar M. (2010). Ecosystem approach for evaluating degradation processes and nature protection in inner asia. Geography, Environment, Sustainability, 3(2), 66-77.

Dong, J., Xiao, X., Sheldon, S., Biradar, C., Zhang, G., Dinh Duong, N., and Moore III, B. (2014). A 50-m forest cover map in Southeast Asia from ALOS/PALSAR and its application on forest fragmentation assessment. PloS one, 9(1), e85801.

Eder J.F. (1990). Deforestation and detribalization in the Philippines: The Palawan case. Population and Environment, 12(2), 99-115.

Engdaw B.D. (2020). Assessment of the trends of greenhouse gas emission in Ethiopia. Geography, Environment, Sustainability, 13(2), 135-146.

FAO (2020). Global forest resources assessment 2020–key findings, Policy research paper.

Fuentes R., and Officer C.P. High conservation value areas management in Palawan Biosphere Reserve.

Fuentes R.T., Pontillas J.F.A., and Pido M.D. (2015). The Role of UNESCO's Man and Biosphere Reserves in Climate Change Adaptation: Experience from Palawan Biosphere Reserve in the Philippines. Our Palawan, 1(1), 49-60. www.wikipedia.org.

Gain A.K., Hossain S., Benson D., Di Baldassarre G., Giupponi C., and Huq N. (2021). Social-ecological system approaches for water resources management. International journal of sustainable development and world ecology, 28(2), 109-124.

Ghazoul J., Burivalova Z., Garcia-Ulloa J., and King L.A. (2015). Conceptualizing forest degradation. Trends in ecology and evolution, 30(10), 622-632.

Gichuki L. (2019). Reviving land and restoring landscapes: policy convergence between forest landscape restoration and land degradation neutrality. IUCN.

Global Forest Watch (2021). Forest Monitoring, Land Use and Deforestation Trends | Global Forest Watch. https://www.globalforestwatch.org/.

Gradel A., Sukhbaatar G., Karthe D., and Kang H. (2019). Forest management in Mongolia–A review of challenges and lessons learned with special reference to degradation and deforestation. Geography, Environment, Sustainability, 12(3), 133-166.

Guiang E. S. (2001). Impacts and effectiveness of logging bans in natural forests: Philippines. Chapter, 4, 103-136.

Houballah M. (2019). Modeling multi-functional forest management through a social-ecological system framework-based analysis (Doctoral dissertation, Université Clermont Auvergne(2017-2020).

Jayathilake H.M., Prescott G.W., Carrasco L.R., Rao M., and Symes W.S. (2021). Drivers of deforestation and degradation for 28 tropical conservation landscapes. Ambio, 50(1), 215-228.

Johnson E.A., and Miyanishi K. (2001). Forest fires. Behaviour and ecological effects. Elsevier, 570.

Johnson K. (1993). Reconciling rural communities and resource conservation. Environment: Science and Policy for Sustainable Development, 35(9), 16-33.

Koike T., Watanabe, M., Hoshika, Y., Kitao, M., Matsumura, H., Funada, R., and Izuta, T. (2013). Effects of ozone on forest ecosystems in East and Southeast Asia. Developments in Environmental Science, 13, 371-390.

Kramer R.A., Richter D.D., Pattanayak S., and Sharma, N. P. (1997). Ecological and economic analysis of watershed protection in Eastern Madagascar. Journal of Environmental Management, 49(3), 277-295.

López D., and Saavedra A. (2021). Mapping forest and agroforestry units for Environmental Planning. Study case transboundary region Mexico-Guatemala. Geography, Environment, Sustainability, 14(1), 63-70.

Matias D.M.S. (2018). Sustainability of Community Forestry Enterprises: Indigenous Wild Honey Gathering in the Palawan Biosphere Reserve, Philippines. Zentrum für Entwicklungsforschung (ZEF).

McDermott M.H. (2000). Boundaries and pathways: Indigenous identity, ancestral domain, and forest use in Palawan, the Philippines. http://dlc.dlib.indiana.edu/dlc/handle/10535/778.

McGinnis M.D., and Ostrom E. (2014). Social-ecological system framework: initial changes and continuing challenges. Ecology and society, 19(2).

Mincey S.K., Hutten M., Fischer B.C., Evans T.P., Stewart S.I., and Vogt J.M. (2013). Structuring institutional analysis for urban ecosystems: A key to sustainable urban forest management. Urban ecosystems, 16(3), 553-571.

NEDA (2022). Palawan. NEDA MIMAROPA. Retrieved August 22, 2022, from https://mimaropa.neda.gov.ph/palawan/

Nigussie Z., Tsunekawa A., Haregeweyn N., Adgo E., Cochrane L., Floquet A., and Abele S. (2018). Applying Ostrom's institutional analysis and development framework to soil and water conservation activities in north-western Ethiopia. Land use policy, 71, 1-10.

Nikitin M.A., Tatarinovich E.V., Rozinkina I.A., and Nikitin A.E. (2019). Effects Of Deforestation And Afforestation In The Central Part Of The East European Plain On Regional Weather Conditions. Geography, Environment, Sustainability, 12(2), 259-272.

Nilsson A.E., Avango D., and Rosqvist G. (2021). Social-ecological-technological systems consequences of mining: An analytical framework for more holistic impact assessments. The Extractive Industries and Society, 101011.

Nolos R.C., Agarin C.J.M., Domino M.Y.R., Bonifacio P.B., Chan E.B., Mascareñas D.R., and Senoro D.B. (2022). Health Risks Due to Metal Concentrations in Soil and Vegetables from the Six Municipalities of the Island Province in the Philippines. International Journal of Environmental Research and Public Health, 19(3), 1587.

NSO (2000). 2000 Census of Population and Housing.

Olabisi L.S. (2010). The system dynamics of forest cover in the developing world: Researcher versus community perspectives. Sustainability, 2(6), 1523-1535.

Ostrom E. (2009). A general framework for analyzing sustainability of social-ecological systems. Science, 325(5939), 419-422.

Ostrom E. (2010). Institutional analysis and development: Elements of the framework in historical perspective. Historical developments and theoretical approaches in sociology, 2, 261-288.

Ostrom E. (2011). Background on the institutional analysis and development framework. Policy Studies Journal, 39(1), 7-27.

Palawan LGU. (n.d.). Palawan INRM Project Proposal. Retrieved December 6, 2021, from https://www.scribd.com/document/478785795/Palawan-INRM-Project-Proposal-pdf.

Palmer K. (2004). Local government law and resource management. New Zealand Law Review, (4), 751-785.

Pamintuan M. (2011). Protect Philippine Forests. Philippine Daily Inquirer, 5.

Partelow S. (2018). A review of the social-ecological systems framework. Ecology and Society, 23(4).

PCSDS (2015): State of the Environment 2015 Updates, Province of Palawan (UNESCO Man and Biosphere Reserve), Philippines. Palawan Council for Sustainable Development, Puerto Princesa City, Philippines.

Perez G.J., Comiso J.C., Aragones L.V., Merida H.C., and Ong P.S. (2020). Reforestation and Deforestation in Northern Luzon, Philippines: Critical Issues as Observed from Space. Forests, 11(10), 1071.

Pichler M., and Brad A. (2016). Political ecology and socio-ecological conflicts in Southeast Asia. ASEAS-Austrian Journal of South-East Asian Studies, 9(1), 1-10.

PSA (2018). Palawan Quickstat. https://psa.gov.ph/content/palawan-quickstat-june-2018.

PSA (2021). Philippine Statistics Authority. https://psa.gov.ph/

Reeves L.E., and Daniels J.C. (2020). Conservation value of secondary forest habitats to endemic frugivorous butterflies at Mount Kanlaon, Negros Occidental, Philippines. Journal of Insect Conservation, 24(6), 913-926.

Richards K.R., and Stokes C. (2004). A review of forest carbon sequestration cost studies: a dozen years of research. Climatic change, 63(1), 1-48.

Seidl R., Thom D., Kautz M., Martin-Benito D., Peltoniemi M., Vacchiano G., and Reyer C. P. (2017). Forest disturbances under climate change. Nature climate change, 7(6), 395-402.

Senoro D.B., de Jesus K.L.M., Nolos R.C., Lamac M.R.L., Deseo K.M., and Tabelin C.B. (2022). In Situ Measurements of Domestic Water Quality and Health Risks by Elevated Concentration of Heavy Metals and Metalloids Using Monte Carlo and MLGI Methods. Toxics, 10(7), 342.

Smith W.H. (2012). Air pollution and forests: interactions between air contaminants and forest ecosystems. Springer Science and Business Media.

Suprapto N., Zamroni A., and Yudianto E.A. (2017). One Decade of the «LUSI» Mud Volcano: Physical, Chemical, and Geological Dimensions. CHEMISTRY, 26(4), 615-629.

Supsup C.E., Asis A.A., Carestia Jr, U. V., Diesmos A.C., Mallari N.A.D., and Brown R.M. (2020). Variation in species richness, composition and herpetological community structure across a tropical habitat gradient of Palawan Island, Philippines. Herpetozoa, 33, 95.

van Beijnen J., and Jose E.D. (2020). Botanical observations from a threatened riverine lowland forest in Aborlan, Palawan, Philippines.

Van Khuc Q., Tran B.Q., Meyfroidt P., and Paschke M.W. (2018). Drivers of deforestation and forest degradation in Vietnam: An exploratory analysis at the national level. Forest policy and economics, 90, 128-141.

Waring R.H., and Schlesinger W.H. (1985). Forest ecosystems. Analysis at multiples scales, 55.

Zambales L.T. (2021). Mining in Palawan: Effect of Environment, Livelihood, Employment, and Health.

Zamroni A., Kurniati A.C., and Prasetya H.N.E. (2020). The assessment of landslides disaster mitigation in Java Island, Indonesia: a review. Journal of Geoscience, Engineering, Environment, and Technology, 5(3), 129-133.

Zamroni A., Trisnaning P.T., Prasetya H.N.E., Sagala S.T., and Putra A.S. (2022). Geochemical Characteristics and Evaluation of the Groundwater and Surface Water in Limestone Mining Area around Gunungkidul Regency, Indonesia. The Iraqi Geological Journal, 189-198.

APPENDIX

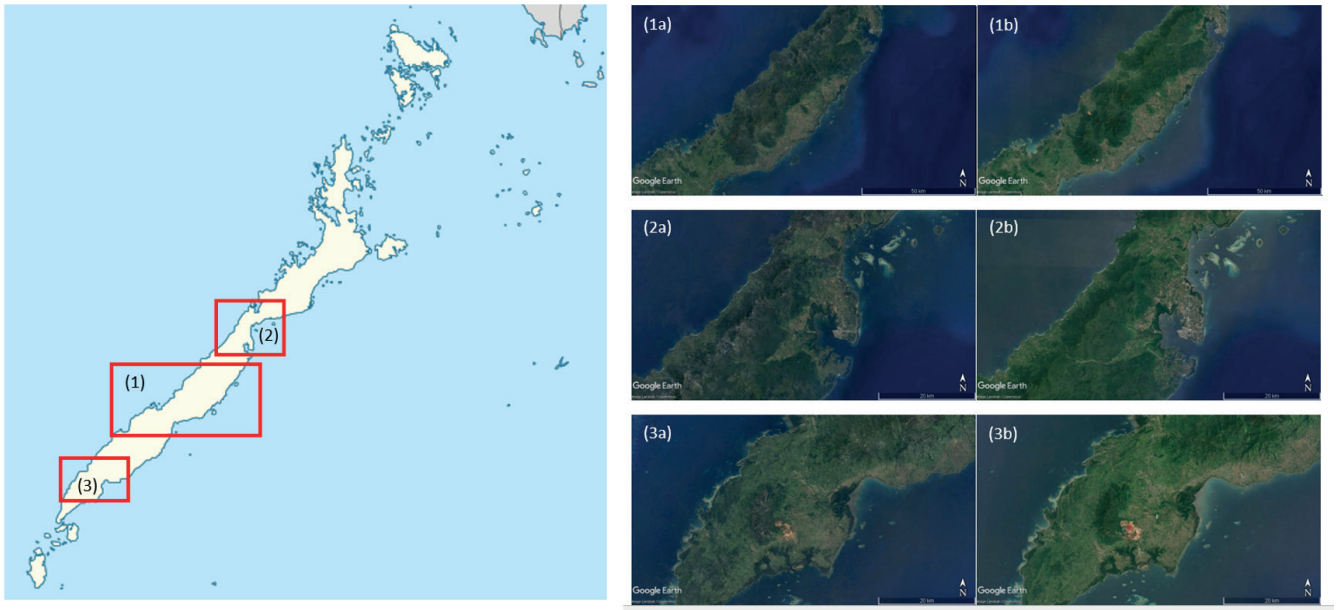

Fig. A1. Land cover change in some parts of the Palawan province in years 2000 (1a, 2a, and 3a) and 2020 (1b, 2b, and 3b)

RESEARCH PAPER

DEVELOPMENT AND EVALUATION OF THE WEBGIS APPLICATION TO SUPPORT VOLCANIC HAZARD MITIGATION IN THE SOUTHERN FLANK OF MERAPI VOLCANO, SLEMAN REGENCY, YOGYAKARTA PROVINCE, INDONESIA

Afrinia Lisditya Permatasari[1]*, Ika Afianita Suherningtyas[1], Putu Perdana Kusuma Wiguna[2]
[1]Universitas AMIKOM, Jl. Padjajaran, Ring Road Utara, Yogyakarta, Indonesia
[2]Universitas Udayana, Jimbaran, Badung Regency, Bali, Indonesia
***Corresponding author:** afrinia@amikom.ac.id
Received: August 21st, 2021 / Accepted: November 11th, 2022 / Published: December 31st, 2022
https://DOI-10.24057/2071-9388-2021-099

ABSTRACT. Merapi Volcano is one of the active volcanoes in Indonesia, which is located in the Central Java and Yogyakarta Province. The eruption of Merapi Volcano is a threat to people living on the slopes of Merapi, especially on its densely-populated southern flank. The purpose of this study was to build a webGIS to support volcanic hazard mitigation regarding Merapi Volcano and evaluate the webGIS system for determining the community's perception. This research was the first to produce a product that is used by government agencies related to volcanic disaster mitigation. webGIS development was carried out using an open source platform. System evaluation was carried out using usability testing. The samples were obtained using systematic the random sampling method of respondents who lived in the villages on the southern flank of Merapi volcano. webGIS was built using LeafletJS and QGIS, combined with spatial data about the evacuation locations, health facilities, evacuation routes, government offices, educational facilities and worship facilities, with a basemap obtained from Openstreet Map and Google Satellite. WebGIS was equipped with a database query feature to make it easier for users to find geographical information. The usability testing results showed that as many as 83% of the respondents were very satisfied with the appearance and information of webGIS, while as many as 82% were very satisfied with the navigation offered via the webGIS display.

KEYWORDS: WebGIS, mitigation, volcanic eruption

CITATION: Permatasari A. L., Suherningtyas I. A., Wiguna P. P. K. (2022). Development And Evaluation Of The Webgis Application To Support Volcanic Hazard Mitigation In The Southern Flank Of Merapi Volcano, Sleman Regency, Yogyakarta Province, Indonesia. Geography, Environment, Sustainability, 4(15), 57-63
https://DOI-10.24057/2071-9388-2021-099

ACKNOWLEDGEMENTS: The writers would like to thank Amikom University for providing research funding, and the local government agencies for data availability.

Conflict of interests: The authors reported no potential conflict of interest.

INTRODUCTION

Indonesia is located in a ring of fire zone, with the characteristics of an archipelago, which is an area where the world's active tectonic plates meet; namely, the Eurasian Plate, the Indo-Australian Plate, and the Pacific Plate (De Bélizal et al. 2012, Wulan et al. 2021). Due to tectonic plate activity, Indonesia has more than 18,000 islands and 127 active volcanoes located along the tectonic faults (Solikhin et al. 2012). Merapi Volcano is one of the most active volcanoes in Indonesia (Hariyono 2018), with the potential to erupt and make an impact on society (Yudistira et al. 2020).

In the 21st century, the most intense eruption to date occurred on October 26, 2010, peaking on November 6, 2010. This eruption led to 275 deaths, 576 people being hospitalized, and 287,131 people becoming refugees, with a calculated loss of Rp 4.23 trillion (280 million USD) (Surono et al. 2012). Merapi Volcano might erupt at any time, posing a huge threat, especially to those living on its southern flank (Jousset et al. 2013). Information on the efforts made to mitigate the results of Merapi Volcano erupting needs to be gathered and disseminated to the public. One way to do this is through the development of a Geography Information System (GIS) for Merapi Volcano disaster mitigation (Sukatja et al. 2014).

Various studies on the provision of eruption disaster information systems have been carried out, such as the research on building a Spatial Data Infrastructure (SDI) for disaster mitigation in Kali Putih, Magelang Regency, which shows the importance of this information regarding the eruption disaster mitigation policies in Magelang Regency

(Permatasari et al. 2020). In addition, the modelling of volcanic eruptions is also important as an early warning system for the communities living on and around Merapi Volcano (Cobar et al. 2016, Santoso et al. 2021). Various efforts to implement Geographic Information Systems (GIS) to mitigate eruption disaster have aimed to improve the disaster management and mitigation efforts. The 3D building model, combined with a webGIS system, creates a Web-based 3D GIS system that can improve the mitigation efforts by additionally considering 3D buildings in regard to the threats of tsunamis and floods. The integrated analysis and visualization capabilities enable the decision makes freely to design scenarios and make evacuation decisions (Hong & Tsai 2022). A WebGIS-based three-dimensional (3D) approach is also applicable for real-time monitoring and to serve as an early-warning system regarding geological disasters. The real time results act as an early warning system when they are received by the sensors in the disaster zone. The system is an effective disaster prediction model, and can successfully realize real-time monitoring and early-warnings about geological disasters (Yang et al. 2015). WebGIS can also fulfil many functions to provide decision support for local disaster prevention and mitigation. In a landslide information system for Lanzhou city, China, a webGIS system faciliates storage and management, query and retrieval, warning and analysis, and web publishing, to support the decision-making based on landslide disaster information (Zhishan et al. 2012).

The WebGIS platform also successfully applied the system to several recent, large magnitude earthquakes. The generated deformation map shows a good agreement when compared to the data based on real earthquakes. WebGIS can act as a database of real earthquake data collected by the community and becomes a voluntary geographic information platform for collecting disaster data for rescue and model validation (Zhao et al. 2020). GIS and WebGIS have been widely used in various scientific fields. GIS also works as a tool for various environmental studies, disasters and hazards and tourism promotion (Warsini et al. 2016, Kusmiyarti et al. 2018; Permatasari et al. 2020; Trigunasih & Wiguna 2020; Permatasari et al. 2021; Sardiana et al. 2021; Suherningtyas et al. 2021; Talib et al. 2021; Wiguna 2021; Muslih et al. 2022; Sukraini et al. 2022). According to interview results with the Agency at Regency level, namely, Planning, Research and Development Agency and Disaster Mitigation Agency of Sleman Regency, the Sleman Regency Government does not have an information system specifically related to the mitigation of a Merapi Volcano eruption, while the national government's webGIS is not detailed and specific about the Merapi volcano eruption, so it is very important to develop and implement one. This research was the first research conducted with aim to build an information system for the mitigation of the eruption of Merapi Volcano. The information system can be implemented in the community and is expected to reduce risk and increase awareness of the community at the southern slopes of Merapi Volcano. The results of this study were expected to provide policy input to the government and stakeholders in efforts to mitigate the disaster of the eruption of Merapi Volcano in an integrated and sustainable manner.

MATERIALS AND METHODS

This research was conducted on the southern flank of Merapi Volcano, which is administratively located in Sleman Regency, especially in Turi, Pakem, Cangkringan, Tempel, Sleman, Ngaglik and Ngemplak Districts, Yogyakarta Province, Indonesia. Fig. 1 shows the research area.

The application's development in this study was divided into four stages; namely, 1) the initiation of the system, 2) the analysis of the system, 3) the system design, and 4) the implementation of the system (Whitten 2007). The system development was carried out using leafletJS and QGIS software. The data for webGIS were collected from local government agencies in Sleman Regency. The data analysis was divided into three steps; namely, (1) data identification, (2) data collection and (3) data entry into webGIS.

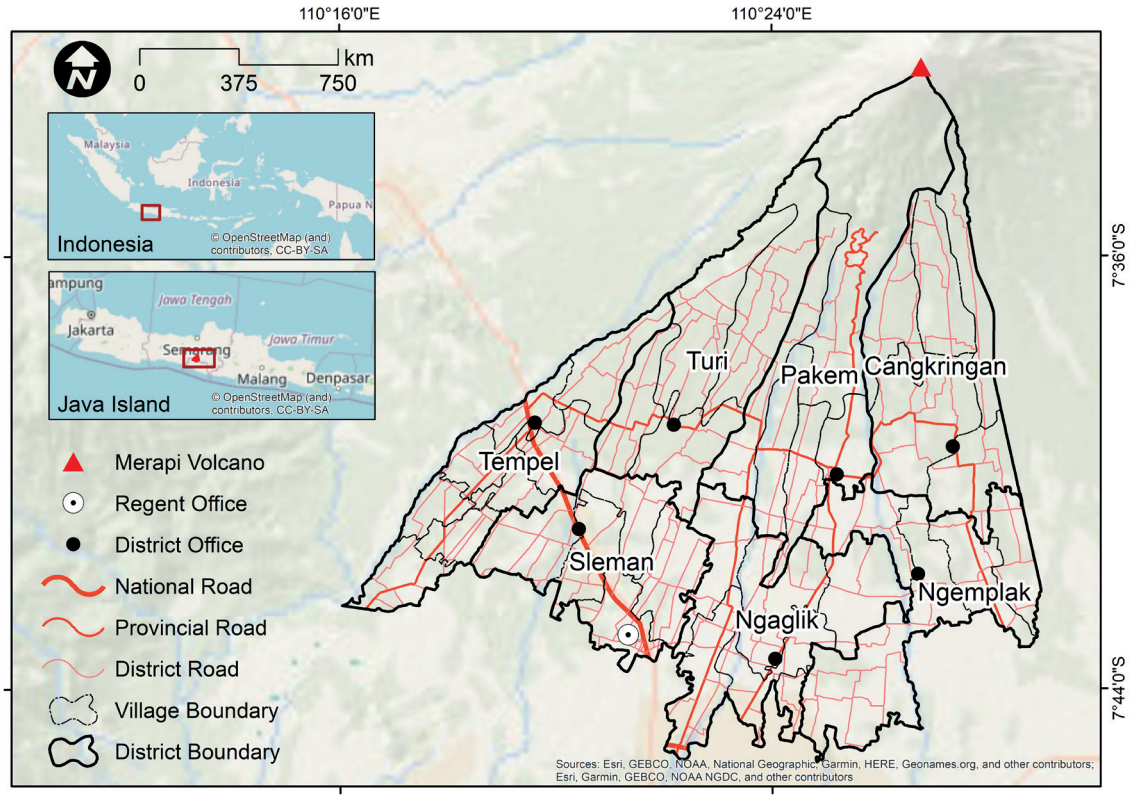

Fig. 1. Research Area

The webGIS was designed using QGIS and libraries from LeafletJS. LeafletJS is an open source JavaScript library that is widely used to build Web-based mapping applications. It supports most mobile and desktop platforms, as well as HTML5 and CSS3, and is used by many web-based mapping site applications (Edler & Vetter 2019).

The webGIS System workflow starts when the user logs in. Entering the system will call up OpenStreetmap and Google Satellite along with thematic data; namely, evacuation routes, river networks and Sabo dam locations, refuge locations, evacuation routes, educational facilities, religious facilities, public facilities, health facilities and government offices. The user can then access the map online. Fig. 2. shows the research flowchart and steps of the application development.

The application development was followed by system evaluation using usability testing (Hertzum 2020). Usability testing was applied by asking the respondents to use the system. The key elements to this technique is the use of traditional testing concepts and techniques such as scenario based testing to measure productivity and learnability of the subject. The assumption of using usability testing is by constructing test cases or tasks to measure the learnability of the application, the developer has a way to measure the quality of both the test and the software. (Mueller et al. 2009). However, evaluation of personalisation system remains a challenge due to thelack of understanding of what factors affect user satisfaction with a personalization system (Anand & Mobasher 2005, Kamarudin et al. 2017). The limitation in using this questionnaire is that it only collects data on display, navigation, and the information, which is an issue in usability testing. The sample for the usability testing were identified by applying random sampling to the inhabitants of the research area. Table 1 shows the questions related to the usability testing.

The respondents were asked to display the main page and map, select a map, display spatial data and select the nearest evacuation point, select an evacuation route, and navigate to the evacuation location. After using the system, the respondents were invited to answer questions related to the usability of the system, using a scale from 1 to 5. A score of 1 indicates dissatisfaction or that the system is not performing very well, while a score of 5 indicates very high satisfaction. The questions covered aspects of the system's display, the ease of navigation, and the completeness of the information displayed.

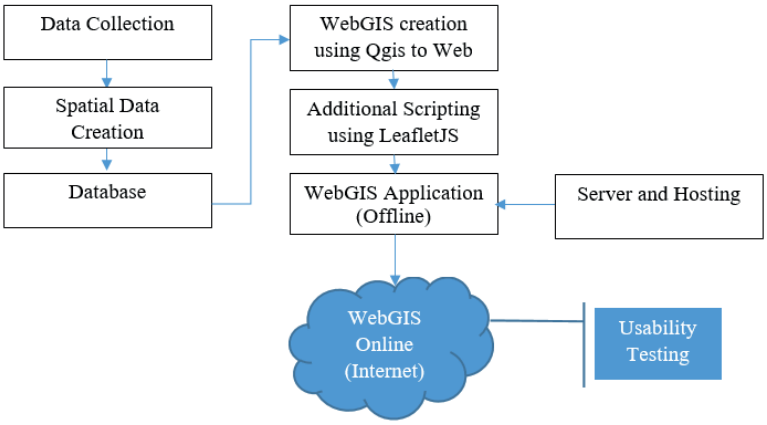

Fig. 2. Steps of the Application Development

Table 1. Questions related to the Usability Testing

No	Questions	Score					% Respondents
		1	2	3	4	5	
	Display (100 respondents)						100%
1	Is the display on the system easy to understand?						
2	Are the colors, layout, and text on the system easy to see and attractive?						
3	Are the image symbols on the system easy to understand?						
	Navigation (100 respondents)						100%
4	Are the pages on the system easy to navigate?						
5	Is the system easy to read?						
6	Are the features in the system easy to use/operate?						
7	Are the menus and displays on the system easy to remember?						
	Information (100 respondents)						100%
8	Is the information on the system easy to use/understand?						
9	Do the specifications on the system meet your needs?						
10	Is the information in the spatial data easy to see/understand?						

Note: Score: 1) Very Not Satisfied, 2) Not Satisfied, 3) Average, 4) Satisfied, 5) Very Satisfied

The method employed to determine the sample was systematic random sampling, which is appropriate for use in area- or region-based research, and involves identifying samples based on a grid system (De Souza & Koizumi 2020). The total number of samples in this study was 100 respondents, aimed to adapt to the large population (Memon et al. 2020). An overview of the sampling technique is shown in Fig. 3.

RESULTS AND DISCUSSION

The webGIS on mitigation of Merapi Volcano eruption was designed to be easily accessible to and used by both the government and public to search, locate and visualize geospatial data related to disaster mitigation regarding a potential eruption of Merapi Volcano. WebGIS was also intended to increase the readiness of the government of Sleman Regency to mitigate the effects of a Merapi Volcano eruption. The data displayed on webGIS were supplied by the Center for Research and Development of Geological Disaster Technology (BPPTKG), the Planning, Research and Development Agency of Sleman Regency, Sleman Regency Health Agency, the Sabo Department of the Ministry of Public Works and Public Housing and the Serayu Opak River Basin Center of the Ministry of Public Works and Public Housing. The available data were relatively comprehensive, ranging from administrative data and basic data (such as road networks, rivers, village government offices, educational facilities and religious facilities). The data were in ESRI shapefile format with UTM coordinates. The only drawback was that the data lack of metadata, so only limited information can be extracted. The thematic data obtained from local governments include spatial data on the disaster-prone areas around Merapi Volcano, the evacuation locations, and the health service locations, plus Sabo dam distribution data and evacuation routes data. Table 2 shows the data displayed on webGIS.

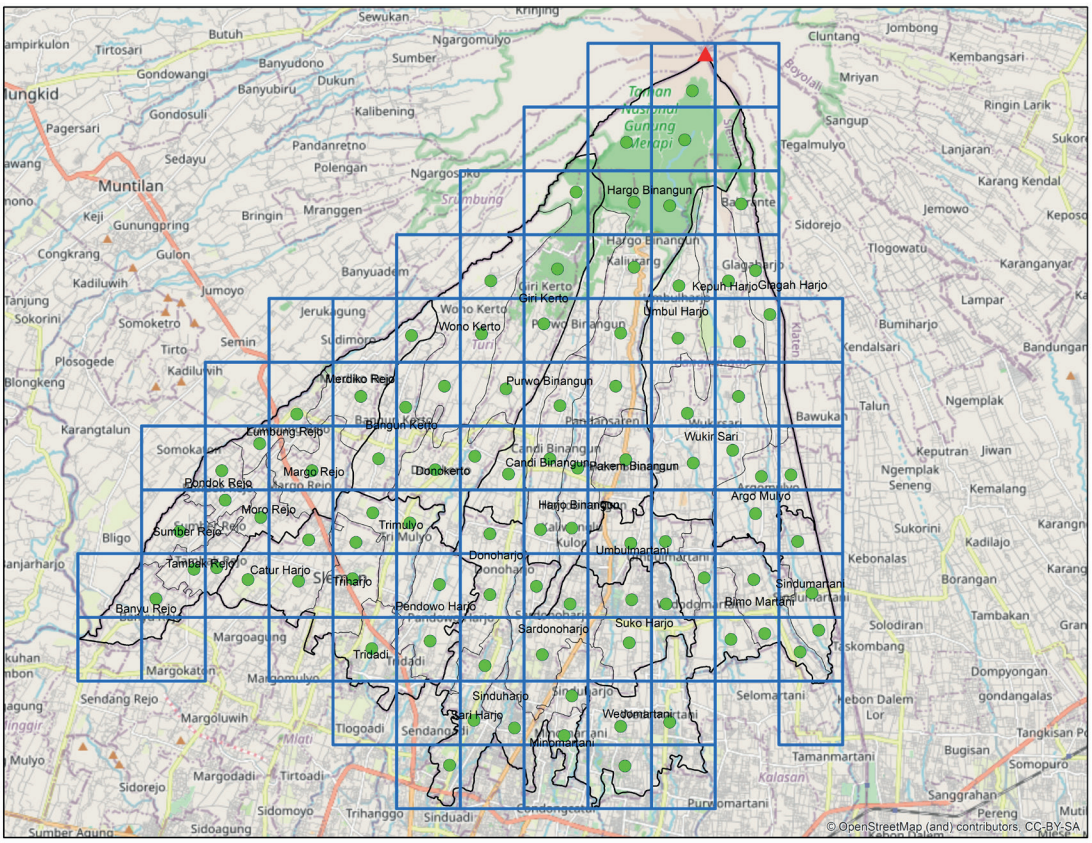

Fig. 3. Grid of the sample location

Table 2. Spatial Data on WebGIS

NNo	Government Agency	Data	Coordinate	Data Type
11	Center for Research and Development of Geological Disaster Technology (BPPTKG)	• Spatial data on the disaster-prone areas around Merapi Volcano	UTM Zone 49S	ESRI Shapefile
2	Planning, Research and Development Agency of Sleman Regency	• Spatial data on the administrative area of Sleman Regency • Spatial data on the road network • Spatial data on the river network • Spatial data on the religious facilities • Spatial data on the educational facilities	UTM Zone 49S	ESRI Shapefile
33	Sleman Regency Health Agency	• Spatial data on the health service locations	UTM Zone 49S	ESRI Shapefile
44	Sabo Department of the Ministry of Public Works and Public Housing	• Sabo dam distribution data	UTM Zone 49S	ESRI Shapefile
65	Serayu Opak River Basin Center, Ministry of Public Works and Public Housing	• Evacuation route spatial data • Village government office spatial data • Spatial data on the evacuation locations	UTM Zone 49S	ESRI Shapefile

The webGIS was equipped with a database query function to allow users to access data which were then displayed in the form of pop-up information. The webGIS also has a dynamic data display. Users can easily select the data from the legend menu to be displayed. Several types of data were also categorized based on colors and symbols to make it easier for users to understand the distribution of the locations; for example, the information on evacuation points was divided into three categories: gathering points, temporary shelter and permanent shelters. The gathering point is used as an initial evacuation place. The Village and District boundary also make it easier for users to identify their location; for example, the initial meeting point is located in Hargobinangun Village, Pakem District, while the temporary shelter point at the Hargobinangun Village Office and the permanent shelter is located in Kledok, Pakem District. By using this information system, the public can be educated, because of the completeness of the information, ease of access and navigation, and attractive display, and it can be accessed at any time. WebGIS, which is available to government agencies in Sleman Regency, can be accessed at http://wigunagis.42web.io/MitigasiMerapi.html#11/-7.6489/110.3752. Fig. 4 shows the display on webGIS on mitigation of Merapi Volcano eruption.

The webGIS was expected to be implemented to increase the level of public awareness about a potential Merapi Volcano eruption. Through usability testing, a total score of 81% (satisfied to very satisfied) for the display criteria, a total score of 81.8% (satisfied to very satisfied) for the navigation criteria and 83.3 % for the information criteria (satisfied to very satisfied). Only 16% to 19% of the respondents has a very not satisfied, not satisfied and average responds. Overall, the respondents were satisfied and very satisfied with webGIS as a way to mitigate the effects of a potential Merapi Volcano eruption. Table 3 shows the total scores for the usability testing.

The respondents also offered suggestions about how webGIS might be improved. They suggested adding a contact person from among the government or volunteers, adding a history of the eruptions of Merapi Volcano and the importance of webGIS developing into a mobile application. These suggestions and inputs were very helpful with regard to further webGIS development. The visualization and data displayed show the potential of web GIS to increase the awareness of the risk of Merapi Volcano erupting and facilitate the planning process by increasing the stakeholders' awareness about the importance of mitigating volcanic eruption risks, including an analysis of safe eruption areas, as well as the potential for evacuation shelter, evacuation routes and the selection of sustainable scenarios to minimize fatalities. However, some potential improvements remain, and the availability and quality of the data on the evacuation sites and evacuation routes must be updated regularly. The webGIS should be updated by developing participatory mapping through citizen and stakeholder engagement.

The webGIS has often been applied in the field of disasters. One example of using webGIS technology for disaster mitigation is urban flood mitigation (Palla & Gnecco 2021). This research concerns the implementation

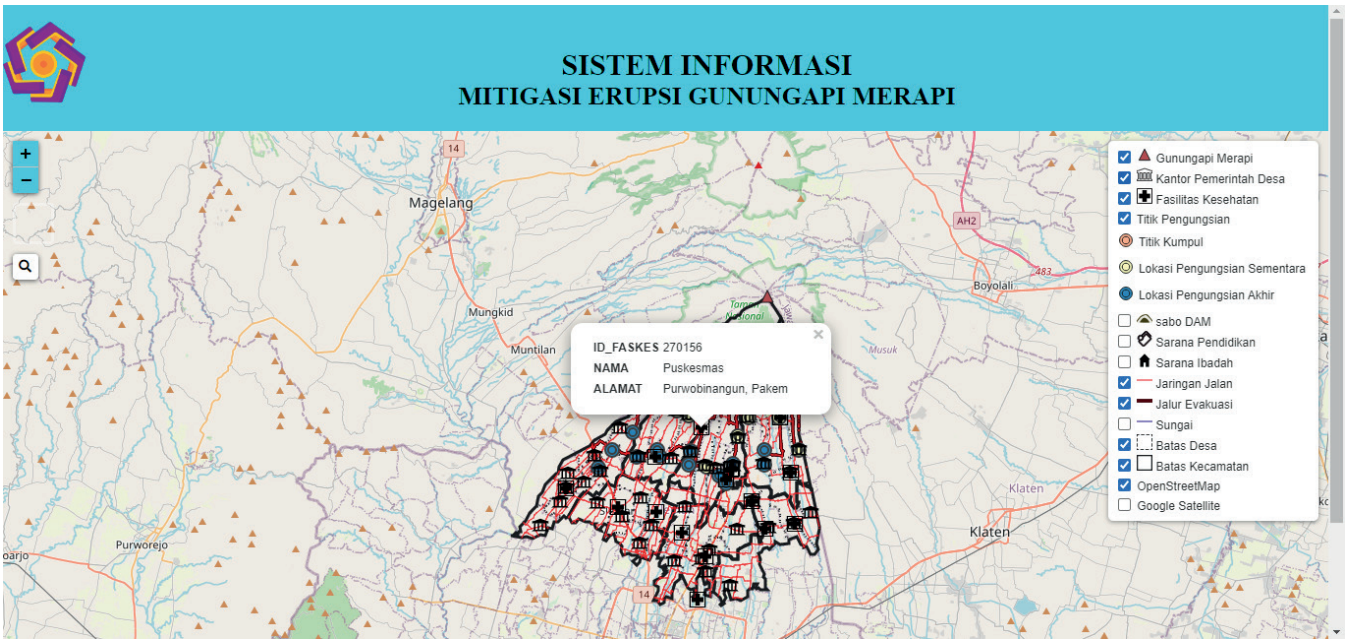

Fig. 4. WebGIS for Mitigating a Merapi Volcano Eruption

Table 3. The Total Scores for Usability Testing

No	Usability of the Website	VNS	NS	A	S	VS	Total
		1	2	3	4	5	
	Average responds (100 respondents)						
1	Display	0,33	3,67	15	39	42	100
2	Navigation	0,25	4,25	13,8	42,3	39,5	100
3	Information	0	6	10,7	37,3	46	100
	AVERAGE	0,19	4,64	13,16	39,53	42,5	100

Note: 1. VNS: Very Not Satisfied, 2. NS: Not Satisfied, 3. A: Average, 4. S: Satisfied, 5. VS: Very Satisfied

of a GIS-based web to support urban flood mitigation and assessing its impact. In this web-GIS application, a special web page is implemented to provide reference studies in the field of urban flood risk mitigation for urban areas. Rocha et al. (2021) studied a multi-hazard webGIS platform for coastal regions, which provides access to a detailed database of past hazardous events, organized along several risk indicators, for the western coast of Portugal. The combination of features on the platform provides a unique repository of hazard information to support end-users in terms of both emergency and long-term risk planning actions. This implementation can be further applied and extended to other coastal zones. Li, et al. (2022) built and analysed the use of webGIS for sustainable natural disaster education for high school students. In the 21st century, webGIS brings opportunities and challenges to the whole educational field, as it is an indispensable supplementary element to improve the quality of education and teaching, so that teaching activities can be effective and students can learn meaningfully (de Lázaro Torres et al. 2017).

Although there are many differences between webGIS platforms, software, databases, processing stages, analysis, and visualisation, the use of webGIS in the field of disasters can support and accelerate the decision-making when a disaster occurs, such as the disaster response, mitigation or reconstruction and recovery activities. Geographic Information System (GIS) and webGIS technology, when applied to disaster management, can help to reduce the loss of life, property and critical infrastructure in the face of natural disasters; facilitate a vulnerability analysis, multi-natural disaster studies, evacuation plans and evacuation shelter plans; and enhance targeted disaster management scenarios, modeling and simulations. With regard to disaster mitigation, GIS can minimize the impact or number of victims of disasters through mapping disaster-prone areas, based on education or increasing public awareness of disaster-prone areas. GIS can identify priority areas in disaster mitigation and also scan the damage and extent of the disaster that has occurred.

CONCLUSION

The webGIS for Merapi Volcano Eruption Mitigation was processed using QGIS software which was published by a free hosting provider. The webGIS contains information on evacuation routes, evacuation gathering points, village government offices, health facilities, religious facilities, and lahar control building points (Sabo dams), which will provide spatial information for mitigation. Based on the results of the usability testing, a total score of 81% and 83.3% (very satisfied) was obtained for the display and system information while, for the information on navigation, a total score of 81.8% (very satisfied) was obtained. Suggestions and input from the users or respondents were considered to improve the quality of webGIS and information for the community, especially related to the south flank of Merapi Volcano.

REFERENCES

Anand S.S., & Mobasher B. (2005). Intelligent Techniques for Web Personalization. In B. Mobasher, & S. S. Anand (Eds.), ITWP 2003, LNAI 3169, 1-36. Springer-Verlag Berlin Heidelberg.

Cobar L.J., Legono D., & Miyamoto K. (2016). Modeling of Information Flow for Early Warning in Mount Merapi Area, Indonesia. Journal of Disaster Research, 11(1), 60-71, DOI: 10.20965/jdr.2016.p0060.

De Bélizal É., Lavigne F., Gaillard J.C., Grancher D., Pratomo I., & Komorowski J.C. (2012). The 2007 Eruption of Kelut Volcano (East Java, Indonesia): Phenomenology, Crisis Management and Social Response. Geomorphology, 136(1), 165-175, DOI: 10.1016/j.geomorph.2011.06.015.

De Lázaro Torres M.L., De Miguel González R., & Morales Yago F.J. (2017). WebGIS and geospatial technologies for landscape education on personalized learning contexts. ISPRS Internatinal Journal of Geoinformation, 6(11), 1-18, DOI: 10.3390/ijgi6110350.

De Souza F.F. & Koizumi H. (2020). Land Readjustment in Denpasar, Indonesia: Effects on Land Management, the Spatial Distribution of Land Prices, and the Sustainable Development Goals. ADBI Working Paper 1148. Asian Development Bank Institute.

Edler D. & Vetter M. (2019). The Simplicity of Modern Audiovisual Web Cartography: An Example with the Open-Source JavaScript Library leaflet.js. KN - Journal of Cartography and Geographic Information, 69(3), 1-12, DOI: 10.1007/s42489-019-00006-2.

Hariyono E. (2018). The Characteristics of Volcanic Eruption in Indonesia Provisional Chapter The Characteristics of Volcanic Eruption in Indonesia. In book: Volcanoes - Geological and Geophysical Setting, Theoretical Aspects and Numerical Modeling, Applications to Industry and Their Impact on the Human Health. Publisher: InTech Open, DOI: 10.5772/intechopen.71449.

Hertzum M. (2020). Usability Testing: A Practitioner's Guide to Evaluating the User Experience: Synthesis Lectures on Human-Centered Informatics. Copenhagen: Morgan and Claypool Publisher, DOI: 10.2200/S00987ED1V01Y202001HCI045.

Hong J.H & Tsai C-Y. (2022). Using 3d Webgis to Support The Disaster Simulation, Management and Analysis – Examples of Tsunami and Flood. The International Archives of the Photogrammetry, Remote Sensing and Spatial Information Sciences, Volume XLIV-3/W1-2020, 2020Gi4DM 2020 – 13th GeoInformation for Disaster Management conference, 30 November–4 December 2020, Sydney, Australia (online), 43-50, DOI: 10.5194/isprs-archives-XLIV-3-W1-2020-43-2020.

Jousset P., Pallister J., & Surono (2013). The 2010 Eruption of Merapi Volcano. Journal of Volcanology and Geothermal Research, 241-242, 121-135, DOI: 10.1016/j.jvolgeores.2013.05.008

Kamarudin, A.N.A., Ranaivo-Malançon, B. & Musa, N. (2017). PIAK: A personalized internet access for kids in Zulikha, J. & N. H. Zakaria (Eds.). Proceedings of the 6th International Conference on Computing & Informatics, 547-552. Sintok: School of Computing.

Kusmiyarti T.B, Wiguna P.P.K., & Ratna Dewi N.K.R. (2018). Flood Risk Analysis in Denpasar City, Bali, Indonesia. IOP Conference Series Earth and Environmental Science, 123(1), 1-13, DOI: 10.1088/1755-1315/123/1/012012.

Li J., Xia H., Qin Y., Fu P., Guo X., Li R., & Zhao X. (2022). Web GIS for Sustainable Education: Towards Natural Disaster Education for High School Students. Sustainability, 14(5), 2694, DOI: 10.3390/su14052694.

Muslih M., Arianti N.D., Somantri, Thamren D.S., Fajri N., & Bulan R. (2022). Utilization of a Web-Based Geographic Information System for Land Mapping and Some Its Overview: A Case Study in Sukabumi District, Indonesia. International Journal of Design & Nature and Ecodynamics, 17(3), 369-374, DOI: 10.18280/ijdne.170306.

Mueller C.J., Tamir D., & Komogortsev O. & Feldman L. (2009). An Economical Approach to Usability Testing, 1, 124-129. Proceedings of the 33rd Annual IEEE International Computer Software and Applications Conference (COMPSAC), DOI: 10.1109/COMPSAC.2009.26.

Memo M.A., Ting H., Cheah J-H., Thurasamy R., Chuah F. & Cham T.H. (2020). Sample Size For Survey Research: Review And Recommendations. Journal of Applied Structural Equation Modeling, 4(2), i-xx.

Palla A. & Gnecco I. (2021). The Web-GIS TRIG Eau Platform to Assess Urban Flood Mitigation by Domestic Rainwater Harvesting Systems in Two Residential Settlements in Italy. Sustainability, 13, 1-17, DOI: 10.3390/su13137241.

Permatasari A.L., Suherningtyas I.A., & Wiguna P.P.K. (2020). Analysis of Local Spatial Data Infrastructure to Support Volcanic Mudflow Mitigation along Putih River, Magelang Regency, Central Java Province, Indonesia. Forum Geografi, 34(1), 66-76, DOI: 10.23917/forgeo.v34i1.11169.

Permatasari A.L., Suherningtyas I.A., & Wiguna P.P.K. (2021). Analysis of Vulnerability to Covid-19 Transmission based on Building Function at Padukuhan Mancasan Kleben, Pandowoharjo, Sleman, Yogyakarta, Indonesia. Forum Geografi, 35(2), 170-179, DOI: 10.23917/forgeo.v35i2.13755.

Rocha M., Oliveira A., Freire P., Fortunato A.B., Nahon A., Barros J.L., Azevedo A., Oliveira F.S.B.F., Rogeiro J., Jesus G., Martins R.J., Santos P.P., Tavares A.O., & Oliveira J. (2021). Multi-Hazard WebGIS Platform for Coastal Regions. Applied Science, 11, 1-16, DOI: 10.3390/app11115253

Santoso A., Parung J., Prayogo D.N., & Lolita A. (2021). Designing an Indonesian Disaster Management Information System with Local Characteristics: A Case Study of Mount Merapi. Journal of Disaster Research. 16(4), 765-777, DOI: 10.20965/jdr.2021.p0765.

Sardiana I.K., Purnawan N.L.R., Wiguna P.P.K., Suyarto R. & Kusmiyarti T.B. (2021). Analysis of Spatial Data Infrastructure to Support Tourism Village Promotion in Badung Regency, Bali, Indonesia. Indonesia Journal of Geography, 53(2), 179-184, DOI: 10.22146/ijg.52556.

Suherningtyas I.A., Permatasari A.L., Wiguna P.P.K., & Adninda G.B. (2021). Assisting smart disaster management for smart city program, case study: Pringgokusuman village, Yogyakarta. IOP Conference Series Earth and Environmental Science, 683(1), 1-8, DOI: 10.1088/1755-1315/683/1/012068.

Sukraini T.T., Yasa I.M.A. & Wiguna P.P.K. (2022). Comparing Choropleth And Graduated Symbols: How Different Map Types Affect Public Understanding In Covid-19 Map Reading In Badung Regency, Bali, Indonesia. eographia Technica, 17(1), 151-167, DOI: 10.21163/GT_2022.171.12.

Surono, Jousset, P., Pallister, J., Boichu, M., Buongiorno, M.F., Budisantoso, A., Costa, F., Andreastuti, S., Prata, F., Schneider, D., Clarisse, L., Humaida, H., Sumarti, S., Bignami, C., Griswold, J., Carn, S., Oppenheimer, C., & Lavigne, F. (2012). The 2010 explosive eruption of Java's Merapi volcano-A «100-year» event. Journal of Volcanology and Geothermal Research, 241-242, 121-135, DOI: 10.1016/j.jvolgeores.2012.06.018.

Solikhin A., Thouret J.C., Gupta A., Harris A.J.L. & Liew S. C. (2012). Geology, Tectonics, and the 2002-2003 Eruption of the Semeru Volcano, Indonesia: Interpreted From High-Spatial Resolution Satellite Imagery. Geomorphology, 138(1), 364-379, DOI: 10.1016/j.geomorph.2011.10.001.

Talib N., Fuad N., Saad N., Zaki N., Hashim N., & Abdullah M. (2021). Towards A Strategic Approach Of Covid-19 Cluster Web Mapping In Malaysia. Geography, Environment, Sustainability, 14(4), 148-154, DOI: 10.24057/2071-9388-2021-088.

Trigunasih N.M. & Wiguna P.P.K. (2020). Land Suitability For Rice Field and Conservation Planning in Ho Watershed, Tabanan Regency, Bali Province, Indonesia. Geographia Technica, 15(1), 124-131, DOI: 10.21163/GT_2020.151.11.

Warsini S., Mills J., West C., & Usher K. (2016). Living Through a Volcanic Eruption: Understanding The Experience of Survivors as a Phenomenological Existential Phenomenon. International Journal of Mental Health Nursing, 25(3), 206-213, DOI: 10.1111/inm.12212.

Whitten J.L. (2007). Systems Analysis and Design Methods. New York: McGraw Hill.

Wiguna P.P.K. (2021). Using Big Global Database to Analyse Impact of Web News to Tourist Visits Due To the 2017 Eruption of Agung Volcano, Bali, Indonesia. Geographia Technica, 16(2), 40-52. DOI: 10.21163/GT_2021.162.04

Wulan M.H., Nurhadi N, & Muryani C. (2021). Vulnerability of Society on Earthquake Disasters in Kayangan, North Lombok. IOP Conf. Series: Earth and Environmental Science, 683, 1-11, DOI: /1755-1315/683/1/012077.

Yang H., Shen D., & Huang H. (2015). A WebGIS-based Monitoring and Early-Warning System for Geological Disasters. 23rd International Conference on Geoinformatics, 1-6, DOI: 10.1109/GEOINFORMATICS.2015.7378718.

Yudistira D., Fadilah R., & Setiawan A. (2020). The Impact of Merapi Mountain Eruption on the Community Economy. Efficient: Indonesian Journal of Development Economics, 3(1), 719-725, DOI: 10.15294/efficient.v3i1.36695.

Zhao R., Liu X., & Xu W. (2020). Integration of Coseismic Deformation into Webgis for Near Real-Time disaster Evaluation and Emergency Response. Environmental Earth Sciences, 79(18), 414, DOI: 10.1007/s12665-020-09153-6.

RESEARCH PAPER

DISCOVERING SPATIAL DEVELOPMENT CONTROL FOR INDONESIA: A SYSTEMATIC LITERATURE REVIEW

Citra Fadhilah Utami[1*], Kosuke Mizuno[1*], Hayati Sari Hasibuan[1], Tri Edhi Budhi Soesilo[1]
[1]School of Environmental Science Programme, University of Indonesia, Salemba Raya Street No. 4 – Central Jakarta 10430, Indonesia
***Corresponding author:** citra.fadhilah@ui.ac.id, kosuke.mizuno@ui.ac.id
Received: October 23rd, 2021 / Accepted: November 11th, 2022 / Published: December 31st, 2022
https://DOI-10.24057/2071-9388-2021-119

ABSTRACT. As a developing country, Indonesia is experiencing rapid growth, necessitating the use of development-control instruments to achieve sustainable development. Furthermore, information about land reform implementation in Indonesia can only be found in academic journals written in Indonesian. As a result, determining the appropriate development-control model in Indonesia is critical. The appropriate concepts and development-control tools for Indonesia are discovered by reviewing papers that implement development control globally and the state of development-control implementation locally in Indonesia. However, by presenting the concept of controlling spatial development—beginning with defining development control, then capturing its typologies globally, and finally discussing the implementation condition in Indonesia—the model can also be adopted in countries with a similar planning system. The main gaps and challenges in implementing spatial development-control tools in Indonesia were identified in the final section of this article. In the meantime, a regulatory zoning system would be successful, but a discretionary system that includes economic development opportunities can be considered by strengthening human resources and institutions. The three elements in development control are spatial planning, land development, and regulation. Furthermore, the community's successful traditional spatial development control can be incorporated into the existing control regulations.

KEYWORDS: Spatial development control, literature review, sustainable development, control regulation

CITATION: Utami C.F., Mizuno K., Hasibuan H.S., Soesilo T.E.B. (2022). Discovering Spatial Development Control For Indonesia: A Systematic Literature Review. Geography, Environment, Sustainability, 4(15), 64-79
https://DOI-10.24057/2071-9388-2021-119

ACKNOWLEDGEMENTS: This research was funded by University of Indonesia-International Indexed Publication (PUTI) 2020, number 626/SK/R/UI/2020.

Conflict of interests: The authors reported no potential conflict of interest.

INTRODUCTION

Sustainable development control is the goal of urban planning, which can be achieved through spatial use control (Gurran et al. 2015; Rowan-Robinson et al. 1995). In this context, spatial development controls have been conducted around the world. Their performance depends on various factors, including planning ability (Gurran et al. 2015), institutional capacity, land administration (Nel 2016a), and the need for community participation (Baics and Meisterlin 2016). It also promotes functional and integrated human settlements, maximizes resource efficiency, and elevates regional identity and a place's unique character (Yudono 2018). Spatial development control is a complex and multi-faceted subject, making it a challenging research field. Vast urban sprawl is a highly relevant topic in increasing urbanization levels worldwide. Spatial development control has arisen since the 1970s, owing to various environmental events that affect physical development and planning (Fuseini and Kemp 2015). Spatial planning helps to achieve a balance in urban development by promoting compact urban development and using undeveloped land versus reusing old urban sites. Sustainable urban development necessitates the prevention of uncontrolled urban sprawl in open spaces (Konyango et al. 2021). The number of journal articles on this subject has been progressively growing. Development control-related studies are becoming internationally widespread. There is an opportunity for a comprehensive, systematic, and up-to-date review of development-control research achievements and challenges.

Furthermore, Indonesia is facing a disruptive urban planning era (Margiansyah 2020; Yudono et al. 2020). The challenge of measuring sustainable development implemented would be an urgent matter in the planning process. Meanwhile, the development control was not fully implemented yet (Firman and Fahmi 2017; Suroso and Firman 2018). This article determines Indonesia's appropriate spatial development control model, considering its implementation challenges. The model developed can also be adopted by other developing countries with similar planning systems.

The purpose of this article is to determine the most appropriate spatial development control tools for Indonesia's condition. It is accomplished by analyzing the general characteristics of researchers of spatial development control implementation worldwide and then evaluating the performance of spatial development

control internationally and locally in Indonesia. From an international research sources, the study investigates spatial development control instruments, as well as their flaws and advantages. The implementation of spatial development control in Indonesia determines the successful technique, the weaknesses of the existing control instruments, and the country's conditions.

LITERATURE REVIEW

Development control is an effort in systematic planning to ensure that the development follows the plan that has been prepared. As a result, extensive urban planning consists of three general stages: planning, implementation, and control (Zhuang et al 2018). Moreover, development control is interpreted as a strategy for protecting an individual's property rights from outside disturbances (Amri and Giyarsih 2022). It should also protect others' rights, so they do not jeopardize public property. So, what is under the regulation of production control? The scope of production control can be very wide, starting with the building exterior, which must comply with the statute.

Spatial development control has existed since the late 19th century when the zoning concept was introduced (Peng et al. 2018). The first study was conducted by Wakeford in the United States in 1990, followed by Davies' study in 1989 on five European countries that began to consider the importance of controlling development (Booth 1993). Zoning regulations are instruments for regulating land use in the United States and several other countries (Aliyah et al. 2017). Zoning divides an area into several parts determined through regulations to separate industrial and commercial development from residential areas (Yu and Hui 2019). This concept then spread to other countries, such as the United States and Canada.

Land development control, such as zoning, is typically justified by planners in terms of social welfare to mitigate market failures, such as negative externalities or social costs, and provide public goods (Acheampong 2019). Spatial use control attempts to incorporate social and environmental considerations into the planning process. The three types of land development control used transaction cost theory to classify various forms and agents of governance in the land development process and the property market. When the state owns the land, the plan requirements are written into the land lease contract with the private agents. Development control takes the form of contractual covenants and deed restrictions when the planner is a private developer (Yu 2020). Private individuals can create, and the government can enforce contractual obligations that limit land development. This type of contract zoning or development control is used in the Netherlands, Israel, and Hong Kong. Coase's description of reality is more in line with Pigouvian social welfare theory in understanding development control as an economic and political planning tool (Lai and Lorne 2013).

According to Amri and Giyarsih (2022), development control can be divided into regulatory and discretionary systems. In the regulatory system, space use is based on legal certainty in the form of zoning regulations. The United States is one of the countries that apply this system, though it first existed in Germany (Amri and Giyarsih 2022). The authorized planning agency decides on a request for spatial development in the discretionary system. England is one of the countries that have adopted this system, which necessitates the ability of good plan human resources. It is since the implementation of this system is heavily reliant on the skills of professional technical planners (Nel 2016b).

Development-control tools typologies

Various forms of spatial use control have existed since the establishment of settlements. The basic objective is to enforce restrictions on space use and development considered important and the general public's desires. Several instruments for spatial development control are based on urban planning objectives (Zhuang et al. 2018), including zoning regulations, the imposition of sanctions, providing incentives and disincentives, and conducting environmental-impact analysis.

The United States introduced the first form of spatial use control based on the land development code (Owusu-Ansah and Atta-Boateng 2016). The code contains development and property use regulations, including zoning, subdivisions, and other related activities. Zoning is a land use management system that focuses on controlling the externalities of each use (Yu 2020). The land use regulation instruments were used to extract public benefits from large-scale developments in different ways, such as density negotiations in exchange for public benefits, incentive zoning programs, inclusionary zoning, transfer development regulation, and impact fees (Kim 2020). Zoning also regulates the floor area ratios and their impact on society and the generated traffic (Bird et al. 2019).

Spatial planning is an important stage of controlling space use (Firman 2004a). Although the spatial plan was not legally binding, development management policies, including site selection notes, land use and construction permits, and fines for unauthorized land occupations, were implemented by city- and district-level planners based on accepted master plans (Deng 2018).

The land development permit system is intended to control land use development (Firman 2004b). Provided processes are transparent, and in line with the principles of administrative justice, the proposed land use management system will also be consistent with the principle of good administration.

MATERIALS AND METHODS

Search and data sources

Two levels of review were applied in this article. This study reviewed internationally published articles on spatial development-control practices obtained from Scopus and ScienceDirect. Further, national articles were also searched on Google Scholar to collect specific situations of planning implementation in Indonesia. To capture the current situation, we focus only on studies published in 7 years, from 2012 to 2020.

Data screening

The papers were then classified using data mining processes, and an overview of tools and implementation of development-control research was provided. Each article was evaluated using a structured data extraction format, considering the research standard. Author, year, title, journal, abstract, keywords, research intent, subjects, comprehensive themes, research methods, and data source were all extracted. The keywords and field of study were then examined in the following stage. We examine the performance of spatial development-control tools, the study method, the implementation challenges, and

the data source.

In the first search for international research sources, 385 articles were found. However, not all of these articles were about urban planning. As a result, a second screening was performed to find related articles. Thirty-nine articles were chosen from 189 urban planning-related articles published between 2012 and 2020 to describe the development-control implementation. Regarding national resources, the phrase «*pengendalian pemanfaatan ruang*» which translates to «development control» in Indonesian, was used to search Google Scholar for relevant articles. Three hundred-one articles about urban planning were gathered in the second step, which is managing the results of the first search. Only 48 articles were chosen for the third step to screen the relevant articles related to urban planning and published between 2012 and 2020. Finally, we chose 26 articles that could provide information on Indonesia's development-control implementation from 2012 to 2020. The international and Indonesia research sources selection processes were examined regarding development-control tools, their performance, the research method used, and the implementation challenges of development-control tools. Figure 1 depicts the article selection process.

The next step was to analyze the number of articles, country of research, and the relationship between research elements using NVIVO 12 and VosViewer as bibliometrics data analysis displays better to understand the general characteristics of spatial development-control studies. A comparative matrix of all selected articles was created to assess the overall performance and challenges of spatial development-control implementation. The current study examines spatial planning control tools, their limitations, and the benefits of foreign posts. The assessment in Indonesia describes the effective strategy, the shortcomings of the existing control tools, and the regional conditions. The sentiment analysis and comparative matrix are used to interpret the discussion and concept of development control. To avoid discrepancies, the authors of this review engaged in intense discussion.

RESULTS AND DISCUSSION

The need to control spatial growth has emerged since the 1970s as a result of numerous environmental events affecting physical development (Fuseini and Kemp 2015). The number of journal publications on this topic has increased significantly. From the 1970s to the end of 2020, 4189 articles were registered in ScienceDirect and Scopus (using the search phrases "development control" and "land use control"; however, only "cities," "urban studies," "land use planning," "development studies," and "regional urban planning" journal categories were considered) showed in Fig. 2. Since 2017, these articles have examined spatial development control in depth around the world. The vast majority of recent studies on the subject have come from China. There is also growing interested in development control in the Asia-Pacific region, including Hong Kong, Malaysia, Australia, and London. Despite the undeniable dominance of the American planning system in this area, development control-related studies are becoming more widespread internationally. A comprehensive, systematic, and up-to-date review of development-control research achievements and challenges exists. Furthermore, this article determines Indonesia's appropriate spatial development-control model to achieve sustainable development. Other developing countries with similar

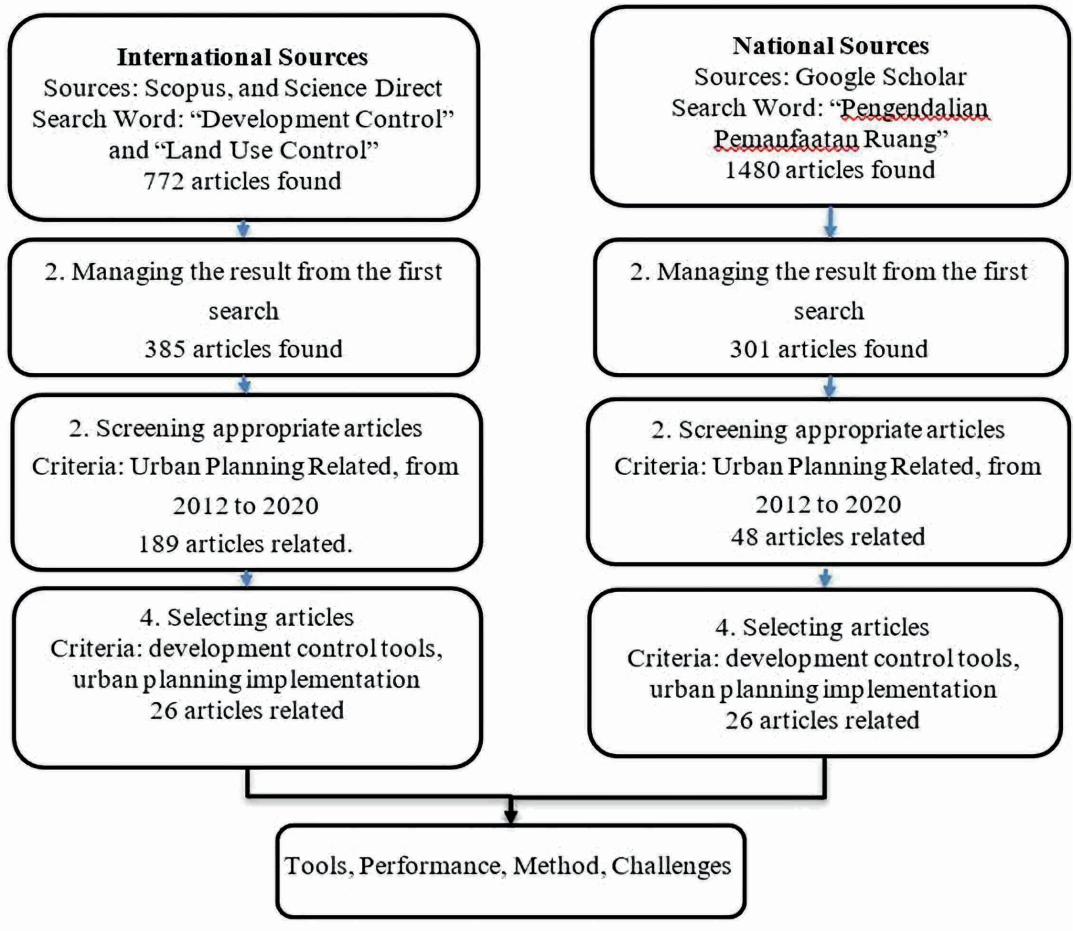

Fig. 1. Article selection process

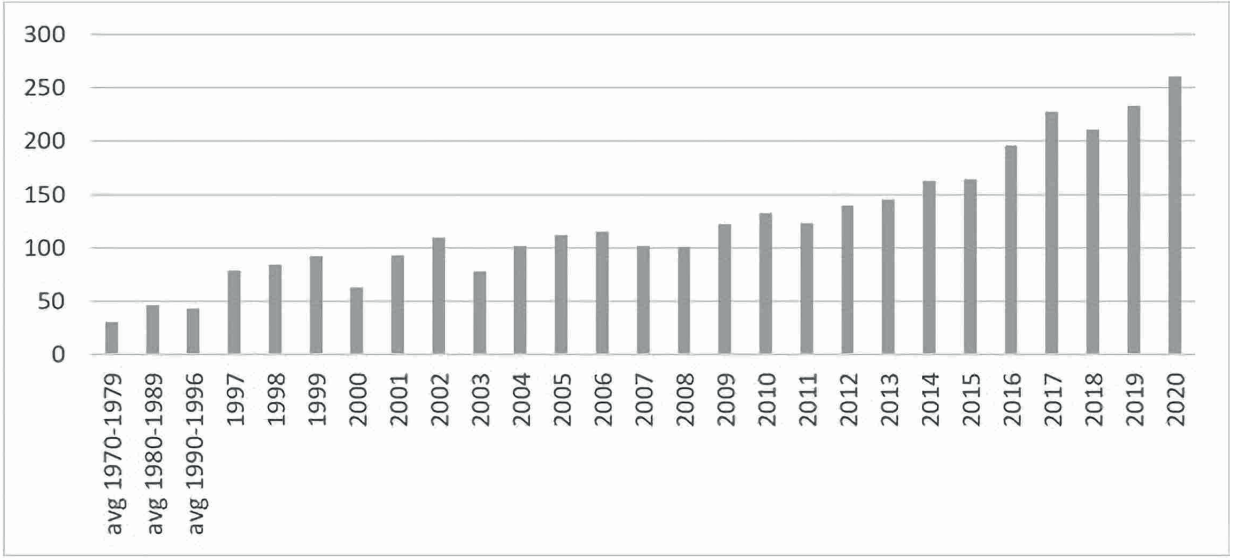

Fig. 2. Number of articles on development control registered in ScienceDirect and Scopus

planning systems can also use the model developed.

A significant amount of research has gone into analyzing the development of control tools. This study divides development control into two types based on a thorough literature review. Each type is addressed in its subsections below. Spatial development in the regulatory system is based on legal certainty in zoning regulations. Although this system originated in Germany, the United States is one of the countries that use it (Amri and Giyarsih 2022). The authorized planning agency decides on a request for spatial development in the discretionary system (Amri and Giyarsih 2022).

The following discussion focuses on spatial use control research. The tools used in various countries are mapped, including those in the Global North, which are developed countries with a well-established planning system, and those in the Global South, which are developing countries with dynamic planning systems in the process of development over the last five years of research. This information aided in describing the study's successes and shortcomings in implementing spatial use control. Figure 3 shows that most Global South countries use the regulatory system at the spatial use control stage, whereas the Global North countries use the discretionary system. However, several countries employ a hybrid system for spatial use control.

The concern of spatial development-control research can change over time depending on the focus of the study. The keywords in the research article can be used to determine the research focus. We can articulate important elements of spatial development control using bibliometric analysis in VosViewer. The results of the VosViewer bibliometrics analysis for international sources are shown in Fig. 4. The color change represents the evolution of the research's focus over time. In 2005, spatial control research concentrated on urban management,

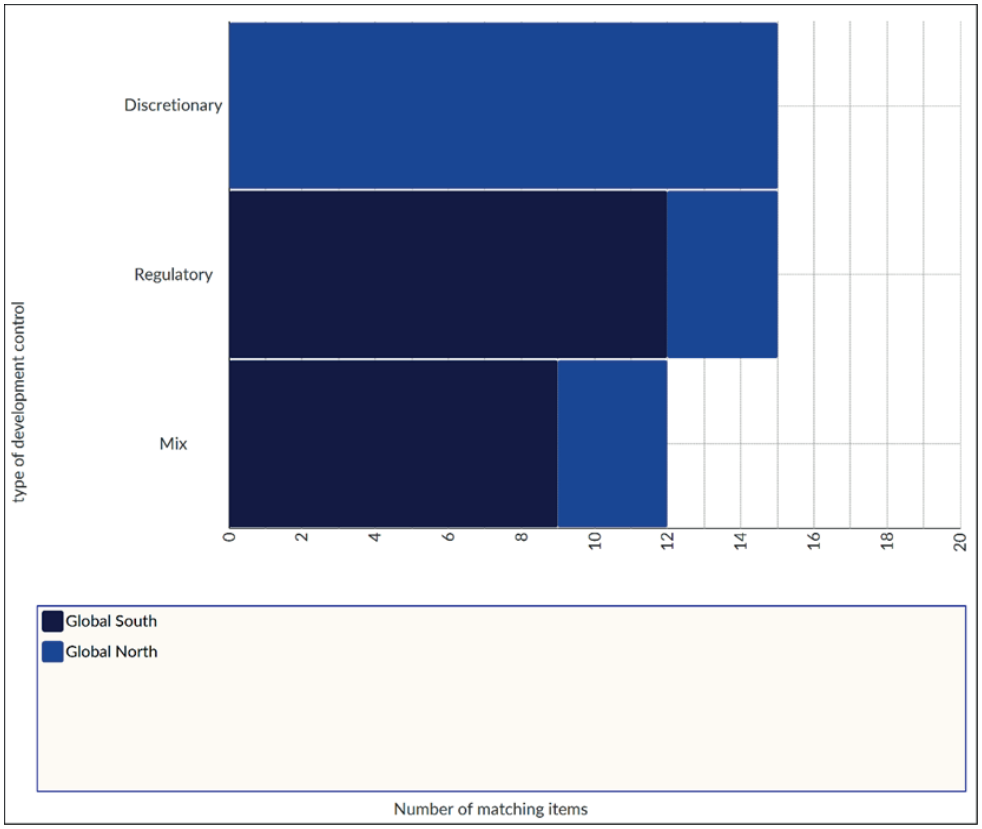

Fig. 3. Type of development control in Global South and Global North County

collaboration, social responsiveness, European countries, and city-level institutions. In 2010, the research emphasis shifted to evaluation, urban form, Ghana, Hong Kong, health impact assessment, informal settlements, and geographic information systems (GIS). Environmental planning, Australia, property rights, zoning, master planning, and regional planning were the elements that became the focus in 2015. The focus of research then shifted to ideology, economic restructuring, and finance over the next five years. At each stage, the main focus was on urban planning, housing, GIS, and urban management, which can be used as a foundation for spatial development control.

A bibliometric review of research papers on space use control from 2012 to 2020 was performed on VosViewer with bibliometric feedback to understand recent research on development control better. Figure 5 depicts the results of the bibliometric analysis. The most recent research on development control divides it into three categories: urban planning, land use, and the legal framework. Research in spatial planning clusters is interested in spatial planning frameworks, design guidelines, zoning with implications for land use laws, zoning negotiations, food systems, immigration, and city expansion. The second cluster of land use research is concerned with land use, the use of historical GIS, urban development, control, China, and development. Meanwhile, the third cluster includes the legal framework for regulating urban growth and the Abercrombie plan.

The matrix in Appendix Table A. 1 maps development-control instruments in various countries based on the most recent research. The conditions that allow the tools to be used are described by success and weakness factors. Understanding human resources and the quality of plans in the drafting process remains a challenge in the regulatory system (Ioannou 2016; Kuusana and Eledi 2015; Shibeshi et al. 2015). The planning phase continues to accommodate progress while providing no direction for urban development (Gurran et al. 2015). Furthermore, land administration issues in the Global South affect the implementation of space use control (Agheyisi 2019; Nel 2016b). The countries of the Global North that use the discretionary system rely on the planning board's decisions. The discretionary system faces several implementation challenges for planning, including requiring committee members to thoroughly understand planning and its social, economic, and environmental implications (Hsu et al. 2016). The economic benefits of this planning transaction are also difficult to quantify, particularly those representing the economic benefits of the entire community and other

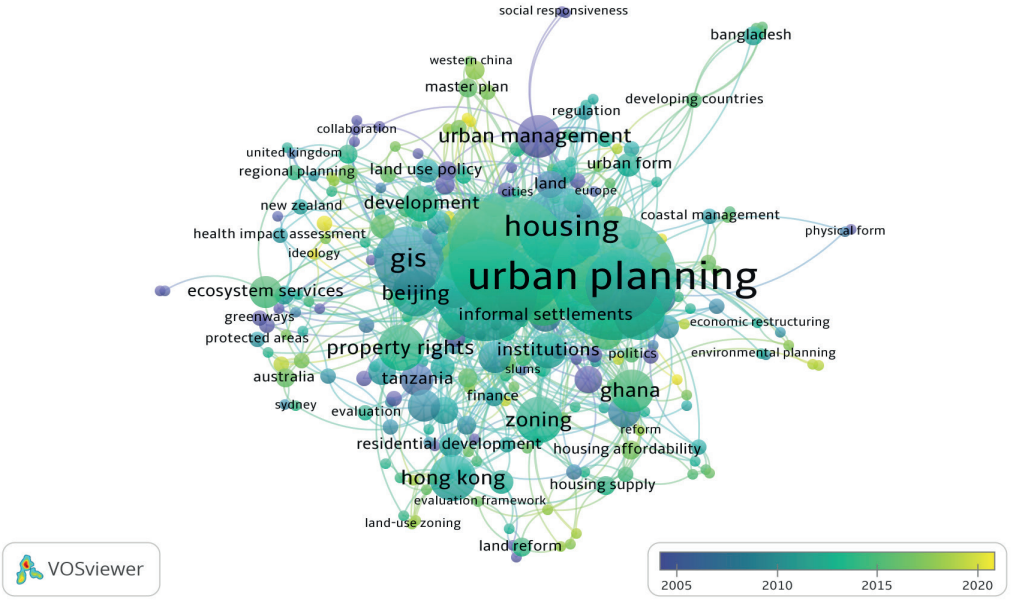

Fig. 4. The relationship between research elements with VosViewer from 2005 to 2020

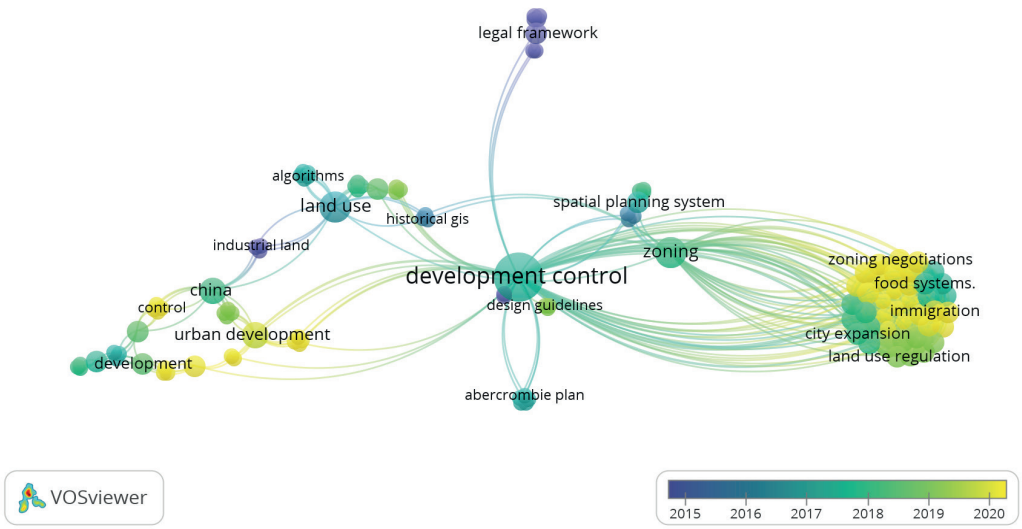

Fig. 5. The relationship between research elements with VosViewer for 2015–2020

social and environmental benefits (Hong et al. 2017). There is an opportunity to use land value capture as a concern to take advantage of land value as an instrument for spatial development control because its implementation is thought to promote city compactness (Kim 2020) effectively. A qualitative approach was used in this study to support the method of describing the planning conditions in the country or city.

Meta-analysis of research on development control in different countries is depicted in Fig. 6 as elements that can be used to draw a big picture of development control (Table 1). The components of creative control research can be classified into five interconnected groups. The area of development control is primarily of public interest, but it also affects private interests. This relates to the scope of the second category. The scope of land and space, particularly land use agreements on private landowners, do not conflict with the public interest. The arrangement is limited to building features visible to the public, such as the building facade. Land use, including improvements to its use; the physical environment, such as circulation, drainage, and green space; and spacing, which includes the basic building coefficient and the building floor coefficient, are all regulated by development control. The social identity of the neighborhood is defined before the building style. Building experts are concerned with the building's material, form, appearance, aesthetic control, and social character. The various instruments used in scope land use, according to the most recent development control articles, include Land Use Ordinance (Ahmad and Anjum 2012), Land Use Control (Abass et al. 2020), Land Subdivision Regulation (Agheyisi 2019), Statutory Planning (Alexander et al. 2012), Land Use Plans (Bidandi and Williams 2020), Development Regulations, Land Allocation (Cirolia and Berrisford 2017), Development Plan Transfer (F (Gurran et al. 2015; Hsu et al. 2016; Kim and Jang 2017). Urban Design includes upzoning (Kim 2020), building permits (Yin and Abdullah 2020), development management systems, and environmental impact assessments of land use policy. Building codes and design guidelines are used to regulate building construction. The final component explains why development control research is important. Researchers are concerned about the impact of construction on pollution, unnecessary noise, fire, health, highway, social character, and the right to peaceful enjoyment of one's own surroundings, so it must be controlled.

Identification of policy issues caused by development-control practices in Indonesia

An overview of the country is required to determine the best development-control model for Indonesia. Indonesia is a country made up of 17,000 islands. It is made up of hundreds of different cultures and ethnicities. This accumulation was built during the Dutch colonial period and is still used today. The most populous and densely populated island is Java, which accounts for only 7% of Indonesia's total land area but is home to 60% of the country's population and Indonesia's dominant ethnic group, the Javanese. The lingua franca maritime traders use is Indonesian, based on the Malay language (Sataloff et al. 2005).

Since the large kingdoms in Indonesia, urban spatial planning has long emerged. De Statuten Van, a modern urban spatial planning document issued by the Dutch government in 1642, was carried out for the city of Batavia. This regulation addresses the construction and maintenance of waterways, housing, and urban expansion, as well as the city government's authority and responsibility. The Dutch government then issued *Decentralisatie Wet*, which governed the formation of municipal and regional governments in 1903. Then came the *Koninklijke Besluit* 1904, strengthened by the *Locale Raden Ordonantie* 1905, which gave the city government the authority to decide on urban development issues. In addition, the Dutch East Indies government drafted a bill on urban area planning in Java in 1939. This bill was renamed *Stadsvorming Ordonantie-Ordinance City Formation* in 1948. Then, an implementing regulation, *Stadsvormingverdoning SVV*, a city formation regulation, was issued to speed up rebuilding war-damaged areas.

The City Development Bill, which regulates provisions in development stages, development financing, development regulations, and urban renovation, was drafted in 1970 in response to the need for urban planning (Sataloff et al. 2005). Then came Law No. 24 of 1992 on spatial planning, which established the stages of spatial planning: planning, utilization, and control. This law exists to regulate spatial planning in Indonesia, considering the following factors: (1) Indonesia as an archipelago with a diverse ecosystem, (2) coordinated and integrated natural

Table 1. The meta-analysis on research on development control in different countries

Domain	Public Interest		Private
Scope	Land – Spatial		Buildings
What to control	Land Use–Physical Environment	Layout, Spacing	Material, form, appearance, aesthetic control, social character
Development control tools	Land use ordinance, land use control, land subdivision regulation, statutory planning, land use plan, development regulation, land allocation development plan transfer development right zoning and land use regulations land use control	Density and scale, density bonuses building permit permission zoning, densities, green spaces, and layouts up zoning planning permits, development-control mechanism, and environmental impact assessment land use regulation urban design	Design guidelines, building code building rules
Impact	polluting industry, excessive noise, fire, health, highway, social character, the right to the quiet enjoyment of one's own surroundings		

resource management, (3) development patterns in a single dynamic environmental system, and (4) the fact that spatial planning can accommodate development developments.

Following the establishment of a regional autonomy government system because of the Reformation Order, Law 26 of 2007 on Spatial Planning was enacted with the goals of (1) wise natural resource management, (2) creating conditions and legal certainty, (3) strengthening national resilience, (4) expanding the existence of space and people's understanding of spatial planning, and (5) disaster mitigation based spatial planning.

At this point, spatial use control is being used in Indonesia. Since Law No. 27 of 2007 on spatial planning, Indonesia has been familiar with spatial use control instruments. The law replaces Law No. 24 of 1992, emphasizing the country's condition, including disaster-prone areas and environmental damage. As a result, urgent spatial development control is established. Furthermore, to exert control over its spatial development, Indonesia employs a mix of regulatory and discretionary systems.

The implementation of spatial development control, according to Indonesia Government Regulation Number 15 of 2015 on the Implementation of Spatial Planning, is an attempt to establish orderly spatial planning in compliance with the stipulated spatial planning, either by Presidential Regulations, Provincial or Regency, or City Regulations. The goal of spatial development control is to ensure that land use plans are consistent with spatial planning plans. Spatial use control is implemented through zoning regulations, spatial use permits, incentives and disincentives, and penalties.

There is a land right in inland use that gives the owner the right to use the land. However, a development right in spatial planning regulates that a plot of land can be used for land use according to the spatial plan. Due to policy differences, land use management as a subsystem of spatial planning has yet to be implemented in Indonesia. The disclosure of information about land ownership and spatial planning impedes land and spatial planning synchronization.

A literature review was conducted on the 26 articles from Google Scholar regarding the implementation of space use control from 2015 to the end of 2020 to determine the performance of spatial use control in Indonesia (Table A. 2 in the Appendix). According to a VosViewer bibliographic analysis (Fig. 6), the most frequently used phrases in articles about development control in Indonesia are spatial planning law, flood and disaster, spatial use management, spatial use changes, and massive development.

The articles discuss specific cases of spatial development control and provide specific conditions for space use control performance. According to Table 2 in the Appendix, not all spatial use control instruments are used. Permits and sanctions are the most used spatial use controls, whereas zoning is not widely used. The consistency of law enforcement is a common barrier encountered when implementing spatial use control in Indonesia. The lack of integrated licensing and spatial planning leads to numerous irregularities, which are not met with legal repression. Furthermore, planners cannot develop plans that serve as the foundation for spatial development control (Murti 2018). The developed plans were more responsive to development but were too late to recognize market developments. The importance of community involvement in developing development control instruments should be emphasized in developing spatial use control instruments (Chandra et al. 2019; Destratianto and Pramono 2020).

According to the bibliometric analysis of international and Indonesia research sources on development control, three important elements for implementing development control are spatial planning, land development, and regulation. The code for development control is shown in Fig. 7 based on the NVIVO12 code analysis.

The elements of development-control implementation are shown in Fig. 8. The three elements, namely, spatial planning, land development, and regulation, should function synergically to make the optimal implementation.

These three components are linked. Spatial planning regulations (such as community planning and construction regulations, land use regulations, regional planning

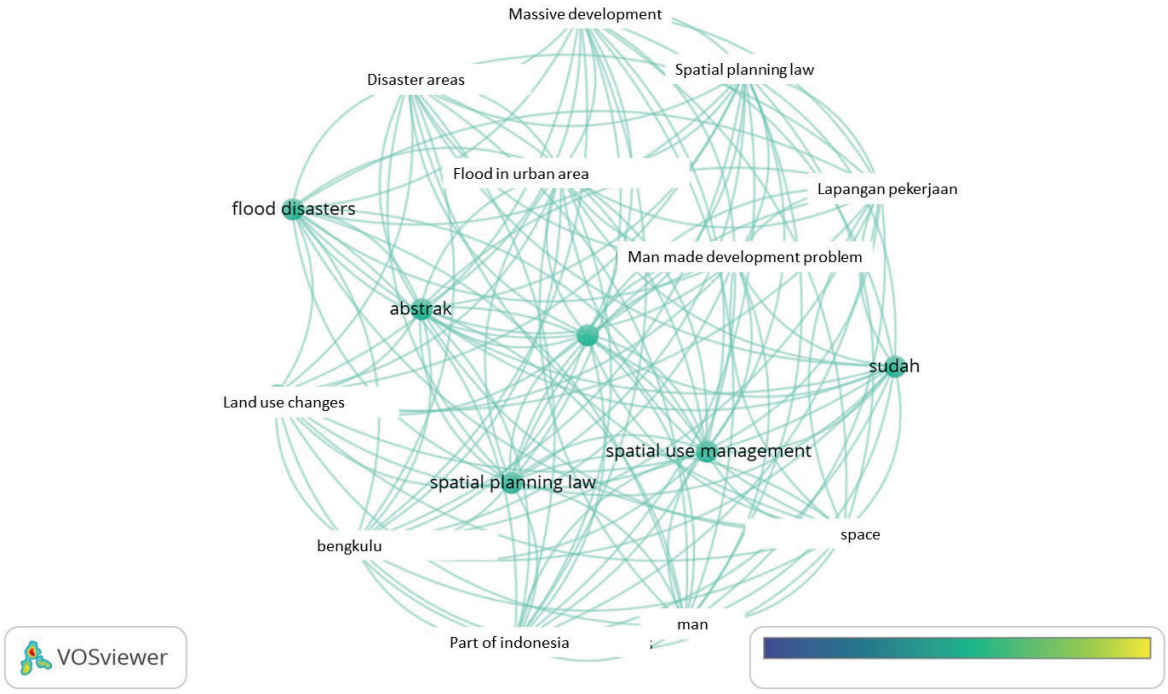

Fig. 6. The relationship between research elements of national development-control research with VosViewer

Fig. 7. Code analysis of development-control research in NVIVO12

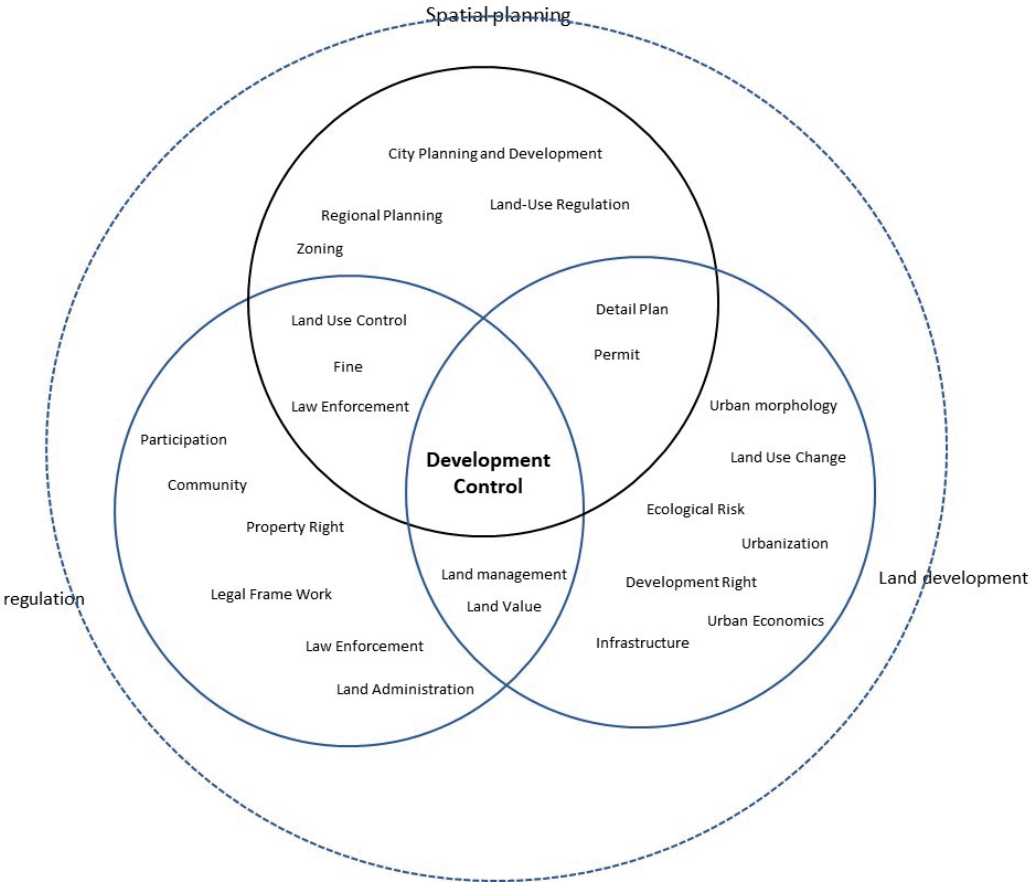

Fig. 8. Three elements of development control

regulations, and zoning regulations) serve as the foundation for managing space utilization in spatial planning elements. Furthermore, the plan must understand the state of soil morphology, land-use changes, ecological risks, and how the community perceives development. Infrastructure and the urban economy could benefit from spatial control. Furthermore, regulations must be enacted to govern the use of this room. Land administration regulations are based on the implementation of land control. The intersection of elements in the performance of commands may be strategic. The comprehensive plan requirement serves as the foundation for licensing. Land conservation and consideration of land values must be the foundation for developing legislation. The fundamental items that must be provided are clarification of land use management rules and regulations and penalties. This feature presents a challenge in its implementation in Indonesia. According to a review of previous research, the need for regional planners who can compile plans and control regional directives has become difficult, to the point where it appears that they only obey market shifts. The community's understanding of spatial planning remains very limited. The limitation of this research is that it is simply a review of numerous studies conducted, so practitioners must gain clarity from managing space use, interacting directly with the group, and direct consulting with experts.

CONCLUSIONS

By examining the interest of each international and Indonesia research sources discussing spatial development control, it is possible to conclude that there are three foundations in development control. The three foundations are the spatial plan, land development, and institution. As a guide in managing the development permit, a detailed plan is required. A spatial plan should consider urban development holistically, taking into account urban economics and ecological risks associated with land-use change. The institution also serves as a foundation for the implementation of development control. Participation of the community, developers, and development of planning officers as the front line of control. Land management could be strategic tools in spatial development control, specifically how to manage property rights and value as the intersection of urban development and institutions.

Spatial use control in Indonesia highlights the importance of better understanding among planners, the government, and the general public. Aside from its economic benefits, existing instruments such as licensing can be a transactional effort to control spatial use. The need for detailed planning as a foundation for controlling is also a major factor in implementing spatial use control. Effective sanctioning efforts should be backed up by legal capacity.

There is an opportunity for land value capture implementation in zoning based on the gaps in the advantages and disadvantages of spatial development control. With a good system, the land value capture implemented in Indonesia includes the success of tax instruments as revenues, though it can be used to regulate zoning. Legalized informal control instruments should provide the opportunity to capitalize on the value of traditional use control.

REFERENCES

Abass K., Buor D., Afriyie K., Dumedah G., Segbefi A.Y., Guodaar L., Garsonu E.K., Adu-Gyamfi S., Forkuor D., Ofosu A., Mohammed A. and Gyasi R.M. (2020). Urban Sprawl and Green Space Depletion: Implications for Flood Incidence in Kumasi, Ghana. International Journal of Disaster Risk Reduction, 51, 101915, DOI: 10.1016/j.ijdrr.2020.101915.

Acheampong R.A. (2019). The Concept of Spatial Planning and the Planning System. In: Spatial Planning in Ghana. The Urban Book Series. Springer, Cham. DOI: 10.1007/978-3-030-02011-8_2.

Agheyisi J.E. (2019). Inter-Communal Land Conflicts in Benin City, Nigeria: Exploring the Root Causes in the Context of Customary Land Supply. Land Use Policy, 83, 532-542, DOI: 10.1016/j.landusepol.2019.02.027.

Ahmad N. and Anjum G.A. (2012). Legal and Institutional Perplexities Hampering the Implementation of Urban Development Plans in Pakistan. Cities 29, 4, 271-277, DOI: 10.1016/j.cities.2011.07.006.

Akil A. (2020). Penyuluhan Mekanisme Pengendalian Pemanfaatan Ruang Wilayah Kota di Kantor Kecamatan Biringkanaya Kota Makassar [Counseling on Urban Spatial Use Control Mechanisms at the Biringkanaya District Office, Makassar City]. Jurnal Teknologi Terapan Untuk Pengabdian Masyarakat, 3, 71-80 (in Indonesian).

Alexander E.R., Mazza L. and Moroni S. (2012). Planning Without Plans? Nomocracy or Teleocracy for Social-Spatial Ordering. Progress in Planning, 77, 2, 37-87, DOI: 10.1016/j.progress.2011.12.001.

Aliyah I., Setioko B. and Pradoto W. (2017). Spatial Flexibility in Cultural Mapping of Traditional Market Area in Surakarta (A case study of Pasar Gede in Surakarta). City, Culture and Society, 10, 36, 41-51, DOI: 10.1016/j.ccs.2017.05.004.

Allouf D., Martel A. and March A. (2020). Discretion Versus Prescription: Assessing the Spatial Impact of Design Regulations in Apartments in Australia. Environment and Planning B: Urban Analytics and City Science, 47, 7, 1260-1278, DOI: 10.1177/2399808318825273.

Amri I. and Giyarsih S.R. (2022). Monitoring Urban Physical Growth In Tsunami-Affected Areas: A Case Study Of Banda Aceh City, Indonesia. GeoJournal, 87, 1929–1944, DOI: 10.1007/s10708-020-10362-6.

Baics G. and Meisterlin L. (2016). Zoning Before Zoning: Land Use and Density in Mid-Nineteenth-Century New York City. Annals of the American Association of Geographers, 106, 5, 1152-1175, DOI: 10.1080/24694452.2016.1177442.

Baker D.C., Sipe N.G. and Gleeson B.J. (2006). Performance-Based Planning: Perspectives from the United States, Australia, and New Zealand. Journal of Planning Education and Research 25, 4, 396-409, DOI: 10.1177/0739456X05283450.

Bidandi F. and Williams J.J. (2020). Understanding Urban Land, Politics, and Planning: A Critical Appraisal of Kampala's Urban Sprawl. Cities, 106, 102858, DOI: 10.1016/j.cities.2020.102858.

Biggar J. and Siemiatycki M. (2020). Tracing Discretion in Planning and Land-Use Outcomes: Perspectives from Toronto, Canada. Journal of Planning Education and Research, DOI: 10.1177/0739456X20904427.

Bird B.W., Barr R.C., Commerford J., Gilhooly W.P., Wilson J.J., Finney B., McLauchlan K. and Monaghan G.W. (2019). Late-Holocene Floodplain Development, Land-Use, And Hydroclimate–Flood Relationships on the Lower Ohio River, US. Holocene, 29(12), 1856-1870, DOI: 10.1177/0959683619865598.

Boamah N.A., Gyimah C. and Bediako Nelson J.K. (2012). Challenges to the Enforcement of Development Controls in the Wa Municipality. Habitat International, 36(1), 136-142, DOI: 10.1016/j.habitatint.2011.06.010.

Booth P. (1993). The Cultural Dimension in Comparative Research: Making Sense of Development Control in France. European Planning Studies, 1(2), 217-229, DOI: 10.1080/09654319308720210.

Budhianti M.I. (2020). Penyimpangan dan Pelanggaran Pemanfaatan Ruang terhadap Rencana Tata Ruang Wilayah yang Telah Ditetapkan Pemerintah Daerah (Studi Kasus di Beberapa Kabupaten/ Kota di Provinsi Jawa Barat). Supremasi Hukum, 16, 58-80 (in Indonesian).

Budiyono (2020). Pengaturan Zoning untuk Pengendalian Pemanfaatan Ruang Kawasan Kotagede (Studi Kasus Kawasan Preservasi Budaya Kotagede). Jurnal Ilmiah PlanoKrisna, 15(1), 79-92 (in Indonesian).

Chandra D., Aulia T.B. and Izziah I. (2019). Kesesuaian Pemanfaatan Ruang Dan Penyelenggaraan Penataan Ruang di Koridor Jalan Teuku Nyak Arief Kota Banda Aceh. Jurnal Arsip Rekayasa Sipil Dan Perencanaan, 2(3), 214-223 (in Indonesian), DOI: 10.24815/jarsp.v2i3.13458.

Cirolia L.R. and Berrisford S. (2017). 'Negotiated Planning': Diverse Trajectories of Implementation in Nairobi, Addis Ababa, and Harare. Habitat International, 59, 71-79, DOI: 10.1016/j.habitatint.2016.11.005.

Collins M.P. (2017). The London County Council's Approach to Town Planning: 1909–1945. London Journal, 42(2), 172-191, DOI: 10.1080/03058034.2017.1305253.

Deng F. (2018). Work Unit and Private Community in the Evolution of Urban Planning in Contemporary China. Planning Theory, 17(4), 533-550, DOI: 10.1177/1473095217734413.

Destratianto D. and Pramono R.W.D. (2020). Efektivitas Implementasi Advice Planning di Perkotaan Banyuwangi [The Effectiveness of Advice Planning Implementation in Banyuwangi Urban]. Jurnal Penataan Ruang, 1(1), 92 (in Indonesian).

Falco E. and Chiodelli F. (2018). The Transfer of Development Rights in the Midst of the Economic Crisis: Potential, Innovation and Limits in Italy. Land Use Policy, 72, 381-388, DOI: 10.1016/j.landusepol.2017.12.069.

Farhat R. (2019). Is Semi-Discretionary Design Review Wieldy? Evidence from Seattle's Program. Planning Practice and Research, 34(1), 103-119, DOI: 10.1080/02697459.2018.1548213.

Fazari S.L. (2020). Penegakan Hukum Lingkungan dan Pemanfaatan Ruang Udara [Enforcement of Environmental Laws and Utilization of Air Space]. Jurnal Ekologi, Masyarakat and Sains, 1(1), 30-36 (in Indonesian).

Ferreira A. (2020). Reconsidering the Merit of Market-Oriented Planning Innovations: Critical Insights on Transferable Development Rights From Coimbra, Portugal. Land Use Policy, 99, 104977, DOI: 10.1016/j.landusepol.2020.104977.

Firman T. (2004a). New Town Development in Jakarta Metropolitan Region: A Perspective of Spatial Segregation. Habitat International, 28(3), 349-368, DOI: 10.1016/S0197-3975(03)00037-7.

Firman T. (2004b). Major Issues in Indonesia's Urban Land Development. Land Use Policy, 21(4), 347-355, DOI: 10.1016/j.landusepol.2003.04.002.

Firman T. and Fahmi, F.Z. (2017). The Privatization of Metropolitan Jakarta's (Jabodetabek) Urban Fringes: The Early Stages of "Post-Suburbanization" in Indonesia. Journal of the American Planning Association, 83(1), 68-79, DOI: 10.1080/01944363.2016.1249010.

Fuseini I. and Kemp, J. (2015). A Review of Spatial Planning in Ghana's Socio-Economic Development Trajectory: A Sustainable Development Perspective. Land Use Policy, 47, 309-320. DOI: 10.1016/j.landusepol.2015.04.020

Gurran N., Gilbert C. and Phibbs P. (2015). Sustainable Development Control? Zoning and Land Use Regulations for Urban Form, Biodiversity Conservation and Green Design in Australia. Journal of Environmental Planning and Management, 58(11), 1877-1902, DOI: 10.1080/09640568.2014.967386.

Hastuti S.D. (2020). Pengendalian Pemanfaatan Ruang Melalui Izin Lokasi dalam Rangka Perolehan Tanah yang Diperlukan Usaha [Control of Spatial Utilization through Location Permits in the Context of Acquisition of Land Required by Businesses]. Jurist-Diction, 3(3), 1099 (in Indonesian), DOI: 10.20473/jd.v3i3.18640.

Hexagraha S.A.A. and Setyorini S.N. (2019). Tinjauan Terhadap Konsep Keadilan Spasial Dan Partisipasi Masyarakat Dalam Perencanaan Dan Pengendalian Pemanfaatan Ruang Pada Program Normalisasi Ciliwung Di Provinsi Dki Jakarta [Review of the Concept of Spatial Justice and Community Participation in Planning and Controlling Space Utilization in the Ciliwung Normalization Program in DKI Jakarta Province.]. Jurnal Hukum and Pembangunan, 49(2), 349 (in Indonesian), DOI: 10.21143/jhp.vol49.no2.2008.

Hong W., Guo R., Su M., Tang H., Chen L. and Hu W. (2017). Sensitivity Evaluation and Land-Use Control of Urban Ecological Corridors: A CASE STUDY of Shenzhen, China. Land Use Policy, 62, 316-325, DOI: 10.1016/j.landusepol.2017.01.010.

Hsu K.C., Lai T.Y. and Li C.N. (2016). Why is There an Urban Pattern Toward Sprawling Development?. Proceedings of the Institution of Civil Engineers: Urban Design and Planning, 169(4), 200-208, DOI: 10.1680/udap.14.00035.

Hu T. and Zhou J. (2018). Co-exist or Integrate ? Reviewing the Spatial Planning Reform of China from the Perspective of Central-Local Relations. International Review for Spatial Planning and Sustainable Development A: Planning Strategies and Design Concepts, 6 (3), 168-184.

Hubbard P. (2015). Law, Sex and the City: Regulating Sexual Entertainment Venues in England and Wales. International Journal of Law in the Built Environment, 7(1), 5-20, DOI: 10.1108/IJLBE-01-2014-0001.

Ioannou B. (2016). Post-colonial Urban Development and Planning in Cyprus: Shifting Visions and Realities of Early Suburbia. Urban Planning, 1(4), 79-88, DOI: 10.17645/up.v1i4.768.

Jaya G.N.P. (2019). Identifikasi Kerjasama Pengendalian Pemanfaatan Ruang dengan Pola Partisipatif di Kota Pamanukan Kabupaten Subang [Identification of Spatial Use Control Collaboration with Participatory Patterns in Pamanukan City, Subang Regency]. Jurnal Pakuan Bidang Keteknikan, 1(33), 1-8 (in Indonesian).

Kim H.R. and Jang Y. (2017). Lessons from Good and Bad Practices in Retail-Led Urban Regeneration Projects in the Republic of Korea. Cities, 61, 36-47, DOI: 10.1016/j.cities.2016.11.004.

Kim M. (2020). Upzoning and Value Capture: How U.S. Local Governments Use Land Use Regulation Power to Create and Capture Value from Real Estate Developments. Land Use Policy, 95, 104624, DOI: 10.1016/j.landusepol.2020.104624.

Konyango C. O., Hayombe P. O. and Owino F. O. (2021). Effectiveness of Planning Tools in Managing the Spatial Stability of Peri-Urban Areas. Architecture Research, 11(2), 31-52. DOI: 10.5923/j.arch.20211102.01.

Kuusaana E.D., and Eledi J. A. (2015). Customary Land Allocation, Urbanization and Land Use Planning in Ghana: Implications for Food Systems in the Wa Municipality. Land Use Policy, 48, 454-466, DOI: 10.1016/j.landusepol.2015.06.030.

Lai L.W.C. and Lorne F.T. (2013). The Fourth Coase Theorem: State Planning Rules and Spontaneity in Action. Planning Theory, 14(1), 44-69, DOI: 10.1177/1473095213510430.

Lawanson T. and Agunbiade M. (2018). Land Governance and Megacity Projects in Lagos, Nigeria: The Case of Lekki Free Trade Zone. Area Development and Policy, 3(1), 114-131, DOI: 10.1080/23792949.2017.1399804.

Lian X. (2018). Review on Advanced Practice of Provincial Spatial Planning: Case of a Western, Less Developed Province. International Review for Spatial Planning and Sustainable Development, 6(3), 185-202, DOI: 10.14246/IRSPSDA.6.3_185.

Margiansyah D. (2020). Revisiting Indonesia's Economic Diplomacy in the Age of Disruption: Towards Digital Economy and Innovation Diplomacy. JAS (Journal of ASEAN Studies), 8(1), 15, DOI: 10.21512/jas.v8i1.6433.

Murti D.P.P.K. (2018). Efektivitas Pasal 72 Huruf A Angka 1 Peraturan Daerah Kabupaten Buleleng No. 9 Tahun 2013 Dalam Pemanfaatan Ruang Sempadan Pantai Kawasan Bali Utara [Effectiveness of Article 72 Letter A Number 1 Buleleng Regency Regulation No. 9 of 2013 in the Utilization of Coastal Border Space in the North Bali Region]. Journal of Chemical Information and Modeling, 53(9), 1689-1699 (in Indonesian).

Nel V. (2016a). A Better Zoning System for South Africa?. Land Use Policy, 55, 257-264, DOI: 10.1016/j.landusepol.2016.04.007.

Nel V. (2016b). Spluma, Zoning and Effective Land Use Management in South Africa. Urban Forum, 27(1), 79-92, DOI: 10.1007/s12132-015-9265-5.

Owusu-Ansah J.K. and Atta-Boateng F. (2016). The Spatial Expression of Physical Development Controls in a Fast Growing Ghanaian City. Land Use Policy, 54, 147-157, DOI: 10.1016/j.landusepol.2016.02.012.

Oya M. (1970). Land Use Control and Settlement Plans in the Flooded Area of the City of Nagoya and its Vicinity, Japan. Geoforum, 4(C), 27-35, DOI: 10.1016/0016-7185(70)90056-4.

Peng J., Pan Y., Liu Y., Zhao H. and Wang Y. (2018). Linking Ecological Degradation Risk to Identify Ecological Security Patterns in a Rapidly Urbanizing Landscape. Habitat International, 71, 110-124. DOI: 10.1016/j.habitatint.2017.11.010.

Pratikto W.A., Suntoyo S., and Sholihin S. (2019). Analisa Pelaksanaan Reklamasi Teluk Lamong Berdasarkan Implementasi UU No. 27 Tahun 2007 [Lamong Bay Reclamation Implementation Analysis Based on the Implementation of Law no. 27 of 2007]. Sewagati, 3(3), 97–102 (in Indonesian), DOI: 10.12962/j26139960.v3i3.6091.

Qodriyatun S.N. (2020). Bencana Banjir: Pengawasan dan Pengendalian Pemanfaatan Ruang Berdasarkan UU Penataan Ruang dan RUU Cipta Kerja [Flood Disaster: Supervision and Control of Spatial Use Based on the Spatial Planning Law and the Job Creation Bill]. Aspirasi: Jurnal Masalah-Masalah Sosial, 11(1), 29-42 (in Indonesian), DOI: 10.46807/aspirasi.v11i1.1590.

Rahmat B. (2020). Implementasi Kebijakan Pengendalian Pemanfaatan Ruang dalam Meningkatkan Pelayanan Pemberian Fatwa Pengarahan Lokasi di Dinas Tata RUang Permukiman Kabupaten Tasikmalaya [Implementation of Spatial Use Control Policies in Improving Services for Providing Fatwas for Location Direction at the Tasikmalaya District Settlement Planning Service]. Jurnal Ilmu Sosial Dan Pendidikan, 1, 16-31 (in Indonesian).

Robb A., Payne M., Stocker L., Middle G. and Trosic A. (2019). Development Control and Vulnerable Coastal Lands: Examples of Australian Practice. Urban Policy and Research, 37(2), 199-214, DOI: 10.1080/08111146.2018.1489791.

Rowan-Robinson J., Ross A. and Walton W. (1995). Sustainable development and the Development Control Process. Town Planning Review, 66(3), 269-286, DOI: 10.3828/tpr.66.3.2671800700r58j52.

Salal R.E.H. and Amirtham L.R. (2021). Impact of Building Regulations on the Perceived Outdoor Thermal Comfort in the Mixed-Use Neighbourhood of Chennai. Frontiers of Architectural Research, 10(1), 148-163, DOI: 10.1016/j.foar.2020.09.002.

Sam I.M., Setiowati and Riyadi R. (2020). Analisis Penguasaan, Pemilikan, Penggunaan Dan Pemanfaatan Tanah Di Sempadan Pantai Di Kelurahan Bintaroe [Analysis of Tenure, Ownership, Use and Utilization of Land on the Coastal Borders in Bintaroe Village]. Jurnal Tunas Agraria, 3, 2 (in Indonesian).

Sari G.D.P. (2020). Implementasi Pengawasan terhadap Pengendalian Pemanfaatan Ruang berdasarkan Peraturan Zonasi Kota Medan untuk Permukiman Zona Perumahan Kepadatan Rendah [Implementation of Supervision of Spatial Use Control based on Medan City Zoning Regulations for Low Density Housing Zone Settlements]. Universitas Muhammadiyah Sumatera Utara, 53(9) (in Indonesian).

Sataloff R.T., Johns M.M. and Kost K.M. (2005). Comparative Planning Cultures. New York: Taylor and Francis Group.

Saunders W., Grace E., Beban J. and Johnston D. (2015). Evaluating Land Use and Emergency Management Plans for Natural Hazards as a Function of Good Governance: A Case Study from New Zealand. International Journal of Disaster Risk Science, 6(1), 62-74, DOI: 10.1007/s13753-015-0039-4.

Sciara G.C. (2020). Implementing Regional Smart Growth Without Regional Authority: The Limits of Information for Nudging Local Land Use. Cities, 103, DOI: 10.1016/j.cities.2020.102661.

Sejati A.P., Sitorus S.R. and Hidayat J.T. (2020). Analisis Keselarasan Pemanfaatan Ruang dengan Rencana Pola Ruang dan Pengendaliannya di Kota Jakarta Timur [Analysis of the Harmony of Space Utilization with the Spatial Pattern Plan and its Control in East Jakarta City]. Tataloka, 22(1), 108-123 (in Indonesian), DOI: 10.14710/tataloka.22.1.108-123.

Shatkin G. (2016). The Real Estate Turn in Policy and Planning: Land Monetization and the Political Economy of Peri-Urbanization in Asia. Cities, 53, 141-149, DOI: 10.1016/j.cities.2015.11.015.

Shibeshi G.B., Fuchs H. and Mansberger R. (2015). Lessons from Systematic Evaluation of Land Administration Systems. The Case of Amhara National Regional State of Ethiopia. World Development, 68, 282-295, DOI: 10.1016/j.worlddev.2014.12.006

Suroso D.S.A. and Firman T. (2018). The Role of Spatial Planning in Reducing Exposure Towards Impacts of Global Sea Level Rise Case Study: Northern Coast of Java, Indonesia. Ocean and Coastal Management, 153, 84-97, DOI: 10.1016/j.ocecoaman.2017.12.007.

Tang B. and Ho W.K.O. (2015). Land-Use Planning and Market Adjustment Under De-Industrialization: Restructuring of Industrial Space in Hong Kong. Land Use Policy, 43, 28-36, DOI: 10.1016/j.landusepol.2014.10.022.

Tenrisau A. (2019). Kebijakan Pengendalian Pemanfaatan Ruang melalui Penegakan Hukum Pidana pada Pelanggaran Rencana Tata Ruang Dihubungkan dengan Undang-Undang No.26 Tahun 2007 tentang Penataan Ruang [Spatial Use Control Policy through Criminal Law Enforcement on Spatial Planning Violations Connected to Law No.26 of 2007 concerning Spatial Planning]. Aktualita, 2(9), 402-421 (in Indonesian).

Van der Sterren M. and Rahman A. (2015). Single Lot on Site Detention Requirements in New South Wales Australia and its Relation to Holistic Storm Water Management. Sustainability of Water Quality and Ecology, 6, 48-56, DOI: 10.1016/j.swaqe.2015.01.001.

Wahidin A.A., Sutaryono and Riyadi R. (2019). Pertimbangan Teknis Pertanahan Sebagai Instrumen Pengendalian Pemanfaatan Ruang Di Kantor Pertanahan Kabupaten Mamuju [Technical Considerations of Land as an Instrument for Controlling Spatial Use in the Land Office of Mamuju Regency]. Jurnal Tunas Agraria, 2(2) (in Indonesian).

Wulansari T.R. (2017). Keselarasan Pengendalian Pemanfaatan Ruang Formal dan Tradisional di Wilayah Desa Adat (studi Kasus: Tiga Desa Adat di Kabupaten Bangli, Provinsi Bali) [Alignment of Formal and Traditional Spatial Use Control in Traditional Village Areas (Case study: Three Traditional Villages in Bangli Regency, Bali Province). Thesis, Bandung Institute of Technology (in Indonesian).

Xiao H., Gao J. and Zou Z. (2017). Reserve Capacity Model Based on Variable Demand for Land-Use Development Control. Transportation Planning and Technology, 40(2), 199-212, DOI: 10.1080/03081060.2016.1266167.

Xu N. (2019). What gave rise to China's land finance?. Land Use Policy, 87, DOI: 10.1016/j.landusepol.2019.05.034.

Yin I., and Abdullah, J. (2020). The development Control of Urban Centre in Kuala Lumpur. Planning Malaysia, 18(3), 313-325, DOI: 10.21837/PM.V18I13.795.

Yu K. and Hui, E.C. (2019). Pogodzinsk Land-Use Planning, Certainty and Flexibility: A Study of Planning Control Decisions on Residential Development in Hong Kong. Habitat International, 83, 85-98, DOI: 10.1016/j.habitatint.2018.11.008.

Yu Z. (2020). The Practice and Principle of City Planning in Contemporary China. Man and the Economy, 7(2), 20200015. DOI: 10.1515/me-2020-0015.

Yudono A. (2018). Why Do Spatial Data and Information Have a Significant Role in Spatial Planning Process?: The Investigation of Spatial Data and Information Usage in Indonesian Spatial Planning Policies. Geoplanning Journal of Geomatics and Planning, 5(1), 131. DOI: 10.14710/geoplanning.5.1.131-146.

Yudono A., Dewi C. and Darmawan M. (2020). An Investigation of Inter-Agency Relationship Respecting One Map Policy: Does the Indonesian Open Spatial Data Policy Reinforce Innovation or Disrupted Bureaucracy?. Systematic Reviews in Pharmacy, 11(12), 897-902, DOI: 10.31838/srp.2020.5.130.

Yustia D.A. (2019). Strategi Pnggabungan Sanksi bagi Pelanggaran HukumTata Ruang dalam Rangka Pemulihan Pemanfaatan Ruang [Strategy for Combining Sanctions for Violation of Spatial Planning Laws in the Context of Restoring Space Utilization]. Jurnal Litigasi, 20(1), 82-115 (in Indonesian).

Zhuang C., Liu J. and Xiong H. (2018). Digital Twin-Based Smart Production Management and Control Framework for the Complex Product Assembly Shop-Floor. The International Journal of Advanced Manufacturing Technology, 96, 1149-1163, DOI: 10.1007/s00170-018-1617-6.

APPENDIX

Table A.1. Mapping table for research development-control systems and tools

Author		Journal	Development Control System and Tools	Country	Method	Comment
1.	Ahmad and Anjum (2012)	Cities	Regulatory – Land Use Ordinance	Pakistan – Global South	Descriptive	Overlapping power and institutions
2.	Abass et al. (2020)	International Journal of Disaster Risk Reduction	Regulatory – Land Use Control	Ghana – Global South	The maximum likelihood classification algorithm	Weak institutions and legislative frameworks affect the regulations made
3.	Agheyisi (2019)	Land Use Policy	Regulatory – Land Subdivision Regulation	Benin, Nigeria – Global South	Descriptive	Need for good land administration. Compilation of a good spatial plan
4.	Alexander et al. (2012)	Progress in Planning	Statutory planning	Israel	Descriptive	Nomocratic tools to promote common values; when "planning for itself," it should use teleocratic tools acting as an organization to realize its goals
5.	Allouf et al. (2020)	Environment and Planning B: Urban Analytics and City Science	Design Guidelines	Australia	Qualitative and quantitative comparative analysis	The victorian system as discretionary development control New South Wales uses a mix of regulatory and discretionary control systems
6.	Baics and Meisterlin (2016)	Annals of the American Association of Geographers	Zoning – building code	New York	GIS method	Land use in a political economy
7.	Baker et al. (2006)	Journal of Planning Education and Research	Density and Scale	US, Australia, and New Zealand	Historical descriptive	Technical staff to undertake comprehensive and legally robust development control
8.	Biggar and Siemiatycki, (2020)	Journal of Planning Education and Research	Density bonuses	Toronto	Descriptive	Consequence for political conflicts over local priorities, democratic accountability, and the built environment
9.	Bidandi and Williams 2020)	Cities	Land use plan	Kampala	Qualitative	Urban land insights and political, revisited urban land policy
10.	Boamah et al. (2012)	Habitat International	Building Permit	Ghana	Quantitative	Enforcement of land use regulation, land value tax
11.	Cirolia and Berrisford (2017)	Habitat International	Development regulation, land allocation	Nairobi, Addis Ababa, and Herare	Qualitative	Negotiated planning . ability architects of the planning discipline or by planners themselves. The planning outcomes in African cities do not reflect clear patterns of data-driven decision making or stakeholder consensus
12.	Collins (2017)	London Journal	Permission Development Plan	London	Historical	Governments, and their advisors, appear to have ignored development plan history
13.	Farhat (2019)	Planning Practice and Research	Design guidelines	Seattle	Qualitative approach	Overlapping design challenges; the importance of a new, mutually agreed upon design

14.	Falco and Chiodelli (2018)	Land Use Policy	Transfer development right	Italy	Comparative	Weak role of public authorities in linking the supply and demand of transferable development rights
15.	Firman (2004b)	Land Use Policy	Land development permits	Indonesia	Descriptive	Giving permission that does not suitable with the room design planning
16.	Ferreira (2020)	Land Use Policy	Transfer development right	Coimbra, Portugal		Reconsidering the merit of market-oriented planning innovations: Critical insights on Transferable Development Rights from Coimbra, Portugal
17.	Gurran et al. (2015)	Journal of Environmental Planning and Management	Regulatory - Zoning and land use regulations	Australia (Sydney)	Spearman correlation	Responsive planning rather than repressive between development pressures and regulatory development control
18.	Hong et al. (2017)	Land Use Policy	Land Use Control	Shenzhen, China	GIS based	Eco-environmental condition of ecological corridors in Shenzhen
19.	Hu and Zhou (2018)	International review for spatial planning and sustainable development A: Planning Strategies and Design Concepts	Development zones	China	Descriptive analytis	Local government-led land development; the-integration of multiple spatial plans
20.	Hsu et al. (2016)	Proceedings of the Institution of Civil Engineers: Urban Design and Planning	Zoning	Taipei	The multinomial logit model	Community involvement
21.	Hubbard (2015)	Geographical Journal	Discretionary-development control, zoning, and change of use regulation	Sydney	Qualitative–descriptive	Sensitive to local contingency and informed by notions of spatial justice
22.	Ioannou (2016)	Urban Planning	Zoning, densities, green spaces, and layouts	Cyprus	Descriptive	Insufficiently capable of providing rational urban development. Planning legislation and a complete planning system exist and have already been in place since 1990, but they do not seem to be efficient
23.	Kim (2020)	Land Use Policy	Zoning-Upzoning	US	Case study	Cities had clear standards or evaluation frameworks for determining: how much value was created, what can be asked for in return, and who should benefit from the value captured
24.	Kuusaana and Eledi (2015)	Land Use Policy	Land Allocation – Regulatory	Ghana – Global South	Explorative and descriptive narrative	Participatory land uses planning, the landowner is not involved
25.	Lawanson and Agunbiade (2018)	Area Development and Policy	Planning permits, development-control mechanism and environmental-impact assessment	Nigeria	Ex ante and ex post project impact assessments	Economic impact of local people on tradable zone

26.	Lian (2018)	International Review for Spatial Planning and Sustainable Development	Land use regulation	Nixia, China	Technical analysis and evaluation	Planning of functional zones and key and core content of technology integration
27.	Nel (2016b)	Land Use Policy	Performance zoning, form-based codes, and local spatial plans	South Africa	Literature	Zoning has been criticized as being an exclusionary, unjust, and unsustainable land use management system
28.	Salal and Amirtham (2020)	Frontiers of Architectural Research	Regulatory-building rules	Chennai India	Steady-state method	Thermal building
29.	Shatkin (2016)	Cities	Land transfer	Jakarta, Chongqing, and Kolkata	Comparative	Land monetization can therefore provide powerful explanatory insights into emergent patterns of social and spatial inequality and political contestation
30.	Robb et al. (2019)	Urban Policy and Research	Discretionary – Land Use Control	Australia	Descriptive	Preserving public beach need for legislative reform or the emergence of incentive-based instruments to complement development control
31.	Sciara (2020)	Cities	Zoning	California	Qualitative analysis	Power retaliation in negotiating zoning
32.	Shibeshi et al. (2015)	World Development	No development control	Ethiopia	Literature reviews, interviews, descriptive statistics	No land use planning control – land administrative not correlated
33.	Saunders et al. (2015)	International Journal of Disaster Risk Science	Mix	New Zealand	Qualitative	Updating hazard information
34.	Tang and Ho (2015)	Land Use Policy	Land use planning regulation	Hong Kong	Johansen cointegration analysis and vector error correction model (VECM)	market competition and segmentation
35.	van der Sterren and Rahman (2015)	Sustainability of Water Quality and Ecology	Water-Sensitive Urban Design	Western Sydney	On-site design modeling	Penguatan local planning
36.	Xiao et al. (2017)	Transportation Planning and Technology	Land use control	China	GA	Decision-makers can make a trade-off between land use potentiality and construction cost
37.	Xu (2019)	Land Use Policy	Land use control	China	Descriptive	Institution building was driven by the party state's idea of "land as resources and asset."
38.	Yin and Abdullah (2020)	Planning Malaysia	Intensity, zoning high-density development	Malaysia	Qualitative and quantitative methods	Development control in the said urban center can identify the latest rank and upgrade or downgrade the growth center
39.	Yu and Hui (2019)	Habitat International	Zoning: Comprehensive Development Area, Greenbelt zone	Hong Kong	Discrete choice (probit) models	Planning schemes based on the Dutch method are more complex to implement. The technical evaluation of government officials is important, as is the arrangement of land ownership.

Table A. 2. Mapping table for research control tools

Article		Control Tools	Performance	Method	Obstacles
1.	Wahidin et al. (2019)	Land technical consideration	Spatial utilization not running optimally owing to vacuum of spatial plan	Qualitative–descriptive	Detailed spatial planning as a base for development permit
2.	Ariffudin (2020)	Detailed spatial plan	There are still many violations	Lack of socialization, knowledge of the officials	Knowledge of officer
3.	Budhianti (2020)	Location permission	HR capacity	Low law enforcement	Qualitative
4.	Budiyono (2020)	Companion zoning	For area preservation	design	Understanding zoning as a control for conservation
5.	Chandra et al. (2019)	Written warning administrative sanctions, temporary suspension of activities, closure of locations, demolition of buildings, and restoration of spatial functions	impact	Questionnaires and interviews	The need for community involvement
6.	Destratianto and Pramono (2020)	Advice planning	not run effectively and efficiently	Qualitative	The public and the private sector do not realize the importance of guiding advice planning
7.	Fazari (2020)	Sanction	Control is not optimal	Qualitative	Weak law enforcement
8.	Febrianda et al. (2020)	Development incentive and disincentive	not implemented yet	Qualitative	Detail spatial planning not stating incentive and disincentive for development
9.	Hastuti (2020)	Location permission	Authority	Literature	Understanding of the license as an instrument of control
10.	Hexagraha and Setyorini (2019)	Strong community involvement	Conflicting administrative and legal powers	Descriptive	Case study
11.	Idris and Amalia (2020)	Permit	Permit does not coherence with plan	Descriptive	Land use change caused by economic, social and physical factor
12.	Iskandar (2020)	Spatial plan	Not functioning optimally	Normative juridic	Increasing op apparatus integrity, the need of legal institution
13.	Jaya (2019)	. permit	Licensing instruments are implemented as a source of regional revenue rather than as part of a control mechanism	Qualitative interview	Regional regulation needs
14.	Murti (2018)	Penalty	Not running effectively	Qualitative interview	Legal factors, law enforcement factors, and community factors are ineffective or not running optimally
15.	Pratikto et al. (2019)	Permission, coordination	Implemented	Literature	Need coordination

16.	Prianto (2019)	Licensing is still a regional income	Not running effectively	Normative law	Understanding of licensing as control
17.	Qodriyatun (2020)	Control of flood causes	Controls are not implemented properly	Study of literature. There are no regulations	Not all violations have been prosecuted. Authority will be transferred to the center
18.	Rahmat (2020)	Fatwas on location direction plans	Fatwas were not thoroughly made and were not followed	Descriptive analysis	Need understanding
19.	Sam et al. (2020)	Incompatibility due to control, ownership, use, and utilization of land			Need reliable land administration
20.	Sari (2020)	IMB (building permit) and non-IMB	Administrative sanctions	Socialization to the community	Knowledge of officer
21.	Sejati et al. (2020)	Control is not optimal	The non-compliance factor	Application of criminal sanctions	Consistency of law enforcement
22.	Tenrisau (2019)	The imposition of criminal sanctions for violations of spatial planning	Not all indications of violations can be identified by the responsible work unit	Secondary literature	There is no detailed 1:5000 plans for proof
23.	Wahidin et al. (2019)	As a building permit	Not running effectively	Not running effectively	Control of traditional spatial development and
24.	Wulansari (2017)	Traditional Baliness building control	Effective implementation	Qualitative	Community influence
25.	Yustia (2019)	Licensing	This has not been fully done by the community	Questionnaire	Role of society

RESEARCH PAPER

ASSESSING THE INTERSECTED RELATIONSHIP BETWEEN LAND USE AND TRANSPORTATION PLANNING

Raed Al Tal[1*], Rawan Theodory[1], Subhi M. Bazlamit[2]

[1]German Jordanian University, School of Architecture and Built Environment, Department of Architecture and Interior Architecture, P.O. Box 35247, 11180, Amman, JORDAN

[2]Al-Zaytoonah University of Jordan, Faculty of Engineering ,Department of Civil Engineering, Amman , Jordan

***Corresponding author:** Raedaltal@Yahoo.com

Received: January 16th, 2022 / Accepted: November 11th, 2022 / Published: December 31st, 2022

https://DOI-10.24057/2071-9388-2022-008

ABSTRACT. This research analyses the causes of traffic congestion in urban corridors. It specifically studies the intersected relationship between land-use and transportation planning by examining Al-Madina Al Monawara street in Amman, the capital of Jordan, as a case study. Techniques implemented in data collection are personal observations, traffic counts, land use maps and questionnaires. The methods applied in analysing the collected traffic counts are: Level of Service (LOS), Automatic Traffic Counters (ATC) and Trip Attraction Analysis (TAA). The outcome of the research verified the relationship between the high level of traffic, where the traffic exceeds the actual capacity of the street by 43%, and the unregulated land use planning where 85% of the existing buildings along the street are commercial. The findings of this research will help to establish an assessment tool for testing the impacts of transportation and land use in congested developing cities. This study is important since transportation solutions receive little attention by planner's development agendas in Jordan and the neighbouring countries.

KEYWORDS: Urban corridors; Traffic congestion; Land-use planning; Transportation planning; Travel behavior; Jordan

CITATION: Al Tal R., Theodory R., Bazlamit S.M. (2022). Assessing The Intersected Relationship Between Land Use And Transportation Planning. Geography, Environment, Sustainability, 4(15), 80-89
https://DOI-10.24057/2071-9388-2022-008

ACKNOWLEDGEMENTS: Thanks for German Jordanian University and Greater Amman Municipality for their logistic help

Conflict of interests: The authors reported no potential conflict of interest.

INTRODUCTION

Land use planning, among other factors such as economic and population growth, plays a vital role in controlling and mitigating traffic congestion in developing cities (Cervero 2013; Kandt 2018; Kesuma et al. 2019). Mixed land use area with dense commercial activities attract higher traffic volumes. Therefore, the integration of land use and transportation planning is crucial to account for traffic congestion solutions (Lucas & Porter 2016). In return, transportation has indirect impact on the spatial distribution of urban activities (Gakenheimer 1999; 2011). Ideally, one should provide a transport system that suits or matches the land use pattern in developing countries as they suffer from traffic congestion. Consequential traffic congestion affects our environment, health, and controls the decisions we make as to where we live, work, and shop (Kesuma et al. 2019; Bharadwaj et al. 2017). Transportation infrastructure consumes 10-25% of urban land. These spaces require available land and consume energy in both construction and maintenance.

In most developing cities, like Amman, mobility is dominated by personal motorization where people prefer to travel by cars. The high dependency on private transportation forms the main challenge facing urban transportation and mobility in Amman. The number of vehicles in Amman (Only those owned by the habitants of Amman, or do they include those coming to Amman every working day from other Jordanian cities is expected to reach 1,170,000 in 2025 out of 1,800,000 in the whole country. It is estimated that 112,000 vehicles enter Amman every day from different parts of the country, where 80% of these are privately owned vehicles. The daily trips in Amman reach seven million, where 70% are private cars and the rest are public transportation. (Smadi 2015).

The high dependency on private transportation primarily resulted from the lack of convenient alternative forms of transport; the horizontal expansion of the city; the lack of integrated transport and planning; psychological and behavioural factors related to the need of the newly rich people to show off and not to walk even 100 m to take the available public transport; and finally public authorities lack of control over transport operators. In general, the urban and transportation bodies in Jordan suffer from shortage in transportation expertise and lack in appropriate valuable data (Cavoli 2017; Shatanawi et al. 2018). Cavoli (2017) stated that Amman does not have a comprehensive urban plan. The Urban Plan of 2009 and Transport Master Plan of 2010 are limited in scope, lack evidence and do not comprise a consultation process. Furthermore, the transport and land use plans are not coordinated. In general, there is a lack of coordination between land use and transportation planning in Jordan.

According to the World Bank Report (2017), Jordan is a lower-middle-income country. Amman, the capital of Jordan is home to almost 42% of Jordan's population.

With the rapid urbanization, Amman's population is expected to increase from 4.4 million residents in 2019 to 6.4 million in 2025 (45% increase) (GAM 2020). From the time of its foundation, Amman growth and expansion are haphazard and uncontrolled due to the continuous political instability in the region which resulted of waves of immigrants and refugees who settled down in the city (Al Tal 2006). Amman's urban form is growing increasingly fragmented. Urban development solutions push towards developing periphery networks on the outskirts of the city. For example the area of Amman jumped over from 5 km^2 in the early 1920s to 680 km^2 in 2006 and then to 1680 km^2 nowadays. It increased 335 times in about one hundred years (GAM 2020). In recent years, congestion has grown to problematic levels in Amman through recent demographic and cultural changes. The distressing increase in population growth and urbanization in Amman results in an increase demand for mobility and affects the land use distribution. The governing institutes approach in planning and transport solutions in Jordan is a reactive approach rather than diagnostic and preventive. All these factors turn Amman into a congested city which increased the cost of productive time, wastage fuel, deteriorating quality of life of its inhabitants and affected the environmental quality. Unfortunately, the arterial streets that connect Amman with the new urban expansion are facing higher traffic densities and received less attention on planning level (Tawil et al. 2014). As a result, commuters in Amman are experiencing long and frustrating commutes to their daily businesses (Fig. 1). Congestion has become a major problem that now threatens numerous aspects of life in Amman.

Study area

Roads are categorized based on their service characteristics. The main considerations in this categorization are accessibility and mobility. The relationship between these two criteria is inversely related, which means the increasing of accessibility reduces mobility and vice versa (Mehdian et al. 2022). Al Madina Al Munawwara street is classified as a collector road due to the high developments around the residential areas and high commercial development along, around, and in the street. It can also be classified as a linear intensified corridor. Corridors are defined by the Urban Hamilton Official Plan (2011) as areas of street-oriented uses which incorporate a mix of retail, employment, and residential properties, developed at overall greater densities, located along arterial roads serving as major transit routes. Corridors link nodes and important areas of activity within Amman and are intended to be key locations for residential intensification. Corridors may form the boundaries of residential subdivisions or neighborhoods, but they should also act

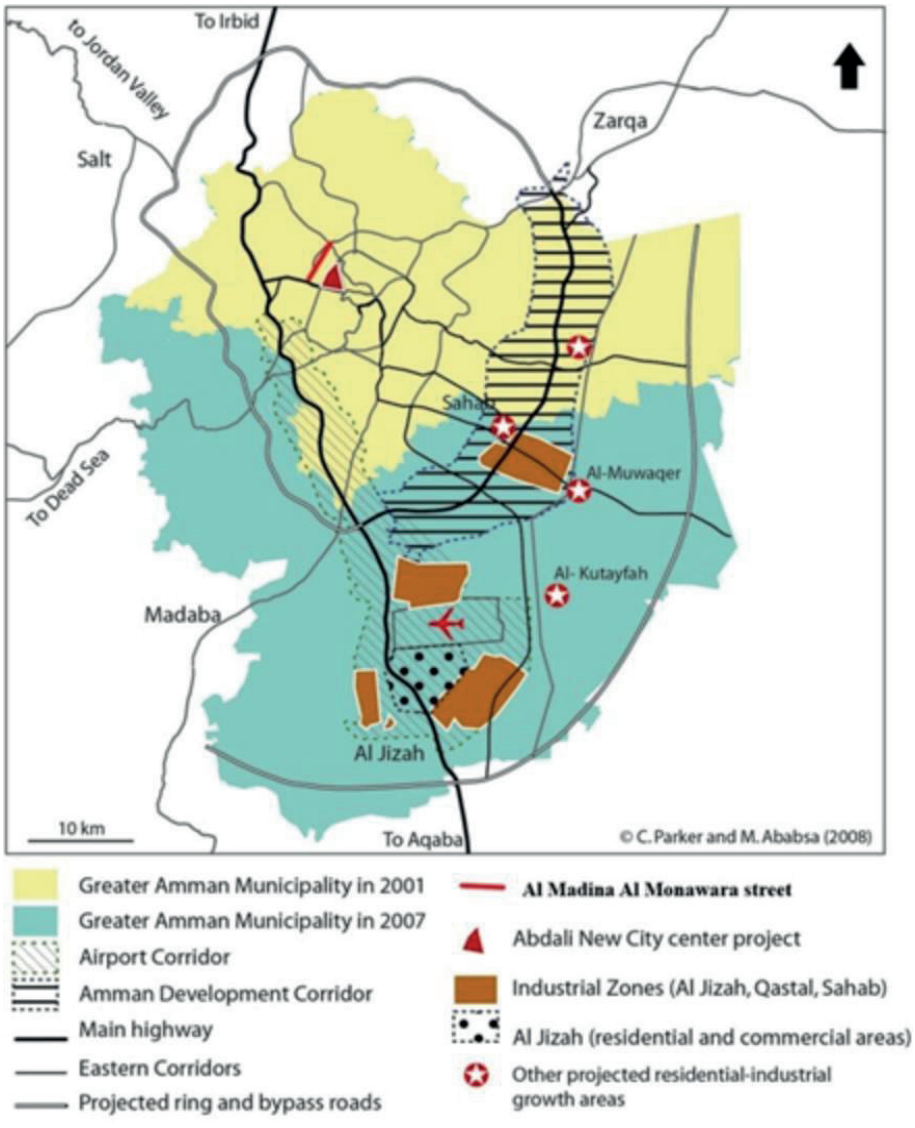

Fig. 1. The arterial streets that connect Amman with the new urban expansion

Source: Ababsa (2013), illustrated by authors (2022)

as a linear focus for activities and alternative uses within the community. They are planned to support development and investment that contribute to the economic and social vitality of a corridor and adjacent neighborhoods.

Al Madina Al Monawara street connects Amman with other governorates, and connect some of the most populous parts of the city. There is high concentration of commercial activities, especially restaurants, that attract large number of people in this street as it serves as a public space, commercial zone and the busiest urban corridor in the city. Urban corridors are defined by the Urban Hamilton Official Plan (2011) as areas of street-oriented uses which incorporate a mix of retail, employment, and residential properties, developed at overall greater densities, located along arterial roads serving as major transit routes. Urban Corridor Planning is focused on changing the City's land development regulations and infrastructure standards to accommodate a broad range of mobility options walking, bicycling, public transit, and driving in order to improve access to jobs, services, entertainment and recreation, now and in the future.

Corridors link nodes and important areas of activity within Amman. They are intended to be key locations for residential intensification. Amman's urban corridors provide a significant opportunity for creating vibrant pedestrian and transit-oriented places through investment in hard and soft infrastructure, residential intensification, infill, and redevelopment.

It is a main access leading to the University of Jordan (Fig. 2). The University of Jordan is the largest university in Jordan which host 49,000 students and 1,500 academic staff. In addition, the street leads to the university hospital that encompasses 64 major, sub-medical and clinical specialties (The University of Jordan 2020). In addition, the street acts as a transition zone between high traffic streets and adjusting neighborhoods. Figure 2 (right) shows that there are over 30 intersected streets on both sides of Al Madina Al Monawara street. The large number of the penetrated streets resulted from the "fine grained urban fabric" of the surrounding neighborhoods. These activities increased both the traffic flow of vehicles, and the load on the street which required more demand for traffic solutions (Al Habashnah 2013; Jawarneh 2021).

The street is divided into three sections defined by four major intersections: section 1 stretches from the Suhaib tunnel to the Al-Haramayn interchange that connects to Mecca street. Another collector street facing traffic problems is in section 2 which stretches from Al-Haramayn interchange to Waha circle, and section 3 stretches from Waha circle to the University Hospital interchange. This study focuses on traffic congestion in section 3, with 1258 meter in length and 30 meter in width (Fig. 2).

The mixture of complementary land uses in section 3 of the street and surrounded area includes housing, retail, offices, commercial services and large number of restaurants and coffee shops. Section 3 mainly attracts people who are looking for places to eat, teenagers to meet, and social interaction, specifically during afternoon and evening hours, to the limit it has been nicknamed "the street of hungers." Less evident but equally powerful is that the street forms a social hub for some of the most important social places such as the bus stop and the shops' steps where the social value has existed due to the existing social encounter, cultural exchange and building values (Fig. 3).

Commercial corridors act as an informal public space, but these corridors are also occupied by more vehicles and left with less space for pedestrian activities (Kamal & Waleed 2019). In this research we refer to the informal public space as a formal space which used for different purpose by people who do not own the space. Commercial corridors can accommodate different modes of transport while creating a safe public space for all commuters and users of the streets. Carmona et. al (2012), identified two

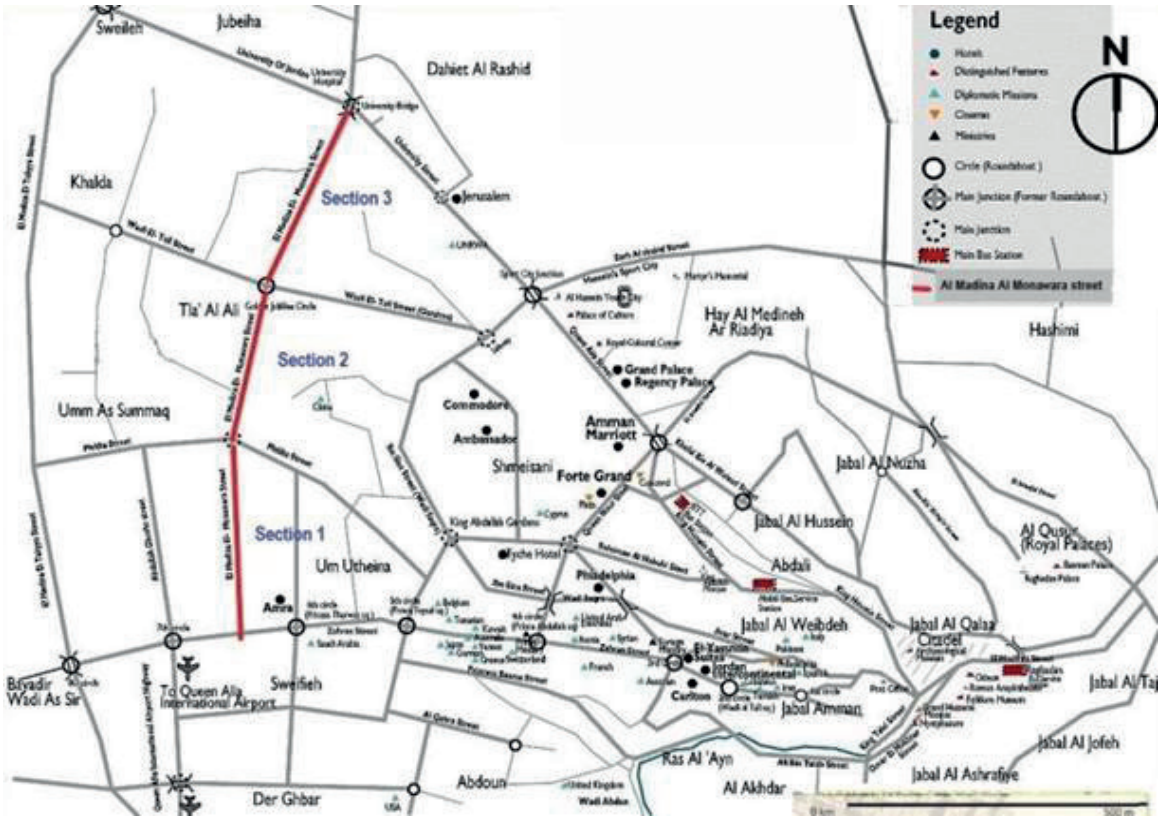

Fig. 2. Al Madina Al Monawara street

Source: Orange Smile illustrated by authors, (2022)

forms of containment of public spaces; the static space, represented by a wide area that suggests calmness and stability. The static space is a place designed to host social gathering and emphasizes the relations between the users. It can be seen in the shape of public, main squares, and residential areas; and the dynamic space which is defined as a space that takes the linear form where it has inspired through the movement like roads, streets or extended spaces such as seaside roads. While the static spaces are formal in layout and use, the dynamic spaces are generally informal spaces. Informal spaces are known in the fields of architecture, planning, design and urban theory as "dead zones" (Doron 2000), "spaces of uncertainty" and "the margin" (Cupers & Miessen 2002). Formal public spaces in Amman such as recreational parks and plazas are minor, while public activities are apparent more strongly within informal or unassigned spaces like streets, sidewalks, stairs, market places, and roundabouts. This research discusses the dynamic form of informal public spaces and its overlap with traffic congestion as Al Madina Al Monawara street acts as informal public space.

METHODOLOGY AND ANALYSIS

This research is based on a mixed method as includes qualitative and quantitative analysis. The qualitative analysis includes personal observations about the site and its traffic conditions; while quantitative analysis includes a study of the socio-economic profile of the area of age, sex, and composition of family, employment statistics, income, vehicle ownership and more. The qualitative analysis covers the land use and traffic survey in terms of type and intensity to conclude? trip attraction analysis. Since travel characteristics are closely related to the land use pattern; inventory of land use is crucial. Techniques implemented for collecting data are personal observations, traffic counts, and land use maps collection from the GAM and questionnaires. The method applied for analyzing collected details for traffic counts are: level of service (LOS) and trip attraction analysis.

The method of traffic counts data was collected through automatic traffic counters (ATC). ATC equipment is a pneumatic tubing that runs across the width of a road. They were temporarily installed to collect traffic speed data (85th percentile)?, vehicle classification and volume of traffic. Traffic data was collected at every intersection feeding Al Madina Al Monawara street. Traffic counts were carried out at 3-time interval; morning (0:00 am–10:00 am), after noon (10:00 pm–17:00 pm) and night (17:00 pm–23:00 pm) on Mondays, Tuesdays and Wednesdays as traffic in the rest of the weekdays is considered to be abnormal traffic movement and not recurrent travel.

Land Use Analysis

The problem of congestion can be reduced by comprehensive planning that considers the different aspects of spatial planning. If land use planning is regulated and accounts for the future number of trips attracted in reference to population growth, road classification and design, it could help to better control future volumes of traffic. The major variables that interplay in the land use pattern are land use intensity and density. Therefore, traffic congestion depends on the kind of land use on any street and its density. According to Kodukula (2018) the more compacted and mixed the land uses are, the less traffic congestion. In the mixed land use zones, commercial activities are placed on the edge boundaries of the residential areas forming commercial ring. Buildings are mostly placed close to the streets to create a vibrant pedestrian environment, provide a storefront character to the street, support future transit service, and encourage walking. Unfortunately, congestion arises in commercial corridors due to increasing number of vehicles on the road when there are the most number of people on these corridors, and the mixed land use zones lack solved planning schemes.

"Exploring the Interrelation between Traffic Congestion and Land uses in Amman: Challenges and Potential" is a recent master thesis by Hamza Jawarneh (2021) which focused on the land use pattern on two neighborhoods: Al-Baraka neighborhood, an adjacent neighborhood to Al-Madina Al Monawara street; and Al-Hasaniyah neighborhood next to Al-Hurriya Street. The findings of thesis revealed that the commercial land use, population density, location in relation to the city, and the inefficient public transportation system are the main causes of traffic congestion in the selected neighborhoods and in Al-Madina Al Monawara street (Fig. 3).

Al-Madina Al Monawara street is located in a very dense restrict with high mixed-use activities and residential types. The urban fabric of the adjacent neighborhoods is a "fine grained urban fabric", consisting of several small blocks close together and defined by street and blocks. The blocks consist of two rows of residential buildings in small land lots units. This layout creates an urban fabric that gradually changed by the time from residential to mixed-use retail facilities and then to a dense urban core that lacks amble public spaces.It causes a flow of vehicles from the neighborhood to Al-Madina Al Monawara street to meet the inhabitants' needs due to the lack of a central area inside the neighborhood that gathers all the needs of the residents. In addition, the longitudinal commercial lands that surround the entire neighborhood, especially restaurants, attract many vehicles from outside the district. To understand the setting of Al Madina street, the Kevin Lynch (1960) urban analysis was used to identify the paths, edges, districts, nodes, and landmarks in and around the case study. Al Madina street is connected with other major streets such as Mecca, Wasfi Al Tal, Zahran, and Queen Rania streets. It includes major nodes in Amman such as Al Kilo and Al Waha circles, and the University Hospital Bridge. The most important landmarks around the site are: King Hussein Cancer Hospital and the University of Jordan; finally the street forms an urban edge between the residential neighborhoods in Khalda district. The land use patterns on the edge of Al-Madina Al Monawara vary in area and usage. The commercial activities, for example, occupy 0.244 km^2 and form 50% of the neighborhood area. The backland uses of the edge buffer zone are residential that occupies 0.277 km^2 and form 46% of the area. Finally, 4% of the neighborhood area are mixed - use facilities (Fig. 3).

Mixed use commercial businesses (office building above a commercial base) form 85% of the existing buildings in the street, and are concentrated along 300-meter length as indicated by the black rectangle in Figure 3. They include a variety of the daily supplies, restaurants, and offices. The remaining 15% are pharmaceuticals, electronic stores, retail, hotels, health care and educational facilities. Restaurants form the higher percentages of these businesses. These local businesses attract recurrent and non-recurrent shoppers, travelers, restaurant customers, employees, health facilities employees and patients, and educational facilities employees and students (Fig. 3). Architecturally, the concentration, variation and the high marketing competitiveness among the commercial and business

activities in the street resulted in visual pollution created by the lack of one architectural language and strict building regulations (Shaban et al. 2018). The architectural design analysis of the building facades in the street by Shaban (2018) revealed that there are undefined architectural statements of the facades where each building owner seeks attention in the mixed use urban context.

The results of the field study and traffic counts show that the intense traffic activities in the study area resulted from the restaurants customers and daily suppliers of supermarkets, bakeries, and toasters, since most of the restaurants are concentrated in the middle section of the street (Fig. 3&4).

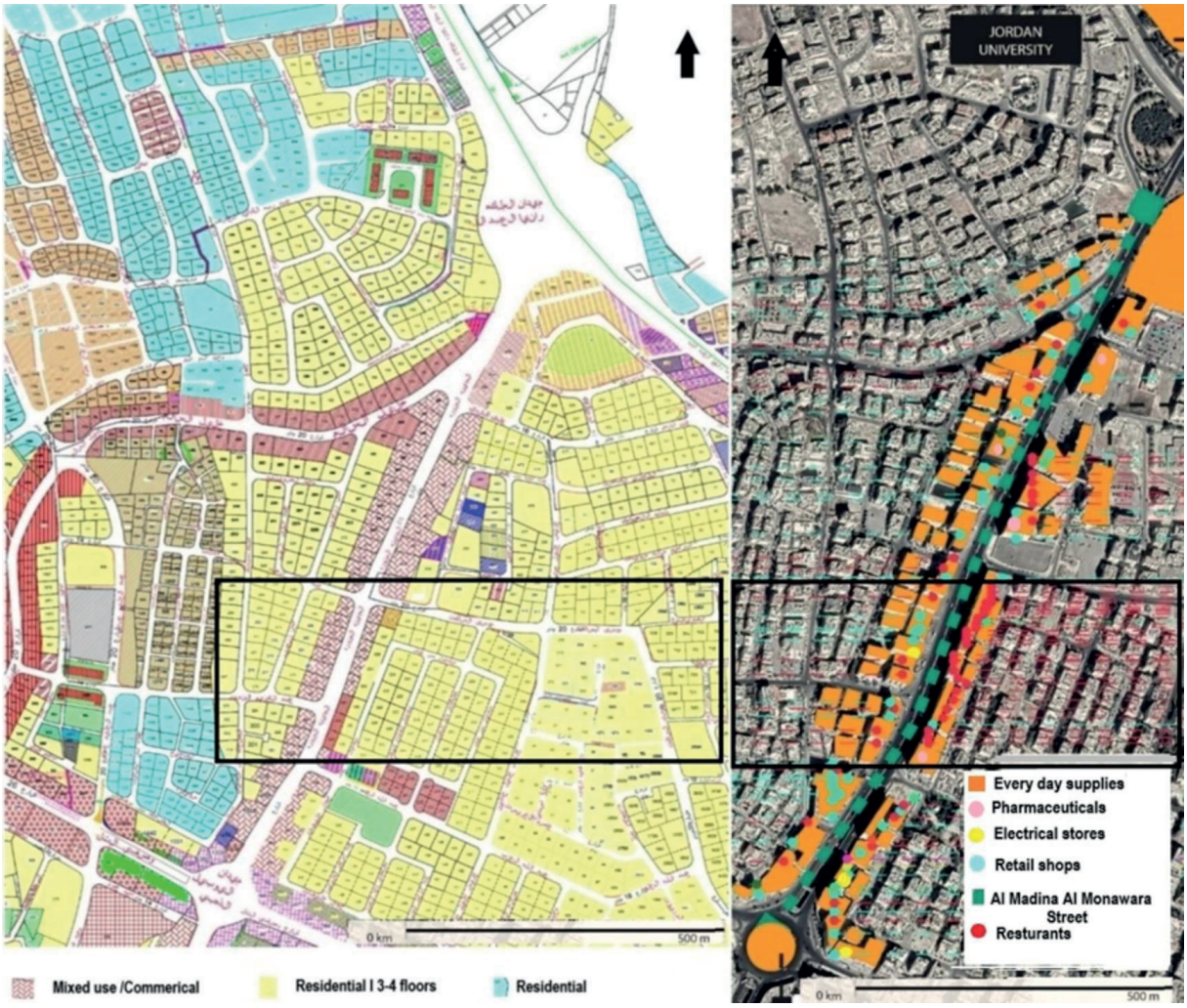

Fig. 3. Left: land use map , Greater Amman Municipality (2021); right: mapping commercial use activities in section 3 Al Madina street

Source: Authors

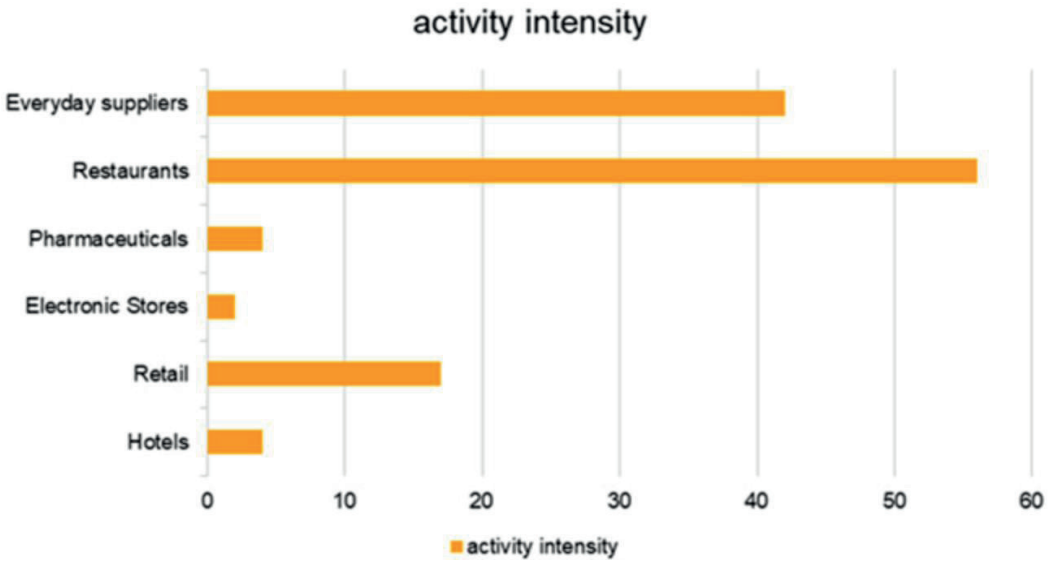

Fig. 4. Activity intensity

Source: Authors

Table 1 shows that traffic counts moving along Al Madina Al Monawara to Waha circle exceed the capacity of the street between 8:00-21:00 and reaches its highest capacity at 19:00 P.M, where the traffic counts exceed the actual capacity of the street by 43%.

General characteristics and field observations in Al Madina Al Monawara street are summarized as follow:

- Common double parking in the busy intersections causes delay, increased volume, and increased reaction time leading to congestion and a higher risk of traffic accidents.
- Only one frontage road on the east lane is available and always congested by food delivery drivers, shoppers running into a stores and restaurants to pick something up quick. It is not wide enough for a car to drive down or park
- Car parking spots are not enough to accommodate the high foot traffic in the street.
- The GAM installed pedestrian fencing and barriers in the middle island of street for redirecting pedestrians away from the dangerous traffic zones, and to save their life .
- Violations have been observed that show some people jumping over the pedestrian fencing.
- It lacks to vehicle-parking because parking facilities need large amount of land and lands are very expensive. There is no bus stop nor bicycle tracks.

Traffic Counts and Analysis

Data includes vehicles count at every entry point and exit of the site, counted at three-time intervals: morning (0:00 am– 10:00 am); afternoon (10:00 am– 17:00 pm); night (17:00 pm– 24:00 pm). Data was collected to analyze the traffic congestion at the street; it was gathered on a Monday, Tuesday and Wednesday as the rest of the weekdays are considered as an abnormal traffic and not recurrent travels. By doing this, the researchers understood the traffic flow behavior in and out the street based on time of day and its relationship to land use. Morning weekday peak hours are (8:00 am– 10:00 am) as the result of commuters from the residential areas around the streets and others from outside of Amman (Fig. 5).

The collected traffic data revealed high consistency in traffic movement on Mondays, Tuesdays, and Wednesdays: the highest traffic rate occurring in the morning;

Table 1. Traffic counts compared to Level of Service LoS/actual Capacity of street

Start Hour	Three-day Average	% of capacity of street compared to three-day average from 0:00 hour to 23:00
0:00	1,365	53.60
1:00	875	34.38
2:00	540	21.21
3:00	357	14.02
4:00	250	9.82
5:00	255	10.01
6:00	686	26.94
7:00	2,104	82.65
8:00	3,035	119.21
9:00	3,046	119.63
10:00	3,149	123.69
11:00	3,220	126.46
12:00	3,312	130.10
13:00	3,411	133.98
14:00	3,521	138.31
15:00	3,543	139.14
16:00	3,505	137.68
17:00	3,580	140.60
18:00	3,543	139.16
19:00	**3,650**	**143.36**
20:00	3,413	134.05
21:00	2,998	117.75
22:00	2,464	96.76
23:00	1,965	77.17

Source: Authors

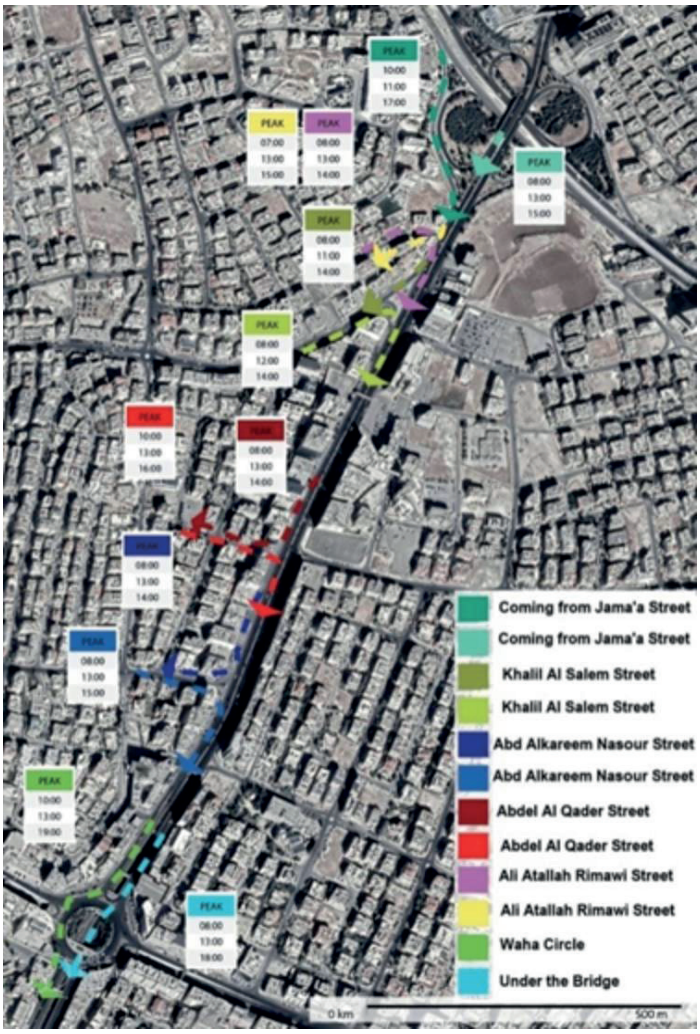

Fig. 5. Peak hours traffic analysis

Source: Authors

commuters of northern areas of the kingdom are using Al Madina Al Monwara street as a connector to the west Amman business concentrations. The same amount of traffic is happening at pm peak hours due to students and staff commuters traveling from Jordan University back to their homes as well as workers in the hospitals at the northern end of the street. Peak hour data is based on Average Weekday Traffic Volumes. It is noted that traffic peaks at the night hours (17:00 pm– 23:00 pm) at a rate of 53%, while morning (0:00 am– 10:00 am) rate is 27%, and after noon (10:00 am– 17:00 pm) rate is 20%. To understand the impact of the land use and the existing landmarks and nodes in the street, the traffic count gives a clear understanding about the size of the traffic passes in the street.

Determination of Capacity & LOS

This section describes the LOS and derives the same for an arterial section of studied street. The road is an arterial road of length 1.24km that links the Waha circle to the University Hospital interchange. Accordingly, the LOS of the project artery is in the direction from the University Hospital interchange towards the Waha circle. The guideline requires the input of an extensive data which are not all readily available for the case; therefore, reasonable assumptions have been made in the absence of the exact available data. While the manual provides for analysis of the LOS for different types of road users in the urban setting, this section only captures the motorized mode of LOS analysis. Road characteristics and Traffic count data are considered as follows:

- The road is observed as a one-way divided road.
- The number of lanes for through traffic is taken as 2.
- Each lane width is considered 3.6m (12ft) with shoulders width of a minimum of 30cm (1ft).
- The speed limit along the section is taken as 80km/h (50mph).
- The section is an arterial street connecting two interchanges with less than 3.2km (2miles) interval.
- The segment length is approximately 1.24km ≈ 0.77 miles
- The proportion of multi-unit truck, PT is assumed 2% of the total traffic volume.
- The proportion of single-unit trucks, PR is assumed 4% of the total traffic volume.

The traffic count data was obtained from the GAM, Department of Traffic Operations. The department has erected automatic traffic count systems at strategic points. The data comprises the hourly average data for the three days, and traffic count data for 12, 16, and 24-hour. Accordingly, the AADT is taken as 57,787 vehicles/day. The K-factor defines the proportion of 24-hour vehicle traffic that is expected during the design hour. Table 2 shows the typical K-factors as defined in HCM 2010.

Considering the recorded peak hour as the design hour, the proportion of traffic in this hour in relation to the AADT is:
Peak Hour Volume = 3,650 vehicles
AADT = 57,787 vehicles;
K-factor = 3650/57787 = 0.063

Table 2. Typical K-factors HCM

Area Type	K-Factor
Urbanized	0.091
Urban	0.093
Transitioning/Urban	0.093
Rural Developed	0.095
Rural Undeveloped	0.100

Source: Florida Department of Transportation (2010)

The D-factor defines the differences that are expected in traffic volume direction at different times such as the demand for entering and leaving the city at different hours of the day. The adopted value for the project road is 0.65.

The Peak Hour Factor (PHF) defines the relationship between the 15-min peak traffic volume and the hourly peak volume. Since only the hourly volume counts are available, PHF is estimated as 0.92 as per the provisions of HCM 2010.

Other parameters are assumed as follow:

•The Density of Accesses (DA) is estimated at 34 per mile.

The following generalized daily service table for an urban street:

•Arrival type is 4.

•Traffic signal cycle time, C = 120 seconds.

•The analysis time, T is estimated to be 0.25hrs.

•Initial Queue delay, D3, for each vehicle is estimated at D D3 = 0 seconds.

•Weighted average Green-to-cycle-length (g/C) = 0.67.

•Saturation flow, So = 1900 passenger cars/hr/lane.

The LOS is determined from the criterion set out by (HCM 2010) (Table 3).

For a travel speed of 70% the base flow speed and a capacity higher than the traffic volume, the LOS of the artery is found to be Class B. The LOS at Al Madina Al Monawara street from the University interchange to Waha circle is 2546 vehicles/hr. The traffic counts calculated as an average from hour 0:00-23:00; it is observed that from hour 7:00 to hour 22:00, the traffic counts are exceeding the capacity of the street traffic counts compared to LOS/ actual capacity of street reaching its highest maximum at hour 13:00, where the traffic exceeds the actual capacity of the street by 90%.

The LOS is determined from the criterion set by the HCM 2010. For a travel speed of 70% of the base flow speed and a capacity higher than the traffic volume, the LOS of the artery is found to be Class B. The LOS at Al Madina Al Monawara street from the University interchange to Waha circle is 2546 vehicles/hr in comparison to the traffic counts calculated as an average from hour 0:00-23:00; it is observed that from hour 7:00 to hour 22:00, the traffic counts are exceeding the capacity of the street, reaching its highest maximum at hour 13:00, where the traffic exceeds the actual capacity of the street by 90%.

Questionnaire and Survey

The questionnaire was carried on both sides of Al Madina Al Monawara street. The 200 questionnaires were distributed on Monday, Tuesday and Wednesday between 11:00 and 20:00. Shop and restaurants opening hours (10:00 am- 22:00 pm) were considered.

They were distributed equally among males and females. This is due to Amman's population equal gender distribution. The age groups 18-24, 25-44, 35-44, and 45-54 appeared to be the largest number of users at the study. The study groups were categorized into students, employees, business owners, retired individuals, and unemployed individuals. The study investigated one person per household as a statistic measure to correlate it to the owned number of vehicles per household.

The results of the questionnaire revealed that vehicle use and dependency referred to comfort and security. While 70% of commuters used their private cars for comfort, 30% used them for security. The study found that most attracted car users are one or two passengers per vehicle. This result indicates that the low vehicle occupancy is one of the major causes in increasing traffic load. Most users suffered from excess traffic mostly in the morning period where travel times exceeded 15 minutes, likely caused by common traffic commutes.

Table 3. LOS Criterion for Urban Roads

	Travel Speed as a Percentage of Base Free-Flow Speed (%)	LOS by Critical Volume –to-Capacity Ratio	
		≤	>
Exhibit 16-4 LOS : Automobile Mode	>85	A	F
	>67-85	B	F
	>50-67	C	F
	>40-50	D	F
	>30-40	E	F
	≤30	F	F

Source: HCM (2010)

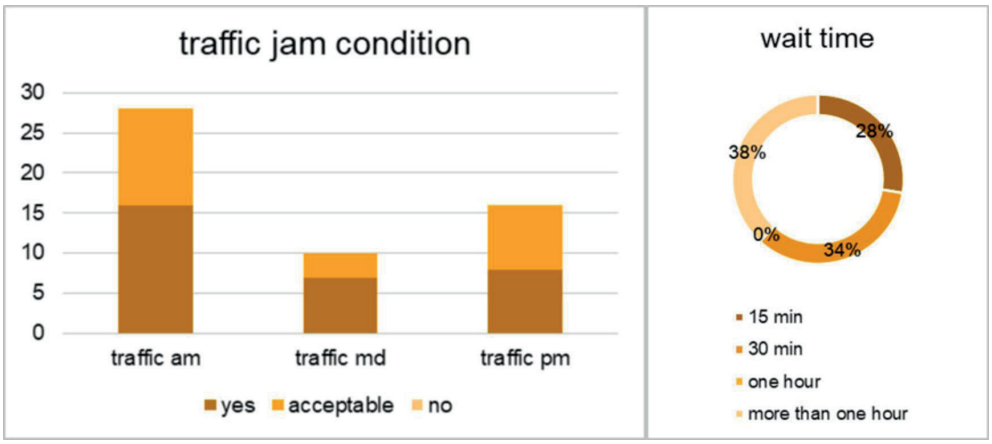

Fig. 6. Traffic jam condition and Wait time

Source: Authors

Table 4. Consequences of traffic congestion according to the surveyed population

Increased traffic and delay	Accidents	Frustration
52.43%	15.53%	32.04%

Source: Authors

Table 5. Mitigation strategies according to surveyed population

Increasing street capacity	Implementing street diversions	Encouraging food delivery	Regulating land use	Expanding parking areas	Decreasing traffic police interventions
10.17%	1.69%	3.39%	0.85%	44.07%	39.83%

Source: Authors

As reported by the surveyed population, the main causes of traffic congestion are unregulated development, unavailable parking areas, sudden stops due to accidents, and unreliable driver behavior. Based on the results of the questionnaire, 38% of users are spending more than an hour, and 62% are spending 15-30 minutes to cross the study area (Fig. 6). The majority of respondents stated that there is a lack of parking spaces. As a result, 79% of commuters continued to drive around to find a parking place, while 21% of commuters drove around more than once to find a parking place. A large number of those interviewed, 97.78%, declared that they will continue on driving around until they find a parking place, while 2.22% of commuters will go around the area until they find parking.Table.4 shows that the consequences of traffic congestion according to the surveyed population are increased delay time, accidents, and frustration.

Table 5. concludes solutions offered by the surveyed population that can help mitigate traffic congestion in Al Madina Al Monawara. Among these solutions are implementing street diversions, encouraging food delivery, regulating land use, expanding parking areas, and decreasing traffic police interventions. The survey revealed that expanding parking areas is one of the highest priority.

CONCLUSIONS AND RECOMMENDATIONS

The study revealed that the traffic counts in Al Madina Al Monwara street exceeds its capacity in relation to the Level of Service (LOS), where the traffic exceeds the actual capacity of the street by 43%. The traffic flow behavior in and out the street based on time of day and its relationship to the commercial activities established along the street. Another major factor is the location of Al Madina Al Monwara street and its relationship to the mixed use urban context. The neighboring residential areas and the educational and health facilities established around the street are the main reasons for the high traffic congestion. An important finding of this study is that Al Madina Al Monawara was developed over time into a densely commercial corridor (85% of the existing buildings along the street are commercials).

In transportation broader scope, the study advises improving the transport options, taking economic measures, introducing smart growth and land use policies, and other programs in the highly dense urban corridors. The transport options can be improved by: Public transit improvement; walking and cycling improvements; ride share/commute trip reduction programs; HOV priority lanes; Flextime/telecommuting; taxi service improvement; improving the condition of roads, infrastructure and sanitation; pedestrian awareness and provision of bridges and pedestrian paths; organizing construction permits for buildings and services.

The study recommended to apply measures in commercial corridors that include redistribution of carriageway space to provide cycle lanes, broader sidewalks, planting strips, bus lanes, redistribution of time cycles at traffic lights in favor of public transport and non-motorized modes, public awareness concepts, citizen's participation and marketing, and as well enforcement and penalizing. It is advised to integrate works of experts from all fields that fall under the spatial planning. As well, the preparation of feasibility and assessment reports that include technical, financial, spatial, and environmental aspects assessments in the mixed use commercial urban corridors.

REFERENCES

Ababsa M. (2013). Altlas of Jordan , Presses de l'Ifpo, Institut français du Proche-Orient. Beirut. https://books.openedition.org/ifpo/5046. [Accessed 8July 2022].

Alhabashneh, F. (2013). [Al Madinah Al Monawarah Street: A model of traffic congestion and chaos day and night]. [online] [Jafranews], (in Arabic with English summary).https://jfranews.com.jo/article/77533.[Accessed 20May 2022].

Al Tal R. (2006). Structures of authority: A sociopolitical account of architectural and urban programs in Amman-Jordan (1953-1999). Unpublished PhD Dissertation, State University of New York, USA.

Bharadwaj S., Ballare S., Rohit, Chandel M.K. (2017). Impact of congestion on greenhouse gas emission for road transport in Mumbai metropolitan region Transportation ReaserchProcedia. (25) 3538-3551, DOI: 10.1016/j.trpro.2017.05.282, https://www.mendeley.com/catalogue/9aa57de5-c805-31d5-9c7c-df109a7ce123/[Accessed 15 May 2022]

Carmona M., Heath T., Oc T., & Tiesdell S. (2012). Public places-Urban spaces. Routledge.

Cavoli C. (2017). «Past, Present and Future mobility challenges and opportunities in Amman», UCL Centre for Transport Studies.

Cervero R.B. (2013). Linking urban transport and land use in developing countries. Journal of Transport and Land Use, 6(1), 7-24, DOI: 10.5198/jtlu.v6i1.425.

Cupers K., Miessen M. (2002). Spaces of Uncertainty, Wuppertal: Verlag Muller and Busmann.

Doron G.M. (2000). The dead zone and the architecture of transgression. City, 4(2), 247-263.

Ekta R., Subhash A., Madha S.V., Poonam S., Anju S., Suraj K. (2021). Traffic Congestion In Azadpur Mandi: A Study On The Largest Vegetables And Fruits Market Of Asia. GEOGRAPHY, ENVIRONMENT, SUSTAINABILITY;14(1):122-13, DOI: 10.24057/2071-9388-2020-209. [Accessed 15 May 2022]

Gakenheimer R. (1999). Urban mobility in the developing world. Transportation Research Part A: Policy and Practice, 33(7-8), 671-689, DOI: 10.1016/S0965-8564(99)00005-1.

Gakenheimer R. (2011). Land use and transport in rapidly motorizing cities: Contexts of controversy. In H. T. Dimitriou & R. Gakenheimer (Eds.), Urban transport in the developing world: A handbook of policy and practice (pp. 40–68). Cheltenham, UK: Edward Elgar Publishing. GAM, (2020). https://www.ammancity.gov.jo/ar/main/index.aspx[Accessed 10 Apr. 2020]

Kamal A., Waleed C. (2019)."Integrating and land use Development approach on the Commercial corridor of Baroshke neighborhood." University ofDuhok.https://www.academia.edu/41583138/Integrating_Transportation_and_Land_use_Development_Approaches_on_the_Commercial_Corridor_of_Baroshke_Neighborhood[Accessed 25 May 2022].

Kandt J. (2018). Heterogeneous links between urban form and mobility: A comparison of São Paulo, Istanbul and Mumbai. Journal of Transport and Land Use, 11(1), DOI: 10.5198/jtlu.2018.1359. [Accessed 22 May 2022].

Kesuma A., Rohman A., Prastyanto A. (2019). Risk analysis of traffic congestion due to problem in heavy vehicles: a concept, OP Conf. Series: Materials Science and Engineering 650:012011, IOP Publishing, DOI:10.1088/1757-899X/650/1/012011.https://iopscience.iop.org/article/10.1088/1757-899X/650/1/012011/pdf. [Accessed 15 May 2022].

Kodukula S. (2018). Integrating Land Use Planning and Urban Transport for Low Carbon Cities. Intergovernmental Eleventh Regional Environmentally Sustainable Transport (EST) Forum in Asia. https://www.researchgate.net/publication/339988778_Integrating_Land_Use_Planning_and_Urban_Transport_for_Low_Carbon_Cities.[Accessed 50 May 2022]

Jawarneh H. (2021). Exploring the Interrelation between Traffic Congestion and Land uses in Amman: Challenges and Potential, Unpublished master thesis, German Jordanian University.

Lucas K., & Porter G. (2016). Mobilities and livelihoods in urban development contexts: Introduction. Journal of Transport Geography, 55, 129-131, DOI: 10.1016/j.jtrangeo.2016.07.007.

Lynch K. (1960). The image of the city. MIT Press.

Mehdian M., Mirzahossein H., Kordani A. (2022). A Data-Driven Functional Classification of Urban Roadways Based on Geometric Design, Traffic Characteristics, and Land Use Features. Journal of Advanced Transportation, https://www.hindawi.com/journals/jat/2022/9970464/

Orange Smile (2022). Detailed hi-res maps of Amman for download or print, https://www.orangesmile.com/common/img_city_maps/amman-map-0.jpg

Shaban L., Suleiman S., Abdel-Aziz D., Isawi H. (2018). Evaluating the Visual Pollution in Urban Corridors-Case of Al-Madina Al-Munawara Corridor, Amman. Research Journal of Applied Sciences, Engineering and Technology 15(8), 288-294. https://www.researchgate.net/publication/325257434_Evaluating_the_Visual_Pollution_in_Urban_Corridors_-_Case_of_Al-Madina_Al-Munawara_Corridor_Amman. [Accessed 2 June 2022]

Shatanawi M., Csete M., Meszaros F. (2018). Road User Charginh? Adaptation to the City of Amman, Conference: III. East-West Cohesion International Scientific Conferenceat: Dunaujvaros, Hungary: University of Dunaujvaros. https://www.researchgate.net/publication/341297205_ROAD_USER_CHARGING_ADAPTATION_TO_THE_CITY_OF_AMMAN. [Accessed 20 May 2022].

Smadi A. (2015). «Sustainable Urban Transport: Amman Context.» https://www.codatu.org/wp-content/uploads/2-.-Ayman-Smadi.pdf. [Accessed 15 April 2021].

Tawil M., Reicher C., Ramadan K., Jafari M. (2014). «Towards More Pedestrian Friendly Streets in Jordan: The Case of Al Medina Street in Amman.» Journal of Sustainable Development, 144-158.https://www.researchgate.net/publication/289064408_Towards_More_Pedestrian_Friendly_Streets_in_Jordan_The_Case_of_Al_Medina_Street_in_Amman. [Accessed 28 May 2022].

The University of Jordan (2020).http://www.ju.edu.jo/Pages/AboutUJ.aspx[Accessed 10 Feb. 2020].

Urban Hamilton Official Plan (2011)https://pub-hamilton.escribemeetings.com/filestream.ashx?DocumentId=170851

World Bank Report (2017). http://pubdocs.worldbank.org/en/908481507403754670/Annual-Report-2017-WBG.pdf#:~:text=The%20World%20Bank%20Annual%20Report%202017%20was%20produced,and%20key%20contributions%20from%20Marjorie%20Bennington%2C%20Denise%20Bergeron%2C[Accessed 15 April 2021].

RESEARCH PAPER

ASSESSMENT OF TEMPORAL VARIABILITY IN THE LEVEL OF POPULATION VULNERABILITY TO NATURAL AND MAN-MADE HAZARDS (THE CASE OF MOSCOW DISTRICTS)

Roman A. Babkin[1], Svetlana V. Badina[1,2*], Alexander N. Bereznyatsky[1,3]

[1]Plekhanov Russian University of Economics, Stremyanny lane, 36, 117997, Moscow, Russia

[2]Lomonosov Moscow State University, Faculty of Geography, GSP-1, Leninskie Gory, 1, 119991, Moscow, Russia

[3]Central Economics and Mathematics Institute of the Russian Academy of Sciences, Nakhimovsky avenue, 47, 117418, Moscow, Russia

***Corresponding author:** bad412@yandex.ru

Received: July 20th, 2022 / Accepted: November 11th, 2022 / Published: December 31st, 2022

https://DOI-10.24057/2071-9388-2022-116

ABSTRACT. The relevance of the study lies in the need for a scientific search for the possibilities of using new types of Big data in studies of the population vulnerability to solve practical problems of improving the safety of urban spaces from natural and man-made hazards. The object of the study is the administrative districts of Moscow; the subject is the temporal patterns of vulnerability of their population to potential natural and man-made hazards. The research question of the study is to develop a typology of Moscow districts and further assess this sustainability in terms of the population vulnerability to natural and man-made hazards. To achieve this research question, a set of tasks was solved: 1. Processing of the mobile operators' data array and further construction of a continuous graph of the Moscow population dynamics in 2019 (with a time cycle of 30 minutes, over 36 million measurements in more than 7 thousand time slices); 2. Empirical justification of natural temporal boundaries of daily, weekly, seasonal cycles of population dynamics in Moscow districts; 3. Justification of key factors and parameters of urban population vulnerability; 4. Development and approbation of the dynamic clustering method of Moscow districts using selected variables and periods. The study is based on the impersonal mobile operators' data on the locations of subscribers for 2019, provided by the Department of Information Technologies of the Moscow city. The method of dynamic cluster analysis is used. Four particular clusterings were obtained that characterize the "behavior" of the settlement system in the main intervals of social time (weekdays and weekends of the cold and warm seasons). Cluster stability matrix allows to identify which of the districts retain their properties during the period under review, and which are characterized by instability of considered indicators of population vulnerability. Depending on the stability of the position of the districts in a particular cluster, "stable", "conditionally stable" and "nomadic" types of districts were identified. The study showed that the first two types include spatial-settlement structures that are stable in time with approximately the same level of population vulnerability during the year, while the third type requires a special differentiated approach to the development of measures to protect the population from natural and man-made emergencies. Calculations have shown that "nomadic" type of districts concentrate on average from 2.2 million people in the summer season to 3 million people in the winter season, that is, a very significant share of the entire population of the capital.

KEYWORDS: mobile operators' data, vulnerability of the urban population, dynamic clustering, typology of urban districts, Moscow, intracity population mobility, social time, time-geography

CITATION: Babkin R. A., Badina S. V., Bereznyatsky A. N. (2022). Assessment Of Temporal Variability In The Level Of Population Vulnerability To Natural And Man-Made Hazards (The Case Of Moscow Districts). Geography, Environment, Sustainability, 4(15), 90-101

https://DOI-10.24057/2071-9388-2022-116

ACKNOWLEDGEMENTS: The research was funded by RFBR and Moscow city Government according to the project 21-35-70004.

Conflict of interests: The authors reported no potential conflict of interest.

INTRODUCTION

One of the key issues in field of monitoring and managing natural and man-made risks is the problem of a reliable population estimates at different time intervals and in different parts of the cities. For instance, in case of a major emergency in the affected area, there may be significantly more people than expected, based on official statistics. This can seriously complicate evacuation and rescue efforts, lead to an increase the number of victims and injured.

Modern Big Data technologies (in our case, mobile operators' data) make it possible to assess the location

of people with high accuracy, including in the poly-time slices. The speed of public life and citizens mobility, which have greatly increased in recent decades, lead to significant fluctuations in the population size and a high degree of uncertainty in the state of urban settlement systems at a certain point in time. However, the movement of the population is subject to cyclic patterns: daily, weekly, and seasonal cycles (Makhrova et al 2022).

In this regard, in this study, it was carried out an attempt to structure a time series of indicators characterizing the present population of Moscow districts, to identify the natural boundaries of different time cycles. The key task of the study is to develop a typology of Moscow districts according to the degree of sustainability of their main population vulnerability characteristics (population density and mobility) in weekly and seasonal cycles. The least sustainable city districts require increased attention, flexible approaches in terms of developing preventive measures to protect the population from potential emergencies.

The selection of key elements of the temporal structure requires consideration of theories that study the cyclical nature of socio-economic processes. Initially, the theory of cycles appeared in economic science and was an attempt to explain the recurring changes in market conditions. The works of many outstanding economists are devoted to the study of multi-temporal market cycles: W. Sombart, N.D. Kondratiev, J. Schumpeter, K. Juglar, S. Kuznets, Yu.V. Yakovets et al (Kondratiev 2003). The issue of cyclicity came to economic geography through the economy, supplemented by social and spatial components. In particular, one can note numerous works on the identification of the urbanization stages by D. Gibbs, L. Klaassen, G. Scimeny, H. Geyer and T. Kontuli (Gibbs 1963; Klaassen and Scimeni 1981; Geyer and Kontuly 1993). One of the modern economic geographers who studies socio-economic cycles and integrates cycles theories with the ideas of T. Hegerstrand is V.L. Baburin (Baburin 2011).

Another direction in the research of cyclicity is the study of the settlement systems dynamics. Thus, pendulum labor migrations and daily population pulsations are the subjects of researches by modern Russian scientists – A.G. Makhrova, P.L. Kirillov, Yu.Yu. Shitova, A.N. Bochkarev et al. (Makhrova et al 2016; Makhrova and Babkin 2018).

Another important research area in the field of population dynamics is related to the study of seasonal changes under the influence of dacha-recreational and rotational migrations: A.G. Makhrova, L.B. Karachurina, P.L. Kirillov and D.Yu. Zemlyansky (Zemlyansky 2011; Makhrova and Kirillov 2015; Karachurina and Ivanova 2017). As an example of short cycles, one can mention weekly cycles, considered by T.G. Nefedova as a special case of "otkhodnichestvo" – "half- otkhodnichestvo-half-pendulum". This type of cycles is widespread in the Moscow oblast and neighboring regions (Nefedova 2015).

Natural and man-made emergencies are also subject to cyclic patterns. The superimposition of the ascending phases of some natural and socio-economic cycles can leads to an increase in damage scale. For instance, the researchers (Zhongrui et al 2003; Kaniewski, et al 2016; Knaub and Ignateva 2022) analyze the relationship between solar activity and the frequency and magnitude of various natural disasters. Studies on the relationship between climate cycles and natural disasters are singled out as a special group (Zhang et al 2010; Luque-Espinar et al 2017, Froude M.J. and Petley 2018). The study (Baida 2019) analyzes the influence of heliophysical and space cycles on hazardous man-made phenomena and processes.

It is important to note that the above works on the cyclicity of population movement are mainly based on imperfect official statistics data. On the contrary, in this study, the use of mobile operators' data made it possible to construct a continuous time series and move to a very large scale – to the level of urban districts, and, accordingly, to obtain the most reliable results.

Turning to the objectives of this study, it is necessary to dwell in more detail on the concept of "social time" and the problem of year periods stratification. Social time is time within the boundaries of social functions, different from standard physical time (Sorokin and Merton 1937). T. Hegerstrand associates it with pacemakers and defines it as time expressed in events, things or conditions (Hägerstrand 1973). The complexity and multicomponent nature of spatial population dynamics requires a systematic consideration of its structure (Fig.1).

In general, spatial dynamics can be divided into two groups: cyclic and non-cyclic. Cyclic dynamics is associated with the natural processes of the settlement system functioning and is subject to certain temporal rhythms. The shortest temporal type of cyclic rhythm is daily dynamics, which is mainly due to the pendulum labor and educational migrations. The longest type is seasonal dynamics, depending on the work-recreation cycle and the seasons change (natural-climatic factor). Between these cycles, there is an intermediate type – weekly dynamics, which is associated with the weekday-weekend cycle of life.

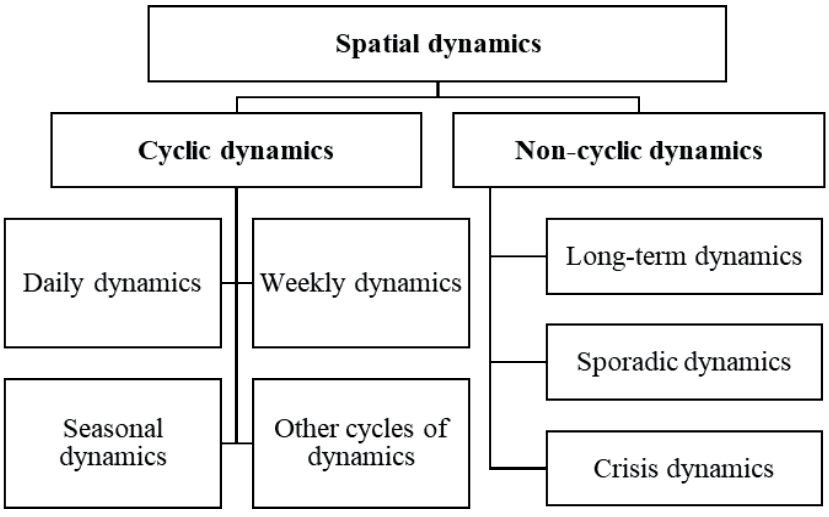

Fig. 1. Types of spatial population dynamics

Source: compiled by the authors

It is convenient to analyze all three cycles using the mobile operators' data, while they are correlated with the main attraction areas for people, which also provides convenience for spatial analysis. A simplified correlation of the pastime (and the corresponding functional zones of urban space) and social time intervals is shown in Table 1.

Thus, the easiest way to determine the presence of citizens at work (study) and at home, since the vast majority of citizens work (study) on a weekday in the cold season, and are at home on a weekday night in the cold season. Recreational activity is most typical for the weekends of the warm season. Finally, temporally distribution of leisure activities is wider, but more typical for weekends. In general, the cyclical movement of people within these four spheres of human activity forms the basis of the settlement spatial dynamics. Disparity in the location of residence places, centers of labor, leisure and recreational attraction is the main factor stimulating population migration and causing regular population fluctuations.

Expanding the spatio-temporal analysis, one can additionally single out places of concentration of dachas or second houses, the main centers of attraction during the various cultural and sports events, the peculiarities of people movement in emergencies, etc. Thus, each type of pulsation is determined by different types of population mobility, which, in turn, have different areas of attraction for commuters. These types can be associated with certain areas of human activity, which takes place in relevant intervals of social time.

The main idea of chronogeography is that the study of various types of people movements must be carried out with close integration of the spatial and temporal characteristics of the data. In this context, the chronogeographic concept and modern possibilities of "big data" open up wide opportunities for the active use of closely related pacemakers and spacemakers[1] in modern economic geography (Table 1).

In this regard, the empirical justification of the time boundaries of different day periods is the most important methodological task. These day periods, on the one hand, will be characterized by a certain structural stability at the selected time interval, and, on the other hand, will differ in different parts of the city (Ahas et al 2015). The typology of urban areas based on the cyclical features of the population distribution will make it possible to identify areas and periods of peak population concentration and, along with this, on the contrary, territories with reduced load.

Thus, the problem of optimizing the territorial structure of settlement can be solved in order to reduce the population vulnerability through specific measures. These include measures to deconcentrate the population, redistribute human flows by locating new places of work, housing, leisure and recreational infrastructure, public transport developing, etc. in areas with potential density increase in certain periods.

Table 1. Correlation between social and physical time

№	Social time element (pacemaker)	Approximate boundaries in terms of physical time	Spacemaker	Clarification
Daily level (daily cycles)				
1	Morning	06:00 a.m. - 12:00 p.m.	Transit from residence place to work place	The time of the beginning of the mass commuters movement from residence places towards work places
2	Day	12:00 p.m. - 06:00 p.m.	Work place	The time of maximum concentration of people in their work places
4	Evening	06:00 p.m. - 12:00 a.m.	Transit from work place to residence place, visits to "third places"	The time of the beginning of the mass commuters movement from work places towards residence places and visits to other places of leisure and consumption
3	Night	12:00 a.m. - 06:00 a.m.	Residence place	The time of maximum concentration of people in their homes
Weekly level (weekly cycles)				
5	Weekday	Monday – Friday	Residence place, work place	The period of the maximum volume of pendulum labor migrations
6	Weekend / holiday	Saturday –Sunday	Residence place, place of the second home / dacha	The period of the minimum volume of pendulum labor migrations
Yearly level (seasonal cycles)				
7	Cold / working / winter season	October – April	Residence place (main house)	The season characterized by the maximum people concentration in their main houses and least recreational mobility (dachas, holidays, etc.)
8	Warm / holiday / summer season	May – September	Place of the second home / dacha	The season characterized by the maximum people concentration in their second (suburban) houses and high recreational mobility (dachas, holidays, etc.)

Source: Orange Smile illustrated by authors, (2022)

[1]By analogy with "pacemakers", which are key time intervals, "spacemakers" are points or areas on which vital activity is attached in space (Petrov 1986)

MATERIALS AND METHODS

The study is based on the impersonal mobile operators' data on the location of subscribers for 2019, provided by the Department of Information Technologies of the city of Moscow. The data represent information about the location of mobile subscribers during the day (with a time fraction of 30 minutes, aggregated in 500 square meters cells), obtained as a result of measuring the location of a mobile phone relative to three cellular stations. The total amount of data involved is 2.5 terabytes (over 36 million measurements in more than 7 thousand time slices during the period from January 2019 to January 2020). Using the set of keys, the cells were linked to the corresponding territories of Moscow and the Moscow Oblast in the context of selected time intervals, reflecting the temporal dynamics in the daily, weekly and seasonal cycles.

The primary task of the study is the empirical substantiation of the natural boundaries of the seasons and intraday cyclicity. The patterns revealed during the construction a continuous series of pulsations of Moscow population during a full year (Fig. 2), made it possible to proceed to a segmented consideration of the year seasons. The pulsation series of the actual Moscow population in January 2019 – January 2020 allowed to see many local extremes within the weekday-weekend cycle (occurring on weekdays, when Moscow's population is higher than on weekends). A noticeable decline in the total population is visible for the May – August period, that is, the dachas-vacation season. In addition, deeper extremes are typical for May holidays, as well as the entire period of New Year's festivities (January 1–7). Another notable distortion of the pulsation series under the influence of events is also Moscow City Day (September 7–8), when the "pit" characteristic of weekends is significantly smoothed out due to the influx of visitors from neighboring regions, as well as Muscovites who remained in the city.

Large cities and urban agglomerations are areas of increased danger first of all due to the high concentration of the population (United Nations… 2019). The territory of Moscow is characterized by an increased likelihood of a wide range of emergencies, both natural and man-made. Additionally, there are higher risks of terrorist attacks. The key natural hazards on the city territory include dangerous hydrometeorological phenomena (Akimov et al 2009), hazardous engineering and geological processes and phenomena (including flooding) (Osipov et al 2011), smoke pollution of vast areas of the city due to massive forest and peat fires in neighboring regions etc. There are some key man-made hazards which should be especially highlighted among the others in the context of Moscow. They include man-made fires, accidents at electric power facilities, accidents at railway and road transport with the release of hazardous substances and the emergence of vast areas of fire, collapse of structural elements of buildings and structures of transport communications, etc.), the emergence of floods due to the potential destruction of water-limiting devices on Moskva river and adjacent water reservoirs. Particular attention should be paid to the dangers associated with potentially hazardous industrial facilities (explosive, chemical, radiation and fire hazardous), institutions working with pathogens of high pathogenicity (Badina et al 2022b).

Therefore, based on the scientific experience in the field of assessing the vulnerability of the urban population to natural and man-made hazards (for instance, (Cutter et al 2003; De Oliveira Mendes 2009; Flanagan et al 2011; Nelson et al 2015; Aksha et al. 2019; Spielman et al 2020; Siagian et al 2014; Ward and Shively 2017), as well as an analysis of the consequences of major natural disasters in Russia and in the world, it was determined that the potentially most vulnerable areas of urban space, other things being equal, are those where at the same time:

1. The population density is higher, because a high population concentration in big cities with their characteristic high building density and infrastructure limitations is a key factor in increasing the risk (Badina 2020; Baburin and Baldina 2021).

2. Variation from Rosstat data is higher, because in Russian practice, the organization of preventive measures to protect the

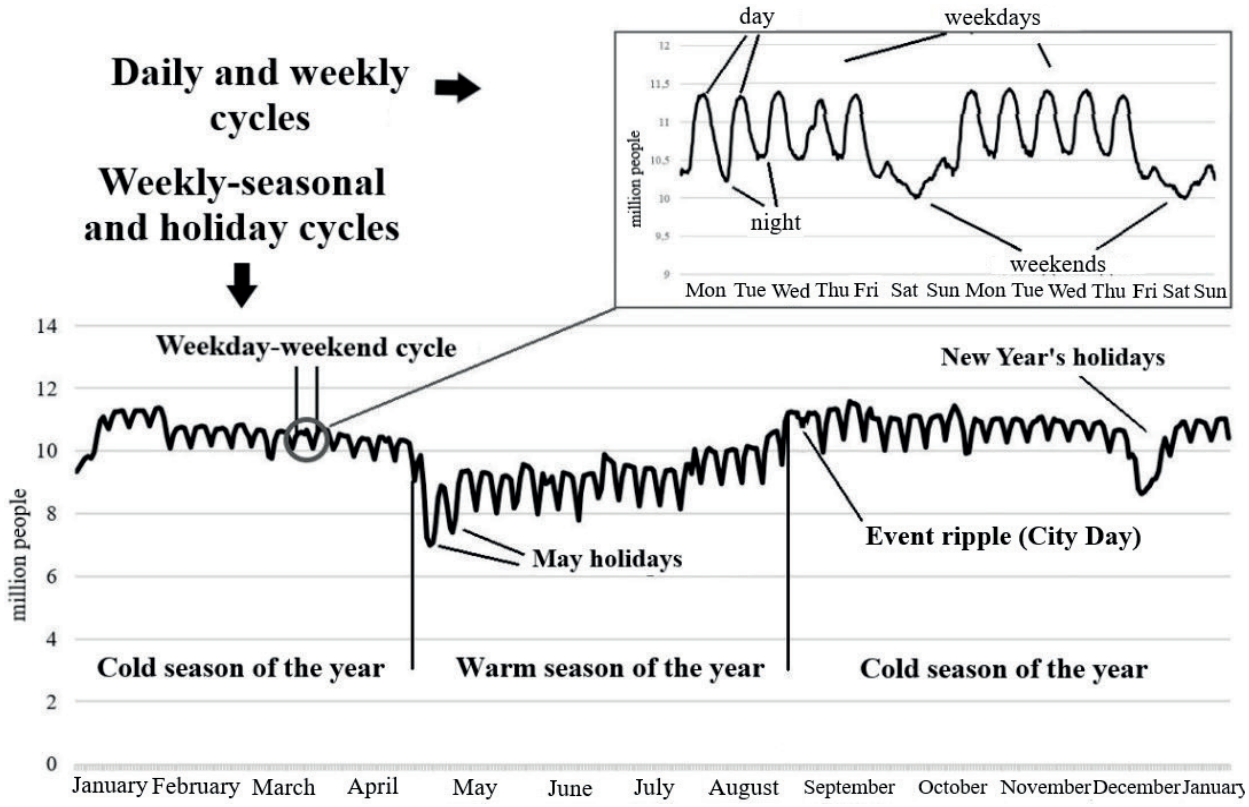

Fig. 2. The pulsation series of the present population of Moscow in January 2019 – January 2020

Source: compiled by the authors based on mobile operators' data

population from emergencies and measures to eliminate the consequences (including population evacuation) are carried out based on official statistics, which, as shown by our previous studies (Badina and Babkin 2021), significantly differ from reality.

3. Dynamic component is higher, since the intensive population movement in the daily cycle on the urban territory increases the uncertainty.

In order to select parameters that could best numerically describe the above characteristics of population vulnerability, about 20 different indicators were calculated, as well as the correlations between them. As a result, for the purposes of Moscow districts typology, according to the degree of present population vulnerability, the following parameters were chosen:

1. Median present population density according to mobile operators' data (persons per sq. km).

2. The ratio of the population size of the district according to Rosstat to the median daily population size according to mobile operators' data (%);

3. General daily gradient (the ratio of the maximum present population size according to the mobile operators' data to the minimum (%)).

The cluster analysis method was used as a typology tool. A detailed description of the methodology and results of cluster analysis carried out on the selected key slice is shown in the previous authors work (Badina et al 2022a). In addition, in this study, an important indicator of the transit flows intensity was considered separately (it was not included directly in the cluster analysis, since it is related to the indicator "Median present population density").

Dynamic clustering will make it possible to identify the typological stability of Moscow districts: how stable is their position within a particular cluster in different phases of the weekly-seasonal cycle. It has great pragmatic importance, since the least sustainable city districts require increased attention, flexible approaches in terms of developing preventive measures to protect the population from potential emergencies.

Dynamic clustering is an iterative cluster analysis based on the three above variables and on four different time periods, each of which characterizes a certain segment of the weekly-seasonal cycles: weekdays of the cold season, weekends of the cold season, weekdays of the warm season and weekends of the warm season. As a result, four particular clusterings are obtained that characterize the "behavior" of the settlement system in the main intervals of social time. After that, a cluster stability matrix is compiled, which allows to identify which of the districts retain their properties, and which are characterized by instability of three considered indicators.

At the same time, the selection of "natural types" of districts is carried out. Depending on how strongly the connection with the "neighbors" is saved according to the initial classification, the stability of the districts with respect to temporal displacements is calculated. The more surviving pairs in each new clustering, the more stable the result.

RESULTS

Static clustering

Based on the study of the pulsation series, it was decided to consider the transitions of districts from group to group, depending on one or another phase of the weekly-seasonal cycle. Consideration of various clustering options is necessary due to the fact that three indicators included in the cluster model are changeable throughout the year and can contribute to the "drift" of the district from one cluster to another.

The most complex (in terms of the number of influencing factors) indicator is the ratio of population density according to Rosstat to the density according to mobile operators' data. In general, the least deviations are typical for the districts of the central business core of Moscow, and the highest deviations – for residential districts, and especially for districts of accelerated housing construction. At the same time, for the vast majority of districts, the maximum deviations are observed on weekends of the warm season, when many Muscovites go to their suburban homes and vacations.

The highest median population density is characteristic of both attractor districts (primarily the Central Administrative District, as well as such subcenter districts as Begovoy, Dorogomilovo, etc.), and some small residential districts. For Moscow districts, this parameter is almost everywhere higher on weekdays of the cold season. The most significant deviations of daily population density gradients are observed in the most attractive districts for business and daytime recreation. The most significant values of daily gradients (2 times or more) are observed in weekdays of both cold (to a greater extent) and warm (to a lesser extent) seasons due to a significant increase in the number of people in the daytime. These values are significantly lower for residential districts, as well as dacha-recreational districts, which, with a certain degree of conventionality, include some districts of New Moscow. The multi-temporal pattern of changes is reflected in various combinations of districts in clusters and, as a result, in the previously mentioned four clustering variants.

The "season" in terms of this study is the time when the pulsation regime and the general characteristics of present population change due to natural seasonality and the prevailing social cycles (Fig. 2). At the previous stage of the study, based on *static clustering* for the general statistical data set (for the whole year), a typology of Moscow districts was created, which reflects the main features of the population spatial dynamics in the context of its vulnerability (Badina et al 2022a). Characteristic names that most fully reflect the essence of each group were given to five selected clusters (Table 2).

Table 2. Characteristics of clusters

Cluster (type of municipalities)	Population density	Intensity of transit flows	Intraday population gradients	Level of official statistics' distortion
Center	very high	very high	very high	low at night, high during the daytime
Transit residential	high	high	average	low
High-density residential	high	average	average	low
Low-density residential	average	average	average	low
Low-density peripherals	low	low	low	high

Source: (Badina et al 2022a)

Dynamic clustering

The most potentially vulnerable districts located in clusters with the maximum values of all four considered indicators. Therefore, these include clusters "Center" and "Transit residential". *Dynamic clustering* made it possible to reveal that each considered time interval is characterized by its own pool of clusters. Therefore, analysis shows six clusters for the weekdays of the cold season: "center", "transit residential", "low-density peripherals", "low-density residential" and two clusters with the characteristics of "high-density residential" (Fig. 3a). For the weekends of the cold season, same as for weekdays, 6 clusters are also identified: "center", "transit residential", "low-density peripherals", "low-density residential" and two clusters with the characteristics of "high-density residential" (Fig. 3b).

Clusters of "Transit residential", "High-density residential" and "Low-density residential" correspond to residential areas of the city, which are characterized by a strong daily outflow of population. In addition, for these clusters official statistics somewhat exaggerate the size of the population. The key difference between the clusters are the population density and the position on the main flows of movement of citizens: the population density reaches the highest values in the clusters "Transit residential", "High-density residential", to which homogeneous arrays of residential buildings are confined. On the territory of most of the municipalities of the "Low-density residential" cluster large areas are occupied by non-residential zones – the territories of small enterprises (primarily communal ones), large parks and urban forests, objects of railway transport infrastructure. For these three clusters the real population density is almost always lower than the official one, therefore, the problem of population vulnerability is the least acute for them.

The cluster "Center", consisting of a group of districts forming the business core of Moscow and concentrating the largest number of transport hubs, are characterized by high values of all considered indicators. They are distinguished by the highest density of the daily population and accordingly the highest intraday gradient of change in the daily population density (in the cluster "Center" these values are higher). Huge flows of people in the morning, afternoon and evening hours greatly increase the potential vulnerability of these territories and require especially close attention. In addition, there are still a number of potentially dangerous industrial enterprises on the territory of these clusters, as well as a number of potentially dangerous research institutes.

A separate category is represented by the areas included in the cluster "Low-density peripherals". This cluster has the lowest intraday population density and the lowest density gradient. This cluster includes many municipalities on the territory of which a large area is occupied by forests and other undeveloped territories – in particular, the municipalities of New Moscow. These are areas of new development, characterized by a low population density (due to the large areas of the districts). However, despite the small overall density, the population concentration here in some areas is very high. In addition, these areas are characterized by the greatest underestimation of real population density and population density by official statistics (2-3 times)[1].

A larger number (8) of clusters is formed in the case of weekdays during the warm season: "transit residential", "low-density peripherals", two clusters each with the characteristics of "center", "low-density residential", and "high-density residential" (Fig. 4a). On the contrary, for the weekends of the warm season, clustering showed only four groups: a highly compressed "center", "low-density peripherals", "low-density residential" and "high-density residential". This period is characterized by low transit, so the cluster of "transit residential" was not formed (Fig. 4b). In the warm season citywide mobility decreases which leads to the "migration" of districts from the most mobile to the more inert clusters (from the cluster "Center (var. 1)" to "Center (var. 2)" ("Subcenter" type) from "Transit residential" to "High-density residential", etc.).

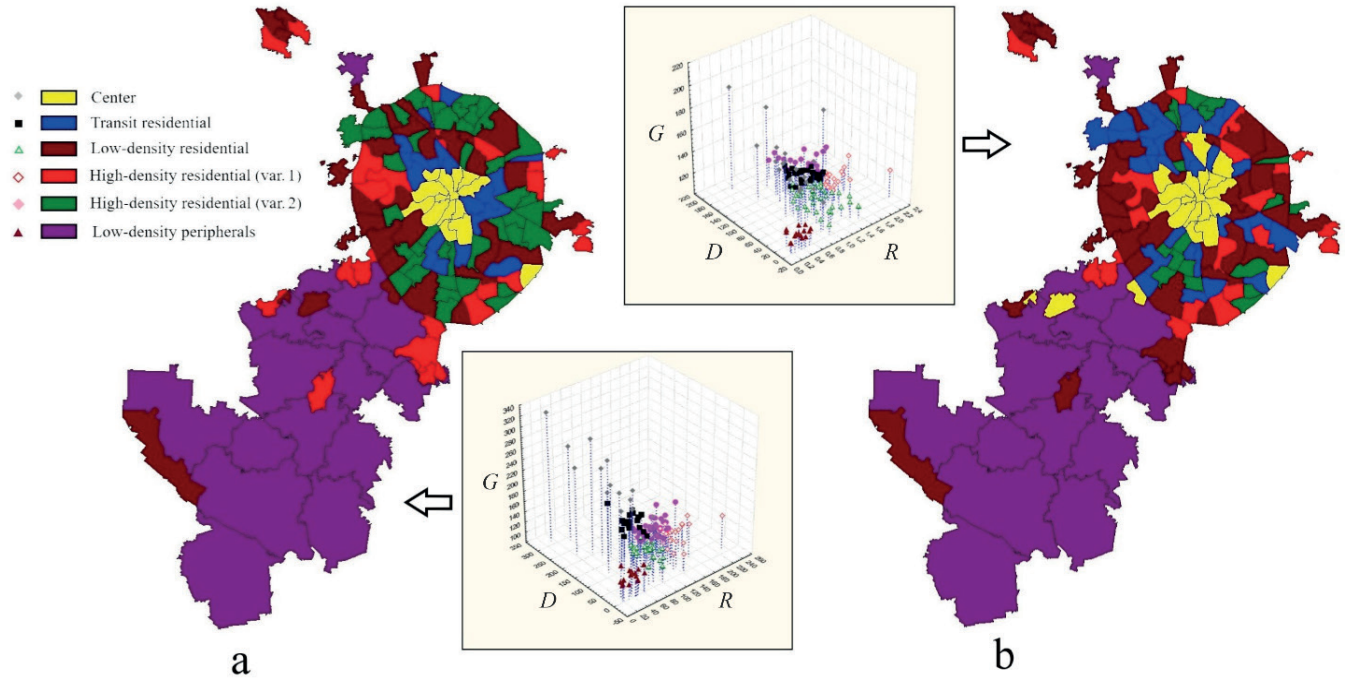

Fig. 3. Clustering for the cold season (a – weekdays, b – weekends). G – total daily gradient, %; D – median population density, people per sq. km; R – the ratio of Rosstat to the median, %

Source: compiled by the authors based on mobile operators' data

[1]As a result of active housing construction and rapid population growth, Rosstat does not have time to track real population changes of these territories providing information with a significant time lag.

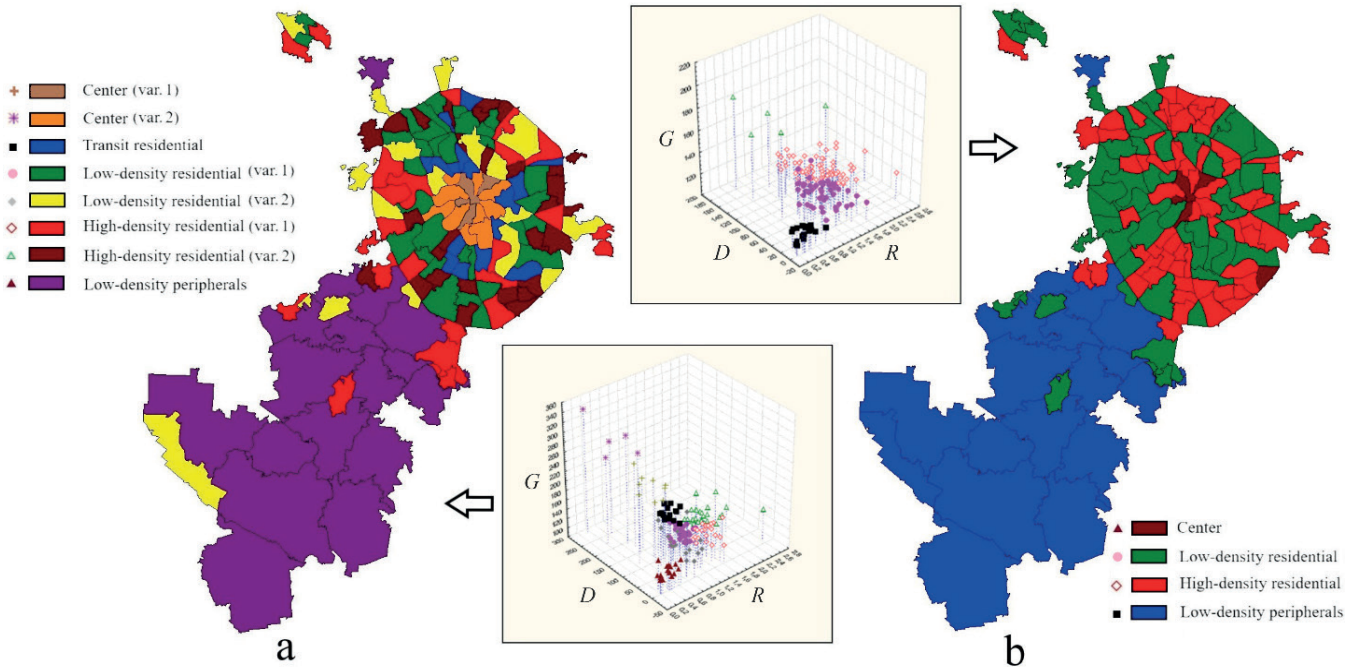

Fig. 4. Clustering for the warm season (a – weekdays, b – weekends). G – total daily gradient, %; D – median population density, people per sq. km; R – the ratio of Rosstat to the median, %

Source: compiled by the authors based on mobile operators' data

Thus, in the territorial aspect, the group of central districts and districts of New Moscow is especially pronounced. The rest of the districts more "wander" between clusters and, accordingly, they are less typologically stable.

The resulting four clussifications clearly demonstrate the transformations of the Moscow settlement system in the weekly-seasonal cycle of social time. Daily cycles are also embedded in the clustering parameters.

According to the results of particular clussification, information about the affiliation of city districts to a particular cluster in different time intervals was processed and a cluster stability matrix *D* was compiled (Fig. 5). Matrix *D* is used to analyze the stability of clusters for various time intervals.

For each classification k=1...4, $D_k=[d_{ij}]$, where d_{ij}=1, if a pair of Moscow districts *ij* belongs to the same cluster, 0 – otherwise, if *i*=*j* matrix value is missing (district is paired with itself). D_k matrices are aggregated into one:

$$D = \sum_{k=1}^{4} D_k$$

The maximum value of the matrix *D* elements is 4. It means that a pair of districts in all four classifications is

	A	B	C	D	E	F	G	H	I
1	**Moscow district**	**Bogorodskoe**	**Veshnyaki**	**Vostochnoye Izmaylovo**	**Vostochny**	**Golyanovo**	**Ivanovskoe**	**Izmailovo**	**Kosino-Ukhtomsky**
2	**Bogorodskoe**		1	3	3	1	1	0	0
3	**Veshnyaki**	1		0	0	4	2	2	2
4	**Vostochnoye Izmaylovo**	3	0		4	0	2	0	0
5	**Vostochny**	3	0	4		0	2	0	0
6	**Golyanovo**	1	4	0	0		2	2	2
7	**Ivanovskoe**	1	2	2	2	2		2	2
8	**Izmailovo**	0	2	0	0	2	2		3
9	**Kosino-Ukhtomsky**	0	2	0	0	2	2	3	
10	**Novogireevo**	1	1	2	2	1	1	0	0
11	**Novokosino**	1	1	2	2	1	1	0	0
12	**Metrogorodok**	0	2	0	0	2	2	3	4
13	**Perovo**	2	1	2	2	1	0	1	0
14	**Severnoye Izmaylovo**	1	0	1	1	0	0	0	0
15	**Sokolinaya gora**	0	2	0	0	2	2	2	2
16	**Sokolniki**	0	1	0	0	1	1	2	3
17	**Preobrazhenskoe**	1	1	2	2	1	1	0	0
18	**Vnukovo**	0	1	0	0	1	1	2	3
19	**Dorogomilovo**	0	1	0	0	1	1	1	1
20	**Krylatskoe**	2	3	1	1	3	3	2	2
21	**Kuntsevo**	0	2	0	0	2	2	3	4
22	**Mozhaisky**	1	3	0	0	3	2	3	3
23	**Novo-Peredelkino**	3	0	4	4	0	2	0	0
24	**Ochakovo-Matveevskoe**	0	2	0	0	2	2	4	3
25	**Prospekt Vernadskogo**	1	1	1	1	1	0	1	0

Fig. 5. Extract from the aggregate matrix D of pairwise connections

Source: compiled by the authors

in the same cluster. The minimum value is 0 (the pair of districts does not belong to the same cluster in any of the classifications).

If at each new time slice the districts keep their connection with their "neighbors" according to the initial[1] classification, then the result of clustering is considered stable regarding time shifts.

The more surviving pairs in each new clustering, the more stable the result. For each Moscow district, the number of all possible pairs with other districts that fall into one cluster in each classification is summed up. From the point of view of the matrix D elements, this operation is formalized in the form of counting the number of value matches (fours, triples, twos and ones) for each district – row. The ratio of counted pairs in one cluster at each time slice to the initial value (of the first clustering) forms a stability metric ρ, $0 \le \rho \le 1$. The higher this value for each district, the more stable its position in the cluster. Accordingly, if this value falls sharply with each new classification, then the district "migrates" between different clusters and the result is unstable. Below is a graphical demonstration of the calculated metrics (Fig. 6). For instance, for one of the districts at the initial classification, 12 pairs of districts were obtained that are in the same class with it. At the next stage, the number of districts pairs of 12 previously considered was reduced to 8. The value of the metric ρ in this case will be $8/12 \approx 0.7$. If the number of obtained pairs is 12, then we get the maximum value of the metric ρ equal to 1.

As can be seen from the graphs, at each new stage of clustering (for a different time slice), the number of surviving pairs decreases. At the same time, in all cases, a set of districts with maximum values of metrics close to one is clearly pronounced. This cluster is the most stable and includes the districts of New Moscow. Such a stable result obtained for New Moscow districts suggests that, despite being included in the administrative-territorial division of Moscow, these districts continue to function as part of the Moscow Oblast in terms of population movement. Thus, the space of Moscow breaks up, in fact, into two cities with different modes of operation.

Classification of districts according to the degree of stability of their position in clusters

Therefore, in order to understand which districts change or retain their affiliation with a particular cluster on weekly and seasonal rhythms, the transitions of districts from one cluster to another within four selected time ranges were analyzed. As a result, three types of districts were identified. Each type includes 11 subtypes (Fig. 7).

1. The first group of municipalities was formed by the "Stable Districts". They do not change their position in the four variants of clustering.

1.1. The subtype "Peripheral" represents the largest and most solid array of districts that are included in the "Low-Density Peripheral" cluster type. All these districts, with the exception of Molzhaninovsky, are located on the territory of New Moscow.

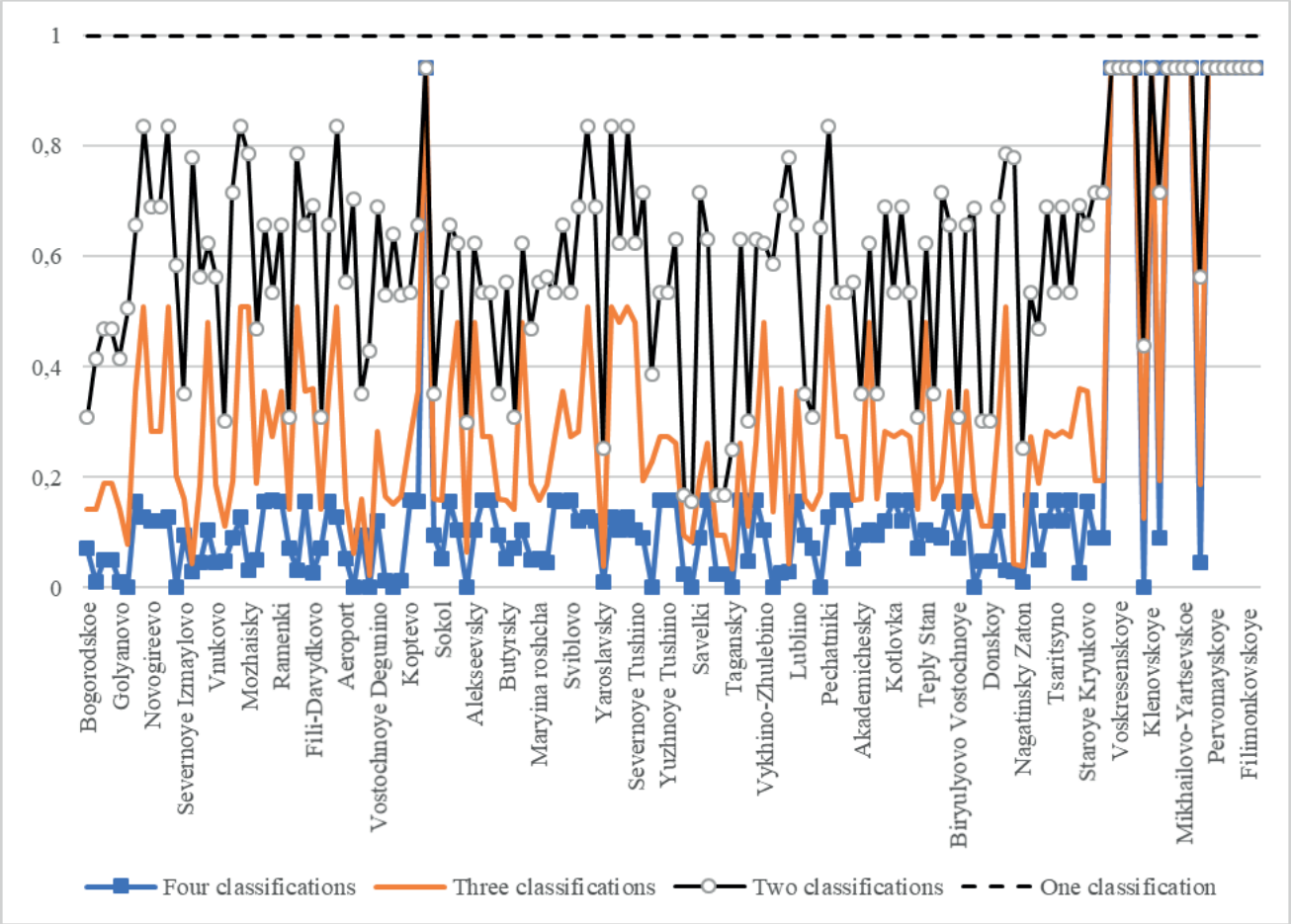

Fig. 6. The value of the stability metric for various clustering options (the case of Moscow districts)

Source: compiled by the authors

[1] "Initial" means the first classification that was made. For instance, firstly, we classify districts for weekdays cold season and it would be initial point for stability analysis. But the first classification could be for weekends warm season and so on. The stability analysis methodology does not depend on which classification comes first.

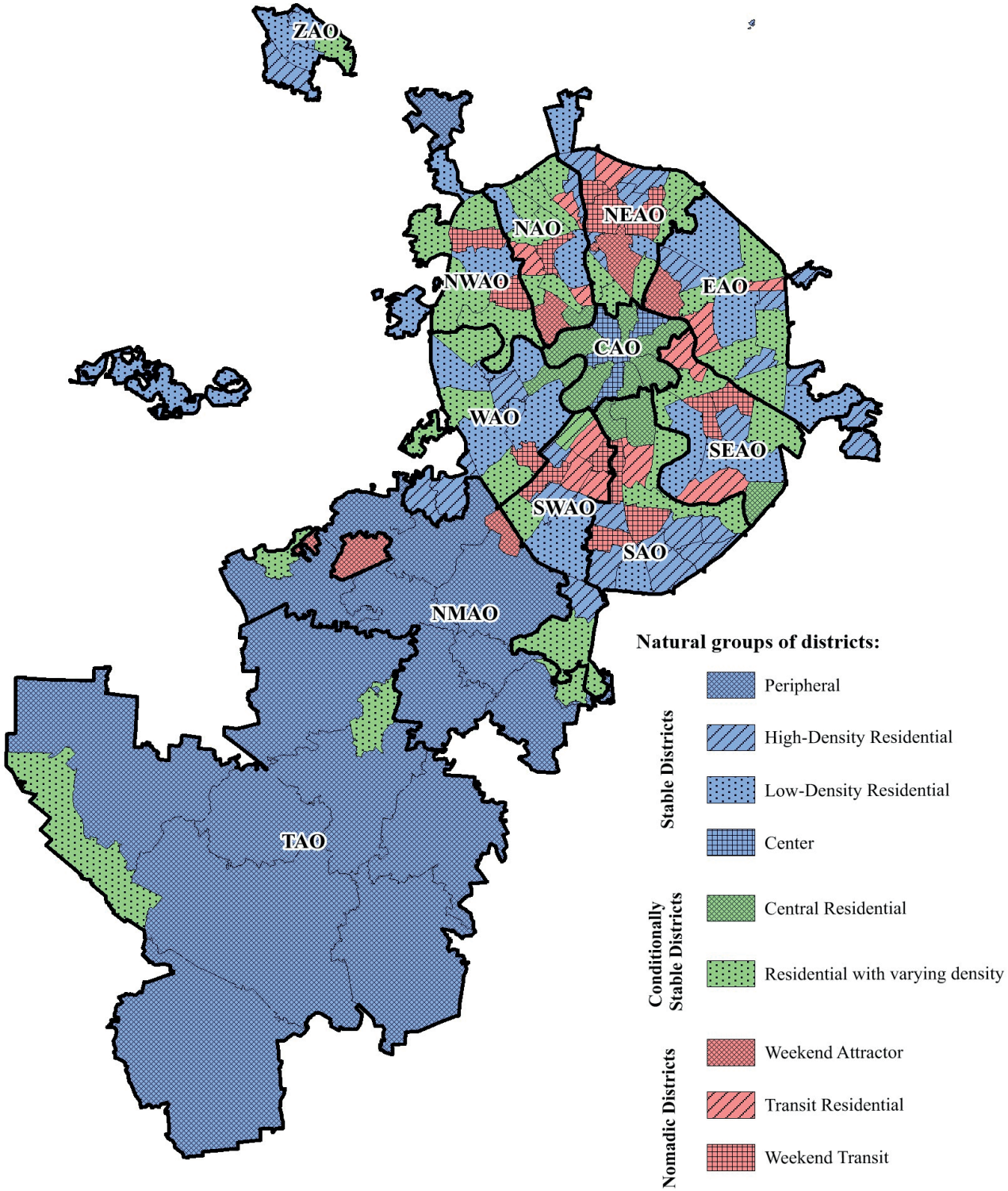

Fig. 7. Natural groupings of districts

Source: compiled by the authors

1.2 and 1.3. The subtypes "High-Density Residential" and "Low-Density Residential" includes scattered sleeping districts[1] of Moscow belonging to the eponymous cluster types.

1.4. The subtype "Center" includes four districts of the center (Arbat, Krasnoselsky, Tverskoy, Yakimanka) distinguished by a stable position in the "Center" cluster.

2. The second group of municipalities consists of "Conditionally Stable Districts", which can slightly change their position depending on the clustering time slice.

2.1. The subtype "Central Residential". This type includes several municipalities of the Moscow center, which, being powerful business attractors, also have a significant housing stock. As a result, in one of the time slices for such districts, the cluster type changes to the "sleeping" one. In most cases, this is the weekend of the warm season.

2.2. The subtype "Residential with varying density" include sleeping areas moving from "Low-Density Residential" to "High-Density Residential" within the week-seasonal cycles.

3. Finally, the third type, which requires special attention, is represented by "Nomadic Districts", which change their cluster type 2 or even 3 times depending on the time slice.

[1] "sleeping districts" or "commuter town" – a residential area of a city (usually in large metropolitan areas or their suburbs), whose residents daily commute to work in the business or industrial center and return home to spend the night

3.1. The subtype "Weekend Attractor" consist a group of districts located close to the city center. These districts moved to the "Center" cluster on the cold season weekends. Characteristic representatives of this type are the Sokolniki and Ostankinsky districts.

3.2. The subtype "Transit Residential" – sleeping districts on weekdays, becoming transit districts for commuting flows to / from the business center.

3.3. The subtype "Weekend Transit" is a group of sleeping districts on weekends moving into the "Transit Residential" cluster. First, these are districts with large transport hubs on their territory, for instance, Tsaritsyno or Shchukino.

The proposed method allows in two iterations (clusterization and identification of natural groups) to carry out a typology of urban districts in order to form approaches to the organization of preventive measures to protect the population from emergencies. The use of the cluster approach in four social time slices makes it possible to consider the stability of the spatial structure of settlement within the framework of weekly-seasonal cycles, and, accordingly, in terms of changes in their vulnerability. Most of the city's districts have a stable position at various time slices in the clustering. Some of them change slightly, for instance, they move from "Low-Density Residential" to "High-Density Residential" types. Finally, about 30 districts are distinguished by transitions between different types depending on the day of the week or the season. These most "unsustainable" or "nomadic" districts due to high uncertainty and the need to use different methods of regulating and controlling human flows will require local-targeted approaches to risk management. In subsequent works, the authors also plan to pay detailed attention to each type of districts, place them in the context of the likelihood of natural and man-made hazards.

DISCUSSION

The application of the dynamic clustering method and the subsequent typology of Moscow districts makes it possible to determine the rank of the vulnerability of various city parts to external shocks. At the same time, it should be noted that this approach, based on dynamic characteristics, does not take into account many other important components of the population vulnerability, such as age-sex composition, income differences, the proportion of youngest children and people with disabilities, people with limited mobility, etc.

Therefore, due to the objective limitations of the data used (problems of the non-personalized nature of data, underestimation of SIM cards of switched off devices, technical interference associated, for instance, with overlapping of signals from neighboring repeaters etc.), as well as the impossibility of taking into account the above significant characteristics of the population vulnerability, the author's approach cannot claim to be universal.

However, in the authors' opinion, despite all the weakness consideration of Moscow districts through the prism of the chronogeographic approach will allow the use of local-targeted approaches to minimizing the emergency consequences for present population. In this logic, the developed typology of Moscow districts in terms of the degree of stability of their main population vulnerability characteristics in weekly and seasonal cycles is the first step towards a more detailed study of natural and man-made risks.

This typology can be used for a wide range of practical tasks, as it well reflects the inequality of social time for different parts of the city. In particular, knowledge about the typological stability of Moscow districts in weekly and seasonal cycles makes it possible to apply appropriate mechanisms to each type in the field of protecting the population from natural and man-made hazards. Depending on the position of the district in the typology, it is proposed to use various methods of regulating and controlling human flows, focusing on individual districts, time slices and cycles that are important for a particular type.

The authors see a promising direction in the development and testing of methods that make it possible to analyze the connection between functional zones in urban space and social time using mobile operators' data. Thus, the temporal and spatial aspects will be best integrated and mutually supplemented, which will allow in the future to obtain the most reliable picture of reality, to identify key patterns.

CONCLUSIONS

The revolution of the last two decades in the field of production and processing of spatiotemporal information has led to a renaissance of chronogeography, which faced insurmountable technological challenges in data collection in the 1980s. Mobile operators' data on a new information and resource basis allow us to continue the traditions of spatio-temporal analysis, which was carrying out by the Institute of Geography of the Academy of Sciences more than 30 years ago.

As the current international and domestic experience shows, Big data and, in particular, mobile operators' data have a great importance for geographical research. This is a very promising and representative tool that can improve the quality of research in many areas. Overcoming technological barriers in obtaining and processing information about the population movement in "real time" mode using mobile operators' data allows in practice to carry out a detailed spatio-temporal analysis of the dynamic characteristics of large city population, which is clearly demonstrated in this article.

Of particular interest is the prospective use of mobile operators' data in the field of assessing and forecasting natural and man-made risks. In this article, to solve the applied problem of assessing the vulnerability of urban areas to potential threats, using the case of Moscow, the authors tried to synthesize three topical elements of modern geographical research – spatiotemporal analysis, Big data and emergency risk assessment. The broad interdisciplinary field of risk research can become a platform for a new era of integration of physical and socio-economic geography.

REFERENCES

Ahas R., Aasa A., Yuan Y., Raubal M., Smoreda Z., Liu Y., Ziemlicki C., Tiru M., Zook M. (2015). Everyday Space–Time Geographies: Using Mobile Phone-Based Sensor Data to Monitor Urban Activity in Harbin, Paris, and Tallinn. International Journal of Geographical Information Science, 29(11), 2017-2039.

Akimov V.A., Durnev R.A., Sokolov Y.I. (2009). Dangerous hydrometeorological phenomena on the territory of Russia. Moscow: FGU VNII GOChS (FC) (in Russian).

Aksha S.K., Juran L., Resler L.M., Zhang Y. (2019). An analysis of social vulnerability to natural hazards in Nepal using a modified social vulnerability index. International Journal of Disaster Risk Science, 10(1), 103-116.

Baburin V.L. (2011). Two-dimensional model of the territorial organization of society. Vestnik Moskovskogo Universiteta, Seriya 5: Geografiya, 1, 3-8 (in Russian).

Baburin V.L. and Baldina S.V. (2021). Forecasting of socio-economic damages from hazardous natural processes for the tourist cluster Resorts of the North Caucasus. Vestnik Moskovskogo Universiteta, Seriya 5: Geografiya, 2, 25-35 (in Russian).

Badina S.V. (2020). Prediction of socioeconomic risks in the cryolithic zone of the Russian Arctic in the context of upcoming climate changes. Studies on Russian Economic Development, 31(4), 396-403.

Badina S.V. and Babkin R.A. (2021). Assessment of Moscow population vulnerability to natural and technogenic hazards. InterCarto. InterGIS, 27(4), 184-201 (in Russian).

Badina S., Babkin R., Bereznyatsky A., Bobrovskiy R. (2022a). Spatial aspects of urban population vulnerability to natural and man-made hazards. City and Environment Interactions, 15, 100082.

Badina S., Babkin R., Mikhaylov A. (2022b). Approaches to assessing the vulnerability of large city population to natural and man-made hazards using mobile operators data (case study of moscow, russia). In: Wohlgemuth V., Naumann S., Behrens G., Arndt HK. (eds) Advances and New Trends in Environmental Informatics. ENVIROINFO 2021. Springer Cham, 171-186.

Baida S.E. (2019). Wave cycles of natural, human-made and social catastrophes. Civil Security Technology, vol. 16, No. 4 (62), 30–-36 (in Russian).

Cutter S.L., Boruff B.J., Shirley W.L. (2003). Social vulnerability to environmental hazards. Social science quarterly, 84(2), 242-261.

De Oliveira Mendes J.M. (2009). Social vulnerability indexes as planning tools: beyond the preparedness paradigm. Journal of Risk Research, 12(1), 43-58.

Flanagan B.E., Gregory E.W., Hallisey E.J., Heitgerd J.L., Lewis B. (2011). A social vulnerability index for disaster management. Journal of homeland security and emergency management, 8(1), article 3.

Froude M.J. and Petley D.N. (2018). Global fatal landslide occurrence from 2004 to 2016. Natural Hazards and Earth System Sciences, 18(8), 2161-2181.

Geyer H.S. and Kontuly T.A (1993). Theoretical foundation of the concept of differential urbanization. International Regional Science Review, 15(2), 157-177.

Gibbs J. (1963). The evolution of population concentration. Economic Geography, 2, 119-129.

Hägerstrand T. (1973). The domain of human geography. In: Chorley R.J. (ed.) Directions in Geography. London: Methuen.

Kaniewski D., Marriner N., Morhange C., Faivre S., Otto T., Van Campo E. (2016). Solar pacing of storm surges, coastal flooding and agricultural losses in the Central Mediterranean. Scientific reports, 6(1), 1-12.

Karachurina L.B. and Ivanova K.A. (2017). Migration of the elderly in Russia (according to the 2010 census). Regional studies, 3(57), 51-60 (in Russian).

Klaassen L.H. and Scimeni G. (1981). Theoretical issues in urban dynamics. In: L.H. Klaassen, W.T.M. Molle and J.H.P. Paelinck (ed.). Dynamics of Urban Development. Aldershot: Gower.

Knaub R.V., Ignateva A.V. (2022). The General Mechanism of the Origin of Natural Disasters in the Global Dimension. IOP Conference Series: Earth and Environmental Science, 988(2), 022068.

Kondratiev N.D. (2003). Large cycles of conjuncture and the theory of foreseeing. Selected Works. Voprosy Ekonomiki, 8, 153-154 (in Russian).

Luque-Espinar J.A., Mateos R.M., García-Moreno I., Pardo-Igúzquiza E., Herrera, G. (2017). Spectral analysis of climate cycles to predict rainfall induced landslides in the western Mediterranean (Majorca, Spain). Natural Hazards, 89(3), 985-1007.

Makhrova A.G. and Babkin R.A. (2018). Analysis of pulsations of the settlement system of the Moscow agglomeration with the use of cellular operator data. Regional studies, 2, (60), 68-78 (in Russian).

Makhrova A.G., Babkin R.A., Kirillov P.L., Starikova A.V., and Sheludkov A.V. (2022). Temporary mobility and population pulsations in space of post-Soviet Russia. Regional Research of Russia, 12(1), 36-60.

Makhrova A.G., Kirillov P.L. (2015). Seasonal pulsation of settlement in the Moscow agglomeration under the influence of dacha and labor pendulum migration: approaches to the study and assessment. Regional studies, 1(47), 117-125 (in Russian).

Makhrova A.G., Kirillov P.L., Bochkarev A.N. (2016). Pendulum labor migrations of the population in the Moscow agglomeration: experience of flow estimates using data from cellular operators. Regional studies, 3(53), 71-82 (in Russian).

Nefedova T.G. (2015). Seasonal work in the system migrations in post-Soviet Russia. Prerequisites. Demoscope Weekly, [online] Available at: http://demoscope.ru/weekly/2015/0641/demoscope641.pdf [Accessed 20 Apr. 2022] (in Russian).

Nelson K.S., Abkowitz M.D., Camp J.V. (2015). A method for creating high resolution maps of social vulnerability in the context of environmental hazards. Applied Geography, 63, 89-100.

Osipov V.I., Burova V.N., Zaikanov V.G. et al. (2011). Map of large-scale (detailed) engineeringgeological zoning of the territory of Moscow. Geoecology, 4, 306-318. (in Russian).

Petrov N.V. (1986). Spatial and temporal analysis in social geography: Main achievements and directions of research. Swedish. shk. [T. Hegerstrand]. Moscow: VINITI (in Russian).

Siagian T.H., Purhadi P., Suhartono S., Ritonga H. (2014). Social vulnerability to natural hazards in Indonesia: driving factors and policy implications. Natural hazards, 70(2), 1603-1617.

Sorokin P.A. and Merton R.K. (1937). Social Time: a methodological and functional analysis. The American Journal of Sociology, 42(5), 615-629.

Spielman S.E., Tuccillo J., Folch D.C., Schweikert A., Davies R., Wood N., Tate E. (2020). Evaluating social vulnerability indicators: criteria and their application to the Social Vulnerability Index. Natural Hazards, 100(1), 417-436.

United Nations, Department of Economic and Social Affairs, Population Division (2019). World Urbanization Prospects: The 2018 Revision (ST/ESA/SER.A/420). New York: United Nations.

Ward P.S. and Shively G.E. (2017). Disaster risk, social vulnerability, and economic development. Disasters, 41(2), 324-351.

Zemlyansky D.Y. (2011). An indicative approach to assessing the seasonal dynamics of population placement in Russia. Regional studies, 3, 83-92 (in Russian).

Zhang, Z., Tian, H., Cazelles, B., Kausrud, K. L., Bräuning, A., Guo, F., Stenseth, N. C. (2010). Periodic climate cooling enhanced natural disasters and wars in China during AD 10–1900. Proceedings of the Royal Society B: Biological Sciences, 277(1701), 3745-3753.

Zhongrui W., Feng S., Maocang T.A. (2003). Relationship between solar activity and frequency of natural disasters in China. Advances in Atmospheric Sciences, 20 (6), 934-939.

RESEARCH PAPER

CONTRIBUTED INDICATORS TO FLUVIAL FLOOD ALONG RIVER BASIN IN URBAN AREA OF INDONESIA

Dwi Ariyani[1,5*], Perdinan[2*], Mohammad Yanuar Jarwadi Purwanto[3], Euis Sunarti[4], Atie Tri Juniati[5], Mochammad Ibrahim[6]

[1]Postgraduate Student of PSL, Bogor Agricultural University, Darmaga Bogor Campus IPB, 16680, Bogor, Indonesia
[2]Department of Geophysics and Meteorology, Faculty of Mathematics and Natural Science, IPB University, Darmaga Bogor Campus IPB, 16680, Indonesia
[3]Department of Civil and Environmental Engineering, IPB University, Darmaga Bogor Campus IPB, 16680, Indonesia
[4]Department of Family and Consumer Sciences, Faculty of Human Ecology, IPB University, Darmaga Bogor Campus IPB, 16680, Indonesia
[5]Civil Engineering Study Program, Pancasila University, Jagakarsa South Jakarta City, 12640, Jakarta, Indonesia
[6]PPK OPSDA 2, Ciliwung Cisadane Natural Resources Maintenance Operations Unit, 13620, Jakarta, Indonesia
***Corresponding author:** perdinan@apps.ipb.ac.id, dwi.ariyani@univpancasila.ac.id

Received: May 4th, 2022 / Accepted: November 11th, 2022 / Published: December 31st, 2022
https://DOI-10.24057/2071-9388-2022-084

ABSTRACT. Flooding is the most common disaster in Indonesia, it is classified as a disaster if it affects humans causing physical and financial losses. Flood damage depends on the type of flood, flow velocity, and duration. The increase in population will cause an increase in infrastructure that will affect the environment, including the carrying capacity of rivers and catchment areas, while flooding in urban areas will also have an impact on infrastructure and assets, increasing flood damage. This study discusses the factors that cause flooding (rainfall, topography, soil type, land slope, distance from rivers, river waste, population density, etc.), as well as various types of floods that occur. The method used in this research was based on the qualitative analysis of the information from the government and literature over the last five years obtained from online databases and search engines. The results of this study can provide a reference for the theory regarding disaster risk assessment and flood hazard prediction in watersheds. This research was conducted in the Ciliwung Watershed (DAS), where the factors and the dominant type of flooding were determined. Knowing the contributing factors can be beneficial for flood risk management. This research focuses on identifying factors that contribute to fluvial flood events and understanding their influence so that a more integrated flood risk management that takes into account the upstream, middle, and downstream parts of the watershed can be arranged in other areas based on the example of measures implemented by the local government in the Ciliwung watershed. This conceptual effort provides a much-needed foundation for developing better mitigation efforts in watersheds.

KEYWORDS: Flood Hazard, Contributing Factor, Flood type, Distance from the river, conceptual study

CITATION: Ariyani D., Perdinan, Purwanto M.Y.J., Sunarti E., Juniati A. T., Ibrahim M. (2022). Contributed Indicators to Fluvial Flood Along River Basin in Urban Area of Indonesia. Geography, Environment, Sustainability, 4(15), 102-114
https://DOI-10.24057/2071-9388-2022-084

ACKNOWLEDGEMENTS: Thanks to the Research Institute of the Faculty of Engineering, the University of Pancasila for the funds provided

Conflict of interests: The authors reported no potential conflict of interest.

INTRODUCTION

According to the United Nations World Health Organization (WHO), a disaster is defined as an event that disrupts normal conditions and causes a level of suffering that exceeds the ability of the affected population to adapt. According to Law No. 24/2007 of the Republic of Indonesia, a disaster is a series of events that threaten and disrupt people's lives and livelihoods caused by natural, non-natural, and man-made factors. According to Omena et al. (2020), disasters can be categorized into natural and non-natural disasters, and as long as an event impacts the functions of the community so that human activities cannot run normally, it can be categorized as a disaster. Based on the above, a flood is classified as a disaster if it causes financial and physical losses, as well as loss of human life. Meanwhile, increased vulnerability to flooding cannot be solely attributed to climate, as it is also affected by population growth, rapid urbanization, and urban sprawl (Pornasdoro et al. 2014). As a result, even though a city is densely populated and has a high economic value, disasters caused by floods can cause a setback in its development for several years (Tingsanchali 2012).

Flood damage depends on the type of flood, flow velocity, and duration. Increased population density coupled with flood-affected infrastructure and assets in cities increases the likelihood of urban flood damage, while the uncontrolled growth of urban settlements reduces

their drainage capacity (Tingsanchali 2012). This paper will discuss the definition of flood hazard, flood event, and flood disasters and the differences between fluvial flooding, flash flooding, and coastal flooding based on flood events that occurred in Indonesia to identify their generic and specific indicators, as well as the methods for their assessment based on event parameters. The study also analyzed flood events in the Ciliwung river basin in order to develop better mitigation efforts in flood management based on the factors that influence flood events in the area, particularly the characteristics of the river, which include its width, order, slope, and other factors that affect the watershed.

MATERIALS AND METHODS

Study Location

This research was conducted on the Ciliwung river, which passes through Bogor Regency, Bogor City, Depok City, South Jakarta, and East Jakarta, and flows into Jakarta Bay. Geographically it spans from 6^0 6′ 00″ to 6^0 46′ 12″ S and from 106^0 48′ 36″ to 107^0 00′ 00″ E (Fig. 1). Its watershed has an area of 386 km^2 and an average slope of 8%, while the average river slope is 0.0146 meters.

Method

This research was conducted based on field observations and a literature review. Field observations were carried out to assess the morphometry characteristics of the watershed. The analysis of watershed morphometry was also carried out using Geographical Information Systems (GIS) for mapping and analyzing land use changes in the Ciliwung watershed over the period of 30 years. The literature search was performed using online databases and search engines. The review includes journals and conference papers identified from SCImago and Google Scholar, reports published by the World Meteorological Organization and government agencies, as well as other reports identified online with a Google search.

This research paper covers the development of a general framework for flood management based on its constituent factors, it discusses several types of floods, such as fluvial, coastal, and flash floods, and focuses on specific and general indicators as well as data sources considered for the establishment of a decision support system in flood management. The general flowchart of the research is presented in Fig. 2 below.

The time frame of the study was limited to the period from 2002 to 2022. The goal of the literature review was to determine contributing factors, assess their magnitude, and identify flood events in various areas in Indonesia, including in the Ciliwung watershed, to distinguish between different types of flooding.

The research followed the flowchart (see Fig. 2) to determine the contributing factors for each flood type based on the literature review and identify the indicator variables. River characteristics were determined using QGIS by mapping USGS satellite data combined with data from the ministry of public works represented by the Ciliwung Cisadane River Basin Center (BBWS Cilincis) and guidelines for watershed characteristics (Ministry Of Forestry Directorate General Of Watershed Development Management And Social 2013). River morphometric characteristics were also estimated based on the river order, which can be determined using the Horton, Strahler, Shreve, and Scheidegger methods. In general, the Strahler method is easier to implement than the other methods. In this method, the upstream river channel without tributaries is assigned an order of 1, after it intersects with another stream of the same order, it is assigned an order of 2, and so on. As a result, the highest order number will correspond to the downstream of the main river (see Fig. 9). The number

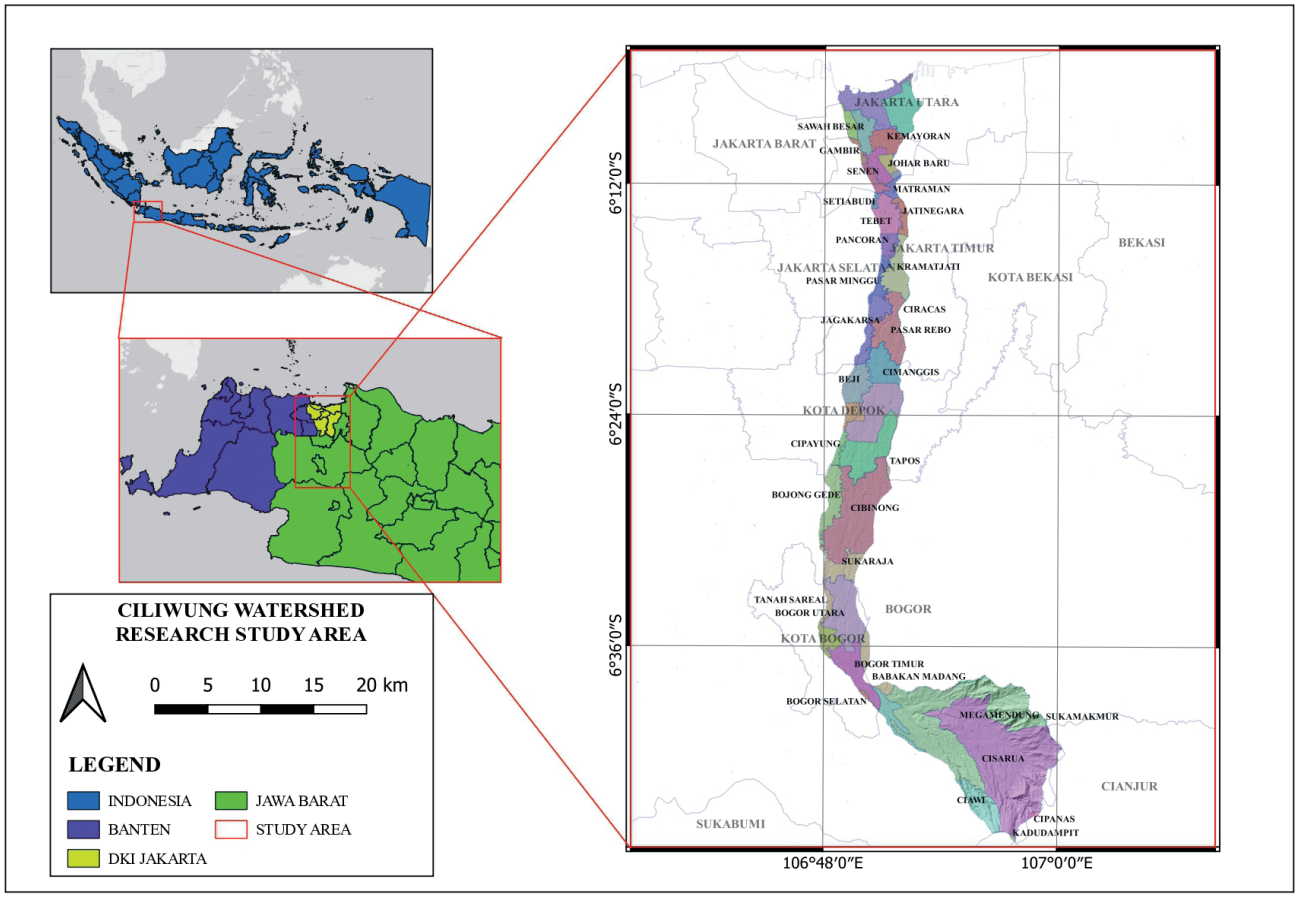

Fig. 1. Study Area

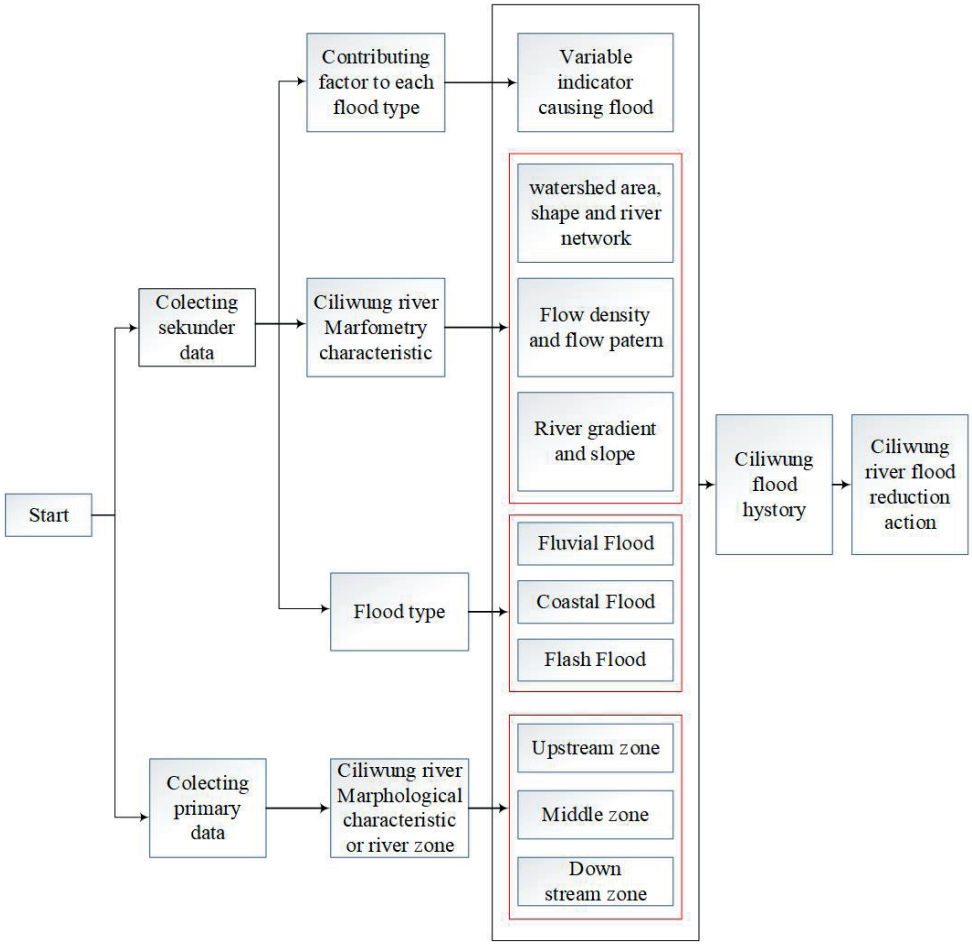

Fig. 2. Research Flowchart

of streams of a certain order can be determined from the bifurcation ratio (Rb) using the following formula:

$$Rb = \frac{N_u}{N_{U+1}} \quad (1)$$

Where:
Rb = River branching rate index
N_u = The number of streams for the order u
N_{U+1} = The number of streams for the order (u+1)

River density is an index that characterizes the drainage network of a watershed and is calculated as the total length of streams (km) per square kilometer of the watershed area. The greater value of Dd indicates better drainage, which results in higher water runoff (less infiltration) and smaller groundwater storage in the area. River density value can be determined as follows:

$$Dd = \frac{\Sigma L_n}{A} \quad (2)$$

Where:
L_n = River Length
A = Watershed area

The Ciliwung river data were obtained based on field observations along the Ciliwung river in the upstream, middle and downstream parts, and included various flooding indicators, as well as river morphometry and morphology characteristics, which were then used to determine the type of floods in the Ciliwung basin.

RESULTS

Types of Floods and their Criteria

Based on the type, floods can be divided into three categories, namely Fluvial Floods (Fig. 3), Coastal Floods (Fig. 4), and Flash Floods (Fig. 5). Fluvial Floods are usually caused by excessive rainfall occurring over a long period and a large area, which can cause large rivers to overflow and inundate the surrounding land. Precipitation in the upstream area will affect the downstream area, even when the downstream area does not receive much rain (Asdak et al. 2018). Coastal Floods in Indonesia include tidal floods, which is a phenomenon of increasing sea level that results in the inundation of tidal areas. Coastal flooding can also be caused by large storms that increase the water level and create high waves (Hanif et al. 2021). Increased flooding in coastal areas will affect both urban and traditional settlements not only due to rising sea levels and climatic factors of the island but also due to population increase in coastal areas (Esteban et al. 2011). Flash floods usually occur on steep slopes due to heavy rainfall, which can cause riverbeds that initially had no water to suddenly overflow. The rainwater that fell on a slope then rushes down the hill with high velocity and gathers in a river at the bottom. Flash floods can be also caused by infrastructure failures such as a broken embankment along the sea or a river, which can also cause water to flow suddenly and with high velocity. (Zanchetta dan Coulibaly 2020).

Contributing Factors to Each Flood Type

Fluvial floods, often called river floods, occur when the flow in a stream exceeds the channel capacity. These fluvial floods are usually observed in areas around rivers and lakes due to high rainfall or melted snow during the rainy season. They are stagnant and can recede after several hours. High rainfall intensity upstream can also cause flooding downstream. Specific indicators of Fluvial Floods are (a) high rainfall (Miftahuljannah dan Ibrahim 2019), (b)

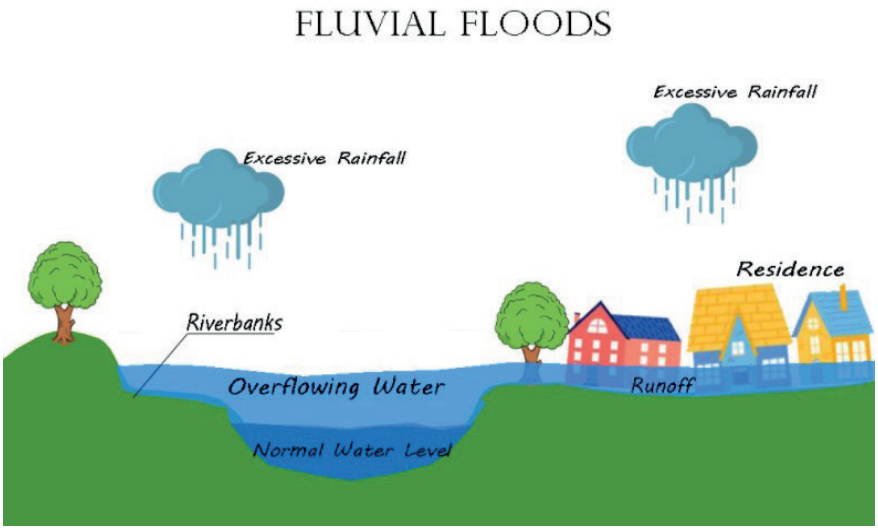

Fig. 3. Illustration of Fluvial Floods

Fig. 4. Illustration of Coastal Floods

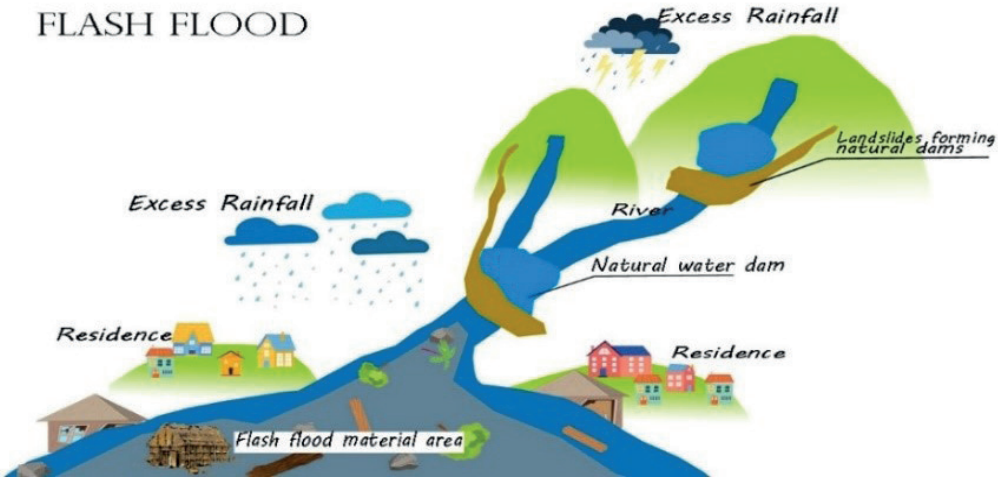

Fig. 5. Illustration of Flash Floods

rainfall intensity in a particular area, (c) channel capacity to accommodate rainfall, (d) watershed characteristics as downstream flooding may occur after a period of time from upstream, (e) type of land cover, which affects the occurrence of flooding, (f) river elevation, which affects the speed of downstream flooding. Examples of fluvial flood events include the Solok floods in 2019, which affected the rivers Sapan Aia Angek, Batang Pagu, Batang Bangko, Batang, and Batang Pulakek, as well as coal irrigation, and were caused by improper functioning of the waterways due to garbage (Miftahuljannah dan Ibrahim 2019). Floods caused by land cover changes also frequently occur in Baleendah Bandung, especially during high rainfall (Barus et al. 2019).

Coastal Floods occur in coastal areas due to rising seawater along with the melting of the north/south poles (Raditya et al. 2020). Specific Indicators of coastal floods also correspond to coastal areas. Floods are higher during the period of high tide, for example, around a full moon, and events are not directly affected by high rainfall. In Indonesia, Modukoro area is affected by both coastal floods and rain floods (Jatmiko 2018).

Flash Floods, or pluvial floods, occur when extreme rainfall events create floods that are not dependent on overflowing water bodies. Pluvial floods can occur in any location, urban or rural, even in areas without surrounding water bodies, and are characterized by a short duration with a relatively high peak discharge (Zain et al. 2021), generally occurs in areas of steep

elevation (Kurniawan 2013). Flash floods generally occur due to landslides in the upstream part of the river. Debris consisting of water, rock, and tree trunks can stem river flow and form natural dams. Landslides are influenced by physical factors such as slope, vegetation density, soil texture, soil permeability, soil solum thickness, and weathering of rock (selvena). Specific Indicators of Flash Floods are the following: (a) occur suddenly, in a short time, (b) large volume of water (peak discharge) (Kurniawan 2013), (c) can be associated with river dam damage due to erosion (Hidayatulloh et al. 2018), (d) travel time from trigger to flood is less than 1 hour (Hidayatulloh et al. 2018), (e) high rainfall (Azmeri et al. 2015, Tewal et al. 2018). (f) the size of the catchment area, which affects the peak discharge, (g) vegetation density, (h) watershed slope, (i) the shape of the watershed (oval, round), a round watershed will be more prone to flooding because more water is accommodated (Savitri dan Pramono 2017), (j) soil permeability.

An example of a Flash Flood incident in Indonesia was observed on 1 Jan 2006, when a disaster occurred in the Kaliputih River, Jember, causing 80 deaths and hundreds of injuries. It was caused by extreme rain damaging a natural dam, which triggered a landslide with a distance of 12.8 km, flood arrival time was 1.7 hours, the speed varied depending on elevation, and the peak discharge was estimated at 891.53 m3/s (Kurniawan 2013, Hidayatulloh et al. 2018). In 2003, a flash flood in the Bahorok Catchment killed 200 people and destroyed nearby buildings. It was caused by heavy rainfall (200-300 mm for the three days before the incident), topographic conditions, soil, and rock structure characteristics. The slope there is more than 40 degrees (Zain et al. 2021). Flash Flood also occurred in Wasior Catchment, in Wasior District, Wondama Bay Regency, West Papua Province, where rainfall reached 179 mm in 10 hours, and with the slope ranging from 5 to 75 degrees, the peak discharge reached 152 m^3/hour. The watershed of Krueng Teungku was flooded three times, in 1987, 2000, and 2013. On 2 January 2013, there was an extreme daily rainfall of 125 mm, leading to a flood with a peak discharge of 34.83 m^3/s and a travel time of about 4 hours (Azmeri et al. 2015). Landslides that triggered flash floods in the Kali river along Manado-Tomohon in North Sulawesi on 15 January 2014 were also caused by very high rainfall of 215 mm in Tondano and 41 mm/day in Tumpaan, the erosion was also strongly influenced by physical factors, such as slope and vegetation density (Tewal et al. 2018). The flash flood in Garut, in the upstream part of the Cimanuk watershed, on 20 September 2016 was very high due to heavy rainfall (110 to 255 mm/day), high soil moisture before the flood (35 to 44 mm), and the forest area covering only 17.9% of the watershed (Savitri dan Pramono 2017). The flash flood in Batu city on 4 November 2021 occurred upstream of Brantas due to the break of the Brantas river bank, while the rainfall in Pasuruan was recorded at 99 mm over the last 24 hours (Davies 2021).

Based on general indicators and specific indicators for each flood type, it can be seen that there are several components that cause flooding, including various indicator variables and sub-indicators, which have a different impact. These indicators, as well as data sources from which they can be obtained, are presented in Table 1 below. Dynamic factor means that the variable can change, while static factor means that the variable either cannot change, or a strong intervention and a long time is needed for changing the variable.

Table 1. Variables/Indicators affecting floods and their data sources

Component	Variable/ Indicator/ sub indicator	Factor	Potential Data	Impact on Flood	Data Source
Hazard (Climate Factor)	Rainfall	Dynamic factor	Design rainfall, rainfall intensity, river discharge, flood return period	Historical changes in rainfall have contributed to approximately one third of cumulative flood damage from 1988 to 2017 with rainfall changes of 20% to 46%, leading to a 36% increase in flood damage (Davenport et al. 2021). Rainfall intensity greater than 70 mm/hour with a return period of 20 years can increase the amount of surface runoff and cause flooding (Yilmaz et al. 2014)	BMKG, BBWS Ciliwung Cisadane
Hazard (non climate factor/ physical factor)	Elevation/Topography	Static factor	Elevation height	The topographic contribution level reaches 96.14% for flood inundation areas, quantitatively it can be stated that lower elevation and smaller topographical variability, can make an area more vulnerable to flooding (Xie dan Zhao 2013)	DEMNAS, USGS
	Slope	Static factor	Percentage of the average slope in the site including sloping or steep areas	Time of concentration (Tc) is influenced by the slope of the land, in areas with a gentle slope, the Tc value and the runoff volume will be smaller, while in areas with a larger slope, the Tc value and the volume of flood runoff will be greater. A slope of 86% will cause an increase in runoff volume of 98% (Elmoustafa 2012)	DEMNAS, USGS
	Soil Type	Static factor	Type of soil on site	A soil erodibility value between 0.02 to 0.04 means that liquid can be absorbed by the porous medium relatively fast before it reaches a saturated state (high permeability), while soil types with an erodibility value between 0.11 and 0.3 have very low permeability (Giatman et al. 2019). Soil types associated with certain land uses in the watershed have a runoff coefficient >0.5, which tends to cause high surface runoff (Basri et al. 2022, Alaoui et al. 2017)	BBWS

Hazard (non climate factor/ social factor)	Land Cover	Dynamic factor	The area of land used for each land cover	Increased change in residential land use by 2.278% can cause an increase in flood discharge of 35% over five years (Wirosoedarmo et al. 2020, Marizan dan Syarifudin 2022, Ariyanto dan Irawan 2020)	BPS, RTRW, Landsat 4, 5 dan 8
	Distance from the river	Dynamic factor	Safe distance from the river	Areas close to rivers are more prone to flooding in the case of fluvial and flash floods (Pham et al. 2020). River borders are determined based on the characteristics of the river and the depth of the riverbed (Presiden Republik Indonesia 2011).	River border regulations
Vulnerability (non-climate factors/ social factor)	Garbage in the river	Dynamic factor	The condition of the garbage in the river during the dry and rainy seasons	Garbage that is thrown carelessly into the river will hinder the flow of water from upstream and result in negative impacts on the environment and humans (Qomariyatus sholihah et al. 2020)	Field Observations
	Population density	Dynamic factor	Total Population, Residential Area	An increase in population can lead to climate change, which causes the intensity and frequency of rainfall to increase (Swain et al. 2020)	BPS
Capacity	Infrastruc-ture	Dynamic factor	Availability of infrastructure for flood management	Infrastructure is one solution in dealing with floods, but infrastructure has an environmental impact and increases the risk of flooding elsewhere. The development of green infrastructure for risk reduction is required for achieving large-scale ecological benefits, social justice, and fiscally functioning local government (Shi 2020)	BPS, BBWS, Provincial SDA Office
	Early warning system	Dynamic factor	Is there an early warning system?	Flood Early Warning Systems (FEWS) are implemented in many parts of the world, but an early warning does not always translate to emergency response for all individuals at risk. In addition to FEWS, warning communication and community response capabilities are also needed (Perera et al. 2020).	Regional Disaster Management Agency
	Institution	Dynamic factor	The relationship between stakeholders in dealing with floods	In handling floods, it is necessary to have a collaborative mechanism in the decision-making process related to efforts to reduce flood risk (Sunarharum 2021, Samaddar et al. 2015)	Relevant agencies/ institutions

History of Flood Disasters in the Ciliwung Watershed

Human civilization is surrounded by various natural hazards that have the potential to cause disasters which are classified according to the type of triggering event (Titley et al. 2021, Bian et al. 2020, Perera et al. 2020). Due to their potential impact on several sectors of society, disasters have been the subject of scientific study in various fields. The development of human civilization over the environment creates the conditions for disasters (Alca´ntara-Ayala 2002). The concept of human-nature relations in the study of natural disasters is associated with the contribution of the geographer Gilbert F. White. His publication "Human adaptation to floods" (Nawaz 2017) studies flooding, risk and risk management, the environment, and climate change (Macdonald et al. 2011). In this context, natural disasters can and should be understood as "non-natural disasters" (Birkmann 2006, Staupe-delgado 2019, Cutter et al. 2008). Flood disasters are caused by natural factors such as extreme rainfall, topography, etc., while non-natural factors significantly influence the change in land use.

In the Ciliwung watershed, flood events continue to increase and occur almost every year, while the most severe floods occurred in 2022, 2007, 2015, and 2020. The history of flood disasters in the Ciliwung watershed and their consequences can be seen in Fig. 6. Floods generally occur due to high rainfall, with the increase in flood discharge directly proportional to the increase in rainfall. Based on the rainfall data for ten years, from 2011 to 2020, the maximum daily rainfall in each year was taken to calculate the design rainfall using various methods for specific return periods, the results of these calculations are presented in Table 2. It can be seen that the flood event in 2020 was caused by a rainfall of 377 mm (Fig. 6), which has a return period of approximately 50 years (design rainfall of 345.92 mm, Table 2).

From Fig. 6 it can be seen that floods are usually caused by rainfall events of more than 100 mm. In addition to extreme rainfall and other natural factors (geographical and physical characteristics), floods can also be caused by man-made factors (Fig. 8). Increased vulnerability to flooding cannot only be attributed to climate as it is also affected by population growth, rapid urbanization, and urban sprawl (Pornasdoro et al. 2014). Land use changes in the Ciliwung watershed from 1990 to 2020 are shown in Fig. 7. The type of land cover significantly affects runoff that causes flooding in an area (Table 1), the results of the land cover analysis in the Ciliwung watershed for 30 years showed a significant change in residential land cover (Fig. 7), which increased from 91,927 km^2 in 1990 to 204,335 km^2 in 2020 and greatly affected surface runoff. In addition, although cities are densely populated and have a high economic value, disasters caused by floods can cause development delays for several years (Tingsanchali 2012). Flood damage

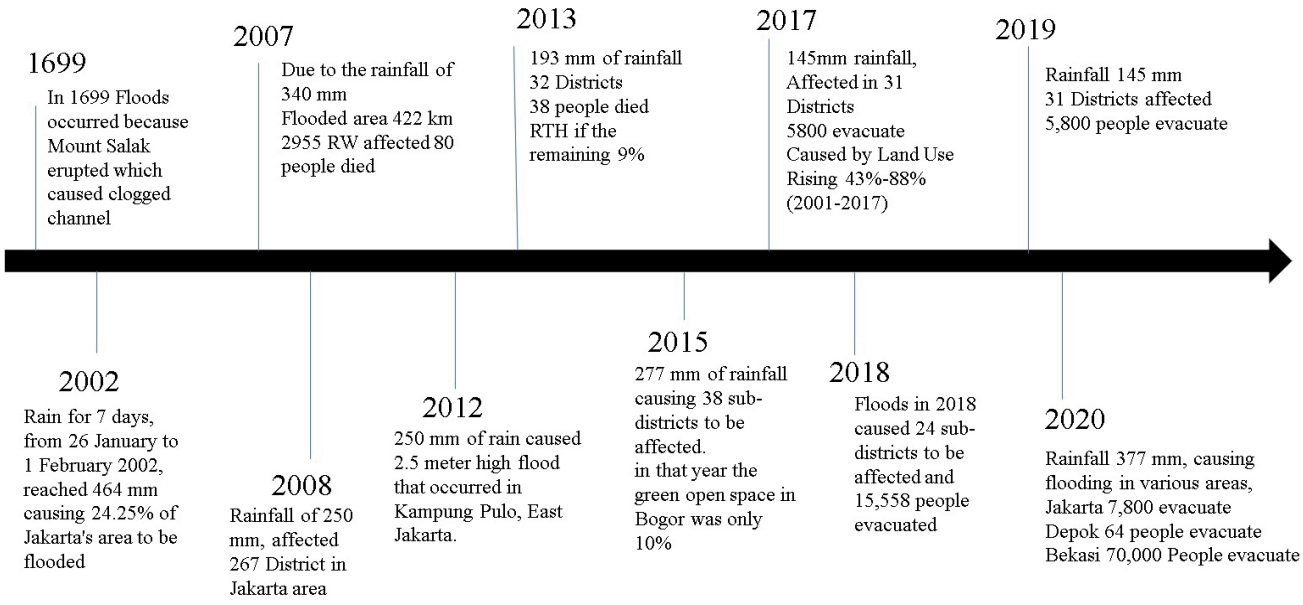

Fig. 6. Flood History in the Ciliwung

Table 2. Design rainfall with return periods of 2, 5, 10, 25, 50, and 100 years

Return Period	Design Rainfall (mm)			
(Year)	Log Pearson Type III	Gumbel	Normal	Log-Normal
2	181.298	180.034	187.748	181.625
5	228.166	233.218	230.770	228.187
10	257.577	268.430	253.305	257.164
25	293.327	312.921	275.242	288.903
50	319.139	345.927	292.741	317.005
100	344.383	378.689	307.082	342.063

depends on the type of flood, flow velocity, and duration of the flood. An increase in population density coupled with the presence of flood-affected infrastructure and assets in a city increases the likelihood of urban flood damage, while the uncontrolled growth of urban settlements reduces their drainage capacity (Tingsanchali 2012).

As shown in Fig. 8, the increase in population can cause land use and land cover changes which put pressure on river areas and change their characteristics such as river width, flow patterns, flow density, and river gradient. In addition, the government carries out various actions to reduce the pressure on river areas by setting zoning, performing flood control, developing infrastructure for river normalization, and providing counseling so that people are aware and do not throw garbage in rivers. Besides that, the increasing population can also lead to air temperature increase in the area, resulting in climate change if not handled properly.

Morphological Characteristics of the Ciliwung River

Based on its morphology, the Ciliwung river can be divided into three zones, the first zone is a sediment supply zone located in the upstream part of the watershed which has a v-shaped valley and is directly connected to the river banks. This zone has a long and steep slope with large sediment grains. The water flows at high speed, resulting in significant erosion from cliffs and the riverbed (Fig. 9). The second zone is the sediment transport zone which is located in the middle part of the watershed, where the river begins to form a floodplain. In this zone, upstream sediment originating from the erosion of cliffs and the riverbed is distributed downstream, thus forming river meanders and filling the floodplain with fine sediments (Fig. 10). And the third zone is the depositional zone, which is located in the downstream part, close to the estuary, and accumulates the sediments originating from zones 1 and 2. In natural conditions, this zone is usually an area of very high potential for wildlife, but in the estuary zone of the Ciliwung river there are many residential areas, and river normalization is carried out by making embankments to prevent flooding (Fig. 11).

Morphometry Characteristics of the Ciliwung Watershed

River morphometry characteristics include watershed area, shape, river network, flow density, flow pattern (Fig. 12), and river steepness gradient. The combination of watershed morphometry factors with other factors that can be changed by humans such as land cover, slope, and slope length will give a different response from the watershed to rainfall, absorption of flow into the soil (infiltration, runoff, groundwater content), and river flow behavior, for example, morphometric characteristics combined with land use will be used to evaluate the occurrence of flooding in the area.

Based on the drainage map of the Ciliwung watershed (Fig. 12), river order according to Strahler was determined, and the obtained results are presented in Table 3.

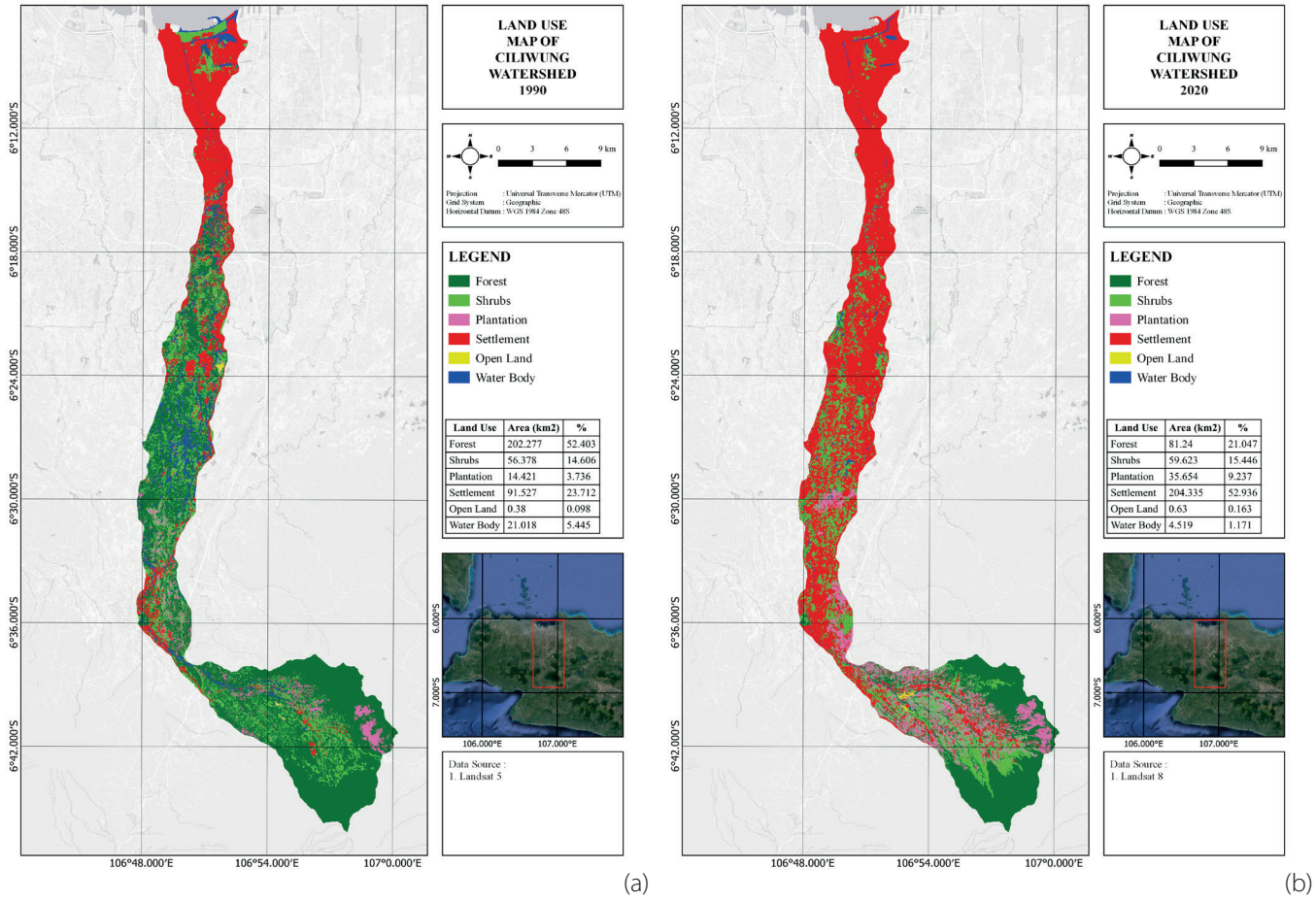

Fig. 7. Land Cover Map (a) 1990 (b) 2020

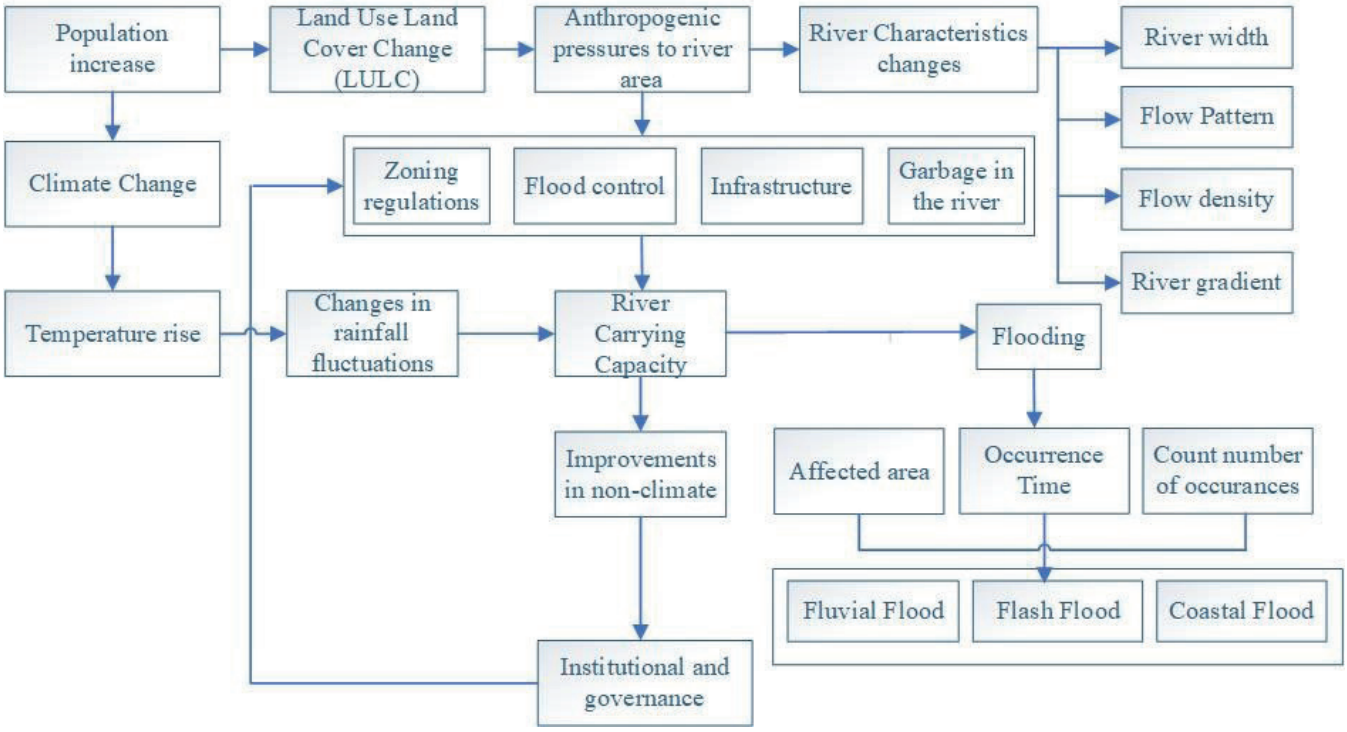

Fig. 8. Identification of factors causing flooding (Mathanraj et al. 2021, Perdinan dan Julie Winkler 2013, Akter et al. 2018, Elmoustafa 2012)

Fig. 9. Sediment Supply Zone/Zone 1 (coordinate '-6.62598, 106.82485)

(a) (b) (c)

Fig. 10. Sediment Transport Zone/Zone 2 (a) coordinate -6.58617, 106.79825, (b) coordinate -6.53742, 106.80347 (c) coordinate -6.50385, 106.79723

Fig. 11. Sediment Deposition Zone/Zona 3 (a) coordinate -6.11865, 106.82867, (b) coordinate -6.15389, 106.83573

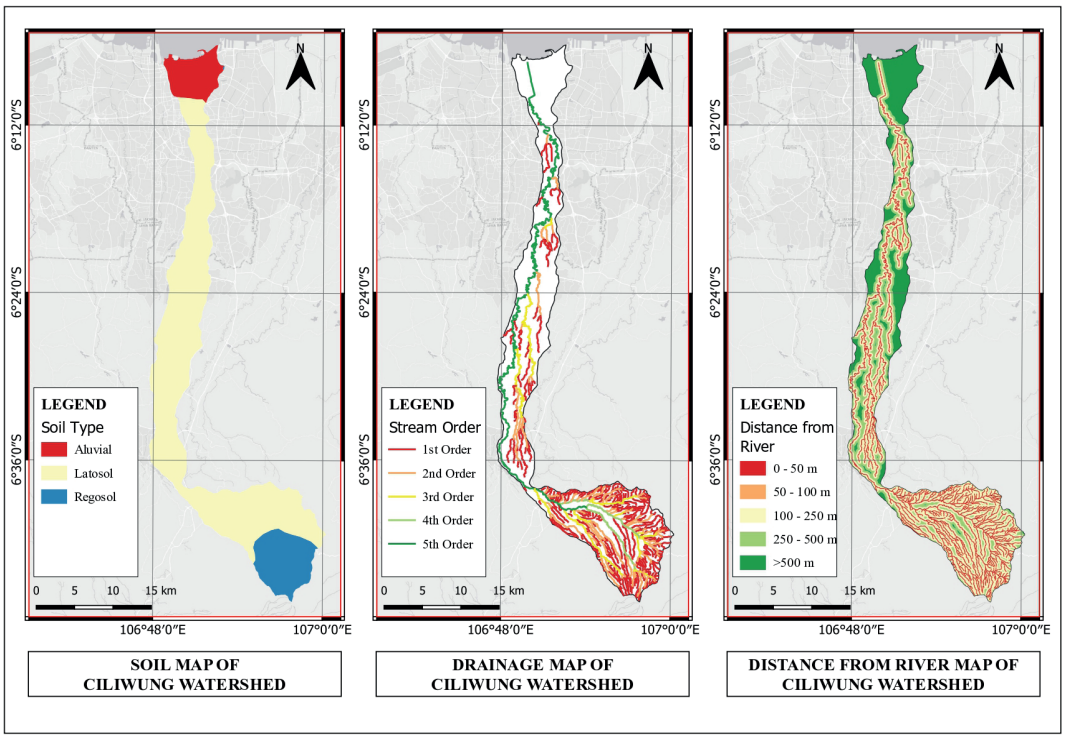

Fig. 12. The Ciliwung Watershed Characteristics, Soil Type, Drainage, and Distance from the River

Table 3. The Ciliwung River Network Order

River Order	River Length (km)	Stream Number	River Branch Index
			Rb = Un/Un+1
1	340.62	325	4.392
2	136.73	74	3.895
3	75.76	19	6.333
4	27.13	3	3.000
5	112.33	1	-
Total	692.57	422	

Based on the obtained values and formula (1), the bifurcation ratio was calculated for each river order. Also, the weighted average branching index (WRb) was calculated, which was equal to 5.392 for order 1, 4.895 for order 2, 7.333 for order 3, and 4 for order 4. These WRb values for each river order result in the weighted average branching index value (WRb average) of 5.05. The length of the river network in the Ciliwung watershed is 692.57 km and the area is 386 km^2, which results in a Drainage density (Dd) of 1.794 km/km^2. The Dd value is calculated based on formula (2) and describes the distance between rivers in the area (Kelaiya et al. 2019, Ali et al. 2018, Dragicevic et al. 2019).

DISCUSSION

Flood events in river areas are influenced by river characteristics. Based on the results of research and field observations, the conditions in the Ciliwung watershed were identified. In terms of morphometric characteristics, the Ciliwung watershed has an area of 386 km^2. According to the guidelines for identifying watershed characteristics issued by the Ministry of Forestry (Ministry of Forestry, Directorate General of Watershed Management and Social Affairs 2013), the Ciliwung watershed belongs to the category of moderate watersheds with an area between 100,000 and 500,000 ha. The Ciliwung watershed has an elongated shape with a rapidly increasing or decreasing peak discharge. The shape of the watershed is determined based on the Rc value, which in this case is 0.122, less than 0.5. Based on the Dd value of 1,794 km/km^2, the density in the Ciliwung watershed can be characterized as good according to the Smith 1950 classification in Raj dan Azeez (2012). According to other classifications, the density of the river network in the Ciliwung watershed is classified as low or medium (1.24 < Dd < 2.49), which also indicates the low infiltration capacity of the watershed. The slope of the watershed is also low, with an average value of 8% it belongs to the category of watersheds with a gentle slope. According to the studies of Lynsley in 1975, if the flow density value is below 1 mile/mile2 (0.62 km/km^2), the watershed will be prone to inundation, and if it is greater than 5 miles/mile2 (3.10 km/km^2), the watershed will often experience drought.

To develop action plans and flood mitigation measures in the Ciliwung watershed, it is necessary to know its characteristics including the river morphometry and morphology, as well as the factors that affect flooding. From the Rb value, it is known that the Ciliwung river is characterized by a rapidly increasing and decreasing flood water level. In this study, it was found that the Ciliwung watershed is dominated by fluvial flooding, which is affected by many factors including the distance of settlements to the river, and the lack of public awareness, which results in a lot of garbage in the river and clogging of the river flow. In addition, the lack of operation and maintenance of infrastructure built by the government in the Ciliwung tributaries, such as the new Situ Weir which is supposed to be used for flood control, has resulted in sedimentation and suboptimal functioning of the lake. As a result, floods continue to occur in the downstream area during the rainy season.

The first recorded case of flooding in the Ciliwung dates back to 1699, or about 323 years ago (Fig. 6), when a flood was caused by the eruption of Mount Salak which blocked the flow of the Ciliwung River and its drainage network. Around that time there was also a flood due to heavy rainfall in January and February which resulted in the inundation of the Old City which used to be the capital of the Dutch colony under the government of Verenigde Oostindische Compagnie (VOC). The next largest flood according to the WHO Emergency Situation Report (2007), occurred in 1714 when the Ciliwung River overflowed due to the clearing of forests in Bogor (Peak Area). Another major flood was recorded in 1996 and led to the inundation of the capital city and ten casualties. From Table 1 it can be seen that flooding in the Ciliwung Watershed (DAS) is usually caused by high rainfall above 100 mm (Fig. 6). Based on the character of events and indicators from Table 1, the floods in the Ciliwung watershed can be classified as Fluvial, which occur due to high rainfall (Fig. 6 and Table 2). The rainfall in certain areas that discharge into the main river through tributaries may result in the cumulative increase of river discharge, which can cause flooding if the carrying capacity of the river decreases. Because of this, rainfall in the upstream area will have an impact on the downstream area as well, while the type of land cover and river elevation will affect the velocity of water that triggers flooding. It was also found that the Ciliwung watershed experienced significant land cover changes from 1990 to 2020 (Fig. 7), as residential land cover increased from 91,527 km^2 to 204,335 km^2, or by 123% over the last 30 years.

However, flood problems do not only come from upstream but also from the middle and downstream, while flood control often does not include certain watersheds or sub-watersheds in flood management units. The novelty of this research is that it describes various factors of flooding that flood management must take into account, it can not include only upstream or downstream, but should be conducted on a watershed level and include comprehensive interventions covering the entire area. This research can be used as a foundation to further explore the factors that form floods in order to develop a more integrated flood management strategy in watershed areas.

In addition, the coordination between different institutions in the Cliwung watershed is also not optimal. Having too many institutions and regional autonomy results in the decentralization of authority, lack of law enforcement in the transition of land use into housing, and difficulties in developing the existing infrastructure in accordance with regional spatial planning. Besides that, infrastructure development is usually not followed by an increase in the capacity of drainage

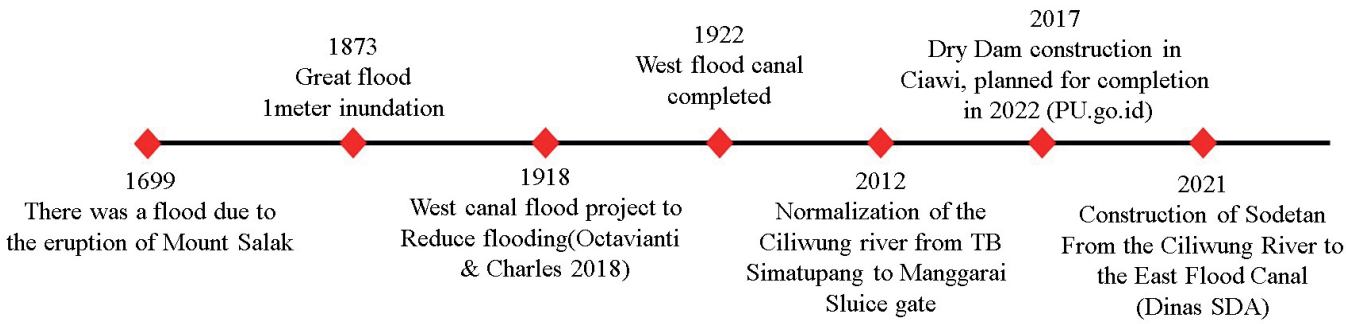

Fig. 13. Mitigation Efforts from the government

channels (especially in the downstream area), which hampers the flow of rainwater and causes inundation.

Based on Fig. 13, what the government has done to reduce the river discharge due to rainfall in the upstream area is building a Dry Dam in Ciawi, according to the PU Dry Dam planning it can reduce flood discharge before the Manggarai sluice gate by 2 to 10% (Prakoso et al. 2020). To reduce flooding in the downstream part, a Flood Sode and the east canal were built by the DKI Jakarta Provincial Natural Resources Service. However, the handling is not maximal in the middle part, where an extended Dam can be constructed along the Cliwung river to include the floodplain and reduce flood discharge downstream. In addition, it is necessary to know the relationship between infrastructure, the economic system, and the role of human factors in assessing and managing risk. In flood management, uncertainty about future conditions is the most important challenge to be faced, which means that strong and resilient measures with good performance in the future should be developed (Jonkman dan Dawson 2012).

Based on the factors causing flooding (Table 1), the government has introduced certain mitigation measures (Fig. 13). To reduce the risk due to the distance of residential areas from the river, the channel was normalized and several pumping stations were built in the downstream area to facilitate faster discharge of water into the sea. The pumping stations pump water in the river at high discharges reducing inundation in the upstream area. To reduce waste in rivers, counseling and assistance were provided to the community in order to change their mindset toward protecting the environment. Another measure was to build the Ciawi weir to reduce runoff in the upstream area of the Ciliwung, which is planned to operate in 2022. However, watershed management to reduce flood risk will not run optimally without the coordination and cooperation between various stakeholders. Stakeholders, whether from the government, the private sector, or the community, in the case of the Ciliwung river management include the Directorate General of Natural Resources, the Ciliwung-Cisadane River Basin Center (BBWS), the DKI Jakarta Provincial Government's Natural Resources Service, the Blood Disaster Management Agency (BPPD), NGOs, river care groups and community leaders. Cooperation and coordination are required to achieve the sustainability of the watershed functions and services. To accommodate the interests of all parties, the government must coordinate and cooperate with them during the planning, implementation, and evaluation process, for example, the improvement of river borders can involve people living near the river banks. The government collaboration with NGOs must be more intense in providing counseling to the community and improving their understanding of the importance of maintaining the sustainability of riverbanks and the proper functioning of rivers as natural drainage. In terms of normalizing riverbanks, it can also be done with an environmental approach, for example, by strengthening riverbanks with plants, which has more economic value and provides additional benefits to the community. However, this can only be applied in the middle part of the Ciliwung area, for the downstream part of the river effective normalization can only be done by building embankments and pumping stations so that water can be quickly discharged into the sea. So, in the case of flood control, maintaining optimal watershed functions and services from upstream to downstream is the responsibility of all relevant stakeholders including the community.

CONCLUSIONS

Based on the discussion above, it can be concluded that to carry out flood management in an area, it is necessary to determine the contributing factors (Table 1). These contributing factors can be used to develop intervention measures and carry out flood risk management. Also, for proper flood management, one must look at the entire watershed unit, not a city or province area. The Ciliwung watershed covers two provinces, namely West Java province, and DKI Jakarta province, where the capital city of Indonesia is located, and because the Ciliwung river is a major cause of flood events in the capital city, most of the government measures for flood control include building infrastructure downstream (Fig. 13). For sustainable flood management in the Ciliwung watershed, it is necessary to know the dominant type of floods in the area, as well as to study the characteristics and nature of the river flow. For example, because the slope of the Ciliwung watershed is not very high, only 8%, the water does not flow downstream quickly, causing inundation in the middle of the Ciliwung river. Mitigation efforts that the government has carried out include diverting the flow of the Ciliwung river to the west and east canal for reducing the flow of water in the central part of the Ciliwung and implementing other flood infrastructure measures such as building the embankments and raising riverbanks so that water can be quickly discharged into the river. In addition, there are also efforts to reduce flood discharge in the upstream area by constructing a dry dam in Ciawi, which is planned to be completed in 2021. However, infrastructure efforts must also be supported by stakeholder participation (Aung dan Lim 2021, Sunarharum 2021, Isa et al. 2019). An example of cooperation between the government and the community showing concern for maintaining and managing the environment could be in preventing people from throwing garbage in the river, especially in the middle Ciliwung area. The results of surveys and research showed that there is a narrowing of the river channel in the middle of the Ciliwung area caused by residential settlements. Due to the proximity of residential areas to the river, garbage is accumulated in the channel, which acts as a flow barrier during rainfall and causes river water to run off to settlements located near the riverbanks.

REFERENCES

Akter T, Quevauviller P, Eisenreich SJ, Vaes G. 2018. Impacts of climate and land use changes on fl ood risk management for the Schijn River , Belgium. Environ. Sci. Policy. 89(July):163–175.doi:10.1016/j.envsci.2018.07.002.

Alaoui A, Rogger M, Peth S, Blöschl G. 2017. Does soil compaction increase floods ? A review. J. Hydrol. 17(December):1–32.doi:10.1016/j.jhydrol.2017.12.052.

Alca´ntara-Ayala I. 2002. Geomorphology , natural hazards , vulnerability and prevention of natural disasters in developing countries. Geomorphology. 47(47):107–124.

Ali U, Ali SA, Ikbal J, Bashir M, Fadhl M, Ahmad M, Al-dharab H, Ali S. 2018. Soil Erosion Risk and Flood Behaviour Assessment of Sukhnag catchment , Khasmir Basin : Using GIS and Remote Sensing. J. Remote Sens. GIS. 7(1):1–8.doi:10.4172/2469-4134.1000230.

Ariyanto L, Irawan AP. 2020. Study of flood discharge due to land use and population change of Way Pisang watershed Study of flood discharge due to land use and population change of Way. IOP Conf. Ser. Mater. Sci. Eng. 1(1007):1–7.doi:10.1088/1757-899X/1007/1/012171.

Asdak C, Supian S, Subiyanto. 2018. Watershed management strategies for fl ood mitigation, A case study of Jakarta ' s fl ooding. Weather Clim. Extrem. J. 21(August):117–122.doi:10.1016/j.wace.2018.08.002.

Aung TM, Lim S. 2021. Evolution of Collaborative Governance in the 2015 , 2016 , and 2018 Myanmar Flood Disaster Responses : A Longitudinal Approach to a Network Analysis. Int. J. Disaster Risk Sci. 12(2):267–280.doi:10.1007/s13753-021-00332-y.

Azmeri, Yulianur A, Listia V. 2015. Analisis Perilaku Banjir Bandang Akibat Keruntuhan Bendungan Alam pada Daerah Aliran Sungai Krueng Teungku Provinsi Aceh. J. Tek. Sipil. 22(3):209–218.

Barus L, Tambunan R, Arif V. 2019. Effect of Changes in Land Use in Flood Disasters in Baleendah District, Bandung Regency. J. Strateg. Glob. Stud. 2(1):25–35.doi:10.7454/jsgs.v2i1.1014.

Basri H, Syakur S, Azmeri A, Fatimah E. 2022. Floods and their problems : Land uses and soil types perspectives. IOP Conf. Ser. Earth Environ. Sci. 1(951):1–9.doi:10.1088/1755-1315/951/1/012111.

Bian G, Du J, Song M, Zhang Xueliang, Zhang Xingqi, Li R, Wu S, Duan Z, Xu C. 2020. Detection and attribution of flood responses to precipitation change and urbanization: a case study in Qinhuai River Basin, Southeast China. Hydrol. Res.:1–15.doi:10.2166/nh.2020.063.

Birkmann J. 2006. Measuring Vulnerability to Natural Hazards: Towards Disaster Resilient Societies. I. Birkmann J rn, editor. United Nations University Press.

Cutter SL, Barnes L, Berry M, Burton C, Evans E, Tate E, Webb J. 2008. A place-based model for understanding community resilience to natural disasters. Glob. Environ. Chang. 18:598–606.doi:10.1016/j.gloenvcha.2008.07.013.

Davenport F V, Burke M, Diffenbaugh NS. 2021. Contribution of historical precipitation change to US flood damages. PNAS. 118(4):1–7.doi:10.1073/pnas.2017524118.

Davies R. 2021 Nov. Berita Banjir Bandang Batu.pdf. Flood List.:1.

Dragicevic N, Karleuša B, Ožani´c N. 2019. Different Approaches to Estimation of Drainage Density and Their Effect on the Erosion Potential Method. water. 11(593):1–14.doi:10.3390/w11030593.

Elmoustafa AM. 2012. Weighted normalized risk factor for floods risk assessment. Ain Shams Eng. J. 3(4):327–332.doi:10.1016/j.asej.2012.04.001.

Esteban MD, Lopez-gutierrez JS, Negro V. 2011. Urban Coastal Flooding and Climate Change Urban Coastal Flooding and Climate Change. J. Coast. Res. 64(October 2014).

Giatman M, Haq S, Andayano T. 2019. Effect of Porosity on Soil Permeability in the Flood Area of Padang City. J. Phhysic Conf. Ser. 1(1387):1–6.doi:10.1088/1742-6596/1387/1/012105.

Hanif M, Putra BG, Hidayat RA, Ramadhan R, Shafrina W, Moh W, Hermon D, Suhana E, Makassar UF. 2021. Impact Of Coastal Flood On Building, Infrastructure , And Community Adaptation In Bukit Bestari Tanjung Pinang. J. Geogr. 21(2).

Hidayatulloh IS, Rahardjo AP, Kironto BA. 2018. Hydrology and Hydraulic Analysis of Nasiri Flash Flood Disaster Event on the 1 st August 2012. J. Civ. Eng. Forum. 4(1):41–50.

Isa M, Fauzi A, Susilowati I, Muhammadiyah U, Tengah J, Economics E, Tengah J. 2019. Flood risk reduction in the northern coast of Central Java Province , Indonesia An application of stakeholder's analysis. J. Disaster Risk study.(Juli):1–9.

Jatmiko DW. 2018. Hydraulics Performance of Coastal Flood Control in Madukoro Area, Semarang City, Indonesia. J. Civ. Eng. Forum. 4(3):189–200.

Jonkman SN, Dawson RJ. 2012. Issues and Challenges in Flood Risk Management—Editorial for the Special Issue on Flood Risk Management. water. October(4):785–792.doi:10.3390/w4040785.

Kelaiya JH, Rank HD, Dwivedi DK. 2019. Evaluation of morphometric characteristics and watershed prioritization of Bhadar basin of Saurashtra region , Gujarat. J. Appl. Nat. Sci. 11(2):273–280.doi:10.31018/jans.v11i2.2032.

Kurniawan YT. 2013. Hydraulic Simulation Of Flash Flood As Triggered By Natural Dam Break. Civ. Eng. Forum. 22(January):1319–1326.

Macdonald N, Chester D, Sangster H, Todd B. 2011. The significance of Gilbert F . White ' s 1945 paper ' Human adjustment to floods ' in the development of risk and hazard management. Prog. Phys. Geogr. 36(1). 36(1):125–133.doi:10.1177/0309133311414607.

Marizan Y, Syarifudin A. 2022. Analysis of Flood Discharge due to Land Used Changes in Keramasan Watershed Palembang , Indonesia. Int. J. Progress. Sci. Technol. 30(2):147–159.

Mathanraj S, Rusli N, Ling GHT. 2021. Applicability of the CA-Markov Model in Land-use / Land cover Change Prediction for Urban Sprawling in Batticaloa Municipal Council , Sri Lanka Applicability of the CA-Markov Model in Land-use / Land cover Change Prediction for Urban Sprawling in Battical. IOP Conf. Ser. Earth Environ. Sci. 620:1–12.doi:10.1088/1755-1315/620/1/012015.

Miftahuljannah, Ibrahim AA. 2019. Flood Disaster Vulnerability Factors in Solok Selatan Regency. Sumatra J. Disaster, Geogr. Geogr. Educ. 3(1):31–35.

Ministry Of Forestry Directorate General Of Watershed Development Management And Social. 2013. Regulation Of The Director General Of Rivershow Management And Social Forestry Region On Guidelines For Identification Of River Watershed Regional Characteristics. Indonesiahlm 1–55.

Nawaz F. 2017. Human perception and responses to flood hazard a case study of district Jhelum. Geol. Bull. Univ. Peshawar. 35(January 2002):139–150.

Omena BEM, Goldenfumb JA, Michelc GP, Cavalcanti JR de A. 2020. Terminology of natural hazards and disasters: A review and the case of Brazil. Int. J. Disaster Risk Reduct.(November):101970.doi:10.1016/j.ijdrr.2020.101970.

Perdinan, Julie Winkler. 2013. Changing Human Landscapes Under a Changing Climate : Considerations for Changing Human Landscapes Under a Changing Climate : Considerations for Climate Assessments. Environ. Manag. 53(July):42–45.doi:10.1007/s00267-013-0125-6.

Perera D, Agnihotri J, Seidou O, Djalante R. 2020. Identifying societal challenges in flood early warning systems. Int. J. Disaster Risk Reduct. 51:1–9.doi:10.1016/j.ijdrr.2020.101794.

Pham BT, Avand M, Janizadeh S, Phong T Van, Al-Ansari N, Ho LS, Das S, Le H Van, Amini A, Bozchaloei SK, et al. 2020. GIS Based Hybrid Computational Approaches for Flash Flood Susceptibility GIS Based Hybrid Computational Approaches for Flash Flood Susceptibility Assessment. Water. 12(683):1–29.doi:10.3390/w12030683.

Pornasdoro KP, Silva LC, Munárriz MLT, Estepa BA, Capaque CA. 2014. Flood Risk of Metro Manila Barangays : A GIS Based Risk Assessment Using Multi-Criteria Techniques. J. Urban Reg. Plan.:51–72.

Prakoso WG, Irawan P, Mahfudz M. 2020. Hydrological Risk Valuation on The Design of Sukamahi Dry Dam , Bogor , West Java. Earth Environ. Sci. 556(1):1–10.doi:10.1088/1755-1315/556/1/012014.

Presiden Republik Indonesia. 2011. Peraturan Pemerintah Republik Indonesia Nomor 38 Tahun 2011 Tentang Sungai. Indonesia: Presiden Republik Indonesia.hlm 1–61.

Qomariyatus sholihah, Kuncoro W, Wahyuni S, Suwandi SP, Feditasari ED. 2020. The analysis of the causes of flood disasters and their impacts in the perspective of environmental The analysis of the causes of flood disasters and their impacts in the perspective of environmental law. IOP Conf. Ser. Earth Environ. Sci. 437:1–7.doi:10.1088/1755-1315/437/1/012056.

Raditya A, Fajrin M, Hayati A, Faqih M. 2020. The Spatial Characteristics of Tidal Flood Vulnerability and Adaptation Strategy in Tambak Lorok Kampung Settlement. IPTEK J. Proceeding Ser. 6(1):363–371.

Raj PN, Azeez PA. 2012. Morphometric Analysis of a Tropical Medium River System : A Case from Morphometric Analysis of a Tropical Medium River System : A Case from Bharathapuzha River Southern India. J. Mod. Hydrol. 2(May 2014):91–99.doi:10.4236/ojmh.2012.24011.

Samaddar S, Misra BA, Tatano H. 2015. Insights on social learning and collaborative action plan development for disaster risk reduction : practicing Yonmenkaigi System Method (YSM) in. Nat Hazards. 75(January):1531–1554.doi:10.1007/s11069-014-1380-4.

Savitri E, Pramono IB. 2017. Upper Cimanuk Flood Analysis. JPPDAS. 1(2):97–110.

Shi L. 2020. Beyond flood risk reduction : How can green infrastructure advance both social justice and regional impact ? Socio-Ecological Pract. Res. 2(4):311–320.doi:10.1007/s42532-020-00065-0.

Staupe-delgado R. 2019. Analysing changes in disaster terminology over the last decade. Int. J. Disaster Risk Reduct. 40(April):101161. doi:10.1016/j.ijdrr.2019.101161.

Sunarharum TM. 2021. Membangun Ketangguhan dan Adaptasi Transformatif : Kasus Pengurangan Risiko Bencana Banjir di Jakarta. Reka Ruang. 3(2):71–80.

Swain DL, Wing OEJ, Bates PD, Done2 JM, K.Johnson, Cameron DR. 2020. Increased Flood Exposure Due to Climate Change and Population Growth in the United States. Am. Geophys. Union.:1–44.doi:10.1029/2020EF001778.

Tewal STR, Sulastriningsih HS, Murdiyanto, Lobja XE, Andaria KS. 2018. Evaluation of Landslide Hazard Levels Post 2014 Flood Disaster in Manado City. Adv. Soc. Sci. Educ. Humanit. Res. 226(1):2014–2016.

Tingsanchali T. 2012. Urban flood disaster management. Procedia Eng. 32:25–37.doi:10.1016/j.proeng.2012.01.1233.

Titley HA, Cloke HL, Harrigan S, Pappenberger, Prudhomme C, Robbins C, Stephens EM, Zsótér. 2021. Key Factors Influencing the Severity of Fluvial Flood Hazard from Tropical Cyclones. J. Hydrometeorol. 22(12 Maret):1801–1817.doi:10.1175/JHM-D-20-0250.1.

Wirosoedarmo R, Anugroho F, Sari NR, Gustinasari K. 2020. The Study Of Land Use Change To Flood Discharge In Gunting Sub-Watershed Of Jombang Regency , East Java – Indonesia. Poll Res. 37(2):355–361.

Xie L, Zhao H. 2013. Correlation between flood disaster and topography: A case study of Zhaoqing City. J. Nat. Disasters. 22:240–245.

Yilmaz AG, Hossain I, Perera BJC. 2014. Effect of climate change and variability on extreme rainfall intensity – frequency – duration relationships : a case study of Melbourne. Hydrol. Earth Syst. Sci.(November 2016).doi:10.5194/hess-18-4065-2014.

Zain A, Legono D, Rahardjo AP, Jayadi R. 2021. Review on Co-factors Triggering Flash Flood Occurrences in Indonesian Small Catchments Review on Co-factors Triggering Flash Flood Occurrences in Indonesian Small Catchments. Earth Environ. Sci. 930(1):1–9.doi:10.1088/1755-1315/930/1/012087.

Zanchetta ADL, Coulibaly and P. 2020. Recent Advances in Real-Time Pluvial Flash. water.(February).

RESEARCH PAPER

PRIELBRUSYE NATIONAL PARK ENVIRONMENTAL CHANGES DUE TO INCREASING TOURISM ACTIVITY

Anna A. Cherkasova[1], Anton A. Iurmanov[1,2], Pravin Kokane[3], Alexey A. Maslakov[4*], Matija Petkovich[5], Marina N. Petrushina[4], Aida Tabelinova[6], Azamat Tolipov[7], Georgy Yakubov[7], Yulia Yushina[8]

[1]All-Russian non-governmental organization Russian Geographical Society, Novaya Ploshchad, 10, bld. 2, 109012, Moscow, Russia

[2]Main Botanical Garden named after N. V. Tsitsin RAS, st.Botanicheskaya, 4, Moscow, 127276, Russia

[3]Department of Geography, University of Mumbai, Santacruz East 400098, Maharashtra, India

[4]Lomonosov Moscow State University, Faculty of Geography, Leninskie Gory, 1, 119991, Moscow, Russia

[5]University of Belgrade, Faculty of Biology, Studentski trg, 16, 11158, Belgrade, Serbia

[6]Lomonosov Moscow State University, Kazakhstan Branch, Faculty of Geography, st. Kazhymukan, 11, 010010, Nur-Sultan, Kazakhstan

[7]Unaffiliated with an organization

[8]Institute of Geography and Water Security, st. Kabanbai batyr/Pushkin, 67/99, Almaty, 050010, Kazakhstan

***Corresponding author:** alexey.maslakov@geogr.msu.ru

Received: June 26th, 2022 / Accepted: November 11th, 2022 / Published: December 31st, 2022

https://DOI-10.24057/2071-9388-2022-108

ABSTRACT. Prielbrusye National Park is one of the most popular tourist destinations in Russia. In recent years internal tourism development, stimulated by restrictive measures (due to the COVID pandemic and geopolitical situation), resulted in significant growth of tourist flow to the national park's territory. A surge in anthropogenic load on the park's geosystems might degrade them and lead to environmental pollution. This research involved chemical studies of natural waters and snow from the south slope of the Elbrus and audit of the most popular tourist trails. The results have shown that in the snow alongside mountain hiking pistes to the Elbrus all the way up to 4,720 m above sea level (a.s.l.) oil stains concentration is up to 38 times higher than maximum acceptable concentration (MAC). Content analysis of heavy metals in snow cover on the Elbrus slopes and in the river Baksan has shown a significant rise in lead load over the period of 2015–2021 from the trace levels to 1.5 MAC, which is the result of increased anthropogenic load on the south slope of the Elbrus mountain. Ground observation of tourist trails has brought to light numerous patches of vegetation trampling, width extension and branching of the main trail, as well as campfire sites. The research results can be used as a rationale to take measures to reduce recreational load, to improve local geosystems' condition and to develop a plan of action on nature conservation within the park's territory.

KEYWORDS: Prielbrusye National Park, Caucasus, tourism, environmental protection, Elbrus

CITATION: Cherkasova A.A., Iurmanov A.A., Maslakov A.A., Petkovich M., Petrushina M.N., Tabelinova A., Tolipov A., Yakubov A., Yushina A. (2022). Prielbrusye National Park Environmental Changes Due To Increasing Tourism Activity. Geography, Environment, Sustainability, 4(15), 115-123

https://DOI-10.24057/2071-9388-2022-108

ACKNOWLEDGEMENTS: The research was carried out as part of a joint expedition of the Rossotrudnichestvo and the Russian Geographical Society as part of the New Generation program. The work of Dr. Alexey Maslakov has been supported by the Interdisciplinary Scientific and Educational School of M.V.Lomonosov Moscow State University «Future Planet and Global Environmental Change». The team would like to thank the Prielbrusye National Park, the Elbrus Alpine Search and Rescue Team of the Ministry of Emergency Situations of Russia, and the Joint-Stock Company KAVKAZ.RF for their help in organizing field work. Laboratory analysis of samples was sponsored by AST-Analitika, LLC.

Conflict of interests: The authors reported no potential conflict of interest.

INTRODUCTION

Given its physiographic features, high mountain territory can be characterized by regular natural processes, including disasters that increased landscape diversity and decreased resilience to anthropogenic load. Intensive recreational development of high mountain regions, first of all of the Greater Caucasus, that has been observed in recent decades, led to an increased anthropogenic load on the terrain. This includes building new innovative skiing and recreational clusters and further development of those in the Russian part of the Northern Caucasus. Such development has also expanded to specially protected natural reserves (SPNR) that were established in areas of diverse landscape and numerous natural attractions, including the oldest Teberda Nature Reserve, the status of which was downgraded to a national park due to intensification in recreational use[1], Caucasus Nature Reserve, and Prielbrusye National Park.

Prielbrusye National Park that was established in 1986 within the territory of the Kabardino-Balkar Republic occupies an area of 101,200 hectares. It includes a well-developed oldest mountaineering and tourism centre Southern Prielbrusye (the upper basin of the river Baksan) and a less developed area of the Malka upstream with a confluent – the river Baksan. The park is located on the north slope of the Central Caucasus along with the highest mountain summit in Russia – the two-headed Elbrus with peaks 5,642 m and 5,621 m high. It is one of the most high-altitude parks in Russia and Europe with complex landscape structure. Altitudinal zonality with high mountain glacial-nival, meadow (subnival, alpine and subalpine) and forest (birch and pine) landscapes, slope-facing landscape contrasts are typical to the study region (Petrushina 1992).

According to the Ministry of Resorts and Tourism of the Kabardino-Balkar Republic, within the 2014–2019 period the tourist flow tended to rise and more than doubled; in 2019 this region was visited by 600,000 tourists; the annual growth was 20%. At the same time, the tourist flow in the Prielbrusye NP more than tripled. COVID-19 pandemic, which started in 2020, has cut the tourist flow to Prielbrusye NP. According to the NP's data, in 2019 SPNR was visited by 209,392 tourists, in 2020 this indicator was a bit lower, equalling 142,284 tourists. In the first nine months of 2021, 572,000 people have already visited this region[2]. In compliance with the national programme aimed at developing a touristic and recreational entity in the Kabardino-Balkar Republic the local authorities plan to increase the tourist flow up to 1 million people by 2025. The programme provides for infrastructure development in the Elbrus and Cheget zones of the Prielbrusye NP, as well as for routing, equipping and marking at least 10 tourist trails a year[3]. Russian Federation's Main State Expert Review Board is known to have approved a construction project on building an additional five-storied hotel of the Ozon hotel chain in Azau; it will accommodate 45 rooms with a total area of 4,280 sq. m[4]. Given hundreds hotels, boarding houses and tourists' and mountain climbers' villages already built, the planned recreational development will result in growing anthropogenic load on landscapes and their degradation, which is already marked out nowadays (Petrushina 2018).

This study aimed to reveal the results of increased recreational load on some ecosystems and their components in Prielbrusye NP. The main study objects were snow cover and river water as one of the indicators of dynamic landscape components' condition. Additional observations were made on some tourist trails.

METHODS

Field studies

Field studies on the territory of Prielbrusye NP were conducted by the International Park School of Russian Geographical society from September 29 to October 10, 2021 (Fig. 1). Field studies were divided into three general directions: 1) snow studies along the main trail for Elbrus summit ascending; 2) water quality studies along the Baksan river – the main water stream of the Prielbrusye National Park; 3) main tourist trails inspection.

Snow cover was studied along the main trail to the Elbrus summit. Pitting snow test was conducted to determine stratigraphy and snow cover density, as well as oil traces and content of heavy metals in the snow (such as Fe, Mo, Pb, Cd, Zn, Ni, Mn, Co, Cr). Description and snow sampling points were located both on the snowcat (ratrack) piste and at some distance from it. The studies of snow cover structure included its description documenting snow decompaction levels and layers of ice; besides, snow density was determined layer by layer using a snow sampler. At the same time, temperature of air was measured, as was that of the snow surface, its middle part, and snow cover floor. After that, the test pit was photographed and snow samples were taken from the pit. At the moment of works above the Mir station (3,450 m a.s.l.) there was a permanent snow cover; that is why the research was conducted at heights ranging from 3,880 m (just above the Gara-Bashi station) to 4,720 m (just above the Pastukhov rocks) (Fig. 2).

To assess the contemporary state of the Baksan streams and their headwaters (the rivers Bolshoi and Malyy Azau and the Azau glacier) water samples were taken to measure concentrations of heavy metals. The points of sampling for water quality were located upstream or downstream from the main recreational entities (Azau Glade, Cheget Glade) and villages (Terskol, Verkhniy Baksan) (see Fig. 1). Evaluation criteria of water quality were maximum acceptable concentration for fisheries, since the susceptibility of aquatic organisms to pollutants is higher. Hydrochemical data was then compared to the previous studies (Reutova et al. 2014, 2018; Chizhova et al. 2017; Dreeva et al. 2017; Kerimov et al. 2018; Atabieva, Cherednik 2020).

During the expedition, sections of the five most popular equipped routes for hiking were also inspected: 1) the trail from the vil. Terskol to the Devichi Kosy waterfall, 2) the

[1]Decree of the Chief State Sanitary Doctor of the Russian Federation dated January 28, 2021 N 2 "On approval of sanitary rules and norms SanPiN 1.2.3685-21" Hygienic standards and requirements for ensuring the safety and (or) harmlessness of environmental factors for humans "(2021). Registered in Ministry of Justice of Russia on 29 January, 2021 N 62296. 1143 p. Available at: http://umka-nadym.ru/media/sub/962/documents/%D0%A1%D0%B0%D0%BD%D0%9F%D0%B8%D0%BD_1.2.3685-21_%D0%BE%D1%82_28.01.2021_2.pdf [Accessed 25 October 2021] (in Russian).

[2]https://tass.ru/ekonomika/13031877?ysclid=l2eszja22l

[3]Decree of the Government of the Kabardino-Balkarian Republic of September 23, 2019 N 167-PP On approval of the state program of the Kabardino-Balkarian Republic "Development of the tourist and recreational complex of the Kabardino-Balkarian Republic", 2019. Available at: https://docs.cntd.ru/document/561556122 (in Russian)

[4]https://kavkaz.rbc.ru/kavkaz/12/08/2020/5f33d30b9a7947c4e05c869c

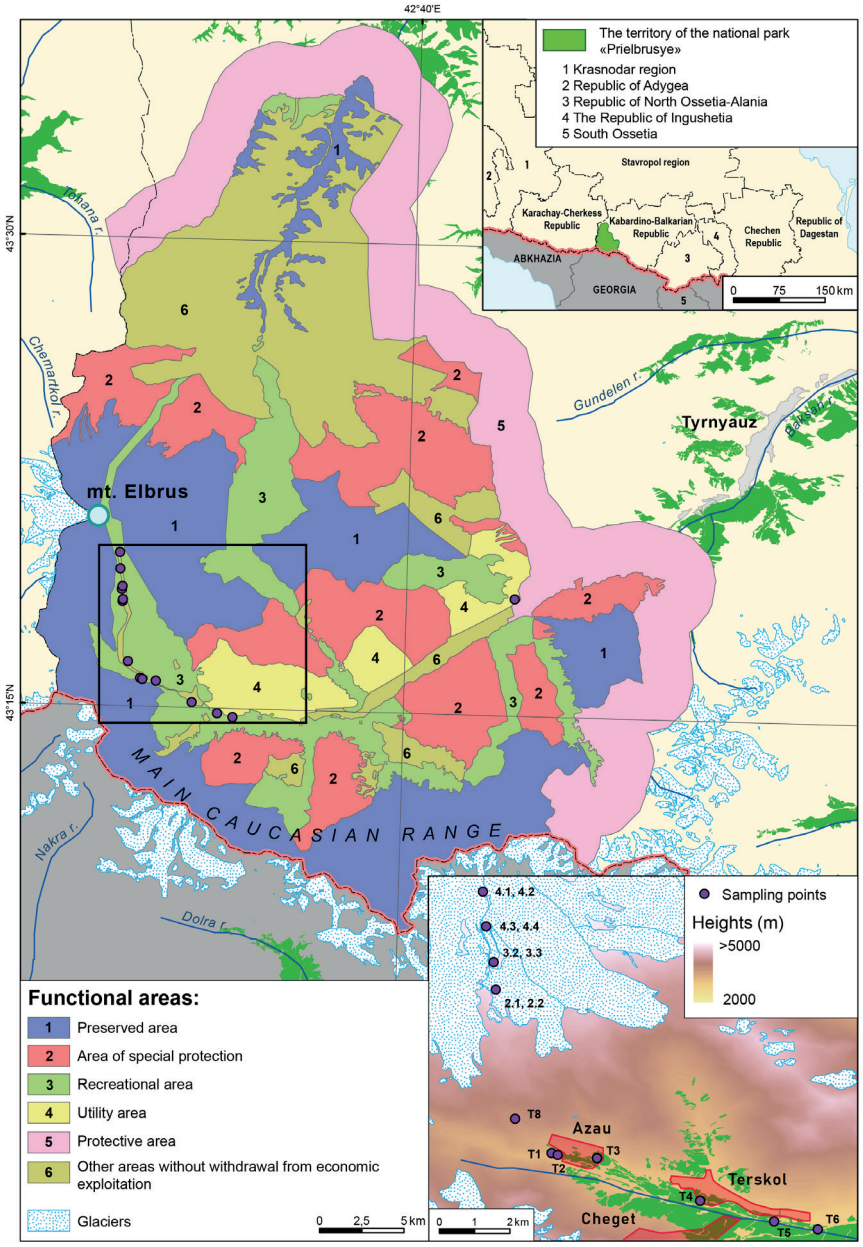

Fig. 1. Study area and sampling points

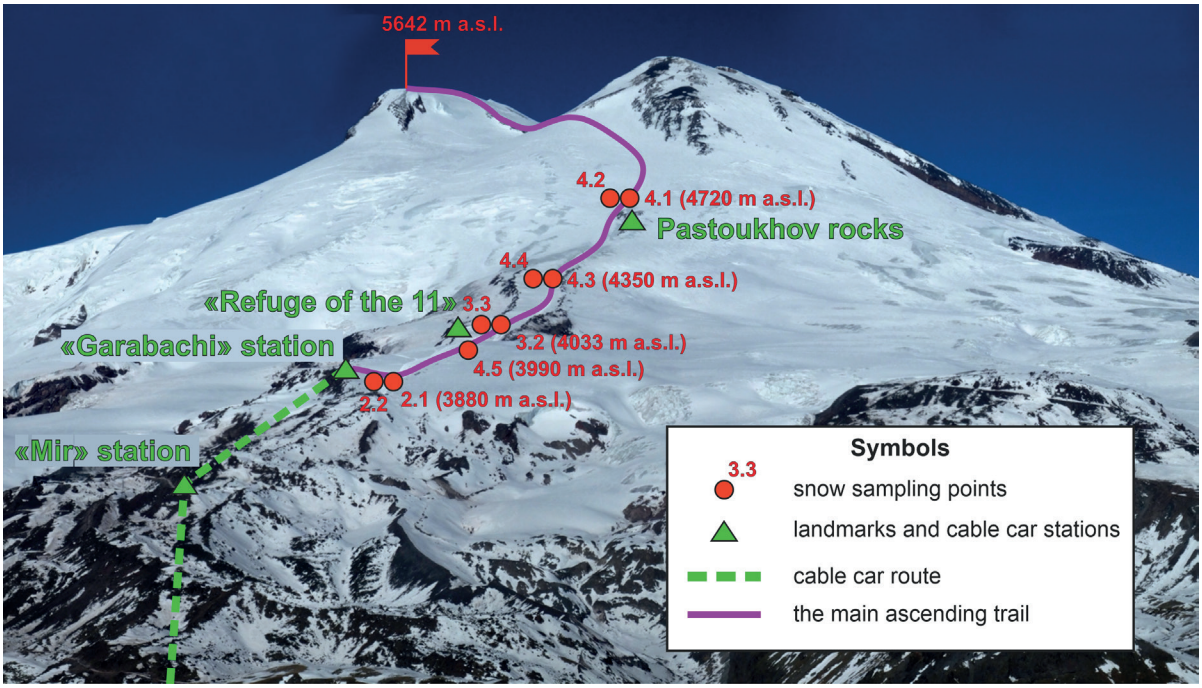

Fig. 2. Location of snow sampling points along the main trail to the Elbrus summit

ecotrail Cheget turn – Azau waterfall, 3) the ecotrail Narzanov Glade – Cheget Glade, 4) the trail Sand Castles from the vil. Elbrus to the Irick-Chat Gorge 5) the trail to Syltran-Kyol lake. Scientific assessment helped to determine the current state of soil and vegetation cover and the consequences of anthropogenic load.

Snow and water samples analysis

The snow samples were collected with plastic shovels, packed in plastic bags and delivered to a facility where the snow thawed in glass reservoirs (jars) at room temperature without being exposed to direct sunlight. After thawing, water was transferred to glass bottles, with a sample size of 1 litre. In situ water samples were taken in plastic bottles. The samples were analyzed within 10 days from the sample date in the Testing Laboratory Center "AST-Analitika", LLC (Saint-Petersburg, accreditation certificate RA.RU.21AK10) in compliance with regulations for defining mass concentration of oil in drinking water, surface water, and wastewater using the method of infrared spectroscopy of federal conservational regulatory document 14.1:2:4.5-95.

Analyzing instrument was spectrometer «Varian» Spectr AA 240FS/120GTA/120PSD. The principle of operation of the spectrometer is to measure the optical density of the atomic vapour of the studied sample and calculate the content of elements according to the calibration characteristics. The spectrometer is built on a modular principle and is equipped with flame and electrothermal atomizers and a hydride attachment. In the flame atomizer, depending on the elements to be determined, a flame of mixtures is used: "acetylene - air" or "acetylene - nitrous oxide". The optical system of the spectrometer is based on a monochromator with a diffraction grating according to the Czerny-Turner scheme. Heavy metals (lead, cadmium, zinc, nickel, manganese, cobalt, chromium) in snow samples were determined according to the Federal Environmental Regulatory Document (FERD) 14.1:2:4.214-06, molybdenum content according FERD 14.1:2:4.140-98, total iron - according to FERD 14.1:2:4.50-96.

The data obtained was then compared to maximum acceptable concentration values for oil (0.3 mg/l) provided by the provisions of the Chief State Sanitary Physician of the Russian Federation of January, 28 2021 on the approval of sanitary rules and regulations 1.2.3685-21 and on the hygienic standards and requirements for safety and (or) harmlessness to humans from environmental factors.

RESULTS

Heavy metals in snow and water

Heavy metals content in natural waters and snow are presented in a table (see Appendix A). According to the data obtained, cobalt and chrome concentrations are lower than MAC and are generally lower than minimal impurities quantitation level. Snow samples were detected lead and zinc MAC overruns. Our data indicates that lead content found in samples from along the snowcat pistes at 4,720 m and 4,356 m heights is triple and double the MAC, correspondingly, as opposed to the samples taken at a distance from the pistes. At the same time, at the heights of 3,880 and 4,033 m (sampling points 2.1, 2.2, 3.1, 3.2) the reverse pattern is observed: lead concentrations on the trail are less than at some distance from it (see Appendix A). Apparently, such pattern is explained by local activities caused by service of alpine huts, confined to this altitude ("Refuge of 11", "Maria" and several unnamed residential cabins). Manganese, molybdenum, and iron contents are mostly noted in river water samples. High manganese content is both registered in the river Malyi Azau, amounting to 3.1 MAC, and in the sample T2, taken downstream the point of its confluence with the river Bolshoi Azau, amounting to 2.6 MAC. Molybdenum concentration in the snow cover is lower than the quantified limit, whereas its content in the river water ranges from 1.7 to 1.9 MAC. Nickel concentration in water starts to noticeably augment in the last three sampling points (T5, T6 and T7) reaching the maximum level of 1.3 MAC downstream the influx of the river Donguz-Orun.

Cadmium content distribution differs from other heavy metals. The maximum was registered in the river Malyi Azau (sampling point T8) and amounted to 1.9 MAC. The values increased gradually from the sampling point T1 (located 300 m downstream from the Azau waterfall), where the concentration adds up to less than 0.001 mg/l, to the sampling point T7 (in the area of Verkhniy Baksan village which is the confluent of the rivers Adyr-su and Baksan), where the descriptor adds up to 0.005 mg/l.

Oil products traces in snow

Laboratory studies have shown that MAC overrun for oil has been registered in all snow samplings with a maximum in points 3.1–3.3 adding up to 10-12 MAC (Fig. 3). Oil pollution was found both along the ratrack and snowcat piste and at a distance of 10–50 m from it or, in other words, in the backcountry. The point 3.3 also evidences maximum above-limit lead concentration (3.5 MAC). It is located near camping sites (Refuge of the 11) where, apart from snowcats performing uphill assistance, snowcats transfer people and cargo from a cableway to huts.

Traces of technical liquids on the fresh snow cover (fallen 1 to 2 days prior to the sample date) were found within the snowcat ascending trail at a distance of every 10 to 30 meters along the trails on the Elbrus slopes (Fig. 4). At least three liquids were identified: fuel, antifreeze substance, and engine oil.

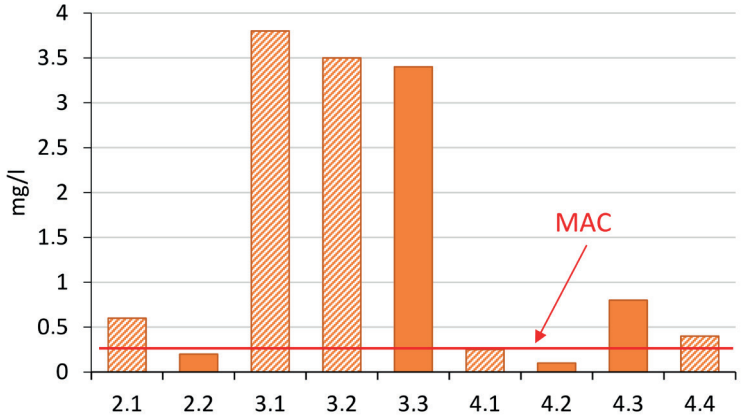

Fig. 3. Oil products concentrations in snow samples. Samples description is given in Appendix A. The concentration values in the hatch have been derived from snowcat trails

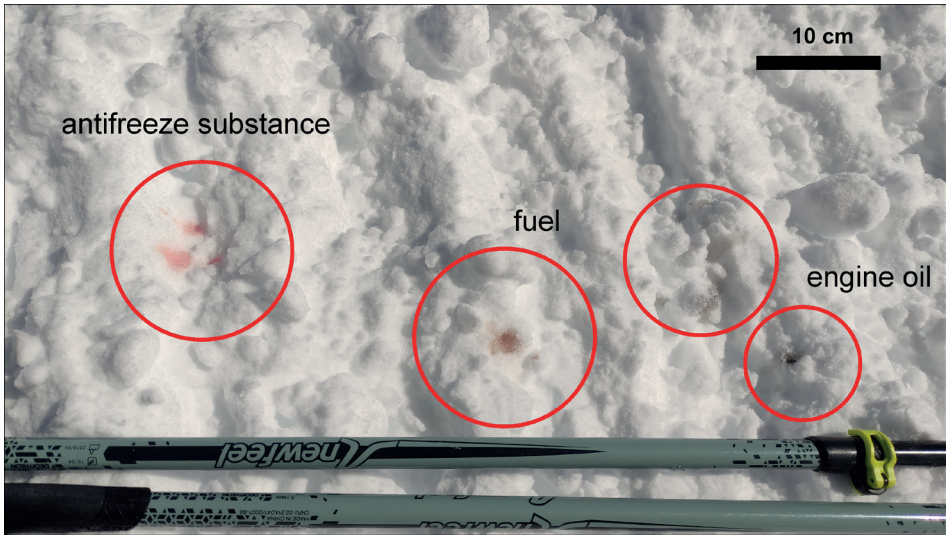

Fig. 4. Technical liquids within the snowcat ascending trail at the altitude of ~4000 m a.s.l. (photo by A. Maslakov, 2021)

Tourist trails impact

Within the framework of field studies, the inspection looked into 5 tourist and sportsmen-heavy equipped functioning trails in Prielbrusye NP. Trails analysis has identified ways of equipping, as well as anthropogenic load on soil and vegetation cover (Table 1).

The trails have been equipped by both national park staff and third parties, including volunteers. As a result, there is a disparity in the style and informativity of the facilities installed. The information board at the beginning of the Irick-Chat Gorge (trail 4) is informative and includes a description of the difficulty, duration, dangerous sections and a map-scheme of the trail itself (Fig. 5a). The information is written both in the Russian and in the English languages. At the same time, the map of functional zoning of the territory of the National Park is presented before the start of the trail to Syltran-Kyol Lake (trail 5) without additional information on the trail (Fig. 5b). The ecotrail "Polyana Narzanov – Polyana Cheget" (trail 3) is better equipped than the others: there are necessary signs and stands along the trail with additional information about flora, fauna, mineral springs, and rivers. All the trails are differently equipped.

The most severe disruption (trampling) was observed near Devichi Kosy (Maiden's Braids) Waterfall (Trail 1) (Fig. 5c) and on the ecotrail Cheget turn– Azau waterfall (trail 2). The highest number of bonfires and a trail width extension (Fig. 5d) were found near the Azau Glade. There is a reduction in the species diversity of vegetation, a decrease in the proportion of forest and post-forest species, a sharp increase in ruderal species, destruction of woody undergrowth and a reduction in the shrub layer and height of herbage. Disturbance of the vegetation cover indicates high recreational pressure in these areas and contributes to the activation of slope processes on the slopes that aren't turfed. The Sand Castles trail in the Irick-Chat Gorge often branches off and there is an extensive area of degraded soil cover on the main trail. Existing trail markings are insufficient to limit anthropogenic load and curb the appearance of branching of a single trail.

Miscellaneous equipment for hiking trails, as well as the chaotic and dense development by private recreational and residential facilities also led to decrease the aesthetic properties of unique high mountain nature.

DISCUSSION

Oil contamination of Elbrus glaciers

Geochemical composition of snow of Mount Elbrus depends both on natural conditions and human impact

Table 1. Examined trails, equipment quality and registered anthropogenic load

№	Trail title	Length of the explored area, km	Elevation difference, m	Equipment along the trail	Traces of anthropogenic load
1	Devichi Kosy (Maiden's Braids) Waterfall	5	704	trail marking, gazebos, litter bins, toilets	Trail width extension, branching of the trail, inscriptions on stones
2	Ecotrail Cheget turn– Azau waterfall	5	332	information boards, direction indicators, gazebos, toilets	Littering, unauthorized bonfires, trail width extension, chaotic choice of tent sites
3	Ecotrail Polyana Narzanov - Polyana Cheget	4	178	information boards, direction indicators, gazebos, bridges, toilets	Movement of prohibited means of transport (ATVs, horses)
4	The Irick-Chat Gorge Sand Castles	2	407	Information boards	Trail width extension, branching of the trail, soil trampling
5	To Lake Syltran-Kyol	5	846	Information boards, trail marking	Chaotic choice of tent and toilet sites

Source: authors' data.

Fig. 5. Tourist trails of the Prielbrusye National Park: (a), (b) information board at the starting points of trails 4 and 5; (c) the downtrodden grass near Devich'i kosy waterfall; (d) trail width extension at the trails 2 (photos by: A. Tabelinova & Yu. Yushina, 2021)

(Vasil'chuk et al. 2020; Chernyakov et al. 2020). The traces of oil concentrations indicate the only latter activity.

According to the emergency services workers who are on duty on the south slope of Mount Elbrus, the movement of snowmobiling equipment on the slope is not regulated or restricted in any way. Taking into account the small flow of tourists during the expedition (due to the off-season), it can be assumed that during the peak of tourist activity in the summer and winter months, the degree of snow pollution and the intensity of traffic on the slope may be several times higher. Uncontrolled traffic, accompanied by the discharge of technical fluids, leads to the pollution not only of the snow cover, but also of the underlying Gara-Bashi and Malyi Azau glaciers. Accumulating in the snowpack every day, oil products and other chemical pollutants (e.g. lead) move from snow to ice at subzero temperatures, accumulating in the glaciers that feed the rivers of the North Caucasus. As the snow fallen in the accumulation zone of a glacier reaches its tongue only several decades or even centuries later, oil contamination can act as a time bomb. Decades later streams and rivers will have elevated concentrations of oil products, which in turn will poison crops, livestock, and local residents.

Given all of the above, special attention should be paid to regulating snowmobile traffic on the south slope of Mount Elbrus and introducing strict environmental measures to reduce snow cover pollution by oil products and other technical fluids.

Potential sources of heavy metals

Heavy metals, especially their soluble phase, have negative effects on biota and humans by accumulating in tissues, inhibiting growth and development, and reducing productivity. However, not only tourism and construction, but also natural conditions can serve as their sources.

Reutova T.V. et al. (2018) recorded distribution of zinc concentrations in water and snow, as well as increased lead content at 4500 m altitude, which is similar to our data. Chizhova Yu.N. et al. (2017) noted that high zinc concentrations in the overlying snow may indicate that dry deposition of aerosols to the surface is the main mechanism of zinc accumulation. In addition, Kerimov A.V. et al. (2018) suggest that volcanic activity is one of the natural sources of zinc and its high concentrations, due to the presence of fumaroles in the area near the peak of Elbrus, may be the result of some volcanic activation.

Dreeva F.R. et al. (2017) in their work note the highest exceedance of MAC for manganese in the area of the confluence of the Baksan and Adyl-su rivers is 7 MAC. The T7 sample we collected 11 km downstream of this point also has elevated values of 2 MAC. Dreeva F.R. et al. (2019) identify manganese as a typical pollutant of the Adyl-su and Irick rivers flowing in the zone of a tectonic fault, where there are many sources of iron- and manganese-enriched carbonaceous mineral waters. Kerimov A.V. et al. (2018) note that molybdenum content in river waters often exceeds the MAC, especially in the Gara-Bashi and Azau rivers. The authors attribute this distribution of concentrations to natural factors. In the work of Reutova T.V. et al. (2014), the maximum nickel concentrations were registered in the estuary of the Terskol River (0.0149 mg/l). The moraine lake of Donguz-Orunkel also showed a high level (0.0137–0.0139 mg/l). In our case the T6 sampling point is located 100 m downstream from the place where the Donguz-Orun River where the maximum level was recorded flows into Baksan.

Although the MAC for fishery reservoirs is 0.005 mg/l, the cadmium clark in river waters is much lower and is only 10-4 mg/l, and in groundwater – $5 \cdot 10^{-5}$ mg/l (Mukha et al. 2012). Reutova T.V. et al. (2014) note in their work that cadmium content in water objects of Elbrus region has ultratrace concentrations and is less than 10^{-4} mg/l. We determined the concentrations of cadmium $1\text{-}9 \cdot 10^{-3}$ mg/l that is 10-100 times higher than the available literature data. According to Vinokurov et al. (2016), the same concentration in this region was once recorded only in the area of influence of the Tyrnyauz tungsten-molybdenum factory. In this way, the obtained results on cadmium concentrations are ambiguous and require further investigations.

The results obtained can be determined by seasonal variations in water flow. Most of the works is devoted to the study of dynamics during winter low-water and summer floods, sometimes spring floods, while our study was conducted in the autumn period. However, it should be noted that the overall pattern of heavy metal distribution over the study area agrees

well with other studies. In general, in 2013 the indicators of heavy metals sampled from the Baksan River described in the work by Reutov T.V. et al. (2018) are predominantly lower than ours. Heavy metal concentrations in the paper were considered by the authors at 8th and 35th km of the road along the Baksan River, which we can compare with our observation points T4 and T7, respectively.

Recommendations on reducing tourist load on ecosystems

Many protected areas, like Prielbrusye National Park, struggle to obtain data on the actual number of tourists to estimate the current strain on the environment. To regulate tourist flows, it is necessary to keep a statistical record of attendance to the most popular trails. In this case, the creation of an electronic registration system could, to some extent, increase the number of recorded tourists. Such a booking system is actively used in Europe and is free of charge. Keeping record of trail attendance will allow tracking statistics on tourist flows as well as identifying the most popular trails that require redirection of tourist flows. For example, the trail to Syltran-Kyol Lake is less popular due to its remoteness from the tourist core area (the Elbrus ski resort) and the lack of a distinct trail surface in the second part of the trail. Redirection of the tourist flow will reduce anthropogenic load on the national park's ecosystems. In addition, it is also recommended to conduct regular monitoring of trails condition, keep the boundaries of the main trail distinct to preventing the trail width extension and the emergence of uncoordinated branches, mark camping sites not only on maps, but also in the field, to conduct phytomelioration and engineering activities to improve the stability of the slopes. There are still problems that have been raised before (Kozova et al. 2010; Petrushina et al. 2010). The information system needs to be improved, especially at the entrances to the park, which is facilitated by having only two entrances due to the natural features of the park. Unfortunately, to date, there is no optimal functional zoning for the national park, with the removal of sloping forest landscapes from the recreational zone. According to the current zoning, the protection area includes predominantly nival-glacial and mountain-meadow landscapes, which are the least accessible to tourists. Forest landscapes, which play important ecological functions, do not fall within this zone and are heavily impacted by human activity. The lack or underdevelopment of wastewater treatment plants is an urgent problem. One of the most important tasks of the national park staff and volunteers is to raise environmental awareness of tourists.

CONCLUSIONS

Based on the conducted research, the following conclusions can be drawn:

1) Heavy metals in natural waters and snow have both natural and anthropogenic sources. Concentrations of cobalt and chromium are below the established MACs and, in most cases, below the limit of determinable impurity levels. Increased content of manganese (1.7–1.9 MAC) and nickel is the result of natural processes. Increased cadmium concentrations have been noted in snow on the slope of Elbrus and in the Baksan River. While in 2012–2015 the content of this element was estimated at a safe "trace" level, in our case concentrations increased to 1.1–1.5 MAC, which appears to be an indicator of anthropogenic pollution. However, our results must be confirmed by repeated studies.There is a significant increase in lead concentrations at sampling points above 3,500 m. Comparison of observation data from 2012–2015 (Reutova et al. 2015), with our results from 2021, shows a sharp increase in lead concentration (the MAC was exceeded in five samples out of eight). This appears to be due to direct contamination from technical fluids (POL, antifreeze) used in snowcats and snowmobiles.

2) Concentrations of traces of oil products exceeding the MAC up to 38 times were recorded along the Elbrus ascending trail up to the altitude of 4720 m, and numerous traces of technical fluids such as fuel, antifreeze, and oil were found on the trail. Uncontrolled traffic on the Elbrus snow cover leads to pollution of the Gara-Bashi and Malyi Azau glaciers, which in the future will reduce water quality in the rivers flowing from the south slope of Elbrus, namely the Baksan and Malka, which carry their waters to the Terek.

3) The most popular trails – Cheget turn – Azau waterfall and Devichi Kosy (Maiden's Braids) Waterfall – show signs of the disturbed soil and vegetation covers, caused by trampling of roadsides, branching of the main trail, as well as activation of slope processes. To reduce the negative impact of sports and tourism activities on the ecosystems in the vicinity of the trails it is recommended to redirect the tourist flow from more popular to less popular trails, to conduct electronic tourist registration, to monitor and equip the trails and to take phytomelioration and engineering measures to improve the stability of slopes near the trails. Tourists' environmental awareness needs to be raised.

The conducted research proves that the increased anthropogenic activity has a negative impact on the natural environment of the Prielbrusye National Park on the south slope of Mount Elbrus. The growth of the tourist flow leads to the degradation of the soil and vegetation cover not only in places of tourist concentration, but also near the equipped tourist trails. Anthropogenic load on geosystems manifests itself through the accumulation of heavy metals and traces of oil products in the natural environment. The results of the research can be used to elaborate plans on the national park's territorial development, to carry out land audits and to justify the need to reduce recreational activity, improve local ecosystems' condition and develop measures of environmental protection in the park territory.

REFERENCES

Atabieva F.A., Cherednik E.A. (2020). Estimation of seasonal variability of the content of heavy metal compounds in river waters of the foothill zone of the Central Caucasus. Water industry of Russia: problems, technologies, management, 3, 68-81 (in Russian).

Chernyakov G.A., Vitelli V., Alexandrin M.Y., Grachev A.M., Mikhalenko V., Kozachek A.V., Solomina O.V., Matskovsky V.V. (2020). Dynamics of seasonal patterns in geochemical, isotopic, and meteorological records of the Elbrus region derived from functional data clustering. Geography, Environment, Sustainability, 13(3), 110-116, DOI: 10.24057/2071-9388-2019-180.

Chizhova Yu.N., Budantseva N.A., Vasilchuk Yu.K. (2017). Heavy metals in the glaciers of the Polar Urals and the Caucasus. Arctic and Antarctica, 1, 10-27 (in Russian with English summary).

Dreeva F.R., Reutova N.V., Reutova T.V., Khutuev A.M., Kerimov A.A. (2017). Exceeding environmental standards for the content of heavy metals in natural waters of the high-mountain zone of the Kabardino-Balkarian Republic. In: Sustainable Development: Problems, Concepts, Models, 132-134, Nalchik, Russia: Kabardino-Balkar Scientific Center of the Russian Academy of Sciences (in Russian).

Kerimov A.M., Kurasheva O.A. (2018). Comparative analysis of heavy metal concentrations in the sources of the Baksan river and the Garabashi glacier (the southern slope of Elbrus). Proceedings of the Dagestan State Pedagogical University. Natural and exact sciences, 1(12), 23-40 (in Russian).

Kozova M., Petrushina M., Paudisheva E., Khoroshev A. (2010). Landscape changes as a consequence of transformational processes in the model areas of the Tatra National Park (Slovakia) and the Prielbrusie State National Park (Russia). In: Landscape ecology – methods, applications and interdisciplinary approach. M. Barancokova, J. Krajci, J. Kollar, I. Belcakova (eds.). Bratislava, Slovakia: Institute of Landscape Ecology Slovak Academy of science, 319-339.

Mukha V.D., Glebova I.V., Gridasov D.S., & Kuznetsova T.V. (2012). The main sorption parameters of the distribution of cadmium ions in the soils of the Central Chernozem region. Bulletin of the Kursk State Agricultural Academy, 2(2), 87-90 (in Russian with English summary).

National Park "Prielbrusye" (2003). Nalchik, Russia: El-Fa, 169 p (in Russian).

Petrushina M.N. Landscapes of the Baksan river basin. Prirodopol'zovanie Prielbrus'ya. Moskva: Izd-vo MGU, 120-152. (In Russian)

Petrushina M.N. Current state of landscapes of Elbrus National Park. In: Current landscape-ecological state and problems of optimization of the natural environment of the regions. Proceedings of the XIII International Landscape Conference dedicated to the centenary of F.N. Milkov, Voronezh, 14-17 May 2018, Voronezh, Russia: Istoki, 1. 412-414 (in Russian).

Petrushina M.N., Chizhova V.P., Kozova M., Paudisheva E. (2010). Tourism Development in National Parks «Prielbrusye» and «Tatransky»: Comparative Analysis. In: Tourism and Recreation: Fundamental and Applied Research. Moscow, Russia, 591-597 (in Russian).

Reutova T.V., Dreeva F.R., Reutova N.V. (2014). Spatial distribution of concentrations of toxic heavy metals in river waters of the mountainous zone of the Kabardino-Balkarian Republic. Proceedings of the Kabardino-Balkarian Scientific Center of the Russian Academy of Sciences, 6, 99-104 (in Russian).

Reutova T.V., Dreeva F.R., Reutova N.V. (2018). The content of impurities in the waters of the mountain rivers of the upper reaches of the Baksan (National Park «Prielbrusye») and its seasonal changes. Water resources, 1(45), 85-92 (in Russian).

Vasil'chuk Yu.K., Chizhova Yu.N., Frolova N.L., Budantseva N.A., Kireeva M.B., Oleynikov A.D., Tokarev I.V., Rets E.P., Vasil'chuk A.K. (2020). A variation of stable isotope composition of snow with altitude on the Elbrus Mountain, Central Caucasus. Geography, Environment, Sustainability, 13(1), 172-182, DOI: 10.24057/2071-9388-2018-22.

Vinokurov S.F., Gurbanov A.G., Bogatikov O.A., Sychkova V.A., Shevchenko A.V., Leksin A.B., & Dudarov, Z.I. (2016). Geochemical features of disposal of buried wastes of the Tyrnyauz tungsten-molybdenum plant by acid leaching. Doklady Academy of Sciences, (4)470, 445-447 (in Russian with English summary).

APPENDIX

Appendix A. Heavy metals concentration in snow and water samples

Sample number	Altitude, (m)	Sampling point description	Microelements' concentration, mg/l									
			Dry residue	Fe	Mo	Pb	Cd	Zn	Ni	Mn	Co	Cr
4.1	4720	Snowcat piste	<50	<0.1	<0.0001	0.0180	0.0073	0.0150	<0.005	<0.001	<0.005	<0.005
4.2	4720	50 meters west of 4.1	<50	<0.1	<0.0001	<0.002	0.0050	0.0203	<0.005	<0.001	<0.005	<0.005
4.3	4356	30 meters west of 4.4	64	<0.1	<0.0001	<0.002	0.0044	0.0170	<0.005	0.0028	<0.005	<0.005
4.4	4356	Snowcat piste	<50	<0.1	<0.0001	0.0130	0.0045	0.0160	<0.005	0.0012	<0.005	<0.005
3.2	4033	Snowcat piste	64	<0.1	<0.0001	0.0080	0.0014	0.0110	<0.005	0.0020	<0.005	<0.005
3.3	4033	10 meters west of 3.2	168	<0.1	<0.0001	0.0210	0.0024	0.0190	<0.005	<0.001	<0.005	<0.005
2.1	3880	Snowcat piste, slightly above the Gara-Bashi Station	126	<0.1	<0.0001	<0.002	0.0057	<0.001	<0.005	<0.001	<0.005	<0.005
2.2	3880	5 meters east of 2.1	<50	<0.1	<0.0001	0.0140	0.0012	0.0150	<0.005	<0.001	<0.005	<0.005
T1	2341	300 meters downstream of the waterfall	104	<0.1	0.00063	<0.002	<0.001	<0.001	0.005	<0.001	<0.005	<0.005
T2	2338	Near Azau tourist camp, below the waterfall, near the sewer. The Baksan river	84	<0.1	0.00063	<0.002	0.0010	<0.001	<0.005	0.026	<0.005	<0.005
T3	2328	Along the road from Azau tourist base to Terskol, in the concrete well	124	0.16	0.0019	<0.002	0.0011	<0.001	0.0051	<0.001	<0.005	<0.005
T4	2141	30 meters downstream from the place of a confluence of the Gara-Bashi river into the Baksan	62	0.16	0.0018	<0.002	0.0016	<0.001	<0.005	<0.001	<0.005	<0.005
T5	2054	The Baksan river below the bridge to Cheget	108	0.11	0.0015	0.0060	0.0016	<0.001	0.0063	<0.001	<0.005	<0.005
T6	2013	The Baksan river 100 meters from the place of confluence of the Donguz-Orun river	52	0.22	0.0005	<0.002	0.0020	<0.001	0.0129	<0.001	<0.005	<0.005
T7	1518	50 meters from the place where the rivers Syltrans, Kyrtyk and Adyr-su join the Baksan	102	0.10	0.0014	<0.002	0.0050	<0.001	0.0090	0.0190	0.0060	<0.005
T8	2802	The Malyi Azau river, ~400 meters east of «Krugozor» cableway station	134	<0.1	0.00167	0.002	0.0093	<0.001	<0.005	0.031	<0.005	<0.005
Maximum acceptable concentration (MAC), mg/l			-	0.1	0.001	0.006	0.005	0.01	0.01	0.01	0.01	0.05

RESEARCH PAPER

RELATIONSHIP BETWEEN URBANIZATION AND ROAD NETWORKS IN THE LOWER NORTHEASTERN REGION OF THAILAND USING NIGHTTIME LIGHT SATELLITE IMAGERY

Nayot Kulpanich[1*], Morakot Worachairungreung[1], Katawut Waiyasusri[1], Pornperm Sae-Ngow[1], Pornsmith Chaysmithikul[1], Kunyaphat Thanakunwutthirot[2]

[1]Suan Sunandha Rajabhat University, Faculty of Humanities and Social Sciences, Geography and Geo-Informatics Program, Bangkok, Thailand, 10300

[2]Suan Sunandha Rajabhat University, Faculty of Fine and Applied Arts, Digital Design and Innovation Program, Bangkok, Thailand, 10300

***Corresponding author:** nayot.ku@ssru.ac.th

Received: August 14th, 2021 / Accepted: November 11th, 2022 / Published: December 31st, 2022

https://DOI-10.24057/2071-9388-2021-096

ABSTRACT. The objective of this research on the relationship between urbanization and road networks in the lower Northeastern region of Thailand was to compare the urban area in 2006, 2013 and 2016 using nighttime light satellite images from the National Oceanic and Atmospheric Administration (NOAA), acquired by the Defense Meteorological Satellite Program (DMSP/OLS) and the Suomi National Polar-orbiting Partnership (Suomi NPP). After that the relationship between urbanization and road network was identified using nighttime light satellite images from these satellites. The nighttime light data was used to determine the urbanization levels, which were then compared with Landsat 8 Satellite images taken in 2016 in order to find the Pearson correlation coefficient. The results indicated that areas with high urbanization identified from the nighttime light satellite images taken by the Suomi NPP Satellite had a day/night band reflectance of 172-255 indicated and were located primarily along the roads. The analysis of these data suggested that urbanization has a significantly positive relationship with the road network at 0.01 level, with R^2 values of 0.800 for urbanization and 0.985 for the road network.

KEYWORDS: nighttime light satellite image, urbanization, road network, lower Northeastern region Thailand, Remote Sensing

CITATION: Kulpanich N., Worachairungreung M., Waiyasusri K., Sae-Ngow P., Chaysmithikul P., Thanakunwutthirot K. (2022). Relationship Between Urbanization And Road Networks In The Lower Northeastern Region Of Thailand Using Nighttime Light Satellite Imagery. Geography, Environment, Sustainability, 4(15), 124-133
https://DOI-10.24057/2071-9388-2021-096

ACKNOWLEDGEMENTS: We would like to thank the National Oceanic and Atmospheric Administration (NOAA), National Aeronautics and Space Administration (NASA) and Japan Aerospace Exploration Agency (JAXA) for providing the data for the research, as well as the U.S. Geological Survey for provideing Landsat 8 Satellite images and Department of Highways, Thailand. Finally, we would like to thank the Geography and Geo-Informatics Program, Faculty of Humanities and Social Sciences, Suan Sunandha Rajabhat University for facilitating this research.

Conflict of interests: The authors reported no potential conflict of interest.

INTRODUCTION

The patterns of land utilization are rapidly changing, significantly affecting people's lifestyles in terms of the economy, society, and the environment (Taati et al. 2015; Heagzy and Kaloop 2015; Waiyasusri and Wetchayont 2020; Zaman et al. 2020). Therefore, the application of remote sensing to monitor, verify and predict land use becomes crucial to monitor, verify and predict land use trends, especially in urban and built-up areas (Ping et al. 2011; Ma and Li 2018; Halder et al. 2021) There are many instruments suitable for this matter, including remote-controlled pilotless aircraft, or drones, and satellite images from natural resource satellites, hyperspectral satellites, etc. (Liu & Yang 2015; Robert Behling et al. 2015). However, the images taken by natural resource satellites are quite large due to the different types of sensors they use, therefore, for studying urbanization it is recommended to use images taken by meteorology satellites (Zhou et al. 2015; Nguyen et al. 2019) In addition, one of the limitations is the long time it takes for satellite to orbit the Earth and then come back to take another picture of the same area, resulting in the lack of data during period. However, the VIIRS/DNB data is currently available to the public from a number of sources, including the Google Earth Engine and Earth Observation Group, Colorado School of Mines. (Puttanapong et al. 2020; Colorado School of Mines 2021)

The study of urban expansion using meteorology satellite images is based on the collection of nighttime light images taken by a satellite of the Defence Meteorological Satellite Program (DMSP) with the Operational Line Scan (OLS) system (hereinafter referred to as the "DMSP/OLS Satellite") from the United States of America (Amaral et al. 2006; Min Zhao 2020), and a satellite of the Suomi National Polar-orbiting Partnership (Suomi NPP) with Visible Infrared Imaging Radiometer Suite (VIIRS) instruments and a Day/Night Band (DNB) sensor

(hereinafter referred to as the "Suomi NPP Satellite") from Japan (Ma et al. 2014; Bennett and Smith 2017). Both satellites collect nighttime light reflectance data for monitoring urbanization (Tong et al.2018). This remote sensing of nighttime light was, applied in the study of urban economic trends and urbanization by Zheng et al (2019) and Zhao et al (2020). In addition, Hasi Bagan & Yoshiki Yamagata (2015) used nighttime satellite images to analyze urban growth, population density, land utilization, and population in Japan from 1990 to 2006. Their results indicated a significant relationship between the land use data, especially in urban and built-up areas, and population. Nighttime light satellite images show illumination in areas of high urbanization and population density (Bagan and Yamagata 2015). Therefore, this methodology could be applied to study urbanization using meteorology satellite images, which are a better instrument for this purpose than other types of satellite images.

In Thailand, there have been many studies on the use of nighttime light and day-night bands. For example, Puttanapong et al. (2020) used nighttime light satellite images from DMSP OLS and Suomi VIIRS to predict the distribution of poverty in Thailand. Nighttime light images were used as one of the geospatial parameters in this prediction. Furthermore, Tepinta (2020) studied the spatial effect of road density on urbanization in Thailand using data from DMSP OLS and the VIIRS project from the Google Earth engine. The results of this study showed a statistically significant correlation between road density and nighttime light (Tepinta 2020).

Furthermore, nighttime light satellite images were used to analyze the spatial cluster of leptospirosis in Thailand during the period from 2013 to 2015. In the study, nighttime light images were used as one of the environmental factors providing a statistically significant contribution to predicting this disease (Luenam and Puttanapong 2020).

The aims of this research was to study urbanization in the lower Northeastern region of Thailand using nighttime light reflectance data collected by the DMSP/OLS Satellite and day/night band reflectance collected by the Suomi NPP Satellite in 2006, 2013 and 2016. In order to analyze urban growth in the lower Northeastern region of Thailand, we aimed to identify the relationship between urbanization and road networks, which can be used to predict urban expansion and prepare an effective development plan without using natural resource satellite images.

MATERIALS AND METHODS

Study area

The study area is located in the lower Northeastern region of Thailand in the middle of the East-West Economic Corridor (EWEC), an Economic Development Program in the Greater Mekong Sub-region (GMS), connecting and promoting trade and culture among the countries in this sub-region with high commercial demand as the key for economic recovery (Ramachandran and Linde 2011; Tansakul et al. 2013; Leisz et al. 2016). The studied territory covers a vast area of 115,402.41 square kilometers, or 22.49% of the country, serves as the gateway to the east border of Thailand, and comprises 12 provinces: Chaiyaphum, Nakhon Ratchasima, Khon Kaen, Maha Sarakham, Kalasin, Roi Et, Yasothon, Ubon Ratchathani, Amnat Charoen, Surin, Si Sa Ket and Buri Ram, as presented in Figure 1.

Thailand's highways

Thailand's highways consist of five levels, particularly special, national, rural, local, and concession highways. National highways also classify into four levels, which are indicated by the number of digits in the highway markers. For example, a single-digit number indicates the main highway that connects to Bangkok, Two digits indicate a principal highway within a region, three digits indicate a secondary regional highway, four digits indicate an intra-province highway connecting a provincial capital to its districts. This study used road network data that included only national highways of the main principal regional, and secondary regional highways.

Fig. 1. Map of the Lower Northeastern Region of Thailand

DATA

Nighttime light images taken by the DMSP/OLS and Suomi NPP meteorology satellites were collected for the analysis of urban and built-up areas, along with the images taken by the Landsat 8 and Sentinel-2 satellites for comparison. These images were then analyzed together with road network data in Thailand using Geographic Information Systems (GIS), as presented in Table 1.

Defense Meteorological Satellite Program (DMSP/OLS)

Defense Meteorological Satellite Program (DMSP) is a program of lower orbit satellites initiated by the United States Department of Defense and managed by the United States Space Force. DMSP is primarily engaged in environmental surveys and monitoring, especially meteorology. DMSP satellites have 7 types of important sensor systems: OLS- Operational Linescan System, SSM/I- Microwave Imager, SSMT/2- Atmospheric Water Vapor Profiler, SSJ/4- Precipitating Electron and Ion Spectrometer, SSM/T- Atmospheric Temperature Profiler, SSIES- Ion Scintillation Monitor, and SSM – Magnetometer. The annual DMSP-OLS NTL composites (i.e., yearly average NTL intensity) from 1992 to 2013 were obtained from the National Oceanic and Atmospheric Administration's National Geophysical Data Center (NOAA/NGDC). The data values range from 0 to 63, (as presented in Table 2.) with 0 representing the background noise. (Lu et. al. 2019)

Suomi National Polar-orbiting Partnership (Suomi NPP)

The Suomi National Polar-orbiting Partnership or Suomi NPP is a weather satellite operated by the United States National Oceanic and Atmospheric Administration (NOAA). Suomi NPP has 5 types of systems for collecting the images: Visible Infrared Imaging Radiometer Suite (VIIRS), Ozone Mapping and Profiler Suite (OMPS), Clouds and the Earth's Radiant Energy System (CERES), Cross-track Infrared Sounder (CrIS), and Advanced Technology Microwave Sounder (ATMS). The Visible Infrared Imaging Radiometer Suite (VIIRS) is the largest instrument aboard NPP. It collects radiometric imagery of the land, atmosphere, ice, and ocean in visible and infrared wavelengths (Keck 2011). Furthermore, VIIRS has a day/night band to detect low levels of visible/near-infrared radiance at night from sources on or near the Earth's surface, which allows to identify lightning flashes from urban areas.

Relationship between DMSP/OLS and Suomi NPP Satellites

The preparation of nighttime light satellite images taken by the DMSP/OLS and Suomi NPP Satellites in 2013 included image analysis to crop the study area and GIS analysis to adjust their reflectance values. The data values ranged from 0 to 63 (64 values) for the DMSP/OLS Satellite (Xiao et al. 2014; Cao et al. 2014; Sun et al. 2020; Gibson and Boe-Gibson 2021), and from 0 to 255 (256 values) for the Suomi NPP Satellite (Stokes and Seto 2019; Sun et al. 2020). Therefore, reclassification of the value was required (Zheng et al. 2019) to divided them into four levels: no urbanization, low urbanization, moderate urbanization, and high urbanization, as presented in Table 2.

Urban and built-up areas were identified from nighttime light satellite images by calculating the digital number of DMSP/OLS and Suomi NPP Satellite images taken in 2013 and employing GIS to convert raster data into a vector before dissolving the reflectance values of the same level to reduce data redundancy. The nighttime light areas in each province were then calculated and identified.

Analysis of the Relationship between Urban Land Utilization and Road Networks Using Landsat 8 Satellite Images

Urbanizations characteristics were identified by analyzing the road network in Landsat 8 Satellite images taken in 2016 using a band composition method for quality detection before cropping the selected areas. Reflectance value adjustments and geometric corrections were required in order to calculate the Normalized Difference Built-up Index (NDBI) (Zha et al. 2003; Chen et al. 2006; Zhang and Jia 2013; Bhatti and Tripathi 2013) using the equation below:

$$NDBI = \frac{SWIR - NIR}{SWIR + NIR} \quad (1)$$

Whereas: NDBI = Normalized Difference Built-up Index
SWIR = Shortwave Infrared Reflectance
NIR = Near Infrared Reflectance

Sentinel-2 Satellite images were used for the geometric correction of the Landsat 8 satellite images in order to identify the area of urban land utilization, while NDBI was used to verify the accuracy of all urbanization levels. The accuracy of Landsat 8 Satellite images was verified by

Table 1. Data used in this study

Description	Year	Source
Nighttime Light Satellite Images Taken by Defense Meteorological Satellite Program (DMSP/OLS)	2006 and 2013	National Oceanic and Atmospheric Administration (NOAA), USA
Nighttime Light Satellite Images Taken by Suomi National Polar-orbiting Partnership (Suomi NPP)	2013 and 2016	National Oceanic and Atmospheric Administration (NOAA), USA
Satellite Images Taken by Landsat 8 Satellite	2016	U.S. Geological Survey, USA
Road Network	2016	Department of Highways, Thailand

Table 2. Day/Night Band Reflectance from DMSP/OLS and Suomi NPP Satellite Images

Urbanization Level	DMSP/OLS	Suomi NPP
No Urbanization	0 - 10	0 - 43
Low Urbanization	11 - 24	44 - 99
Moderate Urbanization	25 - 53	100 - 215
High Urbanization	54 - 63	216 - 255

Cohen's kappa coefficient. Fishnet grids were then drawn on the urban land utilization images and nighttime light satellite images before combining them with the nighttime light images taken by the Suomi NPP Satellite and selecting only the overlaying parts showing high urbanization.

Analysis of the Relationship between Urbanization and Road Network Using DMSP/OLS and Suomi NPP Satellite Images

Road network data overlaid with the nighttime light images taken by Suomi NPP Satellite was selected to analyze the relationship between urbanization and road network using the Pearson correlation coefficient, which was calculated using the equation 2

$$r_{xy} = \frac{N\sum XY - (\sum X)(\sum Y)}{\sqrt{[N\sum X^2 - (\sum X)^2][N\sum Y^2 - (\sum Y)^2}} \quad (2)$$

Where: r_{xy} = Correlation Coefficient
N = Total Number of Data
X = Nighttime Light Satellite Images Taken by Suomi NPP Satellite in 2016
Y = Urban and Built-Up Area, and Transport Network

RESULTS

Comparison of Urban Expansion in the Lower Northeastern Region estimated from Nighttime Light Satellite Images Taken by the DMSP/OLS and Suomi NPP Satellites in 2006, 2013, and 2016.

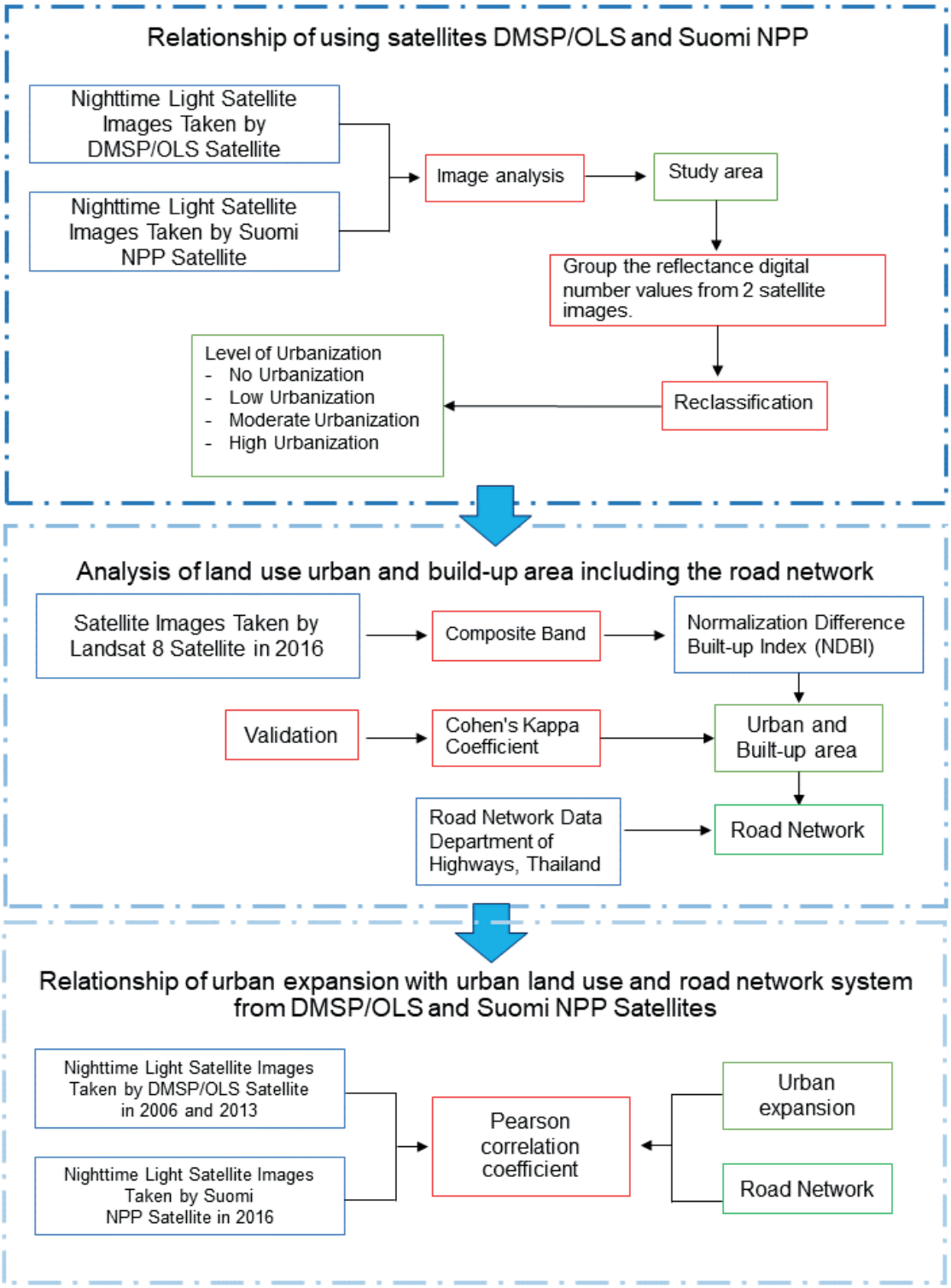

Fig. 2. Research Process

The results indicated that, according to the nighttime light satellite images taken by the DMSP/OLS Satellite, urbanization within the lower Northeastern region of Thailand increased every year as presented in Table 3.

The analysis showed that the area with high urbanization identified from the nighttime light reflectance data collected by the DMSP/OLS Satellite increased from 1,249.02 square kilometers in 2006 to 3,950.37 square kilometers in 2013. In addition, the nighttime light reflectance data collected by the Suomi NPP Satellite showed that by 2016, the urban area increased even further, reaching 13,829.02 square kilometers. This increase in urbanization was observed in all the provinces as presented in Figure 4, and the top 3 provinces with the highest urbanization were Nakhon Ratchasima, Khon Kaen, and Ubon Ratchathani, as presented in Figures 3 and 4 as well as Table 4.

Table 3. Urbanization in the Lower Northeastern Region of Thailand based on Nighttime Light Satellite Images

Urbanization Level		2006	2013	2016
No Urbanization	Day/Night Band Reflectance	0-10		
	Area (km^2)	384,308.55	375,201.72	77,554.25
Low Urbanization	Day/Night Band Reflectance	11-24		
	Area (km^2)	7,867.53	30,296.43	33,855.5
Moderate Urbanization	Day/Night Band Reflectance	25-53		
	Area (km^2)	3,138.75	8,855.73	23,598.5
High Urbanization	Day/Night Band Reflectance	54-63		
	Area (km^2)	1,249.02	3,950.37	13,829.02

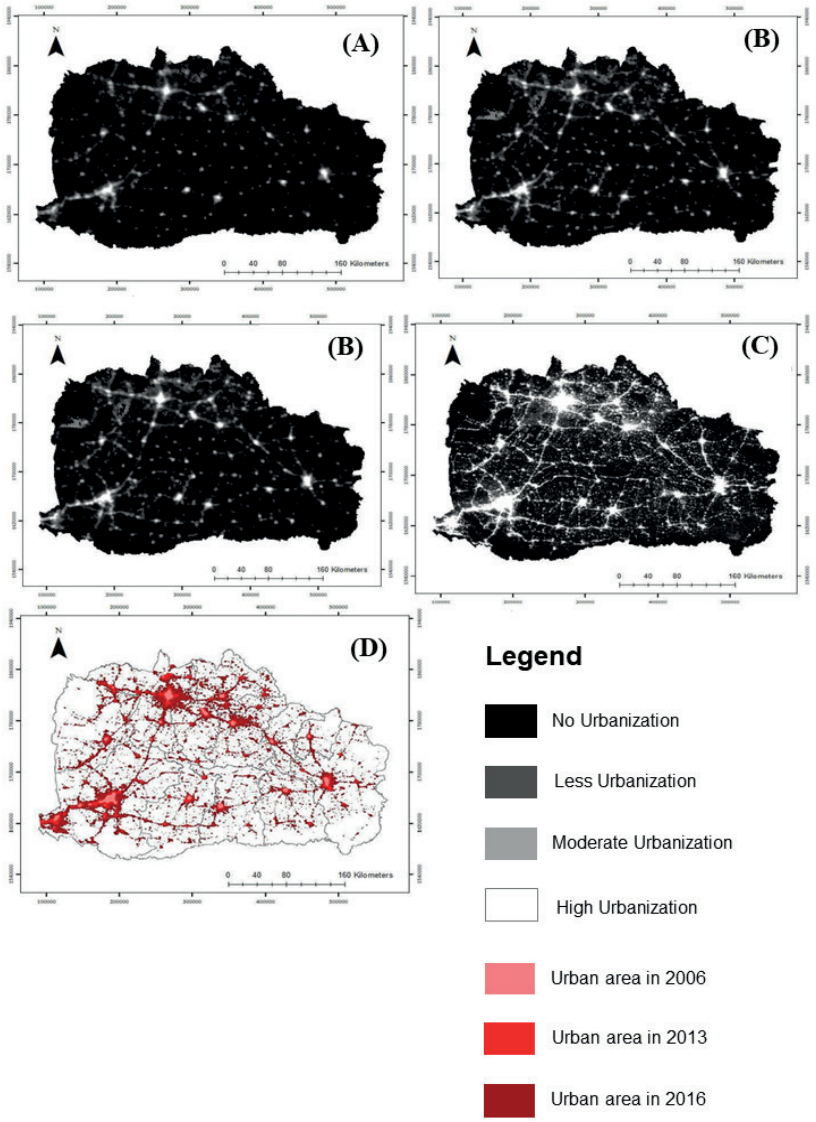

Fig. 3. Night time Light Satellite Images and Urban Expansion in 2006, 2013 and 2016 (A)DMSP/OLS Satellite Image in 2006, (B) DMSP/OLS Satellite Image in 2013, (C) Suomi NPP Satellite Image in 2016, and (D) Urbanization map base on Nighttime Light Satellite Images

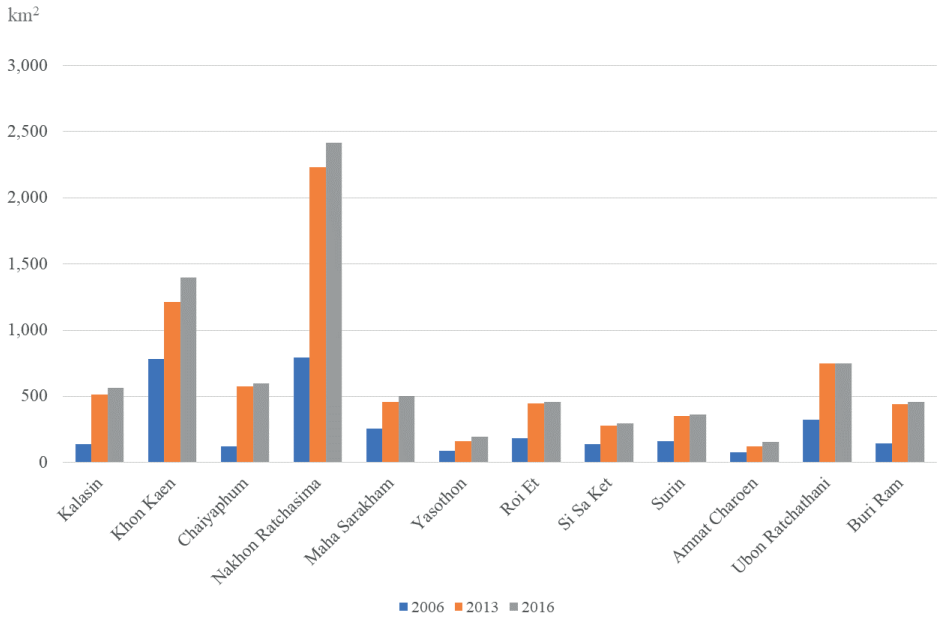

Fig. 4. Urban Area per province based on Nighttime Light Satellite Images

Table 4. Urban Area per province based on Nighttime Light Satellite Images

Province	Urban Area (km²)		
	2006	2013	2016
Kalasin	137.70	513.54	564.25
Khon Kaen	782.46	1,215.00	1,400.00
Chaiyaphum	120.69	557.53	599.25
Nakhon Ratchasima	793.80	228.31	2,418.00
Maha Sarakham	258.39	456.84	501.00
Yasothon	89.10	160.38	193.00
Roi Et	183.06	447.93	456.00
Si Sa Ket	138.51	277.02	296.25
Surin	162.00	349.11	365.00
Amnat Charoen	76.95	124.01	153.25
Ubon Ratchathani	324.00	746.01	750.75
Buri Ram	143.37	442.26	460.00

Relationship between Urbanization and Road Network

Urbanization was divided into four levels: no urbanization, low urbanization, moderate urbanization, and high urbanization. After that nighttime light reflectance data collected by the Suomi NPP Satellite was analyzed to find the relationship between urbanization and road network area, which is presented in Table 5.

The results showed that urban areas are located along Highway No. 2 (Mittraphap Road) and Highway No. 230 in Khon Kaen, Highway No. 231 in Ubon Ratchathani, Highway No. 232 in Roi Et, Highway No. 288 in Buri Ram, and Highway No. 290 in Nakhon Ratchasima, all of which are ring roads. The analysis of nighttime light reflectance indicated a high concentration of residences, shopping malls, commercial buildings and other economic activities along the roads in each province, resulting in high nighttime light reflectance values, as presented in Figure 5.

Table 5. Urbanization Level and Road Network

Urbanization Level	Day/Night Band Reflectance	Road Area (km²)
No Urbanization	0-43	0.44
Less Urbanization	44-99	0.58
Moderate Urbanization	100-215	0.84
High Urbanization	216-255	2.06

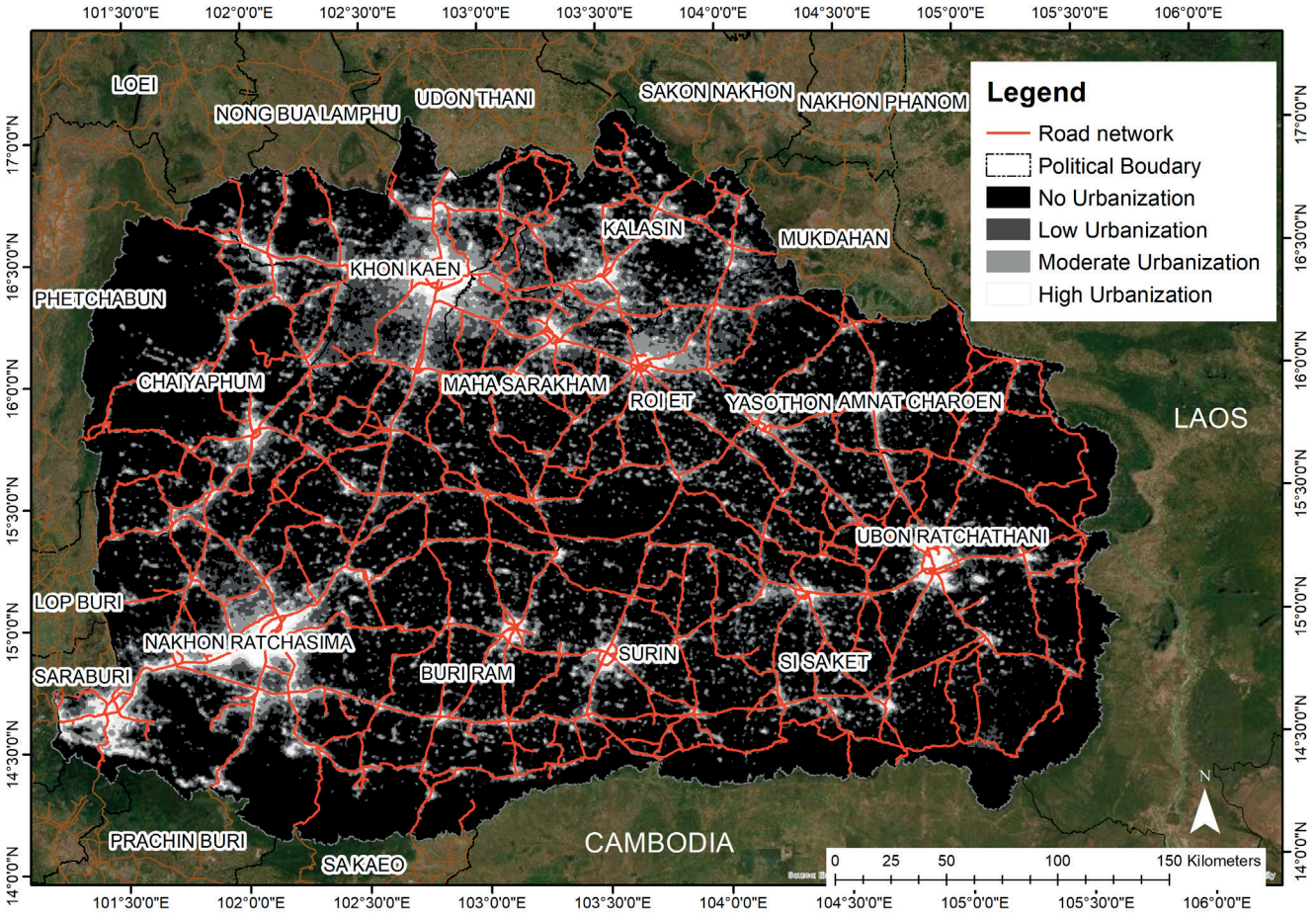

Fig. 5. Road Network and Urbanization base on Nighttime Light Data Acquired by Suomi NPP Satellite in 2016

The Pearson correlation coefficient was calculated found and the correlation was found to be significant at 0.01 level. The data of nighttime light reflectance, urban and built-up areas, and road network are presented in Table 6.

The relationship between the area of urban land use and nighttime light satellite images was found with a correlation coefficient (r) of 0.800. Data from the Department of Highways in Thailand was then used for further analysis. The correlation coefficient (r) between nighttime light satellite images and road network area was found to be 0.985, indicating a significant relationship, as presented in Figures 6 and 7.

Table 6. Comparison of Urban and Built-Up Area Expansion in 2016

Province	Urban or Built-Up Areas in 2016 (km^2)		
	Road Network	Suomi NPP	Landsat 8
Kalasin	0.122	564.25	2,546.53
Khon Kaen	0.410	1,400.00	4,207.02
Chaiyaphum	0.122	599.25	4,371.57
Nakhon Ratchasima	0.485	2,418.00	8,251.13
Maha Sarakham	0.110	501.00	2,288.51
Yasothon	0.092	193.00	1,545.05
Roi Et	0.142	456.00	3,045.25
Si Sa Ket	0.084	296.25	3,689.64
Surin	0.120	365.00	3,726.93
Amnat Charoen	0.057	153.25	1,244.63
Ubon Ratchathani	0.202	750.75	6,375.53
Buri Ram	0.120	460.00	4,439.18

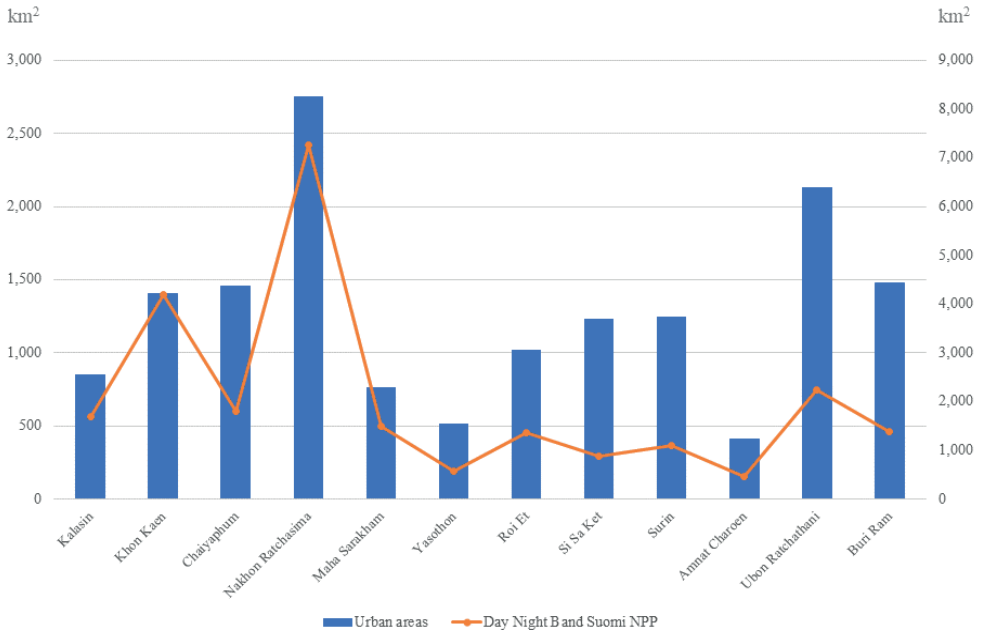

Fig. 6. Relationship between Day/Night Band Captured by Suomi NPP Satellite and Urban Area according to Landsat 8 Data in 2016

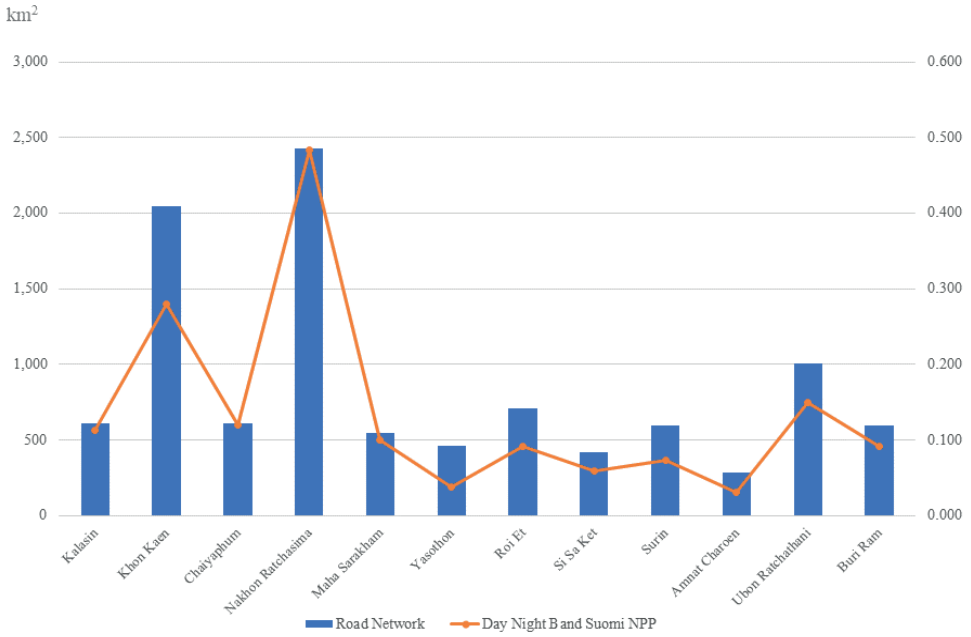

Fig. 7. Relationship between Day/Night Band Captured by Suomi NPP Satellite and Road Network in 2016

DISCUSSION

The nighttime light satellite images taken by DMSP/OLS and Suomi NPP satellites in the lower Northeastern region of Thailand during 2006-2016 can be applied to study the urban area and building expansion over this period (Amaral et al. 2006; Min Zhao 2020; Ma et al. 2014; Mia M. Bennett 2017; Q. Zheng et al. 2019) and replace the analysis using the images from natural resource satellites. This type of analysis can be applied to the regional level as well (Bagan & Yamagata 2015). It was found that the top 3 provinces with the highest urbanization were Nakhon Ratchasima, Khon Kaen and Ubon Ratchathani, the corresponds with the road network expansion surrounding the city centers, which are the key economic areas that include residences, shopping malls, markets, and other related activities (Keeratikasikorn 2018). Moreover, this relationship between the road network and urban areas via the nighttime light images was confirmed using correlation statistics (Tepinta 2020; Sangkasem and Puttanapong 2020). R-square value of the relationship between urbanization and nighttime light satellite images was 0.800, while for one of the relationships between the road network and nighttime light satellite images it was 0.985, which can be considered very high. Therefore, the results of this study can be useful for the agencies that work on monitoring and studying urbanization as well as the relevant local administrative authorities.

The results of this study also showed some patterns of urban development in Thailand. It was found that urban areas will develop primarily from city centers, with the development poles being shopping malls, government offices, stadiums, and other urban areas of high economic activity. For example, Nakhon Ratchasima and Khon Kaen are provinces that developed around their city centers in the past. This happened because the government established a number of regional government centers in the country. In addition, universities such as Khon Kaen University,

and the Rajamangala University of Technology Isan were also established in order to spread higher education into many regions. As a result of such policies, the cities in both provinces have grown considerably. There is also a rapid increase in population and buildings, in Ubon Ratchathani province which has a large area and is located adjacent to Laos and Cambodia. As a result, the expansion of urban areas here occurs mainly from economic development, especially the migration of agricultural workers into the city. Furthermore, an interesting urban expansion pattern was found in this study for Buriram Province, which was associated with the expansion of the city due to the construction of internationally recognized sports facilities, such as football stadiums, and racing tracks that took place in 2014. Therefore, other provinces in the region need to rely on the development of the economy and the infrastructure of the cities for their further growth.

CONCLUSIONS

During this study, while analyzing urban expansion in the lower Northeastern region of Thailand using the nighttime light satellite images taken by the DMSP/OLS and Suomi NPP Satellites, it was found that the data captured by both satellites required conversion in order to obtain compatible values. It was also concluded that nighttime light satellite images taken by the Suomi NPP Satellite were better for the analysis of urban expansion because the DMSP/OLS Satellite data was only available until 2013. Consequently, images from the Suomi NPP, launched in 2011, were required afterwards.

From this study, it can be concluded that (1) urban expansion was analyzed using the nighttime light satellite images taken by the Suomi NPP Satellite and compared with the Landsat 8 Satellite image, which were used to calculate the NDBI, and identify the relationship between the urban area and nighttime light satellite images using the correlation coefficient, it was found that this relationship was highly significant with a coefficient value of 0.800; and (2) the relationship between urbanization and road networks areas was analyzed using the correlation coefficient and it was found that this relationship was also highly significant with a coefficient value of 0.985. The urban and built-up areas can be easily identified from the nighttime light satellite images using the methods employed in this study, as well as compared to the results obtained from the natural resource satellite images.

The present study had two limitations. The first limitation was that the correlation coefficient is only a rough statistical test, future studies regression, and machine learning should be used to analyze the data. The second limitation was that the number of observations used in this study was very small, and a larger area should be chosen for future studies.

REFERENCES

Amaral S., Monteiro A.M.V., Câmara G., and Quintanilha J.A. (2006). DMSP/OLS night-time light imagery for urban population estimates in the Brazilian Amazon. International Journal of Remote Sensing, 27, 855-870, DOI: 10.1080/01431160500181861.

Bagan H., and Yamagata Y. (2015). Analysis of urban growth and estimating population density using satellite images of nighttime lights and land-use and population data. GIScience & Remote Sensing, 52(6), 765-780, DOI: 10.1080/15481603.2015.1072400.

Behling R., Bochow M., Foerster S., Roessner S., and Kaufmann H. (2015). Automated GIS-based derivation of urban ecological indicators using hyperspectral remote sensing and height information. Ecological Indicators, 48, 218-234, DOI: 10.1016/j.ecolind.2014.08.003.

Bennett M.M., and Smith L.C. (2017). Advances in using multitemporal night-time lights satellite imagery to detect, estimate, and monitor socioeconomic dynamics. Remote Sensing of Environment, 192, 176-197, DOI: 10.1016/j.rse.2017.01.005.

Bhatti S.S., and Tripathi N.K. (2014). Built-up area extraction using Landsat 8 OLI imagery. GIScience & Remote Sensing 51(4), 445-467, DOI:10.1080/15481603.2014.939539.

Cao X., Wang J., Chen J., and Shi F. (2014). Spatialization of electricity consumption of China using saturation-corrected DMSP-OLS data. International Journal of Applied Earth Observation and Geoinformation, 28, 193-200, DOI: 10.1016/j.jag.2013.12.004.

Chen X.L., Zhao H.M., Li P.X., and Yin Z.Y. (2006). Remote sensing image-based analysis of the relationship between urban heat island and land use/cover changes. Remote Sensing of Environment, 104(2), 133-146, DOI: 10.1016/j.rse.2005.11.016.

Gibson J., and Boe-Gibson G. (2021). Nighttime Lights and County-Level Economic Activity in the United States: 2001 to 2019. Remote Sensing, 13(14), 2741, DOI: 10.3390/rs13142741.

Halder B., Bandyopadhyay J., and Banik P. (2021). Monitoring the effect of urban development on urban heat island based on remote sensing and geo-spatial approach in Kolkata and adjacent areas, India. Sustainable Cities and Society, 74, 103186, DOI: 10.1016/j.scs.2021.103186.

Hegazy I.R., and Kaloop M.R. (2015). Monitoring urban growth and land use change detection with GIS and remote sensing techniques in Daqahlia governorate Egypt. International Journal of Sustainable Built Environment, 4(1), 117-124, DOI: 10.1016/j.ijsbe.2015.02.005.

Keck A. (2011). NPPNPOESS Preparatory Project Building a Bridge to a New Era of Earth Observations. National Aeronautics and Space Administration (NASA).

Keeratikasikorn C. (2018). A comparative study on four major cities in Northeastern Thailand using urban land density function. Geospatial Information Science, 21(2), 93-101, DOI: 10.1080/10095020.2018.1455320.

Leisz S.J., Rounds E., Thi Bich Yen N., Nguyen Bang T., Douangphachanh S., and Ninchaleune B. (2016). Telecouplings in the East–West Economic Corridor within Borders and Across. Remote Sensing, 8(12), 1012, DOI: 10.3390/rs8121012.

Liu T., and Yang X. (2015). Monitoring land changes in an urban area using satellite imagery, GIS and landscape metrics. Applied Geography, 56, 42-54, DOI: 10.1016/j.apgeog.2014.10.002.

Lu L., Weng Q., Xie Y., Guo H., and Li Q. (2019). An assessment of global electric power consumption using the Defense Meteorological Satellite Program-Operational Linescan System nighttime light imagery. Energy, 189, 116351, DOI: 10.1016/j.energy.2019.116351.

Luenam A., and Puttanapong N. (2020). Modelling and analyzing spatial clusters of leptospirosis based on satellite-generated measurements of environmental factors in Thailand during 2013-2015. Geospatial Health 2020, 15, 856, DOI: 10.4081/gh.2020.856.

Ma T., Zhou C., Pei T., Haynie S., and Fan J. (2014). Responses of Suomi-NPP VIIRS-derived nighttime lights to socioeconomic activity in China's cities. Remote Sensing Letters 5(2), 165-174, DOI: 10.1080/2150704X.2014.890758.

Ma W., and Li P. (2018). An Object Similarity-Based Thresholding Method for Urban Area Mapping from Visible Infrared Imaging Radiometer Suite Day/Night Band (VIIRS DNB) Data. Remote Sensing, 10(2), 263, DOI: 10.3390/rs10020263.

Nguyen T.M., Lin, T.H., and Chan, H.P. (2019). The Environmental Effects of Urban Development in Hanoi, Vietnam from Satellite and Meteorological Observations from 1999–2016. Sustainability, 11(6), 1768, DOI: 10.3390/su11061768.

Puttanapong N., Martinez Jr. A.M., Addawe M., Bulan J., Durante R.L. and Martillan M. (2020). Predicting Poverty Using Geospatial data in Thailand. Asian Development Bank Economics Working Paper Series No. 630, DOI: 10.22617/WPS200434-2.

Ramachandran P., and Linde L. (2011). Integrating spatial support tools into strategic planning—SEA of the GMS North–South Economic Corridor Strategy and Action Plan. Environmental Impact Assessment Review, 31(6), 602-611, DOI: 10.1016/j.eiar.2010.04.002.

Shen P., Zhang J., and Su Z. (2011). The Application of Remote Sensing in the Extraction of Urban land Use Changes. Procedia Environmental Sciences, 10, 1589-1594, DOI: 10.1016/j.proenv.2011.09.252.

Sangkasem K. and Puttanapong N. (2020). Analysis of spatial inequality using DMSP-OLS nighttime-light satellite imageries: A case study of Thailand. Regional Science Policy Practice. 1–22, DOI: 10.1111/rsp3.12386.

Stokes E., and Seto K. (2019). Characterizing urban infrastructural transitions for the Sustainable Development Goals using multi-temporal land, population, and nighttime light data. Remote Sensing of Environment, 234, 111430, DOI: 10.1016/j.rse.2019.111430.

Sun Y., Zheng S., Wu Y., Schlink U., and Singh R. P. (2020). Spatiotemporal Variations of City-Level Carbon Emissions in China during 2000–2017 Using Nighttime Light Data. Remote Sensing, 12, 2916, DOI: 10.3390/rs12182916.

Taati A., Sarmadian F., Mousavi A., Pour C. T. H., and Shahir A. H. E. (2015). Land Use Classification using Support Vector Machine and Maximum Likelihood Algorithms by Landsat 5 TM Images. Walailak Journal of Science and Technology, 12(8), 681-687. Available at: https://wjst.wu.ac.th/index.php/wjst/article/view/1225 [Accessed 31 May. 2021].

Tansakul N., Suanmali S., and Ammarapala, V. (2013). An Analytic Hierarchy Process (AHP) approach to evaluate factors that influence cross border trade facilitation: A case study of East-West Economic Corridor route 2013 10th International Conference on Service Systems and Service Management, Hong Kong, China, 857-862, DOI: 10.1109/ICSSSM.2013.6602573.

Tepinta P. (2020). Effect of Transportation Development on the Urbanization in Thailand. International Journal of Humanities, Arts and Social Sciences, 6(1), 44-62, DOI: https://dx.doi.org/10.20469/ijhss.6.20005-1.

Tong L., Hua S., and Frazier A.E. (2018). Mixed accuracy of nighttime lights (NTL)-based urban land identification using thresholds: Evidence from a hierarchical analysis in Wuhan Metropolis, China. Applied Geography, 98, 201-214, DOI: 10.1016/j.apgeog.2018.07.017

Waiyasusri K., and Wetchayont P. (2020). Assessing Long-Term Deforestation in Nam San Watershed, Loei Province, Thailand Using A Dyna-Clue Model. GEOGRAPHY, ENVIRONMENT, SUSTAINABILITY, 13(4), 81-97, DOI: 10.24057/2071-9388-2020-14.

Xiao P., Wang X., Feng X., Zhang X., and Yang Y. (2014). Detecting China's Urban Expansion Over the Past Three Decades Using Nighttime Light Data. IEEE Journal of Selected Topics in Applied Earth Observations and Remote Sensing, 7(10), 4095-4106, DOI: 10.1109/JSTARS.2014.2302855.

Zaman H.M., Saqib Z., Bokhari A.S., Akhtar N., and Amir S. (2020). The Dynamics Of Urbanizations And Concomitant Land Use Land Cover Transformations In Planned And Quasi-Planned Urban Settlements Of Pakistan. GEOGRAPHY, ENVIRONMENT, SUSTAINABILITY, 13(4), 107-120, DOI: 10.24057/2071-9388-2020-64.

Zha Y., Gao J. and Ni S. (2003). Use of normalized difference built-up index in automatically mapping urban areas from TM imagery. International Journal of Remote Sensing, 24(3), 583-594, DOI: 10.1080/01431160304987.

Zhang A., and Jia G. (2013). Monitoring meteorological drought in semiarid regions using multi-sensor microwave remote sensing data. Remote Sensing of Environment, 134, 12-23, DOI: 10.1016/j.rse.2013.02.023.

Zhao M., Zhou Y., Li X., Cheng W., Zhou C., Ma T., Li M., and Huang K. (2020). Mapping urban dynamics (1992–2018) in Southeast Asia using consistent nighttime light data from DMSP and VIIRS. ISPRS Journal of Photogrammetry and Remote Sensing, 248, 111980, DOI: 10.1016/j.rse.2020.111980.

Zhao N., Cao G., Zhang W., Samson E.L., and Chen Y. (2020). Remote sensing and social sensing for socioeconomic systems: A comparison study between nighttime lights and location-based social media at the 500 m spatial resolution. International Journal of Applied Earth Observation and Geoinformation, 87, 102058, DOI: 10.1016/j.jag.2020.102058.

Zheng Q., Weng Q., and Wang K. (2019). Developing a new cross-sensor calibration model for DMSP-OLS and Suomi-NPP VIIRS night-light imageries. ISPRS Journal of Photogrammetry and Remote Sensing, 36-47, DOI: 10.1016/j.isprsjprs.2019.04.019.

Zhou Y., Smith S.J., Zhao K., Imhoff M., Thomson A., Bond-Lamberty B., Asrar G.R., Zhang X., He C., and Elvidge, C. D. (2015). A global map of urban extent from nightlights. Environmental Research Letters, 10, 054011, DOI: 10.1088/1748-9326/10/5/054011.

RESEARCH PAPER

SURFACE URBAN HEAT ISLAND IN MOSCOW DURING THE COVID-19 PANDEMIC LOCKDOWN IN 2020

Mikhail A. Lokoshchenko[1,2*] and Eugeniya A. Enukova[3]

[1]Lomonosov Moscow State University (MSU), Faculty of Geography, Department of Meteorology and Climatology. Lengory 1, Moscow, 119991, Russian Federation

[2]Obukhov Institute of Atmospheric Physics, Russian Academy of Sciences, Pyzhyovskiy pereulok, 3, Moscow, 119017, Russian Federation

[3]'Dubna' State University, Department of Ecology and Earth Sciences. Universitetskaya str. 19, Dubna, Moscow region, 141980, Russian Federation

***Corresponding author:** loko@geogr.msu.su

Received: October 10th, 2021 / Accepted: November 11th, 2022 / Published: December 31st, 2022

https://DOI-10.24057/2071-9388-2021-116

ABSTRACT. The influence of the COronaVIrus Disease 2019 (COVID-19) pandemic lockdown (the period of strict quarantine measures) in the spring of 2020 on the 'Surface Urban Heat Island' (SUHI) geographical phenomenon in Moscow has been studied. For this purpose, we used the measurements of the surface temperature T_S made by Moderate Resolution Imaging Spectroradiometer (MODIS) radiometer installed on Terra and Aqua satellites. As a result, T_S during the 2020 lockdown, both in the city and surrounding rural zone, was found lower than at the same calendar time in the previous 20 years due to the relatively cold spring.

The SUHI intensity as the difference between T_S inside Moscow and the surrounding rural zone around it during the lockdown was also lower than usual (on average in the previous 20 years), but this decrease is relatively small and non-significant. The Normalized Difference Vegetation Index (NDVI) in Moscow and Moscow region during the lockdown was close to its usual values, but the leaf area index (LAI) was significantly lower than its average values in the previous 20 years. Thus, the weakening of the SUHI during the lockdown in 2020 was caused mostly by lower heat loss due to transpiration in the rural zone. This was associated with the slowdown in vegetation development as a result of the cold spring. Besides, an additional possible reason was the reduction of human activity due to the collapse of many anthropogenic heat sources in the city.

According to long-term MODIS data, the SUHI intensity in Moscow and the surface temperature in Moscow region, as well as the NDVI and LAI values, do not demonstrate statistically significant long-term trends in the spring season over the past 21 years, despite climate changes.

In spring, during faster snow melting in cities, when it still persists in the rural zone, the SUHI intensity can be record high (up to 8 °C).

KEYWORDS: satellite data, surface temperature, surface urban heat island, SUHI intensity, COVID-19 pandemic lockdown, NDVI, LAI, vegetation, snow cover

CITATION: Lokoshchenko M.A., Enukova E.A (2022). Surface Urban Heat Island In Moscow During The COID-19 Pandemic Lockdown In 2020. Geography, Environment, Sustainability, 4(15), 134-144
https://DOI-10.24057/2071-9388-2021-116

ACKNOWLEDGEMENTS: The authors are grateful to Dr. M.V.Zimin and his colleagues from ScanEx Engineering and Technology Center for their help with the software and to Dr. O.V.Tutubalina for her useful advices. This work was supported by the Russian Science Foundation (Project 21-17-00210).

Conflict of interests: The authors reported no potential conflict of interest.

INTRODUCTION

As it is known, at the beginning of 2020, the terrible COVID-19 pandemic quickly spread around the world and caused many dramatic changes in both humankind and natural processes. Studies of the influence of COVID-19 on different geographical phenomena were collected, e.g., at the special issue of GES Journal in Vol. 14, No. 4, 2021 (https://ges.rgo.ru/jour/search/sections/30). Quarantine measures, including self-isolation of people in their houses, were implemented for the first time in most countries in the spring and summer 2020 (later, during the second wave of the pandemic in the autumn of 2020, they were again implemented in many countries, but not in the Russian Federation). As a result, human activity sharply slowed down, including industry, transport, energy sector, etc. The most evident influence of quarantine periods on the geographic envelope is a strong reduction of air pollution, e.g., in Moscow (Ginzburg et al. 2020); in eight cities of Pakistan (Ali et al. 2021); in various locations, especially in small cities in the Middle East (El Kenawy et al. 2021). However, it should also be noted that specific

weather conditions (calm and frequent inversions in anticyclones) lead to an increase in air pollution even during quarantine (Ginzburg et al. 2020). Among other things, the influence of the pandemic also led to the weakening of urban heat islands (UHI) in the surface air layer, e.g., in Moscow, according to Lokoshchenko and Alekseeva (2022). Possible reasons for this effect are the decrease of direct anthropogenic heat emissions and changes in the radiation balance in cities (weakening or disappearance of urban industrial haze, etc.).

Another phenomenon in urban climatology, besides the UHI, is the so-called 'surface urban heat island' (SUHI), i.e., a thermal anomaly in the surface temperature T_S field. This phenomenon has been studied in different cities of the world using satellite data of radiometric measurements (e.g., Rasul et al. 2015; Esau and Miles 2018; Lokoshchenko and Enukova 2020, etc.). The fundamental problems of satellite data use for urban climatology were discussed (Voogt and Oke 2003). As for Moscow, a comparison of satellite data about SUHI and *in situ* data of weather stations about UHI was carried out (Varentsov et al. 2019; Lokoshchenko and Enukova 2020; etc.). The SUHI is created not only due to the higher air temperature T over the city, but also due to different heat losses of the surface for precipitation evaporation and plants transpiration inside and outside cities. Thus, lower plant density in urban areas and artificial rainfall in cities lead to lower heat losses and, as a result, to a higher urban surface temperature.

Meanwhile, the available data on SUHI in the surface temperature field during the global lockdown in the spring of 2020, according to satellite data, are ambiguous. SUHI weakening was noted in several places. This is in the eight largest cities of Pakistan, according to MODIS data (i.e., data from Aqua and Terra satellites equipped with MODIS radiometer), on average by 20% (Ali et al. 2021), as well as in the cities of the United Arab Emirates (UAE), according to MODIS data, at least at night (Alqasemi et al. 2021). The surface of the urban area of New Delhi in April 2020 during the lockdown, according to MODIS data, was even marked by a strong 'cool island' instead of the usual 'heat island' in the T_S field (Mukherjee and Debnath 2020), just as it was observed in the dry season in Erbil (Rasul et al. 2015). The analysis of T_S in the seven biggest Indian megacities in April 2020 (during the lockdown) from Landsat-8 satellite images was presented (Dhruv Nanda et al. 2021). As a result, T_S in April 2020 was found 0.3÷7.1 ºC lower than in April of the two previous years (2018 and 2019) in urban areas of 6 out of 7 mega-urban agglomerations except for Kolkata. A similar analysis was conducted for the urban agglomeration of Yogyakarta, Indonesia, using the data of the same Landsat-8 satellite (Arrofiqoh and Setyaningrum 2021). It showed that T_S during the lockdown in May 2020 was also lower than before the pandemic and after the lockdown. However, neither Dhruv Nanda et al. (2021), nor Arrofiqoh and Setyaningrum (2021) estimated the SUHI values for Indian and Indonesian cities. In other words, it remains unclear whether T_S decreased only in urban areas or in adjacent rural zones as well.

In contrast to these results, the SUHI of cities in the Indus and Ganges basins, according to satellite data in the spring of 2020, increased by 0.2÷0.4 ºC in the daytime. This was due the delay in the winter crops harvest under the quarantine that led to additional greening of the countryside and, consequently to an increase in heat losses by transpiration (Chakraborty et al. 2021). The study of SUHI across 21 metropolitan areas in the Middle East with the use of MODIS data from Aqua satellite also demonstrates mixed results (El Kenawy et al. 2021). The mean intensity of daytime SUHI during the lockdown (from March to June 2020) in different cities either increased or slightly decreased. The intensity of daytime SUHI in many mega-cities such as Tehran, Ankara and Istanbul, showed anomalous increases of even more than 2 ºC compared to the long-term (2003÷2019) average.

Thus, the impact of the lockdown period on SUHI intensity is ambiguous and can be different depending on meteorological and geographic conditions. The main goal of the authors was to assess the influence of the lockdown on the land surface temperature and SUHI intensity for Moscow. To do this, we calculated the values of both parameters during the lockdown in 2020 and compared them with the values for the same calendar time, averaged over the previous 20 years. Another task was to analyze whether the observed differences are associated with additional heat losses by transpiration.

MATERIAL AND METHODS

We used the data from Terra and Aqua satellites launched in December 1999 and May 2002, respectively. These satellites in a Sun-synchronous orbit at an altitude of about 700 km above the Earth are the part of the so-called Earth Observing System (EOS). The imaging bandwidth of both satellites is 2330 km. They are equipped with MODIS radiometers with 36 channels ranging from 0.45 to 14.36 µm. Among other things, MODIS data provide measurements of the standard Land Surface Temperature parameter (LST, or T_S) by spectral brightness in two channels: 31st and 32nd with the wavelengths of 10.78÷11.28 and 11.77÷12.27 µm, respectively. T_S measurements have spatial resolution of 1 km and an accuracy of ±1 ºC for the land (Steitz et al. 1999). Besides T_S, special algorithms also allow calculating additional parameters from MODIS data, including NDVI, LAI, etc. The data from Terra and Aqua satellite images are available at the link:
https://ladsweb.modaps.eosdis.nasa.gov/archive/allData/61/MYD021KM/

Terra and Aqua fly over Moscow region twice a day with an interval of 1 hour and 50 minutes: in the late morning and early afternoon (from 11 to 12 a.m. and from 1 to 2 p.m. Moscow time, respectively) and at night. However, here we considered only daytime images of both satellites since the quality of their night-time data is worse. At night, especially in winter, Moscow is often located on the edge of the image band, which leads to large distortions. The methodical base of our study is detailed by Lokoshchenko and Enukova (2020).

The SUHI intensity (ΔT_S) was calculated as the mean difference of T_S values for the samples of all urban and rural elementary cells with an area of 1 km^2:

$$\Delta T_S = \frac{\sum_{i=1}^{n} T_{U_i}}{n} \frac{\sum_{j=1}^{m} T_{R_j}}{m} \quad (1)$$

where n and m are the number of cells in Moscow and Moscow region, respectively; T_U and T_R are surface temperatures in each cell inside the city and in rural zone, respectively. It is known that in 2012, the city territory was declared to be greatly expanded by 2.4 times, but so-called 'new Moscow' is still a rural area with low population density. Moreover, here we analyzed the period from 2000 to 2020. Thus, most of that time Moscow was in its old borders. That is why Moscow city was considered by authors within its traditional borders from 1992 to 2012, when the so-called 'old Moscow' had the shape of a turtle

(a simple ellipsoid with six outer prominences); and its area was 1081 km^2. The surrounding rural zone was taken as a rectangle circumscribed around the administrative boundaries of Moscow region, including the entire territory of this region and, in addition, the adjacent districts of neighboring regions. Its area is 94,851 km^2. Evidently, both urban and rural areas are not homogeneous because the former includes urban green spaces, whereas the latter includes small towns in the suburbs outside the city borders (Climate of Moscow 2017).

The main problem with the satellite data in mid-latitudes is frequent cloudiness, which greatly reduces the number of images available for the surface temperature analysis; although recently a new approach has been suggested for the analysis of all-weather satellite data about SUHI. It is based on merging of satellite- and ground-based observational data using reanalysis, which allows indirectly reconstructing the LST under clouds (Yangsiyu Liao et al. 2021). As it is known, clouds and wind speed strongly affect the SUHI intensity (e.g., Morris et al. 2001). As a result, the SUHI is stronger in cloudless and calm conditions in anticyclones (e.g., Półrolniczak et al. 2017). This creates a bias in the SUHI intensity satellite estimations without an additional use of the ground-based data.

A clear sky over the entire Moscow region in strong anticyclonic conditions can be observed in rare cases (on average it is only 3% of the total sample of images). Numerical experiments conducted by the authors demonstrate that the analysis of the SUHI intensity is still possible if clouds cover less than 20% of the urban area and less than a half (50%) of the rural zone around the city. In such conditions the possible bias in the SUHI intensity due to clouds is within ±0.2 of the intensity value, i.e., this deviation is relatively small (Lokoshchenko and Enukova 2020). Thus, all images from both satellites were initially tested for a part of an open area without clouds, and then only the cases when this part exceeded critical values, were accepted for further analysis.

The standard normalized difference vegetation index (NDVI) is a well-known parameter regularly measured by satellites since 1981 (EOS Data Products Handbook 2000). It is determined as the ratio of the difference between reflectivity in the red (where it is lower due to radiation absorption by plants) and the near infrared bands of the spectrum to their sum. NDVI calculations using MODIS data are based on the comparison of two channels: 0.62÷0.67 μm (red) and 0.841÷0.876 μm (near infrared) bands. As it is known, NDVI can vary from -1 to 1, but negative values are associated with snow, ice, water, or artificial surfaces such as concrete and asphalt (https://gis-lab.info/qa/ndvi.html). Above green vegetation, NDVI is usually between 0.2 and 0.8, and values exceeding 0.5 indicate dense vegetation. The global distribution of NDVI is presented, e.g., in EOS Data Products Handbook (2000).

Another important parameter that indirectly indicates surface heat losses by transpiration is the so-called 'Leaf Area Index' (LAI). Various methods are used to determine LAI, including direct measurements. Among other things, satellite indirect LAI data are also calculated using MODIS software (e.g., MOD15A2 as one of Standard MODIS LAI/FPAR products) by special spectral analysis of the detected signal. The methodical basis and verification of the LAI measurements are presented by Wenze Yang et al. (2006). However, this parameter is available only outside urban areas and only on average over eight-day periods.

In general, the sequence of our analysis was as follows: preliminary visual selection of suitable images → their processing in the ScanEx Image program → their testing by the criterion of the highest permissible threshold of clouds cover → calculations of the T_S, SUHI intensity, NDVI and LAI mean values → adding them to databases.

RESULTS AND DISCUSSION

Surface Urban Heat Island in Moscow during lockdown in 2020

Strict quarantine measures (a full lockdown) during the COVID-19 pandemic were implemented in Moscow and other Russian cities only once from March 30 to June 8, 2020. At that time, the entire population had to stay inside their houses, except for the workers of the city emergency services. During these 71 days, only 12 images from both satellites were recorded in clear sky or at least with low cloudiness, which meets our criteria (no less than 80% of the urban area and no less than 50% of the outer comparison zone were open and available for analysis). These images are of April 1 (Terra), April 4 (Aqua), April 9 (Terra), April 22 (Terra), May 1 (Aqua), May 2 (both Terra and Aqua), May 3 (both Terra and Aqua), May 11 (both Terra and Aqua), and June 6.

Evidently, this number (12) is less than the classical statistical sample. Nevertheless, it is still enough for the mean value calculation in the first approximation. To test its reliability, we can use the data about T on weather stations. During the COVID-19 strict lockdown the maximum space UHI intensity as a difference between Moscow centre (Balchug station) and rural zone outside the city (on average of 13 rural weather stations) averaged 1.46 ºC per day over 71 days (Lokoshchenko and Alekseeva 2022). Separate calculation of the same parameter only at noon (the closest reading of T to Aqua and Terra flights) during 71 days showed the value of 0.60 ºC. This is not surprising because, as it is known, the UHI is weaker in the daytime. An additional calculation only at noon of nine clear or low-cloud days, when the satellite images were accepted for our analysis, gives nearly the same UHI intensity, and it is 0.58 ºC. Thus, the mean SUHI intensity reflects reality well and is not biased relative to the value for all days of the lockdown.

For the comparison with the lockdown period in 2020, all images from both satellites were analyzed for the same period (from March 30 to June 8) for the entire duration of their flight from 2000 to 2019, and the SUHI intensity in Moscow was calculated for each image. The total sample of images available for the analysis during 20 years until 2020 is 275. Average values of T_S both in Moscow urban area and in the rural zone are presented in Table 1. As it is evident, firstly, the surface temperature in the spring and early summer of 2020 was lower (by 4.3 ºC in Moscow and by 4.1 ºC in Moscow region) than usual for these seasons. Besides, the SUHI intensity as a difference between them was also lower than usual (2.6 ºC, which is 0.2 ºC lower than the average for the previous 20 years). As it was shown above, the SUHI weakening during the global lockdown was observed in many cities in Pakistan (Ali et al. 2021), UAE (Alqasemi et al. 2021), and India (Mukherjee and Debnath 2020; Dhruv Nanda et al. 2021), Indonesia (Arrofiqoh and Setyaningrum 2021), etc. However, this result does not appear to be statistically significant in Moscow conditions, given the large scatter in the data (shown by the confidence intervals in Fig. 1 a).

Let us use the well-known Student criterion Z to evaluate the statistical significance of the differences between conditions in 2020 and in the previous 20 years. It should be noted that Z criterion is parametric and may be used when the distribution corresponds to the Normal law.

Indeed, the SUHI intensity distribution is close to Normal law: Pearson's chi-square (χ^2) test has a relatively low value 10.2 at 6 freedom degrees which is less than the critical value (12.6) for the 5% significance level. So, we can accept correspondence to the Normal law at the 0.95 probability and, hence, correctly use the Student criterion:

$$Z = \frac{(\overline{X} - \overline{Y})}{\sqrt{\sigma^2(X)/n + \sigma^2(Y)/m}} \quad (2)$$

where X and Y are the average values of the two samples; $\sigma^2(X)$ and $\sigma^2(Y)$ are their dispersions; n and m are sample sizes. It was found that for the SUHI intensity Z = 0.39; for the surface temperature in Moscow and Moscow region Z values are 1.86 and 1.90, respectively. Therefore, all three values are less than the critical Z value (1.97) for the 5% significance level. Thus, neither SUHI intensity, nor T_S demonstrate significant differences between the lockdown period in 2020 and the same period on average in 2000÷2019.

It should be noted that during the lockdown in 2020, all images available for the analysis except for only one (of June 6) were taken before May 12. However, the annual course of SUHI intensity has a clear maximum in summer due to intensive vegetation in rural zone and, as a result, intense heat losses by transpiration of plants (Lokoshchenko and Enukova 2020). In other words, in late spring and early summer, the SUHI intensity grows rapidly due to vegetation development outside the city. Therefore, in June it is significantly higher than in March. However, May and early June in 2020 were observed in Moscow by cyclonic weather and high cloudiness (Lokoshchenko and Alekseeva 2022) so only one image was received for the analysis since May 12. That is why the results of comparing the SUHI intensity in 2020 and the 2000÷2019 average for the full lockdown period in 2020 (Table 1) may be distorted. Therefore, all results of the analysis were recalculated within a narrower lockdown period from March 30 only to May 11, not to June 8 (see Table 2 and Fig. 1 b).

As it can be seen from Fig. 1 b, the surface temperature T_S both in Moscow and in the rural zone varies until May 11th in a wide range from 7.8 °C in 2005 to 25.5 °C in 2000, and from 3.8 in 2005 to 23.1 in 2000, respectively (for the full lockdown period in Fig. 1 a) the dynamics is similar). The close relation between T_S inside and outside the city is obvious – the correlation coefficient between mean annual values of both parameters is 0.98. The total sample of all available Terra and Aqua images for the partial lockdown period until May 11th for 21 years is 167, including 11 images in 2020. On average for 2000÷2020, T_S is 18.11 °C in Moscow and 15.56 °C in the outer zone. In the city, this parameter is on average higher each year, so SUHI represents a thermal anomaly that is stable over time.

Table 1. Comparison of different parameters during COVID-19 full lockdown period in 2020 from March 30th to June 8th and at the same time in 2000÷2019 based on Aqua and Terra satellite data

	Moscow	Moscow region (outer zone)	Difference
Surface temperature, °C			
2020 (12)	17.2 ± 7.8	14.6 ± 7.2	2.6
2000÷2019 (275)	21.5 ± 6.4	18.7 ± 6.5	2.8
Normalized Difference Vegetation Index (NDVI)			
2020 (12)	0.28 ± 0.11	0.38 ± 0.13	-0.10
2000÷2019 (275)	0.35 ± 0.16	0.47 ± 0.19	-0.12
Leaf Area Index (LAI): up to June 9			
2020		1.7 ± 0.8	
2000÷2019		2.1 ± 1.3	

The first values are mean; the second are standard deviations (σ). Sample data (number of images) are given in brackets.

Table 2. Comparison of different parameters during COVID-19 partial lockdown period in 2020 from March 30th to May 11th and at the same time in 2000÷2019 based on Aqua and Terra satellite data

	Moscow	Moscow region (outer zone)	Difference
Surface temperature, °C			
2020 (11)	16.7 ± 8.0	14.4 ± 7.5	2.3
2000÷2019 (156)	18.2 ± 6.3	15.6 ± 6.8	2.6
Normalized Difference Vegetation Index (NDVI)			
2020 (11)	0.26 ± 0.09	0.36 ± 0.11	-0.10
2000÷2019 (155)	0.25 ± 0.12	0.34 ± 0.15	-0.09
Leaf Area Index (LAI): up to May 16			
2020		1.2 ± 0.4	
2000÷2019		1.3 ± 0.6	

The first values are mean; the second are standard deviations (σ). Sample data (number of images) are given in brackets.

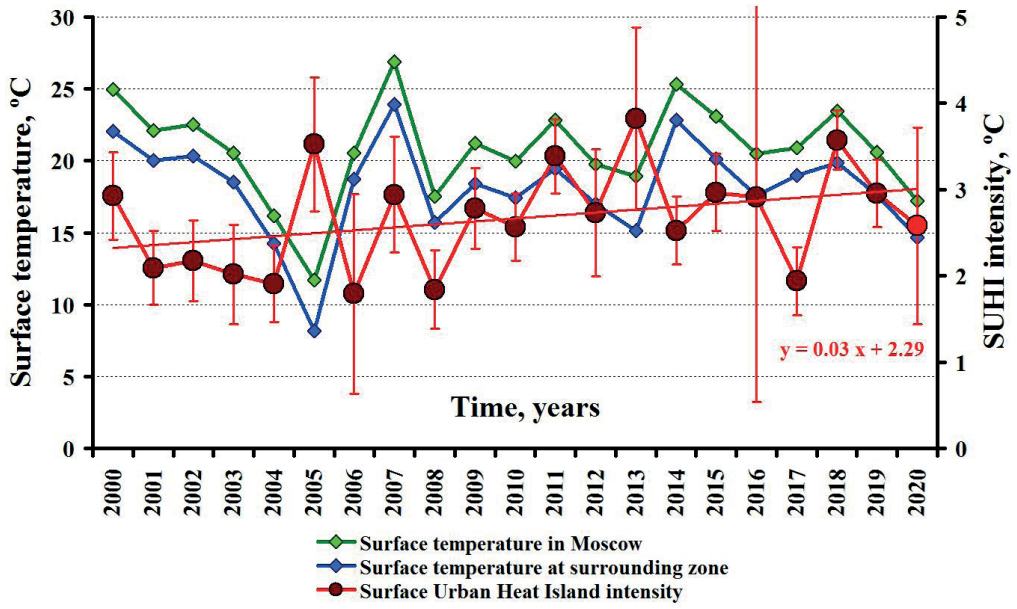

a) Full lockdown period (from March 30 to June 8);

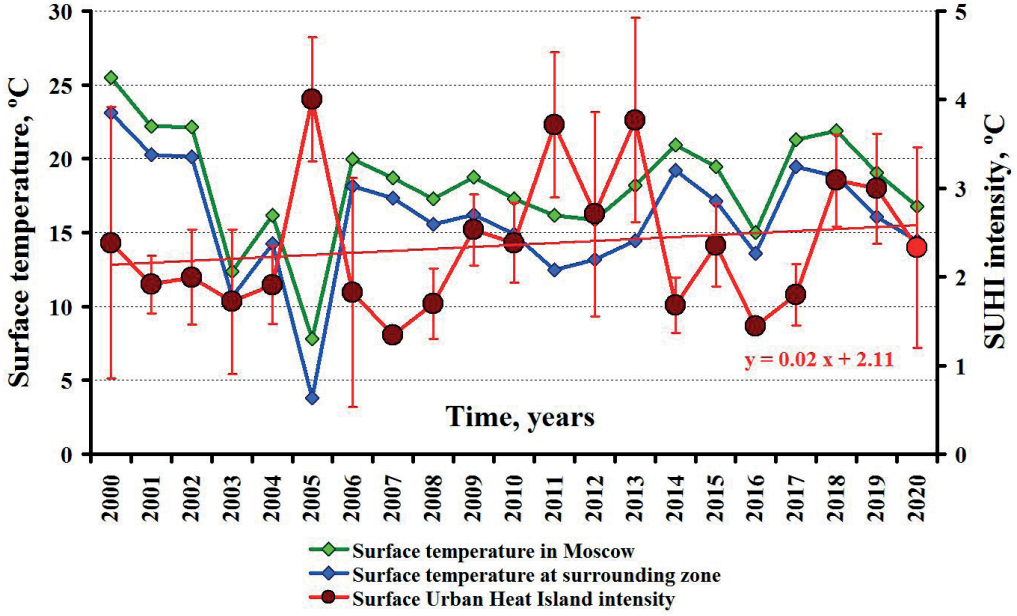

b) Partial lockdown period (from March 30th to May 11th).

Fig. 1. Average surface temperature and Surface Urban Heat Island intensity in Moscow during the lockdown period in 2020 and on the same dates in other years (from 2000 to 2019), in °C

Confidence intervals are calculated with the 0.05 significance level

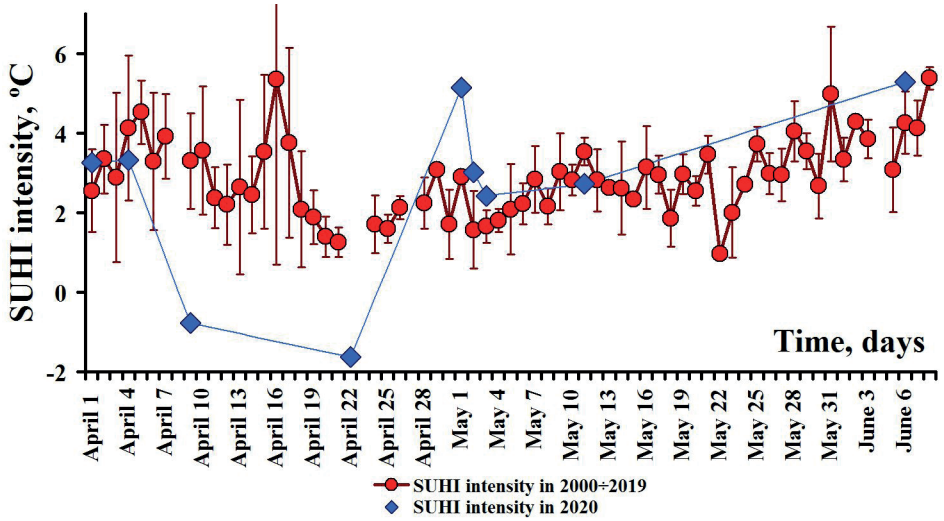

Fig. 2. Surface Urban Heat Island intensity in Moscow on certain days during the lockdown period in 2020 and on average from 2000 to 2019, in °C

Confidence intervals are calculated with the 0.05 significance level

The average annual SUHI intensity during this period varies from 1.3 ºC in 2007 to 4.0 ºC in 2005; on average for 21 years, the SUHI intensity from March 30 to May 11 is 2.55 ºC. Such large changes in this parameter from year to year are explained by the different dates of images taken for studying (early April or May), the presence or absence of snow cover, the degree of vegetation intensity, etc. For example, the SUHI intensity in 2005 was extremely high, since all 12 images before May 11 were recorded in the first decade of April (until April 10), when even in Moscow there was still a heavy snow cover, and its depth was extremely high (from 47 cm (!) in April 1 to 4 cm in April 9). Evidently, in any city there are many surfaces cleared of snow (roads, roofs of buildings, etc.) which contribute to a higher T_S. Besides, snow melts faster in the urban area than in the rural zone, so the difference between T_S inside and outside the city is especially large during the snowmelt. Strong influence of snow cover was also registered in 2013 when it finally disappeared on April 16th in Moscow (according to the data of MSU Meteorological Observatory) and several days later at rural zone. The SUHI intensity in 2013, as it is seen from Fig. 1 a), was 3.8ºC on average of the data of all 12 images during the full lockdown period, but it was equal to 5.4 ºC before and during snow cover disappearing (on average from 5 images from April 12 to April 17) and only 2.7 ºC later (on average from 7 images from May 2 to June 3). It is noteworthy that the highest SUHI intensity value of 7.7 ºC was observed on April 16, i.e. just on the day when snow cover disappeared in the city, but still remained at rural zone.

Regarding ΔT_S values on different days, it should be noted that the maximum value is 7.7 ºC on April 16, 2013, whereas the minimum value is -1.6 ºC on April 22, 2020. Such a high SUHI intensity on April 16, 2013, is not surprising, because the day before, the snow cover depth still was 15 cm in Moscow. Thus, such a strong SUHI is explained by the different rate of snow melting in the city and in the rural zone. On the contrary, only three times the SUHI intensity was negative, so this phenomenon was found as an inverse 'cool island', besides April 22, 2020, in two more cases: April 9, 2020 (-0.8 ºC) and May 2, 2006 (-0.1 ºC). It was shown that cases of a weak 'cool island' involving the entire city are extremely rare in Moscow. For 8 years (from 2008 to 2015) ΔT_S was slightly below 0 ºC in only 8 out of 561 images (Lokoshchenko and Enukova 2020).

In addition to the average value of the SUHI intensity during the lockdown, it is also important to study its dynamics during this period. Fig. 2 shows the values of this parameter during the lockdown in 2020 (either from one image, or an average from two images during the same day). For comparison, the average SUHI intensity for each day was calculated from all available images in 2000÷2019. As it is seen, SUHI in Moscow at the beginning of the lockdown (in the first days of April) was close to its usual intensity. Then it was significantly weaker than on average for 20 years until the end of April so its intensity on April 9 and April 22 was even negative and, finally, except for only one image with an unexpectedly high value (on May 1), it again became close to its usual intensity.

The results for the partial lockdown period are also shown in the two maps in Fig. 3. The spatial distribution of the surface temperature field is calculated using the standard interpolation software Surfer10.1 with a step of 1 ºC. Both maps were created by combining samples of images with a spatial resolution of 15 km by use of kriging interpolation method. The margins of Moscow city and the administrative boundaries of Moscow region are shown with small violet and orange circles, respectively. Both maps demonstrate two major features that are total geographical zoning (general growth of T_S values from northwest to southeast) and, besides, the SUHI as a positive thermal anomaly around Moscow city. As can be seen, on average for 20 years before the pandemic, the surface temperature both in Moscow and in Moscow region was higher than in 2020. The SUHI is expressed in both cases by three closed or semi-closed isotherms but they are quite different: from closed +20 ºC inside the city to semi-closed +18 ºC around the city on average for 2000÷2019, and much lower values from +15 to +13 ºC in 2020 on the right map.

Thus, during the lockdown in the spring of 2020, the SUHI intensity in Moscow was lower than the average for 20 previous years (by 0.3 ºC for the partial lockdown period until May 11 and by 0.2 ºC for the full lockdown until June 8). However, this reduction was found as statistically non-significant with the 0.95 confidence probability. Moreover, the weakening of SUHI in Moscow on average during the lockdown period is caused by extremely low values only in two days (Fig. 2). This result is unexpected, since the UHI in the surface air layer of Moscow during the lockdown was much weaker than in the same period in two previous years (Lokoshchenko and Alekseeva 2022). In fact, in 2018 and 2019 the SUHI as well as the UHI was stronger than in 2020 during the lockdown (as one can see in Fig. 1) but differences for the SUHI, unlike the UHI, are non-significant even for these two years. Possible reason is an additional influence of clouds, which weaken the UHI, as the UHI intensity was calculated for all days of the lockdown whereas satellite data is available only in 9 out of 71 days (Lokoshchenko and

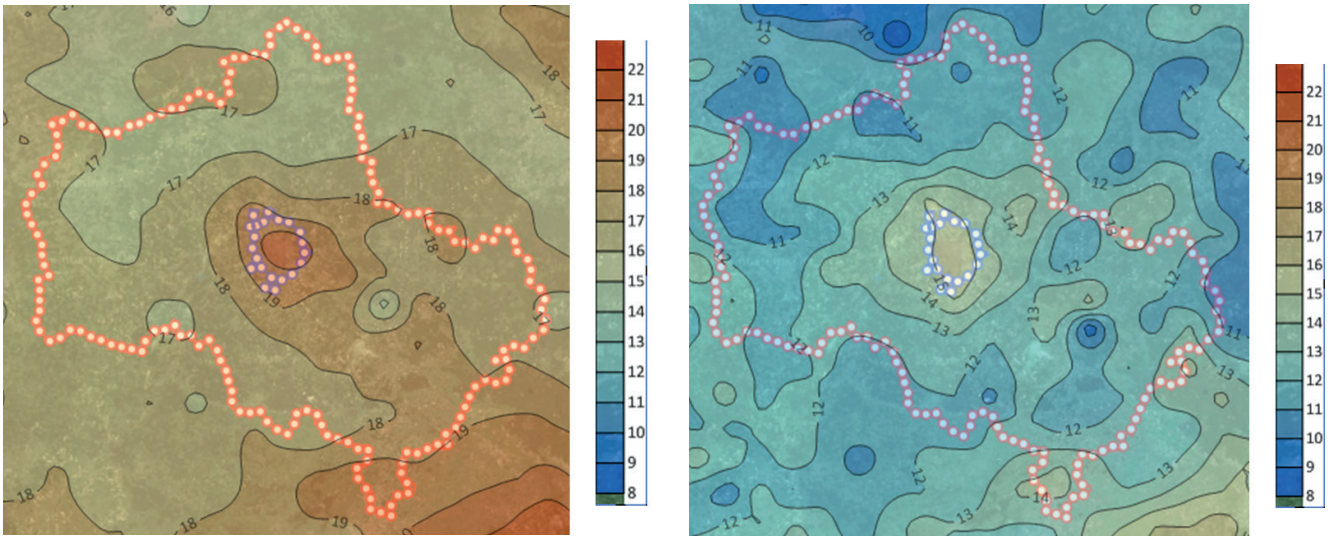

Fig. 3. Maps of the surface temperature T_S in Moscow region on average for the period from March 30 to May 11 in 2000÷2019 (left) and in 2020 (right), in ºC

Orange dots indicate Moscow region boundaries; the violet dots indicate the margins of Moscow city. The scale of T_S is shown to the right of each map

Alekseeva 2022). In other words, in conditions of clear sky the SUHI weakening during the lockdown was not such a strong as the UHI weakening during the entire lockdown period.

To explain this effect in detail, we should also analyze the weather conditions during the lockdown and, besides, should take into account the specifics of the SUHI phenomenon, the intensity of which is sensitive to vegetation activity.

Another additional result of our analysis is the slow changes in the Moscow SUHI intensity in time in the past 21 years. As it can be seen from Fig. 1, both linear trends of this parameter are positive, but the linear regression coefficients are extremely small. The SUHI intensity has been growing since 2000 by an average of only 0.03 °C/year during the full lockdown period and by 0.02 °C/year during the partial one. Evidently, both trends are statistically non-significant due to large dispersions of the mean annual data.

Weather features before and during the lockdown in 2020

Let us discuss the weather specifics in the winter and spring of 2020 in Moscow. Evidently, the weather influences both surface temperature and vegetation activity. The winter of 2019÷2020, which ended shortly before the start of the COVID-19 pandemic, was extremely warm in Moscow. Due to the intense Icelandic Low, strong southern and southwestern flows of warm maritime Polar air masses invaded Moscow region almost continuously, so that in the winter of 2020 there was not a single invasion of cold Arctic air masses. As a result, the air temperature T in Moscow was a record high during the entire season from December 1, 2019 to February 29 (it should be noted that almost regular meteorological measurements started in the city in October 1779). The mean monthly T in December 2019 was +0.6 °C (that is the second record value; since 1779, only once the air temperature in Moscow was even higher in December: +1.3 °C in 2006). In January 2020, the mean monthly T was -0.1 °C, which is a new absolute maximum since 1780 (the next, second record high value of T in January was -1.4 °C in 2007). Mean monthly T in February 2020 was also extremely high, that is -0.3 °C (this was the second record; T was higher only once: +0.2 °C in 1990). Thus, all three winter months in Moscow were extremely warm, so the mean winter air temperature became record high and, for the first time, positive during the history of meteorological measurements: +0.07 °C (see Fig. 4a). Until 2020, the warmest winter in Moscow was 2007÷2008 with the mean T = -2.9 °C which is much less.

March 2020 was also extremely warm in Moscow. The mean monthly T was +4.0 °C, which is the second high record value since 1780, as well as in December and February (only once it was higher in March: +4.9 °C in 2007). The inevitable consequence of such warm winter and early spring is almost snowless conditions. Steady snow cover (i.e., a cover which exists during the longest period in the cold season) in the winter of 2019÷2020 in Moscow appeared extremely late (on January 23), and finally melted extremely early (on March 2). Therefore, it

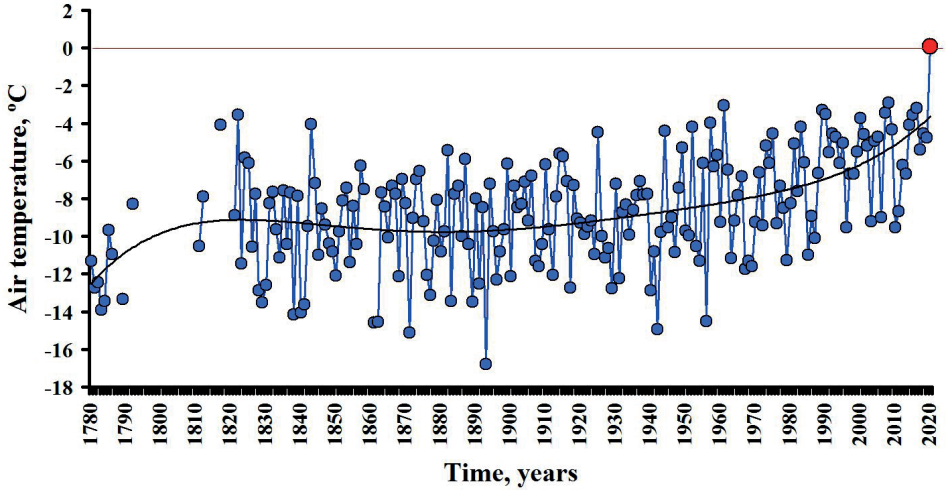

a) Winter (December ÷ February);

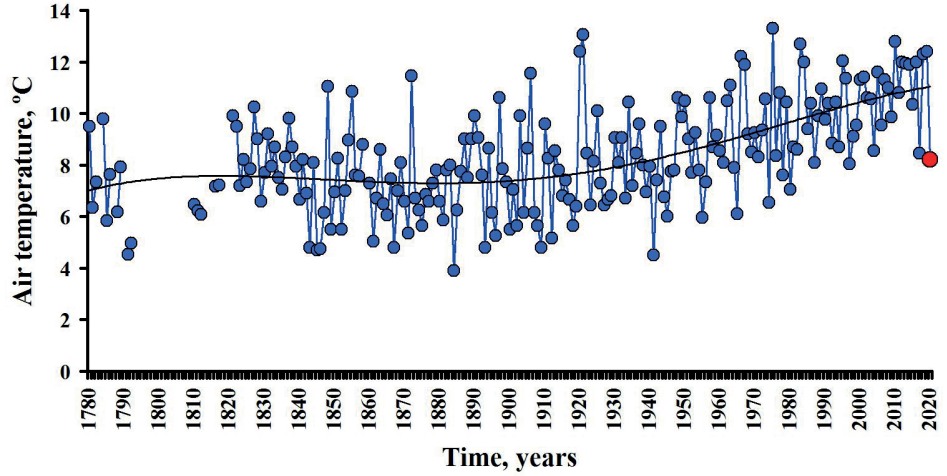

b) Middle and late spring (April and May).

Fig. 4. Long-term dynamics of air temperature in Moscow averaged over certain seasons during the entire history of meteorological measurements, in °C

Data for 2020 is marked with a red dot.
Black lines are the 5th degree polynomial trends

existed for an extremely short time (40 days only). In fact, the lifetime of steady snow cover was even shorter, since in the last days of February it remained only in places. Besides, steady snow cover was extremely thin (the highest depth for the entire cold season was only 15 cm, which is a record low value according to the data of MSU Meteorological Observatory since at least 1954). After March 2, there were only two episodes of short-living snow cover in the city lasting 4 and 3 days (from March 15 to March 18 and from March 31 to April 2).

However, unlike winter and March, the middle and late spring of 2020 in Moscow was cool and cloudy. Moscow was frequently located in frontal zones of Arctic cyclones, or at their rear. Sometimes Russian capital was also near centers of local cyclones. As a result, mean monthly T in April and May (4.8 °C and 11.6 °C, respectively) was significantly lower than the climatic norm for these months (7.0 °C and 13.5 °C, respectively, for April and May, on average for 1981÷2010 in Moscow by the data of MSU Meteorological Observatory). As can be seen from Fig. 4b, such a low mean air temperature in both months in Moscow was registered for the first time since 1997. Thus, we can assume that the unusually early vegetation development in 2020 dramatically slowed down in mid-spring and, as a result, the SUHI intensity decreased in April.

Normalized Difference Vegetation Index (NDVI) during the lockdown in 2020

One of the possible reasons for the SUHI intensity changes is vegetation growth, which leads to additional heat loss by the surface in green rural area compared to urban area. It is difficult to measure directly the heat loss for transpiration by plants. However, we can estimate this indirectly using satellite data for some indexes (e.g., NDVI) which indicate the vegetation intensity.

As well as the SUHI intensity, the NDVI values during the lockdown in Moscow in 2020 are available from the 12 images received from Aqua and Terra satellites for the total period from March 30 to June 8, including 11 images for the period until May 11. As can be seen from Table 1 and Fig. 5, the average NDVI value during the entire lockdown period is 0.28 ± 0.11 (the second value is standard deviation σ) in Moscow and 0.38 ± 0.13 in the outer rural zone outside the city. For an incomplete period only until May 11th (Table 2) NDVI values are 0.26 ± 0.09 and 0.36 ± 0.11 for the city and rural zone, respectively. Both the highest values in different images during the lockdown are 0.50 in Moscow and 0.61 in Moscow region; the lowest values are 0.10 and 0.16 in Moscow and Moscow region, respectively. The highest values were received on the last flight on June 6, whereas both the lowest ones were received on the first flight on April 1.

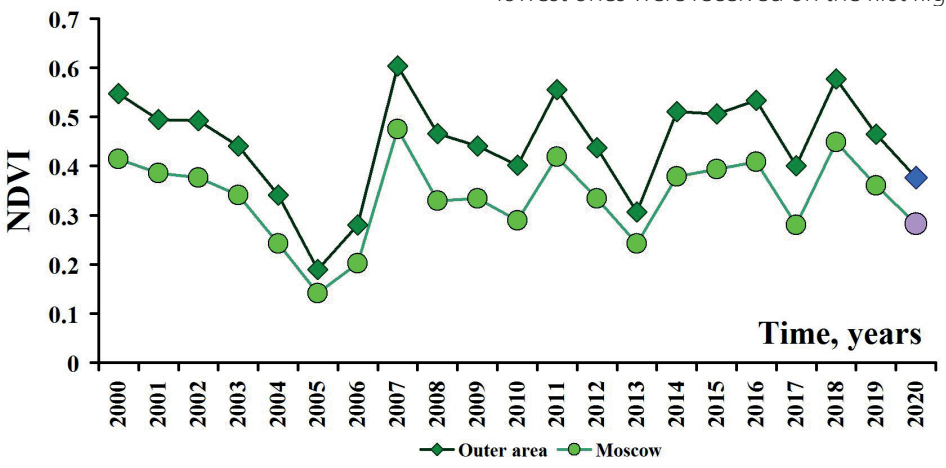

a) Average NDVI for the period from April 1 to June 8 in 2000÷2020;

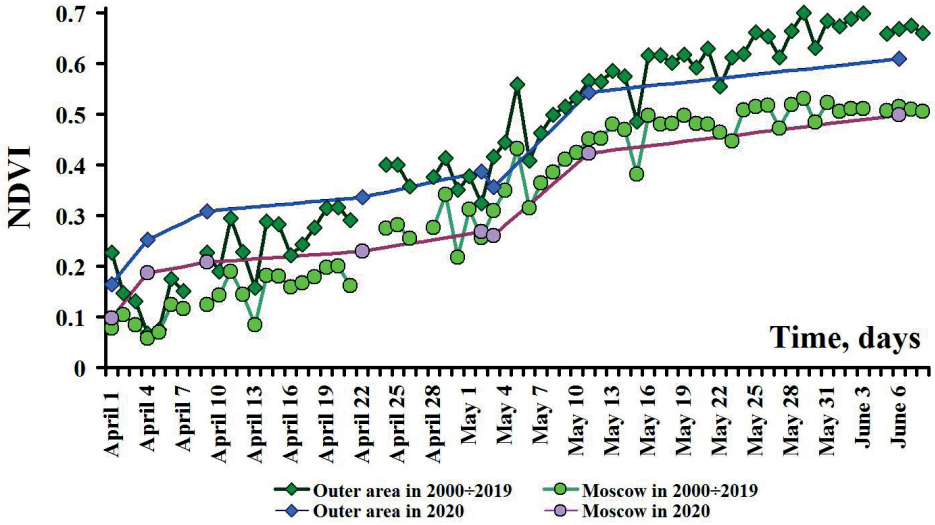

b) NDVI values on certain days from April 1 to June 8 averaged over 2000÷2019 and in 2020.

Fig. 5. Comparison of NDVI values in Moscow and Moscow region based on MODIS data during the lockdown in 2020 and on the same dates in other years (in 2000÷2019)

As can be seen from Table 1, the average NDVI value for 2000÷2019 during the entire lockdown period in 2020 is 0.35 ± 0.16 in Moscow and 0.47 ± 0.19 in Moscow region. For the period from March 30 to May 11, the NDVI values are 0.25 ± 0.12 and 0.34 ± 0.15 in the city and rural zone, respectively. The highest NDVI values for 20 years at the dates of the full lockdown are 0.57 (May 26, 2014) in Moscow and 0.73 (May 29, 2018) in Moscow region. The lowest NDVI values in 20 years are 0.03 and 0.06 in the city and in rural zone, respectively. Both values were measured on April 3, 2011, when the snow cover depth at MSU MO was extremely high for that time, and it was 36 cm. Nearly the same NDVI values in the rural zone (0.06) were observed on April 4 and April 5, 2005, when the snow cover depth was also extremely high: 37 and 34 cm, respectively. Evidently, green vegetation in these conditions is almost absent, except for coniferous trees.

The average NDVI values during the calendar time of the lockdown period in 2020 in different years since 2000 are presented in Fig. 5a. As can be seen, firstly, the NDVI in Moscow region is always higher than in the city, which is not surprising due to the greater number of green areas in the rural zone. Secondly, the difference between average urban and rural values of NDVI is almost always the same (about -0.1) except only for rare cases (e.g., in 2005, when most images were taken in conditions of late snow cover, which remained until April 10, and there was almost no green vegetation both in the city and in the rural zone). Moreover, as it can be seen from Fig. 5a, both NDVI values and their difference in 2020 are quite usual compared to the previous 20 years. Indeed, average values of NDVI for both the city and rural zone for the period until May 11th in 2020 and from 2000 to 2019 are almost the same (Table 2). Their difference on average in the previous 20 years is also close to the value in 2020 (-0.12 for the full lockdown period and -0.09 for the period until May 11). It is noteworthy that the increase in the absolute value of this difference with the lengthening of the averaging period is quite logical due to the rapid vegetation growth in late May and early June.

Besides the average values of NDVI, it is also important to understand the dynamics of this parameter during the lockdown. To do this, the average NDVI values were calculated for certain days both in 2020 and in 2000÷2019 (Fig. 5b). As it can be seen at the beginning of the lockdown period (April 4 and April 9) NDVI was higher than the average for the previous 20 years. In the middle of this period (April 22, May 2, 3 and 11), the values in 2020 and on average for 2000÷2019 are close to each other. Finally, at the end of lockdown (on June 6), the NDVI in the rural zone in 2020 was, on the contrary, lower than usual. The evident reason for such dynamics is, firstly, the extremely hot and almost snowless winter in Moscow, which led to early vegetation development and, secondly, the cold spring, which later slowed down this development. Nevertheless, in general, the NDVI values during the lockdown in Moscow were close to usual ones both in the city and in the rural zone.

Leaf Area Index (LAI) during the lockdown in 2020

One more important parameter, which is available from satellite data, is the Leaf Area Index (LAI). It may be estimated only at rural zone and, hence, cannot indicate SUHI as a difference between values of LAI in urban and rural zones. Nevertheless, it clearly reflects the vegetation development and its changes in time. Thus, the LAI values significantly complement the data about NDVI.

The LAI values were calculated for the outer rural zone (rectangle around Moscow region margins not including the city) for nine separate periods of eight days from March 30 to June 9. The results are presented in Fig. 6 and in Tables 1 and 2. They were received for all years except 2001.

The LAI value in Moscow region averaged over this calendar time is equal to 2.08 for the period of 2000 and 2002÷2019, and 2.06 for the period of 2000 and 2002÷2020. As can be seen, the leaf area index value on average for the full lockdown period in 2020 (1.67) is the lowest among all other years for the period (Fig. 6a), although, taking into account confidence intervals with the 0.95 confidence probability, this reduction is not statistically significant.

The analysis of the average LAI value is insufficient. It is also important to study the dynamics of this parameter during the lockdown. That is why LAI was also compared for each separate 8-day period in 2020 and on average in the previous 19 years (Fig. 6b). It is not surprising that during the spring and early summer, in conditions of developing vegetation, the LAI value averaged over 2000 and 2002÷2019 increased monotonically from 0.77 on March 30÷April 6 to 3.95 on June 2÷9. It is also evident that this growth gradually slows down in June as leaf size approaches its upper limit. As we can see, at the beginning of the lockdown (during the first and second eight-day periods), the LAI in 2020 was slightly higher than usual, evidently due to the warm and almost snowless winter. However, later, their ratio became opposite. During the third and fourth eight-day periods in the second half of April, the LAI value in Moscow region in 2020 was only a bit lower than the average for the previous 19 years, but later the gap between them increased. Since the beginning of May, the difference between LAI values in 2020, and in 2000, 2002÷2019 became statistically significant and in the second half of May its absolute value increased to -1.1÷-1.2. The probable reason for this was the cold spring, which slowed down the development of vegetation. Thus, the LAI dynamics confirms that heat losses by transpiration during the COVID-19 lockdown in 2020 in Moscow region were significantly lower than usual as a result of cool spring.

Influence of different factors on SUHI during the lockdown in 2020

Therefore, after analyzing of all parameters we can define the factors that really influenced on the SUHI in Moscow during the lockdown. Evidently, a decrease in human activity was not the main cause of the SUHI intensity decrease because it was insignificant in the comparison of other years. Apparently, the weakening of the SUHI in Moscow at that time was caused mostly by a slowdown of vegetation development due to specific weather conditions. The Pearson correlation coefficient between monthly-averaged values of the NDVI difference between rural zone and Moscow, and the SUHI intensity (i.e. the T_S difference between Moscow and rural zone) during the period from 2000 to 2019 is -0.47. According to the Fischer's Z-test , this coefficient is statistically significant at the 0.99 probability (for the sample size n = 40 of Aprils and Mays). Thus, the vegetation index really affects the SUHI intensity.

However, a reduction of anthropogenic heat sources during the lockdown is another factor, which, probably, also influenced on the SUHI intensity. Firstly, the contribution of reduced human activity to the weakening of the UHI in the surface air layer in Moscow at that time was shown in (Lokoshchenko and Alekseeva 2022). Evidently, both phenomena (UHI and SUHI) are related to each other. Secondly, we can indirectly demonstrate an impact of the COVID-19 lockdown by comparison of the SUHI intensity

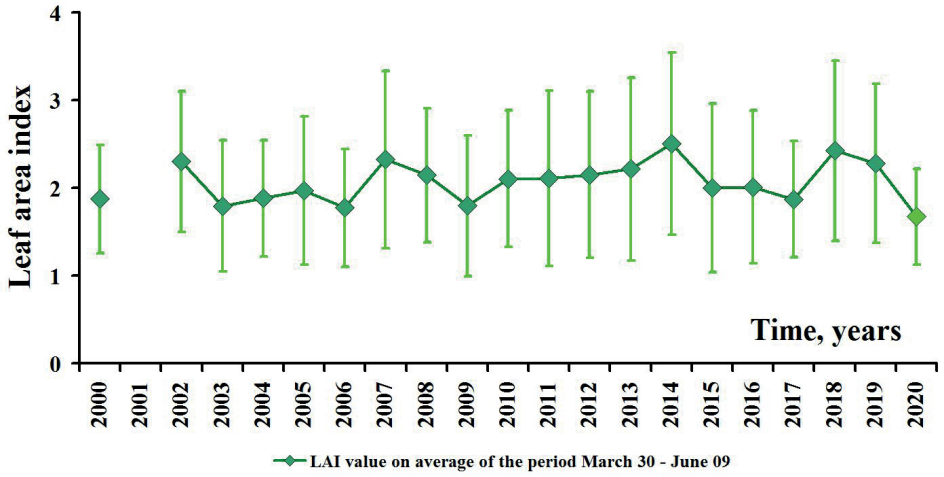

a) LAI values averaged over the period from March 30 to June 9 in 2000 and 2002÷2020;

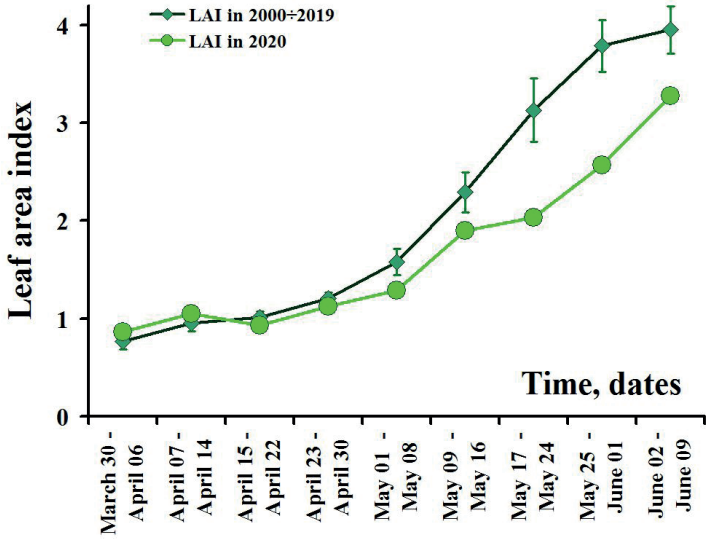

b) LAI values on certain days from March 30th to June 9th averaged over 2000, 2002÷2019 and 2020.

Fig. 6. Comparison of LAI values in Moscow region using MODIS data during the lockdown in 2020 and on the same days in 2000 and 2002÷2019

Confidence intervals are calculated with the 0.05 significance level

during this time and with the same period at some another year. As it is shown above, the SUHI depends on vegetation development. We should take into account a year under similar conditions. As an example, in 2019 an average difference between NDVI values in the city and at rural zone during the lockdown period was the same as in 2020 (-0.10). However, the SUHI intensity in 2019 was noticeably higher than in 2020, and it was 3.0 °C during both the full lockdown period, and non-full period until May 11th. This example indirectly confirms the reduced influence of the human activity on the surface heat balance in 2020.

CONCLUSIONS

1. During the lockdown period in 2020, the surface temperature T_s both in Moscow city and in the surrounding rural zone was significantly lower than usual in this calendar time. Probable explanation is the cool spring.

2. The SUHI intensity in Moscow during the lockdown was also lower than the average for the previous 20 years. A probable explanation of this is the slowdown of vegetation development in the rural zone due to the cold spring which creates a weakening of the SUHI. Besides, the cooling of the surface air layer in Moscow due the reduction of human activity (the weakening of anthropogenic heat sources during the lockdown) could also create an additional weakening of the SUHI. However, the decrease of the SUHI intensity during the lockdown is statistically non-significant.

3. Extremely high SUHI intensity in spring in mid-latitudes is often associated with more rapid snow cover melting in cities.

4. On average of 21 years, the mean NDVI values in April and May are 0.3÷0.4 in Moscow and 0.4÷0.5 in Moscow region. Thus, the difference between the average urban and rural values of NDVI in spring in Moscow region is about -0.1. In the rare cases of deep snow cover in spring, the NDVI values are extremely low (from 0.03 to 0.07) and are close to each other both in the city and in the rural zone.

5. A relation between the monthly averaged differences between urban and rural values of SUHI and NDVI in spring in Moscow region is statistically significant with the 0.99 probability.

6. In conditions of cold spring, LAI values are significantly lower than usual (at the second half of May in Moscow region – 2.0÷2.6 in 2020 and 3.1÷3.8 on average of 19 previous years), which confirms the slowdown in vegetation growth.

7. No significant long-term changes in surface temperature, SUHI intensity, NDVI and LAI values have been found in the past 21 years, according to MODIS data, in Moscow region.

REFERENCES

Ali G., Abbas S., Qamer F.M., et al. (2021). Environmental impacts of shifts in energy, emissions, and urban heat island during the COVID-19 lockdown across Pakistan. Journal of Cleaner Production, 291, 125806.

Alqasemi A.S., Hereher M.E., Kaplan G. et al. (2021). Impact of COVID-19 lockdown upon the air quality and surface urban heat island intensity over the United Arab Emirates. Science of the Total Environment, 767, 144330.

Chakraborty T.C., Chandan S. and Xuhui Lee. (2021). Reduction in human activity can enhance the urban heat island: insights from the COVID-19 lockdown. Environ. Res. Lett., 16, 054060.

Climate of Moscow in conditions of global warming. (2017). Ed. by Kislov A.V. Moscow, Russia: Moscow University Press, 288, [in Russian].

Dhruv Nanda, Deepk R. Mishra and Debadatta Swain. (2021). COVID-19 lockdowns induced land surface temperature variability in mega urban agglomerations in India. Environ. Sci.: Processes & Impacts, 23(1), 144-159, DOI: 10.1039/D0EM00358A.

El Kenawy A.M., Lopez-Moreno J.I., McCabe M.F., Domínguez-Castro F., Peña-Angulo D., Gaber I.M., Alqasemi A.S., Al Kindi Kh.M., Al-Awadhi T., Hereher M.E., Robaa S.M., Al Nasiri N., and Vicente-Serrano S.M. (2021). The impact of COVID-19 lockdowns on surface urban heat island changes and air-quality improvements across 21 major cities in the Middle East. Environmental Pollution, 288, DOI: 10.1016/j.envpol.2021.117802.

EOS Data Products Handbook (2000). Ed. by Parkinson C.L. & Greenstone R. NASA Goddard Space Flight Center Greenbelt, Maryland, 2, 253.

Erlyna Nour Arrofiqoh, Devika Ayu Setyaningrum. (2021). The Impact of Covid-19 Pandemic on Land Surface Temperature in Yogyakarta Urban Agglomeration. Journal of Applied Geospatial Information, 5(1), 480-485, DOI: 10.30871/jagi.v5i1.2784.

Esau I., Miles V. (2018). Exogenous drivers of surface urban heat islands in Northern West Siberia. GEOGRAPHY, ENVIRONMENT, SUSTAINABILITY, 11(3), 83-99, DOI: 10.24057/2071-9388-2018-11-3-83-99.

Lokoshchenko M.A. and Enukova Ye.A. (2020). Urban Heat Island in Moscow Derived from Satellite Data. Russian Meteorology and Hydrology, 45(7), 488-497, DOI: 10.3103/S1068373920070043.

Lokoshchenko M.A. and Alekseeva L.I. (2022). About the Annual Course of Moscow Heat Island and the Impact on it of Quarantine Measures to Prevent the COVID-19 Pandemic in 2020. Izvestiya, Atmospheric and Oceanic Physics, 58(2), 168-177. DOI: 10.1134/S000143382020086.

Morris C. J. G., Simmonds I., and Plummer, N. (2001). Quantification of the influences of wind and cloud on the nocturnal urban heat island of a large city. Journal of Applied Meteorology, 40(2), 169-182, DOI: 10.1175/1520-0450(2001)040<0169:QOTIOW>2.0.CO;2.

Mukherjee S. and Debnath A. (2020). Correlation between Land Surface Temperature and Urban Heat Island with COVID-19 in New Delhi, India. Research Square, 1-11.

Półrolniczak M., Kolendowicz L., Majkowska A. and Czernecki B. (2017). The influence of atmospheric circulation on the intensity of urban heat island and urban cold island in Poznań, Poland. Theor. Appl. Climatology, 127, 611-625, DOI: 10.1007/s00704-015-1654-0.

Rasul A., Balzter H., and Smith C. (2015). Spatial Variation of the Daytime Surface Urban Cool Island during the Dry Season in Erbil, Iraqi Kurdistan, from Landsat 8. Urban Climate, 14, 176-186, DOI: 10.1016/j.uclim.2015.09.001

Steitz D., Kenitzer A., Diller G., Henry K., Ainsworth D., and M. Neiman (1999). Terra: Flag ship of the Earth Observing Sys tem, NASA Press Kit, Release, 99-120.

Varentsov M.I., Grishchenko M.Y. and Wouters H. (2019). Simultaneous assessment of the summer urban heat island in Moscow megacity based on in situ observations, thermal satellite images and mesoscale modeling. GEOGRAPHY, ENVIRONMENT, SUSTAINABILITY, 12(4), 74-95. DOI: 10.24057/2071-9388-2019-10.

Voogt J.A., Oke T.R. (2003). Thermal remote sensing of urban climates. Remote Sensing of Environment, 86, 370-384, DOI: 10.1016/S0034-4257(03)00079-8.

Wenze Yang, Bin Tan, Dong Huang, Miina Rautiainen, Nikolay V. Shabanov, Y. Wang, Jeffrey L. Privette, Karl Fred Huemmrich, Rasmus Fensholt, Inge Sandholt, M. Weiss, Douglas E. Ahl, Stith T. Gower, Ramakrishna R. Nemani, Yuri Knyazikhin, and Ranga B. Myneni (2006). MODIS Leaf Area Index Products: From Validation to Algorithm Improvement. IEEE Transactions on Geoscience and Remote Sensing, 44(7), 1885-1898, DOI: 10.1109/TGRS.2006.871215.

Yangsiyu Liao, Xi Shen, Ji Zhou, Jin Ma, Xiaodong Zhang, Wenbin Tang, Yongren Chen, Lirong Ding and Ziwei Wang (2022). Surface urban heat island detected by all-weather satellite land surface temperature. Science of the Total Environment, 811, 151405, DOI: 10.1016/j.scitotenv.2021.151405.

EDITORIAL

LARGE RIVERS HYDROLOGY AND SEDIMENT TRANSPORT

Anatoly Tsyplenkov[1]*, Sergey Chalov[1], Markus Eder[2], Helmut Habersack[2]
[1]Faculty of Geography, Lomonosov Moscow State University, Moscow, Russia
[2]University of Natural Resources and Life Sciences Vienna, Institute of Hydraulic Engineering and River Research, Vienna, Austria
***Corresponding author:** atsyplenkov@gmail.com
Received: October 29th, 2022 / Accepted: November 11th, 2022 / Published: December 31st, 2022
https://DOI-10.24057/2071-9388-2022-020

ABSTRACT. This paper provides a short overview of the large river research topics discussed during the 4th World's Large Rivers Conference and submitted to the Geography Environment Sustainability special issue. The various aspects of hydrology, sediment transport and river morphology issues are presented based on case studies from Eurasia and Africa.

KEYWORDS: sediment transport, river morphology, river pollution, river geochemistry, Arctic, fluvial processes, flood

CITATION: Tsyplenkov A., Chalov S., Eder M., Habersack H. (2022). Large Rivers Hydrology And Sediment Transport. Geography, Environment, Sustainability, 4(15), 145-147
https://DOI-10.24057/2071-9388-2022-020

ACKNOWLEDGEMENTS: This research was performed according to the Development program of the Interdisciplinary Scientific and Educational School of M.V. Lomonosov Moscow State University, «Future Planet and Global Environmental Change».

Conflict of interests: The authors reported no potential conflict of interest.

INTRODUCTION

Large rivers are particularly vulnerable to conflicting uses and pressures that have risen in recent years. In addition to the lack of an overall assessment of the current status of the World's Large Rivers, the conflicting demands on such rivers, the likely future impacts of anthropogenic activities, and any restoration potential. There is also a lack of an overview assessment of the problems associated with their restoration. This special issue, «Large rivers hydrology and hydrogeochemistry», follows-up the 4th World's Large Rivers Conference, which was held as a hybrid event from the 3rd – the 6th of August 2021 in Moscow and covers two of four thematic focus areas of the conference: Hydrology, Hydraulics and Hydroclimatic Impact (TOPIC I), Sediment transport and river morphology (TOPIC II).

The current issue's Hydrology, Hydraulics and Hydroclimatic Impact section begin with studies by Nasonova et al. (2022) and Vasilenko et al. (2022) exploring the influence of climate change on water and heat flux of Arctic rivers. In contrast to Arctic environments, Houteta et al. (2022) give insights into altering water balance components in sub-tropics due to global warming. Yaitskaya et al. (2022) further describe the necessity of high-quality digital elevation models (DEM) for hydrodynamic modelling, while the study by V. Bondarev (2022) reveals the social consequences of flooding at the beginning of the XXI century. The second part of the issue is devoted to Sediment transport and river morphology studies. It starts with a paper by Schmalfuss et al. (2022) tackling the problem of hydromorphological analysis in hydrology, followed by research focused on bedload sediment measurements (Petrovskaya et al. 2022). The last two papers examine water quality issues associated with sediment load in the Selenga River delta (Zaharova and Belyaev 2022) and Tarbela reservoir (Mazhar et al. 2022). Key aspects addressed by the manuscripts in this volume are visualized in Fig. 1.

Fig. 1. Word cloud showing the most frequently used expressions in this thematic issue (based on manuscript titles and abstracts)

HYDROLOGY, HYDRAULICS AND HYDROCLIMATIC IMPACT

Global warming is expected to majorly impact the pan-Arctic basins, primarily in the north, resulting in changes to air temperature, precipitation, and snowmelt. **Nasonova et al. (2022)** investigate the effects of climate change on five Russian Arctic river basins. The researchers used a SWAP model and data from five global climate models (GCMs) with four different climate change scenarios to come up with projections of how the water balance components (river runoff, evapotranspiration, and precipitation) could be altered. The study found that these components generally increased for all the rivers and varied depending on the natural conditions and scenarios used. The researchers also looked at the uncertainties in the projections, which are caused by using different GCMs and scenarios, and found that the contribution of the GCMs was nearly double that of the scenarios in the 2006-2036 period and then decreased over time.

The water and heat flux changes in the 1930–2018 period from more than 30 gauging stations located in the Russian Arctic are analyzed by **Vasilenko et al. (2022)**. Their analysis revealed that the heat flux from the rivers had not significantly increased in the past three decades, except for the Yenisei and Yana rivers. However, the water temperature of the rivers had increased since 1960, particularly in May and June, but not to a statistically significant extent. It was also determined that dams built along the rivers affected the water temperature in their lower reaches but not further downstream. Finally, the heat flux had decreased by 25% in the Yenisei river's lowlands and estuaries.

The Intergovernmental Panel on Climate Change (IPCC) has determined that sub-tropical areas are particularly vulnerable to the negative repercussions of climate change. The research by **Houteta et al. (2022)** look into water balance components alteration, such as streamflow, evapotranspiration, and land use and land cover (LULC) changes in the Mono River Basin (Togo-Benin) before and after the construction of the Nangbéto dam. The authors noted that a decreased natural vegetation correlated to decreased evapotranspiration and lateral flow. As a result, the paper concluded that sustaining and conserving natural vegetation is crucial for proper water resource management in Mono River Basin.

The following paper discusses digital elevation models creation for the needs of hydrodynamic modelling of the Don and Volga rivers. **Yaitskaya et al. (2002)** used topographical maps, bathymetric surveys, hydrographic maps, and Landsat-8 and Sentinel-2 satellite images to construct DEMs. To assess the accuracy, the article tested various roughness coefficients to see which most accurately represented the fluctuating water stages during events such as flooding from surges. The authors found that the DEMs created enabled them to reproduce the observed dynamics of river discharges and water level fluctuations during high water events, and this was the first time such detailed DEMs had been created for these river deltas.

Scientists have noticed that when it comes to an understanding the social consequences of natural disasters like floods, there is no clear consensus in scientific publications about which consequences should be focused on for proper analysis and management decisions. To see what matters to people in this context, **Bondarev (2022)** looked at over 100 scientific articles on the five biggest flooding disasters of the early 2000s. The results showed that usually, there is a six or seven-year cycle of interest in floods, reaching a peak in the second or third years, though some exceptions occur. As for what matters to us, death losses got the most attention, followed by social solidarity and management problems. Additionally, the study revealed that the level of interest in floods in any given country was linked to its Human Development Index (HDI), meaning that countries with higher HDI rankings were more interested in things like death losses, social solidarity and management than those with lower rankings.

SEDIMENT TRANSPORT AND RIVER MORPHOLOGY

The Biya river, located in the Russian Altai mountains, is an example of a hydromorphological reference system - an area of water relatively undisturbed by humans and thus well preserved. **Schmalfuss et al. (2022)** used aerial imagery, satellite maps, and data on landforms to analyze the Biya in three sections - upper, middle, and lower - and look for differences in topography and hydromorphology. The study showed that the differences in river shape related to the terrain around the river, which supports the idea that understanding a river should include its surroundings. Implementing easily obtainable parameters - like the width of the river channel - can help detect differences in river morphology and improve our understanding of fluvial processes.

Based on the mode of transport, sediment transport in rivers can be divided into suspended, bedload, and suspended bedload material transport (Rhoads 2020). Various methods exist to measure bedload sediment discharge in large rivers, but the empirical equation is the most popular and cost-effective one. **Petrovskaya et al. (2022)** investigated filling a ditch across the Amur River using an echo-sounder measuring device in the summer of 2018. This resulted in 108 measurements used to compare 80 bed load formulas. Researchers used four methods for this comparison: bed form, critical velocity, critical water discharge, and regression approaches. The bed form approach was the most accurate, with 17 out of the 26 formulas showing an error rate of less than 60%. The other 56 formulas had only 5 with an error of less than 60%; these five corresponded to the critical velocity approach.

Suspended sediment is primarily fine inorganic particles of clay and silt and can substantially affect water quality in rivers (Loperfido 2014). Therefore the knowledge of sediment origin can be crucial for sustainable management planning (Walling 2005). The research by **Zaharova and Belyaev (2022)** was conducted using the geochemical fingerprinting method, which uses a quantitative approach to determine sediment origin and associated pollution. Using this method, they found that the majority of sediment on the floodplains of the delta was sourced from floodplains and terraces slopes, and only a small amount originated from remote areas. Additionally, analysis of suspended sediment showed that material from floodplain banks was the dominant source of accumulation. Finally, heavy metals and pollutants were found to accumulate in the lower reaches of the delta during large floods, which could lead to pollutants entering Lake Baikal when the streamflow is lower.

Human activities, such as building dams and other structures, can have a significant influence on lakes and the life in them. This includes changing the sedimentation rate, the availability of light and nutrients, and how often the lake is disturbed. **Mazhar et al. (2022)** collected satellite images from 1990 to 2020 and studied how human activities had changed land use and water quality

in the Tarbela reservoir, the biggest rock-filled dam in the world. They discovered that the amount of built-up areas increased by 630 km^2, reservoir turbidity decreased by 4%, chlorophyll and water increased, and overall water quality improved by 2020. The study suggests that more steps should be taken to decrease sediment and turbidity levels so that the reservoir's life can be extended.

CONCLUSION

In addition to providing economic vitality and habitat diversity, the world's large rivers and floodplains play an essential role in building civilization. Despite the effort to understand large river hydrology over the last few decades, very few hydrological, sediment, and nutrient data are available on large rivers worldwide. (Best 2019). Hopefully, the papers in this special Geography, Environment, Sustainability issue will narrow this gap and allow readers to study the latest developments and advances in World's Large Rivers.

REFERENCES

Best, J. (2019). Anthropogenic stresses on the world's big rivers. Nature Geoscience, 12(1), 7–21. DOI: 10.1038/s41561-018-0262-x.

Bondarev, V.P. (2022) Social consequences of floods: case study of five emergencies in different global drainage basins. Geography, Environment, Sustainability, 4(15), 188-195 DOI:10.24057/2071-9388-2022-102.

Houteta, D.K., Atchonouglo, K., Adounkpe, J.G., Diwediga, B., Lombo, Y., Kpemoua, K.E., Agboka, K. (2022) Changes in land use/ cover and water balance components during 1964-2010 period in the Mono River Basin, Togo-Benin. Geography, Environment, Sustainability, 4(15), 171-180 DOI: 10.24057/2071-9388-2021-098.

Loperfido, J.V. (2014). Surface Water Quality in Streams and Rivers: Scaling and Climate Change. In: S. Ahuja, ed., Comprehensive Water Quality and Purification. Waltham: Elsevier, 87–105. DOI: 10.1016/B978-0-12-382182-9.00064-5.

Mazhar, N., Javid, K., Khan, M.A.N., Afzal, A., Hamayon, K., Ahmad, A. (2022) Index-based spatiotemporal assessment of water quality in Tarbela Reservoir, Pakistan. Geography, Environment, Sustainability, 4(15), 232-242 DOI: 10.24057/2071-9388-2022-077.

Nasonova, O.N., Gusev, E.M., Kovalev, E.E. (2022) Projecting changes in water balance components of Arctic river basins. Geography, Environment, Sustainability, 4(15), 148-157 DOI: 10.24057/2071-9388-2021-144.

Petrovskaya, O.A., Maltsev, A.A. (2022) Testing bed load transport formulas: a case study of the lower Amur multi-beam echo-sounders (MBES) data. Geography, Environment, Sustainability, 4(15), 148-157 DOI: 10.24057/2071-9388-2021-144.

Rhoads, B.L. (2020). River dynamics: geomorphology to support management. New York, NY: Cambridge University Press.

Schmalfuß, L., Hauer, C., Yanygina, L.V., Schletterer M. (2022) Landscape Reading for Alpine Rivers: A Case Study from the river Biya. Geography, Environment, Sustainability, 4(15), 196-213 DOI: 10.24057/2071-9388-2022-046.

Vasilenko, A.N., Magritsky, D.V., Frolova, N.L., Shevchenko, A.I. (2022) Long-term heat flux formation of the large Russian Arctic rivers under the influence of climate-induced and dam-induced effects. Geography, Environment, Sustainability, 4(15), 158-170 DOI: 10.24057/2071-9388-2022-105.

Walling, D.E. (2005). Tracing suspended sediment sources in catchments and river systems. Science of The Total Environment, 344(1), 159–184. DOI: 10.1016/j.scitotenv.2005.02.011.

Yaitskaya, N., Sheverdyaev, I. (2022) Digital elevation model development of the Volga and Don river's delta. Geography, Environment, Sustainability, 4(15), 181-187 DOI: 10.24057/2071-9388-2022-035.

Zaharova, E.D., Belyaev, V.R. (2022) Contribution of the different sources to the formation of alluvial sediments in the Selenga river delta. Geography, Environment, Sustainability, 4(15), 222-231 DOI: 10.24057/2071-9388-2022-098.

RESEARCH PAPER

CLIMATE CHANGE IMPACT ON WATER BALANCE COMPONENTS IN ARCTIC RIVER BASINS

Olga N. Nasonova[1*], Yeugeny M. Gusev[1], Evgeny Kovalev[1]
[1]Water Problems Institute of Russian Academy of Sciences, Gubkina St. 3, Moscow, 119333, Russian Federation
***Corresponding author:** olniknas@yandex.ru
Received: February 23rd, 2021 / Accepted: November 11th, 2022 / Published: December 31st, 2022
https://DOI-10.24057/2071-9388-2021-144

ABSTRACT. Climate change impact on the water balance components (including river runoff, evapotranspiration and precipitation) of five Arctic river basins (the Northern Dvina, Taz, Lena, Indigirka, and MacKenzie), located in different natural conditions, was investigated using a physically-based land surface model SWAP and meteorological projections simulated at half-degree spatial resolution by five Global Climate Models (GCM) for four Representative Concentration Pathways (RCP) scenarios from 2005 to 2100. After the SWAP model calibration and validation, 20 projections of changes in climatic values of the water balance components were obtained for each river basin. The projected changes in climatic river runoff were analyzed with climatic precipitation and evapotranspiration changes. On average, all rivers' water balance components will increase by the end of the 21st century: precipitation by 12-30%, runoff by 10–30%, and evapotranspiration by 6-47% depending on the river basin. The partitioning of increment in precipitation between runoff and evapotranspiration differs for the selected river basins due to differences in their natural conditions. The Northern Dvina and Taz river runoff will experience the most negligible impact of climate change under the RCP scenarios. This impact will increase towards eastern Siberia and reach a maximum in the Indigirka basin. Analysis of the obtained hydrological projections made it possible to estimate their uncertainties by applying different GCMs and RCP scenarios. On average, the contribution of GCMs to the uncertainty of hydrological projections is nearly twice more significant than the contribution of scenarios in 2006–2036 and decreases over time to 1.1-1.2 in 2068–2099.

KEYWORDS: climate change, land surface model, Arctic rivers, hydrological projections, RCP scenarios

CITATION: Nasonova O. N., Gusev Ye. M., Kovalev E. E. (2022). Climate Change Impact On Water Balance Components In Arctic River Basins. Geography, Environment, Sustainability, 4(15), 148-157
https://DOI-10.24057/2071-9388-2021-144

ACKNOWLEDGEMENTS: The authors are grateful to the organizers of the International project ISIMIP for providing global data sets on meteorological data and land surface parameters. This study was carried out within the framework of the State Assignment theme of WPI RAS (№ FMWZ-2022-0001).

Conflict of interests: The authors reported no potential conflict of interest.

INTRODUCTION

It is generally accepted that the pan-Arctic basin will be subject to major changes due to projected global warming, which is expected to be most significant in northern regions, resulting in an increase of air temperature, precipitation and snowmelt. This can lead to significant changes in heat and water balances of drainage area of Arctic rivers, which, in turn, will affect the annual volume of river runoff, as well as the shape and timing of runoff hydrographs. The influence of northern river runoff on the Arctic Ocean is very great. Thus, the influx of fresh water to the Arctic Ocean by means of runoff from the drainage area of the pan-Arctic basin represents about 50% of its net flux (Barry and Serreze, 2000). Taking into account the role of the rivers of the pan-Arctic basin in the transfer of heat, sediment, nutrients and pollutants to the north, changes in the environment caused by climate change, even at low latitudes, can have a significant impact on the freshwater balance of the Arctic Ocean, on the influx the above substances, on sea ice formation, and, ultimately, on the thermohaline circulation and global climate. That is why investigation of the impact of global warming on the hydrological cycle and the dynamics of its components in the Arctic region is very important and relevant.

There are a lot of papers devoted to assessment of changes in Arctic river runoff in the 21st century (see review in (Dai 2016; Gelfan et al. 2022)). They are carried out by global and regional Hydrological Models (HMs) and Land Surface Models (LSMs) using projections of meteorological forcing data from Global Climate Models (GCMs) to project changes in river runoff (e.g., Gusev et al. 2013, 2018; Arnell and Lloyd-Hughes 2014; Gelfan et al. 2017; Gosling et al. 2017; Krysanova and Hattermann 2017; Bring et al. 2017, Nasonova et al. 2019, 2021). However, there are much more studies, which use runoff projections simulated by GCMs (Georgiady and Milyukova 2006; Kattsov et al. 2007; Kislov et al. 2011; Khon and Mokhov 2012; Shkolnik et al. 2014; Koirala 2014; Dobrovolski 2014; Georgievsky and Golovanov 2019) and analyze them for different regions of the globe with or without identifying Arctic river basins. Studies of possible changes in river runoff differ in methods, models, climatic scenarios, climatic periods, and areas used. However, in general, recent studies project an increase in Arctic river runoff by 10-50%, depending on the location of modeling object and climatic scenario.

During the last decade we also performed scenario projections of changes in water balance components for Arctic river basins using our land surface model SWAP (Soil Water – Atmosphere – Plants) and different families of greenhouse gas emission scenarios: IS95, SRES (Special Report on Emissions Scenarios) and RCP (Representative Concentration Pathways). The IS92 family was prepared for the IPCC Second Assessment Report, published in 1995. SRES scenarios were used in the IPCC Third (TAR) and Fourth Assessment Reports (AR4), published in 2001 and 2007, respectively. SRES was replaced by RCP prepared for the IPCC Fifth Assessment Report. The methodological approaches used for the constructions of the above families of scenarious, as well as description and analysis of the scenarious are given in Semenov and Gladilshchikova (2022).

In our earlier studies, we carried out hydrological projections up to the 2060s for the Northern Dvina River basin using SWAP, IS92 scenarios and climate scenario generator MAGICC/SCENGEN, which allowed us to obtained meteorological projections for the ensemble of 16 GCMs (Gusev and Nasonova 2014). The same technique, but with SRES emission scenarios (A1, A2, B1, and B2), was applied to project changes in the water balance components for the Northern Dvina, Olenek, Indigirka, Lena and Ob'-Irtysh basins (Gusev and Nasonova 2014; Gusev et al. 2014, 2016b, 2019a).

The latest RCP scenarios we applied for projecting runoff for the Indigirka, Northern Dvina and Kolyma rivers in (Nasonova et al. 2018). In so doing, meteorological forcing data to drive the SWAP model were simulated by GCM INMCM4.0 for RCP4.5 and RCP8.5 by the end of the 21st century. Five different procedures were used for bias-correction of GCM meteorological outputs to reveal their contribution to the uncertainty in runoff projections.

Participation in the International Inter-Sectoral Impact Model Intercomparison Project, phase 2 (ISI-MIP2) (Krysanova and Hattermann 2017), initiated our implementation of a number of studies aimed at modeling and projecting runoff for 11 river basins located in different regions of the globe and suggested within the framework of the project (e.g., Gusev et al. 2018; Nasonova et al. 2021). In these studies, the projections of forcing data by the end of the 21st century were simulated by five GCMs for four RCP scenarios. It should be noted that there were only two Arctic rivers (the Lena and MacKenzie) among 11 ones.

The present work is a continuation of our ISIMIP-related studies. We will use the same RCP scenarios and GCMs' meteorological outputs to force the SWAP model to simulate hydrological projections. However, here, five Arctic rivers will be involved and the main emphasis will be on the following issues: (1) on the analysis of all components of the water balance, i.e. river runoff projections will be analysed in relation to projected precipitation and evapotranspiration; (2) to identify the causes and patterns of projected changes and find out where the projected changes in the water balance components will be the largest and why; (3) to get more insight in uncertainties of hydrological projections sourced from application of different GCMs and RCP scenarios in order to reveal where the uncertainties are the highest and why.

MATERIALS AND METHODS

As mentioned above, five Arctic river basins were selected for modeling (Fig. 1). Four of them (the Northern Dvina, Taz, Lena, and Indigirka) are situated in Russia, while the MacKenzie is in North America. Some characteristics of the basins are given in Table 1.

The choice of Russian basins was motivated by the fact that they are situated in very contrasting natural conditions. Thus, when moving from the westernmost basin to the east, the climate becomes more and more severe: from temperate in the Northern Dvina basin to subarctic and arctic in the Indigirka basin. The continentality of the climate also increases in the same direction. As a result, the long-term mean annual air temperature, averaged over each basin, decreases from 0.8°C for the Northern Dvina to -5.4°C for the Taz, to -10.2°C for the Lena and to -17.6°C for the Indigirka (Table 1). The Pole of Cold of the Northern Hemisphere with a recorded absolute minimum of air temperature equalled to -67.7°C is located in the Indigirka basin (in Oymyakon). Precipitation also decreases eastward with increasing continentality from 655 mm/year for the Northern Dvina basin to 250 mm/year for the Indigirka; the runoff ratio increases from 0.44 to 0.65 (Table 1). Seasonally frozen soils in the Northern Dvina basin are replaced by permafrost in the other basins.

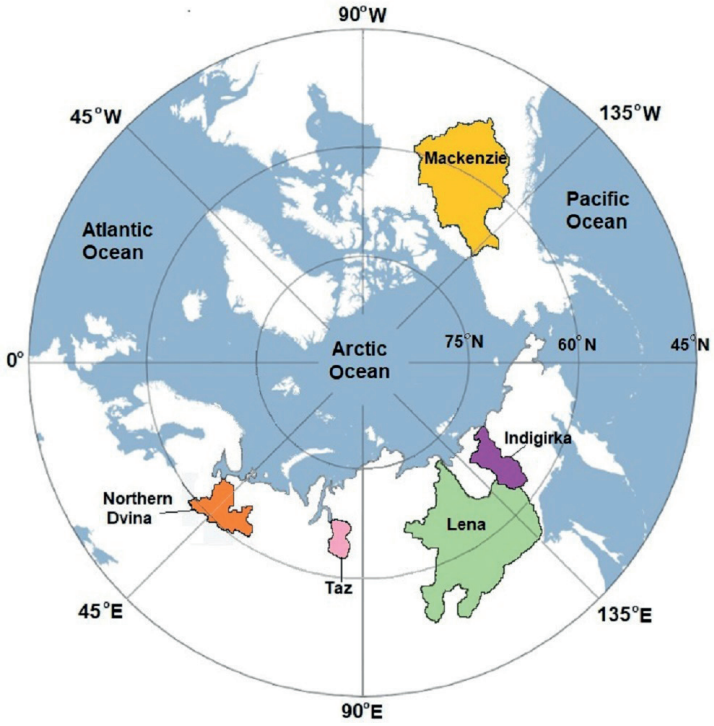

Fig. 1. Distribution of the river basins in the Arctic used in this study

It seemed interesting to complete the picture with the MacKenzie River, which stands apart from the other rivers. Like the Lena River, it is mostly located in the temperate and subarctic zones, but its long-term mean annual air temperature is higher (-4.3°C versus -10.2°C) and permafrost underlies about ¾ of the basin area, while the Lena basin is fully in the permafrost zone. In addition, the MacKenzie has the lowest runoff ratio (0.39) among the rivers (Table 1).

For model simulations, the basins were presented as a set of regular grid cells (with a spatial resolution of 0.5°x0.5° in latitude and longitude) connected by a river network. The number of calculational grid cells for the basins varies from 88 for the Taz River to 1668 for the Lena River (Table 1).

Model

Simulation of river runoff and evapotranspiration for the selected river basins was performed by the spatially-distributed physically-based model SWAP (Gusev and Nasonova 2010). SWAP belongs to the class of land surface models which differ from hydrological models in that they treat not only hydrological processes, but also heat and radiation exchange at the land surface – atmosphere interface. Besides, LSMs require more forcing data including incoming shortwave and longwave radiation, wind speed and air pressure along with precipitation, air temperature and humidity which usually force hydrological models. Output data can reach several dozens variables including different state variables, as well as radiation, heat, and water fluxes. To obtain river runoff at the basin outlet a river routing model was inserted into the SWAP model.

Description of the model and its successful validation performed for experimental sites and for catchments and river basins of different size on a long-term basis and under different natural conditions (from arid to humid and from non-frozen soils to seasonally frozen ones and permafrost) were summarized in (Gusev and Nasonova 2010). Comparison with hydrological models has shown that the LSM SWAP can reproduce river runoff as good as HMs (Nasonova 2011; Nasonova et al. 2009). Taking into account the purpose of the given paper, it should be noted that SWAP has been extensively validated against observed streamflow of northern Russian rivers: the Mezen' (Gusev et al. 2008); Pechora (Gusev et al. 2010); Ponoi, Onega, and Tuloma (Gusev et al. 2011a); Northern Dvina (Gusev et al. 2011b); Olenek and Indigirka (Gusev et al. 2013); Kolyma (Gusev et al. 2015a), Nadym, Pur, and Taz (Gusev et al. 2015b); Lena (Gusev et al. 2016a), and Ob' with Irtysh (Gusev et al. 2019b). The results of validation proved the ability of SWAP to model hydrological processes at high latitudes and in permafrost regions quite adequately.

Meteorological forcing data

Forcing data to drive the SWAP model include incoming longwave and shortwave radiation, air temperature and humidity, precipitation, wind speed, and air pressure. The data were provided within the framework of the ISI-MIP2, in which we participated with SWAP.

For hydrological projections, daily values of forcing data were simulated by five GCMs (GFDL-ESM2M, HadGEM2-ES, IPSL-CM5A-LR, MIROC-ESM-CHEM, and NorESM1-M) for each of four RCP scenarios (RCP2.6, RCP4.5, RCP6.0, and RCP8.5) for the period of 2006–2099. Large numbers in scenarios abbreviations correspond to more aggressive anthropogenic scenarios due to increased emissions of greenhouse gases into the atmosphere and weak measures to limit their release. In addition to the prognostic values, the values of meteorological forcing data simulated by the five GCMs for the historical period (1961-2005) were also provided. They were needed to simulate river runoff using SWAP for the historical period.

Since meteorological outputs from GCMs usually suffer from systematic errors, they were subject to a post-processing bias-correction to the WATCH data within the framework of the ISI-MIP2 project. A detailed description of the bias-correction technique can be found in (Hempel et al. 2013). In so doing it was assumed that the WATCH data, based on ERA-40 reanalysis and hybridized with monthly values of ground-based measurements taken from the Global Precipitation Climatology Center (GPCC) and the Climatic Research Unit (CRU of University of East England) data sets (Weedon et al. 2011), are close to real meteorology.

The WATCH data were also used for calibration and validation of the SWAP model. For this purpose, daily values of meteorological forcing data for the period of 1969–2001 were derived from the WATCH data set for each calculation grid cell of the selected basins.

Model parameters, their calibration and validation

In addition to the forcing data, SWAP needs the land surface parameters for each calculational grid cell. A priori values of vegetation parameters (vegetation class, leaf area index – LAI, albedo, roughness length, greenness fraction, vegetation height, rooting depth) were taken from the global ECOCLIMAP data set (Champeaux et al. 2005), which includes land surface parameters at 1 km spatial resolution. For model simulations, parameter values were aggregated to a half-degree resolution.

A priori soil parameters (porosity, field capacity, wilting point, hydraulic conductivity at saturation, soil matric potential at saturation and B-parameter in parameterisation by Clapp and Hornberger (1978)) were estimated using

Table 1. River basins used in this study with the number of calculational grid cells; gauge stations with coordinates; averaged over 1971-2000 air temperature *T*, precipitation *Pr*, river runoff *R* and runoff ratio *R/Pr*

River basin	Area, km²	Number of grid cells	Streamflow gauge station			*Tr*, °C	*P*, mm/yr	*R*, mm/yr	*R/Pr*
			Name	Latitude	Longitude				
Northern Dvina	348 000	248	Ust'-Pinega	64.13°N	42.17°E	0.8	665	295	0.44
Taz	100 000	88	Sidorovsk	66.60°N	82.28°E	-5.4	650	334**	0.52**
Lena	2 460 000	1668	Stolb	72.37°N	126.80°E	-10.2	384	201	0.52
Indigirka	305 000	243	Vorontsovo	69.58°N	147.35°E	-17.6	250	164*	0.65*
MacKenzie	1 660 000	1128	Arctic Red River	67.46°N	133.74°W	-4.3	435	171	0.39

*1970-1977, 1979-1991, 1993, 1994 (23 years); **1970-1979, 1982,1983,1987-1990,1994-1996 (18 years).

equations by Cosby et al. (1984) and data on soil texture from the ECOCLIMAP.

To improve the quality of hydrological modeling, a number of a priori model parameters, which have the greatest effect on runoff formation, were calibrated. The experience of working with the SWAP model has shown that the following seven parameters can be calibrated for the northern river basins: the hydraulic conductivity at saturation, the soil rooting depth, the soil column depth (from the soil surface to the depth of impermeable layer), snow-free surface albedo, fresh snow albedo, the Manning's roughness coefficient and the effective velocity of water movement in a channel network. For the first four parameters, the correction factors to a priori parameter values were calibrated.

Calibration was carried out against river runoff measured during 7-8 years at streamflow gauge stations (Table 1) located at the basin outlets. In so doing, the large basins of the Lena and Mackenzie rivers were divided into three parts and optimal values of model parameters were obtained for each of them.

Shuffled Complex Evolution method (SCE-UA) was used for automatic calibration (Duan et al. 1992). The objective function represented the Nash and Sutcliffe efficiency

$$NS = 1 - \frac{\sum_{\Omega} \left(x_{cal} - x_{obs} \right)^2}{\sum_{\Omega} \left(x_{obs} - \bar{x}_{obs} \right)^2} \quad (1)$$

where x_{cal} and x_{obs} are calculated and observed values of a variable x (here, monthly river runoff), Ω is a discrete sample set of the variable x.

The search of the maximum value of the objective function during calibration was carried out under the condition that the absolute value of the systematic error *Bias*, calculated as follows

$$Bias = \frac{\sum_{\Omega} \left(x_{cal} - x_{obs} \right)}{\sum_{\Omega} x_{obs}} \cdot 100\,\% \quad (2)$$

cannot exceed 5%.

The calibrated parameters were used for modeling river runoff for the selected basins using SWAP together with forcing data from WATCH and five GCMs. The modeled runoff for the historical period was compared with the available measured runoff at the basin outlets to validate the model.

Projecting changes in river runoff and their uncertainties

For the future period (2006-2099), daily values of river runoff and evapotranspiration were simulated by the SWAP model forced by each of 20 meteorological projections (5 GCMs X 4 RCP scenarios). Then annual values of the water balance components (river runoff – *R*, evapotranspiration – *E*, and precipitation – *Pr*) were calculated. For subsequent analysis, the prognostic period was divided into three parts: P1 (2006-2036), P2 (2037-2067) and P3 (2068-2099). The projected annual water balance components were averaged over each period to obtain their climatic values. Changes in the climatic values of each variable $\Delta X_{GCM,RCP,Pi}$ (X=*R, E, Pr*) obtained for each GCM, each RCP scenario, and prognostic period *Pi* (i=1, 2, 3) were calculated as the difference between the projected value $X_{GCM,RCP,Pi}$ and the historical one $X_{GCM,H}$ (simulated with the same GCM's forcing data and averaged over 1971-2005):

$$\Delta X_{GCM,RCP,Pi} = X_{GCM,RCP.Pi} - X_{GCM,H} \quad (3)$$

Relative changes were calculated as follows:

$$\Delta X_{GCM,RCP,Pi}\,\% = \frac{\Delta X_{GCM,RCP,Pi}}{X_{GCM,H}} \cdot 100\,\% \quad (4)$$

Thus, for each variable X and for each prognostic period, the ensembles of 20 values of $\Delta X_{GCM,RCP,Pi}$ and $\Delta X_{GCM,RCP,Pi}$% were obtained. After that ensemble mean value M and standard deviation STD were calculated. As it was shown in (Gelfan et al. 2017), the interval (M±1.96 STD) can be treated as the index of hydrological projection uncertainty caused by both the climate scenario variability and the climate model structural uncertainty.

Assessment of the contribution of uncertainties in RCP scenarios and GCMs to hydrological projection uncertainty

The obtained changes in the water balance components $\Delta X_{GCM,RCP,Pi}$ and $\Delta X_{GCM,RCP,Pi}$% allowed us to estimate the contribution of GCMs' structural uncertainty and RCP scenarios differences into the uncertainty of the hydrological projections. For this purpose, for each prognostic period and each river, the ranges of variability of ΔX as a difference between the maximum and the minimal values were estimated:

$$Range = \Delta X_{max} - \Delta X_{min} \quad (5)$$

If we use all 20 values of $\Delta X_{GCM,RCP,Pi}$ or $\Delta X_{GCM,RCP,Pi}$% for estimating the range ($Range_{GCM,RCP}$ or $Range_{GCM,RCP}$%), we will obtain uncertainty caused by both GCMs and RCP scenarios. Besides, we can calculate the variation ranges caused only (1) by a scatter among GCM's projections $Range_{GCM}$ (calculated for each scenario and then averaged over the scenarios) and (2) by a scatter due to different RCP scenarios $Range_{RCP}$ (calculated for each model and then averaged over the models). The former indicates the contribution of the climate model structural uncertainty into the hydrological uncertainty, while the latter is associated with the contribution of the climate scenario differences.

RESULTS AND DISCUSSION

Model validation

First of all the calibrated values of model parameters were used to simulate streamflow of the five rivers by the SWAP model using forcing data from WATCH. The results of simulation were compared with corresponding observations at streamflow gauge stations located at the basin outlets. The agreement between simulations and observations for each river basin was assessed on monthly basis using goodness-of-fit statistics such as the Nash-Sutcliffe coefficient of efficiency *NS* and systematic error *Bias*. The results of comparison are presented in Table 2.

As can be seen from Table 2, for the validation period, the worst results in terms of *Bias* were obtained for the Taz River: *Bias*=13.3%. This may be due to deterioration in the quality of measurements after 1979. Thus, there are no gaps in measurements for the calibration period, while for 1980-1996 31% of data are missing and after 1996 measurements are absent.

Fig. 2 shows the progress in SWAP streamflow simulations after calibration of the model parameters. As can be seen, for all rivers, hydrographs simulated by SWAP with calibrated parameters match the observed hydrographs much better than hydrographs simulated with a priori parameters. The worst agreement was obtained for the Lena River: *NS*=0.58 (Table 2). However, in this case,

Table 2. Systematic error (Bias) and Nash-Sutcliffe coefficient of efficiency (NS) for monthly values of streamflow simulated by the SWAP model with optimized parameters for the calibration and validation periods

River	Streamflow gauge station	Calibration period				Validation period			
		Years		*Bias*, %	*NS*	Years		*Bias*, %	*NS*
		Period	Number of years			Period	Number of years		
Northern Dvina	Ust'-Pinega	1973-1979	7	2.67	0.89	1971-2001	31	2.0	0.87
Taz	Sidorovsk	1973-1979	7	0.43	0.93	1971-1996	26	13.3	0.84
Lena	Stolb	1972-1979	8	0.18	0.68	1970-2001	32	-0.49	0.58
Indigirka	Vorontsovo	1973-1979	7	4.60	0.93	1971-1994	24	-2.8	0.89
MacKenzie	Arctic Red River	1973-1980	8	-1.13	0.83	1970-2001	32	4.01	0.76

the systematic error is negligible (*Bias*≈-0.5%) that is much more important for the purpose of the paper, since we will operate with annual values rather than hydrographs.

The results of the comparison led to the conclusion that the obtained optimal values of model parameters can be applied for modeling streamflow for the above rivers.

Before proceeding to hydrological projections until the end of the 21st century using meteorological projections from the aforementioned five GCMs, the simulations with the obtained optimal parameters were performed by SWAP for the historical period (1961-2005) in order to find out how adequately river runoff is reproduced with meteorological outputs from the global models. The simulated annual runoff for each river was compared with observations. Fig. 3 shows comparison of climatic (averaged over historical period) annual values of simulated runoff in comparison with corresponding observed runoff for each river and for each GCM's forcing data.

As can be seen from Fig. 3, the simulated climatic runoff is overestimated, despite the fact that meteorological data from GCMs were bias-corrected to WATCH data (which were used for obtaining optimal parameters). This allowed us to conclude that the meteorological outputs from the above GCMs can be used for hydrological projections, however, to eliminate the impact of systematic errors in the results

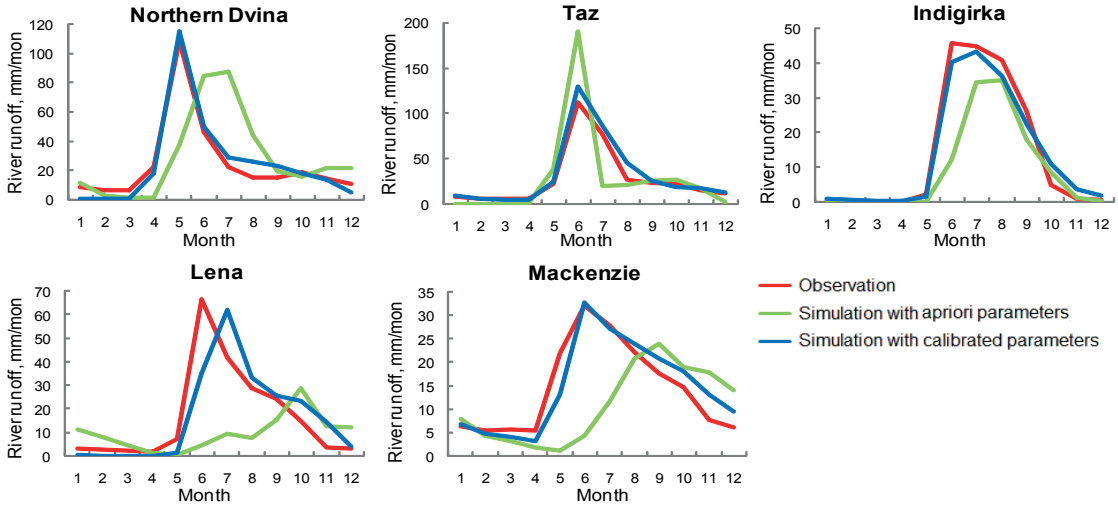

Fig. 2. Averaged over the calculational period monthly hydrographs measured at the river basin outlets and simulated by SWAP with a priori and calibrated parameters

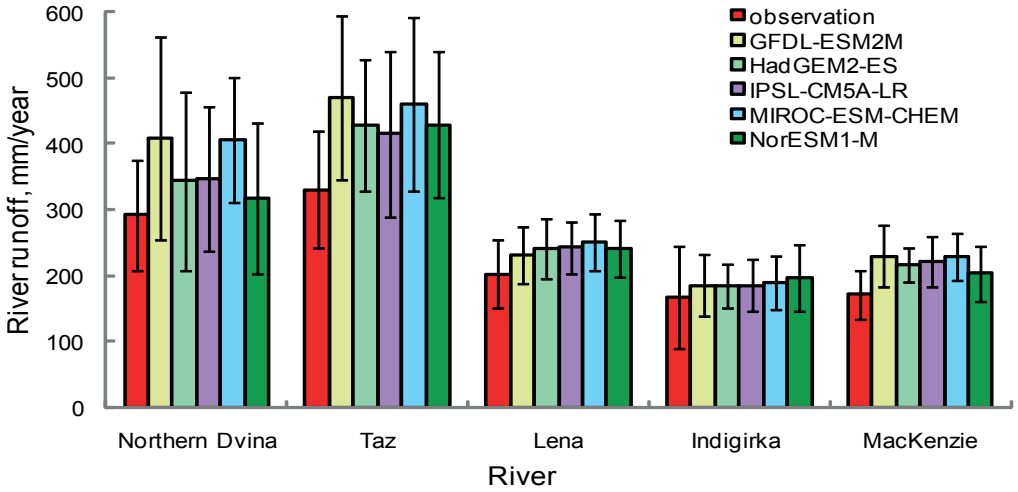

Fig. 3. Climatic annual river runoff observed at the basin outlets and simulated by SWAP driven by meteorological forcing data from 5 GCMs. Vertical bars show the ranges of variability of annual runoff corresponding to MEAN±1.96 STD

of simulations the projected changes $\Delta X_{GCM}=X_{GCM,Pi}-X_{GCM,H}$ in the water balance components will be considered rather than the projected values.

Hydrological projections

The projected changes in annual values of climatic runoff ΔR and precipitation ΔPr calculated by Eqs. (3) and (4) and averaged over the ensemble of five GCMs and four climatic scenarios (i.e., representing the ensemble mean M) are presented in Fig. 4. They are shown for three climatic periods and five rivers. All changes are positive and increase in time, being the largest during the third period P3. For P3, relative changes in runoff range from 10% for the Taz River up to 30% for the Indigirka (Fig. 4a); relative changes in precipitation are in the range of 12–30%, being the lowest for the Mackenzie River and the largest for the Indigirka (Fig. 4c).

In Fig. 4, bars correspond to the intervals of uncertainty in the projected ΔR and ΔPr caused by both the GCMs structural uncertainty and the RCP scenario differences. The largest uncertainty in relative ΔR was found for the Indigirka River. This can be explained by the largest variability of the projected changes in climatic precipitation for this river.

It is interesting to analyze the absolute changes in climatic river runoff (Fig. 4b) in comparison with the absolute changes in precipitation (Fig. 4d) for the third period. For analysis, it is convenient to divide the rivers into two groups: (1) the Taz, Northern Dvina, and MacKenzie with similar ΔR equaled to 44, 42 and 39 mm/year versus large differences in ΔPr equaled to 137, 100 and 55 mm/year, respectively; (2) the Lena and Indigirka with 58 and 67 mm/year increment in runoff versus similar ΔPr equaled to 81 and 79 mm/year, respectively. Both cases can be explained with the help of Fig. 5, which shows changes in forcing data, namely, precipitation and air temperature averaged over each climatic period and for each river basin.

Fig. 5a illustrates how the projected ΔPr partitions between the increments in runoff ΔR and evapotranspiration ΔE. Fig. 5b depicts the projected increase in air temperature ΔT, which leads to an increase in evapotranspiration for all rivers and all periods (Fig. 5a). However, the value of ΔE can be different despite of the same ΔT due to different increases in potential evapotranspiration. As it was obtained in our global simulations with the same models and climatic scenarios, the increase in potential evapotranspiration in 2068-2099 in the areas of the Lena, Indigirka and MacKenzie river basins is much lower than in the Northern Dvina and Taz basins (Nasonova et al., 2021, Fig. 5e). That is why for the Northern Dvina and Taz, ΔE is much larger than for the other rivers.

Contribution of GCMs and climatic scenarios to hydrological uncertainty

Fig. 6 shows projected changes in climatic annual runoff for five rivers and for three climatic periods. In the upper panels, the projections are averaged over the GCMs, therefore, differences between them are due to different RCP scenarios and can be considered as uncertainties sourced from climatic scenarios. For the Northern Dvina (Fig. 6d) and Taz (Fig. 6e), these uncertainties are the lowest. For the other rivers, the uncertainties grow with time and reach the highest values for the Indigirka River; the projected increase in river runoff is minimal for the RCP2.6 scenario and maximum for the RCP8.5 one.

In the bottom panels of Fig. 6, the projections are averaged over the climatic scenarios, hence the scatter among the projected values is caused by differences in the meteorological forcing data from the GCMs and therefore it can be treated as uncertainty sourced from differences in the GCMs structure. This uncertainty also grows with time for all rivers except the Northern Dvina and Taz. In general, it is also greater than the uncertainty caused by RCP scenarios. Again, the Indigirka River has the largest uncertainty (Fig. 6f).

Thus, the obtained results allow us to conclude that the contribution of GCMs to the uncertainties in Arctic river runoff projections is larger than the contribution of the RCP climatic scenarios. This is also confirmed by Fig. 7.

Fig. 7 shows mean variation ranges of projected changes in climatic annual river runoff and precipitation due to differences in GCM forcings, RCP scenarios, and both GCMs and scenarios: $Range_{GCM}$, $Range_{RCP}$ and $Range_{GCM,RCP}$, respectively. They represent uncertainties in hydrological projections caused, respectively, by differences in climatic scenarios, by structural uncertainties in GCMs, and by joint influence of scenarios and GCMs. The ranges were averaged over five rivers for each prognostic period and sorted in increasing order of $Range_{GCM,RCP}$. In general, uncertainties in the projected relative changes in river runoff are somewhat greater than in precipitation. The results presented in Fig. 7

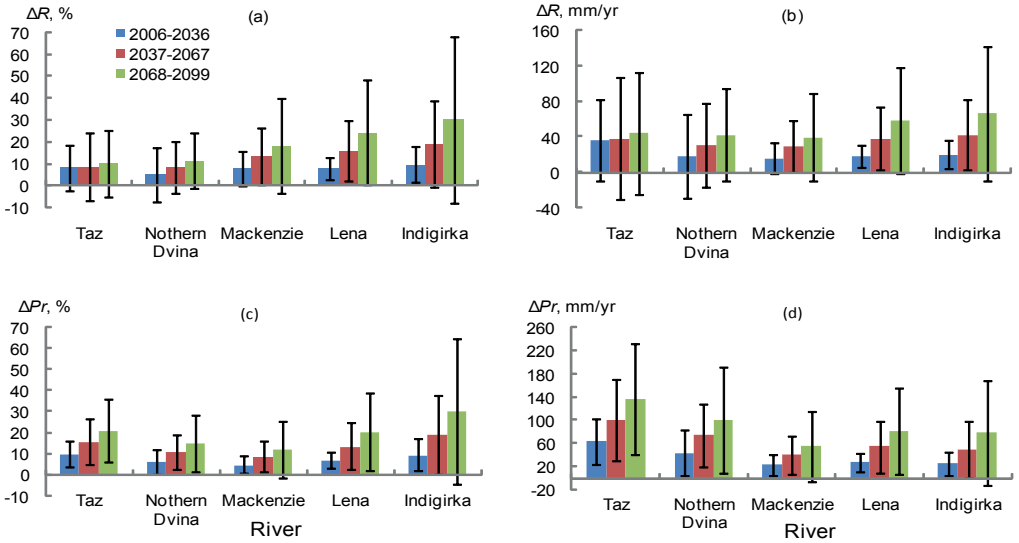

Fig. 4. The projected multimodal and multiscenario changes in (a, b) annual river runoff and (c, d) precipitation, averaged over three climatic periods, and their uncertainties (vertical bars) sourced from different GCMs and RCP-scenarios. Bars are the intervals (M±1.96×STD)

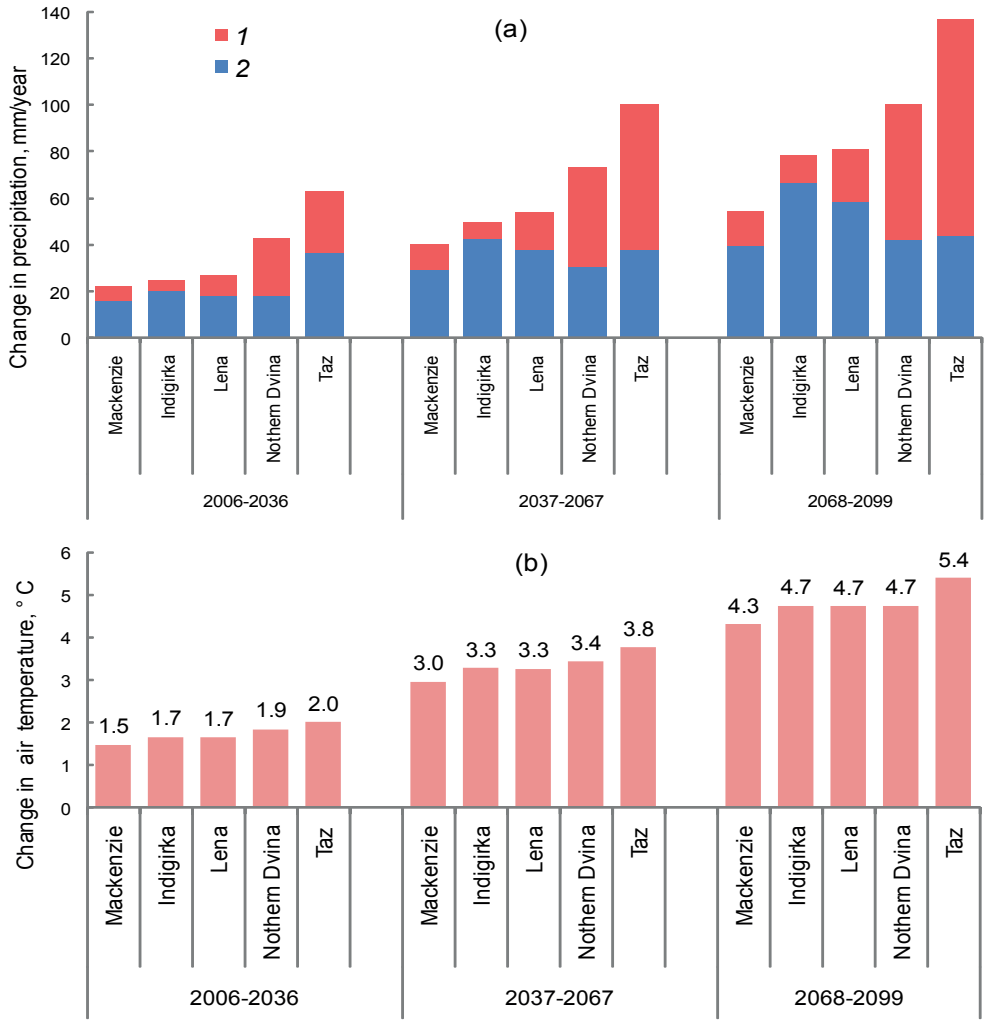

Fig. 5. The projected mean changes in climatic annual (a) precipitation (with partitioning between evapotranspiration – *1* and runoff – *2*) and (b) air temperature

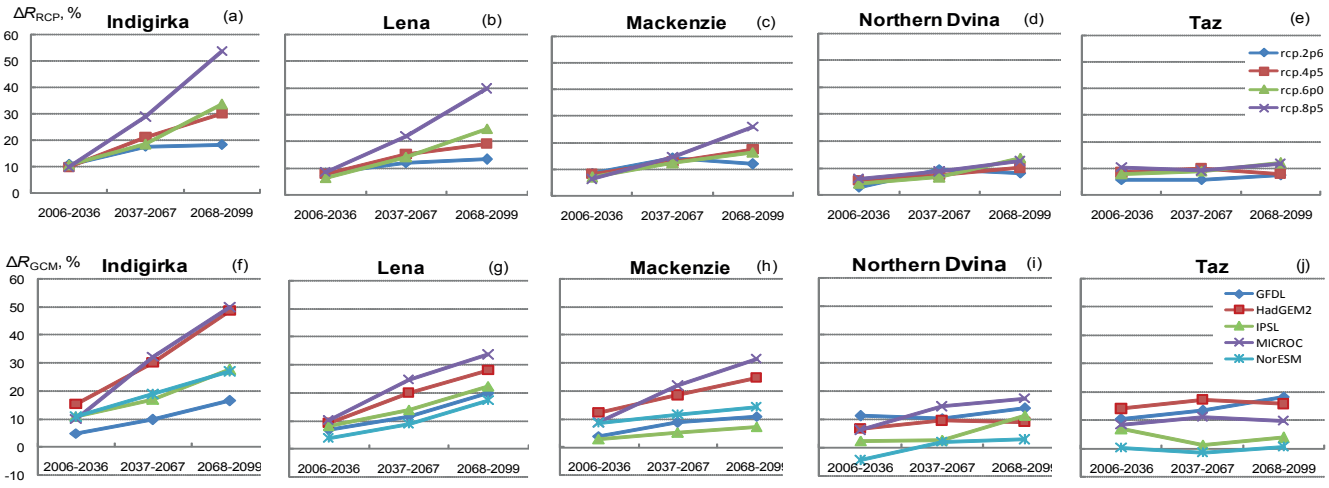

Fig. 6. The projected relative changes in climatic annual river runoff for three climatic periods: (a-e) averaged over five GCMs, (f-j) averaged over four climatic RCP-scenarios

confirm that all types of uncertainties grow with time; the contribution of various RCP scenarios to the uncertainty of precipitation and river runoff is less than that of GCMs, however, it is increasing by the end of the 21st century. Thus, the ratio of $Range\%_{GCM}$ to $Range\%_{RCP}$ decreases with time: for precipitation, from 1.9 for P1 to 1.1 for P3, and for runoff, from 2.2 for P1 to 1.2 for P3 period. As seen, in the third period the GCMs and scenarios make nearly the same contribution to the uncertainty of projected changes in precipitation (Fig. 7 b, d), while the contribution of scenarios is still less in the case of runoff projections (Fig. 7 a, c).

Discussion

The projected changes in Arctic river runoff are in a good agreement with the results found in literature. Thus, in (Bring et al. 2017), simulated by macro-scale hydrological model WBM multimodal and multiscenario (averaged over six GCMs and three RCP scenarios excluding the lowest-emission RCP2.6 scenario) change in annual river discharge for 2061-2090 compared to 1961-1990 is within the range of 0-25% in the region of the Northern Dvina and Taz basins, 25-50% for the most part of Lena, more 50% in the location

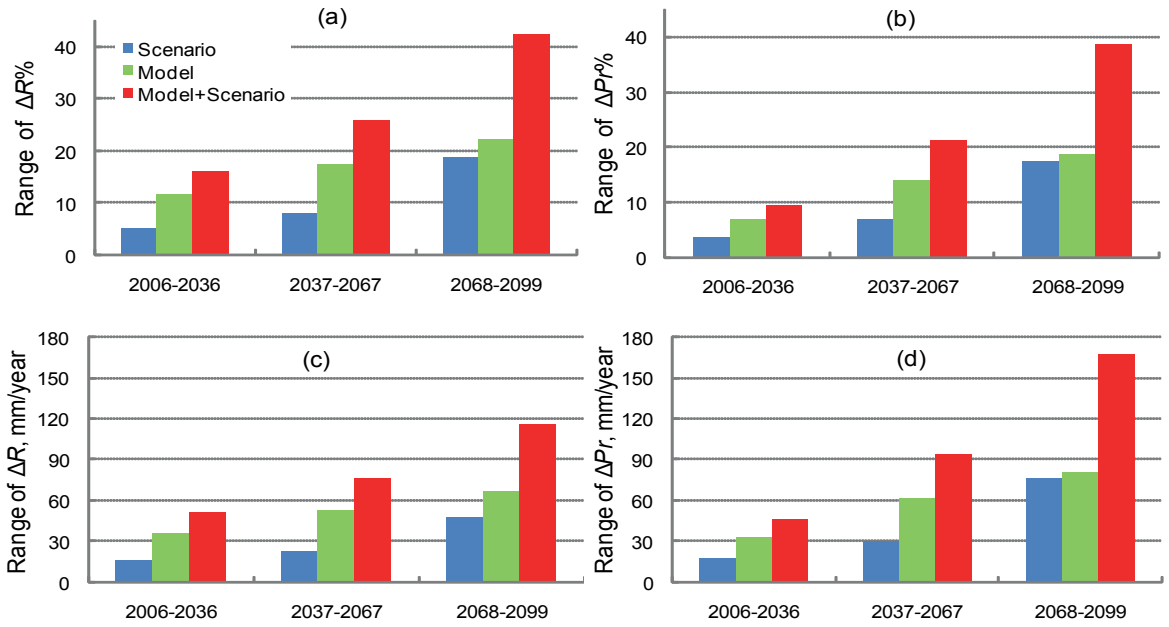

Fig. 7. Averaged over 5 river basins variation ranges of projected changes in climatic values of annual (a, c) runoff and (b, d) precipitation caused by differences in the RCP scenarios (blue), GCMs (green) and both scenarios and models (red)

of Indigirka and mostly 0-25% in the area of MacKenzie basin (Bring et al. 2017, Fig. 3). If we also exclude RCP2.6 scenario, our ensemble-averaged estimates of changes in river runoff are 10, 12, 20, 28 and 39% for the Taz, Northern Dvina, MacKenzie, Lena and Indigirka, respectively. This means that they fall within the above intervals and the directions of increase in the projected changes also coincide. They also coincide with the results published in (Georgievsky and Golovanov 2019), according to which positive changes (for 2041-2060 under RCP4.5 and RCP8.5 scenarios) in annual runoff are projected for the entire pan-Arctic basin of Russia, reaching the highest values in the north-eastern part of Siberia (including, in particular, the Lena and Indigirka basins).

As to uncertainties, our conclusion about the contribution of climate model structural uncertainty and differences in emission scenarios to the overall hydrological uncertainty is consistent with previous studies. The lowest uncertainties in runoff projections were obtained for the Northern Dvina and Taz rivers, higher uncertainties for the Mackenzie and Lena, and the highest ones for the Indigirka. This can be explained by the fact that meteorological outputs from GCMs are more reliable for the East-European and West-Siberian plains of Russia (Kislov et al. 2011). In (Nasonova et al. 2018), the same conclusion was made for the outputs from GCM INMCM4.0, which were of good quality for the Northern Dvina River basin and rather poor for the Indigirka and Kolyma basins.

CONCLUSIONS

Calibration of the most influencing parameters against measured river runoff resulted in significant improvement of SWAP performance with respect to goodness-of-fit statistics and the shape of hydrograph. For the calibration period, absolute value of *Bias* did not exceed 5% for all rivers, *NS* for monthly runoff varied from 0.68 to 0.93 (median value = 0.89). For the validation period, absolute *Bias* did not exceed 3% for 4 rivers, while *Bias*=13.3% for the Taz river, NS varied from 0.58 to 0.89 (median value = 0.84). Hydrological projections up to the end of the 21st century were carried out with the help of SWAP driven by meteorological projections simulated by five GCMs for four climatic scenarios of the RCP family. On the average, for all rivers, precipitation will increase by the end of the 21st century by 12% (Mackenzie) - 30% (Indigirka), runoff will increase by 10% (Taz) – 30% (Indigirka), evapotranspiration by 6% (Mackenzie) - 47% (Taz).

The largest increase in river runoff (averaged over five GCMs) was obtained for the RCP8.5 scenario by the end of 21st century: 12% for the Taz and Northern Dvina rivers, 26% for the Mackenzie, 40% for the Lena and 54% for the Indigirka.

Thus, the runoff of the Northern Dvina and Taz rivers will experience the least impact of climate change under the RCP scenarios, this impact will increase towards eastern Siberia and reach a maximum in the Indigirka basin.

Analysis of the uncertainties in the projected changes in the water balance components has shown that:

- all types of uncertainties increase by the end of the 21st century;
- on the territory of Russia, the uncertainties increase eastward from the lowest values for the Northern Dvina and Taz rivers to the largest values for the Indigirka River;
- the uncertainties in river runoff are in a good agreement with uncertainties in precipitation;
- on the average, the contribution of GCM structural uncertainty to the uncertainty of hydrological projections is nearly twice larger than the contribution of differences in emission scenarios in 2006-2036 and decreases over time to 1.1-1.2 in 2068-2099.

REFERENCES

Arnell N.W. and Lloyd-Hughes B. (2014). The global-scale impacts of climate change on water resources and flooding under new climate and socio-economic scenarios. Climatic change, 122, 127–140, DOI: 10.1007/s10584-013-0948-4.

Barry R.G. and Serreze M.C. (2000). Atmospheric component of the Arctic Ocean freshwater balance and their interannual variability. In: The Freshwater Budget of the Arctic Ocean (Eds: Lewis E.L., Jones E.P., Lemke P., Prowse T.D., and Wadhams P.). New York: Springer, 45-56, ISBN-13: 978-0792364405.

Bring A., Shiklomanov A., and Lammers R.B. (2017). Pan-Arctic river discharge: Prioritizing monitoring of future climate change hot spots. Earth's Future, 5, 72-92, DOI: 10.1002/2016EF000434.

Champeaux J.L., Masson V., and Chauvin F. (2005). ECOCLIMAP: a global database of land surface parameters at 1 km resolution. Meteorol. Appl., 12, 29-32, DOI: 10.1017/S1350482705001519.

Clapp R.B. and Hornberger G.M. (1978). Empirical equations for some soil hydraulic properties. Water Resour. Res., 14(4), 601–604, DOI: 10.1029/WR014i004p00601.

Cosby B., Hornberger G., Clapp R., and Ginn T. (1984). A statistical exploration of the relationships of soil moisture characteristics to the physical properties of soils. Water Resour. Res., 20, 682-690, DOI: 10.1029/WR020i006p00682.

Dai A. (2016). Historical and future changes in streamflow and continental runoff: A review In: Tang Q. and Oki T., eds., Terrestrial Water Cycle and Climate Change: Natural and Human-Induced Impacts, American Geophysical Union, Washington, D.C., 17-37, ISBN: 978-1-118-97176-5.

Dobrovolski S.G. (2014). Assessment of the statistical significance of global changes in the annual river runoff in XXI century due to possible anthropogenic warming of climate. Water Resources, 41(6), 728–737, DOI: 10.1134/S0097807814060049.

Duan Q., Sorooshian S., and Gupta V.K. (1992). Effective and efficient global optimization for conceptual rainfallrunoff models. Water Resour. Res., 28(4), 1015-1031, DOI:10.1029/91WR02985.

Gelfan A.N., Gusev E.M., Kalugin A.S., Krylenko I.N., Motovilov Yu.G., Nasonova O.N., Millionschikova T.D., and Frolova N.L. (2022). Runoff of Russian rivers under current and projected climate change: A review 2. Climate change impact on the water regime of Russian rivers in the XXI century. Water Resources, 22(3), 1-16.

Gelfan A., Gustafsson D., Motovilov Yu., Arheimer B., Kalugin A., Krylenko I., and Lavrenov A. (2017). Climate change impact on the water regime of two great Arctic rivers: modeling and uncertainty issues. Climatic Change, 141, 499-515, DOI: 10.1007/s10584-016-1710-5.

Georgiady A.G. and Milyukova I.P. (2006). River runoff within Lena river basin in conditions of probable global climate warming. Computational technologies, 11(2), 166-174 (in Russian with English summary).

Georgievsky M.V. and Golovanov O.F. (2019). Forcasting changes in river water resources of Russian Federation based on CMIP5 runoff data. Vestnik of Saint Petersburg University. Earth Sciences, 64(2), 206-218, (in Russian with English summary), DOI: 10.21638/spbu07.2019.203.

Gosling S.N., Zaherpour J., Mount N.J., Hattermann F.F., Dankers R., Arheimer B., Breuer L., Ding J., Haddeland I., Kumar R., Kundu D., Liu J. van Griensven A., Veldkamp T.I.E., Vetter T., Wang X., and Zhang X. (2017). A comparison of changes in river runoff from multiple global and catchment-scale hydrological models under global warming scenarios of 1°C, 2°C and 3°C. Climatic Change, 141, 577-595, DOI:10.1007/s10584-016-1773-3.

Gusev E.M. and Nasonova O.N. (2013). A technique for scenario prediction of changes in water balance components in northern river basins in the context of possible climate change. Water Resources, 40(4), 426-440, DOI: 10.1134/S0097807813040040.

Gusev Ye.M. and Nasonova O.N. (2014). Application of a technique for scenario prediction of climate change impact on the water balance components of northern river basins. J. Hydrol. Hydromech., 62(3), 197-208, DOI: 10.2478/johh-2014-0025.

Gusev E.M. and Nasonova O.N. (2010). Modeling heat and water exchange of the land surface and atmosphere. Moscow: Nauka (in Russian), ISBN 978-5-02-036958-0.

Gusev E.M., Nasonova O.N., and Dzhogan L.Ya. (2011a). Modeling river runoff in northwestern Russia with the use of land surface model SWAP and global databases. Water Resources, 38(5), 571-582, DOI: 10.1134/S0097807811050101.

Gusev E.M, Nasonova O.N, and Dzhogan L.Y. (2016a). Physically based modeling of many-year dynamics of daily streamflow and snow water equivalent in the Lena R. basin. Water Resources, 43(1), 21-32, DOI: 10.1134/S0097807816010085.

Gusev E.M., Nasonova O.N., and Dzhogan L.Y. (2015a). Physically based simulating long-term dynamics of diurnal variations of river runoff and snow water equivalent in the Kolyma River basin. Water Resources, 42(6), 834-841, DOI: 10.1134/S0097807815060056.

Gusev E.M., Nasonova O.N., and Dzhogan L.Y. (2010). Reproduction of Pechora runoff hydrographs with the help of a model of heat and water exchange between the land surface and the atmosphere (SWAP). Water Resources, 37(2), 182-193, DOI: 10.1134/S0097807810020065.

Gusev E.M., Nasonova O.N., and Dzhogan L.Y. (2016b). Scenario prediction of changes in water balance components in the Lena basin in the context of possible climate changes. Water Resources, 43(5), 754-765, DOI: 10.1134/S0097807816050079.

Gusev E.M., Nasonova O.N., Dzhogan L.Ya., and Aizel' G.V. (2013). Modeling Streamflow of the Olenek and Indigirka Rivers Using Land Surface Model SWAP. Water Resources, 40(5), 535-543, DOI: 10.1134/S0097807813030056.

Gusev E.M., Nasonova O.N., Dzhogan L.Y., and Ayzel G.V. (2014). Scenario prediction of changes in water balance components of the Olenek and Indigirka rivers in the context of possible climate change in the region of the republic of Sakha (Yakutia). Water Resources, 41(6), 748-762, DOI: 10.1134/S0097807814030099.

Gusev E.M., Nasonova O.N., Dzhogan L.Y., and Ayzel G.V. (2015b). Simulating the formation of river runoff and snow cover in the northern-west Siberia. Water Resources, 42(4), 460-467, DOI: 10.1134/S0097807815040065.

Gusev E.M., Nasonova O.N., Dzhogan L.Ya., and Kovalev E.E. (2011b). Northern Dvina runoff simulation using land-surface model SWAP and global databases. Water Resources, 38(4), 470-483. DOI: 10.1134/S0097807811030043.

Gusev E. M., Nasonova O. N., Dzhogan L. Ya., and Kovalev E. E. (2008). The Application of the Land Surface Model for Calculating River Runoff in High Latitudes. Water Resources. 35(2), 171-184, DOI: 10.1007/s11268-008-2005-7.

Gusev E.M., Nasonova O.N., Kovalev E.E, and Ayzel' G.V. (2018). Possible Climate Change Impact on River Runoff in the Different Regions of the Globe. Russian Meteorology and Hydrology, 43(6), 397-403, DOI: 10.3103/S1068373918060079.

Gusev E.M., Nasonova O.N., Shurkhno E.A., and Dzhogan L.Ya. (2019a). Scenario Forecasting of Changes in Water Balance Components in the Ob–Irtysh Basin in the Context of Possible Climate Change. Water Resources, 46(5), 647-658. DOI: 10.1134/S0097807819050099.

Gusev E.M., Nasonova O.N., Shurkhno E.A., Dzhogan L.Ya., and Aizel G.V. (2019b). Physically Based Modeling of the Long-Term Dynamics of Water Balance and Snow Water Storage Components in the Ob–Irtysh River Basin. Water Resources, 46(4), 493-503, DOI: 10.1134/S0097807819040109.

Hempel S., Frieler K., Warszawski L., Schewe J., and Piontek F. (2013). A trend-preserving bias correction – the ISI-MIP approach. Earth Syst. Dynam., 4(2), 219-236, DOI: 10.5194/esd-4-219-2013, 2013.

Kattsov V.M., Walsh J.E, Chapman W.L., Govorkova V.A., Pavlova T.V., and Zhang X. (2007). Simulation and projection of Arctic freshwater budget components by the IPCC AR4 global climate models. J. Hydrometeorol., 8(3), 571-589, DOI:10.1175/JHM575.1.

Khon V.Ch. and Mokhov I.I. (2012). The hydrological regime of large river basins in northern Eurasia in the XX–XXI centuries. Water Resources, 39(1), 1-10, DOI: 10.1134/S0097807812010058.

Kislov A.V., Grebenets V.I., Evstigneev V.M., Konishchev V.N., Sidorova M.V., Surkova G.V., and Tumel' N.V. (2011). Effects of possible climate warming in the 21st century for Northern Eurasia. Vestnik MGU, Ser. 5, Geography, 3, 3-8 (in Russian with English summary).

Koirala S., Hirabayashi Y., Mahendran R., and Kanae S. (2014). Global assessment of agreement among streamflowprojections using CMIP5 model outputs. Environ. Res. Lett., 9(6), 064017, DOI: 10.1088/1748-9326/9/6/064017.

Krysanova V. and Hattermann F.F. (2017). Intercomparison of climate change impacts in 12 large river basins: overview of methods and summary of results. Climatic Change, 141, 363-379.

Nasonova O.N. (2011). Application of a land surface model for simulating rainfall streamflow hydrograph: 2. Comparison with hydrological models. Water Resources, 38(3), 274-283, DOI: 10.1134/S0097807811030080.

Nasonova O.N., Gusev Ye.M., and Kovalev Ye.E. (2009). Investigating the Ability of a Land Surface Model to Simulate Streamflow with the Accuracy of Hydrological Models: A Case Study Using MOPEX Materials. J. Hydrometeorology, 10(5), 1128-1150, DOI: 10.1175/2009JHM1083.1.

Nasonova O.N., Gusev Ye.M., Kovalev E.E., Ayzel G.V., and Chebanova M.K. (2021). Projected changes in water balance components of 11 large river basins during the 21st century and their uncertainties. Water Resources, 48(5), 666-675, DOI: 10.1134/S0097807821050158.

Nasonova O.N., Gusev Ye.M., Kovalev E.E., Ayzel G.V., and Panysheva K.M. (2019). Projecting changes in Russian northern river runoff due to possible climate change during the 21st century: A case study of the Northern Dvina, Taz and Indigirka rivers. Water Resources, 46(Suppl. 1), S145-S154, DOI: 10.1134/S0097807819070145.

Nasonova O.N., Gusev E.M., Kovalev E.E., and Shurkhno E.A. (2021). Global estimates of changes in the terrestrial water balance components in the context of possible climate changes. Water Resources, 48(4), 459-473, DOI: 10.1134/S0097807821040151.

Nasonova O.N., Gusev Ye.M., Volodin E.M., and Kovalev E.E. (2018). Application of the land surface model SWAP and global climate model INMCM4.0 for projecting runoff of northern Russian rivers. 2. Projections and their uncertainties. Water Resources, 45(Suppl. 2), S85-S92, DOI: 10.1134/S0097807818060271.

Semenov S.M. and Gladilshchikova A.A. (2022). Scenarios of anthropogenic changes in the climate system in the XXI century. Fundamental and Applied Climatology, 8(1), 75-106, DOI: 10.21513/2410-8758-2022-1-75-106.

Shkolnik I.M., Meleshko V.P., Karol I.L., Kiselev A.A., Nadyozhina E.D., Govorkova V.A., and Pavlova T.V. (2014). Expected climate change on the territory of the Russian Federation in the XXI century. Trudy GGO, 575, 65-118 (in Russian).

Weedon G.P., Gomes S., Viterbo P., Shuttleworth W.J., Blyth E., Oesterle H., Adam J.C., Bellouin N., Boucher O., and Best M. (2011). Creation of the WATCH Forcing Data and its uses to assess global and regional reference crop evaporation over land during the twentieth century. J. Hydrometeorol., 12, 823-848, DOI: 10.1175/2011JHM1369.1.

RESEARCH PAPER

LONG-TERM HEAT FLUX FORMATION OF THE LARGE RUSSIAN ARCTIC RIVERS UNDER THE INFLUENCE OF CLIMATE-INDUCED AND DAM-INDUCED EFFECTS

Alexander N. Vasilenko[1*], Dmitry V. Magritsky[1], Natalia L. Frolova[1], Artem I. Shevchenko[2]
[1]Faculty of Geography, Lomonosov Moscow State University, Leninskie Gory 1, 119991, Moscow, Russia
[2]RIHMI-IDC Russian Institute of Hydrometeorological Data-WDC, Obninsk, 249035 Russia
***Corresponding author:** saiiiia24@mail.ru
Received: June 20th, 2022 / Accepted: November 11th, 2022 / Published: December 31st, 2022
https://DOI-10.24057/2071-9388-2022-105

ABSTRACT. The heat flux of the large rivers flowing into the Arctic seas of Russia plays an essential role in the thermal and ice regime of the lower reaches of these rivers and the southern part of the Arctic seas. However, estimates of the total value of heat flux and its spatial-temporal distribution require clarification. In this research, we analyzed monthly, and yearly water temperature data from 55 gauges and water flow data from 35 gauges in the lower reaches of the rivers of the Russian Arctic northerner of 60 N. These rivers are: Onega, Northern Dvina, Mezen, Pechora, Ob, Nadym, Pur, Taz, Yenisei, Khatanga, Anabar, Olenek, Lena, Yana, Indigirka, Alazeya, Kolyma and their main tributaries. The collected data series covers 1930-2018, focusing more on 1960–2018. We used Spearman trend tests and Mann-Whitney U-test to clarify changes in the thermal regime of study rivers. Our estimations showed that heat flux did not significantly increase in the past three decades on most rivers except Yenisei and Yana lowlands. Water temperatures on rivers monotonically increased after 1960, especially in May and June, but without statistical significance. The role of dams in the water temperature regime is observed for nearly 500 km lower dams, but it is not observed in their lowlands and mouths. We also identified the decrease in water temperatures and heat flux in river lowlands, estuaries and deltas up to 25% for Yenisei lowlands.

KEYWORDS: Arctic, water temperature, heat flux, climate changes, reservoir

CITATION: Vasilenko A. N., Magritsky D. V., Frolova N. L., Shevchenko A. I. (2022). Features Of A Long-Term Heat Flux Formation Of The Large Russian Arctic Rivers And Its Transformations In Estuaries Under The Influence Of Climate-Induced And Dam-Induced Effects. Geography, Environment, Sustainability, 4(15), 158-170
https://DOI-10.24057/2071-9388-2022-105

ACKNOWLEDGEMENTS: The research has been performed at the expense of RFBR Grant 18-05-60021, Interdisciplinary Scientific and Educational School of Lomonosov Moscow State University «The Future of the Planet and Global environmental changes» and RSF Grant 21-17-00181 (for the lower reaches of Lena River).

Conflict of interests: The authors reported no potential conflict of interest.

INTRODUCTION

River heat flux plays an important role in hydrological and ecological state of rivers, their thermal and ice regime (Alekseevskiy 2000, 2012). It also takes part in bank erosion in permafrost zone (Costard et al. 2003). River water heat, which is transported from the South to the North with large rivers, is an important component of river valleys climate, ice and thermal regime of arctic sea near shore zones (Golubeva et al. 2015, Park et al. 2020). The role of a heat flux factor depends on thermal conditions, geographical position and basin area, on flow direction, water regime, morphological structure of delta etc.

River heat flux is a function water flow and water temperatures. Annual water flow of Russian Arctic rivers had increased after 1970–1990-s for 7-10%, but statistically significant changes in Russian Arctic rivers are only in North-East of Russia (Frolova et al. 2022). A great range of models as global, as regional ones show that water flow of these rivers will increase for 10-40% to the end of 21 century, first of all with a spring flood reduction and with an increase of summer and autumn water flow (Gelfan et al. 2022). Water temperatures are controlled with air temperatures on monthly and annual time-scale (Hannah and Garner 2015). Significant air temperature increase after the end of 1970-s is observed all around Russia (Doklad 2022). Significant warming in Artic is more intensive, that in southerner regions (IPCC 2014, IPCC 2022). In Russian Arctic annual air temperatures increase for 0.8-1.1°C/decade, and seasonal air temperatures increase for 0.4-1°C/decade (Doklad 2022). Warming is increase from South-West to North-East. Global river water temperature increase is from -1.21°C to 1.076°C (1901–2010) (IPCC 2022), but in Arctic region it is observed (in Russian part) (Vasilenko et al. 2020) and

modeled (Wanders et al. 2019) an increase of annual river water temperatures in past decades. Therefore, changes in a heat flux are expected.

Arctic river heat flux studies began in 1907 (Polinov 1907) and in 1914 (Shostakovich 1914). However, first reliable estimations were obtained in the USSR during the active economic development, expedition and scientific study of the Arctic. In a group of manuscripts (Antonov 1936, Zaikov 1936, Zotin 1947, Korovkin 1940, 1941, Kashcheev et al. 1937, Khmyznikov 1934) there were as heat flux values of some large rivers, as estimations of total heat flux to an Arctic Ocean from Soviet part of basin. There were also several conclusions about a role of a heat flux in Arctic sea ice regime. The next important stage of heat flux studies was release of the series of monographs "Surface water resources of USSR" (Surface water resources of the USSR 1969, 1970, 1972 a,b, 1973 a,b) in 1960–1980. During this stage there were also an expansion of observation network, building dams of a great Asian reservoirs, and projects for the transfer of part of the river water resources to the south. A range of studies, were dedicated to scientific support of these activities (Antonov 1976, Elshin 1981, 1988, Gottlieb et al. 1976, Ivanov and Nikiforov 1976, Ivanov and Kurzhunov 1980, Kurzhunov 1984, Nikiforov et al. 1980, Odrova 1984, 1987, Orlova 1984, Soviet Arctic 1970).

In XXI a new stage of studies began. New hydrological and meteorological data, the building new reservoirs and an increase in the scale of nature management at the catchments of the Arctic rivers, regional climatic changes required new assessments of the heat flux and thermal regime of these rivers, analysis of the adaptation of their thermal regime to these processes, clarification of spatial and temporal patterns, assessment of the contribution of climate induced and anthropogenic factors to the observed changes.

New estimates of the heat flux in the lower reaches and estuaries of the main Arctic rivers, heat inflow into the Arctic seas, new conclusions about trends and cycles in long-term fluctuations in water temperature and heat flux are presented in (Geoecological state 2007, Kosmakov 2001, Magritsky 2009, 2015, Magritsky et al. 2004, Vasilenko et al. 2020; Georgiadi et al. 2018, Lammers et al. 2007, Liu 2004, Liu et al. 2005, Park et al. 2017, Yang et al. 2005). Dam-inducted changes of water temperatures and heat flux of Asian Arctic rivers are in (Geoecological state 2007, Kosmakov 2001, Magritsky 2009, 2015, Magritsky et al. 2004, Yang et al. 2004, Ye et al. 2003, Liu et al. 2005). The estimations of decreasing a heat flux in multichannel big delta of Lena River was done by D.V. Magritskiy et al. (2018). There are a range of new methods to estimate river heat flux from ungauged areas (Geoecological state 2007, Magritsky 2009, 2015, 2021, Lammers et al. 2007, Liu et al. 2005, van Vliet et al. 2011). There are also a range of more complex models, using for future projections of water temperatures and a water heat flux (Mohseni et al. 1998, Park et al. 2017, Toffolon and Piccolroaz 2015, van Vliet et al. 2011). These models are mostly tested by the data from key gages at the Ob, Yenisei and Lena rivers (Park et al. 2017, van Vliet et al. 2011). The dominant role of the thermal factor in the erosion of river banks in permafrost regions was first experimentally confirmed with Costard F. (Costard et al. 2003).

Despite this there are some issues not previously considered, which are related to the thermal state and heat flux of rivers flowing into the Arctic seas, the regularities of their changes over the territory and along the large rivers, anthropogenic influence for these characteristics. The estimates of heat flux in earlier papers were obtained due to short series with the end in the late 1990s – early 2000s, and for a relatively small number of gauging stations. In our study we prolong hydrological data to 2018/2019 and use more posts. The changes in water temperatures and heat flux downstream of the basin outlet station of the Arctic rivers are considered in more detail.

MATERIALS AND METHODS

River water temperature data

Water temperature is measured on gauging stations of the Russian (and former Soviet) Hydrology and Meteorology service (ROSHYDROMET) twice a day, 8 a.m. and 8 p.m. (local time). Temperature on coastal sea stations of ROSHYDROMET (within the river mouths) is measured 4 times a day – 00, 06, 12 and 18 UTC. Measurements at the river gages are not carried out in winter, when the rivers are frozen. In spring, observations often start a few days after ice breaking, sometimes in near-shore polynyas. Annual observation period for the study area is usually from 4 to 8 months. In autumn, measurements are interrupted when the water temperature reaches 0°C or is less than 0.2°C for a few days. It is usually connected with autumn ice run. In May and April all sea coastal waters have negative monthly temperatures, and November water temperatures are also mostly negative.

An important issue with the temperature data is related to the period when it was measured only once a day – in the morning. This was the common practice until the 1950s. According to E.M. Sokolova (1951), morning temperature differs from the average temperature as it is closer to the daily minimum value. On rivers with high water runoff, the difference between the morning and daily average temperature does not exceed 0.1–0.5°C (for monthly values), while on small rivers it can reach 1–2°C. Therefore, we analyzed most of records only after 1960.

Measurements are usually made close to the river bank with flowing water and a depth of at least 0.3–0.5 m. But the water temperature measured near the shore does not show real mean stream temperature due to permafrost rocks, or plant shadowing, or groundwater inflow, or tributary's waters. Information about gauging stations (g.) on large rivers and the difference in temperatures in near-shore zone and mean stream temperature was collected during our and others' field works (Magritsiy et al. 2022), so water temperature data from a several gauges was not use because of a great impact of tributaries. For other cases, which are not covered with field works, we had to use water temperatures, which are measured near a river bank. These temperatures were also used in previous studies (Lammers et al. 2007, Park et al. 2020).

For this research we have selected data from 55 gauging stations from our database, where it is 150 posts (Fig. 1). The main part was made up of data for basin outlet stations and gauges at the mouths of large rivers flowing into the Arctic seas of Russia: Onega, Northern Dvina, Mezen, Pechora, Ob, Nadum, Pur, Taz, Yenisei, Khatanga, Anabar, Olenek, Lena, Yana, Indigirka, Alazeya and Koluma. On the regulated large rivers of the Asian part of Russia (Ob, Yenisei, Vilyui and Kolyma), the data gauges located along the entire length of these rivers, starting from the dam of the reservoirs and ending with the basin outlet station of the river, were used. This is still 28 gauges. The rest is data from gauges on main tributaries of large Arctic rivers.

Due to a lot of gaps in published water temperature data we used in this investigation only those gages, which have in their monthly water temperature records at least

20 years in 1961–1991, and at least 15 years in 1991–2018/2019. Data on water temperature are published by ROSHYDROMET in their annual handbooks as 10-day and monthly average values together with maximum values and dates of their occurrence.

For a largest rivers of the region we also used water temperature and water discharge records from 1936 to 2018. For these rivers we also calculate different statistics for a period before and later than 1970. This year chose because of a beginning of water flow and air temperature changes began after 1970, and a great dams on Ob and Yenisei were built before 1970.

Number of sea coastal stations is decreasing from the West to the East. Measurements in river parts of estuaries and in the deltas are provided within Onega, Severnaya Dvina, Pechora, Ob, Yenisei and Lena rivers' mouths. Sea coastal water temperatures for Russian Arctic seas are in open source mostly from 1977. Lots of stations were closed in 80th and 90th. Near shore zone temperatures was collected from «The Unified State Information System on the situation in the World Ocean» (http://portal.esimo.ru/). We used the information from offshore coastal stations both to analyze seaward transformation of the temperature regime within the mouth.

Water discharge data

Water discharges measurements in Russian Arctic began in 1880s on rivers of the North of European part of Russia. Measurements on most rivers began in the 1930s and 1940s. Most of discharge measurements with the greatest coverage of river basins was from 1960s to 1980s. But since the 1990s a lot of stations were closed and at many gauging stations discharge measurements were terminated. Measurements of water discharge are no longer carried out at the mouth reaches of the Taz, Pyasina, Khatanga, Yana, Indigirka, Alazeya, Kolyma (Kolymskoe-1), Amguema and Anadyr rivers as well as other medium and small rivers flowing into the Arctic seas. At the mouth of the Yenisei River (Igarka) and Lena River (Kyusyur), water discharge measurements are occasional, while in the Lena River delta they are completely abandoned. At the mouths of the Nadym and Pur rivers, water discharge measurements were resumed after a long break in 2010 and 2013.

Water discharges are measured once a 10-day (RD 2020; Instruction 1978) in gauges which have water discharge measurements in their programs. Measurements can be more frequent in the periods of high flow. Daily discharge values are calculated by regional ROSHYDROMET services based on established relationships between water discharge and water stages, measured twice a day. The 10-days mean water discharges are calculated as mean daily discharges for 10-daus period. Monthly discharges are counted as mean from daily ones. Previously obtained empirical dependencies between water levels and discharges, between water discharges at different gauging stations, continue to be officially used to calculate water discharges at some hydrological stations, where water discharges are either no longer measured, or are not measured every year. An example is the situation at the stations of g.Igarka (Yenisei), g.Saskylakh (Anabar) and g.Kolymskoye–1 (Kolyma). Water discharge measurements are provided usually not far than 1 km from a point of water temperature and water level measurements, in a most suitable place on the river. Water discharge data for each station are published in the annual hydrological handbook of ROSHYDROMET as daily, 10-day, monthly and annual average values together with maximum and minimum values and dates of their occurrence.

In total, data on water discharges from 35 stations for the period from 1930 to 2018 year were used. Many of the selected long-term discharge time series had gaps, as well as a late beginning (in the 1960s or 1970s) and an early end of observations, primarily in the 1990s. (mostly in the 1990s). To solve this problem, reconstruction of missing values and lengthening of time series was carried out using one-dimensional and sometimes multiple regression. Water discharges were reconstructed based on the data of analogue stations, which were characterized by an empirical relationship with correlation coefficients (R) greater than 0.7-0.8.

Methods

Heat-flux was calculated using the following equation (Elshin 1981, Magritsky 2009; Methodological recommendations 1961): $W_T = c_p \rho W \bar{T}_w$, where, W_T is heat-flux, Joule (for a month or a decade); c_p is specific heat capacity, which is 4,174-4,212 Joule/(kg×°C) for T_w from 0 to 30 °C; ρ is fresh water density; W is water runoff, m^3 (for a month or a decade); T_w, is mean water temperature for the same time interval. Heat flux over a year or hydrological season is obtained by summing 10-day or monthly values of W_T. It was found that there is a difference between the values of annual heat flux calculated using monthly (main case) and 10-day values, which can be characterized by the coefficient $K_{d/m}=W_T$(decade)/W_T(month) (Magritsky 2021). In the northeast Asian part of Russia, the coefficient $K_{d/m}$ varies from 0.90 to 1.05. For most posts, the calculation of the heat flux is based on monthly data.

Identification and assessment of trends in long-term fluctuations of T_w and the heat flux of rivers of the region was carried out by graphical and statistical methods. The first group of methods included plotting and analysis of the usual timing graphs $T_w=f(t)$, $W_T=f(t)$, as well as

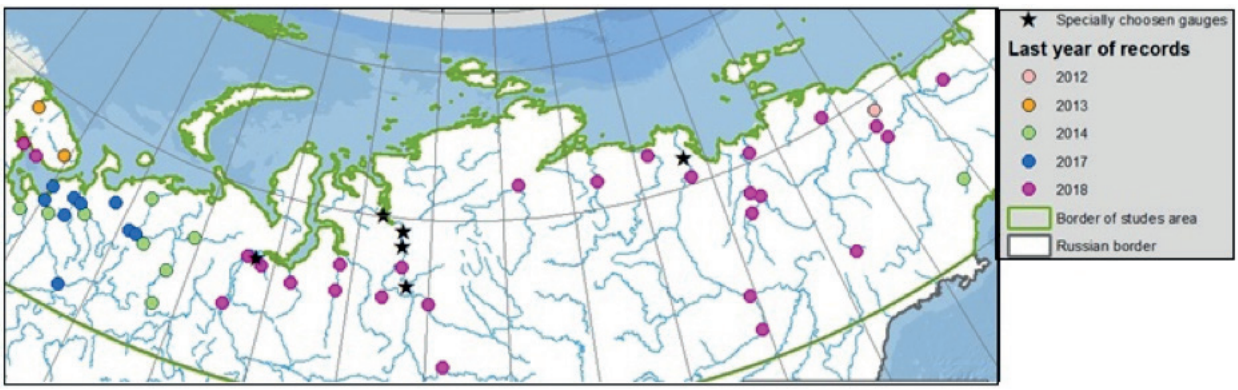

Fig. 1. Geographical location of analyzed gauging stations, and the last year in their water temperature records

differential mass (*St*) and total mass (*Ss*) curves. Ordinates of the differential mass curves were calculated by the formula: $St_i = \sum^{t} (x_i / \bar{x} - 1)$, total mass curves – $Ss_i = \sum^{t} x_i / \bar{x}$, where x_i is value for a certain year. The second group of methods was necessary both for quantifying the main parameters of hydrological characteristics, trend values, etc., and for confirming the statistical significance of the identified trends, the difference in average values and variances of the selected and compared independent long-term periods. Here we used analysis of data series (with a significance level α = 5% for all tests) for homogeneity (using F-test, t-test and Mann-Whitney U-test). Mann-Whitney test was used as main ones, because of it is irrespective from normal distribution and have good results even for a short record. The presence and statistical significance of trends was analyse using Spearman's rank correlation coefficient, which is close to Mann-Kendall test. Although, Pettitt test was used for detecting a "change point" in water temperature and heat stick records. This test is used for detecting "change points" in water flow rows for Russian rivers (Frolova et al. 2022), so it is an opportunity to compare changes in water and temperature regimes of rivers. This test is marked only one point in a row, so local changes were analyzing with trends and comparing statistical characteristics (mean, standard deviations) of two nearest periods. Local increasing or decreasing of water temperatures and heat flux could occur in short time periods (less than 15-20 years). Due to a gaps in records in 1990-s and in past years, such periods length could be not enough to count statistical significance, so we are somewhat cautious about some of the results in the last decade (2011–2020) in the North of European part of Russian Arctic.

It was decided to consider 1961–1990s as the base period, and the 1991–2018/2019 as the modern period. The basis for this decision was the recommendations of the WMO, the features of the initial data on water temperature, and the analysis of graphs. To improve our estimations, we compared differences of mean values of 1991–2018 and 1961–1990 with their standard error of mean (SEM), and also with a SEM of 1960-2018 ($SEM = \sigma / \sqrt{n}$, σ – is standard deviation, n – is a number of values in the series), which helps to separate changes which are driven with changing the length of the record and changes which are driven with another reasons.

The analysis of changes in water temperature and heat flux of rivers by large reservoirs was carried out by comparing changes in the values of T_W and W_T and along the channel of rivers for two or three periods, i.e. statistical and graphical tools. These periods were chosen in such a way that they differed in magnitude of anthropogenic impact on hydrological regime of rivers, but would be similar in temperature conditions and annual/monthly river runoff.

Statistical tests were made using Python. Data was prepared with MS Office Excel. Data analyses were made both using Python and MS Office.

RESULTS AND DISCUSSION

Long-term water temperature and heat flux fluctuations under climate changes

Water temperature in lower reaches and estuaries of large rivers of Russian Arctic is mainly increasing (cf. Fig. 2). However, there are differences in magnitude of changes and in periods of the most changes of water temperatures and a heat flux. The maximum warming of river waters on most rivers is observed in June.

The long-term variability of temperature regime of the large rivers flowing into the White and Barents Seas is caused only by natural causes. The beginning of T_W increase in the lower reaches of these rivers is in good agreement with the beginning of noticeable climatic, first of all air temperature, changes here, dating from the second half of the 70s – early 80s of the XX century. The increase of T_W is found in all months of the warm season of the year. The greatest growth was recorded in June, during the decline of spring flood. The increase was 1.5–2.1°C in 1991–2018 compared with 1961–1990. The same changes of T_W in the same periods are observe on most of rivers of Onega, Severnaya Dvina, Mezen and Pechora watersheds and on Kola Peninsula. However, values of statistical significant T_W changes (due to U-test) are small enough. They are the highest in June in this part of Russian Arctic. The highest changes of T_W in June (2.0-3.0°C) are in Pechora watershed (but not on Pechora itself). In other months of a warm period T_W had changed for less than 1°C in all watersheds of the White and the Barents Seas. The amount of gauges with statistical significance of T_W changes are 31-42% among gauges used in this research (in the Barents and the White Sea watersheds) in July and in August and 62-69% in May and October. Most of gauges have significant changes in June (81%) and September (73%). On Onega, Severnaya Dvina and Mezen lowlands significant changes (due U-test) of T_W are observe from June to September, while on Pechora lowlands significant changes of T_W are observe in all warm months except July and August.

The largest rivers of Asian Part of Russian Arctic are regulated ones, but rivers of their Arctic watersheds are not dam-inducted. T_W increase on gauges of this region for a similar values with T_W of rivers of the White and Barents Seas watersheds. The highest changes are observed in June on large rivers of Kara Sea watershed (2.0-3.0°C). In upstream of Pur river changes of T_W of June is 4.0-5.0°C, but it was a gap of observation in 1990-s so this result is not so reliable as others.

Statistical significance of T_W of rivers of Asian part of Russian Arctic (according to U-test) is observed in 30% of gauges only in May and June. The amount of gauges with significant changes is decrease from June to October. T_W of July and August significantly increase only in a small group of medium rivers of Laptev Sea watershed, especially in Yana and Indigirka watersheds.

Small values of statistically significant changes of T_W accompanied by monotonic trends since 1961 without sharp changes on most of gauges, included gauges on large rivers (Fig. 2). Besides a long-term fluctuations of T_W as annual as monthly ones have gradual character. So in a 20-30 years period substantial T_W changes could be caused by a several extremely hot years. Therefore, differences of means of base period (1961–1990) and modern period (1991–2018) are even less than differences of means of base period and a second half of modern period (Table 1). Significant trends are shown by the color designations in Table 1. Two rows for each gauge are for the differences in T_W in 1991–2018 and 1961–1990, and for the difference in water temperatures 2005–2018 and 1961–1990.

Some differences were found at the years of beginning of a steady increase in seasonal and monthly water temperatures (Pettitt test) after 1960. In different months the median "change point" is from 1989 to 1996 (from May to October except September) and 2000 in September. The median transition year for watersheds (or Arctic parts of watersheds for a large rivers) is in a range from 1983 to 2007. So, main changes in water temperature regime after 1960 is close enough to such changes of air temperature,

Table 1. The value of changes of mean monthly water temperatures in large rivers of Russian Arctic in 1991-2018 in comparison with 1961-1990 and in 2005-2018 in comparison with 1961-1990

River – Gauging station	Periods of mean Tw comparison with 1961–1990	Month							
		April	May	June	July	August	Sept.	October	Nov.
Onega – Porog	1991–2018	0	**0.8**	**0.8**	0.9	**0.6**	0.9	0.8	0.3
	2005–2018	0.1	1.9	0.7	0.7	1.2	1.0	0.6	0.4
Severnaya Dvina – Ust-Pinega	1991–2018	0	**1.0**	**1.6**	**0.9**	**0.6**	**1.1.**	**1.2**	0.1
	2005–2018	0	0.8	0.4	0.3	0.9	0.4	0.4	0.3
Mezen – Dorogorskoe	1991–2018	0	**0.8**	**1.1**	0.3	0.2	0.2	**1.0**	0
	2005–2018	0	1.5	0.6	0.2	1.6	1.3	0.2	0.2
Pechora – Ust-Tsilma	1991–2018	0	**0.6**	**2.1**	**0.9**	**0.5**	**0.5**	**0.8**	**0.1**
	2005–2018	0	0.9	1.8	0.1	-0.1	0.2	1.0	0.1
Ob – Salekhard	1991–2018	0	**0.6**	**2.4**	**1.8**	**0.8**	**0.6**	**0.7**	**0**
	2005–2018	0	-0.1	0.8	0.6	-0.1	1.1	0.9	0
Nadym – Nadym	1991–2018	0	**1.1**	**2.4**	-0.3	0.1	0.2	**0.4**	0
	2005–2018	0	0.1	1.3	0.9	-0.1	1.5	0.6	0
Enisei – Igarka	1991–2018	0	**0.2**	**2.5**	**1.2**	-0.1	0.1	**0.6**	0
	2005–2018	0	0.1	1.9	1.5	-0.7	0.6	0.8	0
Khatanga – Khatanga	1991–2018	0	0	**1.6**	0.1	-0.4	0.4	**0.3**	0
	2005–2018	0	0	1.9	0.2	-0.1	0.8	0.2	0
Anabar – Saskylakh	1991–2018	0	**0.1**	**0.8**	-0.1	0.2	**0.6**	0	0
	2005–2018	0	0.1	2.2	0.8	0	0.9	0.1	0
Olenek – Taimylyr	1991–2018	0	0	**1.9**	**1.5**	**1.1**	**0.4**	0	0
	2005–2018	0	0	1.8	0	-0.1	0.8	0.1	0
Lena – Kyusyur	1991–2018	0	0	**0.9**	**1.2**	**1.1**	0.1	0	0
	2005–2018	0	0	1.5	0	0.4	-0.1	0.2	0
Yana – Yubileinaya	1991-2018	0	**0.1**	**0.7**	**0.8**	**1.3**	**0.4**	0.1	0
	2005–2018	0	0.1	1.7	-0.1	1.0	1.1	0.1	0
Indigirka – Chokurdakh	1991–2018	0	0	**1.2**	**1.0**	**0.9**	**0.9**	**0.1**	0
	2005–2018	0	0.1	1.5	-0.5	0.1	1.0	0,3	0
Kolyma – Srednekolymsk	1991–2018	0	0.1	0.1	**0.5**	**0.7**	**1.1**	**0.4**	0
	2005–2018	0	0.2	0.5	-0.3	0.6	0.9	0.1	0
	Significant trend only in 1961–2018								
	Significant trend in 1961–1990 and 1991–2018								
	Significant trend only in 1991–2018								
1.5	Changes are higher than standard error in 1960–2018, 1961–1190 and 1991–2018								

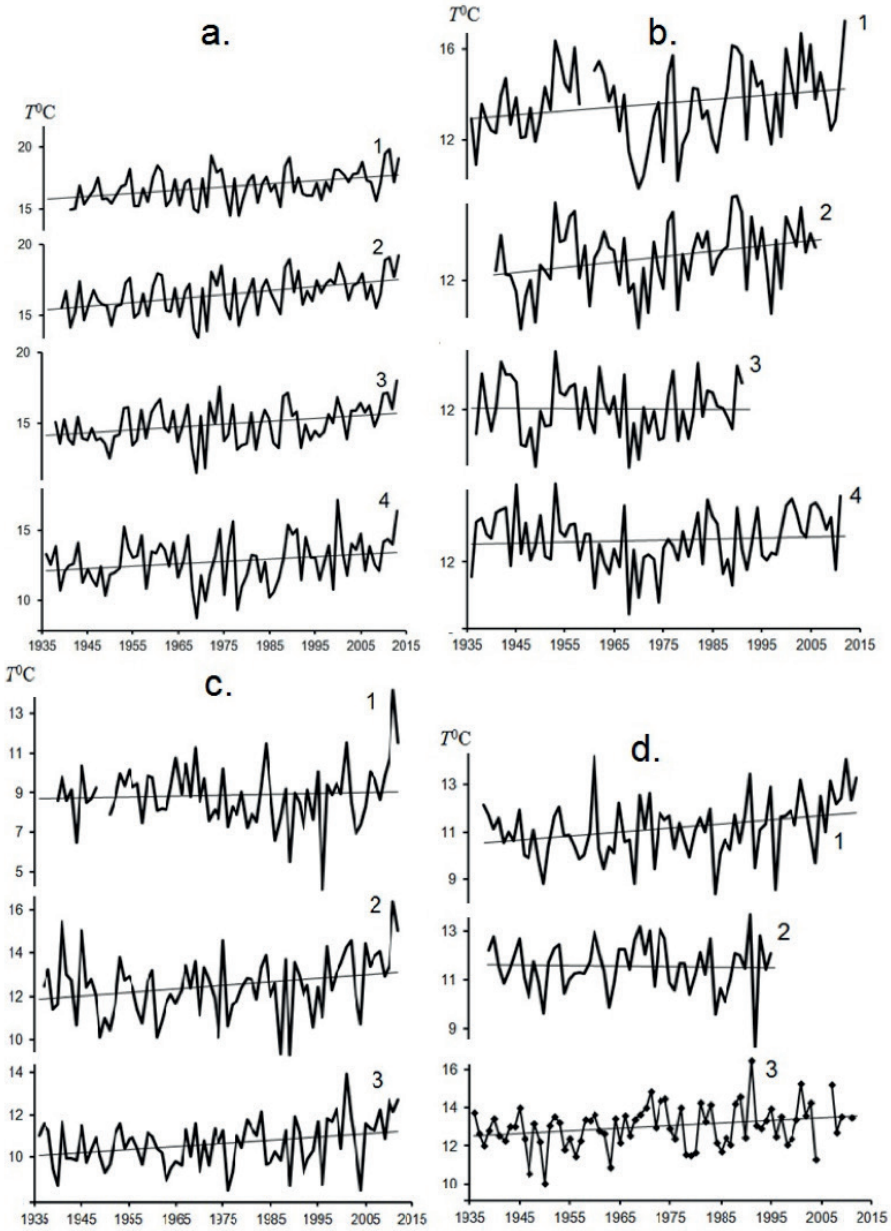

Fig. 2. Long–term changes of mean water temperature in June–August at the basin outlet stations of the large rivers of the Russian Arctic: a. 1 – Onega River (g. Porog), 2 - Severnaya Dvina R. (g. Ust–Pinega), 3 – Mezen R. (g. Malonisogorskaya), 4 – Pechora R. (g. Ust-Tsilma); b. 1 – Ob R. (g. Salekhard), 2 – Nadym R. (g. Nadym), 3 – Pur R. (g. Samburg), 4 –Yenisei R. (g. Igarka); c. 1 – Anabar R. (g. Saskylakh), 2 – Olenek R. (g. Sukhana), 3 – Lena R. (g. Kyushur); d. 1 – Yana R. (g. Yubileinaya), 2 – Indigirka R. (g. Vorontsovo), 3 – Kolyma R. (g. Srednekolymsk)

precipitation and water flow or main changes of T_W started latter (Frolova et al. 2022, Report 2022). In any case increase of water flow and water temperature are going simultaneously at least in past decade, and more often they are going simultaneously since the end of 1990-s.

River heat flux (W_T) is currently either stable or decreasing, despite the increase in water temperatures. An important role plays a choose of periods to compare mean values of a heat flux.

For example, simultaneously with precipitation and air temperature, the annual water runoff of the Severnaya Dvina increased in 1991–2018 by almost 8.4 km^3 (mainly due to the warm season of the year), which entailed corresponding changes in heat flux (W_T) by 11% in comparison with 1961–1990 – from 2.7 to 3 EJ/year (Table 2). The main increase of Sev.Dvina W_T was in 1991–2004. In 2005–2014 annual W_T was the same as in a base period – 2.7 EJ/year. However, it is expected an increase of W_T after 2014 due to several extremal hot summer periods on the North of European part of Russia (Report 2022,). The W_T of the Pechora increased by 8.4% (from 2.7 to 2.9 EJ/year). An increase was in 2005–2018 to 3.0 EJ/year. In 1991–2018 the W_T of the Onega and Mezen rivers changed slightly (in comparison with the base period) – by 1.5-2%.

At the same time, heat flux of Pechora had significantly increase for 11% in 1971–2018 in comparison with 1936–1970. While Onega heat flux had no changes in such periods, and Severnaya Dvina heat flux increased for 4% (statistically insignificantly) in 1971–2018 in comparison with 1936–1970 (Fig. 3).

A specific role is also plays a choose of statistical test for homogeneity of a record. Student t-test marks a heat flux changes as significant ones on more rivers, than a Maan-Whithey U-test (Fig. 3). However, due to a varying normality of records the results of nonparametric analysis are more significant.

The predominant role of natural factors in fluctuations of the heat flux (W_T) is characteristic of unregulated rivers flowing into the Kara Sea. The exceptions are the Yenisei River, regulated by the cascade of big Angara-Yenisei reservoirs, and in a less degree the Ob River, regulated by the Novosibirsk reservoir and a cascade of the Irtysh

river' reservoirs. The main increase in T_W in this sector of the Russian Arctic had been observed since the mid–second half of 1980s (Fig. 2b), and it is continued nowadays. The maximum increase in T_W was recorded in June (2.1-2.4 °C) (Table 1). In the remaining months it was less than 1.1-1.2 °C. The Ob, Nadym and Yenisei rivers are characterized by an acceleration of increasing T_W in June in the last decade (2011–2018) and a decreasing the intensity of T_W rising in other months, except May. Long-term fluctuations of W_T are not so unambiguous. In the mouth of the Ob River, a W_T changes are 9.2%. In 1970s, 1980s and the first half of 1990s the W_T of the Ob River was lowered (Fig. 3, Table 2). Since 1998, the W_T of the Ob River has increased in response to an increase primarily in water runoff, since the water temperature began to rise earlier – from the second half of the 1980s. In the lower reaches of the Yenisei River, low values of W_T were observed from the 1960s to the late 1990s (Fig. 3), despite the positive trend of runoff since the mid-1970s (Frolova et al 2022). A heat flux decreased in comparison with 1936–1970 for 7.2% (Fig. 3). Only since 1999/2000 W_T shows an increase, driven by a significant increase in both runoff and water temperature. Up to this point, T_W changes were positive, but insignificant due to a complex combination of variable fluctuations in spring and summer-autumn air temperatures in different parts of the watershed (http://seakc.meteoinfo.ru/about-centre/bulletin), and also with dam-induced effects. The main reason of small values of long-term heat flux of the Yenisei is the anthropogenic inter-seasonal redistribution of runoff (Magritsky 2008). As a result, the relative discharges of the flood and, in general, the warm season has decreased, and the winter runoff, on the contrary, has increased. Annual heat flux of the Yenisei had increased for 7.8% in 1991–2018. It is worth considering the construction of new reservoirs in the catchment area in recent years.

In the rivers, flowing into the western part of the Laptev Sea, changes in the heat flux in some cases are caused by multidirectional changes of T_W and water runoff, so far with the dominant role of water flow. T_W had significant increase since late 1990-s – early 2000-s in the lower reaches of the Khatanga, Anabar and Olenek rivers, similar to the lower reaches of the Yenisei River (Fig. 2b). Moreover, in the lower reaches of the Anabar River, it was especially sharply after a long period with low TW (with the beginning in the mid–1970s). The maximum warming of river waters, and in all months, was recorded in the lower reaches of the Olenek Rivers – by 1.9, 1.5, 1.1 and 0.4 °C, respectively, in June, July, August and September (Table 1). At the basin outlet stations of the Khatanga and Anabar rivers, a significant increase of T_W occurred only in June – by 1.6 and 0.8 °C, respectively. In the remaining summer months, the changes are small. Anomalies of water flow of the warm period were positive from the mid-1980s to the mid-1990s, after there was a decrease. As a result, since the beginning of the 2000–2010s, there is a tendency to decrease the heat flux in the lower reaches of the Olenek River (Fig. 3). Nevertheless, in 1991–2018 heat flux exceeded by 22.3% (Anabar) and 18.4 % (Olenek) the heat flux of the base period (1961–1990).

Thermal state of the lower reaches of the Lena River does not related to the operation of reservoirs on the Vilyui River, while the temperature regime of the tributary itself has undergone noticeable anthropogenic changes (Magritsky 2015). The heat flux of the lower Lena (g. Kyusyur) in 1991–2018 exceeded its value in 1961–1990 by 5% from 15.8 EJ/year to 16.7 EJ/year. However, this change is not statistically significant, as well as the most changes of a heat flux (Table 2).

Statistically significant climate-driving changes of the heat flux are observed on the rivers between the Lena and Kolyma (Fig. 3). The main increase began in the second half of the 1990s, due to increase of water flow and T_W (Fig. 2d). Water and thermal regime of the Kolyma River is disturbed with the Kolymskoe reservoir (built in 1980) (Magritsky 2008, 2009) and the Ust-Srednekanskoe reservoir (built in 2013). T_W in lower reaches of the Kolyma River increased in 1991–2018 in all months of the warm period. At the mouth of the Kolyma River, there is a positive trend in heat flux fluctuations since mid-1990s. The main reason is climate-driving increase in summer and autumn temperatures

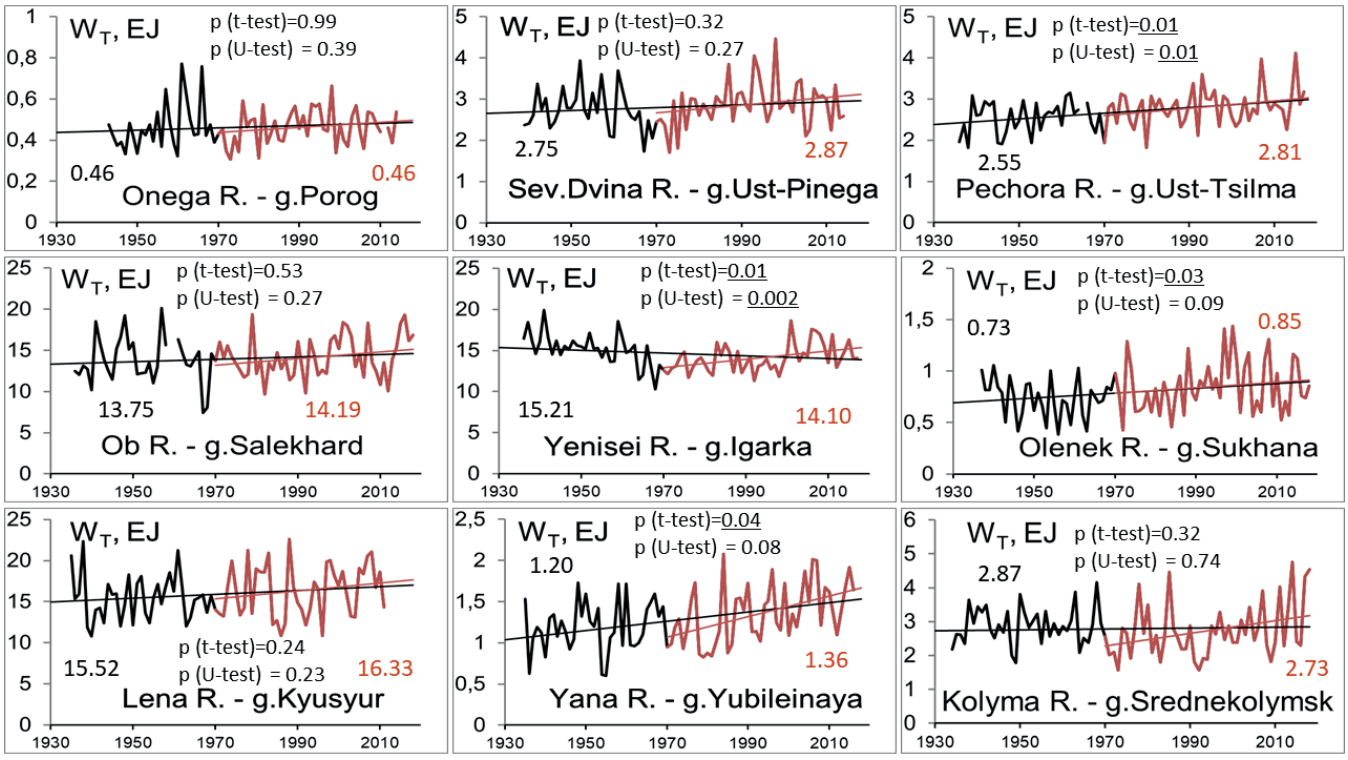

Fig. 3. Long–term changes of annual heat flux (mean heat flux for 1936–1970 subscribed with black, mean heat flux for 1971–2018 subscribed with red)

Table 2. Statistical characteristics of heat flux changes of large Russian Arctic rivers lowlands (significant changes due to U-test are marked with bold)

River – gauge	Mean W_T, EJ/year		Changes, %	U-statistics	p-value
	1961–1990	1991–2018			
Onega – Porog	0,47	0,48	2	304	0,46
Severnaya Dvina – Ust-Pinega	2,70	2,99	11	264	0,09
Pechora – Ust-Tsilma	2,69	2,91	8	294	0,11
Ob – Salekhard	13,40	14,63	9	319	0,12
Yenisei – Igarka*	13,50	14,56	8	278	0,04
Olenek – Sukhana	0,76	0,90	18	295	0,05
Lena – Kusur	15,85	16,65	5	260	0,29
Yana – Yubileinaya*	1,23	1,47	20	220	0,01
Koluma – Srednekolumsk	2,71	2,82	4	411	0,89

(since the late 1980s) and beginning in an increase of water flow in warm season since the mid-1990s (Report 2022, Frolova et al. 2022). This indicates, as in case of lower Yenisei River, intensification of climate changes in recent decades.

Heat flux assessment in large river's mouths based on observation data

The heat flux of the rivers flowing into the seas of the Russian Arctic is quite large, despite the relatively low T_W and the short season of the year with T_W ≥0-0.2 °C. Two factors help this. The first factor is the high water runoff of these rivers and the significant role of water runoff in the formation of the heat flux. The second factor is the similarity of water and temperature regimes. Typical intra-annual changes of T_W in the Arctic zone of Russia consist in a gradual increase of T_W in spring, a maximum in July/August and a slow decrease to autumn. Spring flood (characterized by high water discharges) takes place in spring-summer or only summer months. There are low discharges in low flow season with high water temperatures, but rainfall flood increase the heat flux in summer.

Annual W_T of the large Artcic rivers is at least 62.09 EJ/year (1981–2012). At the same time 45.53 EJ/yr, or 70% is the heat flux of the biggest rivers: Ob, Yenisei and Lena. It is necessary to mention, that an error of estimation of Lena river mean annual heat flux (g. Kyusyur) varies from -0.79 EJ/yr (Magritsky et al. 2018) to 2.7·EJ/yr (Tananaev et al. 2019). There are not such estimations for Ob and Yenisei low reaches. At least 4.25 EJ/yr is a heat flux to estuaries of the White Sea. The share of the Severnaya Dvina is 3.06 EJ/yr. The Pechora has the same value. The heat flux from Kola peninsula to the Barents Sea is at least 0.16 EJ/yr, however it is an absence of data in lots of rivers of this region. The heat flux of the Yana and Indigirka rivers is less than 10% from Lena river's one. W_T of the Indigirka and Kolyma rivers was near the same, before building a new reservoir on the Kolyma River. Total heat flux of individual rivers is increasing in past decades as it was mentioned earlier. It is important to note that in 2013–2018, the annual W_T of most of the rivers changed significantly with the maximum values in the lower reaches of the Olenek River.

The main share of W_T of the large rivers of the White Sea catchment is formed in spring (April–May – 24-28%) and summer (June–August – 58-65%). In other sea catchments summer months play main role: 82% of the Pechora River, 85-92%; to the Kara Sea, 89-96% to the Laptev Sea, 88-92% to the East Siberian Sea, 96% of the Amguema River (Chukchi Sea). The intra-annual distribution of the heat flux in mouths of the large rivers is illustrated in Fig. 4. The transit of heat with medium and small rivers of the Kola Peninsula is observed from May to September. The intra-annual range of fluctuations in monthly heat flux is small (0.03 EJ/year), since significant regulation of runoff by numerous lakes and reservoirs. By September, the heat flux of these rivers decreases to 0.01 EJ/year or less.

Heat flux and water temperature spatial variability

The patterns of changes in T_W and W_T along the large regulated rivers, as well as downstream of the basin outlet stations were studied. The influence of the large reservoirs on the thermal state of the main rivers flowing into the Arctic seas is observed in all seasons throughout hundreds kilometers. The degree and range of this influence depends on next main factors: 1) the size of a reservoir, and a type of regulation and discharge system of Hydro power stations (HPS) dam; 2) flow direction of river and character of climatic zones which it crosses; 3) water and thermal regime of tributaries, and their spatial distribution; 4) channel morphology; 5) additional anthropogenic impact downstream from the reservoir.

The first consequence of the building of large reservoirs on the Ob, Irtysh, Yenisei, Vilyui and Kolyma rivers was a decrease in water runoff during the period with a positive T_W (Magritsky 2008, 2015, Magritsky et al. 2018). The second consequence was a decrease in T_W in some months and an increase in others directly near the dams. For example, near the dam of the Krasnoyarsk HPS, T_W decreased in May-September (by 12.2°C in July and 1°C in September). T_W increased by 1.3°C (in January–March) and 6°C (in October–November). Positive winter TW remain until the mouth of the Angara River. Near the Kolyma HPS, TW decreased by 6.4°C in June and July, and by 1.6°C in August. In September and November–May, the temperature increased by 0.5–1.9°C, in October by 4.4°C. The decrease in water temperature in April, May and June by the Novosibirsk reservoir was about 0.4, 5.0 and 2.0°C, and its increase in August – November is in the range from 0.2 to 2°C. In July, the changes in T_W were insignificant.

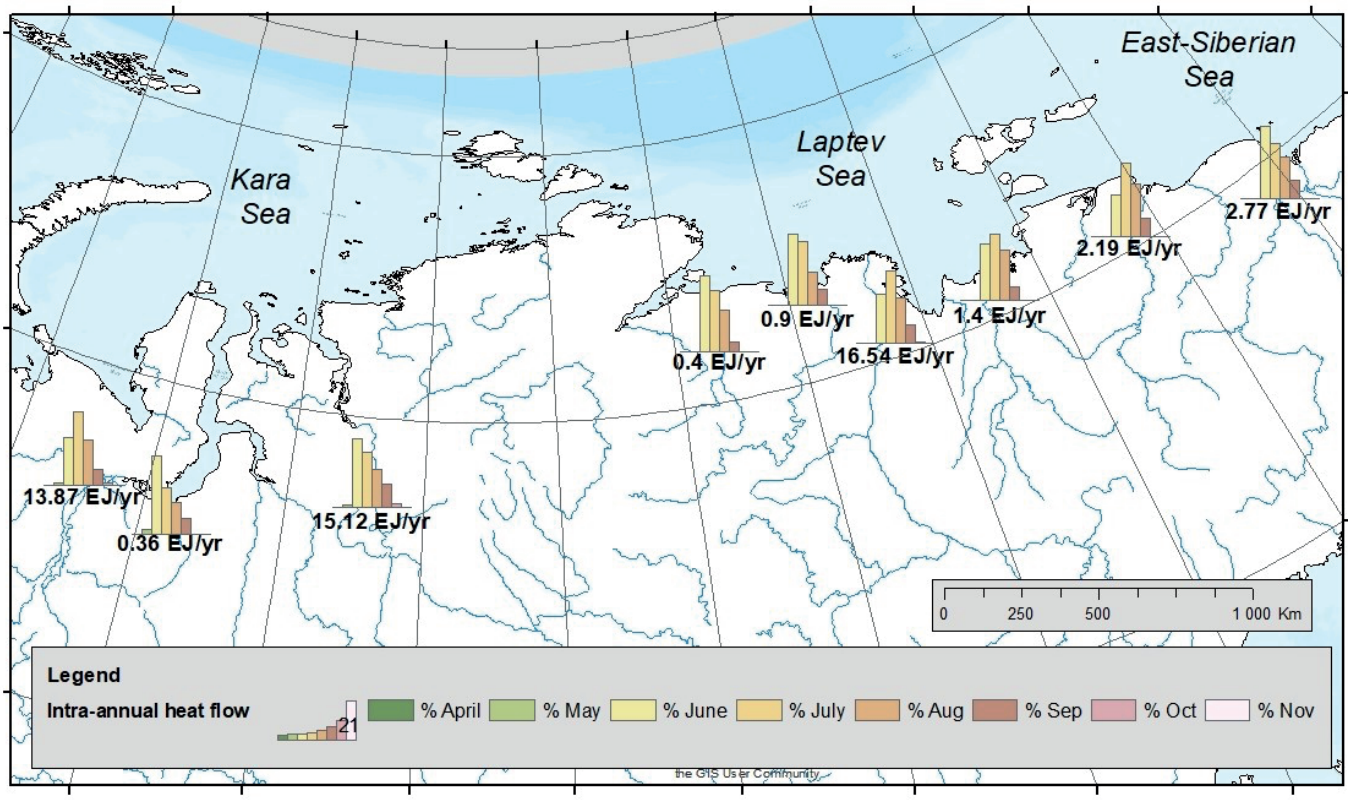

Fig. 4. Relative intra-annual distribution of the heat flux in the mouths of Arctic rivers for the period 1981–2012

The third consequence is the restoration of the natural temperature conditions at a significant distance from the dams. On the Yenisei River, the maximum intensity of temperature restoration in May–October is typical for the first 400-600 km (Kosmakov 2001, Magritsky et al. 2004). In summer, the natural temperature conditions are restored at a distance of 700-750 km, and in winter – 400 km from the dam. On the Kolyma River, the ultimate restoration in November–April was recorded in 40-100 km downstream the Kolyma HPS and in May–October in 230-620 km. In June, the influence of the reservoir may extend to a much greater distance. Downstream, the direct influence of the Novosibirsk reservoir on T_W of the Ob River varies on average from 600-800 km in April, May, August–October to 150-400 km in June–July (Magritsky et al. 2019). The best belongs to November – up to the mouth of the Irtysh River (>1500 km). Larger distances are indicated in (Orlova 1984), smaller ones – in (Beirom et al. 1973). The further observed longitudinal violation of the temperature regime is caused by changes in the water regime of the Ob, the changed role of tributaries, the variability of climatic factors.

The fourth feature is a decrease in the heat flux of regulated rivers. Along the length of the Yenisei River, W_T increases both in natural and regulated conditions. This is due to an increase in water flow towards the mouth of the Yenisei River, which compensates the anthropogenic decrease in W_T. Between Krasnoyarsk and Igarka (a distance of 1765 km), W_T in natural conditions increased almost 4 times. The contribution of the Angara River to heat flux was 29%. Under the new conditions, the W_T at a distance of 40, 448, 934 and 1805 km from the Krasnoyarsk HPS is equal to 45, 61, 79 and 90% of its natural value. At g. Igarka a significant decrease in W_T has been detected since 1964. This period continued until 1998–1999. The impact of the Novosibirsk reservoir on the heat flux also weakens along the length of the Ob river and remains almost unchanged downstream g. Kolpashevo and under the combined influence of the Ob-Irtysh reservoirs. Near the Novosibirsk HPS, W_T is equal to 84% of its natural value. At 23, 564, 1834 and 2699 km downstream, W_T is 88, 95, 95 and 95%. Some aspects of the impact of reservoirs on thermal characteristics are gradually being leveled due to climate warming. For example, since the end of the XX century and at the beginning of the XXI century, an increase in heat flux has been recorded in the estuaries of the Yenisei and Kolyma rivers.

Downstream the basin outlet station of the Arctic rivers and to the sea, a decrease in T_W and W_T usually prevails. The heat flux of the Ob and Lena rivers slightly increases in the pre-estuary sections by 0.87 and 3.4%, respectively. A great longitudinal transformations of W_T and T_W are characterized at the pre-delta reaches of Yenisei River. T_W in May-July gradually decreases downstream g. Igarka (Yenisei R.) (Fig. 5). Moreover, in May and June, there is a slight increase in T_W near g. Potapovo, possibly related to the operation of the Ust-Khantaiskoe reservoir. In August-October, the maximum T_W is observed at the g. Dudinka. But we cannot exclude the influence of the Dudinka River and Dudinka seaport on the measurements at the gauging station. At the same time, heat flux decreases on 4.3 EJ/year. The decrease in W_T is especially noticeable in June (2.45 EJ/month), and its value gradually decreases by September.

In the Arctic river deltas, temperature conditions and heat-flux change under the influence of: 1) the degree of distribution of runoff between the delta branches, 2) the direction and length of the main delta branches, 3) long-term preservation (in riverbeds and on the banks) of river ice and permafrost rocks cooling river waters, 4) marine factors, such as tidal and surge phenomena.

In the meso-tidal delta of the Severnaya Dvina, a comparison of T_W at the delta head (g. Smolny Buyan) and at the sea edge of the delta (g.Severodvinsk and g. Mudyug Island) in 1981–2016 shows a decrease in T_W to the sea in almost all cases (Fig. 6).

A small, within 0.5°C, T_W rising is observed only in October and November. At the same time, in the western part of the sea edge of the delta, the anomaly from the T_W at the delta head is much greater than in the eastern

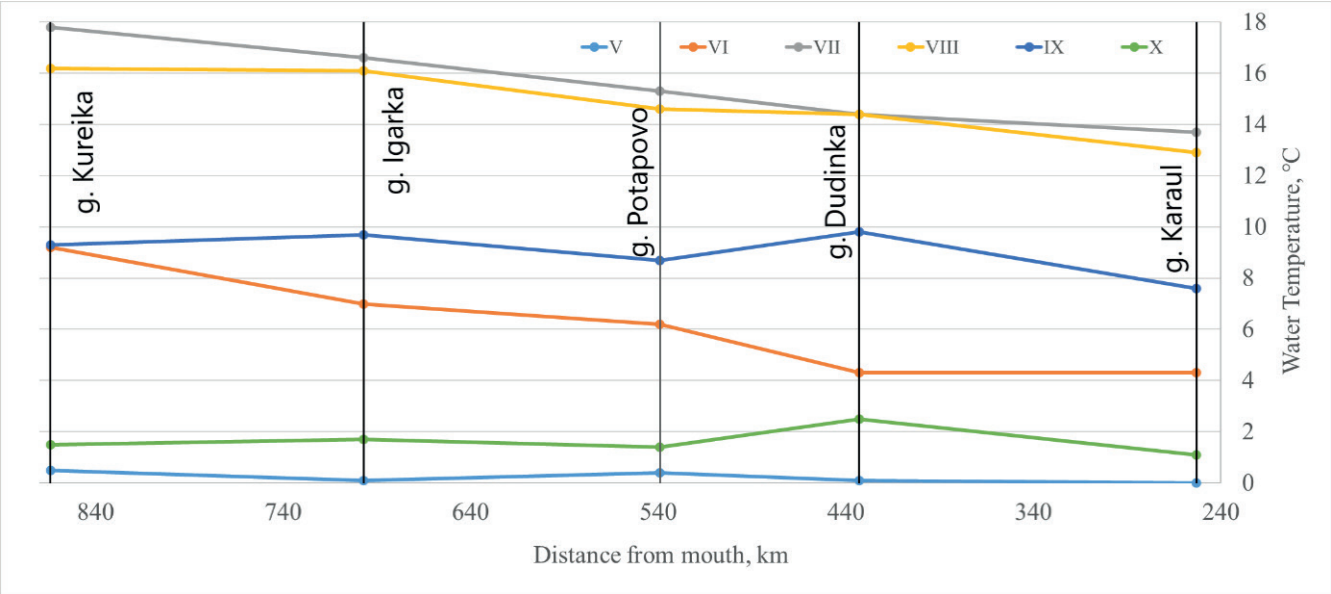

Fig. 5. Changes in average monthly water temperatures from the mouth of the Kureika River to the g. Karaul

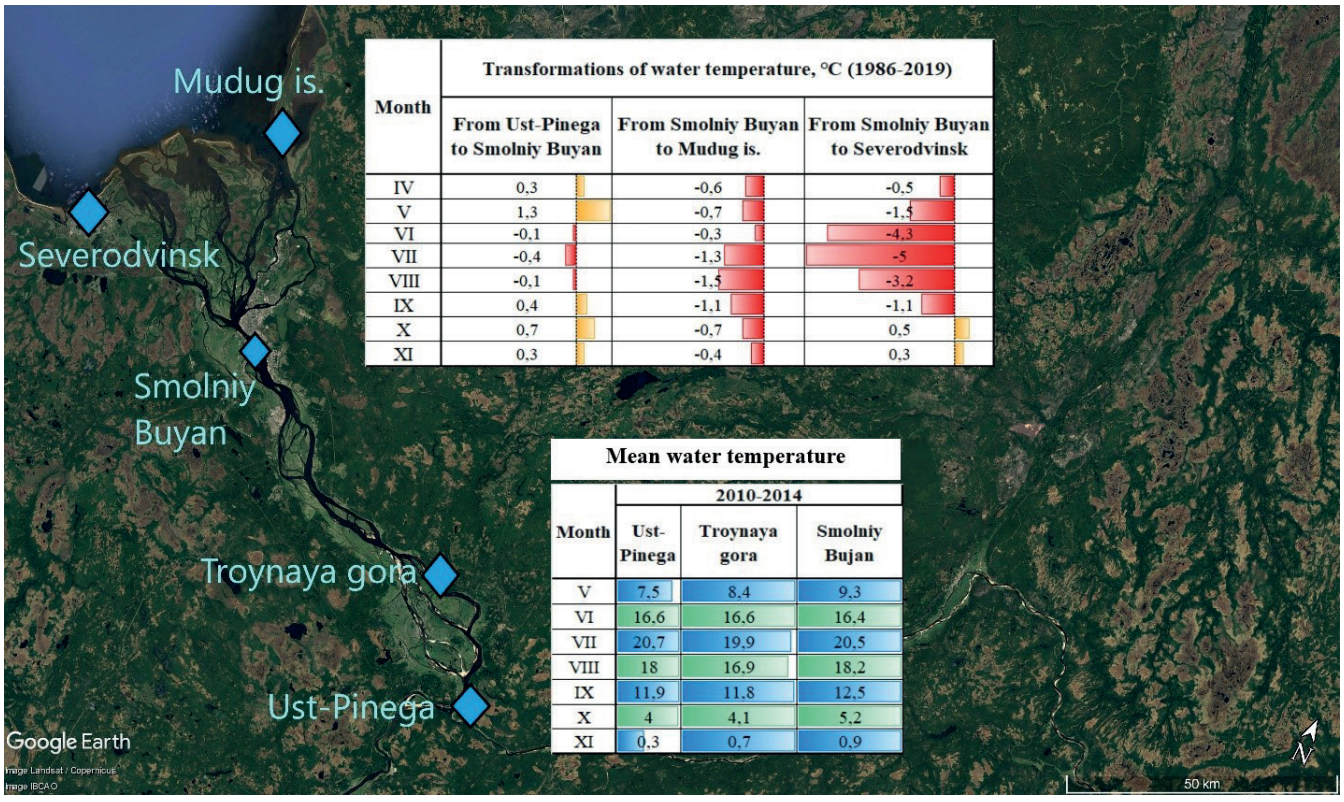

Month	Transformations of water temperature, °C (1986-2019)		
	From Ust-Pinega to Smolniy Buyan	From Smolniy Buyan to Mudug is.	From Smolniy Buyan to Severodvinsk
IV	0,3	-0,6	-0,5
V	1,3	-0,7	-1,5
VI	-0,1	-0,3	-4,3
VII	-0,4	-1,3	-5
VIII	-0,1	-1,5	-3,2
IX	0,4	-1,1	-1,1
X	0,7	-0,7	0,5
XI	0,3	-0,4	0,3

Mean water temperature			
Month	2010-2014		
	Ust-Pinega	Troynaya gora	Smolniy Bujan
V	7,5	8,4	9,3
VI	16,6	16,6	16,4
VII	20,7	19,9	20,5
VIII	18	16,9	18,2
IX	11,9	11,8	12,5
X	4	4,1	5,2
XI	0,3	0,7	0,9

Fig. 6. Transformation of water temperature in the Severnaya Dvina River delta

segment. The greatest difference in temperatures is -4.3 (June), -5 (July) and -3.2°C (August). The difference in temperatures between the delta head and Mudyug Island does not exceed 1.5°C. Tides increase the daily range of fluctuations in TW, which increases towards the sea.

In the micro-tidal (tidal range is less than 2 m) delta of the Pechora, T_w are monitored at the delta head (g. Oksino), on the delta branches of Bolshaya Pechora (g.Naryan-Mar and g. Bolvansky Cape) and Malaya Pechora (g. Andeg) (Fig. 7). T_w in Malaya Pechora are usually slightly higher than in the Pechora River before branching for Bolshaya and Malaya Pechora. In Bolshaya Pechora, T_w increase slightly towards Naryan-Mar in all months except June and July. All changes are quite small, within 0.5°C. However, towards the mouth of the Bolshaya Pechora, T_w decreased in all months in 1977–1996. The largest decrease was observed in June (up to 4.5 degrees Celsius). In July and August, a decrease in T_w by 1.3-1.4°C also prevails. At the same time, June and July-August account for 41% of the annual heat flux of Pechora (g. Oksino).

Presumably, towards the sea, the heat flux decreases together with the water temperature, as in Yenisei lowlands, however data about water flow distribution by delta arms is only for a part of summer period now (Alabyan et al. 2022).

CONCLUSION

The studies carried out on modern and extensive data made it possible to clarify previous estimates of the heat flux of the main rivers of Russian Arctic to their estuaries. The main part of it is formed in the summer months. The long-term variability of the heat flux of rivers is due to climatic reasons, with the exception of the Ob, Yenisei and Kolyma rivers. Rivers without reservoirs have mainly a long-term increase in water temperature and heat flux, especially

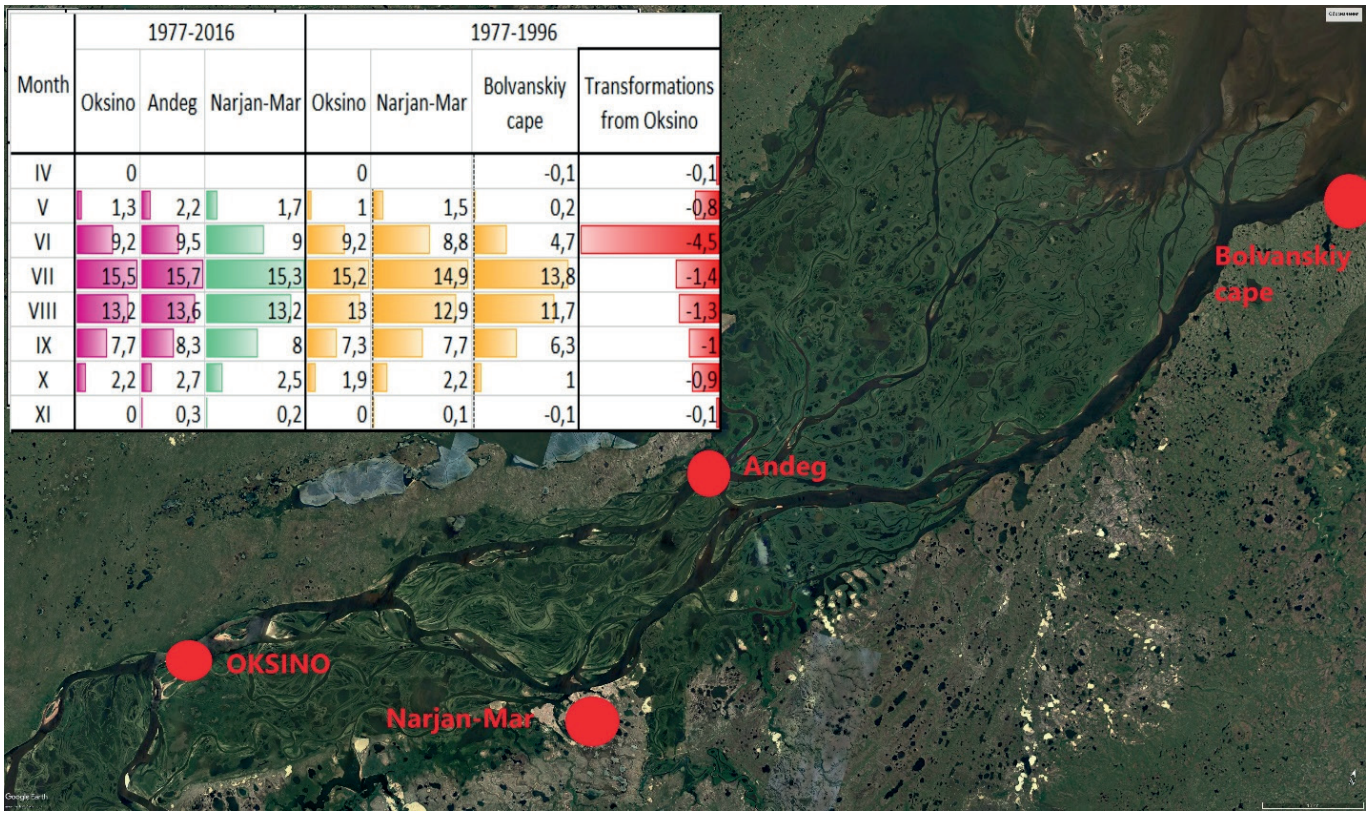

Month	1977-2016			1977-1996			
	Oksino	Andeg	Narjan-Mar	Oksino	Narjan-Mar	Bolvanskiy cape	Transformations from Oksino
IV	0			0		-0,1	-0,1
V	1,3	2,2	1,7	1	1,5	0,2	-0,8
VI	9,2	9,5	9	9,2	8,8	4,7	-4,5
VII	15,5	15,7	15,3	15,2	14,9	13,8	-1,4
VIII	13,2	13,6	13,2	13	12,9	11,7	-1,3
IX	7,7	8,3	8	7,3	7,7	6,3	-1
X	2,2	2,7	2,5	1,9	2,2	1	-0,9
XI	0	0,3	0,2	0	0,1	-0,1	-0,1

Fig. 7. Transformation of water temperature in the Pechora River delta

since mid-1980s and late 1990s. The growth was noted both during spring floods and low water season. However, statistical significance of water temperature and a heat flux changes is still low around the Russian Artic, as a changes of water flow. So reaction of hydrologic parameters for a climate change is lagging.

Building dams on great rivers have a group of consequences. First of all, it is a reduce of water flow in warm period. The second one is increase of water temperatures lower from HPS in several winter and autumn months, and water temperature decrease in other months. Natural water temperature regime returns in a high destination from dams, which can be more than 500 km. Heat flux of big regulated rivers had reduced in general. However, nowadays due to climate driving changes of water and temperature regimes a heat flux of regulated rivers is in general increased. However, in the Ob estuary we observe a small value of heat flux decrease.

REFERENCES

Alabyan A.M., Vasilenko A.N., Demidenko N.A., Krylenko I.N., Panchenko E.D., Popryadukhin A.A. (2022). Tidal dynamic in Pechora delta in summer period. Bulletin of Moscow State University. Series 5. Geography 1, 167-179 (in Russian).

Alekseevskiy N.I. (2012). River flow; geographical role and indicative properties. Questions of Geography, 133, 48-71 (in Russian).

Alekseevskiy N.I. (2000). The concept of geo-runoff and the state of small rivers. Erosion and riverbed processes, 13, 68-77 (in Russian).

Alekseevskii N. (ed) (2007). Geoecological State of the Russian Arctic Coast and the Safety of Nature Development. Moscow: GEOS (in Russian).

Antonov N.D. (1936). The amount of heat transferred by rivers into the Kara Sea. Proceedings of AARI, 35, 23-50 (in Russian).

Antonov V.S. (1976). Great Siberian rivers. Series «Earth Sciences». 10, 1-44 (in Russian).

Beirom S.G., Vostryakov N.V., Shirokov V.M. (1973). Changes in natural conditions at the Middle Ob after the construction of the Novosibirsk HPP. Novosibirsk, AS USSR (in Russian).

Costard F., Dupeyrat L., Gautier E., Carey-Gailhardis E. (2003). Fluvial thermal erosion investigations along a rapidly eroding river bank: Application to the Lena River (Central Siberia). Earth Surf. Process. Landforms, 28, 1349-1359.

Elshin Yu.A. (1981). Heat flux of rivers of the European territory of the USSR. Meteorology and hydrology, 9, 85-93 (in Russian).

Elshin Yu.A. (1988). Heat flux in the Arctic Ocean seas. Water resources, 5, 63-68 (in Russian).

Frolova N.L., Magritskiy D.V., Kireeva M.B., Grigir'ev V.Yu., Gelfan A.N., Sazonov A.A., Shevchenko A.I. (2022) Streamflow of Russian Rivers under Current and Forecasted Climate Changes: A Review of Publications. 1. Assessment of Changes in the Water Regime of Russian Rivers by Observation Data. Water Resources, 49(3), 333-350, DOI: 10.1134/S0097807822030046.

Gelfan A.N., Gusev E.M., Kalugin A.S., Krylenko I.N., Motovilov Yu.G., Nasonova O.N., Millionshchikiva T.D., Frolova N.L. (2022). Runoff of Russian Rivers under Current and Projected Climate Change: A Review 2. Climate Change Impact on the Water Regime of Russian Rivers in the XXI Century. Water Resources, 49(3), 351-365, DOI: 10.1134/S0097807822030058.

Georgiadi A.G., Kashutina E.A., Milyukova I.P. (2018). Long-term Changes of Water Flow, Water Temperature and Heat Flux of the Largest Siberian Rivers. Polarforschung, 87(2), 167-176.

Golubeva E., Platov G., Malakhova V., Iakshina D., Kraineva M. (2015). Modeling the impact of the Lena River on the Laptev Sea summer hydrography and submarine permafrost state. Bulletin of the Novosibirsk Computing Center. Series: Numerical Modeling in Atmosphere, Ocean, and Environment Studies. 15,13-22.

Gottlieb Ya.L., Zhidkikh V.M. et al. (1976). Thermal regime of reservoirs of hydroelectric power plants. Leningrad, Hydrometeoizdat (in Russian).

Hannah D.M., Garner G. (2015). River water temperature in the United Kingdom: changes over the 20th century and possible changes over 21st century. Progress in Physical Geography, 39. 68-92, DOI: 10.1177/030913331455066.

IPCC (2014). Climate Change 2014: Synthesis Report. Contribution of Working Groups I, II and III to the Fifth Assessment Report of the Intergovernmental Panel on Climate Change (Core Writing Team, R.K. Pachauri and L.A. Meyer (eds.)). IPCC, Geneva, Switzerland, 151.

IPCC (2022). Climate Change 2022: Impacts, Adaptation, and Vulnerability. Contribution of Working Group II to the Sixth Assessment Report of the Intergovernmental Panel on Climate Change (H.-O. Pörtner, D.C. Roberts, M. Tignor, E.S. Poloczanska, K. Mintenbeck, A. Alegría, M. Craig, S. Langsdorf, S. Löschke, V. Möller, A. Okem, B. Rama (eds.)). Cambridge University Press. In Press.

Instruction to hydrometeorological stations and posts (1978). Issue 6, part I. Hydrological observations and work on large and medium-sized rivers. Hydrometeoizdat: Leningrad, Russia (in Russian).

Ivanov V.V., Nikiforov E.G. (1976). Ways to assess possible changes in the hydrological regime of the Kara Sea under the influence of the inter-basin transfer of river flow. Proceedings of AARI, 314, 176-182 (in Russian).

Ivanov V.V., Kurszunov A.N. (1980) Heat flux of rivers in the Ob-Taz. Proceedings of AARI, 358, 102-110 (in Russian)

Kashcheev M.A., Kolgushkin V.V., Reshetov V.N., Istomin M.P., Chernyakhovskiy F.G., Shalaev V.A., Schreiber B.E. (1937). Materials on the hydrology of the Anabar River. Proceedings of AARI, 106 (in Russian).

Khmyznikov P.K. (1934). Hydrology of the Yana River basin. Leningrad, AS USSR (in Russian).

Korovkin I.P. (1940). Materials on the hydrology of the Khatanga River. Northern Sea Route, 16, 79-98 (in Russian).

Korovkin I.P. (1941). On the thermal regime and the influence of heat flux of Siberian rivers on ice coverage of seas. Problems of the Arctic, 1, 23-29 (in Russian).

Kosmakov I.V. (2001). Thermal and ice regime in the upper and lower reaches of high-pressure hydroelectric power plants on the Yenisei. Krasnoyarsk, Publishing house «CLARETIANUM» (in Russian).

Kurszunov A.N. (1984). Heat flux of the Yenisei in the estuary region. Proceedings of AARI, 394, 66-74 (in Russian).

Lammers R., Pundsack J., Shiklomanov A. (2007). Variability in river temperature, discharge, and energy flux from the Russian pan-Arctic landmass. Journal of Geophysical Research, 112, 1-15.

Liu B. (2004). Siberia Lena river thermal regimes and changes. MS thesis, USA, University of Alaska Fairbanks, Water and Environmental Research Center.

Liu B., Yang D., Ye B., Berezovskaya S. (2005). Long-term open water season stream temperature variations and changes over Lena river basin in Siberia. Glob. Planet Change, 48(1–3), 96-111, DOI: 10.1016/j.gloplacha.2004.12.007.

Magritskiy D. (2008). Anthropogenic Impact on the runoff of Russian rivers emptying into the Arctic Ocean. Water Resources, 35, DOI: 10.1134/ S0097807808010016.

Magritskiy D. (2019). Water consumption on the catchments of the arctic rivers and into the Arctic zone of Russia: parameters, structure, and many-year dynamics. Water sector of Russia: problems, technologies, management, 3, 20-37 (in Russian).

Magritsky D.V. (2015). Factors and trends of the long-term fluctuations of water, sediment and heat runoff in the lower reaches of the Lena River and the Vilyui River. Bulletin of Moscow State University. Series 5. Geography, 6, 85-95 (in Russian).

Magritsky D.V. (2009). Heat flux of rivers into the seas of the Russian Arctic and its changes. Bulletin of Moscow State University. Series 5. Geography, 5, 69-77 (in Russian).

Magritsky D.V. (2021). A new method for calculating the heat flux of unexplored rivers (using the example of rivers in the North-East of Russia). Current Trends and Prospects for the Development of Hydrometeorology in Russia, Irkutsk, Irkutsk State University, 485-494 (in Russian).

Magritsky D.V., Alexeevsky N.I, Aybulatov D.N., Fofonova V.V., Gorelkin A. (2018). Features and evaluations of spatial and temporal changes of water runoff, sediment yield and heat flux in the Lena River delta. Polarforschung, 87(2), 89-110.

Magritskiy D.V., Chalov S.R., Agafonova S.A., Kuznetsov M.A., Banshchikova L.S. (2019). Hydrological regime of the lower ob in modern hydroclimatic conditions and under the influence of large-scale water management. Scientific Bulletin of the Yamal-Nenets Autonomous District, 1(102), 106-115, DOI: 10.26110/ARCTIC.2019.102.1.015 (in Russian).

Magritsky D.V.; Evseeva L.S.; Reteyum K.F. (2004). Natural and technogenic factors of changes in the thermal flow of northern and southern rivers of Russia. Hydroecology: theory and practice. Problems of hydrology and hydroecology, Issue 2. Moscow, Lomonosov MSU, 213-237 (in Russian).

Magritsky, D.V.; Frolova, N.L.; Agafonova, S.A.; Efimov, V.A.; Vasilenko, A.N.; Sazonov, A.A.; Efimova, L.E. (2022). Hydrological conditions at the mouth of the Kolyma River following the results of the summer complex expedition of 2019. Bulletin of Moscow State University. Series 5. Geography, 1, 1-20 (in Russian).

Methodological recommendations for the compilation of a handbook on water resources. Thermal and ice regime of rivers (1961). Issue 9. Leningrad, State Hydrological Institute: Russia (in Russian).

Mohseni O., Stefan H.G., Erickson T.R. (1998). A nonlinear regression model for weekly stream temperatures. Water Resour. Res. 35(12), 3723-3733, DOI: 10.1029/98WR01877.

Nikiforov E.G.; Moretsky V.N.; Speicher A.O. (1980). Variability of the hydrological regime of the Arctic Ocean and problems arising in connection with the transfer of river flow in its basin. Problems of the Arctic and Antarctic, 55, 67-78 (in Russian).

Odrova T.V. (1984). Conditions for the formation of het flux of Siberian rivers. Dynamics and thermics of rivers and reservoirs. Moscow, Academy of Sciences of the USSR, 239-246 (in Russian).

Odrova T.V. (1987). Changing the regime of the Yenisei and Angara rivers as a result of flow regulation. The impact of hydroelectric power plants on the environment in the Far North, Yakutsk, Academy of Sciences of the USSR, 84-95 (in Russian).

Orlova G.A. (1984). Changes in the thermal regime of the Yenisei and the Ob below the reservoirs of the Krasnoyarsk and Novosibirsk hydroelectric power plants. Ways to transform river flow in the south of Siberia; Novosibirsk, Academy of Sciences of the USSR, 23-39 (in Russian).

Park H., Yoshikawa Y., Yang D.; Oshima K. (2007). Warming water in Arctic terrestrial rivers under climate change. J Hydrometeorol, 18(7), 1983-1995, DOI: 10.1175/jhm-d-16-0260.1.

Park H., Watanabe E., Kim Y., Polyakov I., Oshima K., Zhang X., Kimball J.S., Yang D. (2020). Increasing riverine heat influx triggers Arctic sea ice decline and oceanic and atmospheric warming. Science Advances, 6(45), eabc4699, DOI: 10.1126/sciadv.abc469.

Polilov A.M. (1907). On the influence of Siberian rivers on the waters of the Arctic Ocean and the Kara Sea. St. Petersburg (in Russian).

R 52.08.904-2020 (2020). Organization of observations of water temperature and the state of a water body by automated hydrological complexes. State Hydrological Institute: Saint Petersburg, Russia

Report about features of climate in the Russian Federation territory in 2021. (2022). Moscow, ROSHYDROMET. ISBN 978-5-906099-58-7. (in Russian).

Shostakovich V. (1914). Temperature of Siberian rivers and the amount of heat transferred by them to the Arctic Ocean. Proceedings on hydrography, 33, 123-152 (in Russian).

Sokolova E.M. (1951). Thermal regime of the rivers of the USSR. Proceedings of the State Hydrological Institute, 30(84), 1-74 (in Russian).

Soviet Arctic. Seas and islands of the Arctic Ocean (1970). Moscow, Institute of the Arctic and Antarctic (in Russian).

Surface water resources of the USSR (1970). Vol. 1. Kola Peninsula. Leningrad, Gidrometeoizdat Publ. (in Russian).

Surface water resources of the USSR (1972a). Vol. 3. Northern territory. Leningrad, Gidrometeoizdat Publ. (in Russian).

Surface water resources of the USSR (1973a). Vol. 15. Iss. 3. Lower Irtysh and Lower Ob. Leningrad, Gidrometeoizdat Publ. (in Russian).

Surface water resources of the USSR (1973b). Vol. 15. Vol. 16. Iss. 1. Yenisey River basin. Leningrad, Gidrometeoizdat Publ. (in Russian).

Surface water resources of the USSR (1972b). Vol. 17. Lena-Indigirka area. Leningrad, Gidrometeoizdat Publ. (in Russian)

Surface water resources of the USSR (1969). Vol. 19. North-East. Leningrad, Gidrometeoizdat Publ. (in Russian).

Tananaev N.I., Georgiadi A.G., Fofonova V.V. (2019). Revising Contemporary Heat Flux Estimates for the Lena River, Northern Eurasia. Hydrology research, 5(50), 1440-1452, DOI: 10.2166/nh.2019.062.

Toffolon M.; Piccolroaz S. (2015). A hybrid model for river water temperature as a function of air temperature and discharge. Environ. Res. Lett. 10, 1-11, DOI: 10.1088/1748-9326/10/11/114011.

van Vliet M.T., Ludwig H.F., Zwolsman J.J.G., Weedon G.P., Kabat P. (2011). Global river temperatures and sensitivity to atmospheric warming and changes in river flow. Water Resour. Res., 47, DOI: 10.1029/2010WR009198.

Vasilenko A.N., Magritsky D.V., Frolova N.L. (2020). Regularities of changes in the average annual water temperature of the rivers of the Arctic zone of Russia in connection with climate changes. Water sector of Russia: problems, technologies, management, 2, 8-22 (in Russian).

Wanders N., van Vliet M.T.H., Wada Y., Bierkens M.F.P., van Beek L.P.H. (2019). High-resolution global water temperature modeling. Water Resources Research, 55, 2760-2778, DOI: 10.1029/2018WR023250

Zaikov B.D. (1936). River runoff in the Laptev and East Siberian Seas and the amount of heat transferred by them to these seas. Proceedings of AARI, 35, 51-84 (in Russian).

Zotin M.I. (1947). Water runoff and heat flux into the Laptev Sea. Proceedings of AARI, 198 (in Russian).

Yang D., Liu B., Ye B. (2005). Stream temperature changes over Lena River Basin in Siberia. Geophys. Res. Let., 32, DOI: 10.1029/2004GL021568.

Yang D., Ye B., Kane D.L. (2004). Stream-flow changes over Siberian Yenisei River Basin. J. Hydrology, 296, 59-80.

Ye B., Yang D., Kane D. (2003). Changes in Lena River stream-flow hydrology: human impacts versus natural variations. Water Resour. Res., 39(7), 1-14, DOI: 10.1029/2003WR001991.

RESEARCH PAPER

CHANGES IN LAND USE/ COVER AND WATER BALANCE COMPONENTS DURING 1964–2010 PERIOD IN THE MONO RIVER BASIN, TOGO-BENIN

Djan'na Koubodana Houteta[1,2,3,4]*, Kossi Atchonouglo[2], Julien G. Adounkpe[3], Badabate Diwediga[5,6], Yao Lombo[1], Kossi E. Kpemoua[1] and Komi Agboka[7]

[1]Institut Togolais de Recherche Agronomique (ITRA), Lomé 01BP 1163, Togo
[2]Faculté Des Sciences, Université de Lomé, 01B:P 1515 Lomé, Togo
[3]West Africa Science Service Centre on Climate change and Adapted Land Use, WASCAL-Climate Change and Water Resources, University of Abomey Calavi, 03 PO Box 526 Cotonou, Benin
[4]African Institute for Mathematical Sciences (AIMS), Kigali, Rwanda
[5]Laboratoire de Botanique et Ecologie Végétale, Faculté des Sciences, Université de Lomé, Lomé 01 BP 1515, Togo
[6]UNEP-IEMP, Institute of Geographical Science and Natural Resources Research, The University of Chinese Academy of Science (CAS), 11A Datun Road, Beijing, China
[7]West Africa Science Service Centre on Climate change and Adapted Land Use, WASCAL-Climate Change and Disease Risk Management, University of Lomé, 01 PO Box 1515 Lomé, Togo
***Corresponding author:** koubodana.d@edu.wascal.org; koubo2014@gmail.com
Received: January 4th, 2022 / Accepted: November 11th, 2022 / Published: December 31st, 2022
https://DOI-10.24057/2071-9388-2021-098

ABSTRACT. The Intergovernmental Panel on Climate Change has predicted that sub-tropical regions are more vulnerable to climate change's negative effects (CC). Additionally, to CC, land use and land cover (LULC) changes and dam construction, often neglected, play an important role in the spatial and temporal distribution of water balance components (WBC) for agricultural production and socio-ecological equilibrium. This study aimed to analyze and compare the changes in LULC and WBC for the period before Nangbéto dam construction (1964–1986) and the period after its construction (1988–2010) in the Mono River Basin (MRB). To this end, the study used mainly WBC extracted from the validated Soil and Water Assessment Tool and LULC data of 1975–2000 in the MRB to explore their temporal distributions and the link in their changes. The results showed that mean actual monthly evapotranspiration, percolation, water yield, surface runoff, groundwater, and lateral flow represent 51%, 17.5%, 15.9%, 9.4%; 5.7% and 0.4%, respectively, of total water balance between 1964 and 1986. The same components represented 51%, 9.1%, 20.4%, 6.3%, 10.6% and 2.6%, respectively, between 1988 and 2010. The contribution of these WBC in the mean-annual (1964–1986) period was for actual evapotranspiration (31.3%), water yield (25.9%), percolation (17.7%), groundwater (14.71%), surface runoff (9.94%) and lateral flow (0.40%). Meanwhile, between 1988 and 2010, the contribution of actual evapotranspiration, water yield, percolation, groundwater, surface runoff and lateral flow is 49.8%,19.9%, 11.2%, 10.3%, 6.1%, and 2.5%, respectively. The results showed that the peaks of the actual evapotranspiration, surface runoff, percolation and water yield appeared in September, corresponding to a month after the maximum rainfall in August. However, our more detailed analysis showed that a significant decrease in forest and savanna and an increase in croplands led to a decrease in actual evapotranspiration and lateral flow over the second simulation period compared to the first period of simulation over the MRB scale. These findings showed that sustainable management and conservation of natural vegetation are crucial for integrated water resource management and conservation in MRB.

KEYWORDS: Water balance components, land use/ cover changes, dam construction, temporal analysis, Mono River Basin

CITATION: Houteta D. K., Atchonouglo K., Adounkpe J. G., Diwediga B., Lombo Y., Kpemoua K. E. and Agboka K. (2022). Changes In Land Use/ Cover And Water Balance Components During 1964–2010 Period In The Mono River Basin, Togo-Benin. Geography, Environment, Sustainability, 4(15), 171-180
https://DOI-10.24057/2071-9388-2021-098

ACKNOWLEDGEMENTS: Authors like to thank the German Ministry of Education and Research (BMBF) for their financial through the West African Science Service Center on Climate Change and Adapted Land use (WASCAL) and the Graduated Research Programme on Climate Change and Water Resources at the University of Abomey Calavi Benin. We also thank the International Foundation for Science (IFS) and TWAS-IsDB Collaborative Programmes for support.

Authors acknowledge Togolese and Beninese meteorological and hydrological services for providing historical climatic and discharge data used. We also appreciate the peer review works from anonymous reviewers in strengthening the quality of the paper.

Conflict of interests: The authors reported no potential conflict of interest.

INTRODUCTION

Water is a source of sustainable economic development because it guarantees supply of basic resources to society and ecosystems. Water resources are fundamental to various sectors of activities such as agriculture, industry, domestic water use and sanitation, hydropower generation, health and environmental security (Hanjra and Qureshi 2010). Agriculture, hydropower dams and agricultural land irrigation are the sectors with large water consumption. Actually, water resource management is becoming a more pressing issue due to climate change (CC) impacts (Eusebion and Zong-Liang 2008; Mango et al. 2011). Most researches in water resource management are dealing with complex systems determined by several interactions between natural, socio-economic, political issues and climate change implications (PCCP 2008). As demonstrated by the Intergovernmental Panel on Climate Change (IPCC) in its 2014 report, global climate change, demographic and economic changes will be felt more in tropical and sub-tropical regions (Paeth et al. 2009; Philipp et al. 2018). In most cases, climate variability and human activities are the two major driving factors of hydrological processes and spatial temporal distribution of water balance components (WBC) in any river basin.

In other hand, land use and cover changes (LULCC) usually affect hydrologic cycle through their direct impacts on land surface processes like the amount of evaporation, groundwater infiltration and surface runoff that occur during and after precipitation events (Bronstert et al. 2002; Setyorini et al. 2017). These factors control the water yields of surface streamflow and groundwater aquifers and thus the amount of water available for ecosystem functions and human use (Anderson et al. 2011). For instance, dam construction on a river basin without appropriate management strategies and precautions can induce changes in streamflow with downstream flooding. These LULCC in addition to CC will have consequences on local and regional hydrological regimes. Consequently, the spatial and temporal water resource availability, or in general the water balance, will be significantly affected (Huntington 2006). Therefore, more attention is needed in this sector.

Several studies have investigated the SWAT-simulated hydrological impact of land use change in Iran (Ghaffari et al. 2010). In China, Zuo et al. (2016) assessed the effects of changes in land use and climate on runoff and sediment in China river basin. Others studies assessed future land use changes impacts sed on hydrological process in Canada (Wijesekara et al. 2012) or performed a comparison of hydrological models for assessing the impact of land use and CC on discharge in a tropical catchment (Cornelissen et al. 2013). In Togo, there are few studies on LULCC and water resources in the complex transboundary basin of Mono river (Badjana et al. 2017; Klassou and Komi 2021).

Recently in the MRB, Koubodana et al. (2019) have shown that the watershed landscape is dominated by cropland, savanna, forest and oil palm plantation. LULCC in the MRB is characterized by losses of savanna and increase of cropland between 1975 and 2013, explained by demographic growth in Togo (Koglo et al. 2018; Koubodana et al. 2019). Over the past years, many projects like the Potential Conflict to Cooperation Potential (PCCP 2008), the Integral Water Resource Management in West Africa (SAWES 2011) and the Integrated Disaster and Land Management Project (PGICT) were implemented for promoting sustainable water resource management in the MRB. Previously, Kissi et al. (2015) have analyzed the social vulnerability of flood in the Bas-Mono prefecture embedded in the MRB. Ntajal et al. (2017) have investigated flood disaster risk mapping and analysis while Houngue (2018) has looked at the simulation of high streamflow using lumped hydrological and climate models in the small area of lower MRB. The authors concluded that the source of high streamflow is not only due to climate change but also to the regulation of the Nangbéto dam, land use and the social factors of the communities living in the catchment. In the previous study, Koubodana et al. (2021) have successfully run, calibrated, and validated a semi-distrubuted Soil and Water Assessment Toold (SWAT) model over the MRB in order to. assess streamflow change before dam installation (1964–1986) and for the period after dam installation (1988–2010). The authors suggested that land cover changes impacted on streamflow and probably on the others WBC which need further investigations.

In this study, outputs from the already calibrated and validated SWAT model in Koubodana et al. (2021) were used to analyze the temporal contribution of WBC for sustainable water resource management in the MRB. The specific objectives of the study are to: (i) assess the temporal distribution of WBC for the periods before and after dam construction; (ii) compare the contribution and changes of WBC in the MRB before and after dam construction, and (iii) determine the link between LULCC and WBC changes in the same basin. The results of this study will allow to elaborate strategies for policy makers better planning and sustainable management of water and land resources in the Transboundary Mono River Basin between Togo and Benin.

MATERIAL AND METHODS

Study Area

The MRB is drained by the Mono River and its tributaries. It is a transboundary basin shared by Togo and Benin Republics in the southern parts of the basin. The Mono River is located between 06°16' and 9°20'Northern latitude and 0° 42'and 1° 40' Eastern longitude (Fig. 1). With a perimeter of 872, 092 km, the basin covers a surface area of 22,013.14 km^2, with 88% in Togo (PCCP 2008). Flowing from its main source in the Alédjo mountains in north Togo, to the Atlantic Ocean in the South, the Mono River has a total length of 308.773 km. The elevation of the basin ranges from 12 to 948 m (http://srtm.csi.cgiar.org , [Accessed 10 Apr. 2019]). The watershed shelters the biggest dam of Nangbéto that produces 20% of total hydroelectricity used by the two countries. To increase the electricity supply capacities, Togo and Benin have co-funded the construction project of a second dam on the same river at Adjarala.

The climate is a subequatorial from 0 to 8°N and with two rainy seasons and two dry seasons. It totals 1200 to 1500 mm/year in the mountainous area of the South-West and only 800 to 1000 mm/ year in the coastal zone. From 8 to 10°N, the climate is tropical humid with one rainy season and one dry season (1000 to 1200mm/year). In the winter (December to March), there is an anti-cyclonic high-pressure area centered over the Sahara. It drives the Harmattan, a desiccating, dusty wind that blows rather persistently from the northeast, drying out landscapes all the way to the coast. However, the hydrograph has one peak that indicates that river discharge is mostly controlled by upstream tributaries. The mean annual temperature ranges from 22°C to 30°C and precipitation varies between 800 mm and 1300 mm/year (CILSS 2016; Speth et al. 2010). Precipitation usually reaches the peaks in May-June and September-October.

Human activities in the MRB mainly include the management of the construction of the hydroelectricity

dam, irrigation activities in the downstream, water withdrawal for population needs, agricultural development and fisheries. The rivers shelter the most important reservoir of Nangbéto Dam. The dam is built at 180 km from the mouth of the river and the surface area for water retention that feeds it is 15700 km^2. The second dam under the Adjarala project will be built at 100 km downstream from Nangbéto and, between the two dams, the drained area is 11,000 km^2 (Rossi 1996).

Data

Water balance components datasets

The datasets used in this study are from the validated SWAT model outputs generated by Koubodana et al. (2021). The WBC considered were Precipitation (PCP), actual evapotranspiration (ET), percolation (PERC), surface runoff (SURQ), and groundwater flow (GW_Q), water yield (WYLD) and lateral flow (LAT_Q). These components were extracted from the validated SWAT model for the two periods. The values are provided on daily basis and for each sub-basin or reach point between 1964 and 1986 and from 1988 to 2010. The watershed was divided automatically into 24 sub-basins for the first period of simulation (1964–1986) and 23 for the second period (1986–2010) (Gassman et al. 2007).

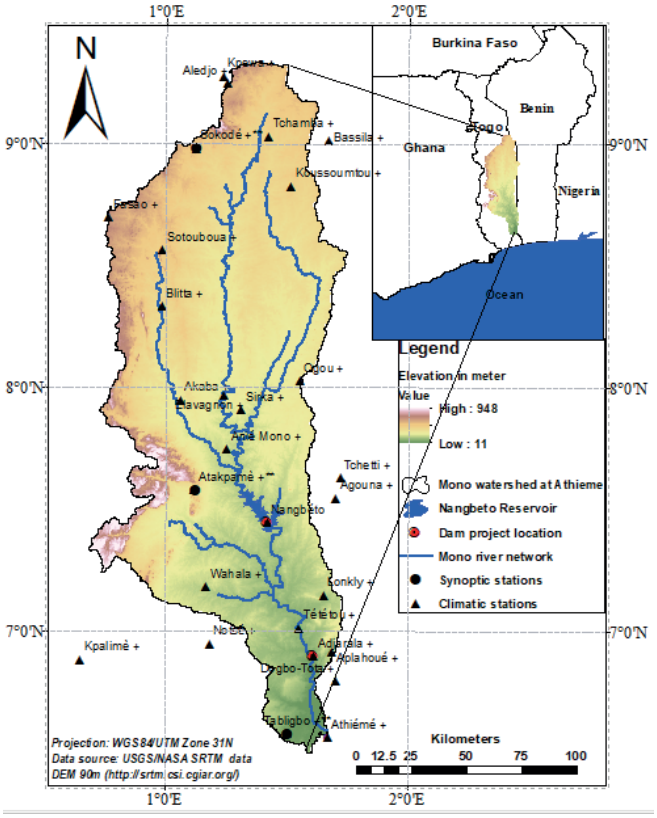

Fig. 1. Study Area (Koubodana et al. 2019)

Land use and land cover change datasets

The LULC maps of 1975 and 2000 were used to reflect on land use/cover patterns for the period 1964–1986 (named as SIM1) and the period 1988–2010 (called SIM2), respectively. The Nangbéto Dam started operating in 1987, which is selected as the turning point of the climate data, because significant changes of land use may play an important role in local WBC. Land use and land cover datasets were initially analyzed (Koubodana et al. 2019). We define cropland and fallow with oil palm as a crop field and fallow land, farms with crops and harvested croplands whereas agriculture represents cultivated areas with seasonal crops dependent on rainfall. Table 1 shows the areal proportions of the LULC units for the two years.

Methods

SWAT model and water balance component outputs extraction

The SWAT model was setup for the MRB by delineating the watershed was divided automatically into 24 sub-basins for the first period of simulation (1964–1986) called SIM1 and for the second period (1988–2011) called SIM2. This resulted in an automatic subdivision of 109 hydrologic response units (HRUs) and 111 HRUs for SIM1 and SIM2 respectively based on the same soil, land use, and slope (Arnold et al. 1998). More detailed characteristics of the input data used for the SWAT model setup can be found in Koubodana et al. (2021). The surface runoff was estimated using the Soil Conservation Service (SCS) curve number method which is a function of land use, soil permeability and antecedent soil water conditions The Hargreaves's method, which requires only minimum and maximum temperature as input data was used for the

Table 1. LULC datasets (Koubodana et al. 2019)

LULC types	SWAT Code	Area [%]	
		1975	2000
Savanna	RNGE	76.03	63.76
Agriculture	AGRR	6.48	21.83
Forest	FRST	5.38	3.03
Gallery and riparian forest	FRSE	5.2	4.28
Degraded forest	RNGB	3.91	1.98
Cropland and fallow with oil palm plantations	OILP	2.22	3.51
Woodland	FRSD	0.43	0.27
Settlements	URBN	0.31	0.49
Water bodies	WATR	0.02	0.52
Wetland-floodplain	WETN	0.02	0.33

evapotranspiration estimation in the model (Hargreaves and Samani 1982; Koubodana et al. 2021). A detailed description of the model setup, sensitivity analysis, calibration, and validation is presented by Koubodana et al. (2021). The SUFI-2 semi-automatic tools for calibration – validation-sensitivity & uncertainty analysis were then used to generate, and to validate a representative SWAT model over the catchment (Abbaspour et al. 2017).

The main WBC were extracted for both the periods before (SIM1) and after (SIM2) dam construction. These data were used to compute the monthly, and annual averages contributions over over the whole catchment. Using SWAT Output Viewer (https://swatviewer.com/, [Accessed 10 Sept. 2019]), it was possible to extract the contribution of each WBC at mean monthly and annual scales. Mean annual and mean monthly values were computed for each WBC contribution considered over SIM1 and SIM2. Therefore, the mean annual and monthly WBC contributions were used to show the percentage of each water balance component at annual and monthly scales.

Analysis of the temporal distribution of water balance before and after dam construction

The temporal distribution of WBC was assessed using Origin 2018 software. Origin is a powerful and full-featured data analysis software (Deschenes and Bout 2000; Gonzalez-Barahona et al. 2008). Origin offers an easy-to-use interface. The graphs plotted by the software and analysis results can automatically update on data or parameter change (https://www.originlab.com/). This software was been used in many previous studies and it has the advantages to be easy handle, generate graph and update data. First, the SWAT models WBC contribution outputs between 1964 and 1986 or between 1988 and 2010 and distributions were averaged at sub-basin level. Next, the temporal contributions of a selected WBC value for the catchment were averaged using Origin 2018 software. Finally, the same software was used to compute the matrix where the component values of the water balance are listed according to month and year for the periods before and after dam construction.

Changes in land use/cover and water balance components before and after dam construction

The study has established the relationship between LULCC and hydrological components before and after dam construction. The SWAT model simulation was divided into two periods: SIM1 period (1964–1986) and SIM2 period (1988–2010). For SIM1, the land use map of 1975 was used as input and with climate variables extended between 1964 and 1986. Meanwhile, the input data for the SIM2 were the land use data of 2000 and climate variables extended between 1988–2010 and Nangbéto reservoir set in 1987. More details about SWAT model setup model sensitivity analysis, calibration, validation and uncertainty analysis can be found in Koubodana et al. (2021). Based on the validated model outputs after its performances and uncertainties analysis during SIM1 and/or SIM2, modelers were able to deduce the impacts of LULCC on hydrological components before and after dam construction in 1987. Thus, the temporal intensity distribution and related statistics of WBC over MRB for SIM1 and SIM2 were respectively generated. Furthermore, the changes between the two periods of hydrological cycle components were computed and comparative methods allowed giving sustainable information for integral water resource management in MRB.

RESULTS

Precipitation temporal distribution and changes before and after dam construction

Fig. 2 underscores the temporal distinction of wet and dry seasons and shows the monthly rainfall patterns for the whole basin between 1964 and 1986 (a) and between 1988 and 2010 (b). The onset of the rainy season is May/June for both periods. The cessation of rains occurs in September/October and October/November for the period before and after dam construction, respectively.

The peak of rainfall is reached in between June and September during SIM1 and July and October during SIM2. The dry season always starts from November/December to March/April of the following year in the two simulations. There is an alteration of unimodal years (1966, 1968, 1979, 1980, 1985 & 1989, 1991, 1993, 1995, 1999, 2002, 2003, 2010) and bimodal years (1964, 1974, 1976, 1978 & 2007, 2009). Rainfall magnitude

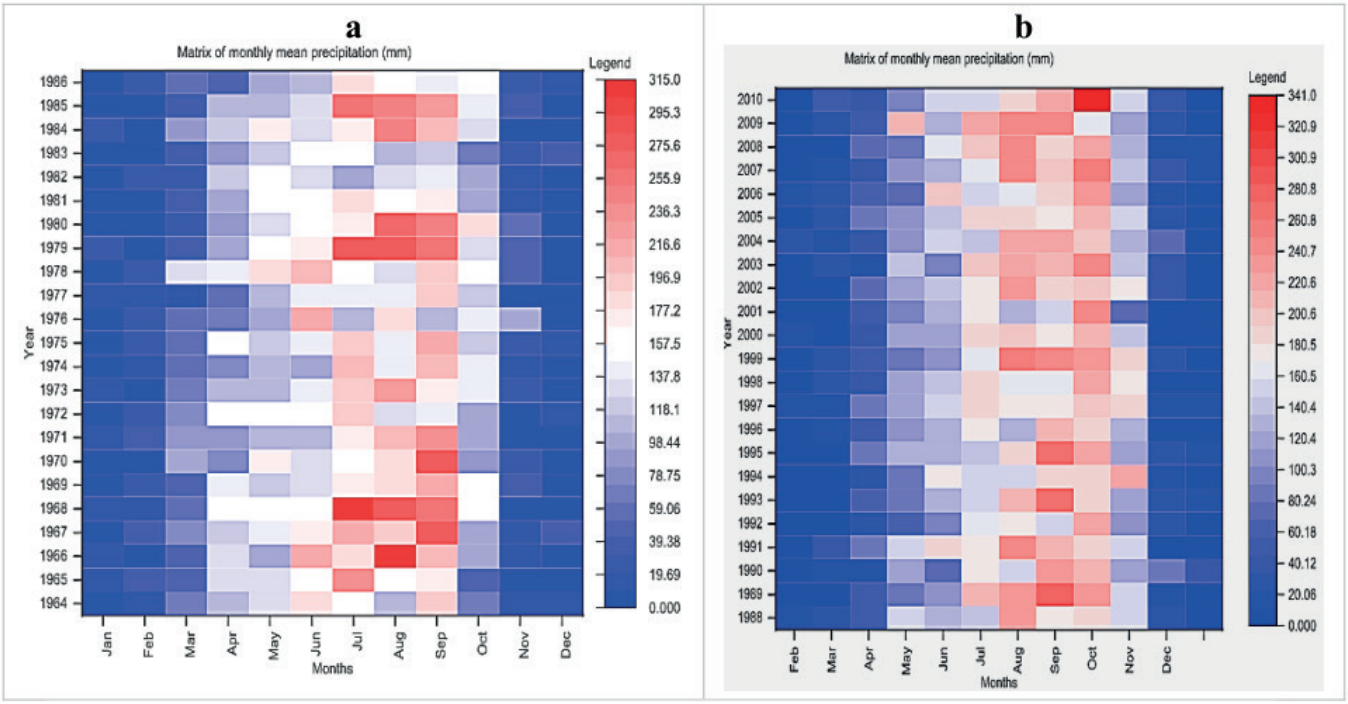

Fig. 2. Matrix [Month-Year] average rainfall evolution over MRB for SIM (a), SIM2 (b)

intensity between 1988–2010 has considerably decreased compared to the period 1964–1986 where there is the inverse situation.

Matrix illustration of water balance components before dam construction (1964-1986)

Fig. 3a to Fig. 3f show the influence of individual water cycle components between 1964 and 1986. These figures showed the distinction between wet and dry months and years over the entire basin. Particularly, actual evapotranspiration (Fig. 3b) ranges from 3.5 to 135 mm/year and the maximum are observed for each year between April and October corresponding to the rainy season. Contrariwise, the minimum of actual evapotranspiration was displayed between November and March which is the dry season. For the other water cycle components such as percolation, surface runoff, groundwater water yield and lateral flow (Fig. 3a, 3c and 3f), the maximum values are observed between August and October which is the period of peak of rainfall over the study area. Some years underline the pronounced lowest value of these variables during this season.

Matrix illustration of water balance components after dam construction (1988–2010)

Over the second period of simulation (SIM2) between 1988 and 2010, the monthly variability of water cycle components per year is presented in Fig. 4. These figures revealed that the high values of actual evapotranspiration are seen between May and October of the year and the other months (November to April) are characterized by the low actual evapotranspiration. For the other components of the hydrological cycle, the maximum is obtained between July and October. There are years with lowest surface runoff over the years of 1988, 1992, 1996, 1997, 2000, 2001, 2002, 2004 and 2005 which are known as drought years in the region.

Land use/cover and water balance component changes before and after dam construction in the Mono River basin

Knowledge about land use and land cover dynamics is of high importance for integral water resource management in a given watershed. Therefore, LULCC were estimated between 1975 and 2000. The major land use changes are observed in savanna, forest, agriculture and cropland (Table 2). Between 1975 and 2000, there is 12.27% of decrease of savanna estimated at 2701.08 Km^2 of losses savanna, 2.35% (517.32 Km^2) of decrease of forest, 15.35% (3379.10 Km^2) increase of agriculture land, 1.29% (283.98 Km^2) increase of Cropland with oil palms as majors land cover over Mono river basin.

LULCC between 1975 and 2000 had repercussions on WBC over the study area (Table 3). Consequently, the results showed that there were significant decreases of forest, savanna and increases of agricultural land involve a decrease of precipitation (PRECIPmm), actual evapotranspiration (ETmm) and lateral flow (LAT_Q_mm) over the second period of simulation compared to the

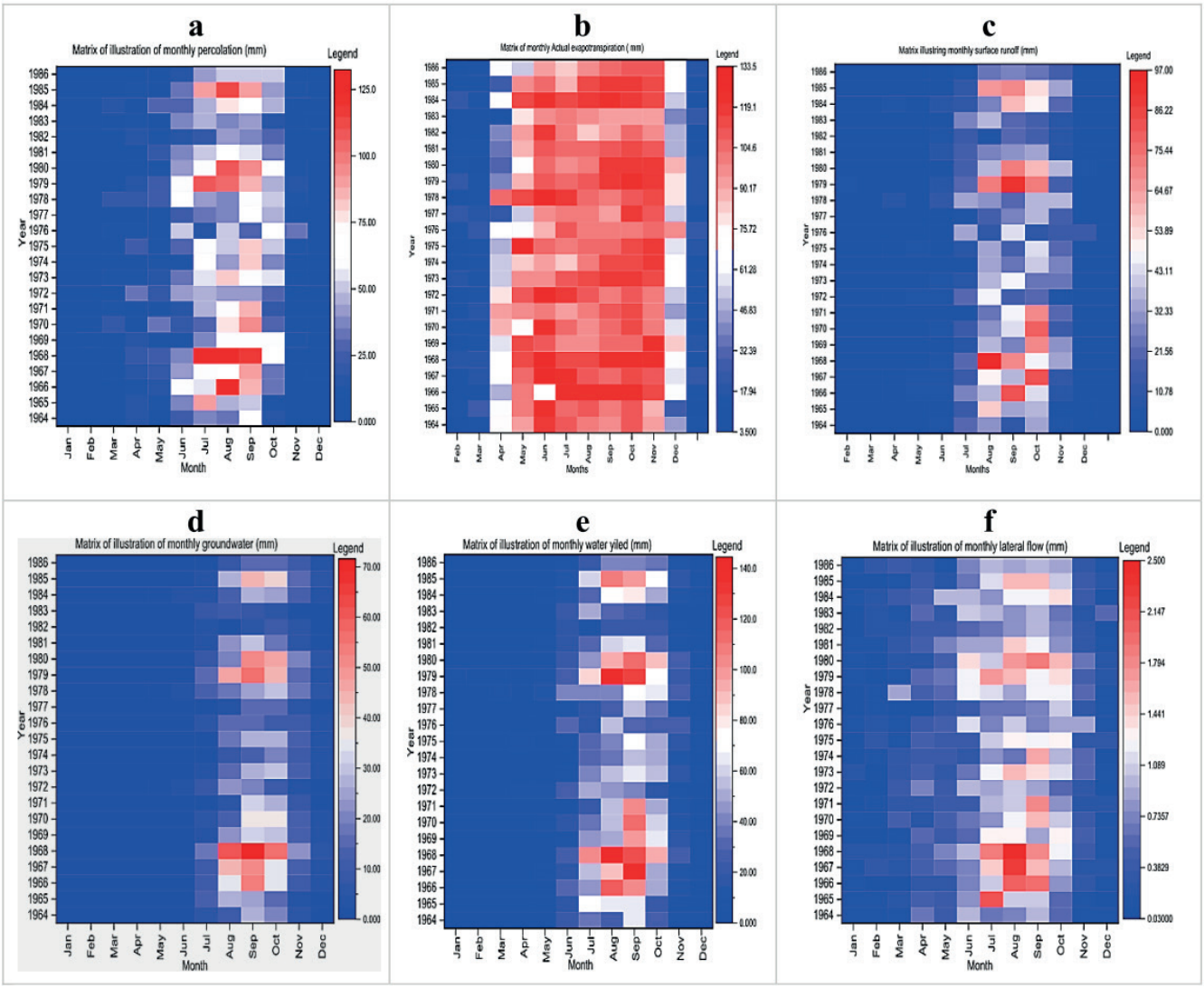

(a) Percolation, (b) actual evapotranspiration, (c) surface runoff, (d) groundwater, (e) water yield and (f) lateral flow

Fig. 3. Matrix [Month-Year] of water balance components contribution between 1964 and 1986

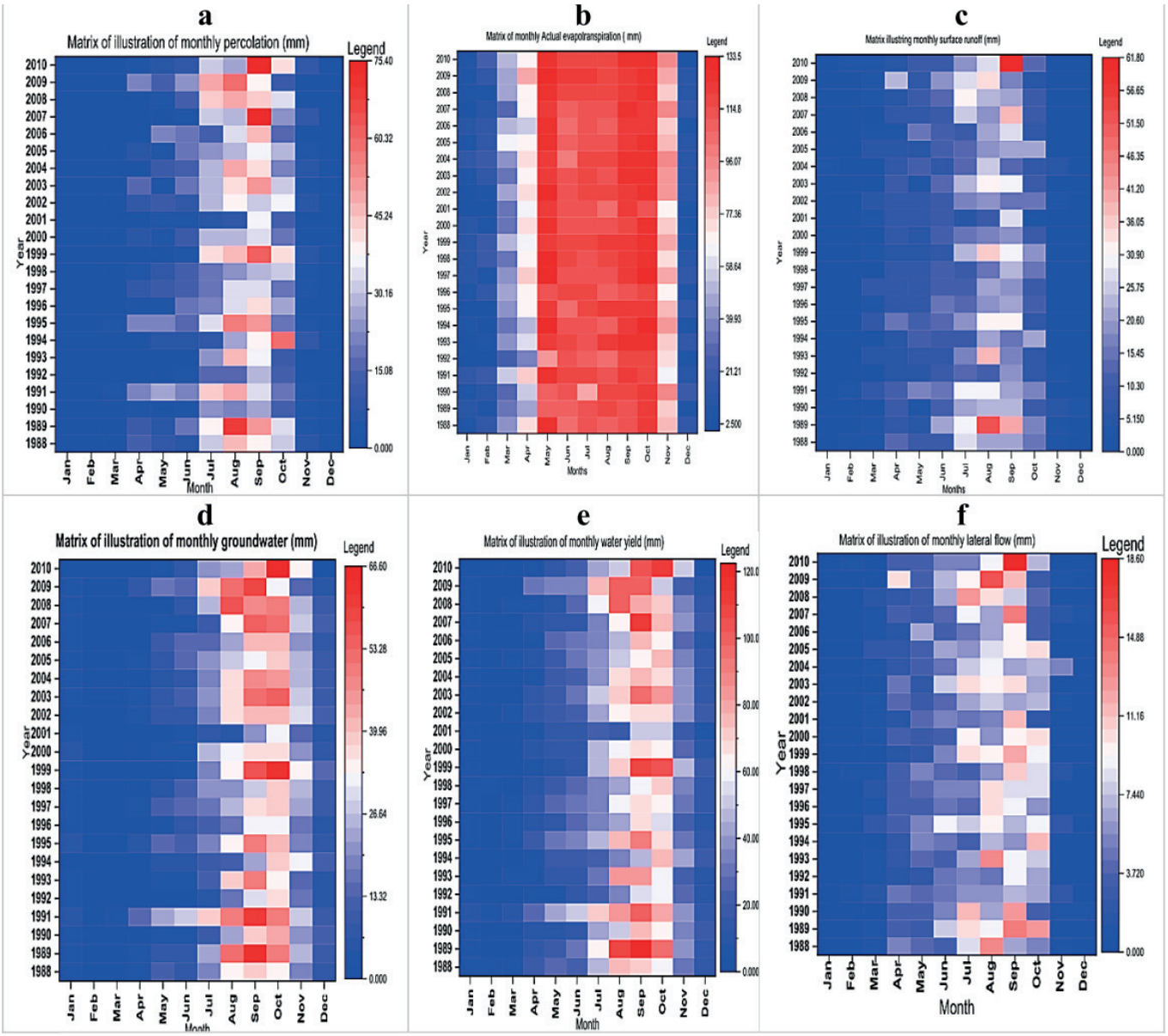

(a) percolation, (b) actual evapotranspiration, (c) surface runoff, (d) groundwater, (e) water yield and (f) lateral flow.

Fig. 4. Matrix illustration of water balance components contribution between 1988 and 2010

Table 2. Statistics of LULC and changes for the period 1975–2000

LULC types	SWAT Code	Year 1975		Year 2000		Change area 1975–2000	
		[Km^2]	[%]	[Km^2]	[%]	[Km^2]	[%]
Forest	FRST	1,184.34	5.38	667.02	3.03	-517.32	-2.35
Savanna	RNGE	1,6737.02	76.03	1,4035.94	63.76	-2,701.08	-12.27
Wetland-floodplain	WETN	4.40	0.02	72.65	0.33	68.24	0.31
Plantation/Agriculture	AGRR	1,426.49	6.48	4,805.59	21.83	3,379.10	15.35
Water bodies	WATR	4.40	0.02	114.47	0.52	110.07	0.50
Settlements	URBN	68.24	0.31	107.87	0.49	39.62	0.18
Gallery and riparian forest	FRSE	1,144.71	5.20	942.19	4.28	-202.53	-0.92
Degraded forest	RNGB	860.74	3.91	435.87	1.98	-424.86	-1.93
Woodland	FRSD	94.66	0.43	59.44	0.27	-35.22	-0.16
Cropland and fallow with oil palms	OILP	488.70	2.22	772.68	3.51	283.98	1.29
-	Total	22,013.70	100.00	22,013.70	100.00	0.00	0.00

first period of simulation. The other components such as percolation (PERCmm), groundwater (GW_Qmm), surface runoff (SURQ_mm) and water yield (WYLDmm) show an increase in the second period of simulation.

DISCUSSION

Temporal analysis of water balance components

In water management strategy planning, the analysis of individual water balance component contribution is a requirement. Sathian and Symala (2009) indicated that precipitation, actual evapotranspiration, percolation, groundwater, surface runoff, water yield and lateral flow were the most important components of water balance in a watershed. Among these components, precipitation is an input in hydrological models such as SWAT while other inputs are predicted due to the paucity of observation data (Ghoraba 2015). Actual evapotranspiration, percolation and water yield component contriburions were the highest components over the two periods of average annual and seasonal timescales as displayed in Table 3.

Actual evapotranspiration is the highest amount of water loss by the watershed in annual and seasonal average scales. The high amount of actual evapotranspiration can be explained by the various types of vegetation and also by the global increase of temperature and particularly in the study area (Koubodana et al. 2021; Lawin et al. 2019). Meanwhile, it is important to note that actual evapotranspiration has increased from 31.33% (1964–1986) to 49.85% (1988–2010) in inter-annual time scale and slightly from 51.02% (1964–1986) to 51.05% (1988–2010) for intra-annual period. This increase of water actual evapotranspiration from the period (1964–1986) to the period (1988–2010) is due to the increase of global land surface temperature since 1970, LULCC or decreasing wind speed (Koubodana et al. 2020, 2019).

The second major WBC is water yield which is net amount of water that leaves the sub-basin or the basin and contributes to streamflow in the reach during the time step. It is computed as WYLD = SURQ + LATQ + GWQ – TLOSS – pond abstractions. Therefore, an important amount of precipitation percentage received by the watershed is lost as streamflow. The percentage amount is ranging from 0.40% (1964–1986) to 2.52% (1988–2010). According to Fig. 2b and Fig. 4b, water yield decreases from 25.95% between 1964 and 1986 to 19.97% between 1988 and 2010 at -average annual timescale whereas Fig. 3b and Fig. 5b show on average seasonal timescale, it amounts has increased from 15.93% (1964–1986) to 20.43% (1988–2010). Lateral flow is the lowest (1988–2010) for average annual time scale and from 0.42% (1964–1986) to 2.59% (1988–2010) for average seasonal timescale. This can be due to the low infiltration rate and also that lateral flow depends on the watershed local slope (Cornelissen et al. 2013) which is not constant in the basin and ranges from 12 to 948m. The results on water cycle components contribution confirmed most analysis performed in West Africa (Akpoti et al. 2016; Begou et al. 2016; Hounkpè 2016;

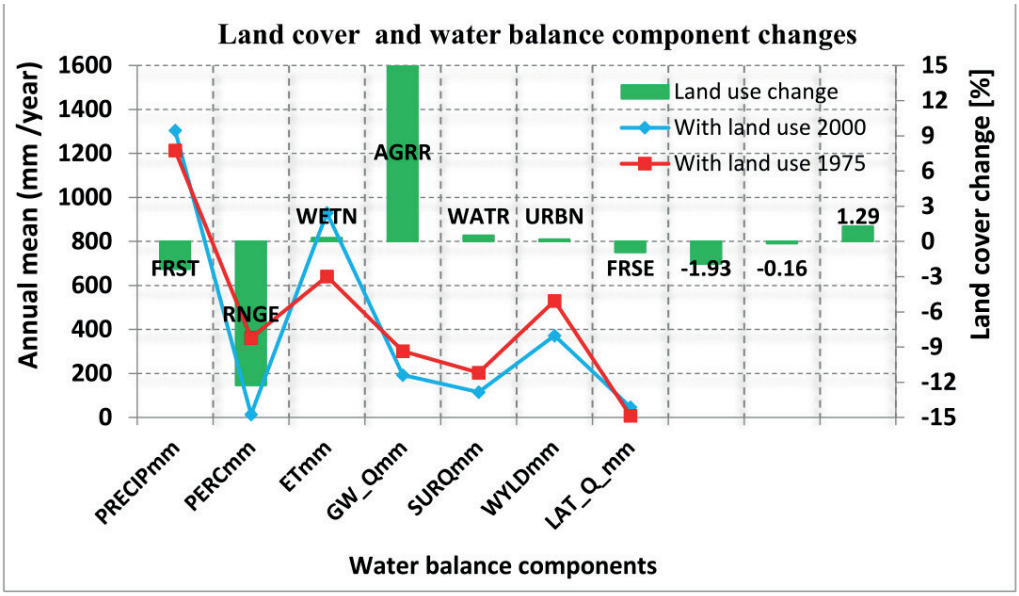

Fig. 5. Land use/cover and water balance components changes between SIM1 and SIM2

Table 3. Water balance component contribution at different time scales

Components	Annual average [%]		Monthly average [%]	
Period	1964–1986	1988–2010	1964–1986	1988–2010
PERCmm	**17.67**	**11.17**	**17.53**	**9.07**
ETmm	**31.33**	**49.85**	**51.02**	**51.05**
GW_Qmm	14.71	10.34	5.67	10.56
SURQmm	9.94	6.15	9.43	6.30
WYLDmm	**25.95**	**19.97**	**15.93**	**20.43**
LAT_Q_mm	0.40	2.52	0.42	2.59
Total	100.00	100.00	100.00	100.00

Kumi M. 2015). For average annual timescale analysis, many years are associated with high and low contribution of surface runoff compared to the average over the period. For example, 1968, 1979, 1980, 1995, 1999 and 2003 runoff contributions are higher and with a positive rainfall index. The years of 1977, 1982, 1983, 1986, 1990 and 2002 present the period with lowest surface runoff and associated with negative rainfall variability index and confirmed the years of drought in West Africa (Koubodana et al. 2020; Oguntunde et al. 2006; Yabi and Afouda 2012).

Rainfall matrix of Fig. 2 shows the average seasonal precipitation from 1964 to 1986 and also from 1988 to 2010 sub-periods. These results confirmed that the climate in the MRB, is unimodal and bimodal according to the past studies (Koubodana et al. 2020; Tramblay et al. 2014).

Fig. 3 and Fig. 4 show the matrix illustration of water cycle components between 1964 and 1986 and from 1988 and 2010 sub-periods. These figures illustrate the dry and wet months and years over the entire basin. It also displays the nature of the season assigned in the basin. The results reported that most of WBC reach their peak between July and October, which is exactly the period of the rainy season in the sub-tropical zone (Djaman et al. 2017; Giertz et al. 2006; Laux et al. 2009). The period of 1964, 1984,1982, 1981, 1977, 1976,1973, 1972, 1988, 1992, 1996, 1997, 2000, 2001, 2002 and 2004 characterized by a very low amount of surface runoff and precipitation are justified by the year where drought occurred in West Africa (Laux et al. 2009; Omotosho and Abiodun 2007; Sylla et al. 2016). For example, 1984, 1982, 1981, 1977, 1976,1973,1972 and 1964 are known in previous analysis as drought years with negative annual rainfall variability index (Descroix et al. 2009; Yabi and Afouda 2012).

Land use/cover and water balance components changes before and after dam construction

Land use and land cover changes are significant between 1975 and 2000 and justified by drivers such as population growth (Ahmad and Quegan 2012; dos R. Pereira et al. 2016). Nevertheless, Koubodana et al. (2019) concluded that the decrease of forest and savanna flowed by an increase of cropland and settlements has occurred in MRB between 1975 and 2000. The combined impacts of land use changes and climate variability induce the increase of precipitation intensity, actual evapotranspiration and lateral flow whereas decrease in percolation, groundwater, surface runoff and water yield were found. One of the reasons for this situation is that the conversion of forest and savanna in cropland caused the change in surface soil layer and vegetation canopy (Wagner et al. 2009). This confirms that LULCC plays an important role in the changes in WBC, water infiltration, evaporation and water movement at local level (Hagemann et al. 2014). The results confirmed the analysis of Koubodana et al. (Koubodana et al. 2019) over the basin. Fig. 5 showed LULCC between 1975 and 2000 have affected water components annual mean for (1964–1986) and (1988–2010) periods respectively. Forest and savanna decreased and could be explained by agriculture expansion, bush fire, timber extraction in response to population needs (Atsri et al. 2018; Koglo et al. 2018; Koubodana et al. 2019). Togo and Benin experience an increase of population which involve more demands for agricultural lands and habit, energy wood consumption. According to Verstraeten et al. (2008), the actual evapotranspiration (ET) is the process from which water is transferred from the soil compartment and/or vegetation layer to the atmosphere. Therefore, any change in land cover (leaf index area) or land use will affect ET intensity. Soil characteristics and climate condition also impacted on water balance components variation (Sciuto and Diekkrüger 2010).

Sources of uncertainty influencing the results of this analysis

Indeed, there are many sources of uncertainty which could affect the results of this study. Some of these include: uncertainty associated with the hydrological modelling and input data quality. In many cases, the analysis of these predictive uncertainty helps in capturing the overall range of expected uncertainty propagated through modelling (Liu and Gupta 2007; Nonki et al. 2021; Zhong-min et al. 2010) . But this study was already subject of uncertainty analysis in Koubodana et al. (2021) . Other studies prefer an ensemble hydrological modeling in order to reduce uncertainties (Gaba et al. 2015; Huisman et al. 2009). The ensemble of the hydrological models could therefore encompass the effects of model uncertainties, because the mean result is a more reliable estimation of hydrology characteristics and increases the confidence of the modeling. In fact, the multi-model approach has been proven to be more robust and exhibits better performance than individual models (Huisman et al. 2009). All these limitations will be considered in furthers analysis in order to minimize uncertainties for formulation of better policies strategies measures at local scale.

CONCLUSION

In this study, outputs on water balance components from a SWAT hydrological model and land use dataset of the years 1975 and 2000 were analyzed in the Mono River Basin over the period before Nangbeto dam construction (1964–1986) and the period after its construction (1988–2010). The results showed that mean monthly actual evapotranspiration, percolation and water yield represent 70% of total water balance in mean monthly and annual time scale. In detail, actual evapotranspiration, surface runoff, percolation and water yield peaks appeared in September corresponding to one month after the maximum rainfall in August. However, more detailed investigation showed that a significant decrease of forest, and savanna and increases of cropland involve an increase of actual evapotranspiration and lateral flow over the second period of simulation compared to the first period of simulation. Therefore, from this analysis it can be concluded that water balance component contribution, the runoff, evapotranspiration and water yield evolution depend strongly on different land-use type change, climate conditions and also on the presence or not of reservoir in the watershed. Finally, there is a strong need to develop sustainable adaptation measures in future studies including ensemble modeling to reduce uncertainties, particularly at local scale where the impact occurs, to mitigate the possible impacts of the projected change in climate.

REFERENCES

Abbaspour K.C., Vaghefi S.A., Srinivasan R. (2017). A Guideline for Successful Calibration and Uncertainty Analysis for Soil and Water Assessment: A Review of Papers from the 2016 International SWAT Conference. Water 10, 1-18, DOI:10.3390/w10010006.

Ahmad A., Quegan S. (2012). Analysis of Maximum Likelihood Classification Technique on Landsat 5 TM Satellite Data of Tropical Land Covers.

Akpoti K., Antwi E.O., Kabo-bah A. (2016). Impacts of Rainfall Variability , Land Use and Land Cover Change on Stream Flow of the Black Volta, West Africa. Hydrology 3, 1–24, DOI: 10.3390/hydrology3030026.

Anderson E.P., Encalada A.C., Maldonado-Ocampo J.A., Mcclain M.E., Ortega H., Wilcox, B.P., (2011). Environmental Flows: a Concept for Addressing Effects of River Alterations and Climate Change in the Andes. Clim. Chang. Biodivers. Trop. Andes 326-338.

Arnold J.G., Srinivasan R., Muttiah R.S., Williams J.R., Arnold J.G., Bednarz S.T., Srinivasan R. (1998). Large Area Hydrologic Modeling and Assessment Part I : Model Development. J. Am. Water Resour. Assoc. 34, 73-89, DOI: 10.1111/j.1752-1688.1998.tb05961.x.

Atsri K.H., Konko Y., Cuni-Sanchez A., Abotsi K.E. (2018). Changes in the West African forest-savanna mosaic, insights from central Togo. PLoS One 13, 10, DOI: 10.1371/journal.pone.0203999.

Badjana H.M., Fink M., Helmschrot J., Diekkrüger B., Kralisch S., Afouda A.A., Wala K. (2017). Hydrological system analysis and modelling of the Kara River basin (West Africa) using a lumped metric conceptual model. Hydrol. Sci. J. 62, 1094-1113, DOI: 10.1080/02626667.2017.1307571.

Begou J.C., Jomaa S., Benabdallah S., Bazie P. (2016). Multi-Site Validation of the SWAT Model on the Bani Catchment : Model Performance and Predictive Uncertainty. Water 8, 178, DOI: 10.3390/w8050178.

Bronstert A., Niehoff D., Gerd B. (2002). Effects of climate and land-use change on storm runoff generation: present knowledge and modelling capabilities. Hydrol. Process. 529, 509-529, DOI: 10.1002/hyp.326.

CILSS (2016). Landscapes of West Africa- A Window on a Changing World. 47914 252nd St, Garretson, SD 57030, UNITED STATES.

Cornelissen T., Diekkrüger B., Giertz S. (2013). A comparison of hydrological models for assessing the impact of land use and climate change on discharge in a tropical catchment. J. Hydrol. 498, 221-236, DOI: 10.1016/j.jhydrol.2013.06.016.

Deschenes L.A., Bout D.A. Vanden (2000). Origin 6.0: Scientific Data Analysis and Graphing Software Origin Lab Corporation (formerly Microcal Software, Inc.). Web site: www. originlab. com. Commercial price: 595.Academicprice: 446.

Descroix L., Mahé G., Lebel T., Favreau G., Galle S., Gautier E., Olivry J.-C., Albergel J., Amogu O., Cappelaere B., Dessouassi R., Diedhiou A., Le Breton E., Mamadou I., Sighomnou, D. (2009). Spatio-temporal variability of hydrological regimes around the boundaries between Sahelian and Sudanian areas of West Africa: A synthesis. J. Hydrol. 375, 90-102, DOI: 10.1016/j.jhydrol.2008.12.012.

Djaman K., Sharma V., Rudnick D.R., Koudahe K., Irmak S., Amouzou K.A., Sogbedji J.M. (2017). Spatial and Temporal Variation in Precipitation in Togo. Int. J. Hydrol. 1, 1-10, DOI: 10.15406/ijh.2017.01.00019.

dos R. Pereira D., Martinez M.A., Pruski F.F., da Silva D.D. (2016). Hydrological simulation in a basin of typical tropical climate and soil using the SWAT model part I: Calibration and validation tests. J. Hydrol. Reg. Stud. 7, 14-37, DOI: 10.1016/j.ejrh.2016.05.002.

Eusebion I.-B., Zong-Liang Y. (2008). Climate Change Impacts on the Water Resources. GEO 387H – Phys. Climatol. 26.

Gaba O.U.C., Biao I.E.E., Alamou A.E., Afouda A.A. (2015). An Ensemble Approach Modelling to Assess Water Resources in the Mékrou Basin , Benin. Hydrology 3, 22-32, DOI: 10.11648/j.hyd.20150302.11.

Gassman P.P.W., Reyes M.M.R., Green C.C.H., Arnold J.J.G. (2007). The Soil and Water Assessment Tool : historical development, applications, and future research directions. Trans. ASAE 50, 1211-1250, DOI: 10.1.1.88.6554.

Ghaffari G., Keesstra S., Ghodousi J., Ahmadi H. (2010). SWAT-simulated hydrological impact of land-use change in the Zanjanrood basin, Northwest Iran. Hydrol. Process. An Int. J. 24, 892-903.

Ghoraba S.M. (2015). Hydrological modeling of the Simly Dam watershed (Pakistan) using GIS and SWAT model. Alexandria Eng. J. 54, 583-594, DOI: 10.1016/j.aej.2015.05.018.

Giertz S., Diekkrüger B., Steup G. (2006). Physically-based modelling of hydrological processes in a tropical headwater catchment (West Africa) – process representation and multi-criteria validation. Hydrol. Earth Syst. Sci. 10, 829-847.

Gonzalez-Barahona J.M., Robles G., Andradas-Izquierdo R., Ghosh R.A. (2008). Geographic origin of libre software developers. Inf. Econ. Policy 20, 356-363.

Hagemann S., Blome T., Saeed F., Stacke T. (2014). Perspectives in Modelling Climate-Hydrology Interactions. Surv. Geophys. 35, 739-764, DOI: 10.1007/s10712-013-9245-z.

Hanjra M.A., Qureshi M.E. (2010). Global water crisis and future food security in an era of climate change. Food Policy 35, 365-377, DOI: 10.1016/j.foodpol.2010.05.006.

Hargreaves G.H., Samani Z.A. (1982). Estimating potential evapotranspiration. J. Irrig. Drain. Div. 108, 225-230.

Houngue N.R. (2018). Assessment of mid-century climate change impacts on Mono river's downstream inflows. Master thesis, Department of Geography, Université de Lomé, Togo, defended in January, 2018.

Hounkpè J. (2016). Assessing the climate and land use changes impacts on flood hazard in Ouémé River Basin, Benin (West Africa). Doctor of Philosophy (Ph.D) thesis in Climate Change and Water Resources at University of Abomey Calavi (Benin Republic); Date of defense: 05 September 2016.

Huisman J.A., Breuer L., Bormann H., Bronstert A., Croke B.F.W., Frede H.G., Gräff T., Hubrechts L., Jakeman A.J., Kite G., Lanini J., Leavesley G., Lettenmaier D.P., Lindström G., Seibert J., Sivapalan M., Viney N.R., Willems P. (2009). Assessing the impact of land use change on hydrology by ensemble modeling (LUCHEM) III: Scenario analysis. Adv. Water Resour. 32, 159-170, DOI: 10.1016/j.advwatres.2008.06.009.

Huntington T.G. (2006). Evidence for intensification of the global water cycle: Review and synthesis. J. Hydrol. 319, 83-95, DOI: 10.1016/j.jhydrol.2005.07.003.

Kissi A.E., Abbey G.A., Agboka K., Egbendewe A. (2015). Quantitative Assessment of Vulnerability to Flood Hazards in Downstream Area of Mono Basin, South-Eastern Togo: Yoto District. J. Geogr. Inf. Syst. 7, 607-619, DOI: 10.4236/jgis.2015.76049.

Klassou K.S., Komi K. (2021). Analysis of extreme rainfall in Oti River Basin (West Africa). J. Water Clim. Chang. 12, 1997–2009, DOI: 10.2166/wcc.2021.154.

Koglo Y.S., Agyare W.A., Diwediga B., Sogbedji J.M., Adden A.K., Gaiser T. (2018). Remote Sensing-Based and Participatory Analysis of Forests, Agricultural Land Dynamics, and Potential Land Conservation Measures in Kloto District (Togo, West Africa). Soil Syst. 2, Pages 1-11, DOI: 10.3390/soilsystems2030049.

Koubodana H.D. (2020). Modeling the Impacts Of Climate Change, Land Use Change And Dam Management On Water Resource In West Africa: Case Of The Mono River Basin, Togo-Benin. PhD Thesis, Graduate Research Program on Climate Change and Water Resources ,University of Abomey Calavi, Benin; defense date: February, 2020.

Koubodana H.D., Adounkpe J., Tall M., Amoussou E., Atchonouglo K., Mumtaz M. (2020). Trend Analysis of Hydroclimatic Historical Data and Future Scenarios of Climate Extreme Indices over Mono River Basin in West Africa. Am. J. Rural Dev. 8, 37-52, DOI: 10.12691/ajrd-8-1-5.

Koubodana H.D., Adounkpe J.G., Atchonouglo K., Djaman K., Larbi I., Lombo Y., Kpemoua K.E. (2021). Modelling of streamflow before and after dam construction in the Mono River Basin in Togo-Benin, West Africa. Int. J. River Basin Manag. 0, 1-17, DOI: 10.1080/15715124.2021.1969943.

Koubodana H.D., Diekkrüger B., Näschen K., Adounkpe J., Atchonouglo K. (2019). Impact of the Accuracy of Land Cover Data Sets on the Accuracy of Land Cover Change Scenarios in the Mono River Basin, Togo, West Africa. Int. J. Adv. Remote Sens. GIS 8, 3073-3095, DOI: 10.23953/cloud.ijarsg.422.

Kumi M A.A. (2015). Predicting Hydrological Response to Climate Change in the White Volta Catchment, West Africa. J. Earth Sci. Clim. Change 06, 1-7, DOI: 10.4172/2157-7617.1000249.

Laux P., Wagner S., Wagner A., Jacobeit J., B, A. (2009). Modelling daily precipitation features in the Volta Basin of West Africa. Int. J. Climatol. 29, 937-954, DOI: 10.1002/joc.

Lawin A.E., Hounguè N.R., Biaou C.A., Badou D.F. (2019). Statistical Analysis of Recent and Future Rainfall and Temperature Variability in the Mono River Watershed (Benin, Togo). Climate 7, 8, DOI: 10.3390/cli7010008.

Liu Y., Gupta H.V. (2007). Uncertainty in hydrologic modeling: Toward an integrated data assimilation framework. Water Resour. Res. 43.

Mango L.M., Melesse A.M., Mcclain M.E., Gann D., Setegn S.G., Melesse A.M., Mcclain M.E., Gann D., Setegn S.G. (2011). Land use and climate change impacts on the hydrology of the upper Mara River Basin, Kenya: results of a modeling study to support better resource management. Hydrol. Earth Syst. Sci. 15, 2245-2258, DOI: 10.5194/hess-15-2245-2011.

Nonki, R.M., Lenouo, A., Tshimanga, R.M., Donfack, F.C., Tchawoua, C., 2021. Performance assessment and uncertainty prediction of a daily time-step HBV-Light rainfall-runoff model for the Upper Benue River Basin, Northern Cameroon. J. Hydrol. Reg. Stud. 36, 100849.

Ntajal J., Lamptey B.L., Mahamadou I.B., Nyarko B.K. (2017). Flood Disaster Risk Mapping in the Lower Mono River Basin in Togo, West. Int. J. Disaster Risk Reduct. 23, 93-103, DOI: 10.1016/j.ijdrr.2017.03.015.

Oguntunde P.G., Friesen J., Giesen N. Van De, Savenije H.H.G. (2006). Hydroclimatology of the Volta River Basin in West Africa: Trends and variability from 1901 to 2002. Phys. Chem. Earth, Parts A/B/C 31, 1180-1188, DOI: 10.1016/j.pce.2006.02.062.

Omotosho J.B., Abiodun B.J. (2007). A numerical study of moisture build-up and rainfall over West Africa 225, 209-225, DOI: 10.1002/met.

Paeth H., Born K., Girmes R., Podzun R., Jacob D. (2009). Regional climate change in tropical and Northern Africa due to greenhouse forcing and land use changes. J. Clim. 22, 114-132, DOI: 10.1175/2008JCLI2390.1.

PCCP (2008). Programme PCCP-from Potential Conflict to Cooperation Potential: cas du basin du Mono(Togo-Benin). Lomé-Togo.

Philipp S., Kling H., Bauer H. (2018). Climate change impact on West African rivers under an ensemble of CORDEX climate projections. Clim. Serv. 11, 36-48, DOI: 10.1016/j.cliser.2018.05.003.

Rossi G. (1996). L'impact des barrages de la vallée du Mono (Togo-Benin). La gestion de l'incertitude. Géomorphologie Reli. Process. Environ. 2, 55-68, DOI: 10.3406/morfo.1996.878.

Sathian K., Symala P. (2009). Application of GIS integrated SWAT model for basin level water balance. Indian J. Soil Cons 37, 100-105.

SAWES (2011). Rapport final Etat des lieux bassin Mono. Aougadougou, Burkina Faso.

Sciuto G., Diekkrüger B. (2010). Influence of Soil Heterogeneity and Spatial Discretization on Catchment Water Balance Modeling Simulaon Model. Vadose Zo. J. 9, 955-969, DOI: 10.2136/vzj2009.0166.

Setyorini A., Khare D., Pingale S.M. (2017). Simulating the impact of land use/land cover change and climate variability on watershed hydrology in the Upper Brantas basin, Indonesia. Appl. Geomatics 9, 191-204, DOI: 10.1007/s12518-017-0193-z.

Speth P., Christoph M., Diekkrüger B. (2010). Impacts of Global Change on the Hydrological Cycle in West and Northwest Africa, Springer S. ed. Springer Berlin Heidelberg, DOI: 10.1007/978-3-642-12957-5_1.

Sylla M.B., Nikiema P.M., Gibba P., Kebe I., Ama N., Klutse B. (2016). Climate Change over West Africa: Recent Trends and Future Projections, in: Hesselberg, J.A.Y. and J. (Ed.), Adaptation to Climate Change and Variability in Rural West Africa. Springer International Publishing, 25-40, DOI: 10.1007/978-3-319-31499-0.

Tramblay Y., Amoussou E., Dorigo W., Mahé G. (2014). Flood risk under future climate in data sparse regions: Linking extreme value models and flood generating processes. J. Hydrol. 519, 549-558, DOI: 10.1016/j.jhydrol.2014.07.052.

Verstraeten W., Veroustraete F., Feyen J. (2008). Assessment of Evapotranspiration and Soil Moisture Content Across Different Scales of Observation. Sensors 8, 70-117.

Wagner S., Kunstmann H., Bárdossy A., Conrad C., Colditz R.R. (2009). Water balance estimation of a poorly gauged catchment in West Africa using dynamically downscaled meteorological fields and remote sensing information. Phys. Chem. Earth 34, 225-235, DOI: 10.1016/j.pce.2008.04.002.

Wijesekara G.N., Gupta A., Valeo C., Hasbani J.-G., Qiao Y., Delaney P., Marceau D.J. (2012). Assessing the impact of future land-use changes on hydrological processes in the Elbow River watershed in southern Alberta, Canada. J. Hydrol. 412, 220-232.

Yabi I., Afouda F. (2012). Extreme rainfall years in Benin (West Africa). Quat. Int. 262, 39-43, DOI: 10.1016/j.quaint.2010.12.010.

Zhong-min L., Rong D.A.I., Bin-quan L.I. (2010). A review of hydrological uncertainty analysis based on Bayesian theory. 水科学进展 21, 274-281.

Zuo D., Xu Z., Yao W., Jin S., Xiao P., Ran D. (2016). Assessing the effects of changes in land use and climate on runoff and sediment yields from a watershed in the Loess Plateau of China. Sci. Total Environ. 544, 238-250.

RESEARCH PAPER

DIGITAL ELEVATION MODEL DEVELOPMENT OF THE VOLGA AND DON RIVER'S DELTA AND APPLICATION IN HYDROLOGICAL MODELING

Natalia A. Yaitskaya[1*], Igor V. Sheverdyaev[1]

[1]Federal Research Centre the Subtropical Scientific Centre of the Russian Academy of Sciences, Yana Fabritsiusa Str.,2/28, Sochi, 354002, Russia

***Corresponding author:** yaitskayan@gmail.com

Received: March 31st, 2021 / Accepted: November 11th, 2022 / Published: December 31st, 2022

https://DOI-10.24057/2071-9388-2022-035

ABSTRACT. The article describes the methodology for constructing digital elevation models for the vast delta areas of the Don and Volga rivers for further use in mathematical models of flooding from surges. The initial cartographic data and features of the delta regions are described. The methods of information processing are considered in detail. An algorithm for constructing a DEM has been developed to obtain highly detailed digital elevation models. The algorithm is based on combining the DEM of individual key features - land, the depths of the hydrographic network and the bathymetry of the receiving reservoir for the river. The topographic maps, maps of the navigable route depths, hydrographic maps, and satellite images Landsat-8 and Sentinel-2 were used to create the DEM of the Don and Volga river. To build individual DEMs, a raster of the absolute depth of the channels, a hydrography DEM, a land DEM, and a shelf DEM were created using geoinformation systems. To assess the possibility of using obtained DEMs in hydrological models based on HEC-RAS, we conducted training and verification calculations of water level during wind surge phenomena in Don Delta using different surface roughness coefficients. The calculation results show good reproducibility of observed water level fluctuation in the Don Delta using obtained DEM with a roughness coefficient of 0.0125. Also, we carried out similar calculations of storm surge phenomena in the Volga Delta using obtained DEM and combinations of various riverbed and not riverbed roughness coefficients. The combination of 0.007 for riverbed and 0.02 for not riverbed surfaces reproduces the observed water level fluctuation during storm surge phenomena in Volga Delta. The constructed DEMs for the Volga and Don deltas made it possible to reproduce the observed dynamics of river discharges and water level fluctuations during surge events. Such detailed DEMs, taking into account all the complexity of the coastal and delta relief, were created for the first time for the Volga and Don.

KEYWORDS: Don River, Volga River, delta, digital elevation model, hydrological modelling

CITATION: Yaitskaya N. A., Sheverdyaev I. V. (2022). Digital Elevation Model Development Of The Volga And Don River's Delta And Application In Hydrological Modeling. Geography, Environment, Sustainability, 4(15), 181-187
https://DOI-10.24057/2071-9388-2022-035

ACKNOWLEDGEMENTS: The research was carried out at the expense of a grant from the Russian Science Foundation (project No. 20-77-00083).

Conflict of interests: The authors reported no potential conflict of interest.

INTRODUCTION

River deltas are among the most densely populated and economically important areas in the world (Vörösmarty et al. 2009). Deltas, as places of mutual influence of river flow and the sea, are characterized by flooding due to short-term level fluctuations caused by wind activity, river flow dynamics, tidal phenomena, or various combinations of these factors (Nienhuis et al. 2020).

Geomorphologically, the river delta is a coastal accumulative lowland at the confluence with the receiving reservoir, cut by branches and channels of the main river channel. Due to its importance in the economy, it is necessary to rationally manage the resources of river deltas, taking into account their natural and hydrological features and characteristic fluctuations in water levels. The development of simulation methods (Blumberg & Mellor 1987, Young 1999, Booij et al. 1999) makes it possible to perform experiments on the calculation of the impact of storms and surges on deltas and near-delta shallow waters, river delta and coastal flooding areas for conditional and real values of sea level and river flow, taking into account the slope of the delta, the type of underlying surface, the properties of soils, near-water vegetation, as well as the presence and characteristics of hydraulic structures on rivers. An important condition for obtaining a qualitative result in this case is an accurate and up-to-date digital elevation model (DEM) of the object of study. Publicly available DEMs with a spatial resolution of at least 30 m/pixel, based on the processing of radar satellite imagery (for example, SRTM (Shuttle…), ASTER GDEM (NASA… 2019), JAXA's Global ALOS 3D World (Takaku et al. 2020)) do not allow detailed studies for vast lowland areas. In this regard, it is necessary to develop DEMs for specific river

deltas using data from various types of maps (topographic, navigation, sailing directions), satellite imagery and field data (Nelson et al. 2009).

The Volga Delta is the largest in Europe (more than 27 thousand sq. km. (Polonskii et al. 1998), although its area varies greatly depending on the water level in the Caspian Sea (Li et al. 2004)) seashore in the Caspian Sea forms a unique natural complex. The flora and fauna of the Delta have been under state protection since 1919, since the formation of the Astrakhan Reserve (Astrakhan...). In 1976, the Volga Delta was included in the list of wetlands of international Ramsar Convention (The List of Wetlands…). Currently, the Volga Delta occupies more than 27 thousand sq km and is a triangle in shape with a peak at the source of the Buzan River (Narimanov town), facing the sea with a height of more than 110 km with a maximum width of more than 250 km. Geographically, the Volga Delta begins at the point of separation from the Volga channel of the Buzan branch (north of Astrakhan) and has up to 500 branches, channels, small rivers and eriks. branches of the delta - Buzan, Bakhtemir, Kamyzyak, Staraya Volga, Bolda, Akhtuba, Kigach. They form systems of smaller streams (up to 30–40 m wide and with a water flow rate of less than 50 m^3/s), which form the basis of the channel network and cut through the sea edge of the delta. Most of the mouth coast of the Volga is a vast shallow area up to 200 km wide and 30-35 km long with depths of less than 1 m, significantly overgrown with aquatic vegetation. The rest of the coast, 15-20 km long, has depths from 1 to 10 m. Due to the Caspian Sea level fluctuations in the XX-XXI centuries the Delta area has changed several times over the past 130 year (Ogorodov et al. 2020). The Volga Delta is characterized by water level fluctuations up to 4-5 m, leading to flooding of large areas due to the flatness of the land surface characteristic of river Deltas. The reasons for such large fluctuations in river levels here may be fluctuations in the Volga river flow and surge processes in the Northern Caspian, caused by south and southeast winds with a constant speed of more than 10 m/s for several hours.

The Don Delta occupies a much smaller area - 540 sq. km, its length is about 30 km, width is about 20 km, the top of the Delta is the source of the river. Mertvy Donets, flowing from the main channel of the Don at the western bridge of Rostov-on-Don. Among the main channels of the Don downstream, the Mertvy Donets, the Kalancha, which is divided into the Mokraya Kalancha and the Bolshaya Kuterma, and the Stary Don branch stand out. In addition, many small rivers and channels have been formed in the Don Delta. Geomorphologically, the Don Delta is a flooded river lowland with a slight elevation in the center (up to 6 m), the hydrography of which is complicated by a large number of ponds, canals, embankments and dams. The Don flows into the Taganrog Bay - a narrow (from 25 to 50 km wide) and shallow (up to 9 m) part of the Sea of Azov, in which navigation channels are arranged in the river. Don and to the port of Taganrog. With stable strong winds (more than 10 m/s) of the western direction in the Don, a surge of water is observed, often leading to partial or complete flooding of the Don Delta, from the east - a surge, during which the small branches of the delta are drained and the bottom of the near-delta part of the Taganrog Bay opens (Matishov et al. 2014a). Since 2013 in the Don Delta area 3 level gauges of Automatic System of Monitoring of Flood Events of Krasnodar Krai (AS MFEKK) were installed – 239, 1001 and 1002 (Monitoring ...). This system allows to get water level observations every 10 minutes. Gauges receive observation in near-real time regime and make it possible to study short-term water level phenomena like wind surgse or seiches.

This article presents the result of the work on the development of the DEM of the Volga and Don Deltas based on a similar set of materials using a single methodology for further use in mathematical models of flooding from surges. Such detailed DEMs, taking into account all the complexity of the coastal and delta relief, were created for the first time for the Volga and Don. In addition, surge flood zone results obtained using hydrological models are presented.

MATERIALS AND METHODS

Features of Deltas, as flat lowlands, crossed by a complex network of permanent and temporary waterstreams, determine the complexity of obtaining plausible DEMs of Deltas using remote sensing methods - orthophotogrammetry, radar imaging. The complexity of forming a DEM based on UAV survey data is due to the large area of the Don or Volga Delta. In addition, to simulate flooding due to surge processes, the reflection in the DEM of the hydrographic network of both permanent and temporary watercourses plays a key role. To build the DEM of the Volga and Don Deltas, data were used on the land relief of the Deltas, on the bathymetry of the Caspian Sea and the Taganrog Bay, on the hydrographic network, transport and hydrotechnical infrastructure. Therefore, the following materials were used to create the DEM of the Volga Delta:

-topographic maps of FSUE "Gosgiscenter" (1:25,000) (Topographic… 2012);

-topographic maps of the USSR General Staff (1:100,000) (Maps of the USSR… 2020);

-maps of the depths of the navigable route of the Volga (Volume 7…);

-hydrographic maps of the Caspian Sea adjacent to the Volga delta (chart 32006, scale 1:200,000) (32006 From Astrakhan…).

The following materials were used to create the Don Delta DEM:

-topographic maps of FSUE "Gosgiscenter" (1:25,000) (Topographic… 2012);

-topographic maps of the USSR General Staff (1:100,000) (Maps of the USSR… 2020);

-maps of the depths of the navigable route of the Don (Volume 8…);

-hydrographic maps of the Sea of Azov adjacent to the Don Delta (chart 33147 scale 1:100,000) (33147 East part of Taganrog…);

-satellite survey Landsat-8 (Landsat 8…) and Sentinel-2 (Sentinel-2…).

The geomorphology of the Don and Volga Deltas is characterized by a low-lying flat surface, in which the hydrographic network of permanent and temporary waterstreams, the bathymetry of the main branches and the adjacent part of the receiving reservoir, as well as a network of hydraulic structures, including road embankments, play a key role. Such small-scale features may be important for flooding processes in the delta. It is difficult to display land topography, bathymetry and various embankments at the same time by common methods of data interpolation for building a DEM, so the algorithm for building a DEM, shown in Fig. 1, was used in the work.

To build individual DEMs, the Topo to Raster ArcGIS10 tool (based on the ANUDEM 5.3 program (Hutchinson et al. 2011)) was used, which allows interpolating height values in each cell of the resulting raster based on an array of point,

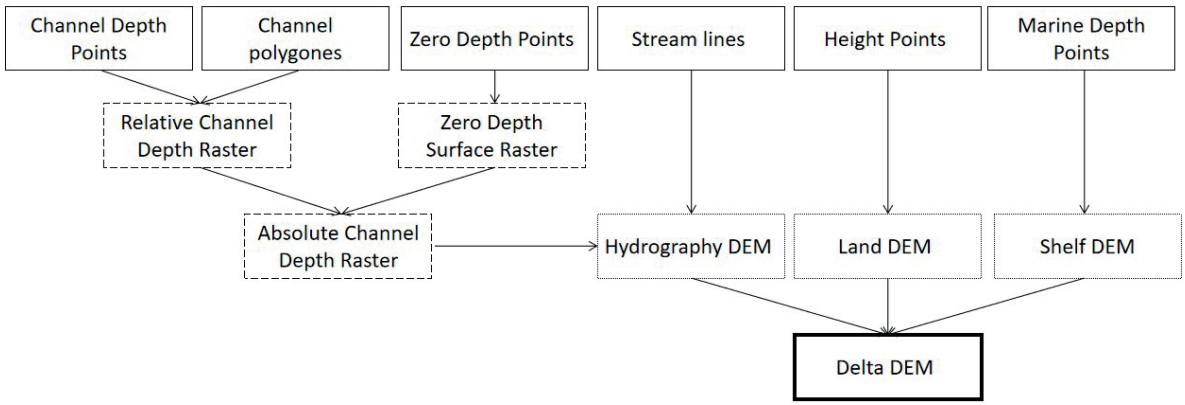

Fig. 1. Algorithm of the delta DEM construction (Yaitskaya et al. 2021)

line and polygonal objects. An important feature of this tool is that that both point values and linear (horizontals, cliff lines) and polygonal (lakes are represented by planes of equal elevation) objects are interpolated. From the point of view of geomorphology, watercourses are characterized by a special structure of the transverse profile.

The DEM of the land was built on the basis of information about the surface topography indicated on topographic maps - points of heights, contours, cliffs, lines of natural waterstreams. To construct the DEM of the hydrographic network, the polygons of the channels, the lines of the hydrographic network, as well as the height marks of the edges of the used topographic maps were used. Depth marks, major channel isobaths, and midstream lines were interpolated into the depth distribution raster within the river channel polygons. The values of the heights of the ridges were interpolated into a raster reflecting the inclined plane of the ridges of the delta hydrographic network. The lines of the hydrographic network were converted to a raster with depth values based on the depths indicated on the topographic maps, or in their absence, the value «1» was set. Further, the values of the depth distribution raster and the linear hydrographic network raster were subtracted from the raster values of the inclined surface. As a result, a DEM raster of the Delta hydrographic network was obtained. Coastal DEMs were built for the Volga Delta on the basis of bathymetric maps, and for the Don Delta on the basis of isobaths obtained as a result of deciphering the drying zones during surges using Landsat-8 and Sentinel-2 surveys (Kleshchenkov & Sheverdyaev 2020).

Checking the finished DEMs of the Volga Delta and the Don Delta was carried out in manual and semi-automatic modes:

Step 1 - sequential visual control of the obtained values of depth marks and correction of inaccuracies;

Step 2 - building «rough» GRID- and TIN-models, which were classified according to the values, the most contrasting coloring was chosen and the «spots» of emissions were already visually visible. In the case of detection of «outliers», we introduced auxiliary elevations and contour lines and built the DEM again.

RESULTS AND DISCUSSION

The obtained DEMs of the Don and Volga Deltas, as well as the computational grids of hydrological models based on HEC-RAS are presented in Figures 2 and 3. The DEM of the Volga Delta is a .tif raster file containing more than 7.1 million cells 100x100 meters on an area of 71100 sq km. Don Delta DEM contains 18.5 thousand cells on area 747.1 sq km. For the model of the Volga Delta, 4 boundaries were established (Fig. 3): for the discharge of the Volga, boundaries were established within the channels near the Nizhnelebyazhye (1) and the Buzan (2), for observing fluctuations of the water level of the boundary in the channel of the Bakhtemir channel near the Olya (3) and at the boundary of the computational grid in the Caspian Sea (4). Since the available daily observations of the discharge of the Volga are available for the Verkhnelyabyazhie (above the branch from the Volga river Buzan) and for the Buzan (respectively below), then for the Nizhnelebyazhie, they were recalculated as observations in Verkhnelebyazhie minus observations in the Buzan.

Within the Don Delta DEM, in the hydrological models based on HEC-RAS (HEC-RAS ...), a computational grid was built covering the Don Delta and floodplain from Zeleny Island within Rostov-on-Don up to the Don mouth area along the meridian 39°12´E (between Stefanidinodar and Morskoy Chulek). The computational grid is a set of cells 100x100 m, complicated by coastlines with a density of up to 50x50 m. Two boundaries were established: in the Don channel at Zeleny Island (upper entrance) and the border in the Delta mouth area, along the meridian 39°12´E (lower entrance). The discharge rate from the Tsimlyansk Reservoir was set at the upper entrance to the model with a delay of 3 days.

To assess the quality of the obtained DEMs and the possibility of using them in hydrological models based on HEC-RAS, we adjusted the surface roughness according to observational data in the Don and Volga Deltas and compared them with each other.

To determine the roughness coefficient in the Don Delta, the water levels were considered at level gauges 239 (the level gauge is located at the confluence of the Temernik with the Don) and 1001 (the level gauge is located in the village of Donskoy at the exit from the Don delta) of AS MFEKK in April-May 2018, when the largest flood in the last 10 years was observed on the river Don, which forced at that time to increase the discharge of water from the Tsimlyansk reservoir of the Don Basin Water Administration (O regime ... 2018). Surge fluctuations in the Don delta are reflected in observations both in the coastal part of the delta (level gauge 1001) and at the top of the delta (level gauge 239). The discharge of the Don is significantly reflected in the water level at the level gauge 239 (Fig. 4a). During April 19-24, 2018, a training period was held (Fig. 4b) - the water level in the Don delta was simulated using various roughness coefficients (0.02, 0.015, 0.0125, 0.01), the level change at the level gauge 1001 and average daily discharge in the Don (according to Razdorskaya station - about 100 km from Rostov-on-Don along the Don). The water levels of roughness 0.0125 turned out to be the most similar to the observed. During May 2018, a verification period took place, when the water levels were calculated using a roughness factor of 0.0125 (Fig. 4c). It is shown that taking into account the jump in the Don flood runoff by

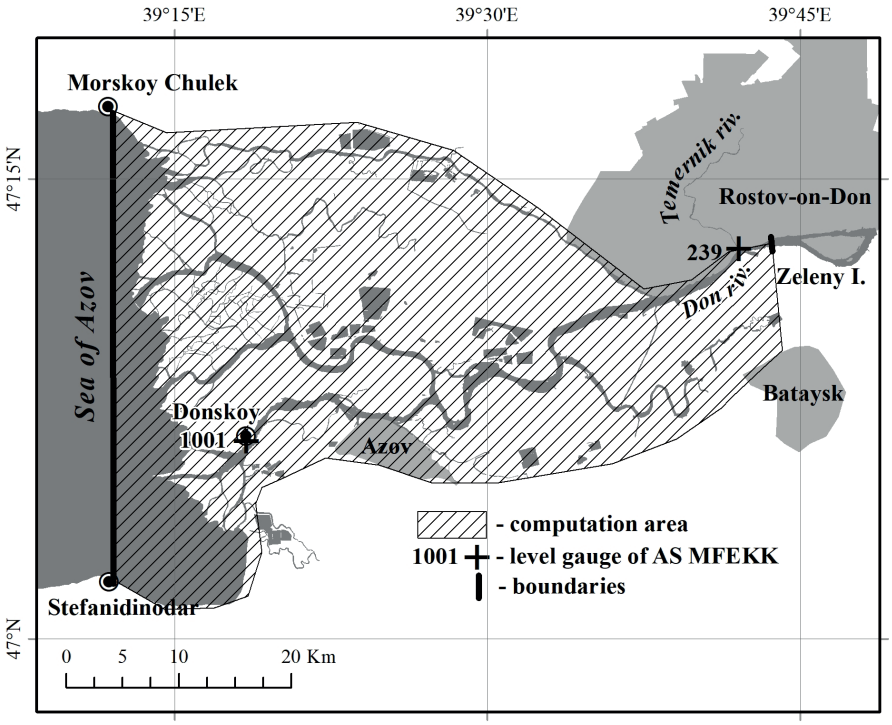

Fig. 2. Hydrography network and computation area of the Don Delta

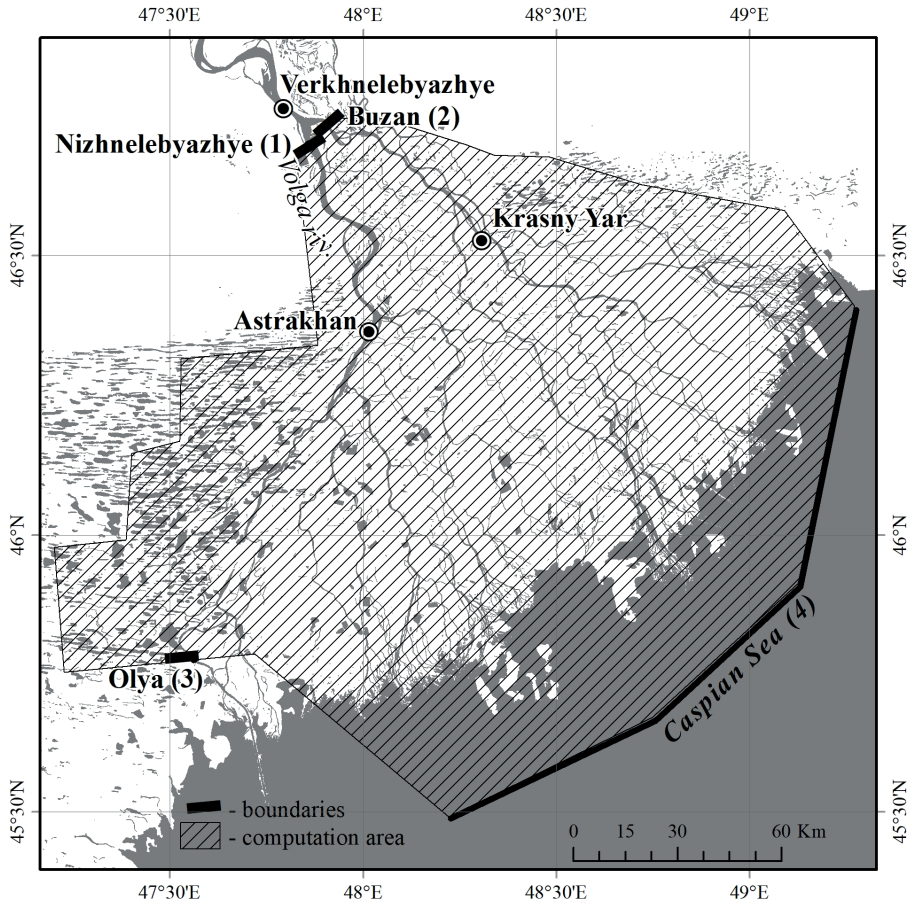

Fig. 3. Hydrography network and computation area of the Volga Delta

300 m^3/s significantly affects both the calculated and the observed water levels.

A number of calculations were carried out with different values of roughness in the channels of the Don delta (Fig. 4b) so that the course of the water level obtained at the confluence of the Temernik with the Don coincided with the value of the level gauge AS MFSKK. These calculations were carried out along the level of April 19-24, 2018, and then the optimal value was checked under the conditions of May 1-31, 2018 (shown in Fig. 4c). The presented results show that the roughness coefficient of the Don delta channel under these conditions is 0.0125, which allows the channel to pass large volumes of water without significant flooding of the floodplain.

To study the roughness coefficient of the Volga Delta, daily observations of level gauges in Astrakhan, Olya, Krasny Yar (Gauge… 2019) and daily observations of expenditures in Verkhnelebyazhye (Volga River) and Buzan (Buzan River) (Gauge… 2019).

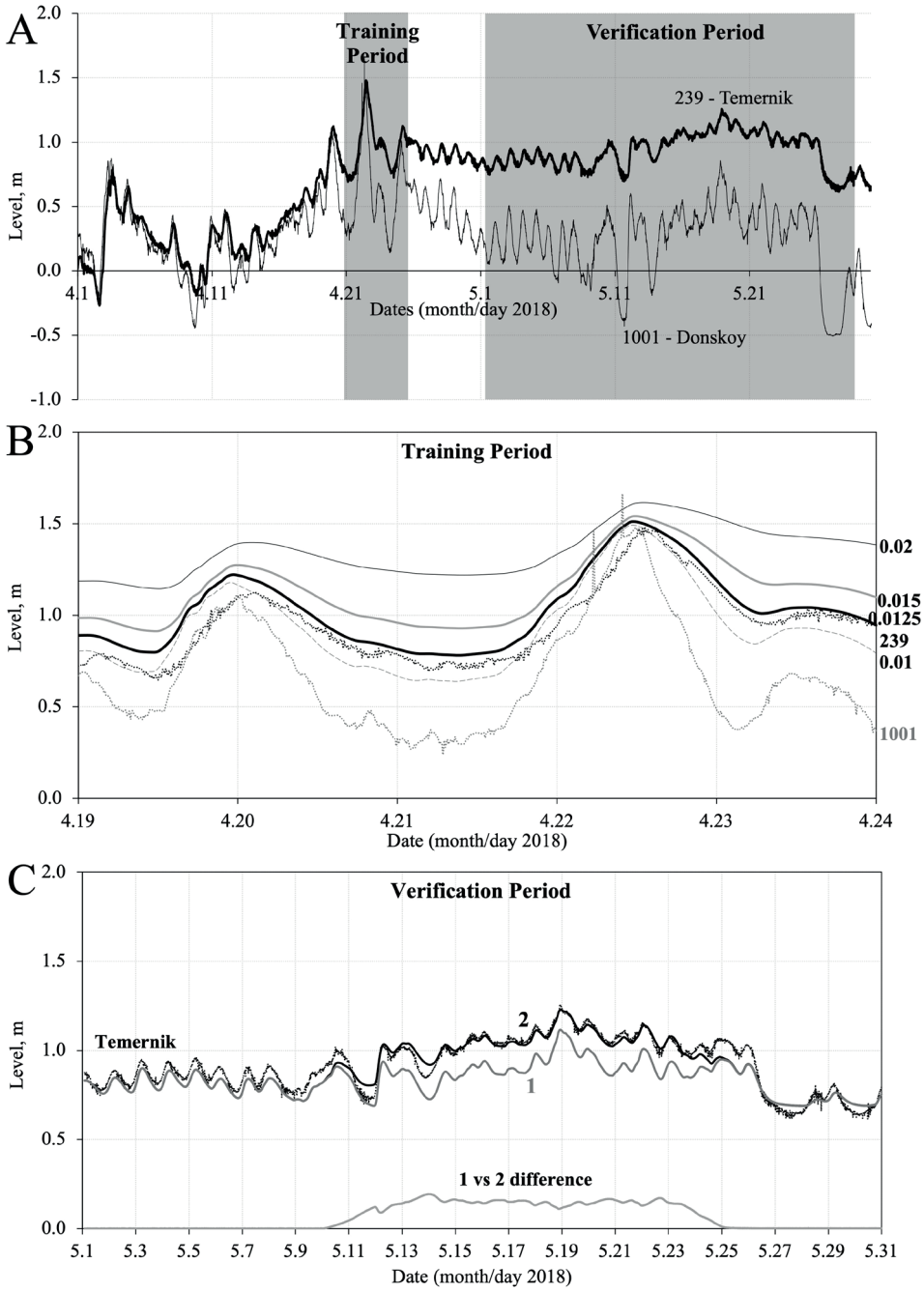

Fig. 4. A – Training and verification periods in April-May 2018 (Flooding period on Don Delta) and level observations at gauges 1001 (Donskoy) and 239 (Temernik). B – Delta roughness coefficient determining at training period in April 2018, C - modeling within Don's discharge 1500 m³/s (1), modeling within discharge 1500 to 1800 m³/s (observed increasing) (2) and Temernik - observed levels at gauge 239

Thus, pairs of scenarios with the same roughness distribution were calculated. Surface roughness was divided into two classes: Riverbeds and Not Riverbeds surfaces (land). It is assumed that the channels of the channels have a reduced roughness due to regular flow, and the land surface, on the contrary, has an increased roughness due to the reed vegetation characteristic of the Volga Delta (Table 1). For the control pair of scenarios, the same roughness was set for both classes - 0.0125 (pairs of coefficients were selected based on the idea that the Volga and Don deltas are in similar climatic conditions according to (Matishov et al. 2014b)).

Table 1. Calculated roughness distributions by class

Scenario	Riverbeds	Not riverbeds
control	0.0125	0.0125
1	0.01	0.02
2	0.0125	0.01
3	0.007	0.02
4	0.0125	0.05

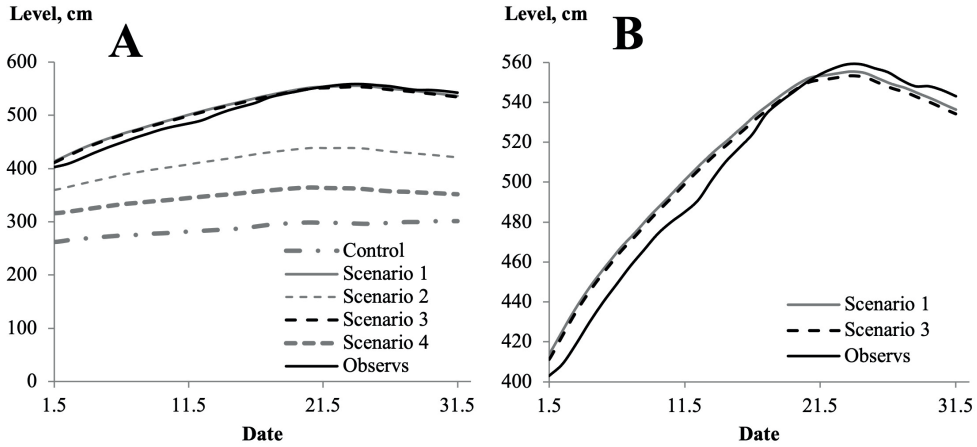

Fig. 5. Comparison of the test calculations results for different scenarios (table 1) with observations from the Astrakhan level gauge: A – results for all scenarios in comparison with observations; B – scenarios 1, 3 and observations, cm

The choice of the optimal variant of the roughness coefficient distribution was carried out on the basis of a comparison of the model level fluctuations in Astrakhan and Krasny Yar with those observed for the corresponding months. Figure 5 shows a comparison of the results of the calculated scenarios with observations in Astrakhan in May 2017.

The control scenario, corresponding to a roughness of 0.0125 for both riverbeds and not riverbeds, does not reproduce the observed level increase in Astrakhan. This is due to the rapid runoff of water both in the channel and on the land surface. Even a small increase in land roughness results in a larger level increase, as scenarios 4 and 2 show. Scenarios 1 and 3, for which the land roughness was 0.2, reproduce the observed level dynamics. We chose the roughness combination for scenario 3 due to the fact that under such conditions the level formed by the river runoff before the surge is somewhat closer to the observed values (Fig. 5B).

CONCLUSIONS

The final result of the work for constructing a DEM for Don and Volga Deltas is presented in the article. This DEM has constructed on the basis of observation data, is the most realistic and has a high level of detail. A method for constructing a DEM is proposed, based on the combination of DEM of individual key features - land, depths of the hydrographic network and bathymetry of a reservoir receiving a river.

The constructed DEMs for the Volga and Don Deltas made it possible to reproduce the observed dynamics of river discharges and water level fluctuations during surge events. However, at the same time, the roughness of the surface of the delta for the Volga and Don was different, and for the Don channels the roughness coefficient was 0.0125, and for the Volga channels – 0.007-0.01, i.e. less. DEMs can be used for retrospective analysis of effects of storm and wind surges in Deltas.

REFERENCES

32006 From Astrakhan to the Astrakhan raid. nteractive marine map. [online]. Available at: https://www.morkniga.ru/r821084-1.html [Accessed 23 Jan. 2021]. (In Russian).

33147 East part of Taganrog Bay. Interactive marine map. [online]. Available at: https://www.morkniga.ru/p150402.html [Accessed 23 Jan. 2021]. (In Russian).

Astrakhan Biosphere Nature Reserve, (2021). History. [online] Available at: https://en.astrakhanzapoved.ru/about-us/history/ [Accessed 20 Jul. 2021].

Blumberg A.F., Mellor G.L. (1987). A description of a three-dimensional coastal ocean circulation model. Three-Dimensional Coastal Ocean Models, American Geophysical Union. Heaps N.S. (Ed.). Washington, American Geophysical Union Publ.: 1-16.

Booij N., Ris R.C., Holthuijsen L.H. (1999). A third-generation wave model for coastal regions 1. Model description and validation. Journal of Geophysical Research: Oceans, 104 (C4), art. no. 98JC02622, 7649-7666, DOI: 10.1029/98JC02622.

Don basin water department of the Federal agency of water resources. (2018). About operating status of the Tsimlyanskoye reservoir in 12.04.2018, 18.04.2018, 24.04.2018, 04.05.2018, 11.05.2018, 17.05.2018 and 24.05.2018. (In Russian). Available at: http://www.donbvu.ru [Accessed 06 Jul. 2018].

HEC-RAS: River Analysis System. (2019). Available at : http://www.hec.usace.army.mil/software/hec-ras/ [Accessed 01 Jul. 2019].

Hutchinson Michael F., Tingbao Xu and John A. Stein. (2011). Recent progress in the ANUDEM elevation gridding procedure. Geomorphometry, 19-22.

Information system of water resources and water management of Russian river basins. [online]. (In Russian). Available at: http://gis.vodinfo.ru/ [Accessed 01 Jul. 2019].

Kleshchenkov A.V., Sheverdyaev I.V. (2020). Changes in the hydrographic network of the Don Delta during downsurge, IV Vinogradov Conference. Hydrology: From Learning to Worldview. Proceedings of international scientific conference in memory of outstanding Russian scientist Yury Vinogradov. Saint-Petersburg, 675-680.

Landsat 8 OLI/TIRS Digital Object Identifier, DOI: /10.5066/F71835S6

Li C.X., Ivanov V., Fan D.D., Korotaev V., Yang S.Y., Chalov R., Liu S.G. (2004). Development of the Volga Delta in Response to Caspian Sea-Level Fluctuation during Last 100 Years. Journal of Coastal Research, 20(2), 401–414, DOI: 10.2112/1551-5036(2004)020[0401:dotvdi]2.0.co;2

Maps of the USSR General Staff - archive of topographic maps. [online]. Available at: https://satmaps.info/genshtab.php [Accessed 01 Jul. 2021]. (In Russian).

Matishov G.G., Berdnikov S.V., Sheverdyaev I.V., Chikin A.L. (2014). The extreme flood in the don river delta, march 23-24, 2013, and determining factors. Doklady Earth Sciences, 455(1), 360-363, DOI 10.1134/S1028334X14030295.

Matishov G.G., Berdnikov S.V., Zhichkin A.P., Makarevich P.R., Dzhenyuk S.L., Kulygin V.V., Yaitskaya N.A., Povazhnyy V.V., Sheverdyaev I.V., Kumpan S.V., Tret'yakova I.A., Tsygankova A.E. (2014). Atlas of Climate Changes in Large Marine Ecosystems of the Northern Hemisphere (1878-2013). Region 1. The Eastern Arctic Seas. Region 2. The Black Sea, the Sea of Azov and the Caspian Sea. Rostov-on-Don, SSC-RAS Publishers, 256. (In Russian).

Monitoting. Emercit. (2021). [online] Available at: www.emercit.com/newmap [Accessed 14 Apr. 2021].

NASA/METI/AIST/Japan Spacesystems and U.S./Japan ASTER Science Team (2019). ASTER Global Digital Elevation Model V003. NASA EOSDIS Land Processes DAAC. [Accessed 20 Feb. 2022], DOI: 10.5067/ASTER/ASTGTM.003.

Nelson A., Reuter H.I., Gessler P. (2009). DEM production methods and sources. Dev. Soil Sci. 33, 65-85, DOI: 10.1016/S0166-2481(08)00003-2.

Nienhuis J.H., Ashton A.D., Edmonds D.A. et al. (2020). Global-scale human impact on delta morphology has led to net land area gain. Nature 577, 514-518, DOI: 10.1038/s41586-019-1905-9.

Ogorodov S.A., Magaeva A.A., Maznev S.V., Yaitskaya N.A., Vernyayev S., Sigitov A., Kadranov Y. (2020). Ice Features Of The Northern Caspian Under Sea Level Fluctuations And Ice Coverage Variations. Geography, Environment, Sustainability, 13(3), 129-138, DOI: 10.24057/2071-9388-2020-77.

Polonskii V.F., Mikhailov V.N., and Kir'yanov S.V. (1998). Volga Mouth Area: Hydrological–Morphological Processes, Pollution Regime, and the Effect of Variations of the Caspian Sea, Moscow: GEOS. (in Russian).

Sentinel-2 Digital Object Identifier, DOI: 10.5066/F76W992G.

Shuttle Radar Topography Mission 1 Arc-Second Global DOI: 10.5066/F7PR7TFT

Takaku Junichi & Tadono Takeo & Doutsu,M. & Ohgushi F. & Kai H.. (2020). Updates of 'AW3D30' ALOS Global Digital Surface Model with other Open Access Datasets. ISPRS - International Archives of the Photogrammetry, Remote Sensing and Spatial Information Sciences. XLIII-B4-2020, 183-189, DOI: 10.5194/isprs-archives-XLIII-B4-2020-183-2020.

The List Of Wetlands Of International Importance (The Ramsar List). [online]. Available at: https://www.ramsar.org/sites/default/files/documents/library/sitelist.pdf [Accessed 23 Jul. 2021].

Topographic maps of FSUE "Gosgiscenter". [online]. Available at: http://retromap.ru/ [Accessed 17 Oct. 2014]. (In Russian).

The Volga River - from the Volgograd hydroelectric complex to Astrakhan. (2021). [online]. Available at: http://roro.pro/tom-7-reka-volga-ot-volgogradskogo-gidrouzla-do-astraxani [Accessed 22 Jan. 2021]. (In Russian).

Volga-Don waterway from Volgograd to Azov Sea. (2021). [online]. Available at: http://roro.pro/volgo-donskoj-vodnyj-put-ot-volgograda-do-azovskogo-morya [Accessed 22 Jan. 2021]. (In Russian).

Vörösmarty Charles J., Syvitski James, Day John, de Sherbinin Alex, Giosan Liviu, Paola Chris (2009). Battling to Save the World's River Deltas. Bulletin of the Atomic Scientists, 65(2), 31-43, DOI: 10.2968/065002005.

Yaitskaya N.A., Sheverdyaev I.V., Magaeva A.A., Brigida V.S. (2021). Reconstruction of dangerous surges in the Northern Caspian based on digital elevation models and hydroligical modeling. Science in the South Russia, 17(3), 18-29, DOI: 10.7868/S25000640210303 (in Russian).

Young I.R. (1999). Wind generated ocean waves. Elsevier ocean engineering book series, vol. 2. Bhattacharyya R., McCormick M.E. (Ed.). Kidlington, Elsevier Publ.: 288.

RESEARCH PAPER

SOCIAL CONSEQUENCES OF FLOODS: CASE STUDY OF FIVE EMERGENCIES IN DIFFERENT GLOBAL DRAINAGE BASINS

Valeriy P. Bondarev[1,2*]

[1]Lomonosov Moscow State University, Faculty of Geography, GSP-1, Leninskiye Gory 1, 119991, Moscow, Russia

[2]Bauman Moscow State Technical University, Faculty of Social Sciences and Humanities, Rubcovskaya naberezhnaya, 2/18, 105085 Moscow, Russia

***Corresponding author:** valery_bondarev@mail.ru

Received: August 6th, 2021 / Accepted: November 11th, 2022 / Published: December 31st, 2022

https://DOI-10.24057/2071-9388-2022-102

ABSTRACT. Identifying social consequences is an essential aspect of considering emergency flood events. There needs to be more consensus in scientific publications on which social consequences of natural disasters, including emergency flood events, should be singled out and considered for the complete analysis of this issue and for further making the right management decisions. To clarify the structure and dynamics of scientific interest in social consequences, a line-by-line content analysis of more than 100 scientific articles on the five largest emergency floods of the early 2010s that occurred in various global basins of the world in countries with different levels of human development was carried out. As a rule, the cycle of interest in the events is 6-7 years, with a peak in the second or third year. There are exceptions to this trend due to either a completely unexpected event or the overlap of several significant events over several years. Social consequences, as the volume of consideration decreases, can be arranged in the following row (by the level of interest, %): death losses (23,1); social solidarity (18,3); management problems (13,4); horizontal mobility (11,3); psychological state (10,9); vertical mobility (7,0); social conflicts (6,2); social adaptation (5,4); health losses (4,4). The relationship of scientific interest in emergency flood events with the country's level of development has been evaluated. There are three types of connection. With the growth of the Human Development Index (HDI), interest in social solidarity, death losses and management problems increases (the correlation coefficient is 0,54; 0,42; 0,31, respectively); However, consideration of vertical mobility, social conflicts and health losses is typical for lower HDI (the correlation coefficient is -0,86; -0,70; -0,47, respectively). The third group of social consequences (social adaptation, horizontal mobility, psychological state of the population) is statistically poorly related to the level of HDI.

KEYWORDS: nature disasters; flood hazard; Human Development Index; climate change; flood risk analysis; flood consequences

CITATION: Bondarev V. P. (2022). Social Consequences Of Floods: Case Study Of Five Emergencies In Different Global Drainage Basins. Geography, Environment, Sustainability, 4(15), 188-195
https://DOI-10.24057/2071-9388-2022-102

ACKNOWLEDGEMENTS: Empirical data and their processing were carried out within the framework of research on state assignment No. 121051100166-4 of the geographical faculty of Lomonosov Moscow State University, theoretical justification and interpretation of the results were carried out according to the plan of the Department of Sociology and Cultural Studies of Bauman Moscow State Technical University. I would like to express special gratitude to Yu.A. Bolkhovitinova, who took an active part in the initial stages of this project and the publication of primary results. I also express my deep gratitude to T.V. Khrapova, who kindly agreed to review the manuscript of the article and make the necessary corrections to it.

Conflict of interests: The authors reported no potential conflict of interest.

INTRODUCTION

Modern society is increasingly viewed from the perspective of the risks it generates (Beck 1996; Giddens 1994; Mythen 2021, etc.). In the theoretical works of U. Beck and A. Giddens and others have shown that we live in an era of risk society characterized by the ubiquity of unlikely, but high-level risks. It is not just humans' health and the environment that are at risk, but the social structure and dynamics of society. In this context, the problems of the social consequences of natural disasters are becoming more acute every year, because the increase in population, the development and complexity of infrastructure, technical innovations lead to an increase in the risk component of society. In order to achieve the Sustainable Development Goals formulated within the framework of the UN (Sustainable Development Goals…), it is necessary to study these risks and create a basis for their forecasting and management.

One of the widespread natural disasters are emergency flood events. A recent report the Intergovernmental Panel on Climate Change (IPCC) showed that rising global

temperatures dramatically affect the water cycle, making flooding more frequent and extreme (AR6 Synthesis Report…). The report of the World Meteorological Organization (WMO) states that from 2000 to 2020, the number of catastrophic floods increased by 134% compared to the period from 1980 to 1999 (2021 State of Climate Services Water…).

Various researchers demonstrate an increase in the risk of emergency flood events in various regions of the world (Alekseevsky et al. 2016; Bloschl et al. 2017; Dobrovolsky 2017; Frolova et al. 2017; Yu Wang, Li 2022). The reasons for the increase in the number of the emergency flood events are natural and anthropogenic factors – changes in the water and climate balance, an increase in population density, the expansion and complexity of infrastructure. In addition, the increase in the volume of information about the emergency flood events is associated with the growing interest in this issue and the development of information technologies.

An important aspect in consideration of emergency flood events is the assessment of their social consequences. Over the past two decades, a number of papers have been published describing and quantifying various consequences of possible and already occurred the events (Convery, Bailey 2008; Xiao et al. 2014; Istomina, Dobrovolskiy 2016; Dar et al. 2018; Karunarathne, Lee 2020; Török 2018; Kroska, et al. 2018; Kirby et al. 2019; Fernández et al. 2019; Mullick et al. 2019; Tate et al. 2021; Emrich et al. 2020). Currently, various risk assessment methods are being created, as well as reducing the impact of emergency flood events (Zemtsov et al. 2016; Mabuku et al. 2018; de Voogt et al. 2019; Hudson et al. 2020; Tanır et al. 2022). One of the other important topics discussed is the problem of prevention and management of social risks arising from emergency flood events. The publications analyze the problems of organizing prevention, mitigating the social consequences of the events, establishing social justice, supporting victims, improving adaptation conditions, alerting, etc. (Brouwer, Van Ek 2004; Norris et al. 2005; Thaler et al. 2018; O'Hare, White 2018; Ciampa et al. 2021; Aznar-Crespo et al. 2021; Kopsidas, Giakoumatos 2021; Mol et al. 2021).

There is no single list of social consequences of emergency flood events. As a rule, while assessing the magnitude and structure of damages, the authors take into account the following points in various combinations: the number of settlements affected by the flood; the amount of material damage; a threat to life; the nature of damage to industrial facilities, residential buildings and road infrastructure; the size and structure of flooding of the developed territory; the degree of disruption of people's way of life and industrial activity; the need for evacuation of local residents; environmental degradation and other characteristics.

Earlier, an analysis of scientific papers was carried out, in which it was shown that several main discussed topics characterizing the social consequences of emergency flood events can be distinguished (Bondarev, Bolkhovitinova 2019). It was possible to establish the most frequently mentioned social consequences in scientific publications:

• Death losses. These are the most obvious and tragic consequences of a natural disaster. Deaths occur not only due to the floods themselves, but also as a result of infrastructure facilities being destroyed at the same time, electric shock, poisoning with chemical compounds, etc.

• *Health losses*. These are injuries, diseases as a result of hypothermia, exacerbation of chronic diseases, malaria, intestinal infections, poisoning, etc. Often there are more victims from the consequences of a disaster than from itself.

• *Socio-psychological state*. Stress and panic may occur. The lack of reliable information generates rumors that have the effect of «infection» and can aggravate the situation.

• *Deviant behaviour,* i.e. the behaviour that violates social norms and informal violations of social norms. Crimes committed during the crisis period are associated with the community's unpreparedness for catastrophic events, confusion and weakening of will and external control, disorganization of public and government authorities, etc.

• *Vertical mobility*. Having lost their housing, job or breadwinner, people often lose their economic and professional status, which can be accompanied by marginalization, to overcome which it is necessary to adapt to new conditions, change the behaviour model and develop a strategy for social adaptation.

• *Horizontal mobility*. Emergency flood events cause an increase in the migration flow. At the same time, it is generally believed that natural disasters usually form short-term internal migration flows, since victims do not have financial opportunities, do not want to change their usual place of residence, etc. Normally, that mass movement of victims occurs if a disaster causes hunger or social tension.

• *Social conflicts*. It usually escalates due to the unfair distribution of social benefits and social, ethnic and other contradictions already existing before the disaster. It could be based on a) the allocation of blame; b) the allocation of resources for rehabilitation and recovery.

• *Social solidarity*. Natural disasters bring not only destructive, but also consensual potential, because they represent an external threat to the affected communities and seek to coordinate actions to solve this problem. Social communication during the tragedy and immediately after it helps to restore mental and emotional balance, as well as to contribute to obtaining the necessary resources.

• *Problems of managerial decision-making* that arise due to the need to make decisions in extreme conditions that are not typical of the ordinary life of the community. Difficulties may arise due to two circumstances: a) strengthening of destructive collective behavior; b) the interests of individual actors who use the current circumstances in their own interests (Gryzunova 2012).

The proposed article develops the approaches and ideas that were formulated in the previous work (Bondarev and Bolkhovitinova 2019), where, using the example of the five largest floods, the main social consequences that can lead to social transformations were considered in general terms. The aim of the work is to identify the structure of interest in the scientific community to various social consequences of emergency flood events.

MATERIALS AND METHODS

The research paper presents the review on social consequences of five large emergency flood events that took place in various global basins (Fig. 1). The large emergency flood events were selected based on several criteria: 1) occurred about the same time (2-3 years); 2) had significant human and economic losses; 3) happened in different global basins; 4) get significant response in the scientific literature; 5) different Human Development Index (HDI) of countries, where the events were take place. All floods were chosen so that they occurred in the early 2010s. Thus, it allows analyzing contemporary events close to us. At the same time, this interval makes it possible to estimate the time of occurrence, growth and decay of interest in the described the emergency flood events.

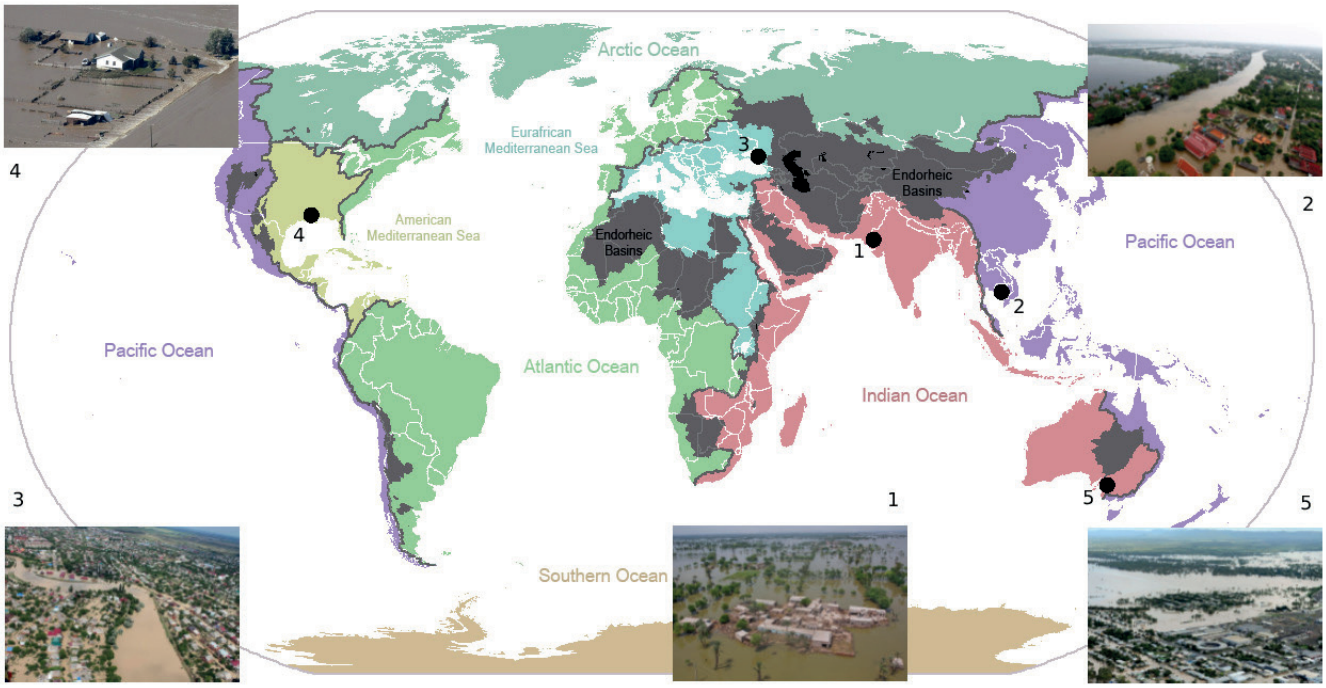

Fig. 1. Location of the large emergency food events within global basins: 1) Pakistan (28.07.2010 – 07.08.2010); 2) Thailand (05.08.2011 – 04.01.2012); 3) Russia (11.07.2012 – 11.07.2012); 4) The USA (12.09.2013 – 19.09.2013); 5) Australia (25.12.2010 – 04.02.2011)

Table 1 presents the main parameters of emergency flood events, which were analyzed in terms of social consequences (The Global Flood Database…; Kronstadt et al. 2010; Kirsch et al. 2012; Natural Disasters 2011...; About catastrophic rain ...; Nearly 35 thousand people…; Volosuhin, Shchurski 2012; Colorado flooding ...; Australian Storms ...; et al.). The Human Development Index was taken from the official UN website (Human Development Reports…), which shows an average achievement in key dimensions of human development: a long and healthy life, being knowledgeable and have a decent standard of living. It allowed us to assess the difference in interest in social consequences due to the level of development of the countries in which the flood occurred.

The cases of flooding from various global basins that occurred in the early 2010s are considered. Floods occurred in various regions of the world on the territory of countries with different Human Development Index (from 0.557 to 0.944). Floods were characterized by significant death losses (from 9 to 1985), affected (from 31 410 to 20 359 496) and economic damages (from $ 600 000 000 to $ 9 500 000 000).

The review is based on content analysis of scientific publications, which were chosen for that purposes, since, unlike media reports that emotionally and subjectively describe natural disasters, scientific publications are processed material obtained during an objective data analysis. The sample set totals 105 articles (21 articles for each emergency flood event). The database was compiled using the Google Scholar system. This search engine is widely known and well-established in the search for scientific publications. The sample set included practically all the articles found that mentioned discussed emergency flood events. Google Scholar made it possible to find

Table 1. Main parameters of the analyzed emergency flood events

Country	River Basin	Global Basin	Dates	Total Deaths	Total Affected	Total Damages ('000 US$)	HDI
Pakistan	The Indus River basin and its surrounding areas	The Indian Ocean	28.07.2010 - 07.08.2010	1 985	20 359 496	9 500 000	0,557
Thailand	The Chao Phraya basin and the Mekong River basin	The Pacific Ocean	05.08.2011 - 04.01.2012	813	9 500 000	40 000 000	0,777
Russia	The Kuban River basin and its surrounding areas	The Eurafrican Mediterranean See	11.07.2012 - 11.07.2012	172	31 410	600 000	0,824
The USA	The Mississippi River basin its surrounding areas	The American Mediterranean Sea	12.09.2013 - 19.09.2013	9 (500 are Missing)	21 900	1 900 000	0,926
Australia	The Murray River basin and its surrounding areas	The Indian Ocean	25.12.2010 - 04.02.2011	35	175 000	7 300 000	0,944

articles from the journals of the largest scientific publishers in the world. Therefore, we can assume that the sample is representative.

The media reflected the main social consequences of the floods under consideration. Most often they indicated death losses. In each case, their specific social consequences were under consideration, which were especially noticeable due to the different flood conditions. Thus, during the flood in Pakistan (July 2010), a huge number of victims was associated with the deterioration of the sanitary and epidemiological situation (Kronstadt et al. 2010). The residents of rural areas were particularly badly affected. Having lost their property and almost all means of livelihood, they lost the chance to restore normal life (Kirsch et al., 2012). The flood in Thailand (July-September 2011) forced a huge number of people to leave their homes, many of them decided to leave their cities forever. This event had a detrimental effect on the economic situation in the country, on migrants, as it weakened their already vulnerable position (Disasters 2011...). Flood in Krymsk (July 2012) (About catastrophic...) it came as an uninspected to the ordinary population and the authorities (Nearly 35 thousand…). The consequences of the flood were aggravated by other unfavourable circumstances (Volosukhin, Shchursky 2012). Flooding in the USA (September 2013) had a strong impact on the transport infrastructure (about 30 bridges and several hundred kilometres of roads were destroyed). At the same time, the least amount of human losses was observed here, as the alert system contributed, as well as the work of more than 50 state and local religious organizations, etc. (Colorado flooding...). Flooding in Australia (January 2011) is also characterized by coordinated actions of the authorities. Due to the high degree of urbanization, about 90 cities were affected (Australian Storms...).

To identify scientific interest in social consequences of emergency flood events, content analysis was used – a method that is used in the processing of voluminous and unsystematic text data to measure and further obtain accurate and objective information (Drisko, Maschi 2016; Bell et al. 2022). The initial category of the study was the social consequence of the flood. The variables of the social consequences caused by the natural (the main topics) disasters under consideration were: death and health losses; social adaptation; horizontal and vertical mobility; psychological state of the population; social solidarity and conflict; management problems.

The mention one of the main topics in the article is taken as a unit of account. The measurement units were the ratio of the total number of mentions of a certain feature to the number of articles describing the emergency flood event, and the average volume of the text of a scientific paper devoted to the consideration of certain social consequences. At the same time, an encoding was developed, as well as a system of indicators. For example, indicators such as «in total died», «drowned in a car», «death occurred as a result of exacerbation of chronic diseases, malaria», etc. were used for the sign of «death of a person».

Correlation analysis was used to further analyze the relationship of scientific interest to the social consequences of the emergency flood events. The ratio of the studied social consequences depending on the human development index (HDI) helped to outline the main trends of scientific interest in the social consequences of the events in the countries with different levels of human development.

THE RESULTS OF THE ANALYSIS TO THE SOCIAL CONSEQUENCES OF THE EVENTS AND DISCUSSION

Any natural disaster, including emergency flood events, has a response in scientific publications, where it is analyzed, the causes of its occurrence are identified, and a forecast of the recurrence of such an event in the future is given. This leads to the improvement of management decisions and the creation of conditions for further reduction of death and material losses, as well as undesirable social transformations. It can be assumed that after a surge of interest in a particular event, the number of mentions of it will decrease over time, and the acquired knowledge will be attached to a body of knowledge about this type of event. To identify the duration of interest in a particular extreme flood event, a graph is constructed (Fig. 2).

According to Fig. 2, the following trend is visible. Immediately after the event, few articles are published, and then their number increases and remains high for several years. Then there is a decline in interest in this event. There are exceptions to the general rule. The first of them is the flood in Krymsk, which caused a wide resonance in Russia. This is confirmed by the increased number of scientific articles in the first year after the flood, as well as the presence of another peak of publications in the third year (the strongest of the five

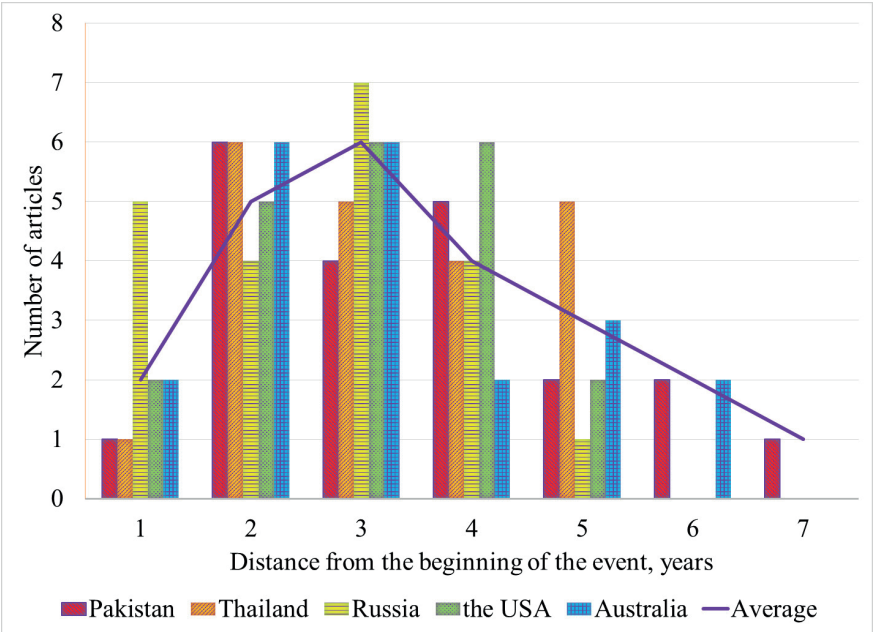

Fig. 2. Dynamics of the number of publications about the emergency flood events depending on the time distance

cases under consideration). Perhaps the first peak is because a catastrophic flood in this region turned out to be a suddenness, which caused the publication of operational data, and a deeper analysis of the situation corresponds to typical peaks of publicability. The second exception is the tragedy in Thailand. In the number of publications, describing this event, cyclicity and a peak are noted in the fifth year. Most likely, this is due to the regularity of catastrophic floods in the region, imposed on the large scale of the event.

Next, the frequency of mentioning in scientific publications of the main social consequences that were caused by the emergency flood events was considered (Fig. 3).

The greatest number of mentions of the social consequences, by which one can assess the general interest in the problem, was revealed in articles about flooding in Pakistan (71). Then there are the considered events that occurred in Thailand (66), Australia (65), the USA (57), and Russia (42). The most considered problems were the death losses, social solidarity and management problems. The problems of the psychological state, as well as horizontal and vertical mobility caused an intermediate interest. The least covered issues were health losses, social conflicts and adaptation.

Death losses are mentioned in almost 65% of articles as the most tragic and obvious consequence of the emergency flood events. However, publications rarely indicate the cause of death. At the same time, it is important to understand that with the development of infrastructure, these losses often occur not from direct impact, but from secondary factors (electric shocks, building collapses, etc.)

The analysis of social solidarity takes the second place in the frequency of mentions. This topic was especially discussed in the cases of the emergency flood events in Russia and Australia. In general, altruistic actions are usually described (monetary donations, gratuitous supply of clothing and medicines, work of volunteers, public organizations, states). In some articles there is information about the opposite trend, namely, the disunity of citizens and an increase in the level of discrimination based on gender, nationality and orientation.

The next frequently discussed social consequence is the reaction of the population to the actions of the authorities during the natural disasters. So, in the USA, management decisions were perceived positively in most cases. Exclusively negative aspects were indicated when describing the floods in Russia and Pakistan. In Thailand, against the background of negative assessments, such a positive factor as the interaction of the authorities with the media was noted twice, in the Australian case there are both positive and negative assessments.

During the emergency flood event, the cases of deviant behaviour are becoming more frequent. House robberies, thefts of essential items collected for victims and fraud on the part of financial criminals are recorded. At the same time, the cases of heroism are also mentioned.

The fifth level of discussion is horizontal mobility (migration). It turned out that there is no direct connection between the intensity of the emergency flood event and horizontal mobility. The decision to move depends not on the level of risk to which the local community is exposed, but on its financial capabilities of individuals living in the region. Unfortunately, the problems of horizontal mobility are not discussed in the Russian case.

The problem of vertical mobility (a movement through a system of social hierarchy or stratification) is also reflected in scientific publications. At the same time, in those countries where local communities do not have flood resistance, the loss of a house, a job or a family breadwinner more often leads to a decrease in social status. Thus, when analyzing the Pakistan case, phrases like «the poor have become even poorer» were often encountered.

The unequal distribution of resources for reconstruction causes an increase in social tension between different groups. The analyzed publications contain information about the formation of a conflict on this issue between individual groups of victims, as well as between the affected people and the authorities. Along with this factor, the following can be distinguished: the existence of personal interests among those making managerial decisions, assigning responsibility to someone for the consequences of flooding, as well as the dissatisfaction of victims with the actions of the authorities during an emergency flood event.

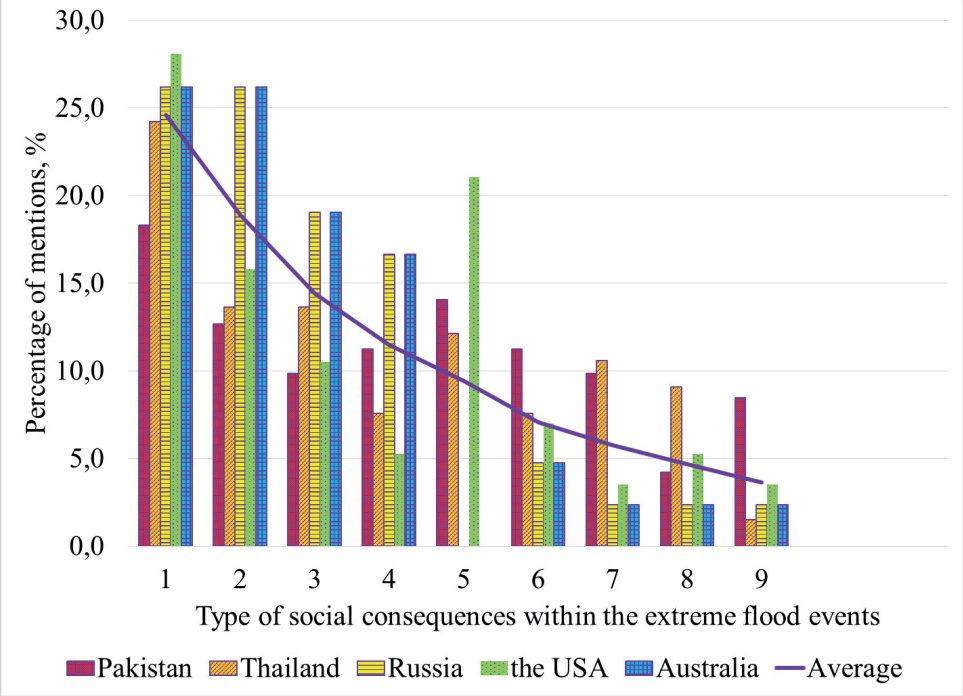

Fig. 3. Percentage of references to the social consequences in the total number of references. 1 – death losses; 2 – social solidarity; 3 – management problems; 4 – psychological state of the population; 5 – horizontal mobility; 6 – vertical mobility; 7 – social conflicts; 8 – social adaptation; 9 – health losses

The publication addresses general issues of community adaptation to the new conditions that developed after the flood. However, depending on geographical and social conditions, the affected population chooses different adaptation strategies. This may also be due to the duration, frequency and intensity of floods, the development of the economy, as well as the general socio-political situation in the country. Thus, when describing the Australian and American floods, the emphasis is more often on active adaptation, while when considering the Pakistan and Thailand cases, passive adaptation, as well as adaptation-avoidance (migration) are more common. It should be noted that in the last two cases, it was extremely difficult for the population to adapt to the prevailing conditions.

The interest in the problem of health losses turned out to be unexpectedly small. The increase in poisoning and the increase in the number of people infected with intestinal infections are discussed. It should be noted that most often scientific publications describing the Pakistan case contain this information, which is directly related to the unsanitary conditions prevalent in this territory.

In general, attention should be paid to the presence of a rather large variability in the general orientation of the topics discussed for each case. So, to emergency flood events in the USA, publications are more focused on describing problems related to the community's resilience to a natural disaster, that is, discussing specific actions taken by the population and authorities to prevent negative consequences from the natural disasters in the future. In Pakistan, the frequency of mentioning of these problems is more acute, since this community is distinguished by a high level of poverty. This explains the increased interest in studying the impact of the emergency flood events on vulnerable segments of the population. In publications about the Russian case, more attention is paid to the civil-legal aspects of the event than to the social ones.

Another important issue is to clarify the dependence of interest in the various social consequences of the emergency flood events, depending on the development of the country. Based on the material under consideration, it is only possible to estimate the corresponding trends in advance. For this purpose, the human development index (HDI) was used as the integral and widespread way to assess the country's development. The results of calculating the linear correlation of this interest with the HDI are presented in Table 2.

As one can see from Table 2, there are three types of statistical association of the social consequences of the events with the level of development of the country. For example, social solidarity, death losses and management problems are discussed more often in countries with higher HDI. That is, we can expect that these problems become more relevant with the development of public relations. At that time, there is an inverse statistical relationship of vertical mobility, social conflicts and health losses with the HDI level. This may mean that the low level of social security, hygiene development, social structure and health care causes many problems with solving these issues. Finally, we can assume that there are issues (social adaptation, horizontal mobility, psychological state of the population) that are not so sensitive to the level of development of society and their discussion is influenced by other circumstances in which the emergency flood events occur. Of cause, these are the first attempts to the problem with used limited data. There is a necessity to improve the knowledge about these interrelations.

CONCLUSIONS

Nature disasters are an element of a risk society, because regardless of the social and spatial position, an individual is in the zone of a potential natural cataclysm. The increase in anthropogenic interference in natural processes, an increase in the number and density of the population, as well as the complexity and increase in the technological infrastructure leads to an increase in the probability of emergency flood events. That inevitably entails a whole range of social consequences, expressed in death and sanitary losses, the emergence of migration flows, changes in the structure and functioning of local communities, the need to improve the systems of social adaptation and local governance.

A detailed analysis of the array of scientific publications of the five largest emergency flood events of the first half of the 2010s allows us to highlight the main topics that are relevant to the social consequences of these disasters: death losses, social solidarity, management problems, psychological state of the population, horizontal mobility, vertical mobility, social conflicts, social adaptation, health losses. The most discussed problems are death losses, social solidarity and management problems. To a lesser extent, scientific articles mention issues of the psychological state of the population, horizontal and vertical mobility. The problems of social conflicts and adaptation in general, as well as sanitary losses as a result of the emergency flood events, do not often fall into the circle of researchers' interests.

Table 2. The average level of interest in different social consequences of the emergency flood events and their correlation with the Human Development Index (HDI)

Social consequences	The level of interest, %	The type of relationship	The coefficient of correlation with the HDI
Social solidarity	18,3	Direct correlation	0,54
Death losses	23,1		0,42
Management problems	13,4		0,31
Social adaptation	5,4	No correlation	0,14
Horizontal mobility	11,3		-0,01
Psychological state of the population	10,9		-0,06
Vertical mobility	7,0	Inverse correlation	-0,86
Social conflicts	6,2		-0,70
Health losses	4,4		-0,47

In scientific publications, it is traditionally accepted to consider negative consequences (individual deaths and sanitary losses, the determination of the socio-psychological state of local community, the formation of conflict situations, and the strengthening vertical and horizontal social mobility). Along with this, there is a tendency to consider positive consequences: the activation of social adaptation processes, changing the level of social solidarity, the necessity to improve the structure of society and the tools of crisis management.

The scientific interest in various social consequences in some cases is due to the human development index (HDI) in different countries. Social solidarity, human losses and management problems are discussed more often in countries with higher HDI. Negative statistic interrelations are observed between vertical mobility, social conflicts and health losses with the HDI level. Sometimes (social adaptation, horizontal mobility, psychological state of the population) individual characteristics of flooding make a greater contribution to the formation of this interest.

REFERENCES

2021 State of Climate Services Water. World Meteorological Organization (WMO). [online] Available at: https://library.wmo.int/doc_num.php?explnum_id=10826 [Accessed 01.08.2022]

About catastrophic rains on the Black Sea coast of the Krasnodar Krai – situation analysis [online] Available at: https://meteoinfo.ru/news/1-2009-10-01-09-03-06/5419-07072012 [Access date 01.08.2022]. (In Russian)

Alexeevsky N.I., Magritsky D.V., Koltermann K.P., Krylenko I.N., Toropov P. (2016). Causes and systematics of inundations of the Krasnodar territory on the Russian Black Sea coast. Natural Hazards and Earth System Science. 16. 1289-1308, DOI: 10.5194/nhess-16-1289-2016

AR6 Synthesis Report: Climate Change 2022. The Intergovernmental Panel on Climate Change (IPCC). [online] Available at: https://www.ipcc.ch [Accessed 01.08.2022]

Australian Storms and Floods: White Paper. «A land ... of droughts and flooding rains». A special report by Zurich risk engineering, Australia & New Zealand. [online] Available at: https://www.zurich.com.au/content/dam/australia/general_insurance/risk_engineering/australian-storms-and-floods- white%20paper.pdf [Accessed 01.08.2022].

Aznar-Crespo P., Aledo A., Melgarejo-Moreno J., &Vallejos-Romero A. (2021). Adapting social impact assessment to flood risk managemen t. Sustainability, 13(6), 3410.

Beck U. (1996). World risk society as cosmopolitan society? Ecological questions in a framework of manufactured uncertainties. Theory, culture & society, 13(4), 1-32.

Bell E., Harley B., & Bryman A. (2022). Business research methods. Oxford university press.

Bloschl G., Hall J., Parajka J. et al. (2017). Changing Climate Shifts Timing ofEuropean Floods // Science, 357(6351), 588-590.

Bondarev V.P., Bolkhovitinova Yu.A. (2019). Social consequences of catastrophic floods. Vestnik of the Moscow University. Series 5. Geography, 5, 21-29.

Brouwer R., & Van Ek R. (2004). Integrated ecological, economic and social impact assessment of alternative flood control policies in the Netherlands. Ecological economics, 50(1-2), 1-21.

Ciampa F., Seifollahi-Aghmiuni S., Kalantari Z., & Ferreira C.S.S. (2021). Flood mitigation in Mediterranean coastal regions: Problems, solutions, and stakeholder involvement. Sustainability, 13(18), 10474.

Colorado flooding one month later: positive signs of recovery. [online] Available at: https://www.fema.gov/news-release/ 201 3/10/1 1/colorado-flooding-one-month-later-positive-signs-recovery [Access date 01.08.2022].

Convery I., & Bailey C. (2008). After the flood: the health and social consequences of the 2005 Carlisle flood event. Journal of Flood Risk Management, 1(2), 100-109.

Dar K. A., Iqbal N., Prakash A., & Paul M.A. (2018). PTSD and depression in adult survivors of flood fury in Kashmir: The payoffs of social support. Psychiatry research, 261, 449-455.

deVoogt D.L., Bisschops S., &Munaretto S. (2019). Participatory social capacity building: Conceptualisation and experiences from pilots for flood risk mitigation in the Netherlands. Environmental Science & Policy, 99, 89-96.

Dobrovolsky S.G. Global Hydrology. Processes and forecasts. (2017). Geos., 526. (in Russian)

Drisko J.W., &Maschi T. (2016). Content analysis. Pocket Guide to Social Work Re.

Emrich C.T., Tate E., Larson S.E., & Zhou Y. (2020). Measuring social equity in flood recovery funding. Environmental Hazards, 19(3), 228-250.

Fernández J., Moshenska G., &Iriarte E. (2019). Archaeology and Climate Change: Evidence of a Flash-flood during the LIA in Asturias (NW Spain) and its Social Consequences. Environmental Archaeology, 24(1), 38-48.

Frolova N.L., Kireeva M.B., Magritday D.V et al. (2017). Hydrological Hazards in Russia: Origin, Classification, Changes and Risk Assessment. Natural Hazards. V. 88. № 1. 103-131.

Giddens, A. (1994) Living in a post-traditional society. Reflexive modernization: Politics, tradition and aesthetics in the modern social order, 56, p.100.

Gryzunova E.A. (2012). Comparative analysis of modern sociological approaches to environmental crises. Vestnik MGIMO-Universiteta. № 5. 195-203. (In Russian with English summary)

Hudson P., Hagedoorn L., &Bubeck P. (2020). Potential linkages between social capital, flood risk perceptions, and self-efficacy. International Journal of Disaster Risk Science, 11(3), 251-262.

Human Development Reports. United Nations Development Program.[online] Available at: https://hdr.undp.org [Accessed 01.08.2022]

Istomina M.N., Dobrovolski S.G. (2016). Floods of the world: quantitative analysis of nature characteristic and parameters of social-economic damages. Water Resourses., 43, 459-471.

Karunarathne A.Y., & Lee G. (2020). Developing a multi-facet social vulnerability measure for flood disasters at the micro-level assessment. International journal of disaster risk reduction, 49, 101679.

Kirby R.H., Reams M.A., Lam N.S., Zou L., Dekker G.G., &Fundter D.Q.P. (2019). Assessing social vulnerability to flood hazards in the Dutch Province of Zeeland. International Journal of Disaster Risk Science, 10(2), 233-243.

Kirsch T.D., Wadhwani C., Sauer L., Doocy S., Catlett C. (2012). Impact of the 2010 Pakistan Floods on Rural and Urban Populations at Six Months. PLOS Currents Disasters. Aug 22. Ed. 1., DOI: 10.1371/4fdfb212d2432.

Kopsidas O.N., & Giakoumatos S.D. (2021). Strategic Planning for Avoidance of Catastrophic Flood Consequences. Journal of Environmental Science and Engineering A 10 (2021), 227-238, DOI: 10.17265/2162-5298/2021.06.004.

Kronstadt K.A., Sheikh P.A., Vaughn B. (2010). Flooding in Pakistan: Overview and issues for congress. DIANE Publishing., 29.

Kroska E.B., O'Hara M.W., Elgbeili G., Hart K.J., Laplante D.P., Dancause K.N., & King S. (2018). The impact of maternal flood-related stress and social support on offspring weight in early childhood. Archives of women's mental health, 21(2), 225-233.

Mabuku M.P., Senzanje A., Mudhara M., Jewitt G., &Mulwafu W. (2018). Rural households' flood preparedness and social determinants in Mwandi district of Zambia and Eastern Zambezi Region of Namibia. International journal of disaster risk reduction, 28, 284-297.

Mol J.M., Botzen W.W., Blasch J.E., Kranzler E.C., &Kunreuther H.C. (2021). All by myself? Testing descriptive social norm-nudges to increase flood preparedness among homeowners. Behavioural Public Policy, 1-33.

Mullick P.D., Ghosh K., & Sen P. An Ethnographic Perception on the Consequences of Social Capital, Flood, Resilience and Disaster Issues in a Rural Setting of West Bengal, India. International Journal for Research in Applied Science & Engineering Technology (IJRASET). 367-374

Mythen, G. (2021). The critical theory of world risk society: a retrospective analysis. Risk Analysis, 41(3), 533-543.

Natural Disasters 2011. Bangkok: Thai Meteorological Department - https://www.tmd.go.th/en/ downloads.php [Access date 01.08.2022].

Nearly 35 thousand people affected by the flood in the Kuban [online] Available at: https://ria.ru/incidents/20120709/695261699.html [Access date 01.08.2022]. (In Russian)

Norris F.H., Baker C.K., Murphy A.D., &Kaniasty, K. (2005). Social support mobilization and deterioration after Mexico's 1999 flood: Effects of context, gender, and time. American Journal of Community Psychology, 36(1), 15-28.

O'Hare, P., & White, I. (2018). Beyond 'just'flood risk management: the potential for—and limits to—alleviating flood disadvantage. Regional Environmental Change, 18(2), 385-396.

Sustainable Development Goals. United Nations. Academic Impact [online] Available at: https://www.un.org/en/academic-impact/page/sustainable-development-goals [Accessed 01.08.2022]

Tanır T., Fındık S.B., Girayhan T.F. &Yorulmaz Ö. (2022). Flood Social Vulnerability Assessment: A case study of Türkiye . Turkish Journal of Water Science and Management, 6 (2) , 237-259, DOI: 10.31807/tjwsm.1089403

Tate E., Rahman M.A., Emrich C.T., & Sampson C.C. (2021). Flood exposure and social vulnerability in the United States. Natural Hazards, 106(1), 435-457.

Thaler T., Fuchs S., Priest, S., &Doorn, N. (2018). Social justice in the context of adaptation to climate change—reflecting on different policy approaches to distribute and allocate flood risk management. Regional Environmenta l Change, 18(2), 305-309.

The Global Flood Database [online] Available at: https://global-flood-database.cloudtostreet.ai/#interactive-map [Accessed 01.08.2022]

Török I. (2018). Qualitative assessment of social vulnerability to flood hazards in Romania. Sustainability, 10(10), 3780.

Volosuhin V.A., Shchurski O.M. (2012). Floods in Kuban. Problems and challenges. Gidrotekhnika., 4, 6-9. (In Russian with English summary).

Xiao L., Fang X., Zhang Y., Ye Y., & Huang H. (2014). Multi-stage evolution of social response to flood/drought in the North China Plain during 1644–1911. Regional Environmental Change, 14(2), 583-595.

Yu Q., Wang, Y., & Li N. (2022). Extreme Flood Disasters: Comprehensive Impact and Assessment. Water, 14(8), 1211.

Zemtsov S.P., Goryachko M.D., Baburin V.L., Krylenko I.N., Yumina N.M. (2016). Integrated assessment of socio-economic risks of hazardous hydrological phenomena in Slavyansk municipal district. Natural Hazards 82(1), 43-61, DOI:10.1007/s11069-016-2290-4.

CASE STUDY

LANDSCAPE READING FOR ALPINE RIVERS: A CASE STUDY FROM THE RIVER BIYA

Lisa Schmalfuß[1*], Christoph Hauer[1], Liubov V. Yanygina[2], Martin Schletterer[3]

[1]Institute of Hydraulic Engineering and River Research, University of Natural Resources and Applied Life Sciences, 1180, Vienna, Austria

[2]Institute for Water and Environmental Problems SB RAS, Ulitsa Molodezhnaya 1, 656038, Barnaul, Russia

[3]Institute of Hydrobiology and Aquatic Ecosystem Management, University of Natural Resources and Applied Life Sciences, 1180, Vienna, Austria

***Corresponding author:** lisa.schmalfuss@boku.ac.at

Received: April 11th, 2021 / Accepted: November 11th, 2022 / Published: December 31st, 2022

https://DOI-10.24057/2071-9388-2022-046

ABSTRACT. Anthropogenic stressors have altered the hydromorphological characteristics of rivers worldwide. Environmental guiding principles are essential for planning sustainable river restoration measures. The alpine river Biya, located in the Russian Altai mountains, originates from Lake Teletskoye and joins the Katun near Biysk, forming the Ob. The Biya represents a hydromorphological reference system in anthropogenically 'least-disturbed' condition. The presented study aimed to assess the river's undisturbed morphology in relationship with the geological history of three different river stretches based on an adapted landscape reading approach using remote sensing information (ASTER GDEM v3). The established widths of the active channel, active floodplain and morphological floodplain as well as the longitudinal section were used to explain the differences between upper, middle, and lower Biya. The results confirm differences in the geological origins between the upper Biya, which has previously been described as the least developed and narrowest, and the other two stretches based on the analyses of morphological parameters. Morphological floodplain width could best explain the differences between upper (0-86 km), middle (86-196 km), and lower Biya (196-301 km). The study further showed a clear relationship between the variations in river patterns and adjacent topographic structures (valley confinements, tributary interactions), highlighting that any assessment of river morphology must consider the wider surroundings of a river stretch. The presented morphological observations and analyses of the Biya show that easily obtainable parameters can detect differences in the morphological history of river stretches within the same catchment, supporting process understanding.

KEYWORDS: hydromorphology, glacial history, sinuosity, channel evolution, remote sensing

CITATION: Schmalfuß L., Hauer C., Yanygina L. V., Schletterer M. (2022). Landscape Reading for Alpine Rivers: A Case Study from the river Biya. Geography, Environment, Sustainability, 4(15), 196-213
https://DOI-10.24057/2071-9388-2022-046

ACKNOWLEDGEMENTS: The authors thank Friedrich Seidl for providing the grain size distribution data that was included in the description of the Biya.

Conflict of interests: The authors reported no potential conflict of interest.

INTRODUCTION

Water covers 71% of our planet (USGS 2019) and contributes majorly to the shape and character of the Earth's surface as it travels from source to sea. River (eco-) systems are the setting of critical environmental processes, like sediment or nutrient transport (Newbold et al. 1982) and connect a wide range of different ecosystems and biotic communities (Vannote et al. 1980), acting on a four-dimensional level (Ward 1989). Connectivity throughout whole river systems is necessary for the functioning of all associated processes (Grill et al. 2015). Changing single parameters within a river's catchment can lead to drastic changes in the dynamic equilibrium (Nanson and Huang 2018). Following centuries of anthropogenic interferences, rivers are affected by a multitude of stressors (Lemm et al. 2020). Rivers are among the most heavily degraded ecosystems in the world (Tickner et al. 2020, Malmqvist and Rundle 2002, Sala et al. 2000), putting freshwater megafauna at severe threat (He et al. 2019, Zarfl et al. 2019, He et al. 2018) and reducing the capacity to further fulfil ecosystem services that human societies rely on (Feio et al. 2022, Abily et al. 2021). The natural regimes of most of the world's larger river systems were altered, and it is assumed that 48% of rivers worldwide are moderately to severely impacted by flow regulation, fragmentation, or both (Grill et al. 2015). Next to these direct anthropogenic impacts, less obvious, indirect changes, like climate or land use change, are continuously transforming hydrological boundary conditions, as well as the sediment cycle, leading to significant alterations in water temperatures and other abiotic habitat factors and consequently destabilising

many riverine ecosystems (Liu et al. 2020, Sala et al. 2000). Ecologically intact, or free flowing rivers have become increasingly rare and are largely restricted to remote areas with lower degrees of human development, usually found in snow climates (Feio et al. 2022, Grill et al. 2019).

There is an urgent need for action and growing demand to reorganise river management based on an international and interdisciplinary approach so that the functionality of the exposed ecosystems is improved and not compromised any further (Feio et al. 2021, Muhar 1996). It is essential that river restoration approaches build on a sound understanding of the complex ecosystem processes (Tickner et al. 2020), also taking into account channel evolution (Scorpio et al. 2020). Our understanding of river morphological processes and interactions must be continuously advanced since it provides the foundation to combat current shortcomings in river health.

When trying to understand why a river looks the way it does, the focus must be put on the temporal context and the geological history of the river's catchment area: Fluvial development is subject to changes in climate as well as tectonic processes (Vandenberghe et al. 2018) that also interact with sediment dynamics and resulting changes in channel bed elevation (Anderson and Konrad 2019). Processes associated with (past) glaciation, for example, exert influence on many rivers in the temperate climate zone. These processes are majorly responsible for reshaping the landscape by eroding older sediments and reorganising river pathways and the sedimentary system through the stages of glaciation (Sokołowski et al. 2021, Comiti et al. 2019, Fildani et al. 2018). Glacial-interglacial cycles are major drivers of river incision and aggradation (Huang et al. 2019 Malatesta and Avouac 2018). Glacial and periglacial erosion provide vast amounts of sediment (Huang et al. 2019). During the glacial retreat, sediment yields increase dramatically, often causing stark and abrupt changes in the landscape, i.e., paraglacial adjustment (Hedding et al. 2020, Williams and Koppes 2019). Non-fluvial deposits associated with previous glaciation may also play a role in the development of channel patterns in fluvially dominated stretches (Hauer and Pulg 2018). In order to account for the decisive effects of (past) glaciation on river and valley formation, the associated semi- and non-fluvial processes acting in postglacial areas must be better included in the analyses of channel evolution (Hauer and Pulg 2021).

This calls for an integrative analysis of river morphology, including a river's geological history and wider morphological context. This need is met with the development of holistic frameworks for the morphological assessment and classification of river systems that try to take into account all associated processes on a catchment scale (e.g., Rinaldi et al. 2016, 2015). Methods like the landscape reading approach (Fryirs and Brierley 2012) aim to relate large-scale landscape features with the region's geological history. It has been adapted and applied by Hauer et al. (2021) to assess paraglacial adjustments and the quaternary development of the river Vjosa highlighting how combined morphological understanding of channel patterns can be used to explain glacially influenced river morphology. These approaches are usually based on large-scale parameters like channel width, or valley width, which are most efficiently assessed using remote sensing techniques.

Remote sensing methods are applied to assess river morphological characteristics across various spatial and temporal scales (Boothroyd et al. 2021, Piégay et al. 2020, Tomsett and Leyland 2019, Hemmelder et al. 2018) as a cost-effective monitoring tool (Bechter et al. 2018) that can help to increase objectivity and comparability (Zhao et al. 2019). They are particularly useful for assessing recent river morphological changes (Langat et al. 2019). Different methodologies have been developed that allow analysing, inter alia, changes in river morphology (Shahrood et al. 2020), river morphological status (Bechter et al. 2018), physical habitat and river health (Zhao et al. 2019), and even river gauging (Hou et al. 2020) based on remote sensing data.

Having established that morphological reference data (e.g., from 'least-disturbed' sites) can serve as valuable environmental guiding principles and support efficient, effective, and sustainable restoration measures (Kujanová and Matouškova 2017, Hey 2006, Newson and Large 2006) while acknowledging that it is next to impossible to find such sites in many regions of the world, like the European Alps (Comiti 2012), we can agree that reference sites must be found elsewhere. 'Least-disturbed' reference sites are not necessarily devoid of any signs of human activity but have suffered the least anthropogenic disturbance within a group of comparable sites (Stoddard et al. 2006). Such regions still exist in less densely populated parts of the world: Anthropogenic impacts in the Altai Mountains, for example, are minimal compared to mountain regions like the European Alps (Volkov et al. 2021). Analyses of such remote areas, especially, rely largely on remotely sensed data.

This study focuses on the morphology of the mountain river Biya in the Russian Altai region (Siberia), which can be regarded as an example of a morphologically least-disturbed river. This river has been studied regarding hydrological properties (Chalov and Ermakova 2011) as well as its geological origins (Baryshnikov et al. 2016). Our study aims to analyse the relationship between the Biya catchment's geological history and its morphological characteristics, described using remotely sensed data based on clearly defined morphological parameters. Following the approach described by Hauer et al. (2021), it shall be illustrated how the evolutionary history of the Biya's different river stretches is reflected by their morphology.

MATERIALS AND METHODS

The study area

The study at hand focuses on the river Biya, one of the two headstreams of the river Ob. The Biya's catchment lies in the Russian part of the Altai Mountains in Siberia (Schletterer et al. 2021). Siberia accounts for 80% of all global freshwater resources, as three of the world's largest and longest rivers (Lena, Yenisei, and Ob) originate there (Klubnikin et al. 2000). The Altai Mountains are among the least disturbed natural areas worldwide and can be considered a center of biological diversity (Dirin and Madry 2017). The area is particularly important for conserving unique habitats characteristic of the Central Asian Mountain System (Chlachula and Sukhova 2011). The area north of Lake Teletskoye, in particular, is reported to have served as a refuge for deciduous plant species during the last glacial maximum (LGM, Hais et al. 2015).

The Biya's origin (Fig. 1A) lies at the outflow of Lake Teletskoye (51°47'13"N, 87°14'49"E, 430 m a.s.l., near the city of Artybash), which is Russia's second deepest natural lake (Dehandschutter et al. 2002). The Biya covers a distance of 301 km until its confluence with the Katun (52°26'12"N, 85°0'47"E, 160 m a.s.l., near the city of Biysk). It has a catchment of about 36,900 km^2. Close to the city Biysk, about 21 km upstream of its confluence with the Katun,

the Biya has an average annual discharge[1] of 476 m^3/s. The chainage information in the following is presented as river kilometres (rkm) starting with 0 at the outflow of Lake Teletskoye. The Biya can be divided into the following three parts: upper Biya (Lake Teletskoye to the mouth of the river Lebed', rkm 0-86) – middle Biya (river Lebed' to Lebyaj'e, rkm 86-196) – lower Biya (Lebyaj'e to the confluence with the Katun, rkm 196-301; sub-stretch division based on *Surface water resources of the USSR 1962*). The most important headstream of the Biya is the Chulyshman (Fig. 1A). Fig. 1C includes additional information on grain size distribution from a Wolman pebble count (Wolman 1954) at three sites along the Biya (Artybash, Kebezen, and Biysk; data kindly provided by Friedrich Seidl). The photographs in Fig. 1B give an impression of the conditions on-site.

In order to discuss hydromorphological processes along a river, it is important to know the river's geomorphological history, which is dependent on its geological setting. The geomorphological development of the Biya valley has, however, not been studied as thoroughly as that of other rivers in the Altai mountains, such as the Katun and the Chuya (e.g., Baryshnikov 2016, Zolnikov et al. 2016, Zolnikov et al. 2015, Baker et al. 1993, Rudoy and Baker 1993). While the Katun still follows its ancient initial course, the Biya, which used to be a small river in the early middle Pleistocene, has grown in length since then: The Biya valley between Lake Teletskoye and the village Turochak (around rkm 75) was formed only in late middle Pleistocene following the beginning of the outflow from the lake. This uppermost part can be described as a mountain river. The lower stretch downstream of Turochak is a well-developed alluvial valley, probably dating back to pre-Quaternary times (Baryshnikov et al. 2016).

In the Biya valley, distinct traces of large-scale flood events can be found: Giant current ripples bear witness to past megafloods caused by glacial lake outburst (Baryshnikov 2016, referring to Baryshnikov 1979). Moraine dam failure caused the catastrophic Biya debris flow (BDF) which initiated the valley incision processes that led to abrupt morphological changes and the development of the river Biya about 37.5 ka before present (Baryshnikov et al. 2016).

Morphological Characterisation

The hydromorphological characterisation of the river Biya was based on the landscape reading approach described by Hauer et al. (2021). This approach aims

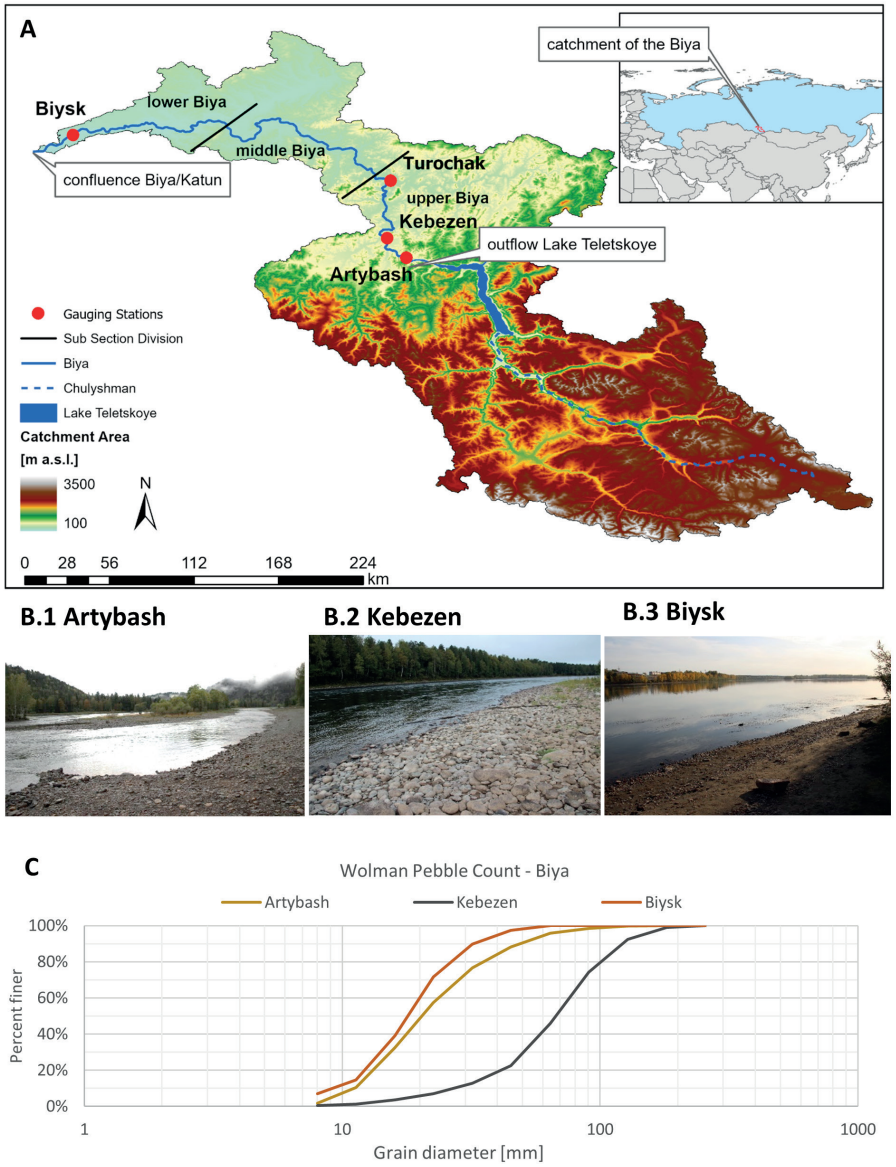

Fig. 1. A: Overview: Catchment of the river Biya. The locations of the four gauging stations are marked in red. Black lines indicate the starting/ending points of upper, middle and lower sections. B: Grain size sampling sites (Artybash, Kebezen, Biysk). Photographs by Martin Schletterer. C: Grain size distribution curves

[1]Russia ArcticNET: https://www.r-arcticnet.sr.unh.edu/v4.0/ViewPoint.pl?Point=6670

to develop an understanding of the morphological background of the area of interest (Fryirs and Brierley 2012). It requires the following three parameters: Active Channel (AC), Active Floodplain (AF), and Morphological Floodplain (MF). While AC and MF were determined during the GIS survey, AF was established from a hydraulic 1D step-backwater model (HEC-RAS) of a flood scenario with a five-year-recurrence interval (HQ5) based on Hauer et al. (2021). In this approach, AF is defined as the wetted cross-section width in the HQ5 scenario. The HQ5 scenario was determined using the long-time data series (*Russia ArcticNET*[1]) for four gauging stations based on a Gumbel distribution (Yue et al. 1999). Channel sinuosity (see below) was added to this set of parameters to allow for a more comprehensive evaluation of the Biya's hydromorphological characteristics. Further differentiation between hydraulic and topographic sinuosity was undertaken to visualise the interactions between the planform river pattern and the surrounding terrain. Next to a geographic characterisation, hydrological and geological boundary conditions were established based on published literature and online data sources (see details below).

A supplementary catalogue of hydromorphological characteristics was established for thirty 10 km-stretches (300 km in total) along the Biya. It is presented as an overview table (Appendix: Tables A.1-3), documenting the morphological variability occurring in a least-disturbed river system. A verbal discussion of the changes in channel characteristics in relation to the surrounding topography emphasises the importance of a holistic approach in applying hydromorphological reference parameters. It is targeted that the results may be used as a basis for ecological guiding principles for river restoration planning in the European Alps.

Hydrological Information

Hydrological information for four gauging stations along the river Biya was taken from the platform *Russia ArcticNET*[2], where monthly discharge values are given for at least three decades. The gauging stations are located at Artybash (rkm 2), Kebezen (rkm 30), Turochak (rkm 81), and Biysk (rkm 280).

GIS Survey

As a first step, the required geometric information was generated and compiled: For this study, remote sensing data represented the most valuable input. Topographic information from ASTER GDEM v3 (Advanced Spaceborne Thermal Emission and Reflectance Radiometer Global Digital Elevation Model, Version 3[3]) was used. The geometric attributes needed for this study were established in ArcMap (ESRI: ArcGIS Desktop 10.8.1) based on ASTER GDEM. Inputs for the analysis of planform morphological parameters (i.e., river axis, active channel width, valley cross-sections and valley width) were largely delineated manually, combining topographic information with recent satellite images. A longitudinal section of the river axis was extracted. Special focus in this study was placed on channel sinuosity.

Sinuosity Calculations

Channel sinuosity is an indicator of the meandering intensity of a river, which is commonly evaluated by a sinuosity index (Mueller 1968). The standard sinuosity index (SSI) quantifies the ratio of the channel length to valley length:

$$SSI = \frac{CL}{VL} \tag{1}$$

where *CL* = channel length, and *VL* = valley length (here: the average between the length of the left and right valley flank).

The total sinuosity of a river is always a combination of hydraulic (i.e., controlled by the river's flow through its flood plain) and topographic (i.e., determined by the shape of the surrounding landscape) sinuosity (Mueller 1968). These two parameters are quantified by the hydraulic (Eq. 2: *HSI*) and topographic (Eq. 3: *TSI*) sinuosity index (calculated based on *CL, VL*, and linear distance, *LD*, between starting and end point of each subsection). Per definition, *HSI* and *TSI* can be added to a total of 1.

$$HSI = \frac{\frac{CL - VL}{LD}}{\frac{CL}{LD} - 1} \tag{2}$$

$$TSI = \frac{\frac{VL}{LD} - 1}{\frac{CL}{LD} - 1} \tag{3}$$

All three sinuosity indices were calculated based on the manually delineated river axis (*CL*) and visually obtained valley borders. The river axis was divided into subsections of 10 km length for which the calculations were performed.

Statistical Testing

All statistical tests were done in R-4.1.1 (R core team, 2021). Differences between the river stretches regarding the landscape reading elements (AC, AF, MF) were assessed with Wilcoxon rank sum tests. Comparisons between all observed parameters (incl. *SSI, HSI/TSI,* and slope) were based on regression analyses using average values for stretches of 10 km length.

RESULTS

For the morphological analyses, the established river stretches (upper Biya: rkm 0-86, n = 85 – middle Biya: rkm 86-196, n = 109 – lower Biya: rkm 196-301, n = 108) were kept. AC, AF, and MF were assessed based on a cross-sectional view at 1 km increments (n =302). Sinuosity values (*SSI, HSI*, and *TSI*) were calculated for stretches of 10 km length (n = 30). The division between upper and middle Biya (and middle and lower Biya) was, in this case, set at rkm 90 (and rkm 200, respectively; $n_{upper} = 9$; $n_{middle} = 11$; $n_{lower} = 10$). The performed analyses (landscape reading elements, hydraulic/topographic sinuosity, and longitudinal profile) show a clear distinction between the upper Biya and the other two sections (Fig. 5), reflecting the differences in the evolutionary history of the upper

[1]Russia ArcticNET: https://www.r-arcticnet.sr.unh.edu (see specifications above)
[2]Russia ArcticNET (Point IDs XXX : 6929 Artybash – 6668 Kebezen – 6669 Turochak – 6670 Biysk):
https://www.r-arcticnet.sr.unh.edu/v4.0/ViewPoint.pl?View=ALL&Unit=ms&Point=XXXX
[3]EarthData: earthdata.nasa.gov, provided by NASA (National Aeronautics and Space Administration) and freely available

river stretch. The statistical analyses showed a relationship between MF and sinuosity (both *SSI* and *HSI/TSI*). Tab. 2 gives an overview of all observed morphological parameters for the upper, middle, and lower Biya. The slope decreases in the downstream direction: While the upper Biya has an average slope of 1.56‰, the gradient of the middle Biya lies only at 0.88‰ and is as low as 0.36‰ in the lower stretch. *SSI* does not show any specific trend. It remains, on average, within the sinuous range (1.06 to 1.25, Brice 1982) for all three stretches. *HSI* and *TSI*, in contrast, show clear increasing (respectively decreasing) tendencies in the downstream direction.

Fig. 2A shows the longitudinal section of the Biya from its origin at Lake Teletskoye down to its confluence with the Katun, separated into upper, middle, and lower stretch. Over a length of about 301 km, the Biya travels roughly 270 m downstream at an average slope of 0.9‰ (compare to sectional slope in Table 2). The locations (river station and orographic side) of all 24 tributaries (*from Russian Water Register*[1]) are indicated in the graph. Additionally, the mean annual discharge at the four gauging stations (Artybash, Kebezen, Turochak, and Biysk, from *Russia ArcticNET*[2]) is included.

Fig. 2B illustrates the development of the three landscape reading elements plus SSI values along the river. SSI is highest where MF peaks. A direct comparison of AC and AF suggests lateral dynamics in the upper Biya are restricted compared to the middle and lower stretch. In the upper stretch, the mean differences between AC and AF amount to 157.45 m, on average, which is less than the mean AC width of 226.82 m. In comparison, differences between AC and AF in the middle and lower Biya come to 532.78 m and 677.95 m, respectively, in both cases exceeding the mean AC widths. This suggests a higher influence of the surrounding topography in the upper Biya.

Fig. 2C shows the ratio between *HSI* and *TSI*. Since HSI and TSI add up to a total of 1, those two values are presented as a stacked bar chart. Hydraulic sinuosity outweighs topographic sinuosity for most of the Biya's length, showing an increasing tendency in downstream direction.

In the upper section (rkm 0-86), the river's valley runs in a rather straight course from south to north (Fig. 3). Over the first 50 km, *HSI* and MF increase rather steadily. Along the upper Biya *SSI* and *HSI* exhibit analogue patterns that correlate visibly with MF values (Fig. 2B and C).

The middle Biya flows towards the northwest over a less mountainous terrain than the upper course. Overall, both valley and river axis show a more complex, winding pattern than in the upper stretch. Three tributary mouths are located within the first ten kilometres of the middle Biya (rkm 86-196). Interestingly, this correlates with an increase in *HSI*, but not in MF. Near rkm 110, the whole valley turns westward, coinciding with a visible drop in *HSI*, indicating topographic constraints. A local peak in *TSI* (rkm 100-110: 80.04%) precedes another peak in HSI (rkm 150-160: 97.91%) which is followed by a reduction in MF (between rkm 160 and rkm 180) and a decrease in HSI that continues until the start of the Biya's lower stretch.

The lower stretch of the Biya (rkm 196-301) starts out with a *TSI*-dominated section (rkm 200-210: 95.81%), after which *SSI*, alongside MF, reaches its peak between rkm 210-220 at the confluence between the Biya and its tributary Souskanikha. *HSI* increases after that local minimum and remains high for most of the remaining lower stretch.

One special focus of the study was the evaluation of channel sinuosity. The goal was to relate sinuosity parameters (*SSI, HSI/TSI*) to the other morphological key parameters. Fig. 3 shows the SSI values for each 10 km-section along the Biya in plan view. Only four stretches (rkm 60-70: 1.55 – rkm 150-160: 1.55 – rkm 160-170: 1.53 – rkm 210-220: 1.74) lie above 1.5. These stretches occur in all three sections of the Biya, one each in the upper and lower stretch, and two adjoining 10 km sections in the middle Biya. None of the three stretches differ significantly from one another regarding sinuosity (SSI, Fig. 5D, mean values: upper: 1.21, middle: 1.18, lower:1.23). The number of observations (n between 9 and 11) is, however, quite low for making statistically meaningful statements. There is a wider range of *SSI*-values occurring in the lower Biya (1 to 1.74), than in the upper stretch (1 to 1.55) with *SSI* values in the middle stretch ranging from 1.02 to 1.55 (Fig. 2B and Fig. 5D).

Next to the planform channel pattern (i.e., considering the x and y dimension), the longitudinal elevation of the three stretches of the Biya was analysed. In contrast to the middle and lower stretch, the upper Biya's longitudinal elevation profile can best be approximated by a linear equation ($R^2 = 0.9827$), while for the other two, a quadratic polynomial equation provides a better fit (Fig. 4).

Fig. 2 shows that the upper, middle, and lower Biya exhibit different morphological characteristics. These are confirmed by the statistical differences between the observed parameters (Fig. 5). Pairwise comparisons between all three stretches were performed using the Wilcoxon rank sum test to test for significant differences

MF (Fig. 5A) differs significantly between all three stretches of the Biya. The difference in MF between the upper Biya (mean: 1866.42 m) and both the middle (mean: 3521.16 m) and lower (mean: 4236.82 m) Biya can be described as highly significant ($p < 0.001$). MF in the middle and upper Biya still differs significantly ($p = 0.002$). AF (Fig. 5B) within the upper Biya (mean: 384.28 m) also shows highly significant differences ($p < 0.001$) from the other two stretches. There is, however, no significant difference between the middle (mean: 955.83 m) and the

Table 2. Elevation and (average) slope, widths of active channel (AC), active floodplain (AF), and morphological floodplain (MF), including standard (SSI), hydraulic (HSI), and topographic (TSI) sinuosity index for the upper, middle, and lower Biya

	River Kilometer		Slope	AC	AF	MF	SSI	HSI	TSI
	Start	End	Average	Average			Average		
	[km]	[km]	[‰]	[m]	[m]	[m]	[-]	[%]	[%]
Upper	0	86	1.56	227	384	1866	1.21	56	44
Middle	86	196	0.88	423	956	3521	1.18	64	36
Lower	196	301	0.36	373	1051	4237	1.23	69	31

[1]Russian Water Register: http://textual.ru/gvr/index.php?card=187196
[2]Russia ArcticNET: https://www.r-arcticnet.sr.unh.edu (see specifications above)

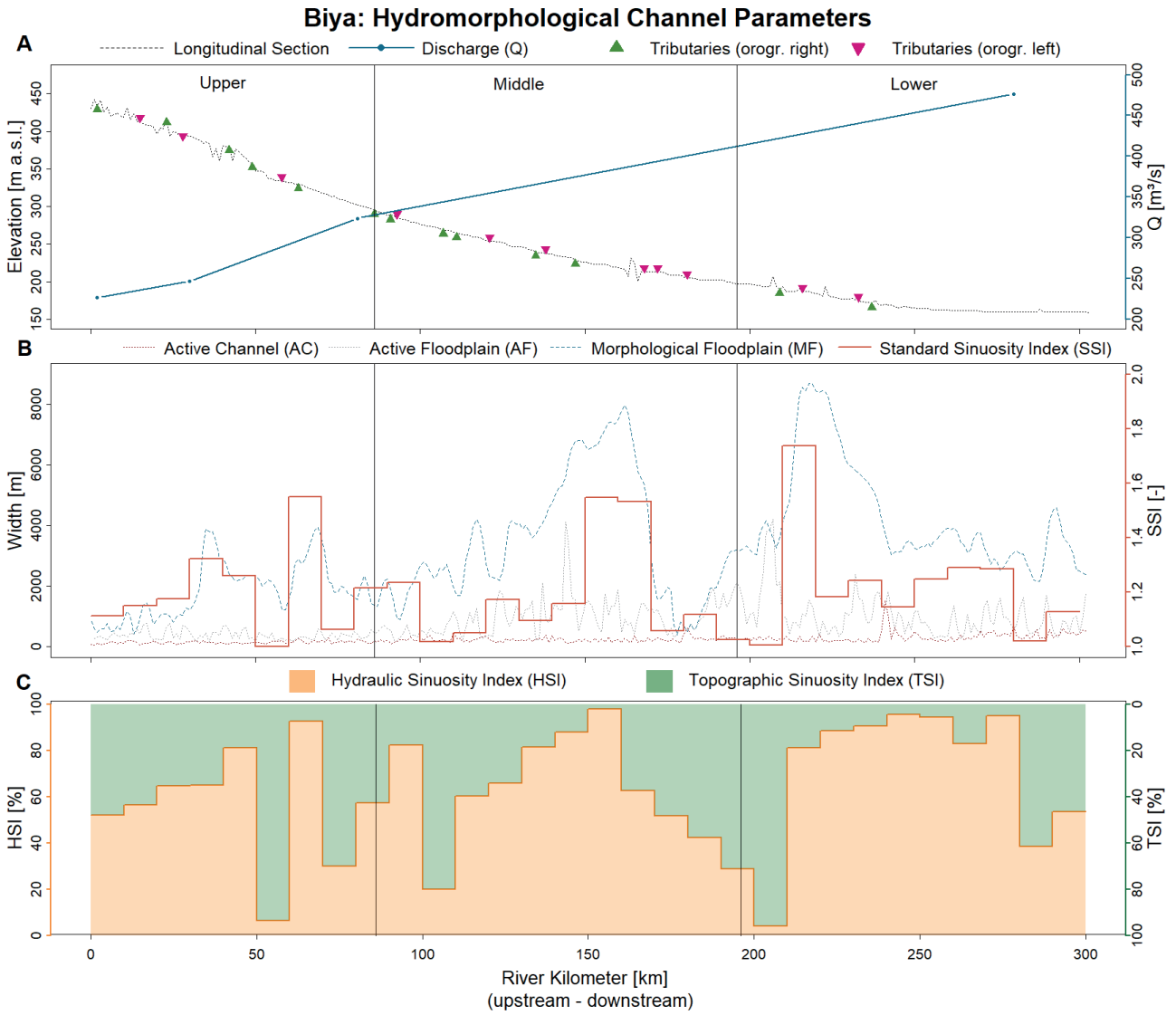

Fig. 2. Overview of the assessed morphological parameters along the Biya. A) Hydrological overview in longitudinal section: Discharge (Q) and tributaries. B) Landscape reading elements (widths of the active channel, AC, active floodplain, AF, and morphological floodplain, MF) incl. standard sinuosity index (*SSI*). C): Hydraulic (*HSI*) vs. topographic (*TSI*) sinuosity index. *HSI* values (orange) can be read on the left-hand y-axis, starting at the bottom with a value of zero. *TSI* values (green) are given on the right-hand y-axis, starting at the top with zero

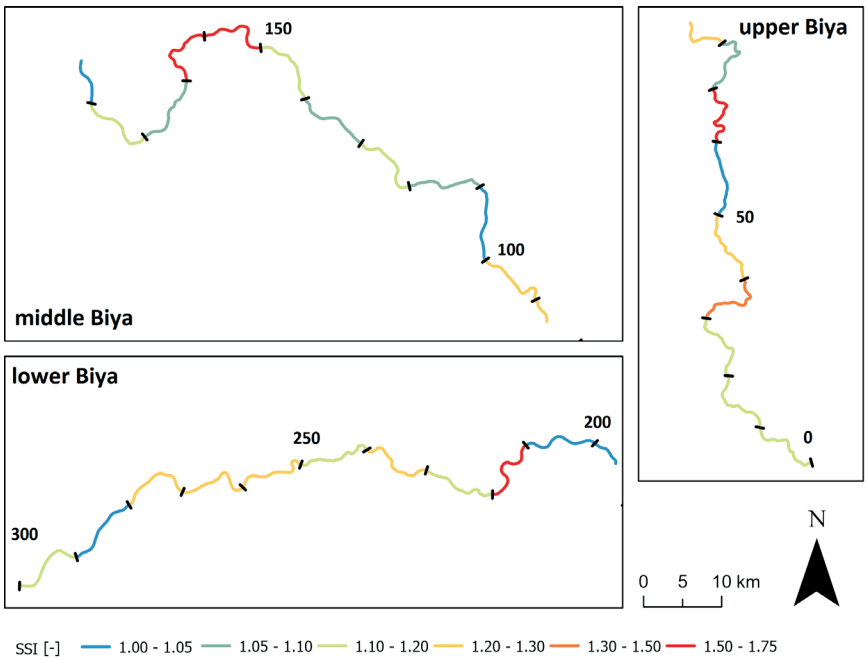

Fig. 3. Plan view of the river Biya including *SSI* values for 10 km sections

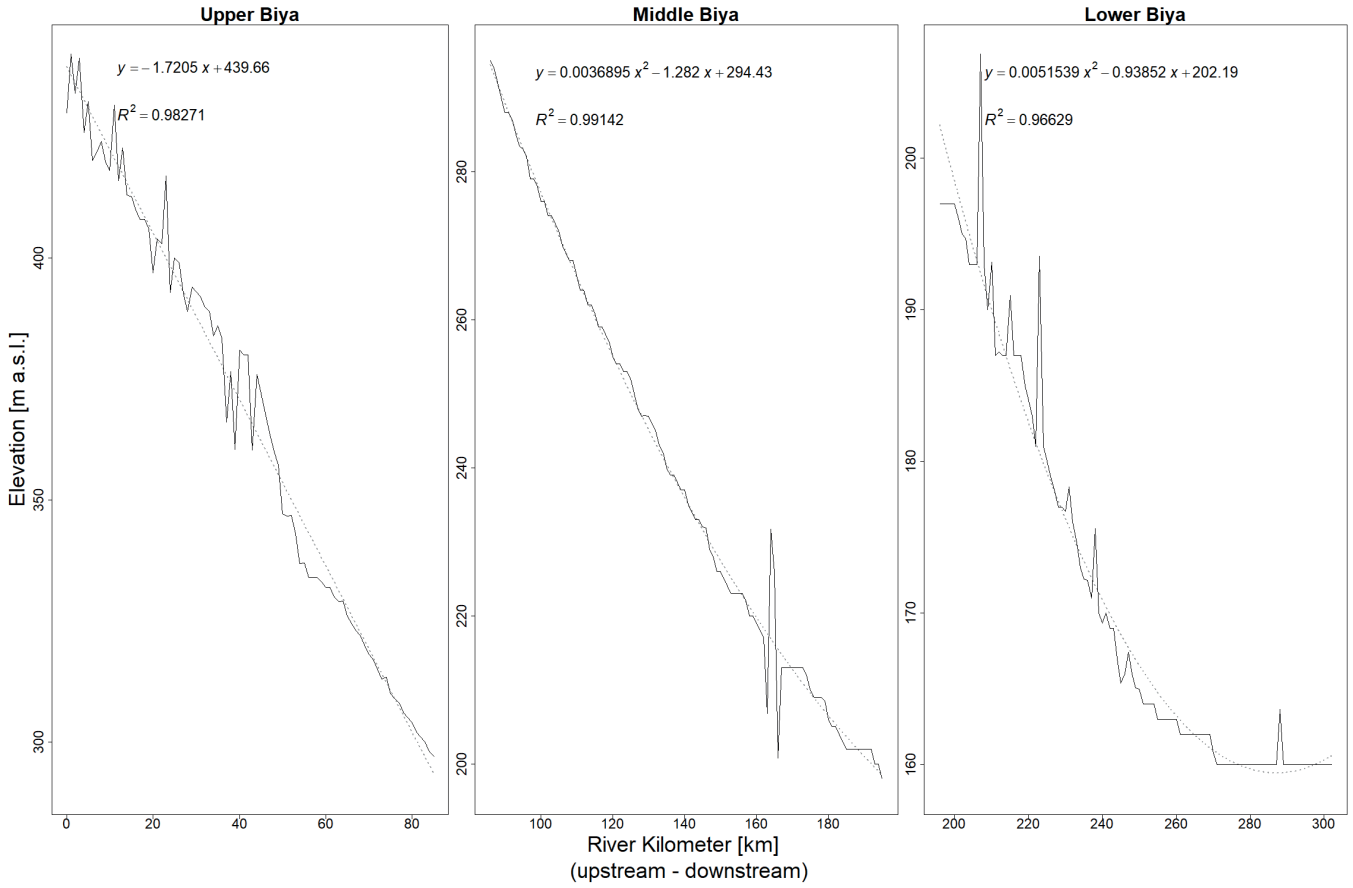

Fig. 4. Longitudinal profiles of the upper, middle, and lower Biya

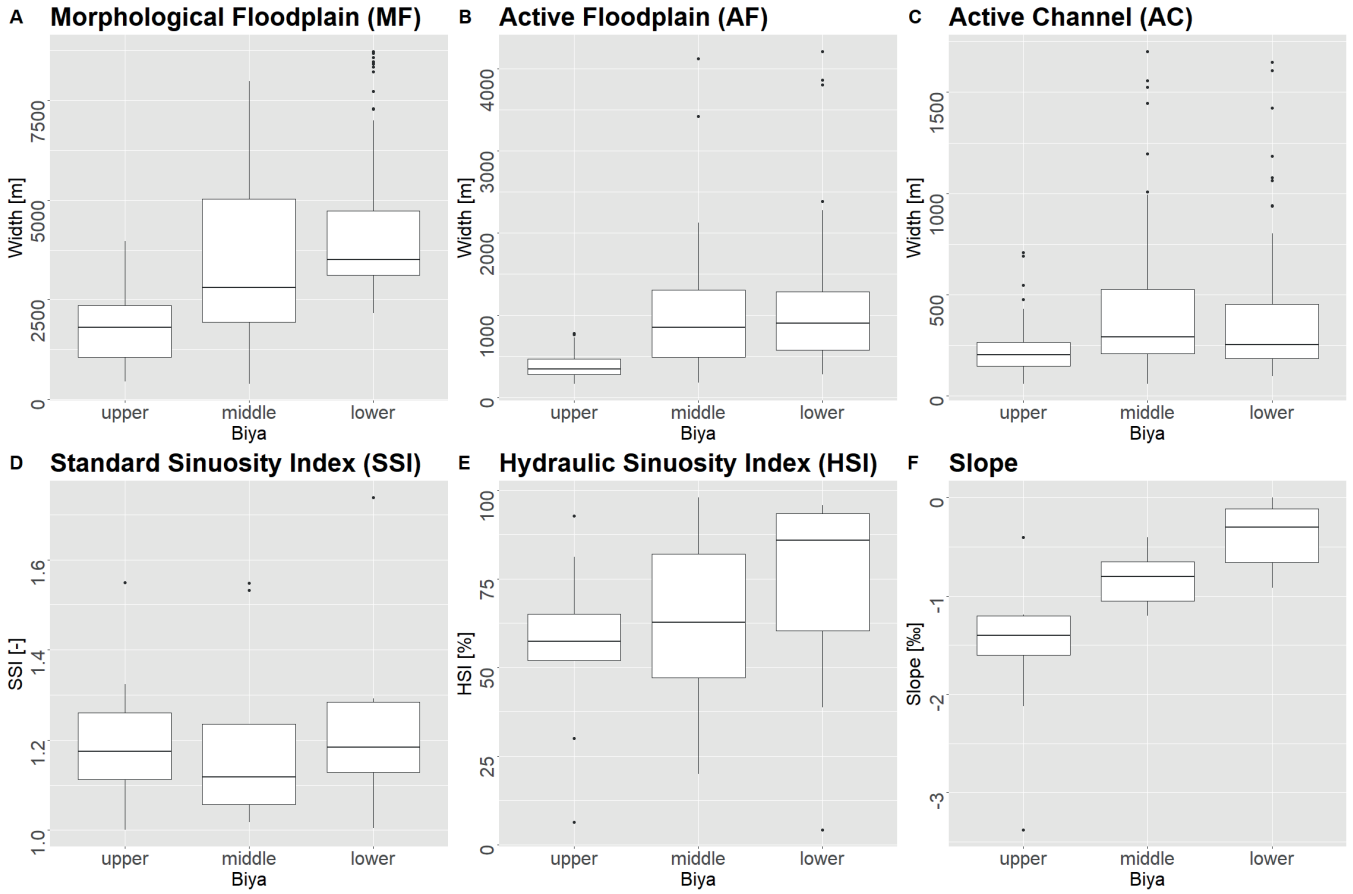

Fig. 5. Boxplots of the assessed morphological parameters

lower (mean: 1051.31 m) Biya regarding AF ($p = 1$). The statistic differences in AC (Fig. 5C) behave similarly: The upper Biya (mean: 226.82 m) differs from the other two stretches at highly significant levels ($p < 0.001$), while there is no significant difference ($p = 0.5$) between AC widths within the middle (mean: 423.06 m) and lower Biya (mean: 373.36 m). Within each of the three stretches, MF, AF, and AC all show highly significant differences from one another ($p < 0.001$).

Regression analyses with all observed parameters (AC, AF, MF, *SSI*, *HSI/TSI*, and slope) were performed using data that had been averaged for stretches of 10 km length. Fig. 6 shows a pairwise arrangement of these values plotted against each other. In most cases, no distinct (linear) relationship could be identified.

Based on these initial analyses (Fig. 6), correlations between MF and sinuosity (*SSI*, and *HSI/TSI*) were suspected. These three relationships are presented in more detail in Fig. 7. As could be expected, higher *SSI* values correlate with higher HSI values (and lower *TSI* values, respectively). Channel 'maturity' (indicated by the ratio between *HSI* and *TSI*, with higher *HSI* values suggesting a more 'mature' stage of the river and a better developed floodplain) is closely related to MF width. Accordingly, higher *HSI* values were also associated with higher MF values. In all cases, the coefficient of determination (R^2) is rather weak: The strongest linear relationship could be identified between *SSI* and *HSI* ($R^2 = 0.37$). The relationships between MF and *SSI* (and MF and *HSI*) are explained by linear regression at R^2 levels of 0.29 (and 0.19, respectively).

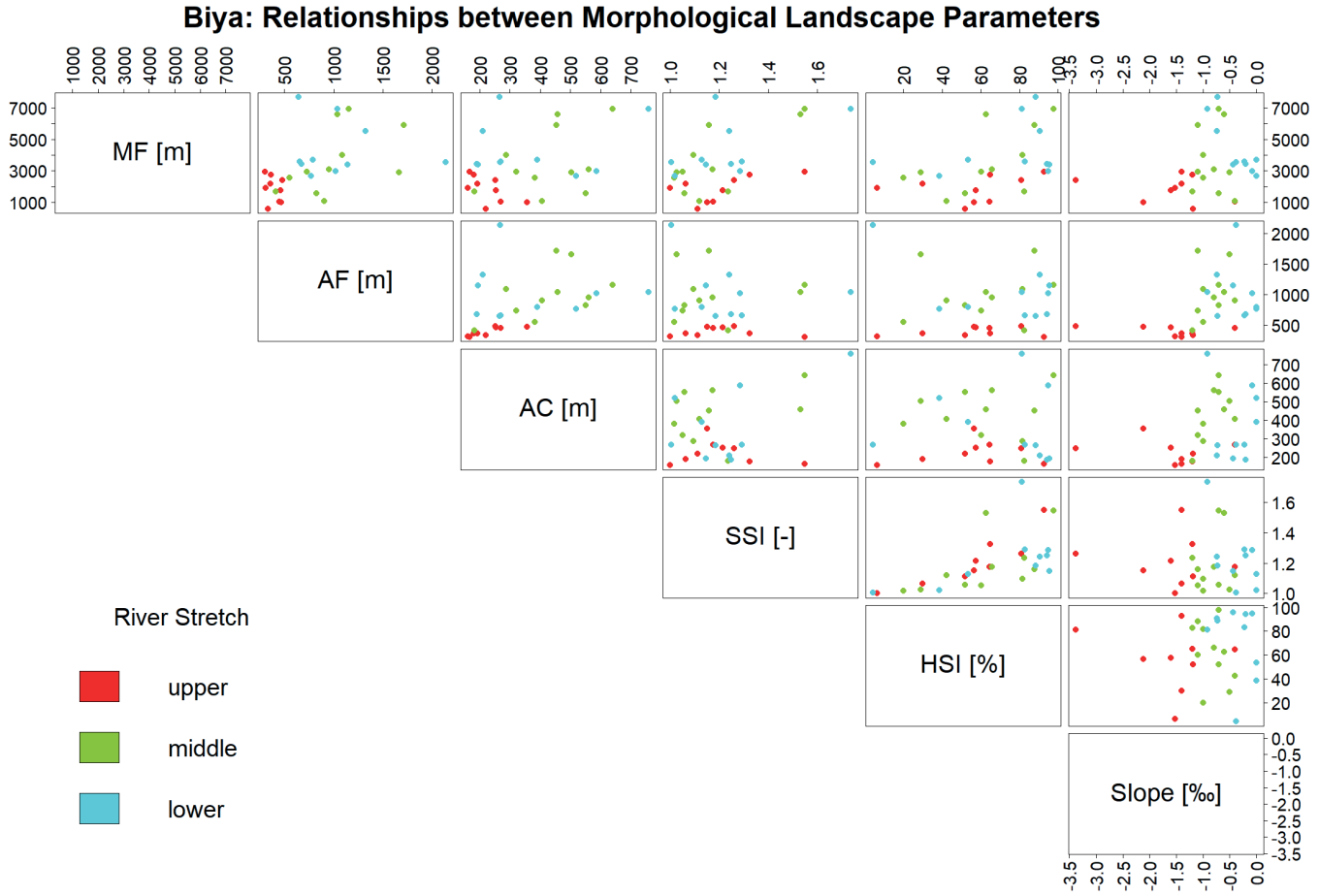

Fig. 6. Regression analyses for the assessed morphological parameters

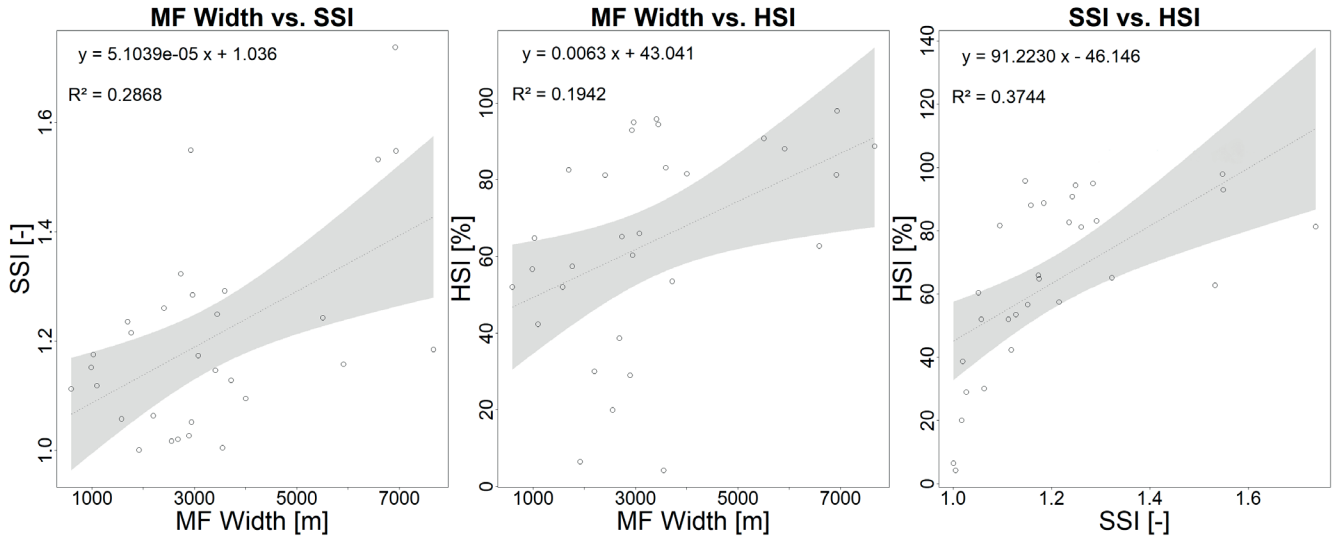

Fig. 7. Linear regression models for the relationships between MF, *SSI*, and *HSI*

DISCUSSION

The appearance and shape of a natural river result from complex morphological processes and interactions, majorly influenced by geological factors and climatic and hydrological controls (Mahala 2020, Castro and Thorne 2019, Stepinski and Stepinski 2005). These boundary conditions define sediment dynamics and determine the interactions between a river and its surrounding topography (Ibisate et al. 2011). Therefore, a profound understanding of a river's geological history is of utmost importance. Periods of glaciation, for example, that date back several thousands of years have strong impacts on today's rivers since glacial processes have provided large quantities of moraine material that gradually enters the sediment cycle (Sokołowski et al. 2021, Huang et al. 2019). Other processes associated with glaciation include the development of glacial lakes that can accumulate large volumes of lacustrine sediments, which may be released through rivers draining these lakes (Baryshnikov 2016). The temporal scale of the associated processes ranges from long-term deposition of lake sediments to rapid onset release events, like glacial lake outburst floods (GLOFs). The after-effects of certain climatic conditions can extend over millennia, so it is essential to consider the whole geological background when assessing a river's morphology. The evaluation of channel sinuosity alongside morphologically significant width parameters (AC, AF, MF) in this study has highlighted the influence of the different geological histories on the morphological characteristics of the upper Biya compared to the middle and lower stretch. The results confirm a distinction based on morphological history and show how different morphological river characteristics result from a river's geological past.

Glaciation and climatic history of the Altai mountains have been described in great depth (Blomdin et al. 2018, Blomdin et al. 2016, Chernykh et al. 2014, Agatova et al. 2012, Surazakov et al. 2007). The Altai mountains have been the scene of some of the largest freshwater megafloods that are known in planetary history (Herget et al. 2020, Bohorquez et al. 2019, Carling et al. 2002, Rudoy 2002). The most recent glacial activity during the Altai mountains' latter half of the holocene seems to have taken place simultaneously with those in the European Alps (Chernykh et al. 2013). It is reported that the maximum extent of glaciation reached the Biya's origin at Lake Teletskoye (Lehmkuhl et al. 2004). As of 2008, only 6.9 km^2 of the Biya's catchment are glaciated, with a clear decreasing tendency (Narozhniy and Zemtsov 2011).

The basin formation of Lake Teletskoye was not caused by quaternary glaciation. The Teletsk graben developed very recently (starting in the Pleistocene) in the contact zone between two Paleozoic blocks as a consequence of shear zone reactivation (Dehandschutter et al. 2002, De Grave and Van den Haute 2002). The formation of the actual lake was, however, a consequence of glacial retreat (about 37.5 ka before present), leaving a moraine-dammed lake (Baryshnikov et al. 2016). The complex tectonic conditions in the upper Biya valley determine the river's outflow direction (Baryshnikov 2016) thereby acting as controls on the course of the river.

Valley shape and different levels of confinement develop in relationship with various geological processes (Fryirs et al. 2016). Measures of confinement and valley width can be used to infer a river's geological history and to interpret its future development (Fryirs et al. 2016 referring to Fryirs and Brierley 2010 and Brierley and Fryirs 2015). Channel sinuosity is often strongly influenced by topographic constraints like valley margins (Woolderink et al. 2021, Fryirs and Brierley 2010, Tímar 2003), acting as a fundamental control on river character and behaviour (Fryirs et al. 2016). Including channel sinuosity and especially TSI in morphological analyses can help to identify interactions between river geometry and such topographic restraints. At the river Biya, high HSI values were associated with higher MF values (i.e., wider valley cross-sections). In this study, the dependence of channel curvature on topographic constraints (indicated by TSI) was shown to decrease in downstream direction, indicating an increasing stage of the river's 'maturity'.

The upper Biya (between Lake Teletskoye and Turochak) has been described as the least developed and narrowest section (Baryshnikov et al. 2016) with mountain river character (Baryshnikov 2016). It was only formed in the late middle Pleistocene when the outflow from Lake Teletskoye began. The remaining part, a well-developed valley is much older (probably dating back to the pre-Quaternary period, Baryshnikov et al. 2016). It could be shown that the upper Biya differs significantly from the other two stretches based on morphological parameters (AC, AF, MF). Glacial processes have determined the morphology of the upper Biya (Baryshnikov et al. 2016). The glacier that used to run through the basin of Lake Teletskoye contributed significantly to sediment production (Baryshnikov 2016). Lacustrine sediment deposits from glacial lakes in the upper Biya's tributary valleys and glacial moraine deposits along the main valley also supplied substantial amounts of sediment. A phase of rapid channel incision of the upper Biya was triggered by a cataclysmic glacial lake outburst event originating from Lake Teletskoye (about 37.5 ka before present, Baryshnikov et al. 2016). This incision into the alluvion is reflected by the limited extent of the active floodplain and restricted lateral dynamics in the upper stretch, indicating a higher sediment supply during the glacial period (Williams and Koppes 2019). The applied method already yielded similar findings at the Vjosa (Hauer et al. 2021). After the rapid incision triggered by the BDF, valley deepening rates slowed to about 0.8-0.9 m per thousand years (Baryshnikov et al. 2016). The upper Biya exhibits a linear longitudinal profile, while the middle and lower Biya follow a concave shape best described by a quadratic polynomial equation. The linear profile is associated with an equilibrium between sediment supply and transport without downstream fining. In contrast, the concave longitudinal profile in the lower Biya is an indicator for downstream fining and channel aggradation (Rice and Church 2001, referring to Mackin 1948). The elevation peaks in the longitudinal profiles (Fig. 4) are most likely caused by uncertainties in the delineation of the channel axis. These errors do, however, not alter the overall characteristic of the longitudinal profile shape of the three sub-stretches.

It could be demonstrated that the upper Biya, which is known to have a different geological background than the middle and lower part (Baryshnikov et al. 2016), significantly differs from the other two stretches based on morphological parameters (AC, AF, MF). The results clearly show that the relatively simple landscape reading approach, according to Hauer et al. (2021), which relies on only three width parameters on a cross-sectional basis, was able to account for the differences in the evolutionary history between the upper Biya and the two remaining sections. This is of particular interest since these parameters are clearly defined and comparably easy to obtain – allowing for a standardised differentiation between river stretches based on their morphological history. The fact that SSI could not be used to explain the differences in channel

evolution between the upper Biya and the remaining river stretch was interpreted as an indicator that the focus should rather be placed on the determining factors behind channel sinuosity and include the wider morphological context. Both the landscape reading approach (after Hauer et al. 2021) and the consideration of hydraulic and topographic sinuosity (after Mueller 1968) have proven useful in this regard.

The most striking constraint to the performed channel pattern analyses was the resolution of the input data at a cell size of 30 m by 30 m. Additional uncertainties within the lowermost 70 km must be mentioned, where catchment borders close in on the river axis and the extent of the morphological floodplain is hard to identify.

Comprehensive assessment of river landscape parameters is a key factor for developing a profound understanding of the complex multi-scale processes operating along and within a river system (see also the review of riverscape approaches by Torgersen et al. 2022). This is especially important when establishing environmental guiding principles and aiming to transfer these observations to other, more heavily disturbed systems. For this purpose, a supplementary catalogue of morphological parameters and verbal descriptions could be established for 10 km stretches along the whole Biya. This comprehensive set of parameters is summarised in Tables A.1-3 (see Appendix).

CONCLUSIONS

In this study of the alpine river Biya, the morphological parameters of a river in the least-disturbed condition were assessed and put into context with its geological history. The concept of 'reading the landscape' (Fryirs and Brierley 2012) in a hybrid approach, including measuring and hydrodynamic-numerical modelling (Hauer et al. 2021) was applied to differentiate between upper, middle, and lower Biya. The study could confirm the differentiation between the upper Biya and the rest of the river based on the different channel evolution history, highlighting the relationship between geological history and channel morphological parameters. Contrary to the initial expectations, channel sinuosity (*SSI*) could not be used to divide the Biya into morphologically meaningful sub-stretches. MF could best explain the differentiation between upper, middle, and lower Biya. The statistical analyses showed a relationship between MF and sinuosity (both *SSI* and *HSI/TSI*). The results of this study confirm that easily obtainable parameters (AC, AF, and MF) can be used to detect differences in the morphological history of river stretches, as was already shown for the Vjosa (Hauer et al. 2021).

REFERENCES

Anderson S.W. and Konrad C.P. (2019). Downstream-propagating channel responses to decadal-scale climate variability in a glaciated river basin. Journal of Geophysical Research: Earth Surface, 124(4), 902-919, DOI: 10.1029/2018JF004734.

Abily M., Acuña V., Gernjak W., Rodríguez-Roda I., Poch M. and Corominas L., (2021)' Climate change impact on EU rivers' dilution capacity and ecological status. Water Research, 199, 117166, DOI: 10.1016/j.watres.2021.117166.

Agatova A.R., Nazarov A.N., Nepop R.K. and Rodnight H. (2012). Holocene glacier fluctuations and climate changes in the southeastern part of the Russian Altai (South Siberia) based on a radiocarbon chronology. Quaternary Science Reviews, 43, 74-93, DOI: 10.1016/j.quascirev.2012.04.012.

Baker V.R., Benito G. and Rudoy A.N. (1993). Paleohydrology of late Pleistocene superflooding, Altay mountains, Siberia. Science, 259(5093), 348-350, DOI: 10.1126/science.259.5093.348.

Baryshnikov G.Y. (2016). Geological and geomorphological background of cataclysmic debris flooding in the Altai mountain rivers. Geography and Tourism, 4(2), 75-81, DOI: 10.5281/zenodo.223926.

Baryshnikov G.Y., Panin A. and Adamiec G. (2016). Geochronology of the late Pleistocene catastrophic Biya debris flow and the Lake Teletskoye formation, Altai Region, Southern Siberia. International Geology Review, 58(14), 1780-1794, DOI: 10.1080/00206814.2015.1062733.

Baryshnikov G.Y. (1979). Revisiting the formation of debris-flow sediment in the Biya valley. Geology and Mineral Resources in Altai Region. Altai University Press, Barnaul, 117-119. (as cited by Baryshnikov 2016)

Bechter T., Baumann K., Birk S., Bolik F., Graf W. and Pletterbauer F. (2018). LaRiMo-A simple and efficient GIS-based approach for large-scale morphological assessment of large European rivers. Science of the Total Environment, 628, 1191-1199, DOI: 10.1016/j.scitotenv.2018.02.084.

Blomdin R., Stroeven A.P., Harbor J.M., Gribenski N., Caffee M.W., Heyman J., Rogozhina I., Ivanov M.N., Petrakov D.A., Walther M. and Rudoy A.N. (2018). Timing and dynamics of glaciation in the Ikh Turgen Mountains, Altai region, High Asia. Quaternary Geochronology, 47, 54-71, DOI: 10.1016/j.quageo.2018.05.008.

Blomdin R., Heyman J., Stroeven A.P., Hättestrand C., Harbor J.M., Gribenski N., Jansson K.N., Petrakov D.A., Ivanov M.N., Alexander O. and Rudoy A.N. (2016). Glacial geomorphology of the Altai and western Sayan mountains, central Asia. Journal of Maps, 12(1), 123-136, DOI: 10.1080/17445647.2014.992177.

Bohorquez P., Jimenez-Ruiz P.J. and Carling P.A. (2019). Revisiting the dynamics of catastrophic late Pleistocene glacial-lake drainage, Altai Mountains, central Asia. Earth-Science Reviews, 197, 102892, DOI: 10.1016/j.earscirev.2019.102892.

Boothroyd R.J., Nones M. and Guerrero M. (2021). Deriving planform morphology and vegetation coverage from remote sensing to support river management applications. Frontiers in Environmental Science, 9, 657354, DOI: 10.3389/fenvs.2021.657354.

Brice J.C. (1982). Stream channel stability assessment. Final Report. (No. FHWA/RD-82/021). United States. Federal Highway Administration. 44 pp.

Brierley G.J and Fryirs K. (2015). The use of evolutionary trajectories to guide 'moving targets' in the management of river futures. River Research and Applications, 32(5), 823-835, DOI: 10.1002/rra.2930.

Carling P.A., Kirkbride A.D., Parnachov S., Borodavko P.S. and Berger G.W. (2002). Late Quaternary catastrophic flooding in the Altai mountains of south–central Siberia: a synoptic overview and an introduction to flood deposit sedimentology. Flood and megaflood processes and deposits: recent and ancient examples, 17-35.

Castro J.M. and Thorne C.R. (2019). The stream evolution triangle: Integrating geology, hydrology, and biology. River Research Applications, 35, 315–326, DOI: 10.1002/rra.3421-

Chalov S. and Ermakova G. (2011). Fluvial response to climate change: a case study of northern Russian rivers. Cold Region Hydrology in a Changing Climate. IAHS, 346, 111-119.

Chernykh D.V., Zolotov D.V., Yamskikh G.Y. and Grenaderova A.V. (2014). Postglacial environmental change in the valley of Malye Chily River (the basin of Lake Teletskoye), northeastern Russian Altai. Physical Geography, 35(5), 390-410, DOI: 10.1080/02723646.2014.929881.

Chernykh D.V., Galakhov V.P. and Zolotov D.V. (2013). Synchronous fluctuations of glaciers in the Alps and Altai in the second half of the Holocene. The Holocene, 23(7), 1074-1079, DOI: 10.1177/0959683612475143.

Chlachula J. and Sukhova M. G. (2011). Regional manifestations of present climate change in the Altai, Siberia. Proc. ICEEA 2nd Int. Conf. on Environmental Engineering and Applications (Shanghai, China, August 19-21, 2011) Int. Proc. of Chemical, Biological and Environmental Engineering and Applications, 17, 134-139.

'Comiti F., Mao L., Penna D., Dell'Agnese A., Engel M., Rathburn S. and Cavalli M., (2019). Glacier melt runoff controls bedload transport in Alpine catchments. Earth and Planetary Science Letters, 520, 77-86, DOI: 10.1016/j.epsl.2019.05.031.

Comiti F. (2012). How Natural are Alpine Mountain Rivers? Evidence from the Italian Alps. Earth Surface Processes and Landforms, 37, 693-707, DOI: 10.1002/esp.226'.

De Grave J. and Van den Haute P. (2002). Denudation and cooling of the Lake Teletskoye Region in the Altai Mountains (South Siberia) as revealed by Apatite Fission-Track Thermochronology. Tctonophysics, 349(1-4), 145-159, DOI: 10.1016/S0040-1951(02)00051-3.

Dehandschutter B., Vysotsky E., Delvaux D., Klerkx J., Buslov M. M., Seleznev V. S. and De Batist, M. (2002). Structural evolution of the Teletsk graben (Russian Altai). Tectonophysics, 351(1-2), 139-167, DOI: 10.1016/S0040-1951(02)00129-4.

Dirin D. and Madry C. (2017). Transformation Processes in Traditional Nature Management Systems in the Altai Mountain Region. 17th International Multidisciplinary Scientific GeoConference, Bulgaria.

Feio M.J., Hughes R.M., Serra S.R., Nichols S.J., Kefford B.J., Lintermans M., Robinson W., Odume O.N., Callisto M., Macedo D.R. and Harding J.S. (2022). Fish and macroinvertebrate assemblages revea' extensive degradation of the world's rivers. Global Change Biology. 00, 1-20, DOI: 10.1111/gcb.16439.

Feio M.J., Hughes R.M., Callisto M., Nichols S.J., Odume O.N., Quintella B.R., Kuemmerlen M., Aguiar F.C., Almeida S.F.P, Alonso-EguíaLis P. et al. (2021). The Biological Assessment and Rehabilitation of the World's Rivers: An Overview. Water, 13, 371, DOI: 10.3390/w13030371.

Fildani A., Hessler A.M., Mason C.C., McKay M.P. and Stockli D.F. (2018). Late Pleistocene glacial transitions in North America altered major river drainages, as revealed by deep-sea sediment. Scientific reports, 8(1), 1-8. DOI:10.1038/s41598-018-32268-7.

Fryirs K.A., Wheaton J.M. and Brierley G.J. (2016). An approach for measuring confinement and assessing the influence of valley setting on river forms and processes. Earth Surface Processes and Landforms, 41(5), 701-710, DOI: 10.1002/esp.3893.

Fryirs K.A. and Brierley G.J. (2012). Geomorphic analysis of river systems: an approach to reading the landscape. John Wiley & Sons.

Fryirs K.A. and Brierley G.J. (2010). Antecedent controls on river character and behaviour in partly confined valley settings: Upper Hunter catchment, NSW, Australia. Geomorphology, 117(1-2), 106-120, DOI: 10.1016/j.geomorph.2009.11.015.

Grill G., Lehner B., Lumsdon A. E., MacDonald G.K., Zarfl C. and Reidy Liermann C. (2015). An index-based framework for assessing patterns and trends in river fragmentation and flow regulation by global dams at multiple scales. Environ. Res. Lett., 10(1), 015001, DOI: 10.1088/1748-9326/10/1/015001.

Grill G., Lehner B., Thieme M. et al. (2019). Mapping the world's free-flowing rivers. Nature, 569, 215–221, DOI: 10.1038/s41586-019-1111-9.

Hais M., Komprdová K., Ermakov N. and Chytrý M. (2015). Modelling the Last Glacial Maximum environments for a refugium of Pleistocene biota in the Russian Altai Mountains, Siberia. Palaeogeography, Palaeoclimatology, Palaeoecology, 438, 135-145, DOI: 10.1016/j.palaeo.2015.07.037.

Hauer C., Skrame K. and Fuhrmann M. (2021). Hydromorphological assessment of the Vjosa river at the catchment scale linking glacial history and fluvial processes. Catena, 207, 105598, DOI: 10.1016/j.catena.2021.105598.

Hauer C. and Pulg U. (2021). Buried and forgotten—The non-fluvial characteristics of postglacial rivers. River Research and Applications, 37(2), 123-127, DOI: 10.1002/rra.3596.

Hauer C. and Pulg U. (2018). The non-fluvial nature of Western Norwegian rivers and the implications for channel patterns and sediment composition. Catena, 171, 83-98, DOI: 10.1016/j.catena.2018.06.025.

He F., Zarfl C., Bremerich V., David J.N., Hogan Z., Kalinkat G., Tockner K., and Jähnig S.C. (2019). The global decline of freshwater megafauna. Global Change Biology, 25(11), 3883-3892, DOI: 10.1111/gcb.14753.

He F., Bremerich V., Zarfl C., et al. (2018). Freshwater megafauna diversity: Patterns, status and threats. Diversity and Distribution; 24, 1395–1404. DOI:10.1111/ddi.12780.

Hedding D.W., Erofeev A.A., Hansen C.D., Khon A.V. and Abbasov Z.R. (2020). Geomorphological processes and landforms of glacier forelands in the upper Aktru River basin (Gornyi Altai), Russia: evidence for rapid recent retreat and paraglacial adjustment. Journal of Mountain Science, 17(4), 824-837.

Hemmelder S., Marra W., Markies H. and De Jong S.M. (2018). Monitoring river morphology & bank erosion using UAV imagery–A case study of the river Buëch, Hautes-Alpes, France. International Journal of Applied Earth Observation and Geoinformation, 73, 428-437, DOI: 10.1016/j.jag.2018.07.016.

Herget J., Agatova A.R., Carling P.A. and Nepop R.K. (2020). Altai megafloods—The temporal context. Earth-Science Reviews, 200, 102995, DOI: 10.1016/j.earscirev.2019.102995.

Hey R.D. (2006). Fluvial Geomorphological Methodology for Natural Stable Channel Design. JAWRA Journal of the American Water Resources Association, 42(2), 357-386.

Huang W., Yang X., Jobe J.A.T., Li S., Yang H. and Zhang L. (2019). Alluvial plains formation in response to 100-ka glacial–interglacial cycles since the Middle Pleistocene in the southern Tian Shan, NW China. Geomorphology, 341, 86-101, DOI: 10.1016/j.geomorph.2019.05.013.

Ibisate A., Ollero A. and Díaz Bea E. (2011). Influence of catchment processes on fluvial morphology and river habitats. Limnetica, 30(2), 0169-182.

Klubnikin K., Annett C., Cherkasova M., Shishin M. and Fotieva I. (2000). The sacred and the scientific: traditional ecological knowledge in Siberian river conservation. Ecological Applications, 10(5), 1296-1306.

Kujanová K. and Matouškova M. (2017). Identification of Hydromorphological Reference Sites Using the New REFCON Method, with and Application to Rivers in the Czech Republic. Ecohgydrology & Hydrobiology, 17, 235-245, DOI: 10.1016/j.ecohyd.2017.06.002.

Langat P.K., Kumar L. and Koech R. (2019). Monitoring river channel dynamics using remote sensing and GIS techniques. Geomorphology, 325, 92-102, DOI: 10.1016/j.geomorph.2018.10.007.

Lehmkuhl F., Klinge M. and Stauch G. (2004). The extent of Late Pleistocene glaciations in the Altai and Khangai Mountains. Developments in Quaternary Sciences, 2, 243-254.

Lemm J.U., Venohr M., Globevnik L., et al. (2021). Multiple stressors determine river ecological status at the European scale: Towards an integrated understanding of river status deterioration. Global Change Biology, 27, 1962-1975, DOI: 10.1111/gcb.15504.

Liu S., Xie Z., Liu B., Wang Y., Gao J., Zeng Y., Xie J., Xie Z., Jia B., Qin P. and Li R. (2020). Global river water warming due to climate change and anthropogenic heat emission. Global and Planetary Change, 193, 103289, DOI: 10.1016/j.gloplacha.2020.103289.

Mackin J.H. (1948). Concept of the graded river, Geol. Soc. Am. Bull., 59, 463-512. (as cited by Rice and Church 2001)

Mahala A. (2020). The significance of morphometric analysis to understand the hydrological and morphological characteristics in two different morpho-climatic settings. Applied Water Science, 10(1), 1-16, DOI: 10.1007/s13201-019-1118-2.

Malatesta L.C. and Avouac J.P. (2018). Contrasting river incision in north and south Tian Shan piedmonts due to variable glacial imprint in mountain valleys. Geology, 46(7), 659-662, DOI: 10.1130/G40320.1.

Malmqvist B. and Rundle S. (2002). Threats to the running water ecosystems of the world. Environmental conservation, 29(2), 134-153, DOI:10.1017/S0376892902000097.

Mueller J. E. (1968). An Introduction to the Hydraulic and Topographic Sinuosity Indexes. Annals of the Association of American Geographers, 58(2), 371-385.

Muhar S. (1996). Habitat improvement of Austrian rivers with regard to different scales. Regulated Rivers Research & Management, 12, 471-482.

Nanson G.C. and Huang H.Q. (2018). A philosophy of rivers: Equilibrium states, channel evolution, teleomatic change and least action principle. Geomorphology, 302, 3-19.

Narozhniy Y. and Zemtsov V. (2011). Current state of the Altai glaciers (Russia) and trends over the period of instrumental observations 1952–2008. Ambio, 40(6), 575-588, DOI: 10.1007/s13280-011-0166-0.

Newbold J. D., O'neill R. V., Elwood J. W. and Van Winkle W. (1982). Nutrient spiralling in streams: implications for nutrient limitation and invertebrate activity. The American Naturalist, 120(5), 628-652.

Newson M. D. and Large A. R. G. (2006). 'Natural' Rivers, 'Hydromorphological Quality' and River Restoration: A Challenging New Agenda for Applied Fluvial Geomorphology. Earth Surface Processes and Landforms, 31, 1606-1624, DOI: 10.1002/esp.1430.

Piégay H., Arnaud F., Belletti B., Bertrand M., Bizzi S., Carbonneau P., Dufour S., Liébault F., Ruiz-Villanueva V. and Slater L. (2020). Remotely sensed rivers in the Anthropocene: State of the art and prospects. Earth Surface Processes and Landforms, 45(1), 157-188, DOI: 10.1016/j.geomorph.2015.05.010.

Rinaldi M., Gurnell A.M., Del Tánago M.G., Bussettini M. and Hendriks D. (2016). Classification of river morphology and hydrology to support management and restoration. Aquatic sciences, 78(1), 17-33, DOI: 10.1007/s00027-015-0438-z.

Rinaldi M., Surian, N. Comiti F. and Bussettini M. (2015). A methodological framework for hydromorphological assessment, analysis and monitoring (IDRAIM) aimed at promoting integrated river management. Geomorphology, 251, 122-136, DOI: 10.1016/j.geomorph.2015.05.010.

Rudoy A.N., (2002). Glacier-dammed lakes and geological work of glacial superfloods in the Late Pleistocene, Southern Siberia, Altai Mountains. Quaternary International, 87(1), 119-140.

Rudoy A.N. and Baker V.R. (1993). Sedimentary effects of cataclysmic late Pleistocene glacial outburst flooding, Altay Mountains, Siberia. Sedimentary Geology, 85(1-4), 53-62, DOI: 10.1016/0037-0738(93)90075-G.

Sala O. E., Stuart Chapin III F., Armesto J. J., Berlow E., Bloomfield J., Dirzo R., Huber-Sanwald E., Huenneke L. F., Jackson R. B., Kinzig A., Leemans R., Lodge D. M., Mooney H. A., Oesterheld M., Poff N. L., Sykes M. T., Walker B. H., Walker M., and Wall D. H. (2000). Global biodiversity scenarios for the year 2100. Science, 287(5459), 1770-1774, DOI: 10.1126/science.287.5459.1770.

Schletterer M., Shevchenko A.A., Yanygina L.V., Manakov Y.A., Reisenbüchler M. and Rutschmann P. (2021). Eindrücke vom Oberlauf des Obs in Russland. Wasserwirtschaft, 111(9-10), 77-85, DOI: 10.1007/s35147-021-0903-7.

Scorpio V., Andreoli A', Zaramella M., Moritsch S., Theule J., Dell'Agnese A., Muhar S., Borga M., Bertoldi W. and Comiti, F. (2020). Restoring a glacier-fed river: Past and present morphodynamics of a degraded channel in the Italian Alps. Earth Surface Processes and Landforms, 45(12), 2804-2823, DOI: 10.1002/esp.4931.

Shahrood A.J., Menberu M.W., Darabi H., Rahmati O., Rossi P.M., Kløve B. and Haghighi A.T. (2020). RiMARS: An automated river morphodynamics analysis method based on remote sensing multispectral datasets. Science of the Total Environment, 719, 137336, DOI: 10.1016/j.scitotenv.2020.137336.

Sokołowski R.J., Molodkov A., Hrynowiecka A., Woronko B. and Zieliński P. (2021). The role of an ice-sheet, glacioisostatic movements and climate in the transformation of Middle Pleistocene depositional systems: a case study from the Reda site, northern Poland. Geografiska Annaler: Series A, Physical Geography, 103:3, 223-258, DOI: 10.1080/04353676.2021.1926241.

Stepinski T. F. and Stepinski A. P. (2005). Morphology of drainage basins as an indicator of climate on early Mars, Journal of Geophysical Research, 110, E12S12, DOI:10.1029/2005JE002448.

Stoddard J.L., Larsen D.P., Hawkins C.P., Johnson R.K. and Norris, R.H. (2006). Setting expectations for the ecological condition of streams: the concept of reference condition. Ecological applications, 16(4), 1267-1276, DOI: 10.1890/1051-0761(2006)016[1267:SEFTEC]2.0.CO;2.

Surazakov A.B., Aizen V.B., Aizen E.M. and Nikitin S.A. (2007). Glacier changes in the Siberian Altai Mountains, Ob river basin (1952–2006) estimated with high resolution imagery. Environmental Research Letters, 2(4), 045017, DOI: 10.1088/1748-9326/2/4/045017.

Surface water resources of the USSR. [Resursy poverkhnostnykh vod SSSR.]. (1962). Vol. 6 Leningrad, "Gidrometeoizdat" [Hydrometeorological Publishing House]: 975 (In Russian)

Tickner D., Opperman J.J., Abell R., Acreman M., Arthington A.H., Bunn S.E., Cooke S.J., Dalton J., Darwall W., Edwards G. and Harrison I., (2020). Bending the curve of global freshwater biodiversity loss: an emergency recovery plan. BioScience, 70(4), 330-342, DOI: 10.1093/biosci/biaa002.

Tímar G. (2003). Controls on Channel Sinuosity Changes: A Case Study of the Tisza River, the Great Hungarian Plain. Quaternary Science Reviews, 22, 2199-2207, DOI: 10.1016/S0277-3791(03)00145-8.

Tomsett C. and Leyland J. (2019). Remote sensing of river corridors: A review of current trends and future directions. River Research and Applications, 35(7), 779-803, DOI: 10.1002/rra.3479.

Torgersen C.E., Le Pichon C., Fullerton A.H., Dugdale S.J., Duda J.J., Giovannini F., Tales É., Belliard J., Branco P., Bergeron N. E., Roy M.L., Tonolla D., Lamouroux N., Capra H. and Baxter C. V. (2022). Riverscape approaches in practice: Perspectives and applications. Biological Reviews, 97(2), 481-504, DOI: 10.1111/brv.12810.

USGS (2019). How Much Water is There on Earth? Available at: https://www.usgs.gov/special-topics/water-science-school/science/how-much-water-there-earth#:~:text=About%2071%20percent%20of%20the,percent%20of%20all%20Earth' s%20water. (Accessed: 21 November 2022).

Volkov I.V., Zemtsov V.A., Erofeev A.A., Babenko A.S., Volkova A.I. and Callaghan T.V. (2021). The dynamic land-cover of the Altai Mountains: Perspectives based on past and current environmental and biodiversity changes. Ambio, 50, 1991-2008, DOI: 10.1007/s13280-021-01605-y.

Wolman M.G. (1954). A Method of Sampling Coarse River-Bed Material. Transactions, American Geophysical Union, 35(6), 951-956.

Vandenberghe J., Kasse C., Popov D., Markovic S.B., Vandenberghe D., Bohncke S. and Gabris G. (2018). Specifying the external impact on fluvial lowland evolution: The last glacial Tisza (Tisa) catchment in Hungary and Serbia. Quaternary, 1(2), 14, DOI: 10.3390/quat1020014.

Vannote R.L., Minshall G.W., Cummins K.W., Sedell J.R. and Cushing C.E. (1980). The river continuum concept. Canadian journal of fisheries and aquatic sciences, 37(1), 130-137.

Ward J.V. (1989). The four-dimensional nature of lotic ecosystems. Journal of the North American Benthological Society, 8(1), 2-8.

Williams H.B. and Koppes M.N. (2019). A comparison of glacial and paraglacial denudation responses to rapid glacial retreat. Annals of Glaciology, 60(80), 151-164, DOI: 10.1017/aog.2020.1.

Woolderink H.A.G., Cohen K.M., Kasse C., Kleinhans M.G. and Van Balen R.T. (2021). Patterns in river channel sinuosity of the Meuse, Roer and Rhine rivers in the Lower Rhine Embayment rift-system, are they tectonically forced? Geomorphology, 375, 107550, DOI: 10.1016/j.geomorph.2020.107550.

Yue S., Ouarda T.B.M.J., Bob´ee B., Legendre P. and Bruneau P. (1999). The Gumbel mixed model for flood frequency analysis. J. Hydrol., 226(1-2), 88-100, DOI: 10.1016/S0022-1694(99)00168-7.

Zarfl C., Berlekamp J., He F., Jähnig S.C., Darwall W. and Tockner K. (2019). Future large hydropower dams impact global freshwater megafauna. Scientific reports, 9(1), 1-10, DOI: 10.1038/s41598-019-54980-8.

Zolnikov I.D., Deev E.V., Kotler S.A., Rusanov G.G. and Nazarov D.V. (2016). New results of OSL dating of Quaternary sediments in the Upper Katun'valley (Gorny Altai) and adjacent area. Russian Geology and Geophysics, 57(6), 933-943, DOI: 10.1016/j.rgg.2015.09.022.

Zolnikov I.D., Deev E.V., Nazarov D.V. and Kotler S.A. (2015). Comparative analysis of megaflood deposits and alluvium of the Chuya and Katun'river valleys (Gorny Altai). Russian Geology and Geophysics, 56(8), 1162-1172, DOI: 10.1016/j.rgg.2015.07.007.

APPENDIX

Table A.1. Summary of the observed morphological parameters along the Biya. Landscape reading elements: Active channel width (AC), active floodplain width (AF), and morphological floodplain width (MF), and sinuosity: Standard (SSI), hydraulic (HSI), and topographic (TSI) sinuosity index

	Section	River Kilometer		Elevation			Slope	AC			AF			MF			Sinuosity			
	Nr.	Start	End	Min.	Max.	Avg.	Avg.	Min.	Max.	Avg.	Min.	Max.	Avg.	Min.	Max.	Avg.	SSI	HSI	TSI	
	[-]	[km]	[km]	[m a.s.l.]			[‰]	[m]			[m]			[m]			[-]	[%]		
upper Biya	1	0	10	420	442	429	-1.19	50	805	384	239	461	335	489	937	630	1.1128	51.98	48.02	upper Biya
	2	10	20	406	432	415	-2.12	45	190	112	241	783	467	445	1453	990	1.1515	56.65	43.35	
	3	20	30	389	417	399	-0.40	42	139	87	226	762	447	809	1297	1032	1.1749	64.74	35.26	
	4	30	40	360	393	382	-1.20	71	163	115	166	506	365	1221	3898	2740	1.3232	65.09	34.91	
	5	40	50	357	381	370	-3.38	65	312	149	269	711	479	2159	2928	2410	1.2603	81.16	18.84	
	6	50	60	333	347	339	-1.52	148	324	232	194	470	310	1211	2363	1920	1.0005	6.40	93.60	
	7	60	70	320	332	327	-1.40	221	503	297	189	598	302	1586	3971	2936	1.5492	92.86	7.14	
	8	70	80	305	318	311	-1.40	180	658	366	212	482	359	1713	3573	2201	1.0634	30.00	70.00	
	9	80	90	290	304	297	-1.60	360	1148	747	275	694	463	1346	2346	1767	1.2153	57.38	42.62	
middle Biya	10	90	100	278	288	283	-1.20	90	595	207	180	735	412	907	2507	1702	1.2355	82.56	17.44	middle Biya
	11	100	110	268	276	272	-1.00	69	197	145	390	904	552	2275	2801	2555	1.0173	19.95	80.05	
	12	110	120	257	266	261	-1.10	106	210	146	255	1285	731	1698	4211	2948	1.0516	60.30	39.70	
	13	120	130	247	255	251	-0.80	87	311	193	338	1840	955	2198	4184	3078	1.1731	65.92	34.08	
	14	130	140	237	247	242	-1.00	133	450	251	230	2126	1088	3616	4577	4007	1.0949	81.56	18.44	
	15	140	150	226	237	232	-1.10	173	337	246	535	4125	1713	4743	6847	5913	1.1579	88.03	11.97	
	16	150	160	220	226	223	-0.70	164	971	301	478	1752	1153	6508	7419	6941	1.5480	97.91	2.09	
	17	160	170	201	232	216	-0.60	186	938	371	429	1882	1039	4590	7979	6594	1.5325	62.74	37.26	
	18	170	180	208	213	211	-0.70	187	708	303	331	1310	828	392	2914	1579	1.0577	51.93	48.07	
	19	180	190	202	206	203	-0.40	199	690	325	502	1783	904	502	1944	1099	1.1183	42.30	57.70	
	20	190	200	197	202	199	-0.50	64	554	225	1265	2133	1661	1965	3326	2899	1.0268	28.95	71.05	
lower Biya	21	200	210	190	207	195	-0.38	72	272	142	630	4205	2135	3036	4163	3555	1.0048	4.19	95.81	lower Biya
	22	210	220	185	193	188	-0.92	73	223	157	416	2143	1039	4094	8713	6926	1.7374	81.27	18.73	
	23	220	230	177	194	181	-0.73	133	267	168	325	1326	646	6212	8452	7672	1.1842	88.67	11.33	
	24	230	240	170	178	174	-0.74	133	395	219	763	2388	1321	4704	5999	5511	1.2423	90.71	9.29	
	25	240	250	165	170	167	-0.44	98	636	224	426	1834	1142	3049	4195	3415	1.1464	95.77	4.23	
	26	250	260	163	165	164	-0.20	146	672	234	300	1186	673	3233	3869	3448	1.2488	94.40	5.60	
	27	260	270	162	163	162	-0.22	137	1008	493	280	1352	658	3115	3912	3595	1.2914	83.06	16.94	
	28	270	280	160	161	160	-0.08	239	841	450	432	1596	1020	2517	3763	2966	1.2847	94.97	5.03	
	29	280	290	160	164	160	0.00	156	1538	505	443	1627	768	2158	3178	2686	1.0200	38.68	61.32	
	30	290	300	160	160	160	0.00	182	562	278	317	1695	789	2517	4591	3718	1.1279	53.44	46.56	

Table A.2. Summary of the observed morphological parameters along the Biya based on 10 km stretches. Verbal and qualitative description (for category definitions cat.A to F see below)´

	Section	River Kilometer		Topographic Structures	Channel		Valley Slopes (orogr. side)		Valley Orientation			Valley Width			
	Nr.	Start	End	Prominent Elements	Type	Width	left	right	current	previous	following	current	previous	following	
	[-]	[km]	[km]	[-]	[cat.A]	[cat.B]	[cat.C]		section [cat.D]			section [cat.E/F]			
upper Biya	1	0	10	Outflow Lake Teletskoye, narrow valley cross sections	3	2	1	1	2		2	1		1	upper Biya
	2	10	20		2	2	2	2/1	2	2	2	2	3	2	
	3	20	30	Valley incision/ topographic constraints that force the valley to bend to the orogr. Right	2	1	2	1/3	2	2	3	1	2	1	
	4	30	40	valley incision followed by significant widening	1	1	2	2	3	2	1	2	3	3	
	5	40	50		2	2	2	2	1	3	1	1	1	3	
	6	50	60	Valley incision at rkm 58/59	1	2	3	3	1	1	2	1	1	1	
	7	60	70	Significant widening	2	2	1	1	2	1	3	2	3	3	
	8	70	80		2	3	2	2	3	2	1/4	2	1	3	
	9	80	90	tributary (orogr. Right) in close vicinity over most part	2	2	1	3	1/4	3	1	2	1	2	
middle Biya	10	90	100	more complex island structure between rkm 94-97	2	2	2	3	1	1/4	2	2	2	1	middle Biya
	11	100	110	more complex island structure around rkm 110	3	3	2	3	2	1	2	1	3	1	
	12	110	120	more complex island structure around rkm 110 and rkm 119	3	3	3	1	2	2	1	2	3	2	
	13	120	130	rkm 120-126	4	2	2	2	1	2	1	2	2	1	
	14	130	140		5	2	2/1	2	1	1	1	1	3	1	
	15	140	150	superordinate valley bend to the orogr. leftbetween rkm 140-175	5	3	3	3	1	1	1	2	3	1	
	16	150	160	superordinate valley bend to the orogr. leftbetween rkm 140-175	4	3	3	3	1	1	3	1	3	3	

middle Biya	17	160	170	superordinate valley bend to the orogr. leftbetween rkm 140-175	5	3	3	2	3	1	2	2	1	3	middle Biya
	18	170	180	superordinate valley bend to the orogr. leftbetween rkm 140-175 followed by superordinate valley bend to the orographic right between rkm 175-190	5	3	2	2	2	3	4/2	2	1	3	
	19	180	190	superordinate valley bend to the orographic right between rkm 175-190, distinctive bend to the left (rkm 180-184) upstream of hill structure	2	2	1	2	4/2	2	3	2	1	1	
	20	190	200	superordinate valley bend to the orogr. Left between rkm 190-210	4	3	1	2	3	4/2	3	2	3	1	
lower Biya	21	200	210	superordinate valley bend to the orogr. Left between rkm 190-210	2	2	1	3	3	3	1	2	3	1	lower Biya
	22	210	220	Significant widening, bend near rkm 220 initiatend by hill structure	2	2	2/1	2	1	3	1	2	3	1	
	23	220	230		2	2	1/2	3	1	1	1	2	3	3	
	24	230	240		2	3	3	3	1	1	1	2	1	3	
	25	240	250		5	3	2	2	1	1	1	1	1	2	
	26	250	260	clear signs of human infrastructure	1	2	2	2	1	1	1	1	2	2	
	27	260	270	clear signs of human infrastructure	2	3	2	2	1	1	1	1	2	2	
	28	270	280	clear signs of human infrastructure	2	3	2	2	1	1	2	1	2		
	29	280	290	clear signs of human infrastructure, valley borders hard to define	5	3	2	2	2	1	2				
	30	290	300	clear signs of human infrastructure, valley borders hard to define, orogr. Left interactions with Katun	2	3	3	2	2	2					

[A]Channel Type	1	one main channel, hardly any developed Islands
	2	1 to 3 developed islands, subordinate sidearms
	3	one well developed Island about every 1 km
	4	more than one (main) channel for more than half of the length
	5	complex, several side arms for (almost) the whole length
[B]Channel Width	1	rather constant channel width
	2	slight channel width variations
	3	strong channel width variations
[C]Valley Slopes	1	steep
	2	flat
	3	flat, dominated by tributary confluence
[D]Valley Orientation	1	straight/unidirectional
	2	sinusoidal
	3	meander bend to the orographic left
	4	meander bend to the orographic right
[E]Valley width	1	rather constant valley width
	2	noticeable valley width variations
[F]Valley Width in Context	1	narrower than previous section
	2	comparable width to previous section
	3	wider than previous section

Table A.3. Summary of the observed morphological parameters along the Biya based on 10 km stretches. Hydrological Information

	Section	River Kilometer		Tributaries*				Discharge (Q)**		
	Nr.	Start	End	Name(s)	orographic side(s)	Catchment Size	Length	Gauging Station	Q_{mean}	
	[-]	[km]	[km]	[-]	[-]	[km^2]	[km]	[-]	[m^3s^{-1}]	
upper Biya	1	0	10	Yurtok	right	?	17	Artybash	226.75	upper Biya
	2	10	20	Pyzha	left	1180	103			
	3	20	30	Kebezenka - Sarakoksha	right - left	? - 3150	16 - 90			
	4	30	40					Kebezen	246.86	
	5	40	50	Tula - stream without name	right - right	384 - ?	54 - 10			
	6	50	60	Bava	left	?	25			
	7	60	70	Tandoshka	right	209	42			
	8	70	80							
	9	80	90	Lebed'	right	4500	175	Turochak	323.83	
middle Biya	10	90	100	Alemchir - Polysh	right - left	? - ?	10 - 13			middle Biya
	11	100	110	Ulmen	right	?	48			
	12	110	120	Ushpa	right	214	24			
	13	120	130	Tibezya	left	?	39			
	14	130	140	Bol. Kuyut - Balyksa	right - left	223 - ?	33 - 31			
	15	140	150	Uchurga	right	?	24			
	16	150	160							
	17	160	170	Kutenek	left	?	14			
	18	170	180	Kozha	left	4210	63			
	19	180	190	Chapshushka	left	?	22			
	20	190	200							
lower Biya	21	200	210	Nenya	right	2210	185			lower Biya
	22	210	220	Souskanikha	left	?	17			
	23	220	230							
	24	230	240	Talitsa - Bekhtemir	left - right	? - 665	28 - 117			
	25	240	250							
	26	250	260							
	27	260	270							
	28	270	280							
	29	280	290					Biysk	476.36	
	30	290	300							

*Information from Russian Water Register: http://textual.ru/gvr/index.php?card=187196
**Data from Russia ArcticNET (Point IDs XXX as in body of text above):
https://www.r-arcticnet.sr.unh.edu/v4.0/ViewPoint.pl?View=ALL&Unit=ms&Point=XXXX

RESEARCH PAPER

TESTING BED LOAD TRANSPORT FORMULAS: A CASE STUDY OF THE LOWER AMUR BASED ON MULTI-BEAM ECHO-SOUNDERS (MBES) DATA

Olga A. Petrovskaya[1*], Andrey A. Maltsev[2]
[1]State Hydrological Institute, Saint-Petersburg, 199004, Russia
[2]Tyumengiprotruboprovod, Tyumen, 625003, Russia
***Corresponding author:** riverchannel@yandex.ru
Received: May 31st, 2022 / Accepted: November 11th, 2022 / Published: December 31st, 2022
https://DOI-10.24057/2071-9388-2022-097

ABSTRACT. The development of bed load calculation methods directly depends on the reliability of the measurement data. The most reliable measurement data remains the data obtained by the volumetric method when observing the filling of reservoirs, borrows, ditches etc. Nevertheless these data are the rarest. In this paper on the base of the data obtained when observing the process of filling of a ditch across the Amur River a comparison of a number of bed load calculation methods is performed. The observations were carried out with a multi-beam echo-sounder during summer floods of 2018, from 21st of July to 22nd of August. Over this time 5 surveys were performed, that allows to have 4 calculation periods for determining bed load yield. The total number of the measurements at different calculation verticals is 108. These data are used for verification of 80 bed load formulas. Four methodological approaches are considered: bed form approach, critical velocity approach, critical water discharge approach and regression approach. The bed form approach has shown the greatest accuracy: 17 formulas out of 26 gave the error less than 60%. For the other 56 methods which were considered only 5 formulas showed the error less than 60%, all of them correspond to the critical velocity approach.

KEYWORDS: bed load measurement, transverse ditch filling, bed load formula, bed load sediments, sediment transport, Amur

CITATION: Petrovskaya O. A., Maltsev A. A. (2022). Testing Bed Load Transport Formulas: A Case Study Of The Lower Amur Using Bed Load Yield Data Obtained With Multi-Beam Echo-Sounders (Mbes). Geography, Environment, Sustainability, 4(15), 214-221
https://DOI-10.24057/2071-9388-2022-097

ACKNOWLEDGEMENTS: The authors would like to thank the Chief Researcher of the Channel Processes Department of the State Hydrological Institute A.B. Klaven and the Leading Researchers V.M. Katolikov, and Z.D. Kopaliany for support and advices in the process of this work.

Conflict of interests: The authors reported no potential conflict of interest.

INTRODUCTION

Bed load transport is difficult to measure. Despite the active development and improvement of the alternative measurement methods bed load traps remain a widely used means of bed load measurement. The first traps appeared at the beginning of the 20th century, and a large number of their designs were proposed later. In 1954, basing on the analyses of the experience in the creation and use of bed load traps accumulated by that time, Shamov (1954) formulated the following conclusions:

• Bed load traps of all designs introduced into the flow radically change the natural structure of the flow, the channel morphology at the places of their installation and the mode of bed load transport.

• All the traps have some design disadvantages that as a rule do not provide a tight coupling of a trap with a bed, taking into account irregularities of river bed and presence of bed forms or cobbles. As a result the bed is washed out in front of the trap inlet, and the natural regime of bed load transport and conditions of sediment entry into the trap are violated.

• In flowing water at considerable depths, with flow velocities of more than 2-3 m/s and intensive bed load transport it is difficult to lower and install the trap on the bed. It drifts with the current.

• When using traps with a mesh bag, the size of the mesh cells affects the trap readings.

Other disadvantages were also mentioned. General conclusion made by Shamov is that "all bed load traps do not satisfy the main requirement that is imposed on them: reliability and accuracy for accounting of bed load".

After Shamov's (1954) generalization the activity of creating new designs of traps was limited in the USSR and there was a reorientation to the search of alternative measurement methods as for the conditions of lowland and mountain rivers.

In other countries the search of more advanced designs of the traps continued, but today we can state that none of Shamov's critical conclusions have been refuted or resolved by these studies.

In the 1960s studies of bed forms intensified and a method of measuring bed load in plain rivers via dunes characteristics progressed. This method was most actively developed in the USSR, where in the period of the 1960-1980s a significant number of measurements were carried out in large, medium and small plain rivers (Snischenko 1966; Korchokha 1968; Kulyomina 1968; Kapitonov et al. 1974; Bashkov et al. 1991). In the USSR and Russia the method is called "iterated lengthwise echo-sounding" (ILES), in English-language literature it is referred to as "bed form velocimetry method".

With the emergence of multi-beam echo-sounders (MBES) this method received a new impulse to development. Baranya and Muste (Muste et al. 2016; Kim et al. 2016) have developed the AMV-method (acoustic mapping velocimetry) that allows to get bed forms characteristics across the width of the river covered by echo-sounder. Abraham with colleagues (Abraham et al. 2015; Baranya et al. 2016; Abraham et al. 2018) have developed the ISSDOT-method (integrated section surface difference over time) which calculates bed load by comparing three-dimensional bed surfaces over consecutive timelines of echo-sounding bypassing the determination of height and velocity of dunes and operating directly with the volume of degradation/aggradation between the surveys.

Despite the prospects of measuring bed load by echo-sounders, the most reliable measurement data remains the data obtained by the volumetric method when observing the filling of reservoirs, borrows, ditches etc. Nevertheless these data are the rarest.

The development of bed load calculation methods directly depends on the reliability of the measurement data. Contrary to the imperfection of the bed load measurement method by traps, these data (along with laboratory data) most often serve as the basis for comparison and derivation of bed load formulas (Kiat et al. 2007; Bombar et al. 2010; Talukdar et al. 2012; Sirdari et al. 2014).

In 2011-2015 the State Hydrological Institute (SHI) carried out studies in which effectiveness of bed load formulas for large rivers was evaluated based on the data obtained by the iterated lengthwise echo-sounding method (Samokhvalova 2011; 2012; 2013; 2014; 2015a; 2015b).

In this paper a comparison of bed load calculation methods is performed on the base of the data obtained by the volumetric method when observing the process of filling of a ditch across the Amur River. The process of the ditch filling was monitored using MBES.

MATERIALS AND METHODS

The source data for this work were obtained during the construction of the reserve line of the Eastern Siberia – Pacific Ocean oil pipeline (ESPO-2) that crosses the Amur River.

This river crossing is located on the Lower Amur, 34 km lower Khabarovsk (Fig. 1). The width of the river in the crossing line at the design water level of 31.5 m of Baltic System of Heights (BS) is 2485 m, mean depth is 6.9 m, maximum depth is 15.9 m.

The Amur flows in the area of monsoon climate and is characterized by high water content during the all warm period of year and low water in winter. In winter the surface of the river is covered by ice. Snow-melt flood begins in March, reaches its peak in May and at the beginning of July rain floods start. In Fig. 2 there is a hydrograph of the Amur near Khabarovsk. Rain floods usually pass from July to September. There are about 3-5 rain floods on average. The highest water levels are observed in this period.

Such long and high floods combined with relatively fine sediments cause a high intensity of bed load transport during the warm period of year. At the considered reach the channel is braided and has a low and wide floodplain with plenty of branches and lakes (Fig. 3). During flooding of the floodplain the finest particles of suspended sediments settle on the floodplain and contribute to stability of many islands in a long-term period. Bed load transport in the river occurs in the form of bars. It causes significant vertical deformations of the channel. In particular from 1941 to 2008 the magnitude of fluctuation of bed elevation was 12 m.

All these circumstances make the pipe-laying by the channel-buried method undesirable. The directional drilling method would be more desirable, but due to the

Fig. 1. The ESPO-2 crossing through the Amur

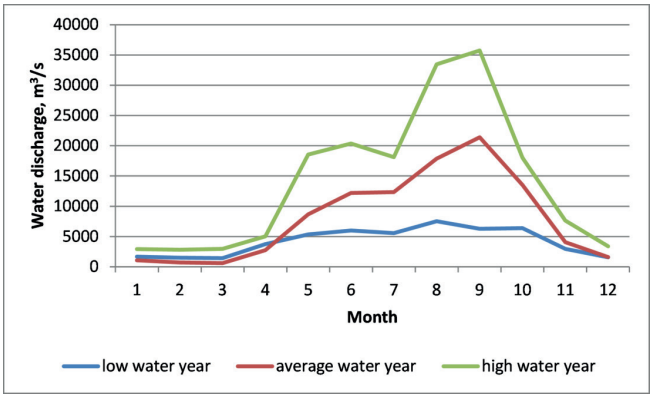

Fig. 2. Hydrograph of the Amur near Khabarovsk

Fig. 3. The ESPO-2 crossing through the Amur on the satellite image

large width of the river it couldn't be implemented. That is why the channel-buried method was chosen.

Due to the fact that in the low water period the surface of the river is covered with ice, the construction works were carried out in the high water period.

In summer 2018 the ditch digging started, but soon the work had to be paused due to high water levels and intensive bed load transport. This circumstance was used for observing of the ditch filling. The observation was carried out in the period from 21st of July to 22nd of August.

The measurements of the ditch filling were carried out by MBES SeaBat T20-R (number of beams 10-1024, swath coverage 165°, depth resolution 6 mm, teledyne INS (heading) 0.015°, teledyne INS (true heave) 2 sm). 5 echo surveys were performed in total: 21st and 27th of July, 1st, 7th and 22nd of August, 2018. Riverbed profiles were plotted for every calculation section of the ditch for each date (Fig. 4).

According to the governing document of the State Hydrological Institute that regulates accounting for channel deformations in construction of pipeline crossings across rivers[1], when width of ditch is significantly larger than length of eddy zone, volume of suspended sediments in total volume of sediments deposited in the ditch is 3-10%. Due to the large width of the Amur River the trenching was stretched out in time, and timelines of the ditch completion were different at different sites. The echo-sounding was carried out on certain dates, so the available profiles register intermediate states of the ditch.

In view of the absence of the ditch profiles fixing its configuration before the beginning of irreversible filling to apply the recommendation of the SHI Standard for evaluation of the part of suspended sediments in the aggradation formed during the calculation period is problematic. There is also no data on suspended load at the study reach of the river for the period of trenching. However due to the fact that the ditch filling occurred in the period of floods, and flow velocities were quite high, and mean concentration of suspended load near Khabarovsk is pretty low and equals 90 g/m^3 (Makhinova et al. 2018), in this work we assume that the ditch was filled only by bed load. The area of aggradation formed between the adjacent echo surveys was assumed to be equal to bed load yield for this period.

Bed load yield measurements were performed for 4 periods (Table 1). The total number of the measurements at different verticals over this time is 108, the total number of the verticals is 32. The location of the measurement verticals is shown in Fig. 5.

These data have been used for verification of bed load formulas. In this work we have tested only a part of methodological approaches, in particular

- bed form approach ($q_b=f(h_D,C_D)$), where h_D – dune height, m, C_D – dune velocity, m/s),
- critical velocity approach ($q_b=f(V_0)$),
- critical water discharge approach ($q_b=f(q_0)$),
- regression approach.

In the first case different combinations of formulas for height and velocity of dunes are considered and calculations are performed using a general formula $q_b=0.6h_DC_D$, where q_b – bed load discharge in bulk volume, m^3/(s·m), 0.6 – dune form coefficient.

80 bed load formulas and their modifications have been tested in total, 26 of them are based on the first methodological approach.

Calculations of bed load discharge and yield have been performed for the verticals of the ditch line for which we have aggradation profiles for the considered period.

Flow characteristics required for the calculations have been taken from a gauge located 120 m upstream from the ditch line. On the 2nd of August there were performed measurements of velocity and depth of flow.

During the all period from 21st of July to 22nd of August water level measurements were being carried out at the gauge section (Fig. 6). Values of flow velocity V for every water level are calculated by the Chezy formula $V=C\sqrt{HI}$, where C – the Chezy coefficient, H – depth of flow, m,

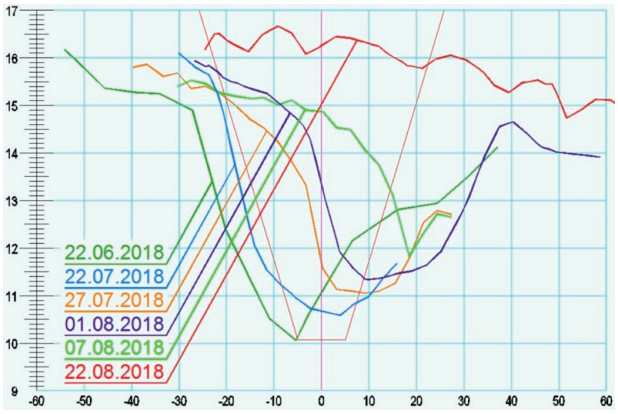

Fig. 4. Steps of the ditch filling

Fig. 5. Location of the measurement verticals

Table 1. Timing and number of bed load yield measurements

Period	Number of days	Number of verticals
from 21st to 27th of July	6	27
from 27th of July to 1st of August	5	28
from 1st to 7th of August	6	31
from 7th to 22nd of August	15	22

[1]Accounting for channel process at river crossings of pipelines: STO SI SHI 08.29-2009, 2009, 175 p.

I – slope, $C=\frac{1}{n}H^{\frac{1}{6}}$, n – roughness coefficient. Roughness coefficients are taken constant for every vertical. Slope is also assumed to be constant and equal to 0.000064. The calculated values of hydraulic characteristics vary within the following limits: 2.58≤H≤16.53 m, 0.49≤V1.48 m/s, the Froude number $0.08 \le Fr = \frac{V}{\sqrt{gH}} \le 0.17$,

where g – gravitational acceleration, m/s^2.

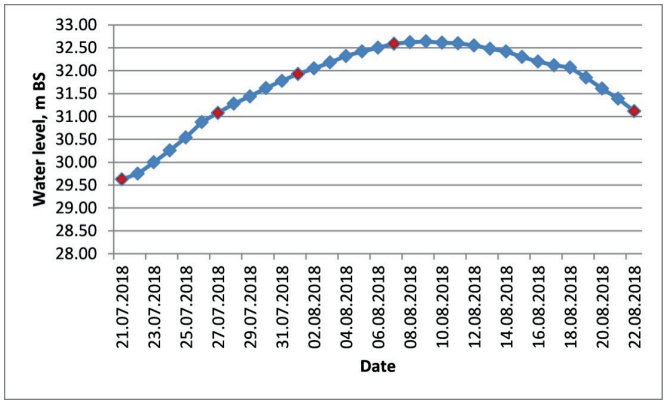

Fig. 6. Graph of water level for the period from 21st of July to 22nd of August (the dates of echo-sounding are highlighted in red)

During these measurements bed sediments were not sampled, but on the other hand an extensive geological examination was performed. As a result of this survey 3 homogeneous geological complexes (HGC) were identified on the river bed. For these complexes averaged particle size distribution curves were calculated. We compared these 3 curves with the curves of bed sediments sampled on this site in 2016 and they appeared to be close (Fig. 7). That is why for our calculations we use these 3 averaged curves. The main parameters of the particle size distribution curves are given in Table 2.

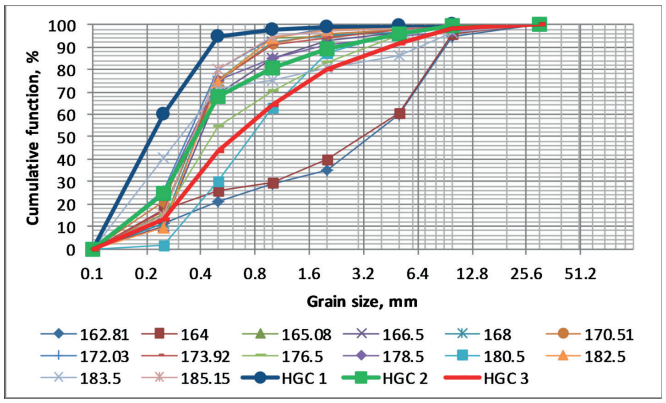

Fig. 7. Particle size distribution curves of bed sediments at different verticals in the crossing line (according to 2016 data) in comparison with the distribution curves of the homogeneous geological complexes identified on the river bed

Flow depth, flow velocity and corresponding bed load discharge in m^3/s/m (by each of the analyzed formulas) are calculated for each average daily level. The resulting bed load discharge is multiplied by the number of seconds in a day (86400) and thus bed load yield per day is obtained. The sum of daily bed load yield values for the considered period is compared with the corresponding value of aggradation. Calculation error is evaluated by the formula

$$\Delta = \frac{\left| Q_{b\,calc} - Q_{b\,meas} \right|}{Q_{b\,meas}} 100\,\%$$

where $Q_{b_{calc}}$ and $Q_{b_{meas}}$ – calculated and measured bed load yield accordingly.

RESULTS AND DISCUSSION

Bed form approach has shown the best result: out of 26 formulas 13 have given the error lower than 50% and 4 more formulas the error less than 60%. Out of 54 other considered methods only 5 formulas have given the error lower than 60%, all of them belong to the critical velocity approach. Expressions of the dune height and velocity formulas which in combination with each other have shown best results are given in tables 3-4. Table 5 contains expressions other bed load formulas (not taking into account dune characteristics) with best results. Table 6 shows mean calculation errors of these formulas. Almost all the formulas except certain specified cases use critical (permissible) velocity V_0, m/s, by V.N. Goncharov (1938)

$$V_0 = 0.96\sqrt{g}H^{0.2}(d+0.0014)^{0.3} \quad (1)$$

Formulas 1-7, 9-11 and 21 have confirmed their effectiveness for large plain rivers identified earlier in studies based on the data obtained by the iterated lengthwise echo-sounding method (Samokhvalova 2012; 2014; 2015a; 2015b). In those studies the total number of bed load measurements was 105, and main hydraulic characteristics of the large rivers varied as follows: 2.90≤H≤13.7 m, 0.72≤V≤2.1 m/s, Fr<0.2, 0.3≤d≤2.9 mm. From the comparison of these hydraulic characteristics with the hydraulic characteristics of the data used in this work it follows that they are very close. Consequently formulas 1-7, 9-11 and 21 can be recommended with greater confidence for bed load calculations in large rivers in the described range of the main hydraulic characteristics. And the circumstance that approximately the same formulas give good results for the both measurement methods implicitly indicates, among other points, the effectiveness of measuring bed load by the ILES method.

CONCLUSION

During the construction of the reserve line of the ESPO-2 oil pipeline across the Amur unique data on bed load transport in a large river were obtained by monitoring the process of the natural ditch filling by MBES.

Table 2. The main parameters of the particle size distribution curves of the homogeneous geological complexes identified on the river bed in the crossing line

Sample	d, mm	d_{50}, mm	d_{90}, mm
HGC 1	0.35	0.25	0.45
HGC 2	1.1	0.40	2.3
HGC 3	1.8	0.65	4.6

Note: d – weighted average diameter, d_{50} – median diameter, d_{90} – particle size for which 90% of the sample is finer.

Table 3. Dune height (h_D, *m*) formulas that showed the least error in bed load calculations

Author	Formula
Kudryashov (1958)	$h_D = d\frac{25.91\left(\frac{V^2}{gH} - 0.251\right)^2 + 1.08}{\left(\frac{V^2}{gH} + 0.07\right)^2}$
Go-Zhen (1960)	$h_D = 0.75\frac{\omega}{0.8V_0}H$
Snischenko (1980)	$h_D = 0.25H \text{ when } H \le 1$ $h_D = 0.2 + 0.1H \text{ when } H > 1$
Kopaliani (1989) (Kopaliani & Gendelman 1989)	$h_D = 0.39d\left(\frac{V}{V_0}\right)^{2.5} Fr^{-3.75}$
Snischenko, Kopaliani (1989) (Kopaliani & Gendelman 1989)	$h_D = 2.1\frac{d}{Fr^{4.1}}\left(\frac{V - V_0}{V_0}\right)^{1.4}$
Noselidze (1992)	$h_D = H\left(0.07\frac{V}{V_0} + 0.02\right)$
Kostyuchenko, Kopaliani (2006)	$h_D = 0.13H$
Samokhvalova (2011)	$h_D = 0.11H$

Note: ω – mean of absolute values of pulsation velocity components, m/s.

Table 4. Dune velocity (C_D, *m/s*) formulas that showed the least error in bed load calculations

Author	Formula
Kudryashov (1958)	$C_D = 0.00788\frac{V^4}{H^{\frac{5}{4}} g^{\frac{3}{2}} d^{\frac{1}{4}}} \text{ when } Fr^2 \le 1$ $C_D = \sqrt[3]{\frac{Igd^2}{H}} - 2.84\frac{gd}{V} \text{ when } Fr^2 \ge 1$
Go-Zhen (1960)	$C_D = 0.26\frac{d}{H}\left(V - 0.8V_0\right)\frac{V^2}{\left(0.8V_0\right)^2}$
Snischenko, Kopaliani, Tvalavadze (1977)	$C_D = 0.032\left(V - V_0\right)\frac{V}{V_0}\left(\frac{d}{h_D}\right)^{0.7}$
Snischenko, Kopaliani (1978)	$C_D = 0.019VFr^{2.9}$
Kopaliani (1989) (Kopaliani & Gendelman 1989)	$C_D = 0.009V\left(\frac{V}{V_0}\right)^2\left(\frac{h_D}{d}\right)^{-0.8}$

Table 5. Bed load formulas that showed the least error

Author	Formula
Shamov (1952)	$q_b=\alpha\sqrt[3]{\overline{d_{max}}^2}\left(\frac{V}{V_0}\right)^3\left(V-V_0\right)\left(\frac{d}{H}\right)^{0.25},\ kg/(s\cdot m)$ α=3, if the largest fraction in the sediment composition is 40-70% of sample weight, α=2.5 – 20-40% or 70-80%, α=1.5 – 10-20% or 80-90% $V_0=3.83\left(\frac{d_{50}}{d_{90}}\right)^{0.2}d^{\frac{1}{3}}H^{\frac{1}{6}},\ m/s$
Goncharov (1962)	$1.\ q_b=\frac{(1+\varphi)}{800}dV_0\left(\frac{V^3}{V_0^3}-1\right)\left(\frac{V}{V_0}-1\right),\ m^3/(s\cdot m)$ $2.\ q_b=1.2(1+\varphi)dV_0\left(\frac{V}{V_0}\right)^{4.33},\ kg/(s\cdot m)$ $V_0=Ig\frac{8.8H}{d_5}\sqrt{\frac{2g\left(\gamma_s-\gamma\right)d}{3.5\gamma}},\ m/s$ when d = 0.15-0.5 mm, φ = 2.25, when d = 0.5-1.5 mm φ =1.23, when d >1.5 mm φ = 1.0.
Grishanin (1969)	$q_b=0.015\left(\frac{V}{V_0}\right)^3d\left(V-V_0\right),\ m^3/(s\cdot m)$
Butakov (1998)	$q_b=0.07\left(\frac{v}{\sqrt{g}}\right)^{\frac{1}{3}}\sqrt{d}V_0\left(\frac{V}{V_0}\right)^3,\ m^3/(s\cdot m)$ $V_0=1.25\sqrt{gd}Ig\frac{8.8H}{d},\ m/s$

Note: α – a coefficient, $\overline{d_{max}}$ – average diameter of the largest sediment fraction which is at least 10% of the composition of the mobile part of bed sediments, m, φ – turbulence parameter, d_5 – diameter of the largest particles which share is 5%, m (accepted equal to d_{95}), γ – specific weight of water, N/m^3, γ_S – specific weight of sediment particles, N/m^3, v – kinematic viscosity coefficient, m^2/s.

Table 6. Error of bed load calculations according to the most accurate formulas

№	Author		Mean error, %
	h_D formulas	C_D formulas	
1	Go-Zhen		45
2	Kudryashov		44
3	Kopaliani		37
4	Kostyuchenko, Kopaliani	Kopaliani	33
5	Samokhvalova	"	33
6	Snischenko	"	33
7	Snischenko, Kopaliani	"	39
8	Noselidze	"	34
9	Kopaliani	Snischenko, Kopaliani	49
10	Kostyuchenko, Kopaliani	"	49
11	Samokhvalova	"	56
12	Snischenko	"	49

13	Noselidze	"	49
14	Kostyuchenko, Kopaliani	Snischenko, Kopaliani, Tvalavadze	51
15	Samokhvalova	"	47
16	Snischenko	"	51
17	Noselidze	"	52
	q_b formulas		
18	Butakov		56
19	Goncharov (1)		38
20	Goncharov (2)		38
21	Grishanin		50
22	Shamov		40

Based on these data a verification of 80 bed load formulas has been performed. Among the considered approaches to bed load calculation (bed form approach, critical velocity approach, critical water discharge approach and regression approach) the bed form approach showed the highest productivity.

11 formulas that previously showed a positive result for the conditions of large plain rivers when tested on the data obtained by the iterated lengthwise echo-sounding method confirmed their effectiveness. They can be recommended with greater confidence for practice in conditions when the Froude number is less than 0.2, flow depth is 2.6-16.5 m, flow velocity is 0.5-2.1 m/s, slope is 0.000064-0.000195 and average particle size of bed sediments is 0.3-2.9 mm.

The fact that approximately the same formulas give good results both for the volumetric method presented in this paper and for the iterated lengthwise echo-sounding method, which was used for testing bed load formulas earlier, implicitly indicates the reliability of measuring of bed load transport by iterated lengthwise echo-sounding.

REFERENCES

Abraham D., McAlpin T., Jones K. (2018). Bed-load measurements on large, sand-bed rivers in the United States. Proc. of the River Flow, 2018, DOI: 10.1051/e3sconf/20184006021.

Abraham D., McAlpin T., May D., Pratt T., Shelley J. (2015). Update on ISSDOTv2 method for measuring bed-load transport with time sequenced bathymetric data. Proc. of the 10th Federal Interagency Sedimentation Conference (April 2015, Reno, Nevada, USA).

Baranya S., Muste M. Abraham D., Pratt T. (2016). Acoustic mapping velocimetry (AMV) for in-situ bedload transport estimation. Proc. of the River Flow, 2016, 1577-1584.

Bashkov A., Kopaliani Z., Snischenko B. (1991). Problems of channel process of small rivers. Reports of the Section of Channel Processes, Water Resources and Water Balance GKNT USSR, 2, 127-141 (in Russian).

Bombar G., Guney M. (2010). Experimental investigation of sediment transport in steady flows. Scientific Research and Essays, 5(6), 582-591.

Butakov A. (1998). Substantiation of a bed load formula by the method of comparative analyses. Transactions of the Academy of Water Management Sciences, 5, 225-238 (in Russian).

Goncharov V. (1962). Stream flow dynamics. Leningrad, Gidrometeoizdat, 274. (in Russian).

Go-Zhen D. (1960) Sediment movement and stability of streams bed: Author's Abstract of Doct. Sci. (Tech.) Diss., Leningrad, 38 p. (in Russian).

Grishanin K. (1969). Stream flow dynamics. Leningrad, Gidrometeoizdat, 428. (in Russian).

Kapitonov N., Karaushev A., Razumikhina K. (1974). Study of bed load transport in tail-bays of hydro power plants. Transactions of the State Hydrological Institute, 120, 98-112 (in Russian).

Kiat C., Ghani A., Wen L. (2007) Development of modified Einstein bed-load equation for sandy stream in Malaysia. Proc. 2nd International Conference on Managing Rivers in the 21st Century: Solutions Towards Sustainable River Basins: Rivers'07 (Riverside Kuching, Sarawak, Malaysia, June 6-8, 2007), 533-538.

Kim D., Ho H., Baranya S., Muste M. (2016) Qualitative and quantitative acoustic mapping of bedform dynamics. Flow Measurements and Instrumentation, 50, 80-89.

Kopaliani Z., Gendelman M. (1989). Channel process and hydraulic resistances. In: Problems of Contemporary Hydrology. Leningrad, Gidrometeoizdat, 288-304 (in Russian).

Kudryashov A. (1958) An experience of studying the regularities of channel processes on mobile-scale models: Author's Abstract of Cand. Sci. (Tech.) Diss., Leningrad, 14 p. (in Russian).

Korchokha Yu. (1968). Study of the dune form of bed load transport on the Polomet' River. Transactions of the State Hydrological Institute, 161, 98-119 (in Russian).

Kostyuchenko A., Kopaliani Z. (2006). Peculiarities of the process and yield of bed load in small rivers. Reports of the 6th All-Russian Hydrological Congress, section 6, 44-49 (in Russian).

Kulemina N. (1968). On the field study of channel process in snow-melt flood. Transactions of the State Hydrological Institute, 147, 52-68 (in Russian).

Makhinova A., Makhinov A., Shuguan L. (2018). The impact of floods on the geochemistry of flood plain landscapes in the river valleys of East Asia (on the examples of the Amur and Yangtze Rivers). Materials of the International Conference "Third Landscape-Ecological Readings "Landscape Geography in the 21st century" dedicated to the 100th anniversary of the birth of G.E. Grishankov" (Simferopol, Russia, September 2018), 115-118 (in Russian).

Muste M., Baranya S., Tsubaki R., Kim D., Ho H., Tsai H., Law D. (2016). Acoustic mapping velocimetry. Water Resources Research, 52, 4132-4150, DOI: 10.1002/2015WR018354.

Noselidze D. (1992) Laboratory studies of structural bed load transport and regulation of channel process at bridge crossings of piedmont rivers: Author's Abstract of Cand. Sci. (Tech.) Diss., Tbilisi, 23 p. (in Russian).

Samokhvalova O. (2011). Calculation of sand dunes height in large and small plain rivers. Vestnik SPBU, ser. 7, 4, 135-148 (in Russian with English summary).

Samokhvalova O. (2012) Bed load assessment in plain rivers. Proc. of the Conference «Contemporary hydrological issues in the research of Polish and Russian MSc and PhD students» (Torun, Poland, 2012), 91-103.

Samokhvalova O. (2013). Calculation of sand dunes velocity in plain rivers. Waterways and Channel Processes, 1, 182-200 (in Russian).

Samokhvalova O. (2014). Selective methodology of bedload discharge calculations in rivers. Proc. of the International scientific conference «Deltas: genesis, dynamics, modeling and sustainable development» (Istomino, Republic of Buryatia, Russian Federation, 2014), 39-44.

Samokhvalova O. (2015a). On the calculation of bed load discharge in large and small plain rivers. Proc. of the 5th International Scientific and Technical Conference "Contemporary Problems of Water Management, Environmental Conservation, Architecture and Civil Engineering" (Tbilisi, Georgia, 2015), 224-234 (in Russian).

Samokhvalova O. (2015b). Calculation of bed load discharge in large and small plain rivers when transport occurs in the form of dunes. Waterways and Channel Processes, 2, 162-177 (in Russian).

Shamov G. (1952). Formulas for permissible velocity and bed load discharge. Transactions of the State Hydrological Institute, 36 (90), 3-17 (in Russian).

Shamov G. (1954). River sedimentation. Leningrad, Gidrometeoizdat, 378. (in Russian).

Sirdari Z., Ghani A., Hassan Z. (2014). Bedload transport of small rivers in Malaysia. International Journal of Sediment Research, 29, 481-490.

Snischenko B. (1966). Movement of sand dunes in natural water flows. Transactions of the State Hydrological Institute, 136, 82-91 (in Russian).

Snischenko B. (1980). On the relationship of sand dunes height with parameters of river flow and channel. Meteorology and Hydrology, 6, 84-91 (in Russian).

Snischenko B., Kopaliani Z. (1978). On the velocity of dunes in rivers and laboratory conditions. Transactions of the State Hydrological Institute, 252, 20-37 (in Russian).

Snischenko B., Kopaliani Z., Tvalavadze O. (1977). On the time scale of channel deformations in mobile-scale modelling of river channels. Transactions of the State Hydrological Institute, 242, 55-60 (in Russian).

Talukdar S., Kumar B., Dutta S. (2012). Predictive capability of bedload equations using flume data. Journal of Hydrology and Hydromechanics, 60(1), 45-56.

RESEARCH PAPER

CONTRIBUTION OF THE DIFFERENT SOURCES TO THE FORMATION OF ALLUVIAL SEDIMENTS IN THE SELENGA RIVER DELTA (EASTERN SIBERIA, RUSSIA)

Ellina D. Zaharova[1]* and Vladimir R. Belyaev[2]

[1]Institute of Geography, Russian Academy of Sciences, 1st Khvostov Lane, 119017, Moscow, Russia

[2]Lomonosov Moscow State University, Leninskiye Gory, 119899, Moscow, Russia

***Corresponding author:** ellina1997zahar@gmail.com

Received: June 3rd, 2022 / Accepted: November 11th, 2022 / Published: December 31st, 2022

https://DOI-10.24057/2071-9388-2022-098

ABSTRACT. Unraveling sources of sediment supply, their temporal and spatial variability is of key importance to determine origin of deposits and to explore the formation mechanism of Selenga Delta landscape units. From an environmental point of view this solution would help to identify the particle-bound pollution sources. We used geochemical fingerprinting (the FingerPro R package), which is a modern quantitative implementation of the method of sedimentary provenance analysis. The main aim was to recognize the main patterns of sediment and associated particle-bound pollutants transport and deposition within the delta. At the old floodplain from 55% to 90% of sediments were delivered from the eroded floodplain and terrace banks upstream and only about 10-15% originates from the remote basin sources. Sedimentary environment in the Khlystov Zaton reveals a greater variety than on the floodplains. 40% of sediments from the upper 5 cm-layer originated from the flood, taking place in 2013, and 30% were the product of floodplain and terraces banks erosion. Nevertheless, analysis of the fine-grained component of suspended sediment sets the material from eroded floodplain banks as the dominant source of accumulation within the delta. This means that the self-absorption is the leading process in the Selenga delta at the moment. Heavy metals and metalloids accumulates in the lower reaches of the Selenga on the floodplain surface, deltaic lakes and oxbows during high floods. Runoff decrease during floods can lead to the release of pollutants into the Lake Baikal.

KEYWORDS: suspended sediment, sediment sources, sediment traps, fingerprinting, Selenga River delta

CITATION: Zaharova E. D., Belyaev V. R. (2022). Contribution Of The Different Sources To The Formation Of Alluvial Sediments In The Selenga River Delta. (Eastern Siberia, Russia). Geography, Environment, Sustainability, 4(15), 222-231
https://DOI-10.24057/2071-9388-2022-098

ACKNOWLEDGEMENTS: The investigation is financially supported by the Russian Geographical Society agreement No. RGO-RFBR 23/2017 «Geochemical barrier zones in freshwater river deltas of Russia». Additional funding was obtained from the he State Task no. FMGE-2019-0005, Institute of Geography RAS, for Ellina Zaharova, State Tasks 1.13 no. 121051100166-4 and I.2 no. 121040100323-5, Faculty of Geography MSU, for Vladimir Belyaev. Authors thanks all members of the Faculty of Geography of LMSU who participated in the field studies or performed analytical work. In addition, we gratefully acknowledge the support of information from M.V.Pavlov and E.A. Illycheva, hydromorpholithogenesis of Selenga river delta expedition leaders, and S.R.Chalov and M.Yu.Lychagin, geochemical barrier zones in freshwater river deltas of Russia project members.

Conflict of interests: The authors reported no potential conflict of interest.

INTRODUCTION

River deltas and estuaries are specific natural geographic objects at locations of river junctions with the receiving waterbody. Deltaic and estuarine geomorphic systems are formed by complex interaction of fluvial (including water and sediment runoff) coastal (waves, changes in the level of the receiving waterbody and surging) and, often, some other (aeolian, biogenic) processes. Such a complex nature and location within the most dynamic contact zone between lithosphere, hydrosphere and atmosphere determines distinctive morphodynamic features of these systems. The Selenga River delta occupies a unique position among all other river deltas, since it is the world's only fluvially dominated river delta formed at the confluence of the Selenga River with the ultra-fresh Baikal Lake (Hume & Herdendorf 1988).

The Selenga River delta region has been studied for nearly a hundred years. Since 2011, scientific research group from V.B.Sochava Institute of Geography SB RAS led by E.A. Ilicheva and M.V. Pavlov concentrated on the delta morphodynamics focusing mostly on the recent transformations of the subaerial deltaic surface. That group employed high-resolution remote sensing (RS) data (spring, 2011) and results of 2003–2013 fieldworks, including repeated geodetic leveling surveys (Ilicheva et al. 2015). Main results describe lateral shifts of the deltaic arms and branches and sedimentation rates at various geomorphic positions. For example, accumulation in the upper section of the Sorokoustnaya arm corresponds to about 1.0-1.5 m since 1986. However, previous study about sedimentation on the deltaic floodplain and oxbow lakes requires further research (Ilicheva et al. 2020).

Suspended sediment provenance data is important for the examination of sediment delivery and construction of catchment sediment budgets (Walling et al. 1984). FingerPro unmixing model allows to reveal potential sediment sources in drainage basins using a number of diagnostic physical or chemical characteristics of sediments (Lizaga et al. 2018). Each source has its own geochemical "fingerprint"- the ratio of heavy metals concentrations or other numeric parameters describing certain characteristics of fine-grained sediment fractions. It can be preliminary suggested that the main sources of floodplain, pools and oxbow lakes deposition include sediment delivery from the large drainage basin of upper and middle Selenga (watersheds and soil downslope washout), as well as bank erosion of sandy deposits of the Late-Pleistocene terraces and old floodplain, located in the lower reaches. Bank erosion sources, situated immediately upstream from the delta apex, have their own individual geochemical fingerprints, depending on the type of eroded material. Suspended sediments coming from basin sources are represented by mixture in which contribution of each individual source cannot be distinguished due to long travel distances and times similar to each other.

The main natural factors influencing the Selenga delta are fluctuations of the Baikal Lake water level, main river hydrological regime and the local landscape characteristics. The sources of suspended load include bank erosion in the main river lower reach, drainage area surface erosion and upstream channel erosion (Potemkina et al. 2019). The tentative hypothesis of this study states that the basin source prevails over others in contribution to sedimentation traps due to the widespread anthropogenic influence throughout the catchment (cultivation, grazing and mineral resources exploration), which enhances fluvial processes including soil, gully and river channel erosion (Bazhenova et al. 1979). However, there are certain facts possibly indicating the opposite. For example, a relatively large river basin with predominantly fine-grained deposits transported through the network of smaller rivers before reaching the main river (it can significantly decrease sediment delivery ratios due to downstream increase of sediment trap efficiency of floodplains) and extensive bank erosion in lower reaches of the main river. Thus, even for deltaic facies, we may observe the predominance of the bank source.

We have employed the fingerprinting approach to establish the ratio of different sediment sources within the heavily polluted drainage basin (i.e. Selenga tributaries catchments and bank source: floodplain and terraces erosion in the lower reaches).

MATERIALS

The Selenga River delta is a large (>600 km^2) fluvially dominated river delta formed on the southeast margin of Lake Baikal. Fluvially-dominated deltas are primarily controlled by the water density difference between the inflowing river water and the standing water on the basin. Located in southern Siberia both the Selenga delta and its basin have a continental semi-arid climate.

Modern delta of the Selenga is situated within the territory bound by the villages of Zhilino, Istomino and Dubinino. The deltaic area consists of two geomorphologically distinct zones, one of which is dominated by the limnic regime and waterlogged landscapes - wetlands, and the other (upper part of the delta) by fluvial conditions (Fig. 1). The annual runoff distribution in the lower reaches is nonuniform. Results of the V.B.Sochava Institute of Geography SB RAS field studies allowed to divide the Selenga River delta into three distinctively different sectors: Selenginskiy, Sredneystevoy and Lobanovskiy, basing on specific features of their morphodynamic regimes (Pavlov et al. 2016).

There are three generations of the deltaic floodplain that can be distinguished on a basis of altitude difference and resulting differences of vegetation communities and sedimentary composition. These will be further referred to as old, middleage and seasonal floodplain levels (Fig. 1). The old floodplain occupies the largest areas of the upper delta, its true altitude is about 460-458 meters (Illycheva et al. 2015).

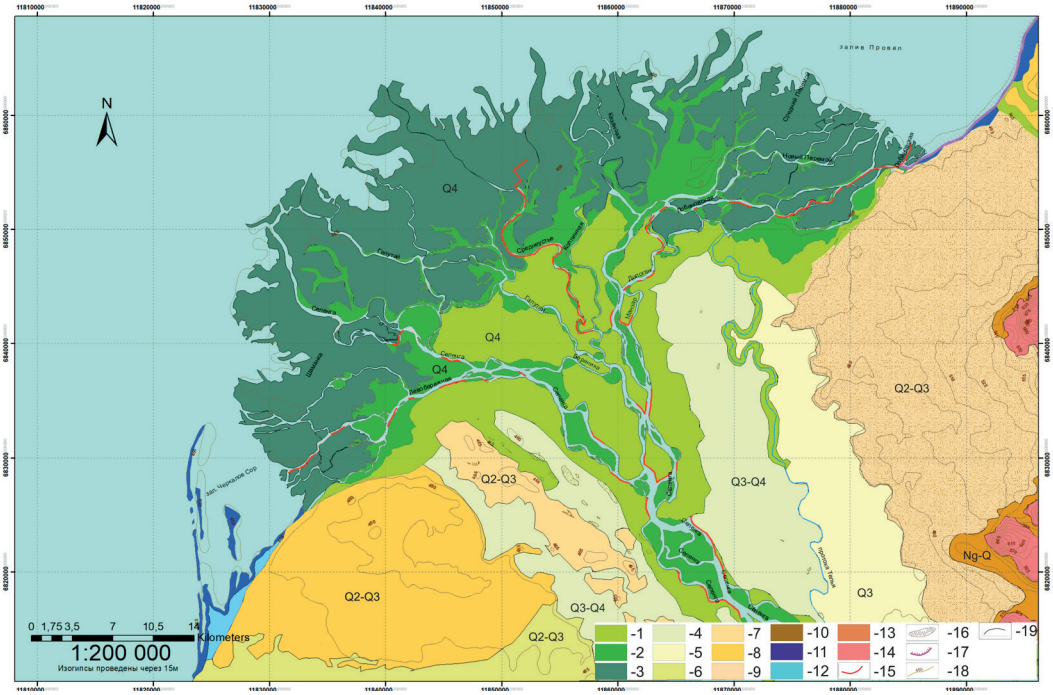

Fig. 1. Geomorphological scheme of the Selenga River Delta (compiled by the author using the following materials: (Budaev and Kolomiets 2014)

Limno/fluvial environments
Flood basins

1-old floodplain 460-458 m. (Q4)
2-middleage floodplain 458-456 m. (Q4)
3-seasonal floodplain 456-454 m. (Q4)
4-Kabansk alluvial terrace 465-460 m. (Q3-Q4)
5-Kudara alluvial terrace (Q3)
6-Terrace formation III (Q3)
7-Terrace formation IV (Q2-Q3)
8-Terrace formation V (Q2-Q3)
9-Terrace formation VI (Q2-Q3)

Systems of seasonally fills

10-Seasonally fills bed and floodplain (Q4)

Baikal basins

11-Lower lake terrace (Q4)
12-Upper lake terrace (Q3-Q4)

Areas dominated by complex tectonic-denudation and denudation topography

13- Piedmonts with low-gradient slopes covered by thin colluvial mantle
14- Dissected low-elevation mountains with moderate to steep slopes

Other landforms

15- Riverbank erosion
16-Sand dunes
17-Ledge associated with seismic fault

Other symbols

18-15 m isohypses
19-Landforms boundary

The middleage floodplain is distributed mainly along the largest arms (Selenginskaya, Levoberezhnaya) and on islands formed by smaller deltaic branches. Geomorphic boundary between the seasonal and middleage floodplains is rather poorly defined. During the fieldwork in 2019-2020 years, the middleage floodplain was completely flooded from 06.08.2019 to 09.08.2019 and from 31.07.2020 to 28.08.2020. The surface of the seasonal floodplain is hidden under water for most of the flood period and appears above the water level only during low levels. In the upper part of the delta, seasonal floodplain is in most cases represented by a narrow strip along the deltaic channels. The width of seasonal floodplain segments rarely exceeds several meters.

METHODS

Three essential geomorphological positions were selected to assess the nature and dynamics of sedimentation in different deltaic zones: the old floodplain surface and the oxbow lake. Data from analysis of the suspended sediment samples collected during the period of 2011-2016 from the Selenga tributaries were used as a prototype of the basin sources (Chalov et al. 2017). The 2013 year fieldwork- end of the flood period (8-20 September), 2011 year fieldwork – summer floods (8-19 August), 2014 year -low water period (4-19 August) and 2016 year – summer-autumn flood (11-30 August) (Fig. 2) (Kasimov et al. 2020; Lychagin et al. 2017; Kasimov et al. 2019).

The bank sources and sediment traps materials were collected at the lower reaches of Selenga river during the 2019-2020 summer expeditions (between 28th of July and 18th of August). Overall, data used in this study were obtained from 19 samples of fresh spring flood deposits from sediment traps, 27 samples from oxbow lake column, 162 suspended sediment samples from the upstream Selenga river (that we consider as a basin source), 68 samples of floodplain and terrace sediments (selected as a channel source) taken throughout the Selenga basin, including the Mongolian part. The samples were mainly taken from the zones of the old floodplain, the terrace and the oxbow lake Khlystov Zaton. The Khlystov Zaton oxbow lake is located in the backarc of a old floodplain at an absolute height of 458.9 m (according to the differential GNSS survey). It remains isolated during the low-water periods, depth ranges from 1 to 2 m (Pavlov 2019).

To assess the accuracy and reliability of the results obtained in this study, we distinguish several floodplain levels characterized by certain elevation intervals and evaluate the sediment contribution from different floodplain parts into fresh sedimentation throughout the delta. Floodplain elevation based on the detailed differential GNSS survey profiles.

Most of the suspended sediment load of the Selenga gets transported during a few high peak discharge flood events. Samples collected in 2011 (low level of water) describe heavy metals composition during low water discharge (Kasimov et al. 2020).

Layer-by-layer samples taken from high floodplains and terraces provide insight into the entire thickness of the eroded banks and contain information for assessment of a potential dispersion of sediment sources. Additional depth-incremental sampling was conducted with 5-cm intervals and 10x10 cm^2 area, total depth reaching down to 60–70 cm. The samples collected from the floodplains and terraces upstream the first bifurcation of the Selenga River delta apex were accounted as the channel source. When channel banks are being eroded dominantly sandy material gets transported into the main channel arms and accumulates on the deltaic surface.

The sediment samples of fresh floods, represented as sediment traps, were collected throughout the delta, in the

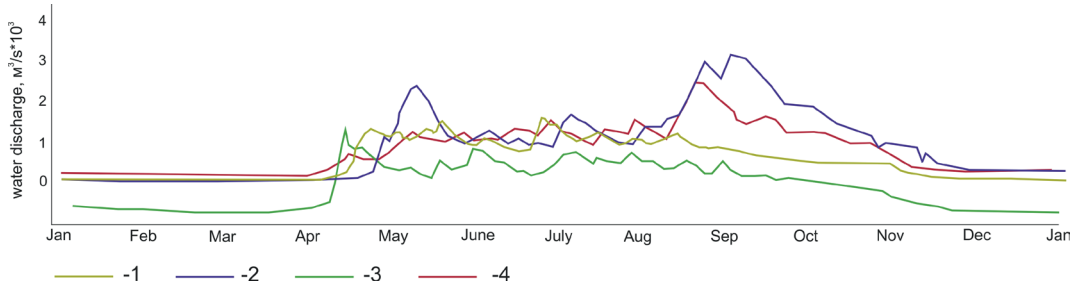

Fig. 2. Daily mean discharges of the Selenga (Kabansk) 1-2011; 2-2013; 3-2014; 4-2016 (gis.vodinfo.ru)

middle and upper course of the Selenginskiy, Sredneystevoy and Lobanovskiy sectors (Fig. 3). The sampling points were eventually selected at the same level as the corresponding old floodplain.

The grain size fractions were separated using the fractionation method by Kachinski (1931). Graph of the nature of hydrodynamics conditions was built on the basis of the dependence of deposits' average diameter from its standard deviation of deposits size. The weighted mean diameter of transported particles varies from fine sand to gravel, depending on the phase of the hydrological regime. Samples from sedimentation traps were matched to

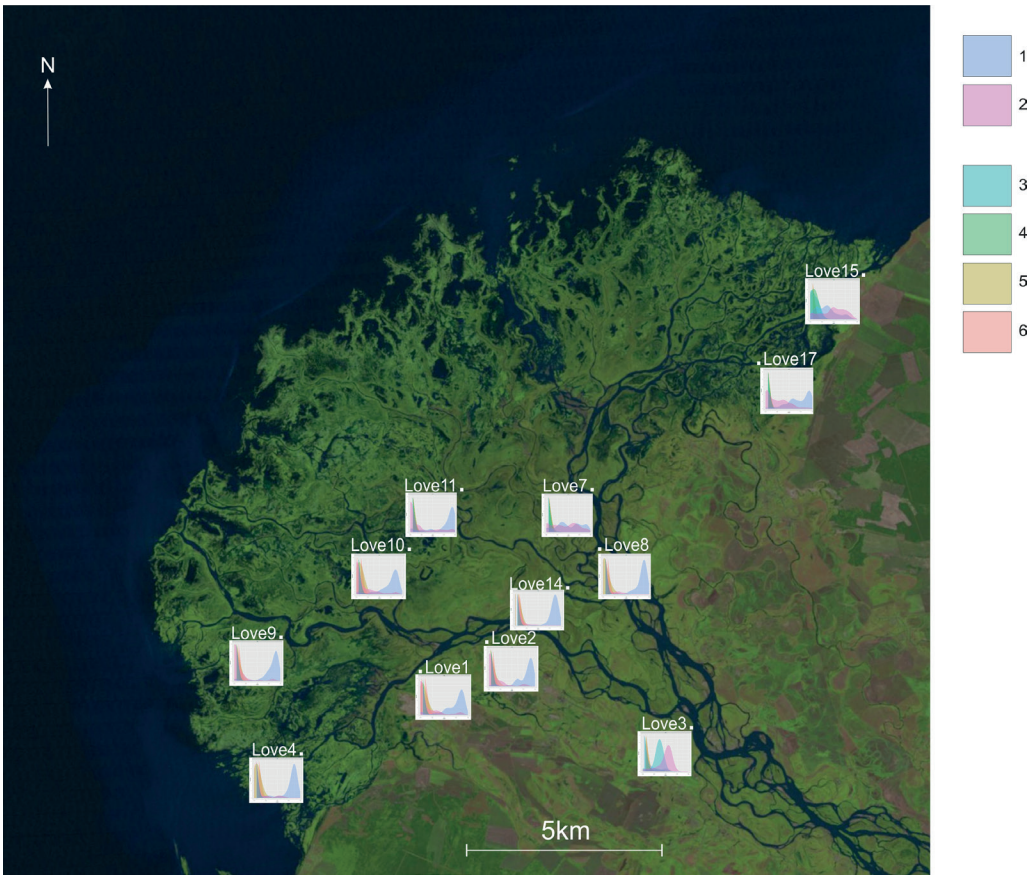

(3)

Fig. 3. Location map for fresh-flood sediment sampling. 1-old floodplain (CE18); 2-Kabansk alluvial terrace (SE-ref-2); 3-flood deposits (2016); 4-flood deposits (4-19 August 2014); 5-flood deposits (8-20 September 2013); 6-flood deposits (8-19 August 2011)

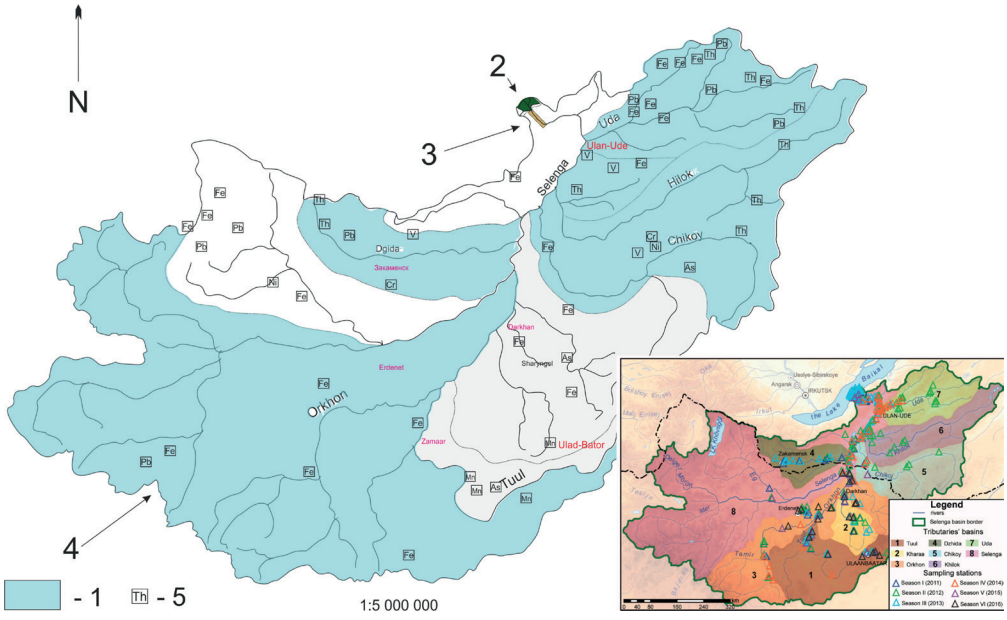

Fig. 4. Scheme of the geochemical fingerprinting method.On the insert map used the sampling stations from the art Kasimov et al. (2020)

1-Proposed river basins
2-Sedimant traps (old floodplain, oxbow lake)
3-Sediment sources in lower reaches of Selenga (bank and bed erosion)
4-Sediment sources of upper reaches of Selenga basin (soil and bank erosion)
5-Heavy metals deposits

the source samples using fingerprinting methods. Geochemical fingerprinting (FingerPro package) is, in fact, a modern implementation of the sedimentary provenances analysis (Fig. 4). ICP-AES analysis of sources and sediment traps samples was applied to define a range of potential fingerprint heavy metals markers: Ag, As, B, Be, Bi, Cd, Co, Cr, Cu, Fe, Hg, Mn, Mo, Ni, Pb, Th, U, V. All source materials were crushed down to 250 µm. Concentration of the technogenic radioactive isotope ^{137}Cs was also used as an additional fingerprinting parameter.

In order to select the most appropriate set of properties to include into the final composition of heavy metals (Lizaga 2018) we used two-stage statistical procedure. At first, we performed the Kruskall-Wallis H-test to establish which properties exhibited signifcant differences between the individual source groups within a particular category of sources (Fig. 5).

In our case, Bi, Cs, Th, U, V, Zn and especially Cs are elements that showed significant differences between the sources. Markers failing this test were removed from the following stage of analysis. Secondly, multivariate discriminant function analysis was applied to the markers selected during the first stage in order to evaluate its input into the source and trap composition. This operation is performed in 50 iterations and is verified each time on the training dataset using cross-validation. The procedure was focused on defining the source proportions allowing to keep the mass balance for all markers. The quality of each candidate is measured using goodness of fit (GOF). Function that describes GOF is based on the sum of the squares of the relative error (Lizaga et al. 2018). In the end, this succession of analytical procedures produced a graph showing the dependence of the source contribution on goodness of fit for each sediment trap.

RESULTS

Spatial differentiation of the fresh flood deposits particle size composition is primarily affected by the water and sediment runoff in the channels. The expected correlation between floodplain height and deposited sediment particle size was not observed. Moreover, granulometry of the fresh floodplain sediments exhibits a large differentiation within each floodplain level. The average thickness and mean particle diameter of the fresh alluvial deposits show a general decrease as one moves from a channel bank to floodplain backarc.

The range of granulometric composition of different samples along the channels is comparable to the grain size differentiation throughout the entire delta floodplain level. Further complicating the overall spatial pattern of sedimentation are marginal channels, floodplain branches, meadow vegetation, and the typical floodplain hollow and ridge topography.

As a result, a range of fresh floodplain sediments can be observed on one floodplain level, from predominantly clayey deposits in the depressions of the floodplain backarc (bluff line, neck cut-off) to sandy deposits along the channel bank where alluvial levees commonly form. Despite the fact that fresh floodplain deposits were sampled at approximately the same geomorphological positions (the edge part of the floodplain), there is a large number of factors that affect its particle size distribution including the sampling points position on a convex or concave river bank, presence of a "flow and sedimentary shadow" in the form of floodplain vegetation, levees, microtopographic depressions, minor channel arms and floodplain branches that strongly affect the water flow and sedimentation patterns.

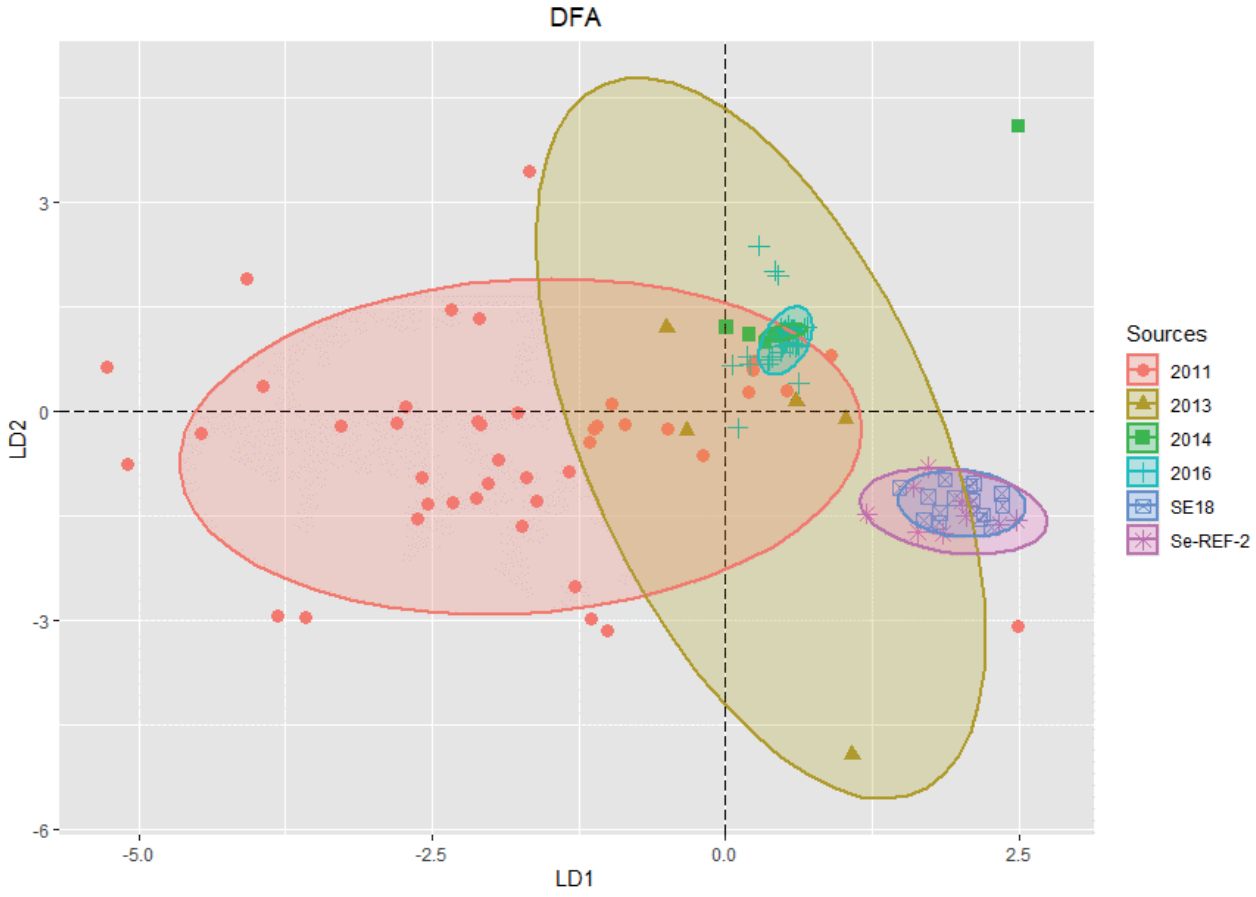

Fig. 5. The results of applying the Kruskall-Wallis test to assess the ability of each tracer property to discriminate between the six main source. 2011-flood deposits (2011); 2013-flood deposits (2013); 2014-flood deposits (2014); 2016-flood deposits (2016); SE18-old floodplain (CE18); Se-REF-2-Kabansk alluvial terrace (SE-ref-2)

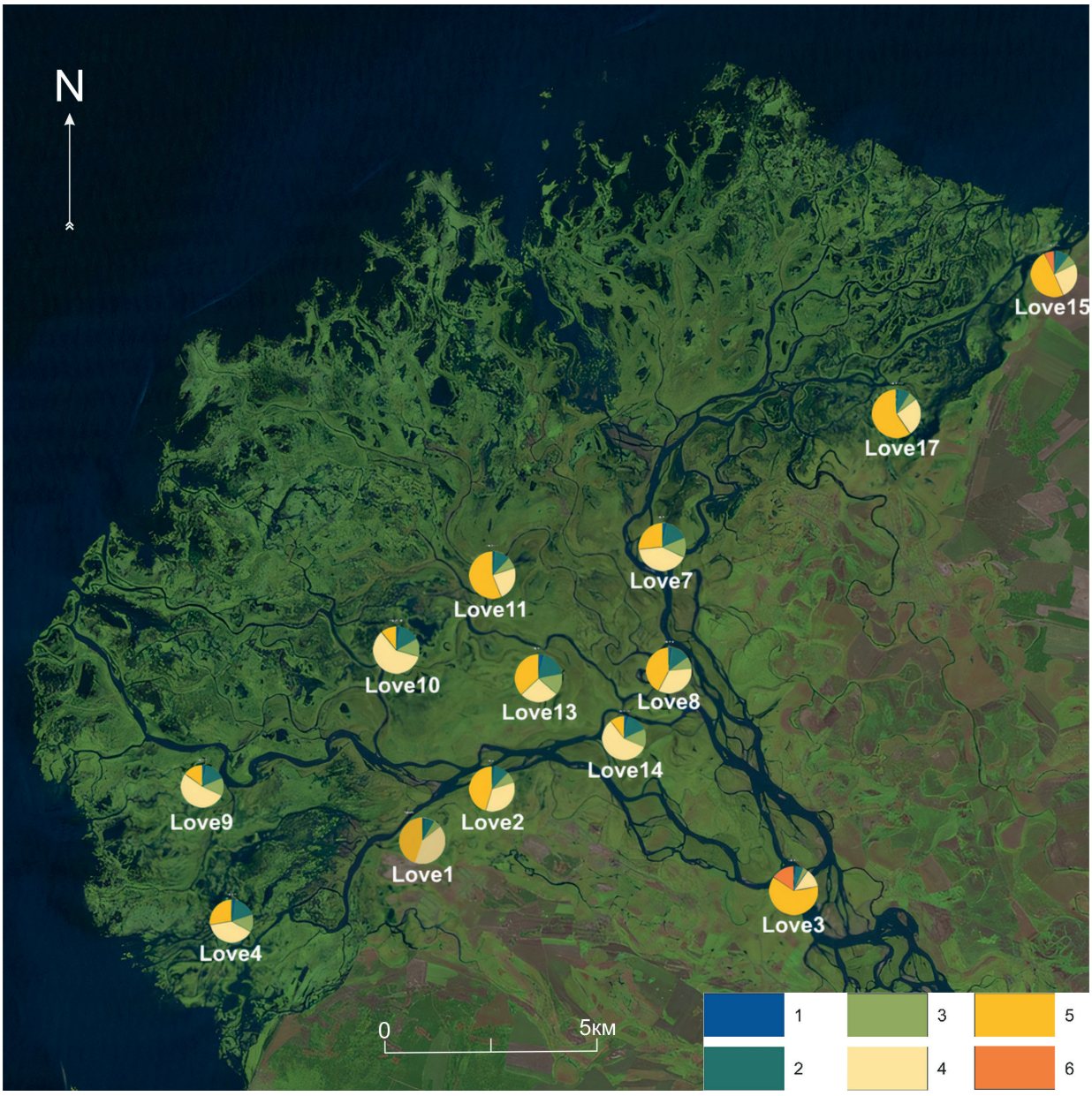

Fig. 6. Grain size composition of fresh flood deposits: 1) <1 μm; 2) 1-5 μm; 3) 5-10 μm; 4) 10-50 μm; 5) 50-250 μm; 6) >1000 μm

The finer-fraction dispersed component of the suspended sediment is the dominant source of accumulation at the floodplain, which distinguishes the latter from other positions. The Selenga floodplain sediments correspond to hydrodynamic conditions of a tranquil flow. Basically, those alluvial facies are composed of the finest material carried by the flow – physical clay (Kachinskiy 1931). At the old floodplain from 55% (Love 3 sampling point) to 90% (Love 14 sampling point) of sediments were delivered from the eroded floodplain and terrace banks upstream and only about 10-15% originates from the remote basin sources.

The most heterogeneous grain-size composition was found in the oxbow lake. Sand fractions in all floodplain lakes indicated high water levels of the main river during floods. Sedimentary environment in the Khlystov Zaton, located in the old floodplain backarc, reveals a greater variety than on the floodplains. 40% of sediments from the upper 5 cm-layer originated from the flood, taking place in 2013 (Tarasov 2019), and 30% were the product of floodplain and terraces banks erosion.

For the oxbow lake Khlystov Zaton, the analysis of sources was carried out for three horizons that differ sharply in sediment proportion: the upper one - presumably accumulated during the last major flood in 2013 (the first 60 cm), the middle one, with the maximum amount of clay in the section (76-77 cm) and the lower one - similar in sediment proportion to the upper horizon. This gives grounds to assume the accumulation of these deposits in the conditions, similar to 2013 flood (Fig. 7).

The nature of sedimentation in oxbows is highly heterogenic. Silt fraction is strongly dominant in sediments, which is common for limnic sedimentation. The increase in standard deviation compared to the floodplain values indicates periods of the hydrodynamic connection with main delta arms. Thus, the finer basin material was delivered into oxbow lakes during high floods (Table 1).

It can be assumed that coarser bank erosion material is deposited on the floodplain, while the basin sources material is carried away with floodplain flows further. Finer deposits of the basin source settle in stagnant water of oxbow lake. The oxbow lake sediments have a more complete size range of sediments and, accordingly, sources than the floodplain. Also, pollutants better retain on the silty sediments surface. Evidently, the use of oxbow lakes as sediment traps is more relevant in studies of sediment sources based on geochemical fingerprinting.

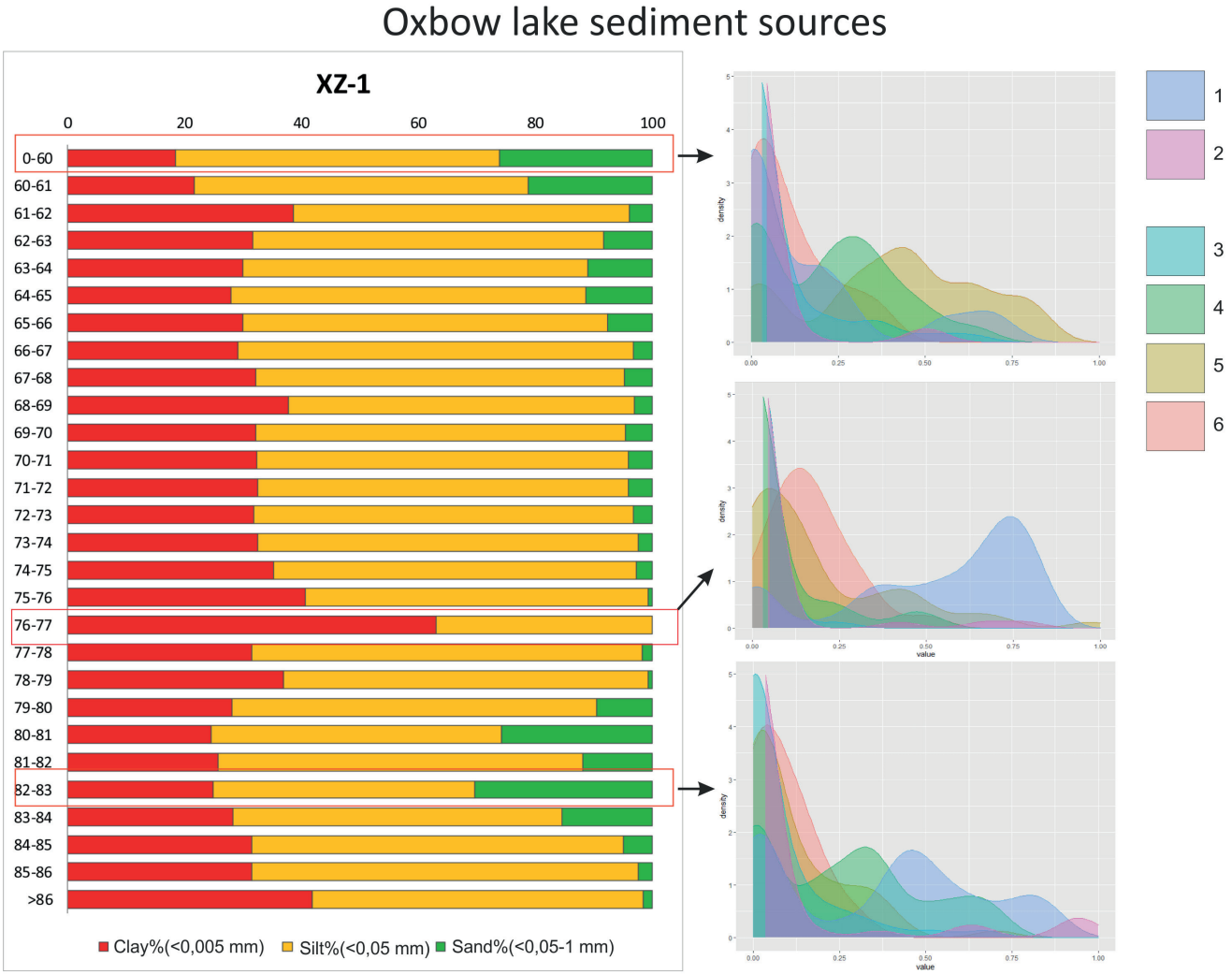

Fig. 7. Similarity of oxbow lake (Khlystov Zaton-XZ-1) sediment geochemical composition (the left figure) and different sources of sediments:

1-old floodplain (CE18); 2-Kabansk alluvial terrace (SE-ref-2); 3-flood deposits (2016); 4-flood deposits (2014); 5-flood deposits (2013); 6-flood deposits (2011) (the right figure)

Despite the confirmation of the hypothesis about the genesis of the source, it is worth taking a closer look at the ratio of the channel sources themselves in the flood deposits in order to reveal their spatial distribution controls. The fresh flood sediment samples acquired in the Lobanovsky sector differ most prominently from the general background (Fig. 2). Major distinctive feature of these samples is the lower contribution of high floodplain material with an increasing proportion of terrace bank erosion products. Apparently, the coarser material of the terrace, picked up by the bottom currents from the eroded left bank, follows the Lobanovskaya channel. This result can be a signal that the main flow is directed to the Lobanovskaya channel, but this statement requires additional studies.

DISCUSSION

The results of genetic analyses of the modern deltaic depositionary facies obtained using the fingerprinting method are quite atypical for the rivers of Eastern Siberia (Potemkina et al. 2011). Despite steep slope and channel gradients in the upper reaches of the Selenga drainage basin, plowing and grazing in the basin, which, as expected, increase the contribution of the basin source for all facies, it is the channel source of sediment that exert dominant contribution in the deltaic floodplain deposition.

Besides elevation, the relative importance of various sources could be affected by the distance from the main bifurcation node. The delta fan is composed of alluvial deposits represented by gravel sands at the head and in the middle of the delta and by fine-grained sands and silts in the estuarine sections (Dong et al. 2016). It serves as a perfect example of the source-to-source differentiation between the head and estuarine section of the delta.

An interesting correspondence between the genetic facies of sediments and the weighted average diameter of sediments was found. Classical ratio for most Siberian rivers is basin source consisting of finely dispersed material, and more coarse-grained corresponding to the channel source (Chalov 2008). For the lower reaches of the Selenga, an opposite relationship is observed: the coarser sediments belong to the basin source. This correlation is clearly illustrated by distribution of sediment sources for oxbow deposits. The oxbow samples exhibit a regular increase of the basin source contribution with a decrease of fine-grained deposits in the sample. It can be suggested that mountainous nature of the upper part of the basin is a reason for the coarser basin material that cannot accumulate on the floodplain surface. Thus, even for floodplain facies, we observe the predominance of the main river lower reach channel bank erosion source.

There are also some sectoral differences of deltaic sedimentation, associated with the contribution of various

Table 1. Contribution of each source types (based on GOF mean) to the samples from oxbow and floodplain from the lower reaches of the Selenga River

			Source types contribution					
			2011 flood deposits	2013 flood deposits	2014 flood deposits	2016 flood deposits	CE18 flood deposits	Se-ref-2 flood deposits
Sediment traps	Floodplain sediments	Love 1	0.06	0.08	0.00	0.00	0.73	0.12
		Love 2	0.04	0.05	0.00	0.00	0.79	0.12
		Love 3	0.03	0.04	0.04	0.35	0.06	0.49
		Love 4	0.06	0.07	0.00	0.00	0.81	0.06
		Love 7	0.02	0.02	0.02	0.01	0.51	0.42
		Love 8	0.05	0.05	0.00	0.00	0.84	0.05
		Love 9	0.05	0.05	0.00	0.00	0.81	0.09
		Love 10	0.06	0.08	0.00	0.00	0.72	0.13
		Love 11	0.01	0.02	0.02	0.00	0.76	0.18
		Love 13	0.00	0.01	0.12	0.05	0.51	0.30
		Love 14	0.05	0.05	0.00	0.00	0.85	0.05
		Love 15	0.01	0.01	0.08	0.08	0.34	0.48
		Love 17	0.01	0.02	0.02	0.00	0.71	0.25
	Oxbow sediments	XZ	0.11	0.41	0.22	0.07	0.16	0.02
		XZ max	0.08	0.12	0.26	0.07	0.37	0.10
		XZ min	0.17	0.19	0.06	0.01	0.54	0.04

* The table shows the contribution of each source as a percentage of the fingerprinting model results. Green color of cells show the high source contribution to sediment traps composition; Red color of cells on the contrary – low source contribution.

channel sources (eroded floodplain banks and the Kabansk terrace banks) among the samples of floodplain sediments (Fig. 3). The main distinctive feature of the Lobanovsky sector samples is noticeable increase of the terrace bank erosion material contribution into the floodplain overbank deposition. One of the possible explanations of variation observed between contributions of the two detected bank sources in different delta sectors is direction of the main flow to the Lobanovskaya channel. However, this assertion requires further research.

The area of the Selenga basin is 447 000 km^2 and each of its parts has its own nature of the morphodynamic regime. This brings up the problems associated with lack of samples of spring floods deposits and suspended materials allowing to establish the relative contribution of different sources throughout the delta. The obtained results reflect the relative contributions of various sources to individual sediment traps represented by each particular sample, and, therefore may not show all variations of sources and accumulation conditions on the floodplain and in oxbows. For this reason, it is important to collect more suspended sediment samples to further decipher spatial and temporal heterogeneity of sediment sourcing and yield.

CONCLUSIONS

The optimum fingerprint set, including, was able to correctly distinguish 80% of the source area samples (Fig. 4). Adding further tracer properties to fingerprint composition does not allow to diversify the sources any further. Sediment transport from the channel to the floodplain and oxbows, depending on increasingly rare high flow events, had the most fine-grained composition. The material sampled in oxbow lakes was deposited in a more heterogenic environment due to the connection with the main delta arms during high flood events.

Fresh flood deposits selected throughout the delta is very different. The most coarsely dispersed silt was collected along the Selenga and Lobanovskaya channels, the maximum coarse fraction is observed in the main channel and the Lobanovskaya channel, the finest material accumulates in the lake part of the Selenga sector delta. The size of the silt most strongly correlates with the water discharge near the sampling point. Therefore, we can talk about the greatest activity and growth of the Lobanovsky sector at the moment.

At the old floodplain 54% of sediments were delivered from the floodplain and terraces bank erosion within the Selenga River lower reach and just 29% originated from the upper and middle parts of the river basin. Sedimentary environment in the oxbow lake reveals a greater diversity than on the floodplains. The 40% of oxbow sediments most similar in geochemical composition to the 2013 flood deposits and 30% - to the products of floodplain and terraces banks erosion. The 45% of pool sediments were most similar to the flood taking place in 2013 and 31% - by the year 2016.

Among the fresh flood deposits samples, there are also some sectoral differences associated with the relative importance of different channel sources: floodplain banks and banks of the Kabanskaya terrace. The main distinctive feature of the Lobanovsky sector samples is the lower

contribution of the eroded floodplain bank material with an increasing proportion of the terrace bank erosion products. This is affected by the direction of main flow: the coarser terrace material uptaken by the strong water flow into the Lobanovsky sector, thus creating the observed distribution of sediment sources. This may indicate more activity in the sector and its growth active aggradation in recent times, but it's requires further research.

Heavy metals and metalloids come from territories of mineral resources exploration, industrial and urban areas, agricultural lands with finer fractions of suspended sediment during high floods. This material accumulates in the lower reaches of the Selenga on the floodplain surface, deltaic lakes and oxbows. Probably, considering the outlined tendency of a recently observed decrease of runoff during floods (Garmaev et al. 2022), increasing concentrations of pollutants can be expected to be carried into Lake Baikal, while lower percentage will remain intercepted within the delta sediment. Further studying. Further research of the sedimentation mechanism would allow to suggest reliable approaches to prevent excessive delivery of pollutants into the unique and vulnerable Baikal Lake ecosystem.

REFERENCES

Bazhenova O.I. et al. (1979). Spatio-temporal analysis of the dynamics of erosion processes in the south of Eastern Siberia.

Bogoyavleskii B.A. (1979). Modeling of the Natural Environment of Lake-Country of the Selenga Delta, Its Dynamics and Forecasting of Development, Proc. 14th Plenary Meeting of the Geomorphological Commission of the USSR Academy of Sciences, 105–128 (in Russian).

Budaev R.Ts., Kolomiets V.L. (2014). Natural and climatic reconstructions of the Late Pleistocene and Holocene of Baikal Siberia based on the results of studying the Ust-Selenga depression eolian morpholithogenesis. Proceedings of the Samara Scientific Center of the Russian Academy of Sciences, 16(1-4), 1059-1062(in Russian).

Chalov R.S. (2008). Comparative analysis of channel processes on mountain, semi-mountain and plain rivers. Geography and natural resources, 29.1, 28-35, DOI: 10.1016/j.gnr.2008.04.006.

Chalov S., Thorslund J., Kasimov N., Aybullatov D., Ilyicheva E., Karthe D., ... & Jarsjö J. (2017). The Selenga River delta: a geochemical barrier protecting Lake Baikal waters. Regional environmental change, 17(7), 2039-2053, DOI:10.1007/s10113-016-0996-1.

Charlton R. (2007). Fundamentals of fluvial geomorphology. Routledge, DOI: 10.1177/0309133308091952.

Collins A.L., Walling D.E., Sichingabula H.M., & Leeks G.J.L. (2001). Suspended sediment source fingerprinting in a small tropical catchment and some management implications. Applied Geography, 21(4), 387-412, DOI:10.1016/S0143-6228(01)00013-3.

Colman S.M., Karabanov E.B., & Nelson III C.H. (2003). Quaternary sedimentation and subsidence history of Lake Baikal, Siberia, based on seismic stratigraphy and coring. Journal of Sedimentary Research, 73(6), 941-956, DOI: 10.1016/j.quaint.2004.11.012.

Dong T.Y., Nittrouer J.A., Il'icheva E., Pavlov M., McElroy B., Czapiga M.J., ... & Parker G. (2016). Controls on gravel termination in seven distributary channels of the Selenga River Delta, Baikal Rift basin, Russia. Bulletin, 128(7-8), 1297-1312, DOI:10.1130/B31427.1.

Ilyicheva E.A. (2021). Exomorpholithogenesis of the Selenga River delta at the present stage of the hydroclimatic cycle. In IOP Conference Series: Earth and Environmental Science (Vol. 885, No. 1, p. 012039). IOP Publishing, DOI: 10.1088/1755-1315/885/1/012039

Illyicheva E.A., et al. (2020). «Formation of floodplains of the delta of the Selenga river.» Geography and Natural Resources 41.S5: 113-119 (in Russian), DOI: 10.21782/GIPR0206-1619-2020-5(113-119).

Illyicheva E.A et al. (2015). Hydromorphological analysis of landscape transformation dynamics of Selenga river delta. Geography and Natural Resources (3), 85-93 (in Russian).

Garmaev E. Zh., Khristoforov A.V., Tsydypov B.Z., Ayurzhanaev A.A., Andreev S.G., Sodnomov B.V., Zhamyanov D.D. (2022). Impact of the global climate change on the transboundary Selenga River water runoff and general principles of its water resources use. Water sector of Russia: problems, technologies, management (in Russian), DOI: 10.35567/19994508_2022_2_7.

Gaspar L., Lizaga I., Blake W.H., Latorre B., Quijano L., & Navas A. (2019). Fingerprinting changes in source contribution for evaluating soil response during an exceptional rainfall in Spanish pre-pyrenees. Journal of environmental management, 240, 136-148, DOI: 10.1016/j.jenvman.2019.03.109.

Hume Terry M., and Charles E. Herdendorf. (1988). A geomorphic classification of estuaries and its application to coastal resource management—a New Zealand example. Ocean and Shoreline Management 11.3: 249-274, DOI: 10.1016/0951-8312(88)90022-7.

Kachinski N.A. (1931). Studies on the Physical Properties of Soil and on the Root-systems of Plants (in Russian), published by Selkolkhozghiz, Moscow.

Kasimov N., Shinkareva G., Lychagin M., Kosheleva N., Chalov S., Pashkina M., ... & Jarsjö J. (2020). River water quality of the Selenga-Baikal basin: Part I—Spatio-temporal patterns of dissolved and suspended metals. Water, 12(8), 2137, DOI: 10.3390/w12082137.

Kasimov N., Shinkareva G., Lychagin M., Chalov S., Pashkina M., Thorslund J., & Jarsjö J. (2020). River water quality of the Selenga-Baikal Basin: Part II—Metal partitioning under different hydroclimatic conditions. Water, 12(9), 2392, DOI: 10.3390/w12092392.

Kasimov N., Kosheleva N., Lychagin M., Chalov S., Alexeenko A., Bazilova V., ... & Dorjgotov D. (2019). Environmental Atlas–monograph "Selenga-Baikal".

Korytny L.M., Il'icheva, E.A. and Pavlov, M.V., (2012) Hydrologo-Morphological Approach to Regionalization of the Selenga River Basin, Geographical Natural Resourses, 33(3), 212–217, DOI: 10.1134/S1875372812030055.

Lizaga Villuendas I., Latorre Garcés B., Gaspar Ferrer L., & Navas Izquierdo (2018). A FingerPro mixing model: An R package for sediment tracing. Water Resources Management 34, 3879–3894, DOI: 10.1007/s11269-020-02650-0.

Lychagin M., Chalov S., Kasimov N., Shinkareva G., Jarsjö J., & Thorslund J. (2017). Surface water pathways and fluxes of metals under changing environmental conditions and human interventions in the Selenga River system. Environmental Earth Sciences, 76(1), 1-14.

Pavlov M.V., Ilyicheva E.A., Vershinin K.E., Kobylkin D.V. (2019). Development of the lakes of the Selenga River delta in the late Holocene. Bulletin of the Buryat State University. Biology. Geography, 3, 31-43.

Pavlov M.V., Illicheva E.A., Savelueva L.A. (2016). Dynamics of the subaerial surface of the Selenga river delta. Geography and natural resources, № 5, 128–136, DOI: 10.21782/GIPR0206-1619-2016-5(128-136).

Potemkina T., Sutyrina E., & Potemkin V. (2019). Changing of the riverine sediment load supply into Lake Baikal: The natural and anthropogenic causes (Russia). Quaternary International, 524, 57-66.

Potemkina T.G. (2011) Sediment runoff formation trends of major tributaries of Lake Baikal in the 20th century and at the beginning of the 21st century. Russian Meteorology and Hydrology, 36(12), 819-825.

Shinkareva G.L. (2018). Geochemistry of heavy metals and metalloids in the components of aquatic landscapes in the Selenga River basin PhD Thesis. Moscow State University, Moscow, Russia.

Tarasov M.K. (2019). Cartographic assessment of the balance of suspended solids in the delta of the Selenga River according to remote sensing data PhD Thesis Moscow State University, Moscow, Russia.

Rusinek O.T., Takhteev V.V., Gladkochub D.P., Hodger T.V., Budnev N.M., Bezrukova E.V. & Kosterin O.E. (2012). Baikal studies. Pub. house of Irkutsk un-that.-291 p. (in Russian).

Estrany J., Garcia C., & Batalla R.J. (2012). Suspended sediment transport in a small Mediterranean agricultural catchment. Earth Surface Processes and Landforms 34(7), 929-940, DOI: 10.1002/esp.1777.

Vermeesch P., & Garzanti E. (2015). Making geological sense of 'Big Data' in sedimentary provenance analysis. Chemical Geology, 409, 20-27, DOI: 10.1016/j.chemgeo.2015.05.004.

Walling D.E., & Kane P. (1984). Suspended sediment properties and their geomorphological significance. In: International Geographical Union Commission on field experiments in geomorphology, 311-334.

Wilkinson S.N., Prosser I.P., & Hughes A.O. (2006). Predicting the distribution of bed material accumulation using river network sediment budgets. Water Resources Research, 42(10), DOI: 10.1029/2006WR004958.

Encyclopedia and news of Priangarye (2022) Rivers of Siberia [online]. Available at: http://irkipedia.ru [Accessed 20 May 2022].

Information system on water resources and water management of Russian river basins (2014) available at http://gis.vodinfo.ru/ [Accessed 17 November 2022]

RESEARCH PAPER

INDEX-BASED SPATIOTEMPORAL ASSESMENT OF WATER QUALITY IN TARBELA RESERVOIR, PAKISTAN (1990–2020)

Nausheen Mazhar[1*], Kanwal Javid[2], Muhammad Ameer Nawaz Khan[3], Amna Afzal[1], Kiran Hamayon[4a&b], Adeel Ahmad[5]**

[1]Department of Geography, Lahore College for Women University, Lahore, Pakistan
[2]Department of Geography, Government College University, Lahore, Pakistan
[3]State Key Laboratory of Information Engineering in Surveying, Mapping and Remote Sensing (LIESMARS), Wuhan University, China
[4a]Department of Geography, Government Associate College for Women Vandala Diyal Shah, Sheikhupura, Pakistan
[4b]Department of Geography, Govt. Graduate College of Science, Wahdat Road, Lahore
[5]Department of Geography, University of the Punjab 54590, Lahore, Pakistan
***Corresponding author:** Nausheen.mazhar@lcwu.edu.pk
****Corresponding author:** adeel.geog@pu.edu.pk
Received: April 17th, 2022 / Accepted: November 11th, 2022 / Published: December 31st, 2022
https://DOI-10.24057/2071-9388-2022-077

ABSTRACT. Anthropogenic activities can greatly influence the lake ecosystems across the globe. Within these ecosystems, the impacts of human activities are most evident on sedimentation, light and nutrient availability, and disturbance frequency. There have been times of natural environmental healing of reservoirs and the present research aims to explore the variations in the water quality of Tarbela reservoir, Pakistan the largest rock-filled dam of the world, from 1990 to 2020. Landsat imagery (Landsat 4-5, 5, 7 and 8) was used to monitor Land Use Land Cover (LULC), Normalized Difference Chlorophyll Index (NDCI), Normalized Difference Turbidity Index (NDTI) and Normalized Difference Water Index (NDWI) in Tarbela reservoir, and its surrounding area from 1990–2020, on decadal interval. The results indicated a significant increase in built-up area, of about 630 km^2, in the western and eastern parts of the reservoir, whereas turbidity level, revealed a substantial decline with 4% decrease observed in the last decade, 2010-2020 thus confirming improved water quality. The study also presented expanse in the spatial coverage of chlorophyll index and water index, indicating increase in residence time of the water. It is concluded that the water quality continued to deteriorate with time, however, 2020 was a year of environmental healing and there was an overall water quality improvement of the reservoir observed. The study recommends policies to be formulated for sediment flushing and turbidity reduction for longer time duration to enhance the life of this mega reservoir.

KEYWORDS: Chlorophyll, Turbidity, Water Index, Landsat, Tarbela

CITATION: Mazhar N., Javid K., Ameer Nawaz Khan M., Afzal A., Hamayon K., Ahmad A. (2022). Index-Based Spatiotemporal Assesment Of Water Quality In Tarbela Reservoir, Pakistan (1990–2020). Geography, Environment, Sustainability, 4(15), 232-242
https://DOI-10.24057/2071-9388-2022-077

Conflict of interests: The authors reported no potential conflict of interest.

INTRODUCTION

Reservoir construction, as an anthropogenic activity continue to alter and influence fluvial processes, including sediment transportation, its resultant altered river geomorphology, geochemical composition of water and ecology (Pogorelov et al. 2021, Condé et al. 2019). The uncontrolled population increase, along with climatic variability, leads to intensive land use practices that impact the water level and clarity of water in inland water reservoirs. A risk assessment approach, in this context, can highlight the magnitude of damage they cause to the lacustrine environment (Ochoa-Contreras et al. 2021; Lymburner et al. 2016).

Inland reservoirs retain the increased sediment and nutrient fluxes, which are induced due to intensified land use practices and human induced disturbances in watershed area, which lead to the eutrophication and degradation of water quality and basin-scale hydrological regimes (Harrison et al. 2010; Lymburner et al. 2016; Zhang et al. 2021). Human induced sediment and nutrient fluxes function as pollutant stressor and impact biodiversity and human consumption (Vörösmarty et al. 2010). Similarly, anthropogenic activities in coastal areas have been said to be responsible for enhanced turbidity in coastal waters (Dorji and Fearns 2017). Land use/land cover change (LULCC), transformation is being experienced in and around growing towns (Amin et al. 2014). In recent decades, the developing countries have witnessed water pollution after unprecedented population growth and industrialization (Singh et al. 2016). Thus, there remains a need for water quality assessment in inland waters by measuring the concentration of human-induced pollutants that degrade the aquatic ecosystem in any water reservoir (Hegazy et al. 2020; Poletaeva et al. 2021).

Inland waters are sensitive to anthropogenic activities and have been affected by environmental disturbances resulting from these anthropogenic activities, which affect

both water quality and hydrological characteristics, which explains the demand for assessing and monitoring water quality parameters (Koronkevich et al. 2019). The present climate change and anthropogenic activities like industrial expansion, urban development, and agricultural practices and natural processes such as precipitation frequency, weathering processes, and transportation of sediments, collectively add sediment flow to reservoirs that affect the water quality and storage capacity of the reservoir simultaneously (Das 2021). Similarly, a recent study pointed out that afforestation schemes like Billion Tree Afforestation Project (BTAP) can decrease the sediment load generation in the catchment area of Tarbela reservoir (Shafeeque et al. 2022).

To study sediment concentration and turbidity level in reservoirs, remotely sensed data is of vital importance for quantification of both variables (Wu et al. 2007; Dorji and Fearns 2017). Turbidity is an important water quality parameter from its optical property perspective. It varies spatio-temporally over large waterbodies. Normalized Difference Turbidity Index (NDTI) for example, has been used for qualitative estimates of turbidity in inland waterbodies around the globe (Garg et al. 2017). Remotely sensed images can assess the dredging impacts on water turbidity (Wu et al. 2007), similarly flat-bed pattern in the lower part of reservoirs can be detected through turbidity currents (Petkovšek 2018). Sedimentation trends and turbidity levels in reservoirs are highly determined by human settlements constructed near them. These settlements add loads of fine suspended sediments to the nearest water body which further accumulate in the bottom of the reservoir and create "muddy water" (Rutherfurd et al. 2020). Sediments from any natural or human source not only decline the water quality of the reservoir but also its water storage efficiency and also lead to other disasters (Petkovšek 2018, Tundu et al. 2018).

Elevated chlorophyll-a (pigment found in all phytoplankton species) concentrations generally indicate a change in the trophic status of a water body, and it is mainly associated with degraded water quality and low biodiversity which adversely destabilizes the ecosystem services and functions (Dalu et al. 2015; Kudela et al. 2015; Masocha et al. 2018). The understanding of the chlorophyll-a spatio-temporal dynamics requires frequent monitoring for water quality management (Andrade 2019). Chlorophyll-a, which is detectable by satellite imagery, therefore, can serve as an indicator of the presence of an algal bloom and is our liable source for water quality (Mishra & Mishra 2012). Various bio-optical algorithms have been designed to retrieve the chlorophyll-a concentration in inland waters, adopting different band combinations. One of the most abundant photo pigments produced by all types of algae is Normalized Difference Chlorophyll Index (NDCI) algorithm (Johansen et al. 2018; Mishra & Mishra 2012). The residence time of water in the reservoirs indirectly leads to eutrophication, as the nutrients get time to stay in water for longer periods (Calijuri et al. 2002). Although eutrophication is a natural phenomenon, however human activities such as, discharge of industrial, agricultural, or domestic effluents, can lead to cultural eutrophication (Rabalais et al. 2009; Bhagowati & Ahamad 2019; Çelekli 2020). The existence of phytoplankton in the in aquatic system, is indicative of enhanced primary productivity (Cai et al. 2011) and leads to high emission of greenhouse gases (Giles 2006; Barros et al. 2011). Being a photosynthetically active pigment, chlorophyll can be used for the determination of phytoplankton biomass (Watanabe et al. 2015).

As novel Coronavirus pandemic hit the world at the end of 2019, there was a halt to major human-induced events due to lockdown and as a result, the natural environment has experienced many changes (Xu et al. 2020). The current study is looking towards the impact of COVID-19 lockdown on the water quality of reservoirs. Globally many rivers, coastal waters and reservoirs examined a profound change in water quality from a positive perspective. Most anthropogenic activities were stopped and inclusion of all pollutants to water channels was declined and most reservoirs regained their clean waters (Dutta et al. 2020; Robin et al. 2021, Arakelov et al. 2021).

Studies have been conducted in past exploring the reservoir sedimentation (Tate and Farquharson 2000; Khan and Tingsanchali 2009; Roca 2012; Mazhar et al. 2021), while others dealt with floor risk assessment (Naz et al. 2019), operational changes in the reservoir (Rafique et al. 2020) and a study even investigated the physiochemical water quality of Tarbela near the federal capital, Islamabad (Ahmed et al. 2015). Although studies have been conducted to spatially monitor the water quality of reservoirs, using remote sensing technology (González-Márquez et al. 2018, Vakili and Amanollahi 2020), however, there has been a gap in terms of assessing this water quality over longer time scales, and the present research aims to fill this gap by exploring the variations in the water quality of Tarbela reservoir for the last 30 years. The study fundamentally has the following objectives: i) to monitor the water quality of Tarbela reservoir from 1990–2020, using remotely sensed data and ii) to explore any changes in the water quality of the reservoir in period under study.

MATERIALS AND METHODS

Study area

Tarbela reservoir, situated in Haripur and Swabi district in Pakistan, about 50 km northwest of Islamabad (Ahmed et al. 2015), is the earth's largest rock filled dam, constructed over River Indus in 1976 (Mazhar et al. 2021). At the time of conception, its main functions were power generation and regulation of seasonal flows for irrigating the Indus plains (Roca 2012). The reservoir had an initial capacity of 11, 600 m^3 (Roca 2012). According to Tate and Farquharson (2000), average daily temperature varies substantially from -7° C in January to 41° C in June, while the relative humidity normally remains low, but more than 50% humidity is witnessed only in pre-monsoon period. The average annual rainfall at Tarbela is around 899 mm, scattered in almost all the months of the year. January and November rarely go rainless. The average inflow in the reservoir is 81, 000 Mcm as shared in TAMS 1998 report (Roca 2012), while Tate and Farquharson (2000) state that snowmelt plays a significant role in raising the peak flows of the reservoir, with snowmelt contributing peak flows as high as 11, 300 m^3s^{-1}, comparatively, rainfall contributes a maximum of 5, 660 m^3s^{-1}.

The geographical coordinates of the reservoir are 34.1438° North latitude and 72.8077° East longitude (Fig. 1). The mean rainfall recorded at Tarbela was 74.41mm for the period 1960-1996 (Tate and Farquharson 2000).

DATA ACQUISITION

The characteristics of Landsat data used in the study are provided in Table 1.

PREPROCESSING

The above-mentioned data was acquired from United States Geological Survey (USGS). Preprocessed Landsat imagery from1990 to 2020 was downloaded from USGS. Preprocessing of data included geometric and radiometric correction, noise removal and cloud cover which was less than 10%. Later, Earth Resources Data Analysis

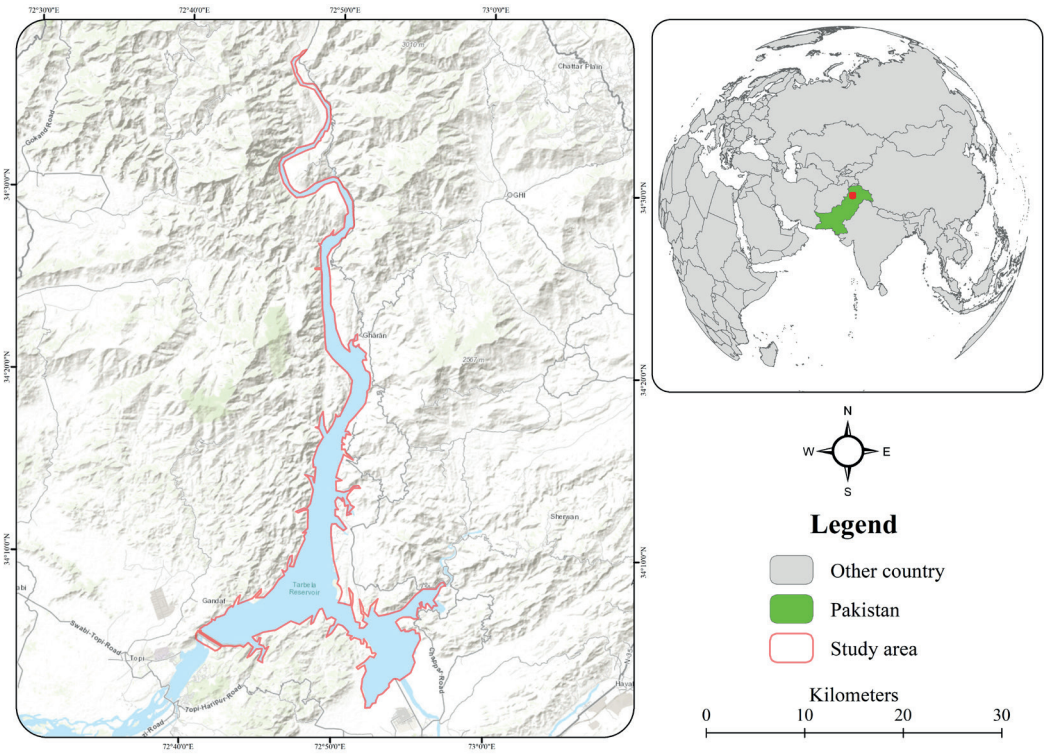

Fig. 1. Study Area Map

Table 1. Characteristics of Landsat data used in the study

Satellite	Sensor	Level	Path	Row	Acquisition Date
Landsat 5	TM	L1	150	36	1990/04/24
Landsat 5	TM	L1	150	36	2000/05/21
Landsat 7	ETM+	L1	150	36	2010/06/02
Landsat 8	OLI	L1	150	36	2020/06/29

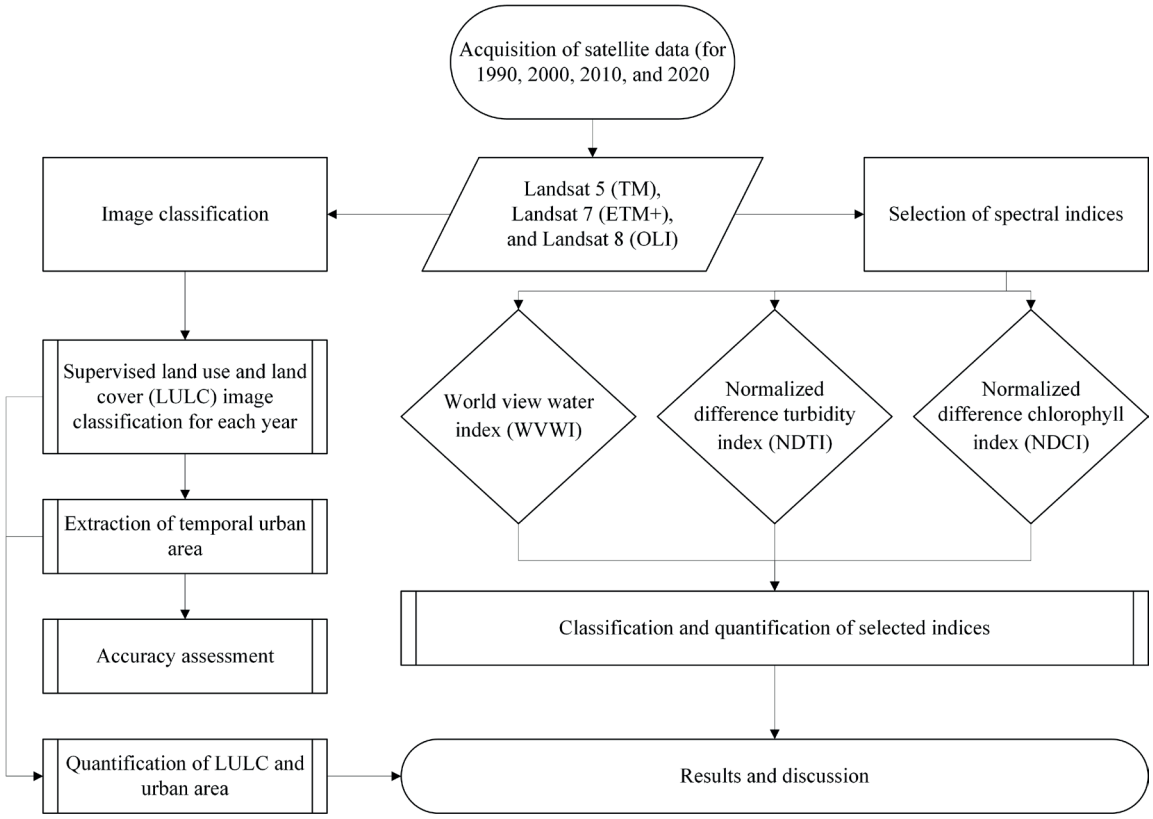

Fig. 2. Methodological Flow chart

System (ERDAS) Imagine was used for layer stacking and mosaicking of images.

Land use land cover classification (LULC)

Land use/land cover change (LULCC) quantification is one of the important applications of earth observation data sets, and it is vital for assessing global environmental change processes and helps in optimizing the maximum use of natural resources in sustainable manner and making new policies (Srivastava et al. 2012; Singh et al. 2016). LULC changes due to afforestation programs also need to be monitored closely through remotely sensed data, as sediment generation rate is impacted by different land uses (Shafeeque et al. 2022). Supervised classification with maximum likelihood algorithm was applied on the Landsat imagery for land use land cover analysis. The study area was broadly classified into five classes, somewhat similar to USGS Level 1 classification scheme (Radhakrishnan 2014; Singh et al. 2016). The waterbody class included all the areas covered by water, including rivers, reservoir, streams, lakes, and ponds: vegetation class included all the sparse forest vegetation and also grass, crops, parks etc. The snow class covered all the pixels showing the presence of snow/ice; the boulder/rocks class covered all the land covered by boulders and rocks within the reservoir boundary and the concrete structures outside the reservoir boundary. The bareland class included the areas without sparse vegetation, without boulders.

To identify the errors, accuracy evaluation is an essential step of image processing procedures (Alam et al. 2019; Hussain et al. 2021; Kumar et al. 2021 & Hussain & Karuppannan 2022). Overall accuracy determines the correctness of the classification process (Mukherjee & Singh 2020; Mishra & Jabin 2020). In order to calculate the accuracy of each class of LULC from LANDSAT images, an accuracy assessment was performed in ArcGIS using the equation 1:

$$= \frac{Total\ Number\ of\ Correct\ Classify\ Pixels\ (Diagonal)}{Total\ Number\ of\ Reference\ Pixels} * 100 \quad (1)$$

Producer's accuracy quantitatively exhibits if all attributes shown in real map are correctly classified (Mukherjee & Singh 2020, Singh & Jabin 2020, Kafy et al. 2021). The Producer Accuracy was calculated through equation 2:

$$= \frac{Number\ of\ Correct\ Classify\ Pixels\ in\ Each\ Category}{Total\ Number\ of\ Reference\ Pixels\ in\ that\ Category\ (The\ Column\ Total)} * 100 \quad (2)$$

In addition, Kappa coefficient measures accuracies between two random values and show reasonable accuracy. Kappa coefficient is regarded as a coefficient of agreement (Mukherjee & Singh 2020; Mishra & Jabin 2020; Gondwe et al. 2021; Bunyangha et al. 2021). The Kappa Coefficient was calculated using equation 3:

$$= \frac{(TS * TCS) - \Sigma(Column\ Total * Row\ Total)}{TS^2 - \Sigma(Column\ Total * Row\ Total)} * 100 \quad (3)$$

According to the assessment results, the overall accuracy of 1990 image was 91.43% with a Kappa coefficient value of 0.89, while the overall accuracy of 2000 image was 90.91% with a Kappa coefficient value of 0.89; the overall accuracy of 2010 image was 86.67% with a Kappa coefficient value of 0.83 and the overall accuracy of 2020 image was 88% with a Kappa coefficient value of 0.85 (table 2).

WORLD VIEW WATER INDEX (WVWI)

World View Water Index (WVWI) has been reported to be a powerful algorithm that detects water or shadows (IMAGINE 2015). This index works with coastal and Near Infrared Reflectance (NIR2) bands, as both these bands have variation in wavelengths, therefore, it provides a reliable threshold to identify water (Wolf 2012) using equation 4.

$$WVWI = \frac{CB - NIR2}{CB + NIR2} \quad (4)$$

NORMALIZED DIFFERENCE TURBIDITY INDEX (NDTI)

The turbidity in inland waters, like ponds and reservoirs, can be monitored through remotely sensed images (equation 5), using the NDTI developed by Lacaux, Tourre et al. (2007).

$$NDTI = \frac{Red - Green}{Red + Green} \quad (5)$$

Moderate Resolution Imaging Spectroradiometer (MODIS) data can also be used to monitor water surface turbidity at both the reservoir level, by analyzing the turbidity pattern variability in each reservoir, and the sedimentation pattern at the water surface can also be retrieved (Condé et al. 2019).

Table 2. Accuracy assessment (%)

Year	1990		2000		2010		2020	
Accuracy	User (%)	Producer (%)	User (%)	Producer (%)	User (%)	Producer (%)	User (%)	Producer (%)
Landcover								
Water	87.5	100	100	100	91.67	68.75	100	83
Vegetation	100	83.33	92.31	85.71	82.35	82.35	90	90
Snow	100	100	100	100	81.81	100	75	100
Boulder/Rock	66.67	100	83.33	90.91	88.89	100	91.66	84.61
Bare Land	100	85.71	80	80	90.9	100	80	88.89
Overall Accuracy (%)	91.43		90.91		86.67		88.00	
Kappa Coefficient	0.89		0.89		0.83		0.85	

NORMALIZED DIFFERENCE CHLOROPHYLL INDEX (NDCI)

Phytoplankton has been used as an organism that is indicative of health of a water body, while phytoplankton cannot exist without chlorophyll. Chlorophyll content in water bodies can be traced through NDCI (equation 6), which can help trace algae growth (Mishra, Schaeffer et al. 2014). It is necessary to monitor chlorophyll content in reservoirs because excessive growth of phytoplankton can lead to eutrophication, thus affecting the efficiency of the reservoir for power generation and provision of irrigation water.

$$NDCI = \frac{Blue}{Red} \quad (6)$$

In order to monitor the settlement expanse during the years under study, Google earth high resolution images were georeferenced and later stretch option of symbology was applied on these images, using Arc GIS 10.3.

RESULTS

LAND USE AND LAND COVER (LULC)

The analysis of Fig. 3 presents the interesting finding that the water class underwent increase in area from 167 km^2 in 1990 to 196 km^2 in 2020, with maximum increase witnessed on the eastern banks of the reservoir. However, the bare land class witnessed the greatest decrease of 3184 km^2 during the period under study. The bare land area was maximum in the year 1990, after which it steadily declined, so much so, that its area was merely 549 km^2 in 2020 (table 3). The bare land area was replaced by vegetation, as this class also underwent massive increase of 2593 km^2 from 1990 to 2020.

Similarly, the boulders/rocks class, also representing the settlement area in the area of interest, experienced a substantial increase of 609 km^2. The snow-covered class existed only in year 1990 and 2010, and its spatial coverage remained less than 50 km^2 and that too limited to only north eastern side of the study area.

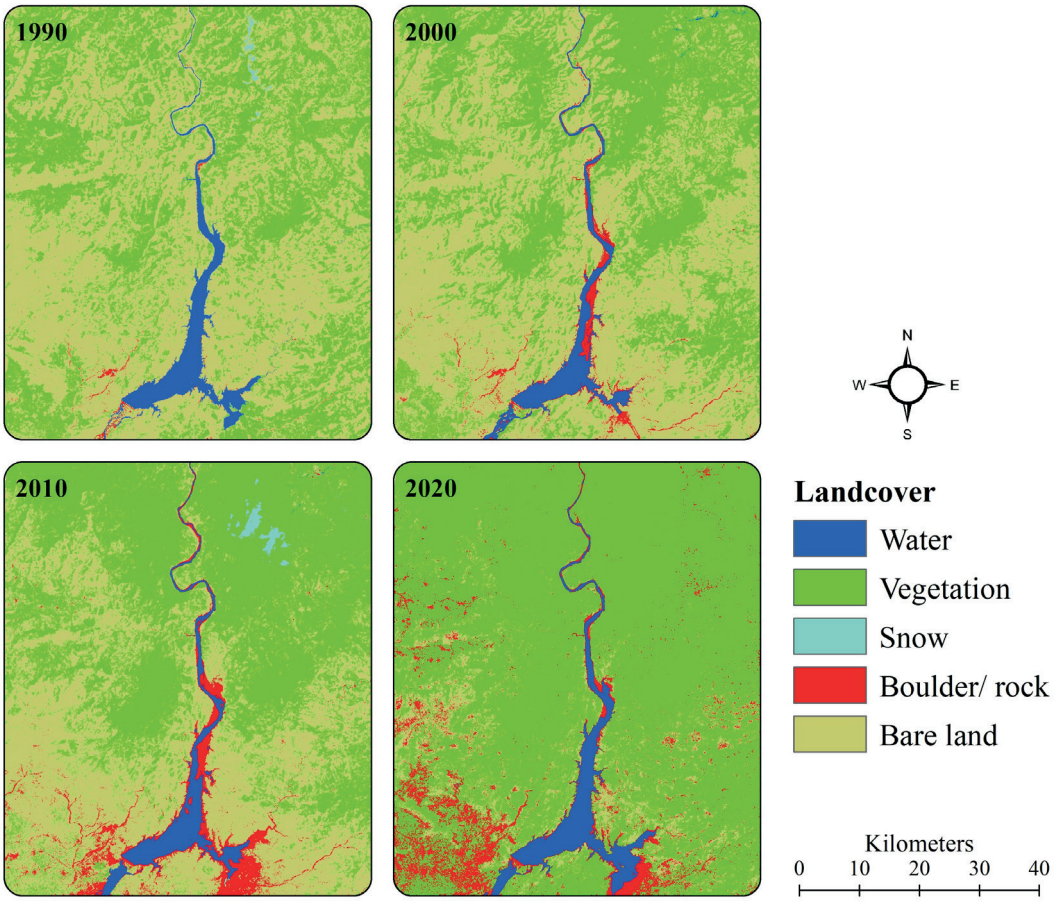

Fig. 3. LULC classification of Tarbela reservoir, 1990–2020

Table 3. Land Use and Land Cover (LULC) characteristics of the study area

Classes	1990 area (sq.km)	2000 area (sq.km)	2010 area (sq.km)	2020 area (sq.km)
Water	167	166	151	196
Bare Land	3733	3424	2680	549
Boulders/Rock	20	90	321	630
Snow	47	0	44	0
Vegetation	2100.94	2388	2872	4694

NORMALIZED DIFFERENCE CHLOROPHYLL INDEX (NDCI)

Figure 4 presents the spatio-temporal variations in the chlorophyll level of the study area. The high NDCI class underwent a decrease of 712%, while the low class of NDCI experienced a decrease of 33%.

The highest NDCI value was recorded in 1990, while the lowest high value of NDCI was identified in 2020. The mean values of NDCI indicate a gradual decrease in the intensification of NDCI from 3.04 in 1990 to 1.12 in 2020 (table 4). Another significant finding is that although the intensity of the high NDCI decreased over the years, however, its spatial coverage significantly increased by 2020. The eastern and western arms of the reservoir, located in the south of the study area appear saturated with high chlorophyll content. This increase in spatial coverage of NDCI shows high eutrophic activity which affects the water quality (Watanabe, Alcântara et al. 2015; Liu, Zhang et al. 2019).

NORMALIZED DIFFERENCE TURBIDITY INDEX (NDTI)

Figure 5 presents the turbidity variation in Tarbela reservoir and its surrounding area. The area covered by high turbidity has declined from 0.15 to 0.09 from 1990 to 2020 (see Table 5) and witnessed a total decrease in spatial coverage by 6%. Whereas there was an increase of 16% recorded for the low NDTI class, which points towards the environmental healing, where the turbidity significantly declined over the years leading to cleaner water concentration in the left and right arm of the reservoir in 2020. The highest spatial coverage of low NDTI was in 2000, while the lowest was observed in the year 1990. However, the mean value of NDTI has increased from -0.13 in 1990 to -0.05 in 2020, which proves gradual decrease in the turbidity level of the waters of the Tarbela reservoir, over the years.

WORLD VIEW WATER INDEX (WVWI)

According to Fig. 6, the spatial extent of water has increased in Tarbela reservoir over the years,

Table 6. World View Water Index (WVWI) characteristics of the study area precisely in year 2020, representing second most widespread spatial coverage of WVWI, after 1990. However, according to Table 4, the highest value of WVWI has decreased by 44% over the years, with highest value of 0.80 recorded in 2000, and lowest value of high WVWI of 0.34 reported in 2020 (Table 6). Similarly, the low WVWI class underwent a 28% decrease from -0.29 in 1990 to -0.57 in 2020. The mean WVWI has also witnessed a decline from 0.13 in 1990 to -0.11 in 2020, thus referring to an overall decrease in intensification of the WVWI values.

SETTLEMENT EXPANSE

Settlement expanse in the study area can be identified through Fig. 7, where shades of brown are indicative of settlement expansion. The same can be seen to be increasing steadily in the south eastern and south western parts of the study area. The rapid expanse of these settlements on the banks of the reservoir hint towards human intervention in the water quality of the reservoir.

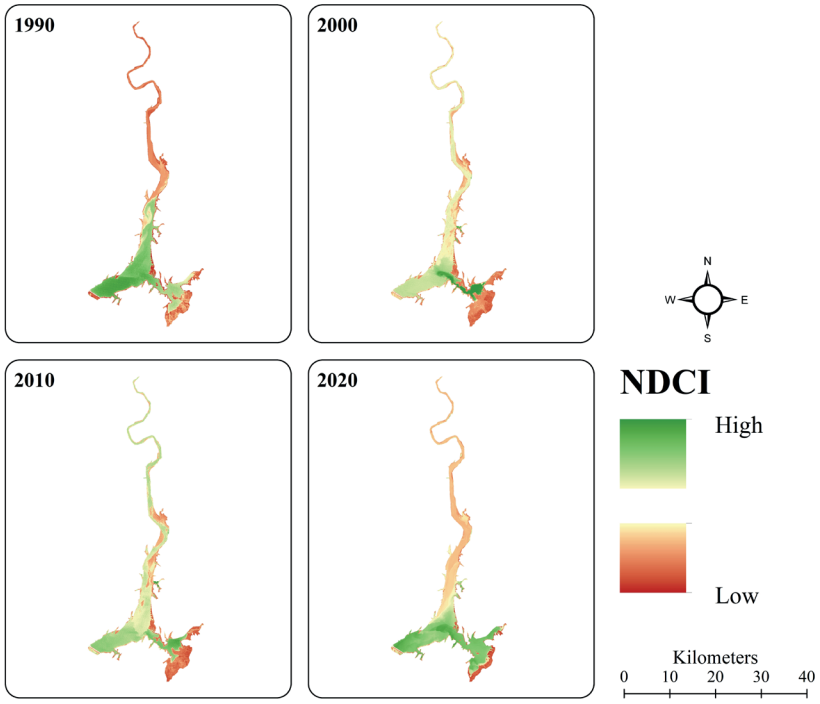

Fig. 4. NDCI of Tarbela reservoir, 1990–2020

Table 4. Normalized Difference Chlorophyll Index (NDCI) characteristics of the study area

Classes	1990	2000	2010	2020
High	4.80	3.04	2.49	1.35
Medium	2.99	2.04	1.86	1.05
Low	1.19	1.05	1.24	0.75
Mean	3.04	1.76	1.79	1.12

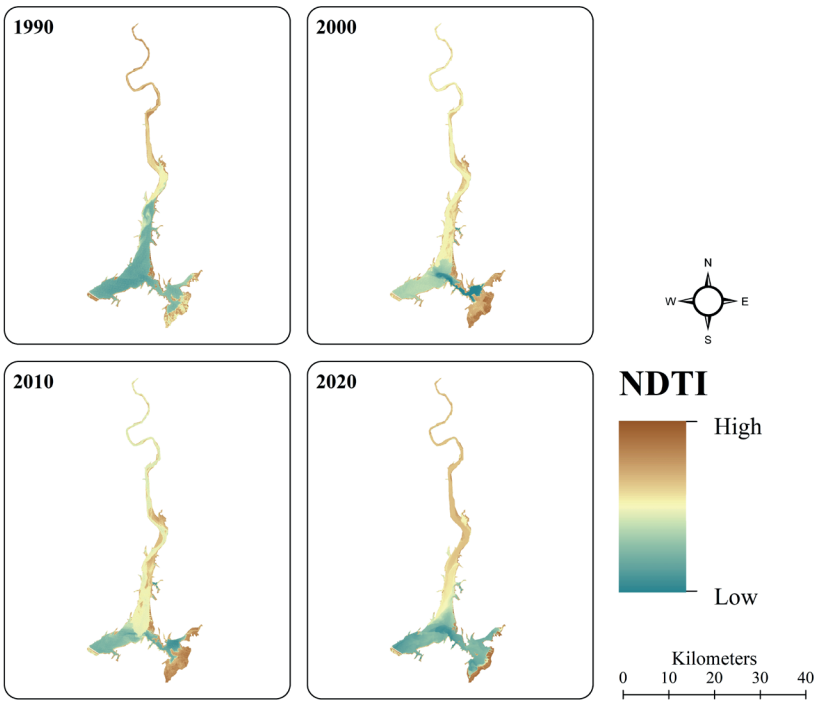

Fig. 5. NDTI of Tarbela reservoir, 1990–2020

Table 5. Normalized Difference Turbidity Index (NDTI) characteristics of the study area

Classes	1990	2000	2010	2020
High	0.15	0.21	0.17	0.09
Medium	-0.07	0.01	0.04	-0.02
Low	-0.30	-0.18	-0.08	-0.14
Mean	-0.13	0.05	0.05	-0.05

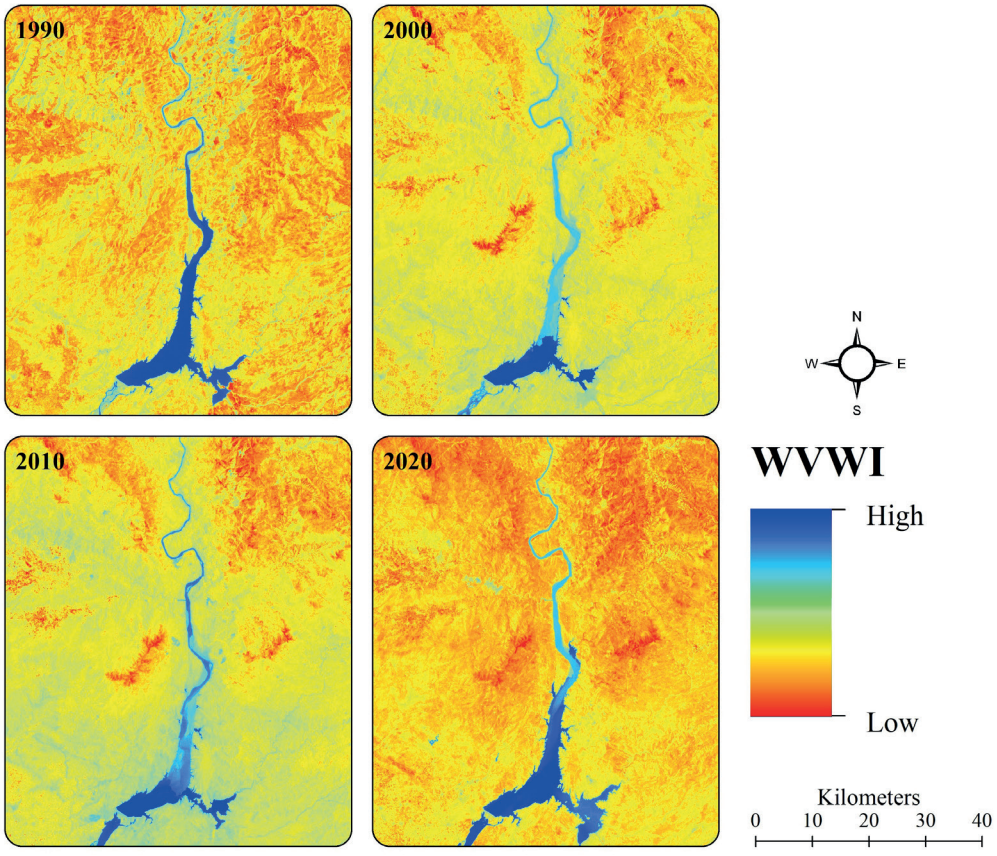

Fig. 6. WVWI of Tarbela reservoir, 1990–2020

Table 6. World View Water Index (WVWI) characteristics of the study area

Classes	1990	2000	2010	2020
High	0.78	0.80	0.63	0.34
Medium	0.17	0.07	0.11	-0.21
Low	-0.11	-0.23	-0.13	-0.46
Mean	0.13	0.28	0.21	0.20

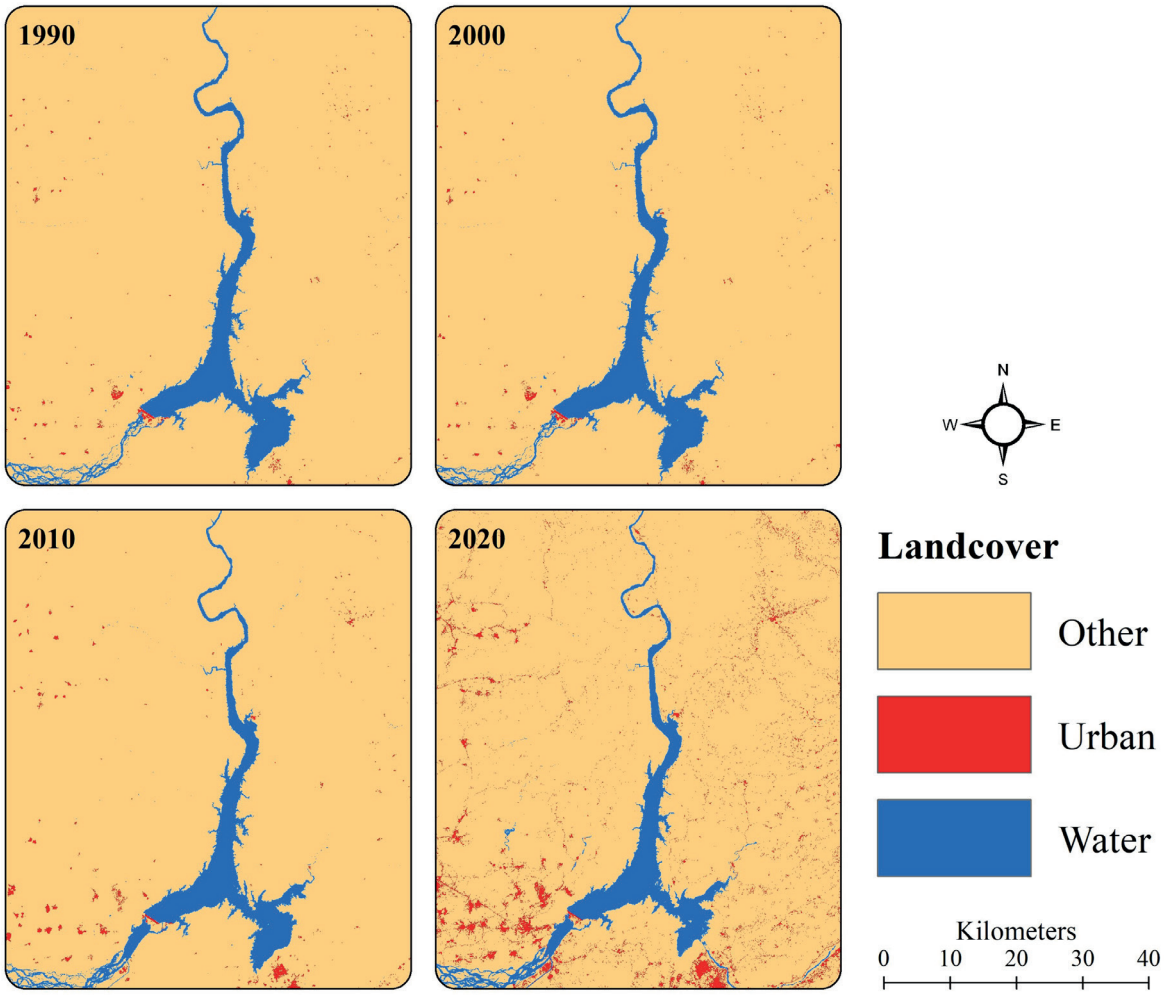

Fig. 6. WVWI of Tarbela reservoir, 1990–2020

DISCUSSION

This study explored the water quality of world's largest earth and rock filled dam, and its surroundings, using geospatial techniques. The results indicated significant increase in built-up area, of about 609 km^2, in the western and eastern parts of the reservoir, from 1990 to 2020. This increase in built up, corresponds with decrease in bare land and increase in vegetation cover over the years and all these directly have impacts on water quality as Srivastava et al. (2012) have mentioned that the combination with remote sensing water quality, the use of multivariate statistical techniques offers a detailed understanding of water quality parameters and possible factors that influence the water quality behavior. The findings of this study can be supported by another recent study where the expanse in vegetation has been reported in the catchment and area around Tarbela reservoir, due to the BTAP project (Shafeeque et al. 2022).

From 1990 to 2010, within the reservoir boundary substantial increase in the boulder class can be identified which is supported by the notion that during the pre-lockdown years, the water drawdown was high from Tarbela for agricultural and hydroelectric power generation purposes, which resulted in the exposure of the boulders lying along the reservoir edges, when the waterlevel went too low. However, in 2020, after Covid-19 related lockdown in Pakistan, an increase in the water level within the reservoir was witnessed which led to the submergence of the boulders within the reservoir boundary. However, an increase in the same category was identified on the south western bank of the reservoir, during the same period, which can be associated with settlement expanse in the region. The Landsat data comparison presents the variation in turbidity, chlorophyll and water area during pre-Covid-19 years and Covid-19 year.

The analysis of the water quality based on turbidity level, revealed a substantial decline in turbidity of the reservoir with 4% decrease observed in the last decade, thus hinting towards the higher turbid waters in Tarbela reservoir, during the pre-covid years. Similar findings by (Yunus et al. 2020) identified lesser suspended particulate matter concentrations in Vembanad lake, India, during the lockdown period. Aman et al. (2020) also concluded

noticeable decline in the suspended particulate matter that causes turbidity, in Sabramati river of Ahmedabad, India during the lockdown period, using OLI-8 imagery.

The study also presented expanse in the spatial coverage of chlorophyll index and water index, indicating increase in residence time of the water (Calijuri et al. 2002), which causes increased rate of eutrophication, and this was witnessed in 2020 NDCI analysis, where although intensity of mean NDCI decreased from pre-covid years to Covid-19 year by 192%, yet its spatial coverage increased. The deposition of dead vegetative matter and suspended sediments can cause decreased capacity of reservoirs (Bishwakarma and Støle 2008), thus contributing towards declined power generation capacity.

CONCLUSION

Based on the aforementioned results and discussion it can be summed up that the Covid-19 related lockdown acted as an environmental healer, which led to repairing of the water quality of the reservoir. The lockdown period led to the closure of factories. and decline in electric and irrigation related water demands, leading to a probable enhanced stay period of water in the reservoir which led to increased NDCI. However, this positive impact of Covid-19 related lockdown requires a more detailed study, where sample collections from the reservoir can help in validating the results obtained from remotely sensed images.

The findings of the study are general in nature as it analyzes and compares the water quality, as gauged by the satellites, on decadal basis. For detailed analysis, future research in 2019 and 2020 is recommended where, month wise comparison of the variables under study can be investigated and variation in water quality can specifically be studies for pre covid and covid year. The findings of the study provide the policy makers with the fruit for thought that measures must be taken for formulating policies regarding sediment flushing and turbidity reduction on larger time scales, and plan for sustainable urban dynamics in Sobra city, located near Tarbela reservoir, and also in the upstream urban centers. Such policies can increase water holding capacity of the reservoir and thus the reservoir can stay functional even for our future generations.

REFERENCES

Ahmed S., Rehman H., Khattak B., et al., (2015). Physicochemical Analysis of Water and Soil of Tarbela Dam in Northwest of Islamabad, Pakistan, with Special Reference to Their Influence on Fish Growth. World Applied Sciences Journal, 33(9), 1446-1449.

Alam A., Bhat M.S., & Maheen M. (2020). Using Landsat satellite data for assessing the land use and land cover change in Kashmir valley. GeoJournal, 85(6), 1529-1543.

Aman M.A., Salman M.S., and Yunus A.P. (2020). COVID-19 and its impact on environment: Improved pollution levels during the lockdown period – A case from Ahmedabad, India. Remote Sensing Applications: Society and Environment, 20, 100382.

Amin A., Fazal S., Mujtaba A., & Singh S.K. (2014). Effects of land transformation on water quality of Dal Lake, Srinagar, India. Journal of the Indian Society of Remote Sensing, 42(1), 119-128.

Andrade C., Alcântara E., Bernardo N., & Kampel M. (2019). An assessment of semi-analytical models based on the absorption coefficient in retrieving the chlorophyll-a concentration from a reservoir. Advances in Space Research, 63(7), 2175-2188.

Arakelov M.S., Lipilin D.A., & Dolgova-Shkhalakhova A.V. (2021). Influence Of Quarantine Measures Against The New Coronavirus Infection Covid-19 On The State Of Black Sea Coastal Waters. Geography, Environment, Sustainability, 14(4), 199-204.

Barros N., Cole J.J., Tranvik L.J., Prairi, Y.T., Bastviken D., Huszar V.L.M., del Giorgio P. and Roland F. (2011). Carbon emission from hydroelectric reservoirs linked to reservoir age and latitude. Nature Geoscience, 4(9), 593-596.

Bhagowati B., & Ahamad K. U. (2019). A review on lake eutrophication dynamics and recent developments in lake modeling. Ecohydrology & Hydrobiology, 19(1), 155-166.

Bishwakarma M., and H Støle. (2008). Real-time sediment monitoring in hydropower plants. Journal of Hydraulic Research, 46(2), 282-288.

Bunyangha J., Majaliwa M.J., Muthumbi A.W., Gichuki N.N., & Egeru A. (2021). Past and future land use/land cover changes from multi-temporal Landsat imagery in Mpologoma catchment, eastern Uganda. The Egyptian Journal of Remote Sensing and Space Science, 24(3), 675-685.

Cai W.-J., Hu X., Huang W.-J., Murrell M.C., Lehrter J.C., Lohrenz S.E., Chou W.-C., Zhai W., Hollibaugh J.T., Wang Y., Zhao P., Guo X., Gundersen K., Dai M. and Gong G.-C. (2011). Acidification of subsurface coastal waters enhanced by eutrophication. Nature Geoscience, 4(11), 766-770.

Calijuri M.C., Dos Santos A.C.A. and Jati S. (2002). Temporal changes in the phytoplankton community structure in a tropical and eutrophic reservoir (Barra Bonita, S.P.—Brazil). Journal of Plankton Research, 24(7), 617-634.

Çelekli A., Kayhan S., & Çetin T. (2020). First assessment of lakes'water quality in Aras River catchment (Turkey); Application of phytoplankton metrics and multivariate approach. Ecological Indicators, 117, 106706.

Condé R.d.C., Martinez J.-M., Pessotto M.A., Villar R., Cochonneau G., Henry R., Lopes W. and Nogueira M. (2019). Indirect Assessment of Sedimentation in Hydropower Dams Using MODIS Remote Sensing Images. Remote Sensing, 11(3), 314.

Dalu T., Dube T., Froneman P. W., Sachikonye M. T., Clegg B. W., & Nhiwatiwa T. (2015). An assessment of chlorophyll-a concentration spatio-temporal variation using Landsat satellite data, in a small tropical reservoir. Geocarto international, 30(10), 1130-1143.

Das S. (2021). Dynamics of streamflow and sediment load in Peninsular Indian rivers (1965–2015). Sci Total Environ. 10 (799), 149372

Dorji P. and Fearns P. (2017). Impact of the spatial resolution of satellite remote sensing sensors in the quantification of total suspended sediment concentration: A case study in turbid waters of Northern Western Australia. PLOS ONE 12(4), e0175042.

Dutta V., Dubey D. and Kumar S. (2020). Cleaning the River Ganga: Impact of lockdown on water quality and future implications on river rejuvenation strategies. Science of the Total Environment, 743, 140756.

Garg V., Kumar A. S., Aggarwal S., Kumar V., Dhote P. R., Thakur P. K., . . . Muduli P. R. (2017). Spectral similarity approach for mapping turbidity of an inland waterbody. Journal of Hydrology, 550, 527-537.

Giles J. (2006). Methane quashes green credentials of hydropower. Nature, 444(7119), 524- 526.

Gondwe J.F., Li S., & Munthali R.M. (2021). Analysis of Land Use and Land Cover Changes in Urban Areas Using Remote Sensing: Case of Blantyre City. Discrete Dynamics in Nature and Society, 2021.

González-Márquez L.C., Torres-Bejarano F.M., Torregroza-Espinosa A.C., Hansen-Rodríguez I.R. and Rodríguez-Gallegos H.B. (2018). Use of LANDSAT 8 images for depth and water quality assessment of El Guájaro reservoir, Colombia. Journal of South American Earth Sciences, 82, 231-238.

Harrison J.A., Bouwman A., Mayorga E. and Seitzinger S.J.G.B.C. (2010). Magnitudes and sources of dissolved inorganic phosphorus inputs to surface fresh waters and the coastal zone: A new global model. Global Biogeochemical cycles, 24(1), GB1003.

Hegazy D., Abotalib A.Z., El-Bastaweesy M., El-Said M.A., Melegy A. and Garamoon H. (2020). Geo-environmental impacts of hydrogeological setting and anthropogenic activities on water quality in the Quaternary aquifer southeast of the Nile Delta, Egypt. Journal of African Earth Sciences, 172, 103947.

Hussain S., & Karuppannan S. (2021). Land use/land cover changes and their impact on land surface temperature using remote sensing technique in district Khanewal, Punjab Pakistan. Geology, Ecology, and Landscapes, 1-13.

Hussain S., Mubeen M., & Karuppannan S. (2022). Land use and land cover (LULC) change analysis using TM, ETM+ and OLI Landsat images in district of Okara, Punjab, Pakistan. Physics and Chemistry of the Earth, Parts A/B/C, 126, 103117.

IMAGINE E. (2015). Hexagon Geospatial. Planetek, ERDAS IMAGINE Tour Guide, PRODUCER Suite of Power Portfolio by Hexagon Geospatial; ERDAS IMAGINE | Hexagon Geospatial: Madison, AL, USA.

Johansen R., Beck R., Nowosad J., Nietch C., Xu M., Shu S., . . . Reif M. (2018). Evaluating the portability of satellite derived chlorophyll-a algorithms for temperate inland lakes using airborne hyperspectral imagery and dense surface observations. Harmful algae, 76, 35-46.

Kafy A.A., Al Rakib A., Akter K.S., Jahir D.M.A., Sikdar M.S., Ashrafi T.J., ... & Rahman M.M. (2021). Assessing and predicting land use/land cover, land surface temperature and urban thermal field variance index using Landsat imagery for Dhaka Metropolitan area. Environmental Challenges, 4, 100192.

Khan N.M., and Tingsanchali T. (2009). Optimization and simulation of reservoir operation with sediment evacuation: a case study of the Tarbela Dam, Pakistan. Hydrological processes: an international journal, 23(5), 730-747.

Koronkevich N.I., Barabanova E.A., Georgiadi A.G., Dolgov S.V., Zaitseva I.S. and Kashutina E.A. (2019). Assessing the Anthropogenic Impact on the Water Resources of Russia. Herald of the Russian Academy of Sciences, 89(3), 287-297.

Kudela R.M., Palacios S.L., Austerberry D.C., Accorsi E.K., Guild L.S., & Torres-Perez J. (2015). Application of hyperspectral remote sensing to cyanobacterial blooms in inland waters. Remote Sensing of Environment, 167, 196-205.

Kumar P., Dobriyal M., Kale A., & Pandey A.K. (2021).

Lacaux J.P., Tourre Y.M., Vignolles C., Ndione J.A., & Lafaye M. et al. (2007). Classification of ponds from high-spatial resolution remote sensing: Application to Rift Valley Fever epidemics in Senegal. Remote sensing of environment, 106(1), 66-74.

Liu X., Zhang G., Sun G., Wu Y., & Chen Y. (2019). Assessment of lake water quality and eutrophication risk in an agricultural irrigation area: a case study of the Chagan Lake in Northeast China. Water, 11(11), 2380.

Lymburner L., Botha E., Hestir E., Anstee J., Sagar S., Dekker A., & Malthus T. (2016). Landsat 8: Providing continuity and increased precision for measuring multi-decadal time series of total suspended matter. Remote Sensing of Environment 185, 108-118.

Masocha M., Dube T., Nhiwatiwa T., & Choruma D. (2018). Testing utility of Landsat 8 for remote assessment of water quality in two subtropical African reservoirs with contrasting trophic states. Geocarto international, 33(7), 667-680.

Mazhar N., Mirza A.I., Abbas S., Akram M.A.N., Ali M., & Javid K. (2021). Effects of climatic factors on the sedimentation trends of Tarbela Reservoir, Pakistan. SN Applied sciecnes, 3(1), 1-9.

Mishra D.R., Schaeffer B.A., & Keith D. (2014). Performance evaluation of normalized difference chlorophyll index in northern Gulf of Mexico estuaries using the Hyperspectral Imager for the Coastal Ocean. GIScience & Remote Sensing, 51(2), 175-198.

Mishra S., & Mishra D. R. (2012). Normalized difference chlorophyll index: A novel model for remote estimation of chlorophyll-a concentration in turbid productive waters. Remote Sensing of Environment, 117, 394-406.

Mishra S., & Jabin, S. (2020, October). Land Use Land Cover Change Detection using LANDSAT images: A Case Study. In 2020 IEEE 5th International Conference on Computing Communication and Automation (ICCCA) (pp. 730-735). IEEE.

Mukherjee F., & Singh D. (2020). Assessing land use–land cover change and its impact on land surface temperature using LANDSAT data: A comparison of two urban areas in India. Earth Systems and Environment, 4(2), 385-407.

Naz S., Ahsanuddin M., Inayatullah S., Siddiqi T. A., & Imtiaz M. (2019). Copula-based bivariate flood risk assessment on Tarbela Dam, Pakistan. Hydrology, 6(3), 79.

Ochoa-Contreras R., Jara-Marini M.E., Sanchez-Cabeza J.A., Meza-Figueroa D.M., Pérez-Bernal L.H., & Ruiz-Fernández A.C. (2021). Anthropogenic and climate induced trace element contamination in a water reservoir in northwestern Mexico. Environmental Science and Pollution Research, 28(13), 16895-16912.

Pervaiz S., Javid K., Khan F.Z., Zahid Y., & Akram M.A.N. (2020). Preliminary assessment of air during COVID-19 lockdown: An unintended benefit to environment. Environment and Natural Resources Journal, 18(4), 363-375.

Petkovšek G. (2018). Long-term modelling of reservoir sedimentation with turbid underflows. Journal of Soils and Sediments, 18(10), 3153-3165.

Pogorelov A., Laguta A., Kiselev E., & Lipilin D. (2021). Features of the long-term transformation of the Krasnodar reservoir, near the mouth of the Kuban River, Russia. Journal of Geographical Sciences, 31(12), 1895-1904.

Poletaeva V.I., Pastukhov M.V., & Tirskikh E.N. (2021). Dynamics of trace element composition of Bratsk Reservoir water in different periods of anthropogenic impact (Baikal Region, Russia). Archives of environmental contamination and toxicology, 80(3), 531-545.

Rabalais N.N., Turner R.E., Díaz R.J., & Justić D. (2009). Global change and eutrophication of coastal waters. ICES Journal of Marine Science, 66(7), 1528-1537.

Radhakrishnan N., Satish Kumar E., & Kumar S. (2014). Analysis of urban sprawl pattern in Tiruchirappalli city using applications of remote sensing and GIS. Arabian Journal Science and Engineering, 39(7), 5555-5563.

Rafique A., Burian S., Hassan D., & Bano R. (2020). Analysis of operational changes of Tarbela reservoir to improve the water supply, hydropower generation, and flood control objectives. Sustainability, 12(18), 7822.

Robin R.S., Purvaja R., Ganguly D., Hariharan G., Paneerselvam A., Sundari R. T., ... & Ramesh R. (2021). COVID-19 restrictions and their influences on ambient air, surface water and plastic waste in a coastal megacity, Chennai, India. Marine pollution bulletin, 171, 112739.

Roca M. (2012). Tarbela Dam in Pakistan. Case study of reservoir sedimentation.

Rutherfurd I.D., Kenyon C., Thoms M., Grove J., Turnbull J., Davies P., & Lawrence S. (2020). Human impacts on suspended sediment and turbidity in the River Murray, South Eastern Australia: Multiple lines of evidence. River Research and Applications, 36(4), 522-541.

Shafeeque M., Sarwar A., Basit A., Mohamed A.Z., Rasheed M.W., Khan M.U., Buttar N.A., Saddique N., Asim M.I., & Sabir R.M. (2022). Quantifying the Impact of the Billion Tree Afforestation Project (BTAP) on the Water Yield and Sediment Load in the Tarbela Reservoir of Pakistan Using the SWAT Model. Land, 11, 1650, DOI: 10.3390/land11101650

Singh, S. K., Singh, P., & Gautam, S. K. (2016). Appraisal of urban lake water quality through numerical index, multivariate statistics and earth observation data sets. International journal of environmental science and technology, 13(2), 445-456.

Srivastava P.K., Mukherjee S., Gupta M. (2010). Impact of urbanization on land use/land cover change using remote sensing and GIS: a case study. Int J Ecol Econ Stat 18(S10), 106-117.

Tate E.L., & Farquharson F.A. (2000). Simulating reservoir management under the threat of sedimentation: the case of Tarbela dam on the river Indus. Water Resources Management, 14(3), 191-208.

Temporal dynamics change of land use/land cover in Jhansi district of Uttar Pradesh over past 20 years using Landsat TM, ETM+ and OLI sensors. Remote Sensing Applications: Society and Environment, 23, 100579.

Tundu C., Tumbare M.J., & Kileshye Onema J.M. (2018). Sedimentation and its impacts/effects on river system and reservoir water quality: case study of Mazowe catchment, Zimbabwe. Proceedings of the International Association of Hydrological Sciences, 377, 57-66.

Vakili T., & Amanollahi J. (2020). Determination of optically inactive water quality variables using Landsat 8 data: A case study in Geshlagh reservoir affected by agricultural land use. Journal of Cleaner Production, 247, 119134.

Vörösmarty C. J., McIntyre P. B., Gessner M.O., Dudgeon D., Prusevich A., Green P., ... & Davies P.M. (2010). Global threats to human water security and river biodiversity. Nature, 467(7315), 555-561.

Watanabe F.S.Y., Alcântara E., Rodrigues T.W.P., Imai N.N., Barbosa C.C.F., & Rotta L. H.D.S. (2015). Estimation of chlorophyll-a concentration and the trophic state of the Barra Bonita hydroelectric reservoir using OLI/Landsat-8 images. International journal of environmental research and public health, 12(9), 10391-10417.

Wolf A.F. (2012). Using WorldView-2 Vis-NIR multispectral imagery to support land mapping and feature extraction using normalized difference index ratios. In Algorithms and technologies for multispectral, hyperspectral, and ultraspectral imagery XVIII, 8390, 188-195.

Wu G., de Leeuw J., Skidmore A. K., Prins H.H., & Liu Y. (2007). Concurrent monitoring of vessels and water turbidity enhances the strength of evidence in remotely sensed dredging impact assessment. Water Research, 41(15), 3271-3280.

Xu H., Yan C., Fu Q., Xiao K., Yu Y., Han D., ... & Cheng J. (2020). Possible environmental effects on the spread of COVID-19 in China. Science of the Total Environment, 731, 139211.

Yunus A.P., Masago Y., & Hijioka Y. (2020). COVID-19 and surface water quality: improved lake water quality during the lockdown. Science of the Total Environment, 731, 139012.

Zhang G., Ding W., Liu H., Yi L., Lei X., & Zhang O. (2021). Quantifying Climatic and Anthropogenic Influences on Water Discharge and Sediment Load in Xiangxi River Basin of the Three Gorges Reservoir Area. Water Resources, 48(2), 204-218.

ges.rgo.ru/jour/

ISSN 2542-1565 (Online)